

https://dspace.org/

# Naturally occurring asbestos (NOA) and asbestos contamination of the environment: Implications for in-situ risk assessment and rehabilitation

**Schapira, Jessica Shaye**

**2023-01**
University of the Witwatersrand, Johannesburg
https://hdl.handle.net/10539/42851
Schapira, Jessica Shaye. (2023). Naturally occurring asbestos (NOA) and asbestos contamination of the environment: Implications for in-situ risk assessment and rehabilitation. [PhD thesis, University of the Witwatersrand, Johannesburg]. https://hdl.handle.net/10539/42851

Downloaded from a DSpace repository. https://dspace.org/

# Naturally occurring asbestos (NOA) and asbestos contamination of the environment: Implications for *in-situ* risk assessment and rehabilitation




by

Jessica Shaye Schapira

A thesis submitted to the Faculty of Science, University of the Witwatersrand, Johannesburg, in fulfilment of the requirements for the degree of Doctor of Philosophy

School of Geosciences and School of Molecular and Cell Biology

University of the Witwatersrand

Johannesburg September 2023

# Declaration

I declare that this thesis is my own, unaided work. It is being submitted for the Degree of Doctor of Philosophy at the University of the Witwatersrand, Johannesburg. It has not been submitted before for any degree or examination in any other University.



Jessica Shaye Schapira (signature)

4th day of September 2023, Springs, South Africa

# Abstract

The risk associated with asbestos minerals is an enduring global concern, especially with regards to exposure at the sources. The risks connected to exposure in their natural contexts (i.e., derelict mine sites and naturally occurring asbestos) form the subject of this study. These sites are plentiful throughout Southern Africa (and Africa) and are considered as unconfined, thereby constituting large environmental and human health risks. Asbestos in these settings is not inherently hazardous unless dispersed from its sources into environmental systems, such as the atmosphere, where it may be inhaled. Compared to occupational asbestos exposure, environmental sources present unique challenges with respect to their potential risks. Literature focused on these sites is lacking and without extensive knowledge the risks remain greatly unknown, and thus asbestos site assessment frameworks are imperative. South Africa, with its geological richness, allows for all aspects of environmental asbestos to be studied in its natural context.

In this research, mineral fibres from derelict asbestos mine sites were characterised mineralogically and geochemically to identify and assess their human health hazard potential, to define the degree of toxicity and to determine the potential negative environmental effects. High concentrations of heavy metals, including copper, iron, magnesium, manganese and zinc detrimental to human health and environmental functioning were measured in these fibrous minerals using X-ray fluorescence (XRF) . The chemical stability of four asbestos minerals was studied using batch isothermal dissolution tests in acidic solutions and their stability determined as follows: chrysotile < crocidolite < amosite < anthophyllite. Significant inferences can be made regarding the persistence of asbestos particles in their natural environments from dissolution kinetics mechanisms.

The mineralogical, geochemical, and microbiological characterisation of solid asbestos mine waste rock substrates indicate that their properties, such as low macro and micronutrients and lack of properties of true soils, strongly alkaline pH and low to zero microbial abundance and diversity present significant challenges to rehabilitation strategies. Such parameters are identified as important baseline conditions that need to be considered prior to rehabilitation implementation, if long-term, self-sustaining ecological restoration is to be achieved on these sites.

Present bio-solutions to ensure asbestos mine land rehabilitation success are discussed and the potential of using available agronomic bio-fertilisers (microbial strain *Pseudomonas fluorescens*) is examined. The growth-based assays indicate that this micro-organism is suitable for an environmental biotechnology applied to ecosystem restoration of asbestos-mining lands.

Naturally Occurring Asbestos (NOA) occurrences are highly dependent upon the geological conditions, and understanding these in a large variety of settings may allow the development of predictive strategies necessary for *in situ* identification and hazard assessment required for health risk mitigation in the context of mining and other geologically disruptive activities. A variety of natural asbestos rock samples was examined, showing how geological databases relevant for predicting natural occurrences of asbestos provide baseline data required for mitigating asbestos exposure risks.

# Acknowledgements

The Centre of Excellence for Integrated Mineral and Energy Resource Analysis (CIMERA) is thanked for funding this project.

I am grateful to my supervisors Professor Robert Bolhar, Dr Sharad Master and Professor Karl Rumbold for all their support and counsel in their respective fields constituting this multi-interdisciplinary research.

I would like to thank Dr Loic Le Bras for mentoring, supporting, and guiding me through my PhD journey.

Many thanks to Professor Robert Bolhar for allowing me to pursue my curiosity into aspects not considered as conventional geosciences and keeping me on track.

Special thanks to Professor Karl Rumbold for taking a chance on me and teaching me invaluable microbiological laboratory skills.

Thank you to Dr Sanchia Moodley and Sasha Richardson (School of Molecular and Cell Biology, University of the Witwatersrand) for their patience and governance in the MSB laboratory.

Thank you to Eric Cousins (First Quantum Minerals Limited (FQML), Professor Paul Nex (Economic geology, University of the Witwatersrand) and Oliver Barker (Banzi Geotechnics Pty) for providing all the samples studied.

Thank you to Alicia Greyer (Microbial Biological Fertilizers International (MBFi)) for providing the biofertilizer studied.

# Table of contents


| Chapters | Contents | Page number |
|---|---|---|
| | | |
| Declaration | | 2 |
| | | |
| Abstract | | 3 |
| | | |
| Acknowledgements | | 5 |
| | | |
| Contents | | 6 |
| | | |
| Structure of thesis | | 10 |
| | | |
| List of figures | | 12 |
| | | |
| List of graphs | | 26 |
| | | |
| List of tables | | 27 |
| | | |
| Nomenclature | | 33 |
| | | |
| Chapter 1 | Introduction | 34 |
| 1.1. | General introduction | 34 |
| 1.2. | Asbestos | 37 |
| 1.2.1. | Brief overview of asbestos mineralogy | 38 |
| 1.2.2. | Asbestos toxicity and sources of exposure | 40 |
| 1.2.3. | Asbestos-related lung diseases (ARLDs) | 42 |
| 1.2.4. | Defining the term 'asbestos' | 43 |
| 1.3. | Project overview | 45 |
| 1.3.1. | Derelict asbestos mine lands (DAMLs) | 45 |
| 1.3.2. | Managing and rehabilitating DAMLs | 48 |
| 1.3.3. | Conventional technologies for asbestos remediation | 55 |
| 1.3.4. | Bio-augmentation-assisted rehabilitation of DAMLs | 59 |
| 1.3.5. | Naturally occurring asbestos (NOA) | 71 |
| 1.4 | Aims and objectives | 72 |
| 1.5. | References | 74 |
| | | |
| Chapter 2 | Mineralogical, petrological, and geochemical characterisation of chrysotile, amosite and crocidolite asbestos from mine waste in Southern Africa in the context of hazard evaluation and rehabilitation | 95 |
| 2.1. | Introduction | 96 |
| 2.2. | Materials and methods | 97 |
| 2.2.1. | Sampling locations and geological background | 97 |
| 2.2.2. | Polarising light microscopy (PLM) | 100 |
| 2.2.3. | Crushing | 101 |
| 2.2.4. | X-ray diffraction (XRD) | 101 |
| 2.2.5. | X-ray fluorescence (XRF) | 102 |
| 2.2.6. | BET-$N_2$ specific surface area (SSA) | 102 |
| 2.2.7. | Bio-durability tests | 102 |
| 2.3. | Results | 103 |
| 2.3.1. | Bulk material description | 103 |
| 2.3.2. | Polarising light microscopy (PLM) | 107 |
| 2.3.3. | X-ray diffraction (XRD) | 113 |
| 2.3.4. | X-ray fluorescence (XRF) major and trace elemental analysis | 117 |
| 2.3.5. | BET-$N_2$ specific surface area (SSA) | 118 |
| 2.3.6. | Bio-durability tests | 119 |
| 2.4. | Discussion | 121 |

| | | |
|---|---|---|
| 2.5. | Implications for the environment and rehabilitation | 127 |
| 2.6. | Conclusion | 129 |
| 2.7. | References | 129 |
| | | |
| Chapter 3 | Using kinetics models to study mechanisms of asbestos dissolution for inferences of chemical stability in the natural environment | 145 |
| 3.1. | Introduction | 145 |
| 3.2. | Materials and methods | 148 |
| 3.2.1. | Asbestos samples | 148 |
| 3.2.2. | Isothermal dissolution experiments | 149 |
| 3.2.3. | Heterogenous solid-liquid kinetics models | 149 |
| 3.3.4. | Solid-state kinetics models | 150 |
| 3.2.5. | Statistical analysis | 153 |
| 3.3. | Results | 153 |
| 3.3.1. | Bulk geochemistry of asbestos samples | 153 |
| 3.3.2. | Mass loss and pH measurements | 156 |
| 3.3.3. | Solid-liquid kinetics | 157 |
| 3.3.4. | Solid-state kinetics | 162 |
| 3.4. | Discussion | 165 |
| 3.4.1. | Mass loss and pH | 165 |
| 3.4.2. | Conversion curves and dissolution mechanisms | 167 |
| 3.4.3. | Solid-liquid dissolution mechanisms | 168 |
| 3.4.4. | Solid-state dissolution mechanisms | 169 |
| 3.5. | Conclusion | 171 |
| 3.6. | References | 172 |
| | | |
| Chapter 4 | Preliminary characterisation of mineralogical and microbiological constraints of banded-iron formation hosted asbestos mine dumps as substrates for the long-term revegetation and phyto-stabilisation by native plant species | 188 |
| 4.1. | Introduction | 188 |
| 4.2. | Materials and methods | 190 |
| 4.2.1. | Sample location and collection | 190 |
| 4.2.2. | Mineralogical characterisation and pate-pH-conductivity 1:10 (w/v) | 192 |
| 4.2.3. | Analysis of mine waste microbial community by culture-dependent methods | 193 |
| 4.2.4. | Analysis of mine waste microbial community by culture-independent methods | 194 |
| 4.3. | Results | 199 |
| 4.3.1. | Mineralogy, pH and EC | 199 |
| 4.3.2. | Culture-dependent methods | 200 |
| 4.3.3. | Culture-independent methods | 200 |
| 4.4. | Discussion | 200 |
| 4.5. | Conclusion | 205 |
| 4.6. | References | 206 |
| | | |
| Chapter 5 | Rhizosphere competence and abiotic stress tolerance of commercially sold *Pseudomonas fluorescens* bio-fertiliser: implication for their bioremediation potential | 212 |
| 5.1. | Introduction | 213 |
| 5.2. | Materials and methods | 216 |
| 5.2.1. | Microorganisms, maintenance, and storage | 216 |
| 5.2.2. | Media composition and preparation of experimental plates | 217 |
| 5.2.3. | Detection of motility | 218 |
| 5.2.4. | Detection of fluorescence | 218 |
| 5.2.5. | pH tolerance tests | 219 |
| 5.2.6. | Temperature tolerance tests | 219 |
| 5.2.7. | Salinity tolerance tests | 219 |
| 5.2.8. | Heavy metal (HM) tolerance tests | 219 |
| 5.3. | Results | 220 |
| 5.3.1. | Effect of media composition on colony morphology, colour and growth | 220 |
| 5.3.2. | Abiotic stress tolerance and growth | 226 |
| 5.3.3. | Heavy metal (HM) tolerance and growth | 227 |
| 5.4. | Discussion | 228 |

| | | |
|---|---|---|
| 5.5. | Conclusion | 231 |
| 5.6. | References | 231 |
| | | |
| Chapter 6 | Crocidolite and amosite asbestos occurrences and mineralisation in the Precambrian Banded Iron Formations of South Africa: Implications for iron and manganese ore mining and significance for field identification and *in situ* hazard evaluation | 236 |
| 6.1. | Introduction | 236 |
| 6.2. | The geographical and geological context of BIF-hosted amphibole asbestos in South Africa | 238 |
| 6.3. | Methodology | 240 |
| 6.3.1. | Samples | 240 |
| 6.3.2. | Determination of carbonate presence | 242 |
| 6.3.3. | Distinguishing fibrous and pseudo-fibrous minerals | 242 |
| 6.4. | Results | 243 |
| 6.5. | Discussion | 278 |
| 6.6. | Geological factors potentially responsible for BIF hosted asbestos mineralisation | 288 |
| 6.7. | Hawks-eye (sample 12): pseudo-morphic replacement of crocidolite by quartz or crack-seal fracture filling? | 295 |
| 6.8. | Implications for *in situ* asbestos identification and hazard assessment | 302 |
| 6.9. | Conclusion | 303 |
| 6.10. | References | 304 |
| | | |
| Chapter 7 | Fibrous minerals and Naturally Occurring Asbestos (NOA) in the metacarbonate-hosted Fe oxide-Cu-Au-Co mineralised rocks from the Guelb Moghrein Mine, Akjoujt, Mauritania: Implications for *in situ* hazard assessment and mitigation protocols | 314 |
| 7.1. | Introduction | 315 |
| 7.2. | Geological background and mineralisation | 316 |
| 7.3. | Materials and methods | 318 |
| 7.3.1. | Sample location and collection | 318 |
| 7.3.2. | Sample characterisation | 320 |
| 7.3.3. | Fibre subsample extraction; distinguishing fibrous and pseudo-fibrous minerals, and acid test on fibre (determination of carbonate presence) | 322 |
| 7.3.4. | Mineralogical and geochemical investigation | 322 |
| 7.3.5. | Polarised light microscopy (PLM) | 322 |
| 7.3.6. | X-ray diffraction (XRD) | 323 |
| 7.3.7. | X-ray fluorescence (XRF) | 323 |
| 7.3.8. | BET-$N_2$ specific surface area (SSA) | 324 |
| 7.4. | Results | 324 |
| 7.4.1. | Sample characterisation | 324 |
| 7.4.2. | Polarised light microscopy (PLM) | 334 |
| 7.4.3. | X-ray diffraction (XRD), X-ray fluorescence (XRF) and BET-$N_2$ specific surface area (SSA) (sample 1) | 337 |
| 7.5. | Discussion | 340 |
| 7.6. | Implications for *in situ* identification and health risk assessment | 343 |
| 7.7. | Conclusion | 344 |
| 7.8. | References | 344 |
| | | |
| Chapter 8 | Toxic element enrichment and potential ecological risks from asbestos-bearing mine wastes | 350 |
| 8.1. | Introduction | 350 |
| 8.2. | Methodology | 352 |
| 8.2.1. | Chemical analysis of asbestos | 352 |
| 8.2.2. | Pollution Indices for assessing metal contamination in asbestos rock samples | 352 |
| 8.2.3. | Ecological risk assessment | 357 |
| 8.2.4. | Health risk assessment | 358 |
| 8.2.5. | Statistical analysis | 359 |
| 8.3. | Results | 359 |
| 8.3.1. | Heavy metal concentrations | 359 |
| 8.3.2. | Contamination level of heavy metals in different asbestos mine wastes | 361 |
| 8.3.3. | Ecological risk assessment | 365 |

| | | |
|---|---|---|
| 8.3.4. | Health risk assessment | 367 |
| 8.3.5. | Statistical analysis | 368 |
| 8.4. | Discussion | 370 |
| 8.5. | Conclusion | 372 |
| 8.6. | References | 372 |
| | | |
| Chapter 9 | The importance of functional integration of independent studies to the environmental management of asbestos-polluted mine land | 384 |
| 9.1. | Introduction | 384 |
| 9.2. | Multi-faceted approach to remediation | 384 |
| 9.3. | Conclusion | 390 |
| 9.4. | References | 391 |
| | | |
| Chapter 10 | Conclusions | 402 |
| | | |

# Structure of thesis

Part 1 (chapter 1) provides an introduction and background to the research. The issue of environmental asbestos in South Africa is multifaceted and complex hindering governmental, public, and environmental health protection strategies.

Part 2 (chapters 2 and 3) identifies and describes the historical issue of asbestos mine waste and its relationship to healthy living and sustainable environments. Asbestos fibre exposure for Derelict Asbestos Mine Lands (DAML) is examined in terms of environmental and human health risks. In chapter 2 the mineralogy and geochemistry of solid asbestos mine waste is characterised and evaluated as the essential baseline knowledge for predicting the environmental and human health impacts of these sites. This data allows for the potential fibre toxicity of asbestos fibres polluting DAMLs to be estimated, with relevance for developing countries without available *in vivo* experimental and exposure data required for risk evaluations. Additionally, this data allows an understanding of the extent to which asbestos minerals polluting DAMLs may induce environmental hazards and risks in the surrounding area. The chemical stability of asbestos fibres in terrestrial environments is examined in chapter 3 using dissolution experiments. The rates and mechanisms of asbestos dissolution allow inferences of the persistence of asbestos minerals in asbestos mine waste relevant for risk assessments.

Part 3 (chapter 4 and 5) explores the short-term nature of asbestos mine dump rehabilitation and potential solutions based on biotechnology. Asbestos mine dumps are mostly devoid of vegetation and unproductive, acting as a perennial source of asbestos fibre emissions. The social and environmental impacts of asbestos mine wastes in DAML are considerable; literature suggests that current rehabilitation methods for DAMLs are not suitable for mitigating their negative impacts in the long-term. In chapter 4 the mineralogy and microbiology of solid asbestos mine waste is evaluated to determine the physicochemical, mineralogical, and microbiological limitations for rehabilitation. The combined properties of asbestos mine dumps dictate the success and long-term trajectory of rehabilitation. Thus, these baseline evaluations are crucial for both identifying the issues likely to affect revegetation and driving how rehabilitation is conducted. Baseline data is essential for assessing the long-term viability of the selected rehabilitation design, providing key knowledge

for predicting the environmental impact. Chapter 5 explores whether commercially available biofertilisers may provide a viable solution to revegetation and rehabilitation of asbestos mine dumps. Here, the commercially-sold biofertilizer, *Pseudomonas fluorescens*, is evaluated for whether it demonstrates favourable characteristics indicating adaptability and tolerance to abiotic stresses important in the context of remediation of contaminated soils; it can act as a bio-inoculant for plant growth promotion of asbestos contaminated sites.

Part 4 (chapter 6 and 7) focuses on the lack of national management policies for preventing the risks of asbestos exposure during industrial activities; it presents geology-based solutions to improving frameworks for protection plants. Datasets pertaining to the geologic settings of asbestos formation are demonstrated as important tools for land managers and safety and health administrators involved in geologically disturbing industries. Chapters 6 and 7 examine NOA and provide geobiological correlation and characterisation required for mitigation of environmental asbestos exposure. Geological knowledge of NOA allows asbestos emission prediction and control strategies to be implemented prior to mining activities and thus the amelioration of asbestos release.

Part 5 (chapter 8, 9 and 10) aims to integrate the ideas and results of the individual sub-studies into an encompassing and comprehensive research project that has overall scientific value.

# List of figures.

Figure 1.1: Potential hazards of fibre release and dispersion of environmental asbestos into the environment and the risks to human and environmental health

Figure 1.2: Two environmental asbestos exposure sources of focus of this research

Figure 1.3: Schematic illustration of asbestos mineral groups, asbestos mineral types and their chemical formula

Figure 1.4: Major categories of asbestos-related lung diseases and schematic illustration of pathologic features of each

Figure 1.5: Methodology followed using the rehabilitation priority index to identify and monitor the status of asbestos mine rehabilitation.

Figure 1.6: Steps involved in asbestos mine dump rehabilitation using encapsulation and soil remediation approaches.

Figure 1.7: Typical trajectory followed by current mine rehabilitation practices (adapted from Huang *et al.,* 2012)

Figure 1.8: Assumptions of current rehabilitation strategy (adapted from Huang *et al.,* 2012)

Figure 1.9: Airborne and subsurface dispersion of asbestos fibres

Figure 1.10: 'Encapsulation' rehabilitation method of asbestos contaminated soils, dumps, tailings and mine sites

Figure 1.11: Problems facing the current 'encapsulation' rehabilitation method of asbestos contaminated soils, dumps, tailings and mine sites

Figure 1.12: Recognition and evaluation of potential problems associated with reclamation

Figure 1.13: Flow chart depicting the mechanical/physical processes resulting in asbestos fibres dispersion and distribution in the environments (adapted from Vignaroli *et al.,* 2014; Lucci *et al.,* 2018).

Figure 2.1.: Graphical abstract showing typical layout and interrelationships between rural communities and DAMLs in Southern Africa.

Figure 2.2: (A) Chrysotile rock sample; (B) length of fibres spanning the width of veins; (C) individual masses of matted white fibres and (D) parting at the centre of the vein width halving the length of the cross-vein fibres

Figure 2.3: (A) Amosite rock sample and (B) matted and splintery fibres

Figure 2.4: (A) Crocidolite rock sample and (b) showing slight curvature of poly-filamentous bundles

Figure 2.5: Chrysotile fibre bundle (PPL). Notice the break in the bundle in the top right.

Figure 2.6: Chrysotile fibre bundle (XPL)

Figure 2.7: Partially altered chrysotile fibres shown by amorphous, irregular material and cloudiness (PPL)

Figure 2.8: Partially altered chrysotile fibres shown by amorphous, irregular material and cloudiness (XPL)

Figure 2.9: Extremely fine amosite fibres showing parallel alignment and matting (PPL)

Figure 2.10: Extremely fine amosite fibres showing parallel alignment and matting (XPL)

Figure 2.11: Amosite fibres at maximum angle of pleochroism showing heterogenous colours (PPL)

Figure 2.12: Amosite fibres at maximum angle of birefringence showing heterogenous interference colours (XPL)

Figure 2.13: Poly-filamentous crocidolite (PPL)

Figure 2.14: Poly-filamentous crocidolite (XPL)

Figure 2.15: Crocidolite fibres with spayed ends (PPL)

Figure 2.16: Crocidolite fibres with spayed ends (XPL)

Figure 3.1: Dissolution models of solid particles (modified from Safari *et al.,* 2009)

Figure 3.2: pH of the acidic solution versus time during the dissolution of asbestos particles

Figure 3.3: Diagram showing biphasic dissolved mass fraction, α, released from chrysotile, amosite, crocidolite and anthophyllite rocks in acidic solution consisting of an initial rapid stage followed by a slower later phase, when plotted vs t.

Figure 3.4: Experimental data fitted to shrinking core models for the entire dissolution reaction (0 to 720 hours). Y-axis represents the left-hand side of the shrinking core equations. The suitability of the models was evaluated using the correlation coefficient $r^2$.

Figure 3.5: Experimental data fitted to shrinking core models for the first 48 hours (fast stage). The Y-axis represents the left-hand side of the shrinking core equations. The suitability of the models was evaluated using the correlation coefficient $r^2$.

Figure 3.6: Experimental data fitted to shrinking core models for 48 – 720 hours (slow stage). The Y-axis represents the left-hand side of the shrinking core equations. The suitability of the models was evaluated using the correlation coefficient $r^2$.

Figure 3.7: Experimental data fitted to solid-state kinetics models

Figure 3.8: Schematic diagram showing surface chemical and diffusion control reactions of shrinking core model (SCM).

Figure 4.1: Google Earth image of derelict amosite mine, Penge, Limpopo

Figure 4.2: Google Earth image of derelict crocidolite mine, Postmasburg, Northern Cape. Notice the blue colour of the crocidolite.

Figure 4.3: Bacterial and fungal media used for culture-dependent microbial analysis

Figure 4.4: Microbial enumeration in LB broth for (a) powdered asbestos rock material and (b) asbestos mineral fibres

Figure 4.5: ZR Soil Microbe DNA Kit Miniprep™ (Zymo Research, Irvine, CA, USA) (ZR kit)

Figure 4.6: Qubit 2.0 Fluorometer

Figure 4.7: Thermal cycler apparatus used for PCR analysis

Figure 4.8: Horizontal gel electrophoresis tank

Figure 4.9: Bio-Rad ChemiDoc machine for gel visualisation of DNA

Figure 4.10: Edaphic conditions characterising DAMLs and the surrounding environments.

Figure 5.1: Graphical abstract showing practical science for allowing environmental sustainability progress under the biotechnology development limitations of developing countries.

Figure 5.2: Applications of biotechnology and alternative applications of agricultural and in environmental. (a) Antibiotic production; (b) genetic engineering for human application; (c) genetic engineering for plant and animal applications; (d) decontamination, biomonitoring, biosensors, and pollution prevention, and (e) fermentation products (adapted from Gavrilescu, 2010)

Figure 5.3: (a) Morphology and (b) fluorescence of PGPR *Pseudomonas fluorescens* on Pseudomonas agar over 3 days of incubation

Figure 5.4: (a) Morphology and (b) fluorescence of PGPR *Pseudomonas fluorescens* on Kings B agar over 3 days of incubation

Figure 5.5: (a) Morphology and (b) fluorescence of PGPR *Pseudomonas fluorescens* on LB agar over 3 days of incubation

Figure 5.6: (a) Morphology and (b) fluorescence of PGPR *Pseudomonas fluorescens* on nutrient agar over 3 days of incubation

Figure 6.1: Two structural basins of the Transvaal Supergroup: Griqualand West Basin and Transvaal Basin (adapted from Hodgson, 1977)

Figure 6.2: Composite seam of oxidised crocidolite (griqualandite) displaying ‘corrugated’ or cone structures and bifurcation of thin magnetite seams.

Figure 6.3: Oxidised crocidolite fibres: (a) Disseminated magnetite crystals in the upper portion of the fibre seam derived from the upper magnetite screen; (b) fragments of the magnetite layers scattered throughout the fibres derived from the magnetite bands overlying and underlying the cross-fibre and (c) texture and colour of the soft, ochreous, matted fibrous griqualandite material that resulted from the oxidation of crocidolite.

Figure 6.4: Oxidised, simple crocidolite cross-fibre seam showing magnetite screen at the upper bounding surface.

Figure 6.5: Three silvery crocidolite seams within a ‘sandy’ jasper host rock

Figure 6.6: Irregular upper bounding surface of thickest seam due to local warping of bedding

Figure 6.7: Composite crocidolite seam in banded chert

Figure 6.8: Composite seam of cross-fibre crocidolite having a wavy central magnetite parting and interface buckling at the upper bounding surface.

Figure 6.9: Composite cross-fibre seam that exhibits variation in fibre lengths. The seam in the upper portion of the image has irregular and wavy bounding surfaces resulting in length variations in cross-fibres. The seam in the lower portion of the image shows wavelike behaviour of the fibres due to irregular wave-like magnetite partings resulting in variations in fibre length.

Figure 6.10: Spherulites of fibrous riebeckite associated with irregular magnetite layers disrupting crocidolite cross-fibres.

Figure 6.11: Discoloured, oxidised and silicified composite seam in thinly banded shaly material and brown jasper. Side views are shown in (a) and (c) and the back view in (b).

Figure 6.12: Brown acicular amphibole cross-fibre seam with planar bounding surfaces

Figure 6.13: Composite seam composed of cross-fibre crocidolite in lenses of mass fibre riebeckite

Figure 6.14: Blue coloured riebeckite rich bands composed of complex, interwoven, dis-orientated acicular crystals

Figure 6.15: Section through the seam to show the variation in the small fibre seams due to irregular pinch and swell behaviour of bounding surfaces

Figure 6.16: (a) Pinch-and-swell structures and (b) green and black cross-fibres characterising the sample.

Figure 6.17: Carbonate-rich rock containing cross-fibre brown acicular amphibole with large magnetite dispersed through the fibres and concentrated at the bounding surfaces.

Figure 6.18: Silicified crocidolite seam in banded jasper and ironstone showing a complex composite structure.

Figure 6.19: Wavelike behaviour and subsequent rapid variation of fibre lengths. The wavy seams above and below one another have extremely similar profiles formed during fibre growth.

Figure 6.20: Three different cone-in-cone structures lying next to one another along the same plane (a) (0.8 cm L x 0.7 cm H); (b) (0.8 cm L x 1 cm H); (c) (0.9 cm L x 0.4 cm H) (L = length; H = height). Cone in the seam contains a number of subsidiary cone-shaped layers of magnetite resulting in cone-in-cone structures.

Figure 6.21: Silicified mix Hawks-eye and Tigers-eye simple seam showing many kink bands across length of seam.

Figure 6.22: Compact, columnar quartz material comprising the bedding-parallel cross-fibre seam

Figure 6.23: Silicified simple cross-fibre seam

Figure 6.24: Various orientations assumed by the fibres across the width of the seam

Figure 6.25: Mixed fibre orientations exhibited across the length of the seam

Figure 6.26: Silicified Hawks-eye seam showing a cone-in-cone structure at the lower margins, marginal ‘fibrous’ quartz at the lower seam margin and deformation structures.

Figure 6.27: Different structural features associated with the cone-in-cone structure. The dashed purple lines outline two magnetite laminae fundemental to the two separate cone structures highlighted in the figure. Lower dashed purple line shows the discontinuous magnetic screen following the upper surface of the cone shaped cross-fibre crocidolite seam indicating that the unequal growth of the fibres resulted in their movement and shape. The ruptured magnetite is separated by orange-brown chert. Upper dashed purple line shows warped, curved and disrupted segments and/or remnants of what was a previously connected and continuous magnetite band between the crocidolite seam and lower contant chert wall rock. The pinch-and-swell and subsequent conical appearance of the chert laminae indicate a pressure phenomenon resulting in the upward transfer of wall material in isolated areas along the lower seam contact. The minute fractures are observed in the figure and trend more or less perpendicular to the bedding planes crest of the cone (shown by the red dashed lines) and represent small-scale faulting, which typically accompanies folding of rock laminae. The magnetite laminae display drag structures on either sides of these fractures, which can be observed in the top left portion of the figure. The above features provide evidence for small scale folding after consolodation of the rock. Formation of the fibres resulted in the observed conical proturbance of the enclosing rock into the crocidolite seam. Massive reibeckite pods, infered from macroscopic investigations, shown in the yellow ovals, are composed of randomly orientated, slender riebeckite needles forming intricately interlocking aggregates and giving a mesh appearance. These reibeckite pods occur between the cone and the fragmented piece of the magnetite bands following the curvature of the outer cone surface.

Figure 6.28: Back view of the sample showing various structures that will be described separately in the images corresponding to the blocks.

Figure 6.29: Complex dislocation structures between magnetite and bedding parallel fibrous quartz veins. Also notice the greyish blue slip fibre riebeckite at the upper left part of the image.

Figure 6.30: Thin bedding-parallel quartz veins lying above the seam between chert and magnetite laminae.

Figure 6.31: Gradation of colour across the direction of the fibrous quartz vein from yellow to blue indicating an increased infilling of fibrous riebeckite material within the bedding-parallel fibrous quartz veins.

Figure 6.32: Dislocation structures formed between magnetite layers and marginal fibrous quartz

Figure 6.33: Close up image of the planar features observed in this specimen

Figure 6.34: The images above show the (a) side view (1); (b) side view (2) and (c) front view of a Tigers-eye rock specimen.

Figure 6.35: Cone microstructures observed on the upper bounding surface and protruding from persistent central partings dividing the seam into two portions. Notice the magnetite screens making up the marginal bounding surface and the central discontinuity across the seam.

Figure 6.36: The image shows the same cone structure photographed using different light sources to highlight the various components of this peculiar structure.

Figure 6.37: Highly unusual cone structure formed by large, coarse, multi-coloured, and interlocking quartz crystals. The cone shape is outlined by dark-grey magnetite laminae of varying thickness.

Figure 6.38: Silicified crocidolite cross-fibre seam showing mixed fibre orientations

Figure 6.39: Silicified; mixed fibres orientation and extremely compact cross-fibres

Figure 6.40: Crocidolite from the Malips Drift area of the Pietersburg District of Limpopo

Figure 6.41: Single folded crocidolite cross-fibre seam

Figure 6.42: Different stages of weathering and subsequent effects on cohesion of fibres within a single sample (A). The fibrous mass presents a deep blue, compact, smooth, silky-lustrous surface,

parallel oriented fibres, fibre bundles; (B) lavender blue, non-lustrous, fluffy, moderately compact fibre bundles and, (C) grey, ashy, dull, fluffy, loose, poorly compact fibrous mass rather than bundles of parallel fibres.

Figure 6.43: Close up view showing different stages of alteration reflected in fibre colour, 'wooliness' and cohesion.

Figure 6.44: Amosite asbestos cross-fibre seam in host rock containing grunerite needles giving the rock a speckled or 'sugary' appearance.

Figure 6.45: The walls of the cross-fibre bands shown in this image are irregular and wavy with the upper bounding surface being the more extreme of the two.

Figure 6.46: Cusp and lobe upper bounding surface and approximately planar lower bounding surface with cone structure filled with fibres. Notice the loose, long, and relatively stiff, amosite fibres on the surface of the seam.

Figure 6.47: Amosite rock sample (side view 1)

Figure 6.48: Amosite rock sample (side view 2)

Figure 6.49: Jagged and uneven upper bounding surface formed due to the unequal growth of fibres.

Figure 6.50: Jagged and uneven upper bounding surface formed due to the unequal growth of fibres and the cross-cutting relationship of the fibres with the bedding-planes of the host rock.

Figure 6.51: Amosite asbestos rock sample; notice the wavy, uneven, and unclear bounding surfaces due to overgrowth of grunerite needles.

Figure 6.52: Amosite seam having a waste cone that does not contain any amosite fibres.

Figure 6.53: Five stages in the development of spherulite fibres (adapted from Keller, 1958 and Genis, 1961)

Figure 6.54: Inclined orientation of fibres owing to sliding of opposite bounding surfaces (a) movement along one bounding surface; (b) movement along both bounding surfaces; and (c) shearing of the cross-fibres in the direction of greatest movement (adapted from Hanekom, 1966).

Figure 6.55: The conversion of layers of mass fibre into composite crocidolite seams with partings of magnetite. The conical structures occur in the lower portion of the seam only (adapted from Fockema, 1967).

Figure 6.56: Crack-seal deformation: (a) elastic strain, (b) fracture, (c) sealing, (d) later fracture, (e) overgrowth and sealing, and (f) development of fibrous microstructure by repeated crack-seal increments (adapted from Cox and Etheridge, 1983)

Figure 6.57: Dilation growth during the force of asbestos fibre crystallisation/growth. The amphibole asbestos cross-fibre seams are formed by dilation growth shown in (a) to (d) where space is progressively created by the force of crocidolite/amosite fibre growth along their lengths.

Figure 6.58: Image showing Hawks-eye rock sample

Figure 6.59: Small deformation structures observed in the Hawks-eye rock sample

Figure 6.60: Proposed model for the history and formation of crocidolite and Hawks-eye in sample 12 (figure 5)

Figure 6.61: Proposed model for the history and formation of crocidolite and Hawks-eye in sample 12 (figure 5) continued

Figure 6.62: (1) Un-altered sample, cohesion is substantial, releasability is low; (2) beginning of alteration, discolouration, cohesion progressively decreases, releasability is the greatest; (3) moderate alteration, oxidation, pseudo-fibrous, loss of aerodynamic fibrous morphology, low

dispersibility potential and, (4) silicification, cohesion is great, no potential of airborne and waterborne releasability and dispersion. The progressive loss of cohesion of fibres in host rock followed by release of fibre bundles and subsequent from fibre release is shown by the arrow in (a). However, the integrity of the fibrous structure is intact and thus the highest potential for airborne release is approached (c). Following (c) the structural integrity of the fibres breaks down and therefore the hazards of fibre dispersion decrease along (b) with loss of morphological parameters pertinent to toxicity

Figure 7.1: Graphical abstract of work investigated in the study

Figure 7.2: Regional geological setting of the Guelb Moghrein Fe oxide Cu-Au deposit (taken from Kolb and Petrov, 2016)

Figure 7.3: Schematic illustration of the Fe oxide-Cu-Au-Co mineralised meta-carbonate deposit of the Guelb Moghrein (adapted from Sakellaris, 2007)

Figure 7.4.: Photographs of different parts of the Guelb Moghrein mine

Figure 7.5: Flowchart of the geology-based approach for macroscale characterisation corresponding to geological and structural features of the asbestos hazard associated meta-carbonate rocks examined.

Figure 7.6: Rock sample 1 showing least altered siderite with white to clove brown coloured, ‘slip-fibre’ type poly-filamentous, parallel arranged fibre bundles on the surfaces. Curvature of fibres and bundles, and splayed and/or frayed fibre bundle ends are observed.

Figure 7.7: Rock sample 2 showing long pebble-like, low clast/matrix ratio siderite breccia surrounded by very long, fine fibrous amphibole.

Figure 7.8: Sample 3 to 6 showing discrete, white to clove brown parallel-arranged fibre bundles ranging in length from 11 to 6 cm. The bundles of fibres demonstrate ridged acicular habit. The

bundle ends shown in sample 4 are splayed and having longitudinal splitting in flexible fibres. Matted fibre masses are shown in the surface of sample 5.

Figure 7.9: Sample 7 showing (a) white fibres occurring as mats encompassing and surrounding different minerals. The flexible white fibrous bundles form around mineral grain boundaries; within cleavage planes and fractures they directly replace siderite, and (b) fibre bundles occur as fracture filling in fractured siderite crystals. The fibrous amphibole grews as fracture filling material in siderite microfractures and shows clear crystallographic preferred orientation with respect to the fracture.

Figure 7.10: Textures observed between fibrous amphiboles, sulphides, and magnetite within the siderite host rock.

Figure 7.11: Sample 8 showing (a) white to tan coloured vein filling asbestos in siderite organised in bundles structure; bundles have a curvilinear trend orientated parallel to trend of the vein wall. Fibre bundle ends show individual fibrils disseminated/splaying into the siderite matrix and the boundary between the vein and the host rock is sharp; (b) showing replacement of siderite along cleavage cracks by fibrous amphiboles

Figure 7.12: Textures observed in sample 8 of fibrous amphibole replacing siderite along cleavage cracks and grain boundaries forming thin sub-parallel bands

Figure 7.13: Sample 9 showing large mats of fibrous mineral replacement of siderite overprinting original rock mineralogy and texture in both (a) and (b).

Figure 7.14: Sample 10 (a and b) show replacement of siderite by fibrous amphiboles along grain boundaries and cleavage cracks. The orientation of fibre growth conforms to that of the cleavage microcracks and boundaries of the siderite grains.

Figure 7.15: Sample 11 showing large mats of replacement material having an elongated crystal habit covering original mineralogy and rock textures.

Figure 7.16: Photomicrographs of fibrous-acicular bundles sample 1 in (a) plane polarising light and (b) cross-polarising light. The fibre bundles show heterogeneous birefringence colours and the red oval highlights splayed ends of the asbestiform component.

Figure 7.17: Photomicrographs of fibrous-acicular bundles sample 1 in (a) plane polarising light and (b) cross-polarising light. Heterogenous pleochroic and birefringence colours are observed along the length of the crystals. Notice the lenticular inclusion within the fibre bundle.

Figure 7.18: X-ray diffraction and Rietveld refinement diffractogram of fibrous material sub-sampled from sample 1

# List of graphs

Graph 2.1: Diffractogram and relative phases (weight %) of the chrysotile sample

Graph 2.2: Diffractogram and relative phases (weight %) of the amosite sample

Graph 2.3: Diffractogram and relative phases (weight %) of the crocidolite sample

Graph 2.4: The dissolved mass fraction of the asbestos samples over time (hours)

# List of tables

Table 2.1: Location coordinates and description of sampling locations

Table 2.2: Fibre lengths for 21 counts for each mineral in hand sample

Table 2.3: The values of 2 and intensity (I) recorded for each the peaks of each phase from the X-ray diffraction record (λ (Co*K*α) = 1.78892)

Table 2.4: Reduction of data from X-Ray Diffractogram (λ (Co*K*α) = 1.78892). The value of $I/I_1$ (relative intensity %) is determined from equation 1, where $I_1$ is intensity of the highest peak of the phase and *d* (Å) is calculated from equation 2 assuming *n* = 1.

Table 2.5: Abundance (%) of mineral phases detected by XRD analysis

Table 2.6: Major element analysis (n = 2)

Table 2.7: Trace element analysis (n = 2)

Table 2.8: BET surface area report

Table 2.9: The measured mass (mg) of the solid asbestos sample residue after each time interval during dissolution in acidic solutions

Table 2.10: The dissolved mass fraction (DMF) calculated for the asbestos samples

Table 2.11: Threshold values of heavy metals in the lungs (ppm)

Table 3.1: Shrinking Core Models

Table 3.2: Solid-state rate expressions for different reaction models

Table 3.3: Integral and Differential Forms of Model Equations used in Master Plots

Table 3.4: XRD analysis showing percentage of mineral phases in asbestos-bearing rock samples (n = 2)

Table 3.5: XRF analysis of major elements (n = 2)

Table 3.6: XRF trace element concentrations (n = 2)

Table 3.7: Weight of the solid residue measured at each time interval (n = 2)

Table 3.8: pH of the solution measured at each time interval (n = 2)

Table 3.9: Apparent rate constants and correlation coefficients for kinetics models during the entire dissolution process

Table 3.10: Apparent rate constants and correlation coefficients for kinetics models during the fast reaction stage

Table 3.11: Apparent rate constants and correlation coefficients for kinetics models during the slow reaction stage

Table 3.12Overall dissolution reaction and relative kinetic parameters of each asbestos-bearing sample to selected solid-state reaction models

Table 3.13: Statistical regression and correlation values of master plots

Table 3.14: Total dissolution rates calculated for the four samples using a non-linear expression.

Table 4.1: Location co-ordinates and description of sampling locations

Table 4.2: Description of the banded-iron formation-hosted amosite and crocidolite asbestos deposits in South Africa

Table 4.3: Mineralogical characterisation of asbestos mine waste rock samples

Table 4.4: DNA quantification

Table 5.1: Media used and their composition

Table 5.2: Heavy metal concentrations and volumes added to agar plates

Table 5.3: Effect of media composition on colony morphology and growth

Table 5.4: Effect of media composition of pigment and fluorescence

Table 5.5: Abiotic stress tolerance and growth results of PGPR *P. fluorescens*

Table 5.6: Heavy metal (HM) tolerance results of PGPR *P. fluorescens*

Table 6.1: General parameters of the naturally occurring asbestos-bearing rock specimens studied including 'type-area', sample numbers, sizes, fibre-lengths, and magnetic properties

Table 6.2: Summary of sample description, lithology and carbonates, deformation character and morphological and structural features

Table 6.3: Summary of sample alteration status, fibrous or pseudo-fibrous classification, cohesion, releasability and potential hazard

Table 6.4: Geological history, meso-structural analysis of different crocidolite and amosite seams, primary and secondary structural elements, and potential mechanisms of formation

Table 7.1: General macroscopic description and lithotype category of the different fibrous mineral containing rock fragments studied

Table 7.2: The values of 2 and intensity (I) recorded for each peak of each phase from the X-Ray diffraction record (λ (Co*K*α) = 1.78892)

Table 7.3: Reduction of data from X-Ray Diffractogram (λ (Co*K*α) = 1.78892). The value of $I/I_1$ (relative intensity %) is determined from equation 1 where $I_1$ is intensity of the highest peak of the phase and *d* (Å) is calculated from equation 2 assuming *n* = 1

Table 7.4: Major (oxide wt%) and trace element (ppm) concentrations of fibrous material subsamples extracted from sample 1, values of elements in the human lungs (ppm) (Vanoeteren *et al.,* 1986) and the threshold values (ppm) for metals in soils (Toth *et al.,* 2016)

Table 8.1: Classification of degree of enrichment based on the enrichment factor values

Table 8.2: Division of $I_{geo}$ values into quality classes

Table 8.3: Crustal abundance, WHO permissible limits and UICC asbestos standards

Table 8.4: Classification of contamination factor into degree of contamination

Table 8.5: Classification of degree of contamination based on $C_d$ values

Table 8.6: Interpretation of contamination based on the modified degree of contamination values

Table 8.7: Interpretation of pollution load index based on PLI values

Table 8.8: Classification of ecological risk level using potential ecological risk index ($E_r^i$) values

Table 8.9: Ecological risk level interpretation of risk index (RI) values

Table 8.10: Threshold values for heavy metal (ppm) in the lungs

Table 8.11: The chemical composition of major heavy metals (ppm) of concern in the asbestos mine wastes studied

Table 8.12: Enrichment factor values of the studied asbestos mine wastes

Table 8.13: Geo-accumulation indices of the metals in the studied asbestos mine wastes

Table 8.14: Contamination factor values of the studied asbestos mine wastes

Table 8.15: Degree of contamination values of the studied asbestos mine wastes

Table 8.16: Modified degree of contamination values of the studied asbestos mine wastes for each background value

Table 8.17: Pollution load index values of the studied asbestos mine wastes

Table 8.18: Individual potential ecological risk factor values of the studied asbestos mine wastes

Table 8.19: Ecological risk index values of the studied asbestos mine wastes

Table 8.20: HQ values of the studied asbestos mine wastes

Table 8.21: Pearsons rank correlation matrix for chrysotile (n = 66)

Table 8.22: Pearsons rank correlation matrix for amosite (n = 66)

Table 8.23: Pearsons rank correlation matrix for crocidolite (n = 55)

Table 8.24: Pearsons rank correlation matrix for anthophyllite (n = 45)

# Nomenclature

ARDs – Asbestos-related diseases

ARLDs – Asbestos-related lung diseases

DAML - Derelict asbestos mine lands

DME – Department of Minerals and Environment

DMR – Department of Minerals and Resources

HM – Heavy metals

NOA - Naturally occurring asbestos

PCR – Polymerase chain reaction

PGPR – Plant growth promoting rhizobacteria

PLM – Polarising light microscopy

RPI - Rehabilitation priority index

XRD – X-ray diffraction

XRF – X-ray fluorescence

# Chapter 1 – Introduction

## 1.1. General introduction

Industrialisation and the extraction of natural resources have resulted in considerable environmental contamination and the dispersion of numerous toxic materials in various contaminated sites. Asbestos, due to its unique properties, was one such natural resource that was extensively mined for its use in countless commercial products (David *et al.,* 2020). High tensile strength, non-flammability, sound thermal and electrical insulation, and resistance to physical and chemical agents are just a few of the "excellent" mineral properties of asbestos fibres (Tabata *et al.,* 2016; Gaggero *et al.,* 2016). The myriad uses of asbestos in manufactured products, warships, building and cars during the mid-20$^{th}$ century was attributed to such properties (Bartrip, 2004). However, following the discovery that the chemical and physical properties of asbestos, although having a superior industrial functionality, are in fact toxic to humans, a widespread ban on its usage was implemented (Guthrie, 1997). In the wake of its global ban, society is now confronted with a considerable amount of asbestos-containing waste and the clean-up of such sites is necessary for the preservation of human health (David *et al.,* 2020).

In South Africa, which was the third largest producer of asbestos products, the mining of this mineral occurred from the late 1800s to 2002 and was used for a wide variety of industrial applications (Nelson *et al.,* 2011). South Africa contains and possess reserves of all the three varieties of asbestos, which are chrysotile, crocidolite and amosite, making it unique in the world (Hart, 1988). The long history of mining and manufacturing has made asbestos a priority contaminant concern in South Africa with a wide spectrum of potentially contaminated sites (Nelson *et al.,* 2011). A treacherous legacy of contaminated soil, water and air remains in the wake of rapid worldwide industrialisation, leaving behind an unsuitable environment for sustaining life. Asbestos is one such recalcitrant inorganic/mineral contaminant, being listed as the third most abundant pollutant on a global scale, shown to be a potent hazard for human health. Globally, asbestos-related diseases (ARDs) acquired environmentally are still of significant concern (Ndlovu *et al.,* 2013). Historical and poorly regulated asbestos mining operations in South Africa have resulted in the widespread and seemingly unassailable contamination of the environment. Although occupational exposures diminished in the wake of the asbestos mining cessation in South Africa, this tenacious,

contemporary, and vast environmental contaminant is indicative of an indeterminate and conceivably boundless ARD epidemic (Ndlovu *et al.,* 2013).

The relationship between ARDs, such as malignant mesothelioma, and exposure to environmental asbestos sources, including both NOA and abandoned asbestos mines, has been shown recently in numerous studies (Noonan, 2017; Krówczynska and Wilk, 2018; Vimercati *et al.,* 2018; Visona *et al.,* 2018; Xu *et al.,* 2018; Lee *et al.,* 2021). The airborne dispersion of asbestos fibres through human activities and natural rock weathering increases the potential for inhalation of fibres and is the basis of the risks to human health (Harper, 2008; Culley *et al.,* 2010; Bloise *et al.,* 2012, 2014; Punturo *et al.,* 2015). The potential hazards of fibre release and dispersion of environmental asbestos into the environment and the risks to human and environmental health are diagrammatically represented in figure 1.1.

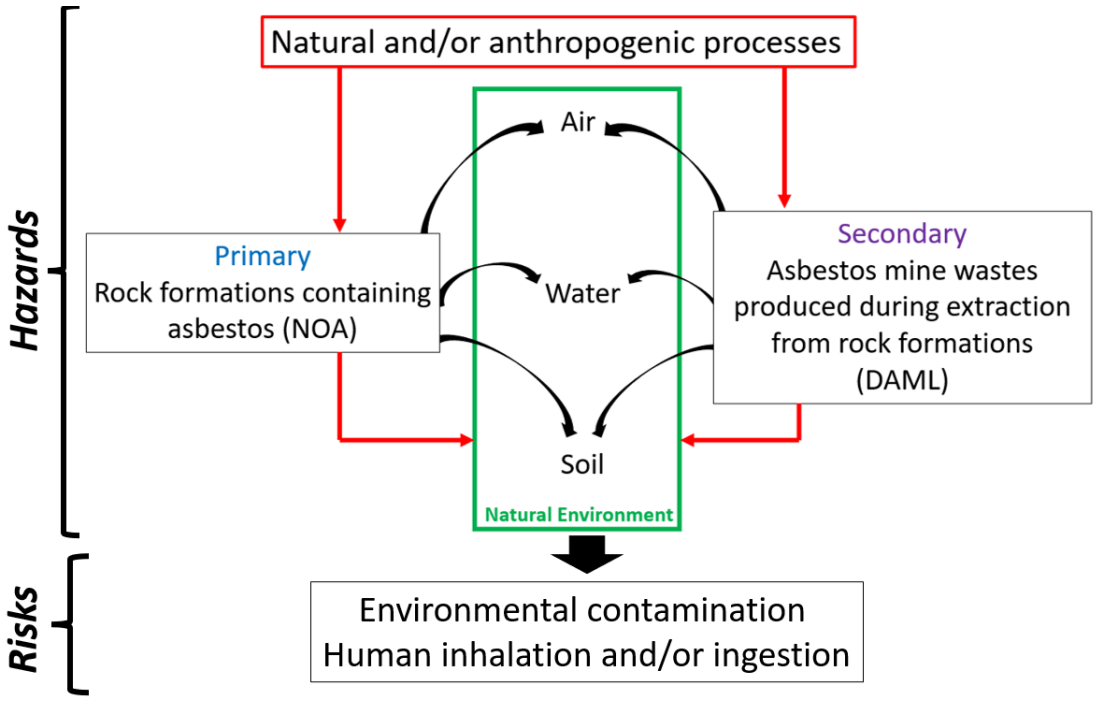


Figure 1.1: Potential hazards of fibre release and dispersion of environmental asbestos into the environment and the risks to human and environmental health

Scientific studies form the foundation upon which solving complex environmental issues are based. Without such studies the very standing of the methods, implementation, management, and monitoring of current asbestos mine reclamation strategies is questioned (Van Druten and Bekker, 2017). Thus, a critical restriction to successfully developing and executing asbestos mine

rehabilitation is the disconnect between the scientific community and both industry and governmental sectors. This lack of co-operation indicates that asbestos mined land rehabilitation is constrained by lack of transparency and assurance issues as information sharing is yet to be established. The massive expenses involved in rehabilitation is another significant issue in South Africa, as in many other developing countries. Furthermore, costs which depend upon the rehabilitation goals and criteria, as well as inadequate knowledge of abandoned asbestos mine sites, result in poor cost-estimation and therefore wastage of finances (Mhlongo and Amponsah-Dacosta, 2016). Suffice to say, to avoid squandering any funding provided, effective engagement between scientists, communities and officials is essential for implementing site management and risk mitigation strategies (Cornelissen *et al.,* 2019). In this thesis, the topic of asbestos in terms of environmental exposure sources is investigated in the context of developing countries. The two environmental exposure sources of asbestos studied in this research are graphically outlined in figure 1.2.

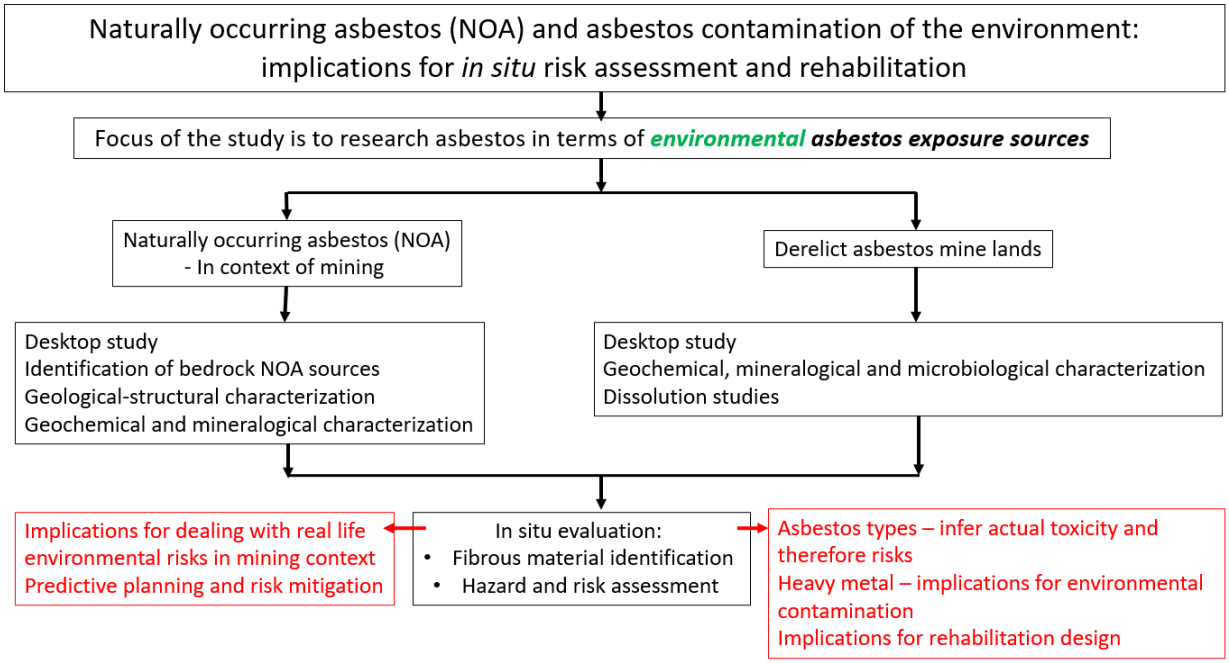


Figure 1.2: Two environmental asbestos exposure sources of focus of this research

## 1.2. Asbestos

The generic term ‘asbestos’ is designated to the six types of naturally occurring and commercially exploited mineral fibres belonging to two mineral groups: Amphiboles and serpentines (figure 1.3) (Cambell and co-workers, 1977; Van Gosen, 2007).

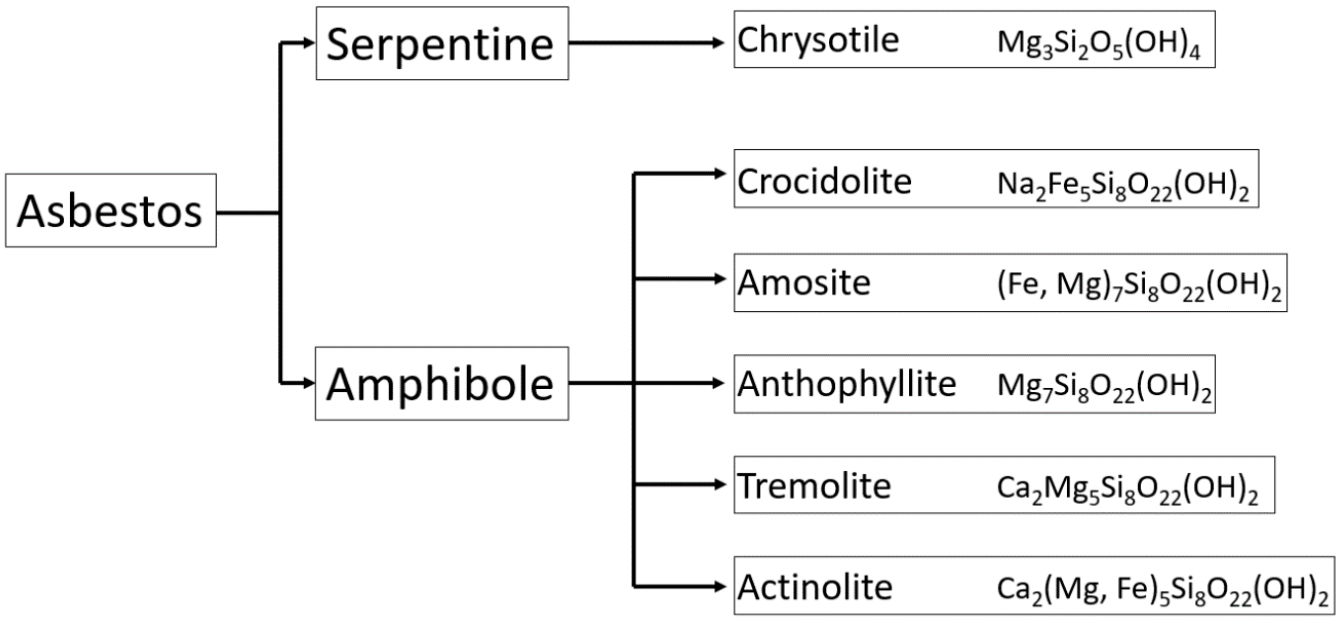


Figure 1.3: Schematic illustration of asbestos mineral groups, asbestos mineral types and their chemical formula

Translated as ‘inextinguishable flame’, the Greek-derived name for the miracle mineral, asbestos, is a term used to delineate one of the oldest and vastly used minerals known to mankind. However, centuries on asbestos use developed into among the greatest controversial topics surrounding the commercial and industrial mineral industry (Hart, 1988; Virta, 2002). Centrally contributing factors to these controversies include: A comprehensive absence of understanding of minimum safe exposure quantities; its carcinogenic identity; prolonged latency period for disease development and its extensive use for over 100 years (Virta, 2002). The physical and chemical properties of each species is different with their fibrous nature being the only feature they have in common (Hodgson, 1977).

### 1.2.1. Brief overview of asbestos mineralogy

The serpentine variety of asbestos, known as chrysotile, is a hydrous magnesium silicate (Abbott, 1983). In the serpentine mineral group the crystal structure is formed by a $(Si_4O_{11})_n^{6n-}$ composed tetrahedral silicate double layer sheet (Daghino *et al.,* 2009). Each $SiO_4$ tetrahedron can share three oxygen atoms with adjacent tetrahedra and/or an octahedral sheet of brucite (Daghino *et al.,* 2009). Apical oxygen of the silica tetrahedra $(Si_2O_5)_n^{2n-}$ layer comprising the phyllosilicate, chrysotile, is shared with the Mg octahedra $[Mg_3O_2(OH)_4]_n^{2n-}$, which forms the brucite-like layer (Daghino *et al.,* 2009). In the 1:1 trioctahedral phyllosilicate, chrysotile, Mg is substituted by $Fe^{2+}$ (Anastasiadou *et al.,* 2010). A single Mg-octahedral sheet bound to a Si-tetrahedral sheet comprise the structure of this 1:1 phyllosilicate (Gidarakos *et al.,* 2008; Anastasiadou *et al.,* 2010). The lateral dimensions of the ideal Si-tetrahedral sheet and the Mg-octahedral sheet have slightly different values (Wicks and O'Hanley, 1988). The curling of this mineral, with its outside brucite-like sheet, forms due to the slight misfit between these two layers (Daghino *et al.,* 2009). A lateral misfit, due to these dimensional differences, occurs along the C and Y axes between the tetrahedral and octahedral sheet (Smith, 1972; Wicks and O'Hanley, 1988; Hardy and Aust, 1995). Compensation for this misfit results in the curling of the larger octahedral Mg sheet over the smaller tetrahedral silica sheet, which subsequently generates the tubular morphology of chrysotile (Anastasiadou *et al.,* 2010). Additionally, the hydroxyl ions ($OH^-$) are exposed on the outer surface of the octahedral Mg sheet (Anastasiadou *et al.,* 2010). Four reactive sites are produced by the tubular structure of chrysotile, namely: (i) The ends of the fibre; (ii) the outer hydroxyl sheet; (iii) the interior of the hollow central channel and (iv) the exposed edges of the curled sheet (Smith, 1972).

Modulating the toxicity of chrysotile is the occurrence of iron that substitutes Mg in the octahedral layer (Gazzano *et al*., 2005). Both ferric and ferrous iron can replace outer layer magnesium in chrysotile, whereas in the inner silica layer, silicon can be replaced by ferric iron (Pollastri *et al.,* 2015). However, the greatest fraction of iron in chrysotile is found to be present in the outer layer (Pollastri *et al.,* 2015). The impurity, brucite, is typically contained in chrysotile fibres and due to dissolution of $Mg^{2+}$ and $OH^-$, pH of the fibre suspension increases (Mohanty *et al.,* 2018). Even though both pure brucite and the brucite-containing outer layer of chrysotile have an identical formula, $Mg(OH)_2$, in chrysotile the magnesium atom shares an oxygen atom with silicon, causing the $Mg^{2+}$ dissolution from chrysotile to significantly decrease compared to that from brucite (Lin and Clemency, 1981). While chrysotile toxicity is attributed to iron, the backbone of the mineral is made

up mostly by Mg and Si atoms, and the persistence and structure of this mineral is affected by their removal (Daghino *et al.,* 2009). The trace to minor amounts of iron in the structure of chrysotile is accounted for by the modest degree to which the magnesium ions are substituted with iron ions (Hardy and Aust, 1995). Depending on the geological source the extent at which $Fe^{2+}$ ions replace $Mg^{2+}$ ions can vary in chrysotile and there may be up to 5% of iron contained in natural chrysotile (Daghino *et al.,* 2005). Chrysotile fibre bundles are green, yellow, or grey in colour, but when fibres are individually separated from the bundles, they appear white in colour, hence the term 'white' asbestos. Chrysotile asbestos deposits are found in two distinct geological settings in South Africa (Abbott, 1983). The first of these occurrences is chrysotile veins within serpentinised ultramafic rocks and the second is as chrysotile veins in narrow layers of serpentinised dolomitic limestones. When compared to the amphiboles, chrysotile is less friable and more flexible (Skinner *et al.,* 1988).

The chemical composition of the amphibole fibres is more complex and the idealised chemical formulae of the five different amphiboles, although their structures are the same, vary in composition (Speil and Leineweber, 1969). A direct consequence of this variability in composition is the fact that a mixture of many different ions can be accommodated in the space between the silicate ribbons of the silicate framework that forms the fibres (Speil and Leineweber, 1969). Sandwiched between two double silicate chains, octahedrally coordinated cations, including iron, compose the amphibole minerals, amosite and crocidolite (Hardy and Aust, 1995). Both silica and other cations, predominantly magnesium and iron, are co-ordinated by the oxygen atoms (Hardy and Aust, 1995). The $(Si_4O_{11})_n^{6n-}$-composed double-tetrahedral chain (corner linked $SiO_4$ tetrahedra) is the basic structural unit forming the crystal structure of the amphiboles (Daghino *et al.,* 2009). Oxygen atoms are shared between these silicate double chains and the edge-sharing $MO_6$ octahedra alternate layers (Daghino *et al.,* 2009). Standing for a variety of cations, the M in $MO_6$ can include the cations: $Ca^{2+}$, $Mg^{2+}$, $Fe^{3+}$ or $Fe^{2+}$ (Daghino *et al.,* 2009). In the amphibole asbestos minerals, iron is present as part of the mineral stoichiometry, whereas in the serpentine, chrysotile, iron is present as an impurity (Hardy and Aust, 1995). Compared to chrysotile the amphiboles are more brittle and less structural deformation is accommodated by these fibres during abrasion or mechanical treatment (Skinner *et al.,* 1988).

Fibrous amphibole found in minor quantities within siliceous dolomite is potassium richterite and the calcium-magnesium amphibole asbestos tremolite, which typically occurs as silky, light-coloured, and long fibres (Abbott, 1983). The light-coloured, brittle anthophyllite asbestos is a rhombic iron-magnesium hornblende and has a comparably poorly developed fibre structure

(Abbott, 1983). Small and irregular deposits of tremolite and anthophyllite asbestos occur in ultramafic intrusions and in the related amphibolite and greenstone (Coetzee *et al.,* 1976). Anthophyllite asbestos is a grey-brown coloured asbestiform mineral with the ideal formula being $(Mg, Fe)_7Si_8O_{22}(OH)_2$ (Gaffney *et al.,* 2017). Unlike the other amphibole asbestos minerals, which have a monoclinic crystal system, anthophyllite is orthorhombic (Gaffney *et al.,* 2017). Commercially, anthophyllite was mined sparsely and occurs mostly as a contaminant in talc and other asbestos minerals (Gaffney *et al.,* 2017). Banded ironstones or fine-grained chert ferruginous metasediments host amosite and crocidolite asbestos deposits only (Abbott, 1983). Amosite ($MgFe_6[(OH)Si_4O_{11}]_2$) is an iron-magnesium silicate found predominantly in the Limpopo and Mpumalanga Provinces (Hart, 1988). Crocidolite ($Na_2(Fe^{3+})_{2}\text{-}(Fe^{2+}, Mg)_3Si_8O_{22}(OH)_2$), a complex sodium-iron silicate (Hart, 1988), occurs in the form of asbestos that is most frequently studied and is one of the most formidable carcinogenic fibrous substances (Martino *et al.,* 2003). Being closely associated with their parent rocks, all forms and types of asbestos are metamorphic minerals (Hodgson, 1977).

### 1.2.2. Asbestos toxicity and sources of exposure

The hazard posed by mineral fibres and dusts depends on their chemical composition, surface area, solubility, shape, size and abundance all of which mediate the associate carcinogenic, toxic and health effects following inhalation as indicated in toxicological and epidemiological studies (Mossman *et al.,* 1990). The durability/bio-persistence (Aust and Lund, 1990, Aust *et al.,* 2000; Fubini and Mollo, 1995), high aspect ratio (Miserocchi *et al.,* 2008; Tomatis *et al.,* 2010) and iron content (Turci *et al.,* 2011; Pascolo *et al.,* 2013) of asbestos make them extremely toxic Group 1 carcinogens (Mohanty *et al.,* 2018). The accumulation and the manifestation of health problems including mesothelioma, asbestosis and lung cancer result from the exposure and internalisation of these micro- to nano- sized asbestos fibres particularly in the lungs (Kilburn, 2000; David *et al.,* 2020). The inhalation of the fibres is the primary risk and is considered carcinogenic even at low levels of exposure (Nelson *et al.,* 2011). Following inhalation, the deposition of asbestos either in the lungs or along the airway (i.e., nose, throat, and trachea) depends on the dimensions of the fibres (Morgan, 1997). Once in the lungs the fibres may be translocated to various other tissues and organs (Boutin *et al*., 1996). Lung carcinoma, pleural mesothelioma or asbestosis are caused following internalisation and the gradual accumulation of the micro-sized fibres in the lungs (Kilburn, 2000). Asbestos toxicity is a result of numerous factors all of which involve both the physical and chemical

characteristics of this fibrous mineral (Berry *et al*., 2000). The shape, size and extremely insoluble nature of asbestos minerals makes them highly bio-persistent once inhaled (Fubini and Otero-Arean, 1999). This bio-persistence allows the fibres to reside in the lungs for longer periods of time, which is directly proportional to the amount of damage caused (Fubini and Otero-Arean, 1999). The inhalation of airborne asbestos fibres is a major carcinogenic concern that has been well-documented (Holmes *et al.,* 2012). Numerous forms of cancer, such as diffuse thickening of the lung, mesothelioma and asbestosis have been linked to asbestos exposure (Moldoveanu *et al.*, 2009). The removal of asbestos fibres from the lungs through the engulfment by macrophages and other immune cells is hindered by their long aspect ratio and high resistance to chemical attack (Tomatis *et al.,* 2010). As a result, excessive reactive oxygen species (ROS) are produced by macrophages causing DNA damage and inflammation, which are subsequently the precursors for resultant tumour development (Mohanty *et al.,* 2018). The increased production of ROS is also a result of increased oxidative stress facilitated by the presence of iron in the asbestos fibres (Pascolo *et al.,* 2013). The accepted mechanisms of asbestos fibre toxicity directly involve the presence of iron ions (Prandi *et al.,* 2002) as they constitute the active centres at the lung/fibre interface where the release of reactive oxygen species and free radicles takes place following inhalation (Fubini *et al.,* 1995). The overall pathogenicity is initiated by such reactions (Prandi *et al.,* 2002). Thus, a first-order mechanism in the fibre toxicity reduction of asbestos minerals is the removal of iron from both its surface and crystal structure (Foresti *et al.,* 2009). The mechanisms of asbestos-induced carcinogenesis are regarded by three major hypotheses, being (1) oxidative stress hypothesis, (2) protein adsorption hypothesis and (3) chromosome tangling hypothesis (Toyokuni, 2009). The oxidative stress hypothesis states that the phagocytic cells engulf the asbestos mineral fibres but are incapable of digesting them resulting in the accumulation of high concentration of iron species and the production of large quantities of free radicles (Liu *et al.,* 2013). The protein adsorption hypothesis postulates that the negative or positive charge of the surface of asbestos fibres concentrates proteins and molecules (Toyokuni, 2009; Liu *et al.,* 2013). The chromosome tangling hypothesis suggests that asbestos fibres tangle with chromosomes during cell division because they enter the nucleus in addition to the cytoplasm (Toyokuni, 2009; Liu *et al.,* 2013).

There are six scenarios that asbestos exposure may be distinguished and categorised into (Liu *et al.,* 2017; Lee *et al.,* 2018):

1. Direct occupational asbestos exposure

2. Para-occupational asbestos exposure
3. Other non-environmental and non-occupational asbestos exposure
4. Neighbourhood environmental asbestos exposure
5. Exposure to environmental pollution of asbestos containing wastes or products
6. Environmental exposure to asbestiform or asbestos minerals occurring in their geological settings

### 1.2.3. Asbestos-related lung diseases (ARLDs)

Lung carcinoma, pleural mesothelioma, benign pleural responses, or asbestosis are caused following internalisation and the gradual accumulation of the micro-sized fibres in the lungs (figure 1.4) (Moldoveanu *et al.*, 2009).

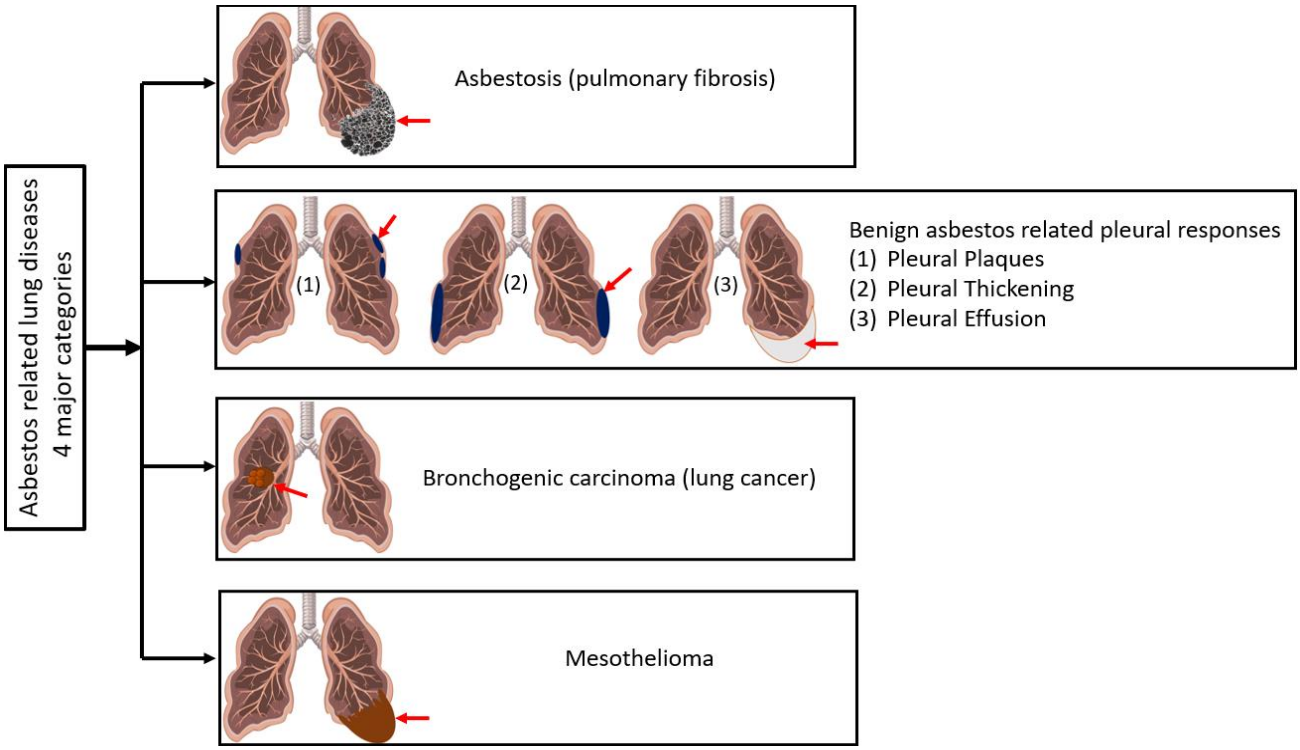


Figure 1.4: Major categories of asbestos-related lung diseases and schematic illustration of pathologic features of each

There are numerous types of asbestos-related diseases, which include both diseases of the pleura and diseases of the lung parenchyma (Ndlovu *et al.,* 2013). Malignant mesothelioma, thickening and pleural plaques comprise the pleura diseases category and asbestosis and lung cancer comprise the lung parenchyma diseases category (Rees *et al.,* 1999; Ndlovu *et al.,* 2013). The global scientific community, to date, agrees that, based on scientific evidence, there is no safe level or threshold of asbestos fibre exposure below which the risk of mesothelioma is negligible (Ramazzini, 2011; Gualtieri *et al.,* 2012).

### 1.2.4. Defining the term 'asbestos'

The regulatory and commercial term, asbestos, is applied to define a group of naturally occurring silicate minerals with a specific fibrous crystal habit and unique chemical, physical and technological properties (Jones, 2010; Williams *et al.,* 2013). Asbestos minerals occur in poly-filamentous bundles (USGS, 2001). These easily separated fibres are thin, flexible, and long (USGS, 2001). Chrysotile is the single asbestiform variety contained in the serpentine group. Anthophyllite, amosite (grunerite), tremolite, actinolite and crocidolite (riebeckite) are the five asbestiform varieties comprising the amphibole group (Cambell and co-workers, 1977). Chrysotile is curly and pliable, whereas the amphibole varieties are dustier and have a needle or rod shape (Mossman and Gee, 1989; Mossman *et al.,* 1990). Several properties are shared amongst these fibrous minerals qualifying them as asbestiform fibres (Whittaker, 1979). These properties include high aspect ratios (length: diameter); they resemble organic fibres macroscopically; they occur in bundles that are easily separated from the matrix hosting them and the fibrous bundles may be cleaved into thinner fibres (Whittaker, 1979; Hodgson, 1986; Skinner *et al.,* 1988). Additionally, as all these asbestos fibres are silicates, several other properties such as chemical and thermal stability, incombustibility and a low electrical conductivity are exhibited amongst them (Skinner *et al.,* 1988). There is a broad variety of industrial applications in which asbestos fibres are used because of such properties shared amongst them (Hart, 1988).

The term asbestiform is used in asbestos identification methods (HSG 248, USEPA 600/R-93/116) as a mineralogical designation applied to an array of minerals that display the following attributes:

1. Capable of being separated into extremely thin fibrils;

2. Having an aspect ratio between and ranging from 20:1 to 100:1, or higher for fibres having lengths > 5 µm;

And two or more of the following:

1. Bundles composed of parallel fibres;
2. Fibre bundles displaying frayed ends;
3. Fibres in the form of thin needles;
4. Individual fibres forming matted masses;
5. Fibres showing curvature along their lengths.

The difficulty experienced using the above classification is that numerous minerals, which are not classified as asbestos under the regulatory definition, may show these properties such that, for example, gypsum occurring in the asbestiform habit may never be declared as asbestos.

Furthermore, the ISO 22262-1:2012E, in addition to the above characteristics, defines asbestos as: ‘’*term applied to a group of silicate minerals belonging to the serpentine and amphibole groups, which have crystallised in the asbestiform habit, causing them to be easily separated into long, thin, flexible, strong fibres when crushed and processed*.’’

The identification of asbestos in section 7.2.3.7 of ISO 22262-1:2012E is discussed as follows:

*A detailed description for the morphology that is characteristic of asbestos is as follows. This morphology is characteristic of the larger fibres seen in stereomicroscope examinations and of fibres selected from laboratory samples for PLM identification of fibre type.*

*In the light microscope, the asbestiform habit is generally recognised by the following characteristics:*

*a) the presence of fibre aspect ratios in the range of 20:1 or higher for fibres > 5 µm;*
*b) the capability of longitudinal splitting into very thin fibrils, generally > 0.5 µm in width;*
*c) in addition, observation of any of the following characteristics for the fibre type under consideration provides additional confirmation that the fibres are asbestiform:*

*1) parallel fibres occurring in bundles,*

*2) fibre bundles displaying splayed ends,*

*3) fibres in the form of thin needles,*

*4) matted masses of individual fibres,*

*5) fibres showing curvature.*

Over the last decade the term asbestos has be defined in four different ways (Glenn *et al.,* 2008):

1. Commercial asbestos definitions emphasise the attributes of asbestos that award commercial worth, such as high chemical and mechanical durability, high tensile strength and heat resistance, and low electrical and thermal conductivity.
2. Regulatory asbestos definitions are mainly designated for the occupational situation to identify and distinguish regulated asbestos minerals and asbestos-containing materials (ACM) from non-regulated mineral fibres.
3. Mineralogical and geological asbestos definitions provide criteria such as crystal structure, morphology and formation mechanisms implementing traditional analytical techniques to discriminate between asbestiform and non-asbestiform minerals.
4. Analytical asbestos definitions supply guidelines and tools required by analysts and laboratories to distinguish, characterise, and count regulated morphologies to ascertain their concentration in liquids, solids, tissues or air.

The inconsistencies of the above asbestos definitions present a problem and complications emerge when undertaking health risk assessments (Strohmeier *et al.,* 2010). Additionally, the incorporation of other non-asbestos asbestiform minerals into the regulatory asbestos definition has been suggested.

## 1.3. Project overview

### 1.3.1. Derelict asbestos mine lands (DAMLs) of South Africa

Historical asbestos mining operations have left a legacy of widespread environmental contamination globally. However, in comparison to North America and Europe, the quantity of modern environmental asbestos exposure sources that litter the land in rural provinces of South Africa is inconceivable. Intense mining of asbestos began in South Africa in the 1930's and grew significantly over subsequent decades (McCulloch, 2003; Virta, 2002). However, at the antipode to its beneficial mineral characteristics are physical and chemical properties discovered to be lethal to humans and its mining and usage was banned in 2002 (Braun and Kisting, 2006). Decades of asbestos mining and use in South Africa followed by its cessation have left a legacy of widespread asbestos-associated pollution of the environment (Ndlovu *et al.,* 2013). The now defunct mines, mine dumps, tailings dams and other industrial and environmental sources of asbestos exposure where merely abandoned upon the transition from 'miracle mineral' to one of the greatest industrial hazards ever known to man. With the sudden vanishing of the personnel responsible came a long trail of sick and dying people. Adding further insult to injury, poor efforts to mitigate the health risks to these deserted high-risk communities have followed in the years after the banning with these people still being forced to live in the shadow of the past (Ndlovu *et al.,* 2013). Any visitor, from developed countries to the former asbestos mining regions in the Northern Cape, Northwest, Limpopo, or Mpumalanga would be struck by the unimaginable number of potential environmental asbestos exposure sources faced by nearby rural communities (Braun and Kisting, 2006). Of these sources, the 'rehabilitated', partially rehabilitated and unrehabilitated mine dumps that dot the landscape throughout the rural provinces are of particular concern to nearby communities as the subsequent 'invisible epidemic' of asbestos-related diseases (ARDs) that infest the population persists (Braun and Kisting, 2006; Nelson, 2012; Ndlovu *et al.,* 2013). In addition to the numerous people who lost their lives following exposure during the mining and milling era of asbestos (Sluis-Cremer, 1970), new asbestos-related diseases continue to persist in members of communities living in these antecedent mining areas long after the closure of these asbestos mines (Braun and Kisting, 2006). This is attributed to the airborne release of fibres from the numerous un-rehabilitated, inadequately and/or unsuccessfully rehabilitated mine dumps (Le Roux, 2007).

The asbestos mine dumps were formed through the accumulation of rock and mineral waste emerging from the mining sites (Kwata, 2019). The mine waste, dumps and tailings are extremely rich in the mined asbestos type as only long fibres were targeted for extraction with shorter fibres being discarded alongside the host rock as waste material (IARC, 1977; Harrington and McGlasham, 1998; Kwata and Mojo, 2017). The DME (Department of Minerals and Environment) selects the

asbestos mine dump sites as a priority for rehabilitation based on the variety of asbestos mineral fibre present, proximity to human communities, dump size and pollution vectors (Kwata, 2019). However, both the environmental and human health impacts of asbestos mineral fibres and dusts are influenced by specific properties governed by their mineralogical and geochemical characteristics (Entwistle *et al.,* 2019). The complex nature of, and human and environmental exposure to, asbestos mineral fibres necessitate procedures that account for this complexity if the attenuation of the human health and environmental impacts is to be conducted correctly.

The health hazards presented by some mineral fibres have, over the last decades, been the focus of rigorous and ingenious multidisciplinary research aimed at understanding the mechanisms by which fibrous minerals generate pathogenic and carcinogenic effects in humans (Gualtieri, 2018; Bloise *et al.,* 2020). This research is done adopting two approaches: First is the more traditional biological approach and the second is the more recent geochemical/mineralogical approach (Bignon and Jaurand, 1983; Bellmann and Muhle, 1994; Bernstein *et al.,* 2008; Andreozzi *et al.,* 2009; Aust *et al.,* 2011; Bernstein *et al.,* 2013; Ballirano and Cametti, 2015; Bernstein and Pavlisko, 2017; Gualtieri *et al.,* 2017; Gualtieri *et al.,* 2018; Gualtieri, 2018). These scientific studies are largely designed to identify the major risk factors associated with different types of mineral fibres with the goal of providing scientific data that will encourage local and/or national authorities to act and implement preventative measures to save lives. In developed countries, such research has a profound impact in directing governmental management plans and actions to mitigate the risks of environmental exposure to mineral fibres and subsequently reducing the burden of asbestos-related diseases (ARDs). Management assistance derived from complex and cost-intensive scientific research designed for developed countries is often assumed to serve as ideal models for developing countries. These scientific studies are adopted to lower the burden of ARDs and, albeit effective for developed countries, they tend to follow a reductionist approach that simply does not lend aid or practicality when considering asbestos exposure and environmental issues in developing countries. Typically, risk factors associated with these inhabited environments and ecosystems, in developing countries such as South Africa, are fundamentally intertwined with the very livelihoods of the communities in question. Therefore, the reductionist approach, whereby the hazard is identified, and communities are immediately relocated or restricted so that rehabilitation strategies may be implemented, overlooks the interdependencies of the subsistence of these, often rural, impoverished communities on the very land that is essentially poisoning them. Thus, addressing the double burden of asbestos-

related diseases that developing countries face requires a holistic ecological perspective to health. However, the mineralogical and geochemical characteristics of asbestos mineral fibres directly influences its toxicity and thus the degree of hazard posed by the waste rocks. The exclusion of these investigations during rehabilitation prioritisation is a direct contradiction to the aims and objectives of the regulatory guidelines, which dictate the specification of human and environmental risks of the mineral fibres at derelict mine sites. Several cost-effective analytical techniques may be employed to conduct mineralogical and geochemical characterisation of asbestos-containing mine rock wastes to gauge their individual potential toxicity on human health and the environment to satisfy the standards set by developed countries and the WHO.

Asbestos-bearing rocks are reservoirs of large varieties and concentrations of heavy metals, which may be released into the environment, either directly via weathering or indirectly in airborne fibres and mineral dusts, and adversely affect human and ecosystem health (Bloise *et al.,* 2008; Ho *et al.,* 2013). The major aim of this study is to use and compare more traditional mineralogical and geochemical methods that are relatively cost-effective and easily accessible to study and diagnose abandoned asbestos-containing mine wastes, thereby emphasising the importance, feasibility, and absolute necessity of the inclusion of geological assessments for establishing effective environmental monitoring systems.

### 1.3.2. Managing and rehabilitating DAMLs

Numerous studies have demonstrated the health risks related to asbestos fibre exposure over the last few years. Today, the scientific community widely accepts that environmental exposure to and the inhalation of asbestos mineral fibres results in the development of detrimental health issues, including lung cancers and malignant mesothelioma (Hillerdal, 1999; Berry and Gibbs, 2008; Gamble and Gibbs, 2008; Baumann *et al.,* 2015). In South Africa, the historical mining of asbestos occurred in four provinces, namely the Northern Cape, Northwest, Limpopo, and Mpumalanga (Jones, 2010). Many derelict and ownerless mines and their associated environmental and health impacts occur throughout South Africa because of historical mining operations conducted with little to no consideration for the environment and no strict legal obligations or regulations pertaining to environmental protection and restoration (Hobbs *et al.,* 2008). Derelict asbestos mines threaten human health and life and pose environmental issues (Cornelissen *et al.,* 2019). To safeguard the public and the environment it is therefore required that these mines be rehabilitated.

Derelict and abandoned mines in South Africa are managed using a developed national strategy, and currently various government-funded projects are being undertaken to deal with these historical mining sites and their associated health and environmental issues (Cornelissen *et al.,* 2019). The rehabilitation of asbestos mine sites, dumps and tailings in South Africa is conducted in accordance with the technical guidelines developed by the Department of Minerals and Environment (DME). Rehabilitation is being conducted by private companies, which are awarded the tender. Prioritisation is important to tackle asbestos mine lands as a huge budget is needed for rehabilitation and it is impossible for many of these sites to be addressed concurrently (UNEP, 2001). Asbestos mine sites in South Africa are prioritised for rehabilitation using a basic risk analysis method that includes three main metrics: (i) health and safety risks, (ii) environmental risks and (iii) land utility risks (Cornelissen, 2017). The health and safety risks are determined by evaluating the proximity of human settlements to the asbestos site and assessment of mineral release, exposure, and consequence (Cornelissen, 2017). The environmental risks are determined by assessing qualitative parameters, such as proximity to natural and protected environments, release of asbestos mineral fibres into water courses and rivers and potential environmental degradation impacts (Cornelissen, 2017). Land utility risk assessments are done through the determination of the derelict mine sites' potential to hinder economic development in the location and adversely affect current and future uses of the land (Cornelissen, 2017). The data obtained from this risk analysis technique serves as the foundation upon which asbestos mine sites are ranked for further investigations and prioritised for subsequent rehabilitation.

The scientifically-based method known as the Rehabilitation Prioritisation Index (RPI), developed in 2007 monitors the rehabilitation status of derelict asbestos mines through comprehensively assessing pre-determined qualitative and quantitative data (figure 1.5) (Bezuidenhout *et al.,* 2013). The RPI is utilised by the South African Department of Minerals and Energy to aid in the proper monitoring of asbestos mines for long-term rehabilitation (Van Rensburg *et al.,* 2008). The parameters included in the quantitative data are physical and chemical soil properties, small mammal surveys, soil microbial activity, cover depth and vegetation properties (Bezuidenhout *et al.,* 2013). The qualitative data parameters include water control structure damage, footprint area, secondary pollution, erosion or flood damage and land use (Bezuidenhout *et al.,* 2013). However, this methodology does not incorporate the geological aspects of these sites.

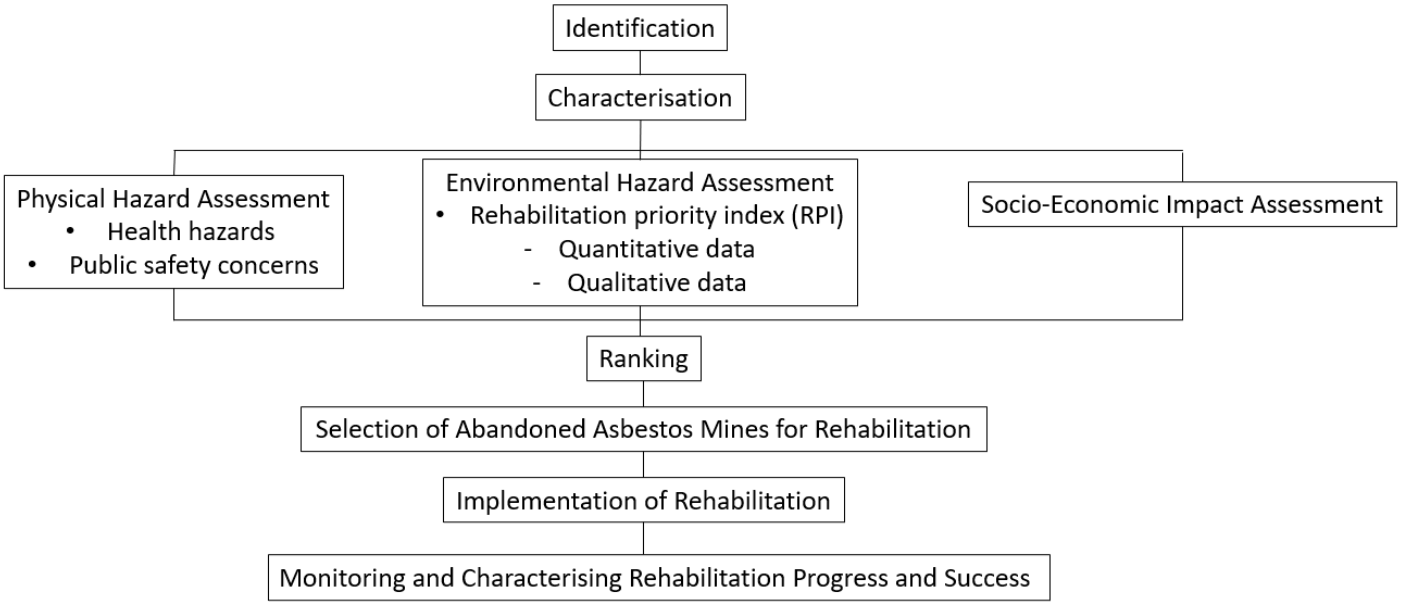


Figure 1.5: Methodology followed using the rehabilitation priority index to identify and monitor the status of asbestos mine rehabilitation (Ndlovu *et al.,* 2013)

In addition to the quantitative and qualitative parameters already discussed, the main factor influencing the decision-making about selection of the site for rehabilitation is its proximity to nearby communities (Cornelissen *et al.,* 2019). Proximity to derelict asbestos mine sites affects the dosage via dispersion and degree of soil contamination by asbestos experienced by surrounding populations.

Following this criterion, the encapsulation method is adopted and is the most common method for asbestos mine dump rehabilitation. Encapsulation includes mine dump grading, stabilising, soil capping and phyto-stabilisation using indigenous vegetation (Wallis *et al.,* 2020). The primary and secondary aims of asbestos mine site rehabilitation are to (i) eliminate asbestos fibre dispersion and create a self-sustaining ecosystem, and (ii) return the mine land to an ecologically stable environment (Mchaina, 2001; Liebenberg-Weyers, 2010; Lima *et al.,* 2016). Confinement via soil capping and revegetation is then implemented and plant establishment and development are encouraged using agronomic approaches whereby organic matter, fertilisers and other amendments are added to the topsoil (i.e., soil remediation). Following the establishment of vegetation, the guidelines state that the rehabilitated mine dumps be maintained and monitored for the subsequent three to five years. Research on asbestos mine dump rehabilitation methods is encouraged in the technical guidelines and the DME is dedicated to applying new, suitable, and successful asbestos rehabilitation methodologies (Matsabatsa, 2009).

Broadly, the encapsulation method is divided into two stages, the first is geotechnical and the second containment (soil capping, soil remediation and phyto-stabilisation via revegetation) (figure 1.6). The geotechnical part involves stabilising the waste material through grading, in which the slope angles of the mine dumps are reshaped to a maximum of 18° and stabilised. Slope reshaping is done to decrease the rate of erosion and permit rainwater infiltration into the soil. The dumps are then covered with a 30 to 50 cm layer of asbestos-free topsoil to prevent the exposure and release of the asbestos fibres into the environment (Matsabatsa, 2009). Erosion control measures are then applied to the site and native species of vegetation planted on the topsoil. Drain and contour construction are typical erosion prevention measures used for restricting the rate of water flow (Matsabatsa, 2009). Additionally, cut-off trenches and retaining walls may be constructed to divert the flow of water from adjacent catchment areas and augment the location of the toe of the mine dump below the 1:100 annual flood line (Matsabatsa, 2009).

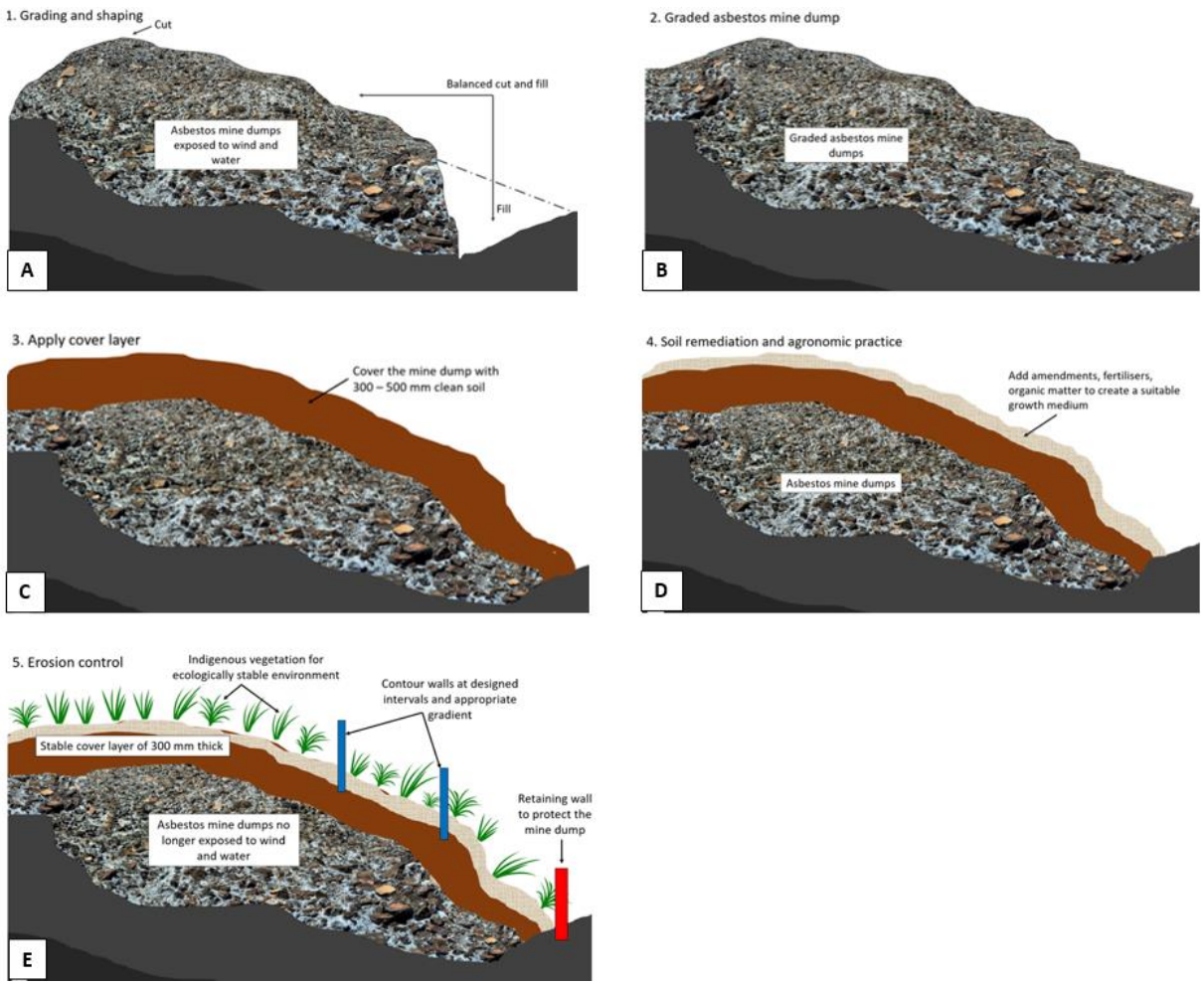


Figure 1.6: Steps involved in asbestos mine dump rehabilitation using encapsulation and soil remediation approaches

To date, it has been recorded that government has spent ~ ZAR 800 million (US$65 million) to rehabilitate 40 of the 249 derelict asbestos mines (Cornelissen *et al.,* 2019). The rehabilitation strategies implemented to address asbestos-related environmental pollution in South Africa have proven, in large, ineffective, and unstainable in the long term. Short-lived rehabilitation practices, poor vegetation cover, lack of microbial baselines and non-existent mineralogical and geochemical standards (Mendez and Maier, 2008 a,b; Matsabatsa, 2009; Liebenberg-Weyers, 2010; Sheoran *et al.*, 2013; Schimmer, 2017) shroud current asbestos rehabilitation practices, and specifications are suspicious and questionable. In addition, the lack of access to and available literature on these steps of the rehabilitation process and subsequent environment parameter values for monitoring and management, contribute to the ambiguity regarding the governing agenda of these rehabilitation projects. This short-lived success of the major costly, taxpayer-funded rehabilitation programmes are typically explained by organisational, structural, and economic challenges (Cornelissen *et al.,* 2019) and using individual parameters, such as hostile conditions, poor nutrients etc. (Matsabatsa, 2009; Liebenberg-Weyers, 2010) To date such excuses have satisfied authorities, industry, and the public (figure 1.7).

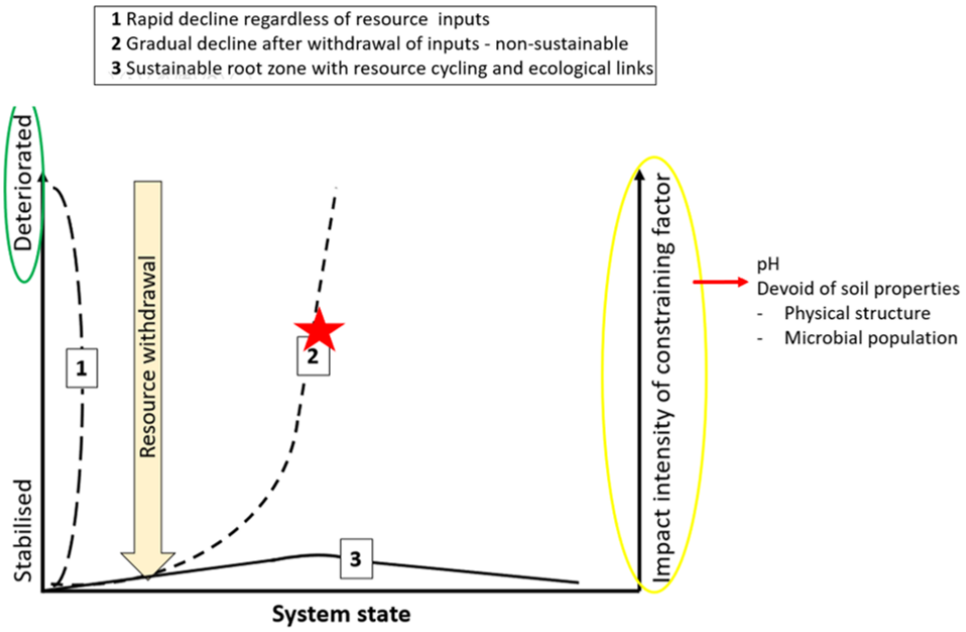


Figure 1.7: Typical trajectory followed by current mine rehabilitation practices (adapted from Huang *et al.,* 2012)

Governmental and environmental agencies involved in derelict asbestos-mine land management have mostly adopted the soil remediation approach to evaluate the rehabilitation requirements. This approach treats asbestos mine dumps and rock wastes as 'pseudo-soil' instead of artificially created poly-mineral parent materials (figure 1.8) (Wu *et al.,* 2019). Under this approach, mine dumps and tailings are dealt with using ameliorative practices that allow for the immediate revegetation (Schimmer, 2017). Although successful for contaminated soils, this technique does not account for extensive mineralogical and geochemical alterations of the asbestos rock wastes and thus will only provide short-term improvements of geo-chemical features restricting the survival and growth of native plants used to revegetate these complex man-made environments (Wu *et al.,* 2019).

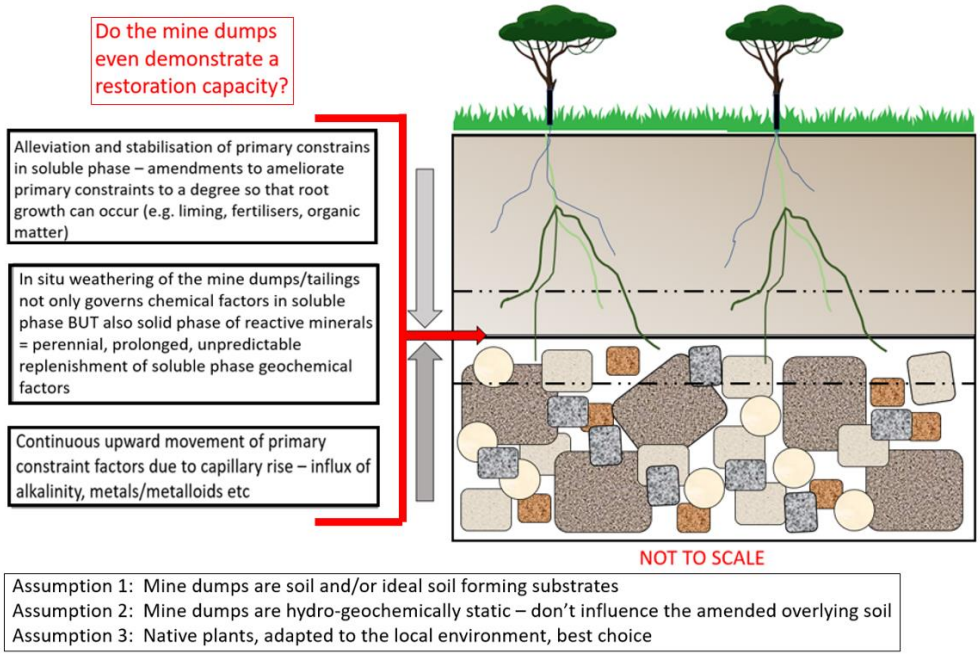


Figure 1.8: Assumptions of current rehabilitation strategy (adapted from Huang *et al.,* 2012)

Mine dumps are large stockpiles of hydraulically-undersaturated, porous post-mining landforms established by the accumulation of waste rocks during mining and are considerably exposed to atmospheric and surficial conditions (Amos *et al.,* 2015). Waste rocks comprise the low-grade bedrocks and undesirable commodity excavated and transported away to get access to the desired and profitable ore (Vriens *et al.,* 2020). Waste rocks are granular, and course broken, poly-mineral/lithological rocks forming a heterogenous mixture that ranges from sand to boulder in size (Vriens *et al.,* 2020). The vast textural properties and size range of waste rocks results in non-uniform hydrodynamic actions (Vriens *et al.,* 2020). These dumps are composed of a collection of both the

growth by addition of short, unwanted asbestos fibres, gangue, and other rock material associated with the unearthed deposit during mining activities (Kwata, 2019). The rocks and minerals comprising the asbestos mine dumps are often affiliated with unique, geologically ancient terrains in exceptionally old and climatically stable landscapes (e.g., Beukes, 1973). These landscapes comprise diverse suites of vegetation assemblages and communities of micro-organisms that are well-adapted to the deeply weathered, shallow and acidic soils of this ecosystem (Hopper *et al.,* 2016). The artificial, poly-mineral, un-weathered and vastly different asbestos mine dumps represent potentially hostile and extremely challenging substrate for the endemic, highly specialised and range-restricted taxa of the associated deeply weathered ancient landscape (Cross and Lamber, 2017).

### 1.3.3. Conventional technologies for asbestos remediation

Traditionally, excavation and burial in confined landfills provided a means for chemically contaminates soil remediation through 'off-site' management (Anderson *et al.,* 2003). Although this practice is cheap it does conflict with recommendations of recycling and sustainable land use (Promentilla and Peralta, 2003; Leonelli *et al.,* 2006; Tam and Tam, 2006; Paglietti *et al.,* 2016). Furthermore, such a remediation method simply relocates the contamination problem to another location and is an extremely costly endeavour (Anderson *et al.,* 2003) and do not definitely abolish the problems associated with the release of asbestos fibres (Paglietti *et al.,* 2016). Additionally, the transportation and relocation of the pollutant involves potentially great environmental risks to the contamination of areas along the route of transport (Anderson *et al.,* 2003). Soil washing is alternative method to landfill burial whereby inorganic contaminants are removed from the soil (Anderson *et al.,* 2003). However, residue containing high metal concentrations is produced during this technique requiring further treatment (Anderson *et al.,* 2003). Due to this numerous physical and chemical treatments have been proposed in scientific papers which are aimed at the detoxification of asbestos containing materials and wastes (Linton *et al.,* 2012). A few such asbestos containing waste treatment processes will be described with focus on the environmental and economic advantages and disadvantages.

Currently, asbestos-contaminated sites in the United States are treated using the remediation plan whereby uncontaminated soils are used to cap the waste piles (Mohanty *et al.,* 2016a). However, fibers contained in these capped piles can pose threats to nearby human populations (Gonneau *et al.,* 2016). Such strategies are further hindered by the fact that the capping material

when subjected to long-term erosion risks the re-exposure of the asbestos fibres (Mohanty *et al.,* 2016a). Additionally, such a strategy relies on the assumption that there is no movement of the asbestos fibers through the sub-surface soil, another route allowing the potential for re-exposure (Mohanty *et al.,* 2016b). The question then arises if whether asbestos movement in the subsurface soil followed by the potential for groundwater contamination may result from the typical geochemical and hydrological conditions in the soil (Mohanty *et al.,* 2016b). Under three different geochemical conditions: ionic strength, pH and dissolved organic carbon (DOC), an asbestos-fiber suspension was injected through a soil and saturated sand column and the fibre mobility was examined (Mohanty *et al.,* 2016b). In the absence of fluvic acid (DOC), irrespective of the water's pH and ionic strength, the asbestos fibres were not mobile (Mohanty *et al.,* 2016b). however, in the presence of fluvic acid, nearly 60% of the asbestos fibres injected moved through the column (Mohanty *et al.,* 2016b). The charge reversal of asbestos fibres subjected to fluvic acid enhances mobility by lowering the ability of the fibres to attach to sand or soil grains (Mohanty *et al.,* 2016b). The potential of asbestos exposure via groundwater must be considered when evaluating the effectiveness of remediation strategies over the long-term.

Vitrification thermally converts the waste into a homogenous and stable glass eventually leading to the media being fused (Colombo *et al.,* 2003). There is complete destruction of the asbestos fibres as the temperatures used in this process are between 1200-1600 °C which are extreme (Tu *et al.,* 2010). The volume of waste is reduced, and the harmful fibres are destroyed using vitrification processes making this treatment desirable (Dellisanti *et al*., 2009). The cost of doing this treatment is exorbitant as large amounts of electricity are required which is a major drawback in using vitrification in asbestos remediation (Gomez *et al*., 2009).

Thermal Treatment of asbestos is based on the principle that at high temperatures asbestos fibres become unstable (Zaremba *et al.,* 2010). During heating, water that is chemically combined to the asbestos is released resulting in the formation of new mineral phases as the crystal structure is changed (Kusiorowski *et al.,* 2013). Due to the high temperatures required and prolonged duration of the treatments this method is extremely energy consuming and so very expensive (Zaremba *et al.,* 2010).

Chemical treatments, with the use of various fluxes, the chemical degradation of asbestos has been carried out in attempt to alter the fibrous chrysotile asbestos form into an amorphic one. Even the nanoscale reduction of asbestos fibre size in strongly acidic environments has been stated in some reports to have no effect on the toxicity as it persists regardless of size (Wypych *et al*., 2005).

When roasted at 700°C, Domka *et al.,* 2001 found some desired effect however the results were not encouraging. Turci *et al*., 2007 found that suspended chrysotile asbestos fibres treated with oxalic acid and subjected to power ultrasound were not detoxified but only disintegrated into nano-sized particles.

The inefficiency, high cost and potential for hazardous by-product generation are all disadvantages hindering the promotion of contaminated site remediation through conventional methods (Bahi *et al*., 2012). Furthermore, although conventional methods may provide a means of suitably controlling contamination, these technologies in many instances are unable to remove the toxic compound polluting the environment (Bahi *et al*., 2012). As biological methods minimize secondary pollutants and are operated easily, they provide a solution to the drawbacks of conventional technologies (Iram *et al*., 2013). Indeed, new remediation strategies, such as bioremediation, are urgently required and should be explored extensively.

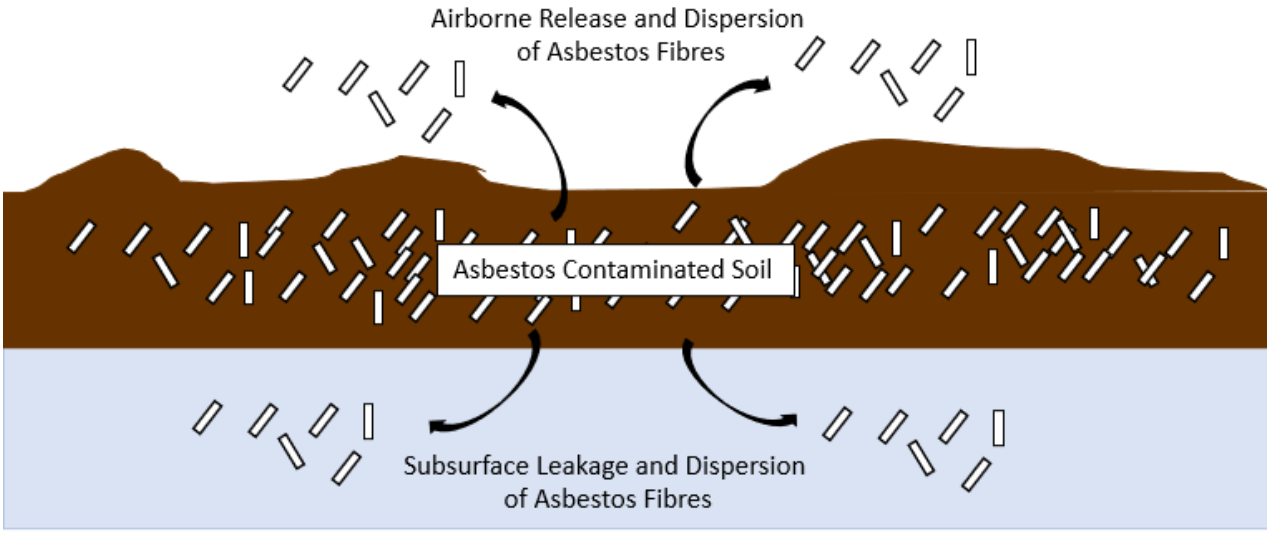


Figure 1.9: Airborne and subsurface dispersion of asbestos fibres

Furthermore, the issue is not solely related to airborne dispersion of fibres, but also the release of toxic elements within the asbestos fibre structure (Apollaro *et al.,* 2018). Factually, the various asbestos minerals contain an extensive quantity of toxic species and elements (Apollaro *et al.,* 2018). The carcinogenesis effects of asbestos due to the existence of trace metals, especially iron, has been fully recorded (IARC, 1993; IARC, 2012). Chrysotile, amosite, crocidolite and anthophyllite could be a consequential provenance of these threatening trace elements.

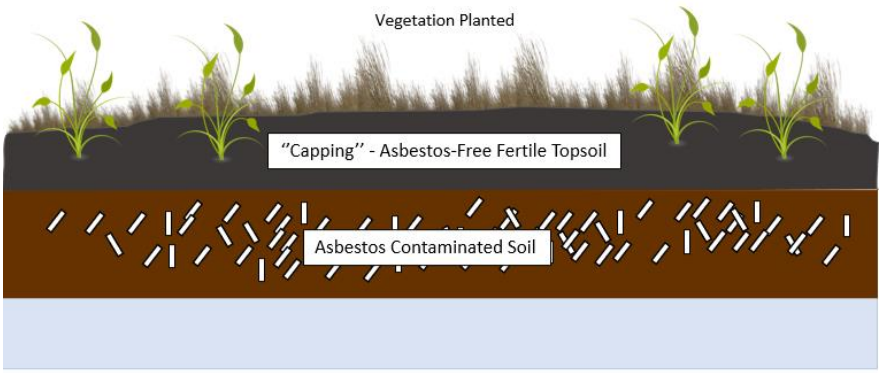


Figure 1.10: 'Encapsulation' rehabilitation method of asbestos contaminated soils, dumps, tailings and mine sites

Capping or encapsulation rehabilitation methods do not provide a decontamination solution but rather confinement efforts, and thus cannot free a contaminated area of these carcinogenic contaminants (Otness *et al.,* 2003). Such confinement methods do not bestow an indefinite or long-term solution as environmental factors, such as erosion and runoff, work to chip away at the constructed contaminant confining barrier (Wallis *et al.,* 2020).

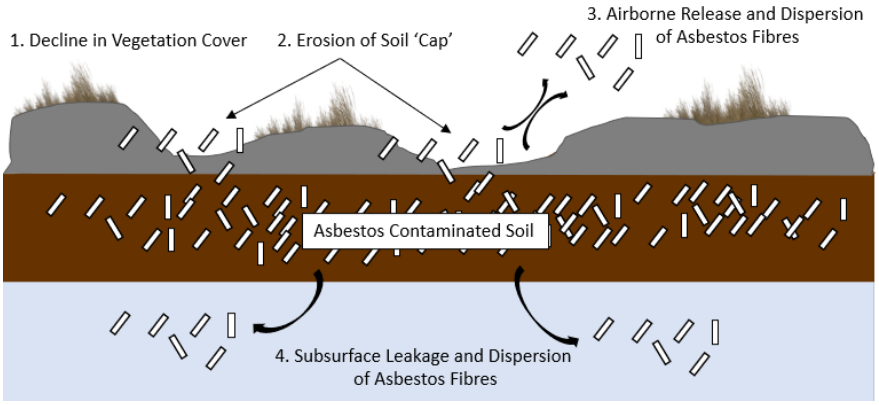


Figure 1.11: Problems facing the current 'encapsulation' rehabilitation method of asbestos contaminated soils, dumps, tailings and mine sites

The infirmity of these solutions has meant that the negative impacts of forsaken mines and tailings are only the tip of the iceberg as hazardous waste materials from these operations have farther dispersed to litter human inhabiting zones surrounding the former mining areas, substantially fuelling the health and environmental risks (Braun and Kisting, 2006). To a greater degree, asbestos contaminated soils are often associated with the presence of co-contaminants, such as heavy metals and nutrient impoverishment (Gonneau *et al.,* 2017). The effectiveness of the capping and re-

vegetation rehabilitation method is severely affected by the addition of these limiting factors above that of those of the primary contaminant, asbestos (Gonneau *et al.,* 2017). The co-occurrence of heavy metals, nutrient deficiency and extreme pH values of the asbestos contaminated soils further facilitate the scarcity and poor diversity of vegetation cover (Bendire *et al.,* 2016). The ineffectiveness of plant establishment and growth on these capped sites has left the 'rehabilitated' sites open to the effects of weathering and erosion that ultimately result in the wind and water dispersion of both asbestos fibres and heavy metal co-contaminants (Boularbah *et al.,* 2006a; Boularbah *et al.,* 2006b).

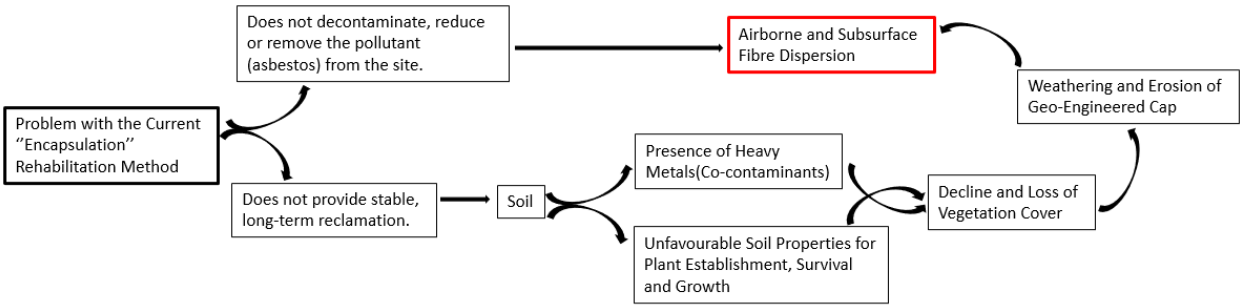


Figure 1.12: Recognition and evaluation of potential problems associated with reclamation.

The establishment of vegetation is one of the main objectives for the rehabilitation of any mine, being displayed as the apparent answer to attaining rehabilitation success on discarded mine sites. Thus, there is urgent need to improve plant survival and establishment on these capped sites; detoxify the recalcitrant pollutants *in situ* and diminish the presence and effects of any other co-contaminants characterising these sites, such as heavy metals, to mitigate the effects to both humans and the environment.

### 1.3.4. Bio-augmentation assisted rehabilitation of DAMLs

Bioremediation exposes environmental contaminants to microorganisms, and their associated microbial processes subsequently degrading or transforming them into less toxic or harmless forms (Garbisu and Alkorta, 2003). Bioremediation provides an environment-friendly and cost-effective method for the removal or degradation of recalcitrant pollutants in contaminated environments. Naturally-occurring mitigation processes, including bioaugmentation, biostimulation and natural attenuation, are exploited in bioremediation technologies and use any biological organism to remediate the environment to its original state (Rimmer *et al.,* 2006; Nie *et al.,* 2009).

*In situ* and *ex situ* are the two methods by which bioremediation may be implemented according to EPA (2001, 2002 and 2006). This classification is based on the location where the contaminants are being treated (Boopathy, 2000). *In situ* bioremediation accomplishes remediation without the excavation or removal of the contaminated water or soil, whereby certain microorganisms are introduced to the site of contamination (Girma, 2015). To reduce expense and dust creation the elimination of the pollutant proceeds directly where it occurs or at the location of contamination (Girma, 2015). This method allows large volumes of soil to be treated without the release or spread of the contaminant (Girma, 2015). As *in situ* methods accomplish degradation with the use harmless microbial organisms it a far safer method for degrading harmful compounds as well as being significantly cheaper than methods involving the relocation of contaminants. Thus, it is considered a superior method to cleaning contaminated environments (Girma, 2015). The introduction of engineered systems to a particular site is done when the conditions of the contaminated site are not suitable (Girma, 2015). The acceleration of degradation process is achieved when engineered bioremediation encourages the growth of microorganisms through the enhancement of the physicochemical conditions (Evans and Furlong, 2003). Remediation following the excavation or removal of contaminated soils is known as *ex situ* bioremediation (Girma, 2015). *Ex situ* bioremediation is classified as either a solid phase system or slurry phase systems, depending on the state of the contaminant to be removed (Cunningham and Philip, 2000). Bioaugmentation is defined as the addition of biological amendments to contaminated sites to increase the degradation rate of the contaminant or recovery rate of the site (Garbisu and Alkorta, 2003). Oxidising, binding, immobilising, volatising and the transformation of heavy metals are the various different methods by which microbes restore the environment (Adams *et al.,* 2015). By understanding the mechanism controlling growth and activity of microorganisms in the contaminated sites, their metabolic capabilities and their response to environmental changes. Bioremediation, through the designer microbe approach, can be made successful (Adams *et al.,* 2015). By measuring the release of K and Mg, Calvaruso *et al.* (2006) observed that the weathering rate of biotite varied with the strain of bacteria present in the soil. Influencing the microbial weathering ability in the field, the microcosm experiments (not in vitro) conducted by Calvaruso *et al*. (2006) demonstrated the importance of abiotic and biotic parameters. Successful soil augmentation requires the selection of a microbial inoculant that is easily cultured, fast growing and can survive in a wide range of environmental conditions at high concentrations of contaminants (Mrozik and Piotrowska-Seget, 2010). The survival of strains introduced into the soil is one of the major difficulties associated with bioaugmentation

procedures (Thompson *et al.,* 2005). The effectiveness of bioaugmentation is influenced by both biotic and abiotic factors and the effect they have on the survival of the introduced microorganisms (Bento et al., 2005). Moreover, the efficiency of bioaugmentation is also determined by the soil type, nutrient content and aeration (Bento *et al.*, 2005). Being an *in-situ* treatment, bioaugmentation, provides a safe and economic alternative to commonly used physicochemical strategies (Adams *et al.,* 2015). To optimize bioaugmentation and to guarantee a reliable process, two major requirements must be fulfilled, irrespective of the soil physico-chemical characteristics. Firstly, the survival of the microbes must be ensured. This can be achieved using protective carriers in which the microorganisms are immobilised (Cassidy *et al.,* 1996; Gentry *et al.,* 2004; McLoughlin, 1994). Secondly, the soil conditions must favour the synthesis of siderophores (Ams *et al.,* 2002; Sharma and Johri, 2003). Both cell growth and the siderophore activity can be increased by supplying substrates, such as glucose, glycerol, lactose, and mannitol, to the microbial cells (Gram, 1996; Duffy and Defago, 1999; Diaz de Villegas *et al.,* 2002). The colocation of inoculant strain and the carbon substrate was shown by Duquenne *et al. (*1999) to enhance the survival of immobilised cells in the soil. The growth of inoculated cells rather than the indigenous microbial population in the soil is selectively promoted by this co-location (Duquenne *et al.,* 1999). Inoculum survival in soil is the principle weakness of bioaugmentation (Singer *et al.*, 2005). The frequent disappearance of inoculants in the soil soon after their introduction results from the competitive, predatory and inhibitory ecology of live soil (van Veen *et al.*, 1997; Gentry *et al.*, 2004). Repeated delivery of liquid inoculants (Newcombe & Crowley, 1999; Silva *et al.*, 2004) can enhance the survival after introduction into the soil as well as formulation (Bashan, 1998; Lewis and Papavizas, 1991).

Most asbestos-contaminated sites are a consequence of human activities such as asbestos mining and other industrial processes (Martino *et al.,* 2004). The detrimental health effects related to asbestos have deemed fibrous asbestos-rich soils an exposure hazard to surrounding communities (Martino *et al.,* 2004). Thus, the presence of fibrous asbestos minerals represents an important environmental issue with removal being impossible and no strategy for the *in-situ* inactivation currently available (Martino *et al.,* 2004). In response to the growing need to address the contamination of soils with the toxic mineral asbestos, numerous physical and chemical remediation technologies have been developed, including soil capping, washing, vitrification, thermal desorption, encapsulation, and excavation (Khan *et al*., 2004; Mulligan *et al*., 2001). Unfortunately, these techniques are often labour intensive, expensive, and frequently leave the soil highly disturbed

(Marques *et al*., 2009). Bioremediation, however, takes advantage of the naturally occurring processes by which microorganisms sequester, detoxify or immobilize heavy metals consequently 'cleaning' contaminated soils (Pilon-Smits, 2005). As the chemical reactivity of iron contained within asbestos minerals contributes to its overall toxicity (Mohanty *et al.,* 2018) a potential remediation strategy may involve targeting the iron in the asbestos as a means of detoxifying the mineral in soils. The carcinogenicity of asbestos is primarily due to its iron composition. The removal or extraction of the iron from the asbestos would provide a potential solution to supressing its carcinogenic nature. The extraction of iron from asbestos fibres by various chelators has been reported in numerous in vitro experiments (Lund and Aust, 1990; Werner *et al*., 1995). Furthermore, this extraction has been shown to modify the surface properties of the fibres (Fubini *et al.,* 1995) and in some cases even promoting the disruption of several subsurface layers (Prandi *et al*., 2002). Different amounts of iron characterise different types of asbestos, a property that contributes to determining asbestos toxicity (Fubini and Otero-Arean, 1999). In the soil environment, bacteria can release organic compounds such as siderophores that modify metal bioavailability and mobility (Gadd, 1993). Siderophore mediated iron solubilisation is a commonly occurring interaction between bacteria and biologically unavailable iron (Gadd, 1993). This interaction may be exploited for remediation purposes to mobilise iron from asbestos minerals (Mohanty *et al.,* 2018). Under iron-limiting conditions, iron may be solubilised from the asbestos minerals by siderophores (Indiragandhi *et al.,* 2008). Using biological agents to target and treat contaminated sites is the new technology known as bioremediation (Prince, 1996). Bacteria introduced into the asbestos contaminated soils provide a hypothetical bioremediation strategy as siderophores released during their growth could be used to mediate the depletion of iron from the fibres subsequently lowering its toxicity (Martino *et al.,* 2004).

Currently, soil capping is the recommended method of asbestos remediation (Wallis *et al.,* 2020), however, this method is cost excessive and only provides an interim solution as the contaminant persists on site (Vidali, 2001) necessitating exploration into new, innovative, environmentally friendly, and economically feasible remediation strategies. A more effective approach is to destroy, if possible, or transform the toxic pollutants into innocuous substances (Vidali, 2001). Bioremediation is one such option (King *et al.,* 2007; Bhattacharya *et al.,* 2015), and is defined as the process in which living organisms, particularly micro-organisms, are used to biologically degrade and/or transform organic (Mueller *et al.,* 1996) and inorganic contaminants (Vidali, 2001) into a less toxic state (Wallis *et al.,* 2020).

Geological sites associated with fibrous asbestos minerals (i.e., serpentine and amphiboles) are ecologically consequential environments (Daghino *et al.,* 2012). These asbestos-related sites are copiously distributed throughout the globe and contain, in addition to the various toxic asbestos mineral fibres, harmfully high heavy metal concentrations, nutrient deficiencies, extreme pH values and slow rock weathering (Kazakou *et al.,* 2008; Daghino *et al.,* 2012; Wallis *et al.,* 2020). The occurrence of endemic species tolerant to the extreme properties characterising these geological locations means that these sites represent unique biodiversity hotspots (Daghino *et al.,* 2005; Daghino *et al.,* 2006; Daghino *et al.,* 2012). Asbestos-contaminated sites and their associated co-contaminants (i.e., heavy metals, pH variability etc.) drives the existence and evolution of special stress tolerant and heavy metal rich adapted micro-organisms and flora (Daghino, 2005; Wallis *et al.,* 2020), which is of great scientific and ecological relevance (Weissenhorn *et al.,* 1993). It has been shown that asbestos-contaminated soils exhibit an array of indigenous micro-organisms that possess mechanisms allowing them to thrive by overcoming the toxic effects of their surroundings (Daghino *et al.,* 2012; Ndeddy Aka and Babalola, 2017). The ability of asbestos inhabiting micro-organisms to grow and thrive on these oxidative and heavy metal-rich substrates is extremely important as such microbes are tolerant to hostile conditions and unfavourable environmental factors unlike those inhabiting non-contaminated soils and sites (Weissenhorn *et al.,* 1993). Autotrophic and heterotrophic asbestos-inhabiting bacteria and fungi could be sourced from these sites and explored as suitable agents for bioremediation purposes (Umrania, 2006; Daghino *et al.,* 2012). Autotrophic microorganisms use photosynthesis or chemical energy to produced their own food, whereas heterotrophic microorganisms obtain food from utilising organic compounds in their surroundings (Umrania, 2006).

Organisms living in close association with minerals and rocks, known as lithic microbial communities, inhabit one of the most omnipresent niches on the planet and unexpectedly persist in hostile environments (Ronholm *et al.,* 2018). The community composition of lithic micro-organisms is controlled by micro-environmental factors (mineralogy, texture, and rock chemistry) and biogeographic parameters (nutrients, light, water availability and climate) (Ronholm *et al.,* 2018). A fundamental feature of lithic microbial communities are microbe-mineral interactions, which involve both the micro-organisms and the mineral (Ronholm *et al.,* 2018). Minerals and rocks are modified by micro-organisms through chemical and physical actions that include metal cycling, weathering, and soil formation (Walker *et al.,* 2005; Walker and Pace, 2007). The mineralogical and chemical properties of minerals and rocks are likely to influence the selection of microbial communities on

account of the intimate interaction of mineral and microbe, however, very little information on the details of how this is achieved is known (Walker and Pace, 2007). Currently there is little information pertaining to lithic bacterial and fungal communities residing directly on or within asbestos rocks and minerals as most investigations focus on the microbial inhabitants within the soils associated with asbestos-bearing geological sites. Due to this, investigations into bacterial and fungal community residing on the asbestos rock material itself are important as these species are especially interesting as agents for bioremediation of inorganically contaminated sites. The ability of micro-organisms to survive on toxic materials stems from their capability to metabolise its resources and thus contaminants often provide potential sources for microbial agents for bioremediation of certain inorganic pollutants such as asbestos and heavy metals (Moorthy *et al.,* 2010; Torres *et al.,* 2017). Knowledge acquired will serve as a guide in selecting favourable microbial isolates that can be employed to improve or develop environmental 'clean-up' biotechnological systems. In water, all asbestos fibres are very poorly soluble, however, research using *in vitro* treatments with various chelators (Werner *et al.,* 1995; Lund and Aust, 1990) have reported their ability for iron extraction from the fibres; surface property modifications and even, over extended periods of time, the promotion of several subsurface layer disruption (Fubini *et al.,* 1995). Additionally, asbestos minerals are extremely resistant to weathering however certain fungal species. *Verticellum leptobactrum, Paecilomyces lilacinus* and *Aspergillus fumigatus* have been observed to biodegrade these fibres by extracting the iron or disrupting the magnesium-silicate framework of the asbestos minerals (Daghino *et al*., 2008). In *in vitro* conditions, the effective reduction in the cytotoxicity of the asbestos, chrysotile, was observed following the siderophore release by some fungal species (Martino *et al.,* 2004; Daghino *et al.,* 2005). In *in vitro* situations, the fungi *Verticillium* species, *Paecilomyces* species and *Fusarium oysporium*, were reported by Daghino *et al. (*2006) to have reduced the damaging effects of asbestos on naked DNA through the removal of iron. *Aspergillus fumigatus* was observed by Daghino *et al. (*2008) to be a potent asbestos bioremediatory. In serpentine rocks growing in close proximity to asbestos, the lichen forming fungus, *Xanthoparmelia tinctina*, was reported to have mediated the removal of magnesium from the asbestos fibres both *in vitro* and *in situ* (Favero-Longo *et al.,* 2005; Favero-Longo *et al.,* 2007). Serpentine rocks are a wealthy source of chrysotile asbestos and Crawford *et al. (*2000) demonstrated that two *Penicillium* strains could effectively mobilise silica and magnesium from this asbestos. Soils rich in asbestos were shown by Favero-Longo *et al. (*2006) to be effectively colonised by the plants, *Thalaspi sylvium* and *Minuartia larcifolia*, and the lichens, *Scoliciosporumumbrinum* and *Candelariella vitelline*. Fungal

species, including *Verticellum leptobactrum, Paecilomyces lilacinus* and *Aspergillus fumigatus*, have been reported for their capacity to biodegrade the highly resistant asbestos minerals (Bhattacharya *et al.,* 2015). The proceeding of this weathering occurs either by the siderophore-mediated iron extraction from the asbestos or by the disruption of the asbestos mineral's magnesium-silicate framework (Daghino *et al.,* 2008).

As naturally occurring asbestos is known for its toxicity and poses serious environmental and epidemiologic concerns, such minerals offer batches for the isolation of microbes naturally adapted to their mineralogical and chemical features potentially able to weather this recalcitrant mineral.

Upon examination into the contemporary state of this insidious asbestos legacy, certain questions become apparent. Why is it that this 'grandfather's' problem still burdens antecedent mining communities, particularly in South Africa? Why are current methods so ineffective at mitigating risk of exposure? The rehabilitation of asbestos mine dumps in South Africa is conducted in accordance with the technical guidelines developed by the Department of Minerals and Environment (DME), whereby the mine dumps are covered with asbestos-free topsoil on top of which indigenous vegetation is planted (Otness *et al.,* 2003; Boularbah *et al.,* 2006a, b; Bendire *et al.,* 2016; Gonneau *et al.,* 2017). Capping rehabilitation methods do not provide a decontamination solution but rather confinement efforts and thus cannot free a contaminated area of these carcinogenic contaminants (Gonneau *et al.,* 2017; Arunakumara *et al.,* 2014). To a greater degree, asbestos-contaminated soils are often associated with other contaminants, such as heavy metals and nutrient impoverishment (Patel *et al.,* 2016; Ahemad, 2019). The effectiveness of the capping and re-vegetation rehabilitation method is severely limited by the above factors. The ineffectiveness of plant establishment and growth on these capped sites has left the 'rehabilitated' sites open to the effects of weathering and erosion that ultimately result in the wind and water dispersion of both asbestos fibres and heavy metal co-contaminants (Boularbah *et al.,* 2006a, b; Bendire *et al.,* 2016). The establishment of vegetation is displayed as the apparent answer to attaining rehabilitation success on discarded mine sites. Thus, there is urgent need to (1) improve plant survival and establishment on these capped sites; (2) detoxify the recalcitrant pollutants *in situ* and (3) diminish the presence and effects of any other co-contaminants to mitigate the health effects on both humans and the environment. The present scenario of environmental asbestos pollution calls for immediate attention towards the remediation and detoxification of these hazardous agents to provide a healthy living environment for humans and the implementation of bio-augmentation, in addition to ongoing

rehabilitation strategies, has been proposed as an inexpensive and environmentally friendly approach to ameliorate reclamation and reduce the risk from chronic exposure to toxic fibres.

Bio-augmentation is the inoculation of a contaminated site with specific strains or consortia of micro-organisms to improve the biodegradation capacity of the system for a specific pollutant (Adams *et al.,* 2015). Bioremediation by means of bio-augmentation is, in many cases, considered when the harmful compound is one that resists indigenous microbial degradation and persists in the environment indefinitely (Adams *et al.,* 2015). Bio-augmentation experiments require detailed understanding of several important parameters (Vogel, 1996): Characteristics of the contaminant, the chemical and physical properties of the soil environment and microbiology and methodology (Vogel, 1996). These parameters and the effects that they have on one another must be extensively understood to achieve conditions that will optimise the bioremediation of the pollutant (Bento *et al.,* 2005).

Successful soil augmentation requires the selection of a microbial inoculant that is easily cultured, fast growing; occurs and survives in a wide range of environmental conditions and can withstand high concentrations of contaminants (Mrozik and Piotrowska-Seget, 2010). The survival of strains introduced into the soil is one of the major difficulties associated with bio-augmentation procedures (Thompson *et al.,* 2005). The effectiveness of bio-augmentation is influenced by both biotic and abiotic factors and the effect they have on the survival of the introduced micro-organisms (Bento et al., 2005). Moreover, the efficiency of bio-augmentation is also determined by the soil type, nutrient content and aeration (Bento *et al.*, 2005). Being an *in-situ* treatment, bio-augmentation provides a safe and economic alternative to commonly used physicochemical strategies (Adams *et al.,* 2015). To optimise bio-augmentation processes and to guarantee a reliable process, two major requirements must be fulfilled, irrespective of the soil physicochemical characteristics.

Firstly, the survival of the microbes must be ensured. This can be achieved using protective carriers in which the micro-organisms are immobilised (Cassidy *et al.,* 1996; Gentry *et al.,* 2004; McLoughlin, 1994).

Secondly, the soil conditions must favour the synthesis of siderophores (Ams *et al.,* 2002; Sharma and Johri, 2003). Both cell growth and the siderophore activity can be increased by supplying substrates, such as glucose, glycerol, lactose, and mannitol, to the microbial cells (Gram, 1996; Duffy and Defago, 1999; Diaz de Villegas *et al.,* 2002). Under various environmental conditions certain factors are key for the production and function of siderophores (Winkelmann, 2004; Winkelmann, 2007). In soil, essential for the growth of soil microorganisms, iron is a limiting bioactive metal with

a concentration low ($10^{-7}$ M) enough to limit the growth of soil microorganisms ($10^{-8}$ – $10^{-6}$ M) (Gurinot, 1994). To acquire iron several strategies in rhizobacteria have been developed, with the major one being the production and utilization of siderophores (Gurinot, 1994). To denote the relatively low molecular weight carriers of Fe (III), Lankford (1973) was the first to propose the generic term, siderophore, which are encountered most in the aerobic and facultative anaerobic microbial species (Neilands, 1982). On Earth, iron is the fourth most abundant element existing predominantly in its ferric ($Fe^{3+}$) form (Rashid *et al.,* 2016). In most minerals, iron occurs with oxygen in octahedral coordination (Poole and McKay, 2003; Kraemer, 2004). Fe(III) and Fe(II) are the two stable oxidation states seen by this transition metal (Poole and McKay, 2003; Kraemer, 2004). The chemical behaviour of iron is strongly influenced by the oxidation state (Poole and McKay, 2003; Kraemer, 2004). The presence of oxygen determines the redox potential of soils (Poole and McKay, 2003; Kraemer, 2004). The speciation of iron is dramatically affected by oxic conditions (Poole and McKay, 2003; Kraemer, 2004). Except for the genus *Lactobacilli* and *Streptococcus sanguis*, iron is essential for all living organisms (Lindsay and Riley, 1994) and iron is one of the key micronutrients for fertile soil (Rashid *et al.,* 2016). The maintenance of enzymatic function and many metabolic processes depends on the presence of iron (Lindsay and Riley, 1994). In the electron transport chain, iron, specifically serves as a component of iron-sulfur centers of cytochromes (Lindsay and Riley, 1994). In energy producing pathways of anaerobic bacteria, iron may also serve as a terminal electron acceptor (Nealson and Daad, 1994). Oxygen metabolism, electron transfer and DNA and RNA synthesis are some of the enzymatic processes that iron has been proven to catalyse (Touati, 2000; Verkhovtseva *et al.,* 2001). Iron-bearing minerals such as goethite, ferrihydrite and hematite are common in the Earth's crust, but as these minerals have very low solubilities the $Fe^{3+}$ ionic concentrations and $Fe^{2+}$ under oxic conditions are very low (Poole and McKay, 2003; Kraemer, 2004). In aerated circumneutral pH soils, iron is restricted to insoluble compounds as ferrous iron is auto-oxidised to ferric iron rendering it biologically unavailable (Ma, 2005). The low dissolved $Fe^{3+}$ concentrations and poor solubility of ferric iron minerals under oxygenated conditions makes iron a limiting nutrient (Konhauser *et al.,* 2011). Iron concentrations are reported to be between $10^{-10}$M and $10^{-9}$M at circumneutral pH and oxic conditions (Poole and McKay, 2003; Kraemer, 2004). The internal iron concentration of $10^{-6}$ M is maintained and required by bacteria regardless of the external iron concentration (Kenneth *et al.,* 2003). The evolution of sophisticated mechanisms in bacteria that accurately adjust, in response to prevailing levels of iron limitation, the level of siderophore production comes to no surprise given the importance of iron as a key growth-limiting

factor for most bacteria (Andrews *et al.*, 2003; Parrow *et al.*, 2013; Frawley and Fang, 2014). Overcoming the iron limitation is accomplished by many bacteria and fungi through the production and excretion of siderophores (Ma, 2005). Siderophores are low-molecular weight ferric iron specific chelators produced in conditions, where iron is limited (Drechsel and Winkelmann, 1997). Deriving its name from the Greek term, siderophore, meaning iron carries have a molecular weight ranging between 600 to 1500 Daltons (Ishimaru, 1993). A large multi-enzyme structure containing a peptide backbone, including one of three iron coordinating ligands which surround $Fe^{3+}$ in an octahedral configuration, constitutes a complete siderophore (Chu *et al.,* 2010). Siderophores are as diverse as the microorganisms that produce them (William *et al.,* 2012). The development and diversity of siderophores is thought to have been facilitated by the evolutionary pressures of bacteria on microorganisms unable to utilise siderophore (William *et al.,* 2012). These enormously abundant low molecular weight organic compounds specifically complex dissolved Fe(III) (Rashid *et al.,* 2016) and dominate ferric iron speciation in soils (Konhauser *et al.,* 2011). The siderophore association constant for ferric iron ranges between $10^{12}$ and $10^{52}$ (Neilands, 1982). The soluble nature and availability of reaction sites on which the central Fe(III) cation can bind are the two properties of siderophores making them exemplary Fe(III) chemical agents (Konhauser *et al.,* 2011). The dissolved form of Fe(III) is maintained by the siderophores exceedingly stronger binding capacity for Fe(III), being several times higher than that of the common organic acids found in the soil (Konhauser *et al.,* 2011). The colocation of inoculant strain and the carbon substrate was shown by Duquenne *et al. (*1999) to enhance the survival of immobilised cells in the soil. The growth of inoculated cells rather than the indigenous microbial population in the soil is selectively promoted by this co-location (Duquenne *et al.,* 1999). Inoculum survival in soil is the principle weakness of bio-augmentation (Singer *et al.*, 2005). The frequent disappearance of inoculants in the soil soon after their introduction results from the competitive, predatory, and inhibitory ecology of live soil (van Veen *et al.*, 1997; Gentry *et al.*, 2004). Repeated delivery of liquid inoculants (Newcombe and Crowley, 1999; Silva *et al.*, 2004) can enhance the survival after introduction into the soil as well as formulation (Bashan, 1998; Lewis and Papavizas, 1991).

Commercially formulated inoculants are applied readily and this is not a time-consuming application presenting a major advantage over inoculants specifically prepared in the laboratory (Bashan, 1998). As these formulations are environmentally friendly, they adhere to 'green movements' and are viewed as more acceptable than remediation methods involving chemicals (Bashan, 1998). These inoculants are also cost effective as dictated by the market and, thus, for large

scale bioremediation purposes are regarded as a feasible possibility (Bashan, 1998). A key factor for successful treatment in bio-augmentation is applying suitable micro-organisms (Nopcharoenkul *et al.,* 2011). Micro-organisms suitable for bio-augmentation are easy to culture, grow fast, are resistant to high pollutant concentrations and are capable of surviving in the environmental conditions of the site to be remediated (Cunliffe *et al.,* 2006; Mrozik and Piotrowska-Seget, 2010). The bacterial populations degrading the hazardous compound must be monitored throughout the treatment period for maintaining and operating of suitable treatment conditions which render bioremediation successful (Sayler *et al.* 1995; Phrommanich *et al.* 2009).

The success or failure of biological inoculants is crucially dependent on the formulation (Bashan, 1998). In general, there is a progressive decline of the bacterial population shortly after their introduction into the soil which prevents the development of a sufficiently large microbial population (van Elsas *et al*., 1986; Heijnen and van Veen, 1991; van Veen *et al.,* 1997). Such a phenomenon is a result of the unpredictable and heterogeneous nature of the soil environment as well as the presence of competitive native micro-organisms, which are often better adapted to the environment (van Elsas and van Overbeek, 1993). A suitable micro-environment must be provided by inoculant formulations to prevent the rapid decline of bacteria introduced into the soil (Heijnen, 1992; Bashan, 1998). The survival of microbial inoculants introduced into the harsh soil environment requires effective inoculant formulations designed to ensure longer survival by providing a dependable source of beneficial bacteria (Heijnen *et al*., 1992; Roszak and Colwell, 1987). Liquid-based inoculants are new formulations that facilitate introduction of high cell numbers and increase survival of micro-organisms in soil (Trevors *et al.,* 1992). In addition to containing the desired micro-organisms and their nutrients, liquid bio-inoculants also contain cell protectants that are specialised for increasing the tolerance of the organisms to adverse conditions (Bashan, 1986; Trevors *et al.,* 1992).

Prior to the use of applications such as bio-augmentation, one option to store commercial inoculums is liquid formulation (Nopcharoenkul *et al.,* 2011). The cost-effectiveness and easy preparation and application of liquid formulations make them more advantageous over other storage techniques (Melin *et al*., 2006, 2011). The preparation of liquid formulations requires the suspension of bacterial cells in appropriate solutions (Nopcharoenkul *et al.,* 2011). Prolonged storage of the cells can be mediated by adjusting the water activity and adding protective agents, such as glutamate, sorbitol, glucose, lactose, trehalose, xanthan, glycerol polyvinyl alcohol etc. (Abadias *et al*. 2003; Torres *et al*. 2003; Tittabutra *et al*. 2007; Albareda *et al.* 2008; Liu *et al*. 2009).

For decades the introduction of desired bacteria and fungi into the soil has occurred for agricultural purposes (Van Veen *et al.,* 1997). These inoculations have been done to stimulate plant growth, supply nutrients, improve the structure of soil and control plant pathogen activity (Wilson and Lindow, 1993). In more recent years, there have been other objectives for the introduction of microbial organisms into the soil (Van Veen *et al.,* 1997). These include the bioaccumulation of inorganic compounds, microbial leaching (Van Veen *et al.,* 1997) and the bioremediation of pollutants in the soil (Middeldorp *et al.,* 1990). There have been many inoculations of microorganisms into the soil that have successfully fulfilled their purpose, however, many failures have also been reported (van Elsas and Heijnen, 1990; Akkermans, 1994). Such failures raise concern about the degree at which these microbial releases have sufficient practical potential in soil remediation objectives (Van Veen *et al.,* 1997). Following the introduction into the soil, a pivotal factor involved in leading to failure is the rapid decline in the size of the active cells population below levels required for the objective to be achieved rendering them ineffective to their purpose (Van Veen *et al.,* 1997).

The application requires that certain ecological conditions on which the effective level of introduced microorganisms is dependent upon be present (Van Veen *et al.,* 1997). When in the soil system, the process in which the introduced microorganisms are to be involved in gives them a selective advantage, then only a minimal number of active cells is initially required for effective application (Van Veen *et al.,* 1997). Maximum numbers of active cells are, however , initially required when the occurrence of such an ecological selectivity is unlikely to be achieved in soil (Van Veen *et al.,* 1997). The survival of introduced microorganisms is largely determined by abiotic soil factors, such as temperature, pH, substrate availability, moisture content and texture, thus a critical assessment of these factors is required before each introduction (Gray, 1975). The physiological and genetic constitution of the inoculant determines its response to the prevailing conditions of the soil (Gray, 1975). Thus, the ability of the introduced microorganisms to deal with the effects of the various soil factors differs in accordance with the inoculants' ability to cope with fluctuation and adverse conditions (Gray, 1975).

Comprising an important group of bacteria relevant to environmental applications, such as bioremediation, is the genus *Pseudomonas* (Dowling and O'Gara, 1994; Timmis, 1994). Feast and famine conditions are often assumed to be experienced by bacteria inoculated into soil, whereby there is a fluctuation between periods of apparent inactivity and those of sporadic growth (Van Elsas

and Van Overbeek, 1993). Such fluctuations are due to nutrient and energy sources distributed heterogeneously in small amounts (Van Elsas and Van Overbeek, 1993). Stress resistance is induced by pseudomonads during the transition from growth to inactivity (Givskov *et al.,* 1994, Sarniguet *et al.,* 1995, Van Overbeek *et al.,* 1995), and the production of secondary metabolites is increased and thus their ability to degrade xenobiotics (Canosa *et al.,* 1999, Sze *et al.,* 1996). Carbon limitation, as suggested by indirect evidence, affects pseudomonads in bulk soil (Van Overbeek *et al.,* 1995). Hence, in the soil Van Overbeek *et al. (*1995) found that *Pseudomonas fluorescens* strain R2f developed a stress-resistant state. This stress resistance was comparable to that developed by cells starved in culture and the addition of glucose to the soil could prevent it (Van Overbeek *et al.,* 1995). Reported gene technology has, during recent years, provided direct information on the major nutrient availability to pseudomonads. The availabilities of nitrogen, iron and phosphate to pseudomonads have been revealed by studies exploiting whole-cell biosensors as not severely limited in natural bulk soil (Jensen *et al.,* 1998, Jensen and Nybroe, 1998, Kragelund *et al.,* 1997, Loper and Henkels, 1997). However, nitrogen limitation of an introduced pseudomonad may result from the enrichment of plant residues into the soil (Jensen and Nybrow, 1998). As a consequence, the dynamic changes in the carbon and nitrogen availabilities in the heterogeneous soil environments limits the proliferation of pseudomonads. The fate of *Pseudomonas* inoculants in the soil may be better understood if the spatial and temporal variabilities in available nitrogen and carbon sources are known.

### 1.3.5. Naturally occurring asbestos (NOA)

In addition to environmental (i.e., non-occupational) exposure to asbestos from derelict asbestos mine lands (DAML), awareness of environmental exposure to naturally occurring asbestos (NOA) has increased in recent years. Unlike the various asbestiform minerals at DAML, those found in NOA outcrops do not conform to those defined under the regulatory designation of asbestos (Harper, 2008). The all-encompassing term given to asbestos minerals found in rocks, sediments and soils in their natural state is Naturally Occurring Asbestos (NOA) (Baumann *et al.,* 2015; Cavallo, 2020). The release of airborne asbestos from natural occurrences has recently been shown to increase the risks of malignant mesothelioma in surrounding and exposed populations raising worldwide concern (Petriglieri *et al*., 2020). The naturally occurring asbestos (NOA) hazard emerges in natural environments, when airborne fibres are produced during mechanical and physical

disturbances such as human activities and erosion (Carbone *et al.,* 2011; Baumann *et al.,* 2013; Vignaroli *et al.,* 2011, 2014) (Figure 1.9). The fibres are extensively dispersed due to their small size and low density resulting in contamination of various environmental systems (Lucci *et al.,* 2018).

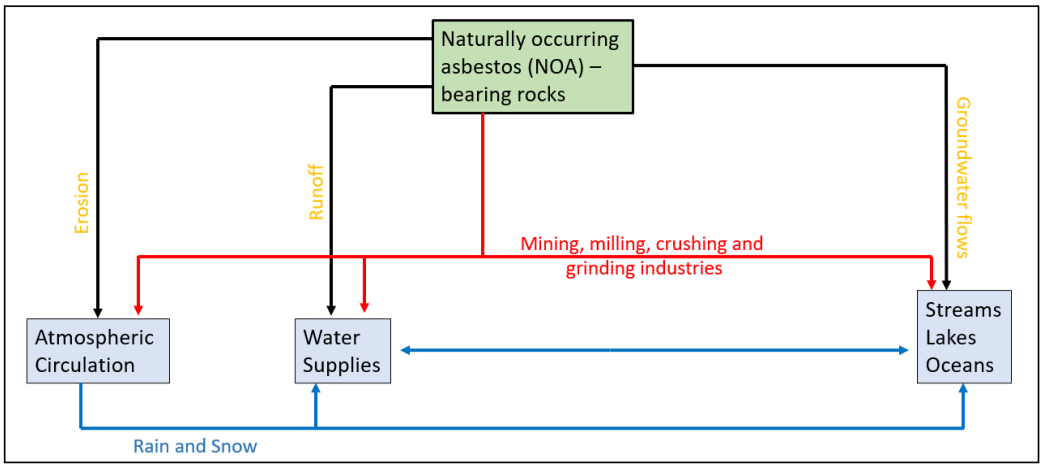


Figure 1.13: Flow chart depicting the mechanical/physical processes resulting in asbestos fibres dispersion and distribution in the environments (adapted from Vignaroli *et al.,* 2014; Lucci *et al.,* 2018)

Anthropogenic (mining, grinding, crushing, and milling) and natural (weathering, erosion and transport) processes represent a critical source of fibrous asbestos (Lucci *et al.,* 2018) and both may incite a strong and unassailable environmental hazard (Vignaroli *et al.,* 2011; Vignaroli *et al.,* 2014). The increased awareness of the risks posed by the environmental exposition of asbestos from NOA geological units has led to the renewed nterest in the *in-situ* identification and characterisation of regulated asbestiform and non-regulated fibrous minerals. In this study, NOA is studied using the real-life procedures used by the mining industry in the context of in-field fibrous mineral identification. A broad variety of amphibole asbestos rock samples were presented to demonstrate the visual variability and its impact of recognition of hazardous asbestos-bearing materials in their natural setting.

## 1.4. Aims and objectives

The aim of this thesis is to identify and examine the multifaceted avenues of environmental asbestos presenting major environmental and public health issues, specifically those in developing countries such as South Africa, and relate this to the current policy and strategy challenges.

The main objectives of this research are to:

- Collect and examine asbestos material from exposed derelict asbestos mine dumps in Southern Africa.
- Mineralogically and geochemically characterise chrysotile, amosite, and crocidolite mine waste to provide baseline data relevant to hazard assessments and rehabilitation planning in the context of the developing world.
- Test and classify the dissolution mechanisms of chrysotile, amosite, crocidolite and anthophyllite asbestos to infer chemical stability in the natural environment.
- Provide a preliminary characterisation of the bulk mineralogical and microbial properties of amosite and crocidolite mine waste constraining rehabilitation success.
- Use a culture-based strategy to examine colony morphology expressions, abiotic stress tolerance and heavy metal tolerance of *Pseudomonas fluorescens* to evaluate the potential to increase asbestos rehabilitation efforts.
- Collect numerous NOA rock samples, investigate the geological-structural associations of asbestos mineralisation in their host rocks and define asbestos-related lithologies and structures.

| Manuscript # | Manuscript title | Manuscript status |
|---|---|---|
| 1 | Rhizosphere competence and abiotic stress tolerance of commercially sold *Pseudomonas fluorescens* bio-fertiliser: implication for their bioremediation potential | Published |
| 2 | Mineralogical, petrological, and geochemical characterisation of chrysotile, amosite and crocidolite asbestos from mine waste in Southern Africa in the context of hazard evaluation and rehabilitation | Submitted for publication |
| 3 | Fibrous minerals and Naturally Occurring Asbestos (NOA) in the metacarbonate-hosted Fe oxide-Cu-Au-Co mineralised rocks from the Guelb Moghrein Mine, Akjoujt, Mauritania: Implications for *in situ* hazard assessment and mitigation protocols | Submitted for publication |

## 1.5. References


Abadias, M., Usall, J., Teixido, N. and Vinas, I. (2003): Liquid formulation of the postharvest biocontrol agent Candida sake CPA-1 in isotonic solutions. *Phytopathology*, **93**, 436– 442.

Abbot, P. (1983): A review of asbestos resources. M. Sc. Dissertation, Rhodes University, Grahamstown, South Africa.

Adams, G.O., Fufeyin, P.T., Okoro, S.E. and Ehinomen, I. (2015): Bioremediation, Biostimulation and Bioaugmention: A Review. *International Journal of Environmental Bioremediation and Biodegradation,* **3** (1), 28–39.

Ahemad, M. (2019): Remediation of metalliferous soils through the heavy metal resistant plant growth promoting bacteria: Paradigms and prospects. *Arabian Journal of Chemistry*, **12**, 1365 – 1377.

Ahmad, S., Lee, S.Y., Kong, H.G., Jo, E.J., Choi, H.K., Khan, R. and Lee, S.W. (2016): Genetic Determinants for Pyomelanin Production and Its Protective Effect against Oxidative Stress in *Ralstonia solanacearum. PLOS ONE*, **11**, e0160845.

Albareda, M., Rodriguez-Navarro, D.N., Camacho, M. and Temprano, F.J. (2008): Alternatives to peat as a carrier for rhizobia inoculants: solid and liquid formulations. *Soil Biology and Biochemistry*, **40**, 2771–2779.

Amos, R.T., Blowes, D.W., Bailey, B.L., Sego, D.C., Smith, L. and Ritchie, A.I.M. (2015): Waste-rock hydrogeology and geochemistry. *Applied Geochemistry*, **57**, 140–156.

Ams, D.A., Maurice, P.A., Hersman, L.E. and Forsythe, J.E. (2002): Siderophore production by an aerobic *Pseudomonas mendocina* bacterium in the presence of kaolinite. *Journal of Organic Chemistry,* **188**, 161–170.

Anastasiadou, J., Axiotis, D. and Gidarakos, E. (2010): Hydrothermal conversion of chrysotile asbestos using near supercritical conditions. *Journal of Hazardous Materials*, **179**, 926–932.

Andreozzi, G.B., Ballirano, P., Gianfagna, A., Mazziotti-Tagliani, S. and Pacella, A. (2009): Structural and spectroscopic characterization of a suite of fibrous amphiboles with high environmental and health relevance from Biancavilla (Sicily, Italy). *American Mineralogist*, **94** (10), 1333–1340.

Aust, A. and Lund, L. (1990): The role of iron in asbestos-catalyzed damage to lipids and DNA. *Biological Oxidation Systems*, **2**, 597–605.

Aust, A.E., Cook, P.M. and Dodson, R.F. (2011): Morphological and Chemical Mechanisms of Elongated Mineral Particle Toxicities. *Journal of Toxicology and Environmental Health*, Part B, **14**, 40–75.

Aust, E.A., Lund, L.G., Chao, C.C., Park, S.H. and Fang, R. (2000): Role of iron in the cellular effects of asbestos. *Inhalation Toxicology*, **12**, 75–80.

Ballirano, P. and Cametti, G. (2015): Minerals in the human body. Crystal chemical and structural modifications of erionite fibers leached with simulated lung fluids. *Am. Mineral.*, **100** (4), 1003–1012.

Ballirano, P., Bloise, A., Gualtieri, A.F., Lezzerini, M., Pacella, A., Perchiazzi, N., Dogan, M. and Dogan, A.U. (2017): The crystal structure of mineral fibres. In A.F. Gualtieri, Ed., Mineral fibres: Crystal chemistry, chemical physical properties, biological interaction and toxicity Vol. 18, pp. 17–64. European Mineralogical Union and the Mineralogical Society of Great Britain & Ireland, UK.

Bartrip, P.W. (2004): History of asbestos related disease. *Postgraduate Medical Journal*, **80** (940), 72-76.

Bashan, Y. (1986): Alginate beads as synthetic inoculant carriers for slow release of bacteria that affect plant growth. *Applied Environmental Microbiology*, **51**, 1089–1098.

Bashan, Y. (1998): Inoculants of plant growth-promoting bacteria for use in agriculture. *Biotechnology Advances*, **16** (4), 729 - 770.

Bashir, S.T., Yang, L., Liggat, J.J. and Thomason, J.L. (2018): Kinetics of dissolution of glass fibre in hot alkaline solution. *Journal of Material Sciences*, **53**, 1710–1722.

Baumann, F., Ambrosi, J.P. and Carbone, M. (2013): Asbestos is not just asbestos: an unrecognised health hazard. *Lancet Oncology*, **14** (7), 576–578.

Baumann, F., Buck, B.J., Metcalf, R.V., McLaurin, B.T., Merkler, D.J. and Carbone, M. (2015): The presence of asbestos in the natural environment is likely related to mesothelioma in young individuals and women from Southern Nevada. *J. Thorac. Oncol*., **10**, 731–737.

Bento, F.M., Camargo, F.A.O., Okeke, B.C. and Frankenberger, W.T. (2005): Comparative bioremediation of soils contaminated with diesel oil by natural attenuation, biostimulation and bioaugmentation. *Bioresource Technology,* **96**, 1049 – 1055.

Bernstein, D., Dunnigan, J., Hesterberg, T., Brown, R.,Velasco, J.A.L., Barrera, R., Hoskins, J. and Gibbs, A. (2013): Health risk of chrysotile revisited. *Crit. Rev. Toxicol*., **43** (2), 154–183.

Bernstein, D. and Pavlisko, E.N. (2017): Differential pathological response and pleural transport of mineral fibres. Chapter 12. In: Gualtieri, A.F. (Ed.), Mineral fibres: crystal chemistry, chemical-physical properties, biological interaction, and toxicity. EMU Notes in Mineralogy, 18, 417–434.

Bernstein, D. M., Rogers, R. and Smith, P. (2005): The biopersistence of Canadian chrysotile asbestos following inhalation: Final Results Through 1 Year After Cessation of Exposure. *Inhalation Toxicology*, **17** (1), 1-14.

Bernstein, D., Castranova, V., Donaldson, K., Fubini, B., Hadley, J., Hesterberg, T., Kane, A., Lai, D., McConnell, E.E., Muhle, H., Oberdorster, G., Olin, S. and Warheit, D.B. (2005): Testing of fibrous particles: short-term assays and strategies: report of an ILSI Risk Science Institute Working Group. *Inhalation Toxicology*, **17**, 497-537.

Bernstein, D., Dunnigan, J., Hesterberg, T., Brown, R., Velasco, J.A.L., Barrera, R., Hoskins, J. and Gibbs, A. (2013): Health risk of chrysotile revisited. *Crit. Rev. Toxicol*., **43** (2), 154–183.

Bernstein, D.M., Donaldson, K., Decker, U., Gaering, S., Kunzendorf, P., Chevalier, J. and Holm, S.E. (2008): A biopersistence study following exposure to chrysotile asbestos alone or in combination with fine particles. *Inhal. Toxicol*., **20**, 1009–1028.

Bernstein, D.M., Dunnigan, J., Hesterberg, T., Brown, R., Velasco, J.A.L., Berrera, R., Hoskins, J. and Gibbs, A. (2013): Response to Murray M. Finkelstein, letter to editor re Bernstein et al: Health risk of chrysotile revisited. *Critical Reviews in Toxicology*, **43** (2), 154–183.

Bernstein, D.M., Dunnigan, J., Hesterberg, T., Brown, R., Velasco, J.A.L., Berrera, R., Berry, G. and Gibbs, G.W. (2008): Mesothelioma and asbestos. *Regul. Toxicol. Pharmacol*., **52**, S223–S231.

Berry, G., Newhouse, M.L. and Wagner, J.C. (2000): Mortality from all cancers of asbestos factory workers in east London 1933-80. *Occupational and Environmental Medicine*, **57**, 782–785.

Beukes, N.J. (1973): Precambrian iron-formations of Southern Africa. *Economic geology*, **68**, 960–1004.

Bezuidenhout, J.J., Liebenberg, D., Claassens, S. and Van Rensburg, L. (2013): Application of evolutionary algorithms to develop a rule set for assessing the rehabilitation status of asbestos mines in South Africa. *Environ. Earth Sci.*, **70**, 3267–3275.

Bignon, J. and Jaurand, M.C. (1983): Biological *in vitro* and *in vivo* responses of chrysotile versus amphiboles. *Environ. Health Perspect*., **51**, 73–80.

Bloise, A., Barca, D., Gualtieri, A.F., Pollastri, S. and Belluso, E. (2016): Trace elements in hazardous mineral fibres. *Environmental Pollution*, **216**, 314-323.

Bloise, A., Barrese, E. and Apollaro, C. (2009): Hydrothermal alteration of Ti-doped forsterite to chrysotile and characterization of the resulting chrysotile fibers. *Neues Jahrbuch für Mineralogie Abhandlungen*, **185**, 297-304.

Bloise, A., Belluso, E., Barrese, E., Miriello, D. and Apollaro, C. (2009): Synthesis of Fe-doped chrysotile and characterization of the resulting chrysotile fibers. *Crystal Research and Technology*, **44**, 590-596.

Bloise, A., Belluso, E., Critelli, T., Catalano, M., Apollaro, C., Miriello, D. and Barrese, E. (2012): Amphibole asbestos and other fibrous minerals in the meta-basalt of the Gimigliano-Mount Reventino unit (Calabria, South-Italy). *Rendiconti della Società Geologica Italiana*, **21**, 847-848.

Bloise, A., Belluso, E., Fornero, E., Rinaudo, C., Barrese, E. and Capella, S. (2010): Influence of synthesis conditions on growth of Ni-doped chrysotile. *Microporous and Mesoporous Materials,* **132**, 239-245.

Bloise, A., Catalano, M., Barrese, E., Gualtieri, A.F., Gandolfi, N.B., Capella, S. and Belluso, E. (2016): TG/DSC study of the thermal behaviour of hazardous mineral fibres. *Journal of Thermal Analysis and Calorimetry*, **123**, 2225-2239.

Bloise, A., Catalano, M., Critelli, T., Apollaro, C. and Miriello, D. (2017): Naturally occurring asbestos: Potential for human exposure, San Severino Lucano (Basilicata, southern Italy). *Environmental Earth Sciences*, **76** (19), 648.

Bloise, A., Critelli, T., Catalano, M., Apollaro, C., Miriello, D., Croce, A., Barrese, E., Liberi, F., Piluso, E., Rinaudo, C. and Belluso, E. (2014): Asbestos and other fibrous minerals contained in the serpentinites of the Gimigliano-Mount Reventino Unit (Calabria, S-Italy). *Environmental Earth Sciences,* **71**, 3773-3786.

Bloise, A., Fornero, E., Belluso, E., Barrese, E. and Rinaudo, C. (2008): Synthesis and characterization of tremolite asbestos fibres. *Eur. J. Miner.*, **20**, 10271033.

Bloise, A., Punturo, R., Catalano, M., Miriello, D. and Cirrincione, R. (2016): Naturally occurring asbestos (NOA) in rock and soil and relation with human activities: the monitoring example of selected sites in Calabria (southern Italy). *Italian Journal of Geosciences*, **135**, 268-279.

Bloise, A., Ricchiuti, C., Punturo, R. and Pereira, D. (2020): Potentially toxic elements (PTEs) associated with asbestos chrysotile, tremolite and actinolite in the Calabria region (Italy). *Chemical Geology*, **558**, 119896.

Braun, L. and Kisting, S. (2006): Asbestos-Related Disease in South Africa: The Social Production of an Invisible Epidemic. *American Journal of Public Health*, **96** (8), 1386 – 1396.

Campbell, W.J. and co-workers (1977): **Selected Silicates Minerals and Their Asbestiform Varieties**. IC 8751, U.S. Bureau of Mines, Washington, D.C., p. 5 - 33.

Carbone, M., Baris, Y.I., Bertino, P., Brass, B., Comertpay, S., Dogand, A.U., Gaudino, G., Jube, S., Kanodia, S., Partridge, C.R., Pass, H.I., Rivera, Z., Steele, I., Tuncer, M., Way, S., Yang, H. and Miller, A. (2011): Erionite exposure in North Dakota and Turkish villages with mesothelioma. *Proc. Natl. Acad. Sci. USA*, **108** (33), 13618–13623.

Cassidy, M.B., Lee, H. and Trevors, J.T. (1996): Environmental applications of immobilized microbial cells: a review. *Journal of Industrial Microbiology,* **16**, 79–101.

Cavallo, A. (2020): Environmental asbestos contamination in an abandoned chrysotile mining site: the example of Val Malenco (central Alps, northern Italy). *IUGS*, **43** (3), 851–858.

Coetzee, C.B. (1976): Mineral Resources of the Republic of South Africa. *Geol. Surv. S. Afr. Handbook*, **7**, 462p.

Cornelis, P. (2010): Iron uptake and metabolism in pseudomonads. *Appl. Microbiol. Biotechnol*., **86**, 1637–1645.

Cornelissen, H. (2017): The Development of a Qualitative Ranking Tool for the Preliminary Selection of Abandoned Asbestos Mine Sites for Rehabilitation. Proceedings of the 3rd World Congress on New Technologies (NewTech'17) Rome, Italy. Paper No. ICEPR 145.

Cornelissen, H., Watson, I., Adam, E. and Malefetse, T. (2019): Challenges and strategies of abandoned mine rehabilitation in South Africa: The case of asbestos mine rehabilitation. *Journal of Geochemical Exploration*, **205**, 106354.

Culley, M.R., Zorland, J. and Freire, K. (2010): Community responses to naturally occurring asbestos: implications for public health practice. *Health education research*, **25**, 877-891.

Cunliffe, M., Kawasaki, A., Fellows, E. and Kertesz, M.A. (2006): Effect of inoculum pre-treatment on survival, activity, and catabolic gene expression of *Sphingobium yanoikuyae* B1 in an aged polycyclic aromatic hydrocarbon-contaminated soil. *FEMS Microbiology and Ecology*, **58**, 364– 372.

Daghino, S. (2005): Asbestos hazard in Western Alps: the use of soil fungi in bioremediation of asbestos fibres dispersed in the environment; a chemical-molecular integrated analysis. PhD thesis, University of Torino (Italy) and University "J. Fourier" of Grenoble (France).

Daghino, S., Martino, E., Fenoglio, I., Tomatis, M., Perotto, S. and Fubini, B. (2005): Inorganic Materials and Living Organisms: Surface Modifications and Fungal Responses to Various Asbestos Forms. *Chemistry: A European Journal*, **11**, 5611–5618.

Daghino, S., Murat, C., Sizzano, E., Girlanda, M. and Perotto, S. (2012): Fungal Diversity Is Not Determined by Mineral and Chemical Differences in Serpentine Substrates. *PLoS ONE*, **7** (9), e44233. doi:10.1371/journal.pone.0044233.

Daghino, S., Turci, F., Tomatis, M., Favier, A., Perotto, S., Douki, T. and Fubini, B. (2006): Soil fungi reduce the iron content and the DNA damaging effects of asbestos fibres. *Environmental Science and Technology*, **40**, 5793–5798.

Daghino, S., Turci, F., Tomatis, M., Girlanda, M., Fubini, B., and Perotto, S. (2009): Weathering of chrysotile asbestos by the serpentine rock-inhabiting fungus *Verticillium leptobactrum*. *FEMS Microbiol. Ecol*., **69**, 132–141.

David, S.R., Fritsch, S., Forster, A., Ihiawakrim, D. and Geoffroy, V.A. (2020): Flocking asbestos waste, an iron and magnesium source for *Pseudomonas. Science of the Total Environment,* **709**, 135936.

David, S.R., Ihiawakrim, D., Regis, R. and Geoffroy, V.A. (2020): Iron removal from raw asbestos by siderophores-producing *Pseudomonas. Journal of Hazardous Materials,* **385**, 121563.

Duffy, B.K. and Defago, G. (1999): Environmental factors modulating antibiotic and siderophore biosynthesis by *Pseudomonas fluorescens* biocontrol strains. *Applied and Environmental Microbiology,* **65**, 2429–2438.

Duquenne, P., Chenu, C., Richard, G. and Catroux, G. (1999): Effect of carbon source supply and its location on competition between inoculated and established bacterial strains in sterile soil microcosm. *FEMS Microbiology Ecology*, **29**, 331–339.

Entwistle, J.A., Hursthouse, A.S., Marinho Reis, P.A. and Stewart, A.G. (2019): Metalliferous Mine Dust: Human Health Impacts and the Potential Determinants of Disease in Mining Communities. *Current Pollution Reports*, **5**, 67–83.

Fubini, B. and Mollo, L. (1995): Role of iron in the reactivity of mineral fibres. *Toxicology Letters*, **82–83**, 951–960.

Fubini, B. and Otero-Arèan, C. (1999): Chemical aspects of the toxicity of inhaled mineral dusts. *Chemical Society Reviews,* **28**, 373-381.

Fubini, B., Bolis, V., Cavenago, A. and Volante, M. (1995): Physicochemical properties of crystalline silica dusts and their possible implication in various biological responses. *Scandinavian Journal of Work, Environment and Health*, **21**, 9-15.

Fubini, B., Gianello, E., Volante, M. and Bolis, V. (1990): Chemical functionalities at the silica surface determining its reactivity when inhaled: formation and reactivity of surface radicals. *Toxicology and Industrial Health,* **6**, 571-94.

Fubini, B., Mollo, L. and Giamello, E. (1995): Free radical generation at the solid/liquid interface in iron containing minerals. *Free Radical Research*, **23**, 593 – 614.

Gaffney, S.H and Simmons, B.D. (2017): Anthophyllite asbestos: state of the science review. *Journal of Applied Toxicology*, **37** (1), 38–49.

Gaffney, S.H., Grespin, M., Garnick, L., Drechsel, D.A., Hazan, R., Paustenbach, D.J., Gaggero, L., Caratto, V. and Ferretti, M. (2016): Self-sustained combustion synthesis and asbestos-bearing waste: Scaling up from laboratory towards pre-industrial size plant. *Energy Procedia*, **97**, 515-22.

Gamble, J.F. and Gibbs, G.W. (2008): An evaluation of the risks of lung cancer and mesothelioma from exposure to amphibole cleavage fragment. *Regul. Toxicol. Pharmacol*., **52**, 154–186.

Gazzano, E., Foresti, E., Lesci, I.G., Tomatis, M., Riganti, C., Fubini, B., Roveri, N. and Ghigo, D. (2005): Different cellular responses evoked by natural and stoichiometric synthetic chrysotile asbestos. *Toxicology and Applied Pharmacology*, **206**, 356–364.

Gazzano, E., Turci, F., Foresti, E., Putzu, M.G., Aldieri, E., Silvagno, F., Lesci, I.G., Tomatis, M., Riganti, C., Romano, C., Fubini, B., Roveri, N. and Ghigo, D. (2007): Iron loaded synthetic chrysotile: a new model solid for studying the role of iron in asbestos toxicity. *Chemical Research in Toxicology*, **20**, 380–387.

Gentry, T.J., Rensing, C. and Pepper, I.L. (2004): New approaches for bioaugmentation as a remediation technology. *Critical Reviews in Environmental Sciences and Technology*, **34**, 447–494.

Gidarakos, E., Anastasiadou, K., Koumantakis, E. and Stappas, N. (2008): Investigative studies for the use of an inactive asbestos mine as a disposal site for asbestos wastes. *Journal of Hazardous Materials*, **153**, 955–965.

Glenn, R.E., Lee, R.J., Jastrem, L.M., Bunker, K.L., Van Orden, D.R. and Strohmeier, B.R. (2008): Asbestos: By any other name, is it still? *Chemical Regulation Reporter*, **32** (21), 22–33.

Gonneau, C., Miller, K., Mohanty, S.K., Xu, R., Hwang, W., Willenbring, J.K. and Casper, B.B. (2017): Framework for assessment and phytoremediation of asbestos-contaminated sites. *Environmental Science and Pollution Research*, **24**, 25912–25922.

Gram, L. (1996): The influence of substrate on siderophore production by fish spoilage bacteria. *Journal of Microbiological Methods*, **25**, 199–205.

Gualtieri, A.F. (2017): Introduction. In: A.F. Gualtieri, Ed., Mineral fibres: Crystal chemistry, chemical physical properties, biological interaction, and toxicity. Vol. 18, pp. 1–15. European Mineralogical Union and the Mineralogical Society of Great Britain & Ireland, UK.

Gualtieri, A.F. (2018): Towards a quantitative model to predict the toxicity/pathogenicity potential of mineral fibres. *Toxicology and Applied Pharmocology*, **361**, 89–98.

Gualtieri, A.F., Andreozzi, G.B., Tomatis, M. and Turci, F. (2019): Iron from a geochemical viewpoint. Understanding toxicity/pathogenicity mechanisms in iron-bearing minerals with a special attention to mineral fibres. *Free Radical Biology and Medicine*, **133**, 21–37.

Gualtieri, A.F., Lusvardi, G., Zoboli, A., Di Giuseppe, D. and Gualtieri, M.L. (2019): Bio-durability and release of metals during the dissolution of chrysotile, crocidolite and fibrous erionite. *Environmental Research*, **171**, 550–557.

Gualtieri, A.F., Mossman, B.T. and Roggli, V.L. (2017): Towards a general model to predict the toxicity and pathogenicity of mineral fibres. In: Gualtieri, A.F. (Ed.), Mineral Fibres: Crystal Chemistry, Chemical-physical Properties, Biological Interaction and Toxicity. European Mineralogical Union, London, pp. 17–64.

Gualtieri, A.F., Pollastri, S., Gandolfi, N.B. and Gualtieri, M.L. (2018): *In vitro* acellular dissolution of mineral fibres: A comparative study. *Science Reports*, **8**, 7071.

Gualtieri, A.F., Viani, A., Sgarbi, G. and Lusvardi, G. (2012): *In vitro* bio-durability of the product of thermal transformation of cement–asbestos. *Journal of Hazardous Materials*, **205–206**, 63–71.

Hardy J.A. and Aust A.E. (1995): The effect of iron binding on the ability of crocidolite asbestos to catalyse DNA single-strand breaks. *Carcinogenesis*, **16**, 319-325.

Hardy, J.A. and Aust, A.E. (1995): Iron in asbestos chemistry and carcinogenicity. *Chemistry Reviews*, **95**, 97–118.

Harper, M. (2008): 10th Anniversary critical review: Naturally occurring asbestos. *Journal of Environmental Monitoring*, **10**, 1394-1408.

Harrington, J.S. and McGlasham, N.D. (1998): South African asbestos: Production, exports, and destinations, 1959–1993. *American Journal of Industrial Medicine*, **33**, 321-326.

Hart, H.P. (1988): Asbestos in South Africa. *Journal of the Southern African Institute of Mining and Metallurgy*, **88** (6), 185–198.

Health and Safety Executive (2005): HSG 248, 'Asbestos: the analyst's guide for sampling, analysis and clearance procedures,' HMSO, London.

Heijnen, C. E. (1992): Population dynamics of bacteria introduced into bentonite-amended soil. Ph.D. thesis. Wageningen Agricultural University, Wageningen, The Netherlands.

Hillerdal, G. (1999): Mesothelioma: Cases associated with non-occupational and low dose exposures. *Int. J. Occup. Environ. Med*., **56**, 505–513.

Ho, C.M., Yau, S.K.W., Lok, C.N., So, M.H. and Che, C.M. (2010): Oxidative dissolution of silver nanoparticles by biologically relevant oxidants: a kinetic and mechanistic study. *Chemistry - an Asian Journal*, **5**, 285–293.

Ho, C.P., Hseu, Z.Y., Chen, N.C. and Tsai, C.C. (2013): Evaluating heavy metal concentration of plants on a serpentine site for phytoremediation applications. *Environ. Earth Sci.*, **70**, 191–199.

Hobbs, P., Oelofse, Z.H.H. and Rascher, J. (2008): Management of environmental impacts from coal mining in the upper Olifants river catchment as a function of age and scale. CSIR natural resources and the environment, Pretoria, South Africa.

Hodgson, A.A. (1977): Nature and paragenesis of asbestos minerals. *Philosophical Transactions Royal Society of London A,* **286**, 611–624.

Hodgson, A.A. (1986): **Scientific Advances in Asbestos, 1967 to 1985**. Anjalena Publication, Crowthorne, UK, p. 10 -117.

Holmes, A., Morgan, A. and Sandalls, F.J. (1971): Determination of iron, chromium, cobalt, nickel, and scandium in asbestos by neutron activation analysis. *Am. Ind. Hyg. Assoc. J.*, **32** (5), 281–286.

Holmes, E.P., Wilson, J., Schreier, H. and Lavkulich, L.M. (2012): Processes affecting surface and chemical properties of chrysotile: Implications for reclamation of asbestos in the natural environment. *Canadian Journal of Soil Science,* **92**, 229–242.

Huang, L., Baumgartl, T. and Mulligan, D. (2012): Is rhizosphere remediation sufficient for sustainable revegetation of mine tailings? *Annals in Botany*, **110**, 223–238.

IARC (1977): Some miscellaneous pharmaceutical substances. *IARC Monogr. Evaluation Carcinogenic Risk Chemistry Man.*, **13**, 1–255.

IARC, (2012): A Review of Human Carcinogens. Part C: Arsenic, Metals, Fibres, and Dusts. International Agency for Research on Cancer, Lyon, France.

Indiragandhi, P., Anandham, R., Madhaiyan, M. and Sa, T.M. (2008): Characterization of plant growth-promoting traits of bacteria isolated from larval guts of diamondback month *Plutella xylostella* Lepidoptera: Plutellidae. *Current Microbiology*, **56**, 327 - 333.

International Standardization Organization (2012): ISO 22262-1:2012 'Air quality – Bulk materials – Part 1: Sampling and qualitative determination of asbestos in commercial bulk materials,' ISO, Geneva.

Jones, R.R. (2010): Risk-based assessment of environmental asbestos contamination in the Northern Cape and Northwest Provinces of South Africa. D. Phil. Thesis, Department of Environmental Sciences, Rhodes University, Grahamstown.

Kamp, D.W., Graceffa, P., Pryor, W.A. and Weitzman, S.A. (1992): The role of free radicals in asbestos-induced diseases. *Free Radic. Biol. Med.*, **12**, 293–315.

Kazakou, E., Dimitrakopoulos, P.G., Baker, A.J.M., Reeves, R.D. and Troumbis, A.Y. (2008): Hypotheses, mechanisms and trade-offs of tolerance and adaptation to serpentine soils: from species to ecosystem level. *Biology Reviews*, **83**, 495–508.

Kilburn, K.H. (2000): Indoor air effects after building renovation and in manufactured homes. *The American Journal of Medical Sciences,* **320** (4), 249–54.

Kwata, M.G. (2019): The application of the modified crude settleable dust approach as a viable asbestos mineral test method. PhD thesis, Department of Environmental Sciences, University of South Africa, South Africa.

Kwata, M.G. and Moja, S.J. (2017): Characterization of Settleable Dust and Surface Dust Samples from the Old and Abandoned Asbestos Mine Dumps in the Limpopo Province,South Africa. *Journal for Pollution Effect Control*, **5** (4), 111-120.

Lee, Y.J., Lim, S.S., Baek, B.J., An, J.M., Nam, H.S., Woo, K.M., Cho, M.K., Kim, S.H. and Lee, S.H. (2016): Nickel (II)-induced nasal epithelial toxicity and oxidative mitochondrial damage. *Environ. Toxicol. Pharmacol*., **42**, 76–84.

Lewis, J. A. and Papavizas, G. C. (1991): Biocontrol of plant diseases: the approach for tomorrow. *Crop Protection,* **10** (2), 95-105

Liebenberg-Weyers, D. (2010): A multidisciplinary approach for the assessment of rehabilitation at asbestos mines in South Africa. MSc dissertation, Northwest University, Potchefstroom.

Lima, A. T., Mitchell, K., O'Connell, D. W., Verhoeven, J. and Van Cappellen, P. (2016): The legacy of surface mining: Remediation, restoration, reclamation, and rehabilitation. *Environmental Science and Policy*, **66**, 227–233.

Liu, J. and Hurt, R.H. (2010): Ion release kinetics and particle persistence in aqueous nanosilver colloids. *Environmental Science Technology*, **44**, 2169–2175.

Liu, J., Sonshine, D.A., Shervani, S. and Hurt, R.H. (2010): Controlled release of biologically active silver from nano silver surfaces. *ACS Nano*., **4**, 6903–6913.

Liu, J., Tian, S.P., Li, B.Q. and Qin, G.Z. (2009): Enhancing viability of two biocontrol yeasts in liquid formulation by applying sugar protectant combined with antioxidant. *Biological Control,* **54**, 817–824.

Lucci, F., Della Ventura, G., Conte, A., Nazzari, M. and Scarlato, P. (2018): Naturally occurring asbestos (NOA) in granitoid rocks, a case study from Sardinia (Italy). *Minerals*, **8**, 442.

Lucci, F., Ventura, G.D., Conte, A., Nazzari, M. and Scarlato, P. (2018): Naturally Occurring Asbestos (NOA) in Granitoid Rocks, A Case Study from Sardinia (Italy). *Minerals*, **8** (442), 1 - 23.

Matsabatsa, G.M. (2009): Post-closure environmental impacts of asbestos mining in Penge, Limpopo Province, South Africa. MSc dissertation, University of the Witwatersrand, Johannesburg.

McCulloch, J. (2003): Asbestos mining in Southern Africa, 1893 - 2002. *Int. J. Occup. Environ. Health*, **9**, 230–235.

McDonald, A., McDonald, J. and Pooley, F. (1982): Mineral fibre content of lung in mesothelial tumours in North America. *Ann. Occup. Hyg.*, **26**, 417–422.

McDonald, J. and McDonald, A. (1997): Chrysotile, tremolite and carcinogenicity. *Annuals of Occupational Hygiene*, **41**, 699–705.

Mchaina, D. (2001): Environmental planning considerations for the decommissioning, closure, and reclamation of a mine site. *International Journal of Surface Mining, Reclamation and Environment*, **15** (3), 163–176.

McLoughlin, A.J. (1994): Controlled release of immobilized cells as a strategy to regulate ecological competence of inocula. *Advances in Biochemical Engineering/Biotechnology*, **51**, 1–45.

Mendez, M.O. and Maier, R.M. (2008a): Phytoremediation of mine tailings in temperate and arid environments. *Reviews in Environmental Science and Biotechnology,* **7** (1), 47-59.

Mendez, M.O. and Maier, R.M. (2008b): Phytostabilization of mine tailings in arid and semiarid environments- an emerging remediation technology. *Environmental Health Perspectives*, **116** (3), 278-283.

Mohanty, S.K., Gonneau, C., Salamatipour, A., Pietrofesa, R.A., Casper, B., Christofidou-Solomidou, M. and Willenbring, J.K. (2018): Siderophore-mediated iron removal from chrysotile: Implications for asbestos toxicity reduction and bioremediation. *Journal of Hazardous Materials*, **341**, 290–296. http://dx.doi.org/10.1016/j.jhazmat.2017.07.033

Moorthy, K., Lavanya, V., Malarvizhi, A., Arul Sheeba Malar, S., Bharathy, G., Arjunan, S., Gnanendra, T.S. and Thajuddin, N. (2010): Isolation of soil bacteria for bioremediation of hydrocarbon contamination. *Biosciences, Biotechnology Research Asia*, **7** (2), 901 – 906.

Mossman, B.T. and Gee, J.B.L. (1989): Asbestos related diseases. *The New England Journal of Medicine,* **320**, 1724 -1730.

Mossman, B.T., Bignon, J. and Corn, M. (1990): Asbestos: scientific developments and implications for public policy. *Science,* **247**, 294-301.

Mossman, B.T., Lippmann, M., Hesterberg, T.W., Kelsey, K.T., Barchowsky, A. and Bonner, J.C. (2011): Pulmonary endpoints (lung carcinomas and asbestosis) following inhalation exposure to asbestos. *Journal of Toxicology and Environmental Health*, **14**, 76-121.

Mrozik, A. and Piotrowska-Seget, Z. (2010). Bioaugmentation as a strategy for cleaning up soils contaminated with aromatic compounds. *Microbiological Research*, **165**, 363 - 375.

Muhle, H. and Bellmann, B. (1997): Significance of the bio-durability of man-made vitreous fibres to risk assessment. *Environmental Health Perspectives*, **105**, 1045.

Ndeddy Aka, R. Jr and Babalola, O.O. (2017): Identification and characterization of Cr-, Cd-, and Ni-tolerant bacteria isolated from mine tailings. *Bioremediation Journal*, **21** (1), 1-19. DOI: 10.1080/10889868.2017.1282933.

Ndlovu, N., teWater Naude, J. and Murray, J. (2013): Compensation for environmental asbestos-related diseases in South Africa: a neglected issue. *Global Health Action*, **6** (19410), 82 – 88.

Nelson, G. (2012): Living in the shadow of a dust cloud: occupational respiratory diseases in the South African mining industry, 1975 to 2009. PhD thesis. University of the Witwatersrand, Johannesburg.

Nelson, G., Murray, J. and Phillips, J.I. (2011): The Risk of Asbestos Exposure in South African Diamond Mine Workers. *Annals of Work Exposure and Health*, **55** (6), 569–577.

Noonan, C.W. (2017): Environmental asbestos exposure and risk of mesothelioma. *Ann. Transl. Med.*, **5**, 234–244.

Nopcharoenkul, W., Pinphanichakarn, P. and Pinyakong, O. (2011): The development of a liquid formulation of *Pseudoxanthomonas* sp. RN402 and its application in the treatment of pyrene-contaminated soil. *Journal of Applied Microbiology*, **111**, 36–47.

Pascolo, L., Gianoncelli, A., Schneider, G., Salome, M., Schneider, M., Calligaro, C., Kiskinova, M., Melato, M. and Rizzardi, C. (2013): The interaction of asbestos and iron in lung tissue revealed by synchrotron-based scanning X-ray microscopy. *Scientific Reports*, **3** (1123), 1 - 11.

Patel, P.R., Shaikh, S.S. and Sayyed, R.Z. (2016): Dynamism of PGPR in bioremediation and plant growth promotion in heavy metal contaminated soil. *Indian Journal of Experimental Biology,* **54**, 286 – 290.

Petriglieri, J.R., Bersani, D., Laporte-Magoni, C., Tribaudino, M., Cavallo, A., Salvioli-Mariani, E. and Turci, F. (2021b): Portable Raman Spectrometer for *in situ* Analysis of Asbestos and Fibrous Minerals. *Appl. Sci*., **11**, 287.

Petriglieri, J.R., Laporte-Magoni, C., Salvioli-Mariani, E., Ferrando, S., Tomatis, M., Fubini, B. and Turci, F. (2021a): Morphological and chemical properties of fibrous antigorite from lateritic deposit of New Caledonia in view of hazard assessment. *Science of the Total Environment*, **777**, 146185.

Petriglieri, J.R., Laporte-Magoni, C., Salvioli-Mariani, E., Tomatis M., Gazzano, E., Gunkel-Grillon, P., Turci, F., Cavallo, A. and Fubini, B. (2020): Identification and Preliminary Toxicological Assessment of a Non-Regulated Mineral Fibre: Fibrous Antigorite from New Caledonia. *Environmental and Engineering Geoscience*, **26**, 89–97.

Phrommanich, S., Suanjit, S., Upatham, S., Grams, S.V., Kruatrachue, M., Pokethitiyook, P., Korge, G. and Hofmann, A. (2009): Quantitative detection of the oil-degrading bacterium *Acinetobacter* sp. strain MUB1 by hybridization probe based real-time PCR. *Microbiology Research*, **164**, 486–492.

Pollastri, S., D'Acapito, F., Trapananti, A., Colantoni, I., Andreozzi, G.B. and Gualtieri, A.F. (2015): The chemical environment of iron in mineral fibres. A combined X-ray absorption and Mössbauer spectroscopic study. *Journal of Hazardous Materials*, **298**, 282–293.

Pollastri, S., Gualtieri, A.F., Gualtieri, M.L., Hanuskova, M., Cavallo, A. and Gaudino, G. (2014): The zeta potential of mineral fibres. *Journal of Hazardous Materials*, **276**, 469-479. *Applied Geochemistry*, **49**, 46–56.

Prandi, L., Tomatis, M., Penazzi, N. and Fubini, B. (2002): Iron cycling mechanisms and related modifications at the asbestos surface. *Annual Occupational Hygiene*, **46**, 140 –143.

Punturo, R., Bloise, A., Critelli, T., Catalano, M., Fazio, E. and Apollaro, C. (2015): Environmental implications related to natural asbestos occurrences in the ophiolites of the Gimigliano-Mount Reventino Unit (Calabria, Southern Italy). *International Journal of Environmental Research*, **9**, 405-418.

Punturo, R., Cirrincione, R., Pappalardo, G., Mineo, S., Fazio, E. and Bloise, A. (2018): Preliminary laboratory characterization of serpentinite rocks from Calabria (southern Italy) employed as stone material. *J. Mediterr. Earth Sci*., **10**.

Ronholm, J., Goordial, J., Sapers, H.M., Izawa, M.R.M., Applin, D.M., Pontefract, A., Omelon, C.R., Lamarche-Gagnon, G., Cloutis, E.A. and Whyte, L.G. (2018): Characterization of Microbial Communities Hosted in Quartzofeldspathic and Serpentinite Lithologies in Jeffrey Mine, Canada. *Astrobiology*, **8** (8), 1–15. DOI: 10.1089/ast.2017.1685

Roszak, D. B. and Colwell, R.R. (1987): Survival strategies of bacteria in the natural environment. *Microbiology Reviews*, **51**, 365–379.

Sayler, G., Layton, A., Lajoie, C., Bowman, J., Tschantz, M. and Fleming, J. (1995): Molecular site assessment and process monitoring in bioremediation and natural attenuation. *Applications in Biochemistry and Biotechnology*, **54**, 277–290.

Schimmer, C. (2017): Synergistic use of soil microbes and plants to facilitate rehabilitation on gold tailings materials. M.Sc. Dissertation, School for Geo- and Spatial Sciences, North-West University, Potchefstroom.

Skinner, H.C.W., Ross, M. and Frondel, C. (1988): **Asbestos and other fibrous materials – mineralogy, crystal chemistry, and health effects**. Oxford University Press, New York (NY).

Sluis-Cremer, G. (1970): Asbestosis in South African asbestos mines. *Environmental Research,* **3,** 310–319.

Smith, I.C.R. (1972): Kinetic study of dissolution of asbestos fibres in water. *Journal of Colloid Interface Science*, **40** (2), 253–262.

Speil, S. and Leineweber, J.P. (1969): Asbestos minerals in modern technology. *Environmental Research*, **2**, 166–208.

Thompson, I.P., Van der Gast, C.J., Ciric, L. and Singer, A.C. (2005). Bioaugmentation for bioremediation: the challenge of strain selection. *Environmental Microbiology*, **7** (7), 909 - 915.

Tomatis, M., Turci, F., Ceschino, R., Riganti, C., Gazzano, E., Martra, G., Ghigo, D. and Fubini, B. (2010): High aspect ratio materials: role of surface chemistry vs. length in the historical long and short amosite asbestos fibres. *Inhalation Toxicology*, **22**, 984–998.

Torres, E.M., Hess, D., McNeil, B.T., Guy, T. and Quinn, J.C. (2017): Impact of inorganic contaminants on microalgae productivity and bioremediation potential. *Ecotoxicology and Environmental Safety*, **139**, 367–376.

Torres, R., Usall, J., Teixido, N., Abadias, M. and Vinas, I. (2003): Liquid formulation of the biocontrol agent *Candida sake* by modifying water activity or adding protectants. *Journal of Applied Microbiology*, **94**, 330–339.

Van Druten, E. and Bekker, M. C. (2017): Towards an inclusive model to address unsuccessful mine closures in South Africa. *Journal of the Southern African Institute of Mining and Metallurgy*, **117** (5), 485–490.

Van Gosen, B.S. (2007): The Geology of Asbestos in the United States and Its Practical Applications. *Environmental & Engineering Geoscience*, **8** (1), 55–68.

Van Rensburg, L., Claassens, S., Bezuidenhout, J.J. and Jansen van Rensburg, P.J. (2008): Rehabilitation of asbestos mining waste: a Rehabilitation Prioritisation Index (RPI) for South Africa. *Environ. Geol.*, **57** (2), 267–273.

Vidali, M. (2001): Bioremediation: An Overview. *Pure and Applied Chemistry,* **73** (7), 1163–1172.

Vimercati, L., Cavone, D., Lovreglio, P., De Maria, L., Caputi, A., Ferri, G.M. and Serio, G. (2018): Environmental asbestos exposure and mesothelioma cases in Bari, Apulia region, southern Italy: A national interest site for land reclamation. *Environ. Sci. Pollut. Res. Int*., **25**, 15692–15701.

Virta, R.L. (2002): Asbestos: Geology, Mineralogy, Mining and Uses. Reston, VA: US Geological Survey.

Visonà, S.D., Villani, S., Manzoni, F., Chen, Y., Ardissino, G., Russo, F., Moretti, M., Javan, G.T. and Osculati, A. (2018) Impact of asbestos on public health: A retrospective study on a series of subjects with occupational and non-occupational exposure to asbestos during the activity of Fibronit plant (Broni, Italy). *J. Public Health Res*., **7**, 1519–1524.

Vogel, T.M. (1996): Bioaugmentation as a soil bioremediation approach. *Current Opinion in Biotechnology,* **7**, 311–316.

Walker, J.J. and Pace, N.R. (2007): Endolithic microbial ecosystems. *Annual Reviews in Microbiology*, **61**, 331–347.

Walker, J.J., Spear, J.R. and Pace, N.R. (2005): Geobiology of a microbial endolithic community in the Yellowstone geothermal environment. *Nature*, **434**, 1011–1014.

Wallis, S.L., Emmett, E.A., Hardy, R., Casper, B.B., Blanchon, D.J., Testa, J.R., Menges, C.W., Gonneau, C., Jerolmack, D.J., Seiphoori, A., Steinhorn, G. and Berry, T-A. (2020): Challenging Global Waste Management: Bioremediation to Detoxify Asbestos. *Frontiers in Environmental Sciences*, **8** (20), 1 - 14.doi: 10.3389/fenvs.2020.00020.

Weissenhorn, I., Leyval, C. and Berthelin, J. (1993): Cd-tollerant arbuscular mycorrhizal (AM) from heavy metal polluted soils. *Plant Soil*, **157**, 247-256.

Wu, C.H., Wood, T.K., Mulchandani, A. and Chen, W. (2006): Engineering plant–microbe symbiosis for rhizoremediation of heavy metals. *Appl. Environ. Microbiol.*, **72**, 1129–1134.

Wu, L., Jacobson, A.D., Chen, H.C. and Hausner, M. (2007): Characterization of elemental release during microbe–basalt interactions at T = 28°C. *Geochimica et Cosmochimica Acta*, **71**, 2224–2239.

Wu, S., Liu, Y., Southam, G., Robertson, L., Chiu, T.H., Cross, A.T., Dixon, K.W., Stevens, J.C., Zhong, H., Chan, T-S., Lu, Y-J. and Huang, L. (2019): Geochemical and mineralogical constraints in iron ore tailings limit soil formation for direct phytostabilization. *Science of the Total Environment*, **651**, 192–202.

Xu, R., Barg, F.K., Emmett, E.A., Wiebe, D.J. and Hwang, W.T. (2018): Association between mesothelioma and non-occupational asbestos exposure: Systematic review and meta-analysis. *Environ. Health*, **17**, 90–103.

# Chapter 2 - Mineralogical, petrological, and geochemical characterisation of chrysotile, amosite and crocidolite asbestos mine waste from southern Africa in context of hazard evaluation and rehabilitation

## Abstract

Derelict asbestos mine dumps, tailings and contaminated soils in southern Africa pose considerable harm to human, environmental and socio-economic health. Cost, time, legislation, and the vast number of these sites make rehabilitation a massive undertaking. Developing complete criteria necessitates sufficient baseline data, such as asbestos mine waste characterisation, to be acquired by industry and regulators before-hand so that the subsequent rehabilitation design is realistic, informed, and achievable in terms of best policy science. However, mineralogical, and geochemical data sets for the actual hazardous geological material of concern from southern African derelict asbestos mines remain largely non-existent and little published and up-to-date literature is currently available. The health hazards of asbestos exposure from environmental settings received much attention in recent years and asbestos fibre heavy metal concentration data have shown to be consequential with respect to the toxicity to both human and environmental health. The aim of this study is to collect and analyse three types of asbestos mineral fibres from derelict asbestos mines in Southern Africa, namely chrysotile from Havelock mine (Eswatini, formerly Swaziland); amosite from Penge mine (Penge, South Africa) and crocidolite from Prieska mine (Prieska, South Africa) to provide mineralogical and geochemical data to evaluate real-life hazards in rural and asbestos-fibre contaminated regions. The samples were subjected to macroscopic examination, polarising light microscopy, X-ray fluorescence (major and trace elemental analysis), X-ray diffraction (including Rietveld refinement), specific surface area analyses and bio-durability tests. Data is used to define and discuss their potential toxicities on both human health and the environment in the context of developing countries. Further implications of this study may extend to preliminary information on the mineralogical and geochemical status of asbestos mine waste and its importance as baseline data for rehabilitation considerations.

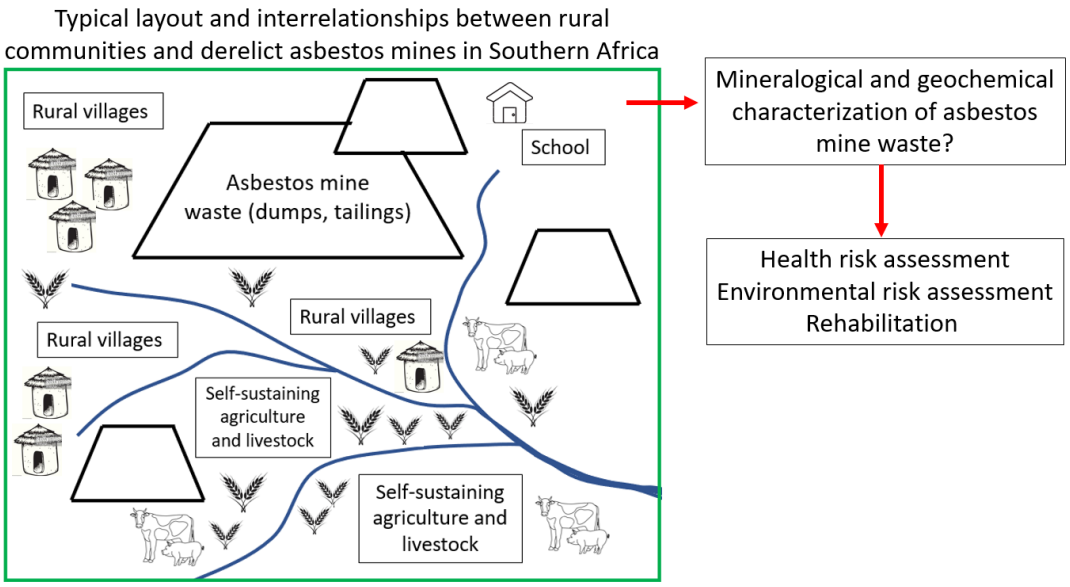


Figure 2.1.: Graphical abstract showing typical layout and interrelationships between rural communities and DAMLs in Southern Africa

## 2.1. Introduction

South Africa is endowed with considerable mineral wealth, but at the same time also faces tremendous environmental and human health problems resulting from mining. Approximately 6000 derelict mines exist in South Africa, which pose significant health and environmental concerns (Cornelissen *et al.,* 2019). Of these, 249 are abandoned asbestos mines, of which only ~40 have been rehabilitated (Cornelissen *et al.,* 2019). A legacy of pollution remains in the wake of the asbestos mining industry, and the enormous quantities of rock-waste generated by decades of asbestos mining continue to pose an insurmountable health and environmental risk to surrounding communities, especially those in developing countries (Harris and Kahwa 2003). Historically, poorly regulated asbestos mining operations in South Africa have resulted in the widespread and seemingly unassailable contamination of the environment. Although occupational exposures diminished in the wake of the asbestos mining cessation in South Africa, this tenacious, contemporary and vast contamination of the environment by asbestos is indicative of an indeterminate and conceivably boundless epidemic of asbestos-related diseases (ARD) (Ndlovu *et al.,* 2013).

The regulatory and commercial term, asbestos, is applied to define a group of naturally occurring silicate minerals with a specific fibrous crystal habit and unique chemical, physical and technological properties (Williams *et al.,* 2013). There are six types of asbestos minerals that fall into

one of two groups, namely serpentine and amphiboles (Hodgson, 1977). The physical and chemical properties of each species is different with their fibrous nature being the only feature they have in common (Hodgson, 1977).

The toxicity and carcinogenic effects of asbestos-mineral fibres are related to their physical and chemical properties including durability and/or bio-persistence; high aspect-ratio and their chemical composition (Mossman *et al.,* 2011; Pugnaloni *et al.,* 2013; Bloise *et al.,* 2016a, b).

Geochemical and mineralogical characterisation of asbestos-bearing mine rocks is important for both human and environmental health risk assessment and quantification that impact on risk mitigation interventions (Higueras *et al.,* 2012). Moreso, baseline geochemical and mineralogical data on asbestos fibre waste dumps are important for directing rehabilitation interventions and therefore are important to consider when dealing with such sites (Higueras *et al.,* 2012). However, the costs involved in these assessments are a major issue for developing countries. The aim of this paper is to use traditional mineralogical and geochemical methods, typically involved in the characterisation of inorganic fibrous minerals, to demonstrate the importance of incorporating geologic-based delineation in derelict asbestos mine site rehabilitation programmes. This chapter further highlights the necessity of mineralogical and geochemical knowledge in the context of asbestos mine reclamation by emphasising its benefits and indicating its possibility in fund-limited, developing countries, by using relevant scientific methods that are also cost-effective, relatively rapid, and easily accessible.

## 2.2. Materials and Methods

### 2.2.1. Sampling locations and geological background

Three different asbestos rock samples were investigated in this study (table 2.1), namely: (i) Chrysotile from Bulembu (Havelock Mine), Swaziland; (ii) amosite from Penge, Lydenberg District, South Africa and (iii) crocidolite from Prieska Division, Northern Cape, South Africa.

Table 2.1: Location co-ordinates and description of sampling locations

| | **Chrysotile** | **Amosite** | **Crocidolite** |
|---|---|---|---|
| | | | |
| **Sampling locations** | Havelock Mine, Bulembu, Swaziland (Eswatini) (figure 1) | Penge, Sekhukhune District, Limpopo, South Africa (figure 2) | Prieska Division, Northern Cape, South Africa (figure 3) |
| **Location coordinates** | 25°57'21''S 31°07'51''E | 24°25'07''S 30°20'14''E | 28°19'01''S 23°06'05''E |
| **Climate** | Humid sub-tropical | Sub-tropical | Semi-arid |
| **Biome** | Grassland | Savanna | Savanna |
| **Occurrence** | Cross-vein fibres (growth of fibres at right angles to the walls of cracks) | Cross-fibre seams in banded ironstones | Cross-fibre seams in banded ironstones |
| **Number of samples collected** | Three | Two | Two |

In southern Africa, the Havelock orebody is one of the largest chrysotile asbestos deposits (Anhaeusser, 1976). The Havelock asbestos deposits occur as ultramafic lenses within the Swartkoppie Formation of the Onverwacht Group in the south-eastern part of Precambrian layered ultramafic complexes of the Barberton greenstone belt (Hunter and Jones, 1969; Viljoen and Viljoen, 1969). Dunite, lherzolite and harzburgite primarily comprise these ultramafic complexes with the main minerals being clinopyroxene, orthopyroxene, olivine, and chromite (Abbott, 1983). The chrysotile asbestos occurs as serpentinite lenses or pods within the main lithological components of the Swartkoppie Formation (van Biljon, 1964). The differentiated and serpentinised ultramafic bodies contain units of pyroxenite, metagabbro, dunite and peridotite where relict and strongly altered olivine, clinopyroxene, orthopyroxene and chromite are the major rock forming minerals (Abbott, 1983). The asbestos deposits are localised within the deformation zones of the host rocks (van Biljon, 1964; Anhaeusser, 1976) and hydration resulted in the partial or complete serpentinisation of the ultramafic rock (Abbott, 1983). Chrysotile asbestos formation requires a specific combination of folding, faulting, shearing, serpentinisation and metamorphism (Abbott, 1983). The chrysotile asbestos mineralisation occurs in the form of cross-fibres in a stockwork of veins (Hart, 1988). Chrysotile fibre genesis is structurally controlled by the host rocks and usually occurs as cross-fibre veins forming as the final products of the serpentinisation (Abbott, 1983). The vein material is provided by the host rocks and reflects its composition (Riordon, 1955). Host rocks with abnormally high iron contents result in the formation of dark green, harsh fibres (Riordon, 1955). Host rocks with low iron, calcium and aluminium content and high silica and magnesia content lead to the

development of softer, silky fibres (Riordon, 1955). The chrysotile fibres are perpendicular to the walls of the veins and are arranged together in parallel bundles.

The amosite samples were collected from Penge, Limpopo Province where they occur as layered, extensive continuous seams within Banded-Iron Formations (BIF) (Cairncross, 2004). Situated in the metamorphic aureole of South Africa's Bushveld Complex, the Penge Iron Formation of the Transvaal Supergroup is a unique succession as it contains both amosite and crocidolite asbestos (Dreyer and Sohnge, 1992; Miyano and Beukes, 1997). The distribution of amosite and crocidolite asbestos seams in the Penge Iron Formation are controlled by bulk-rock composition. However, some evidence exists that with increasing metamorphic grades, amosite replaced crocidolite (Miyano and Beukes, 1997). The fibrous amosite units occurring in the BIF are in transitional contact with and underlain by a thick dolomitic sequence (Abbott, 1983). An angular disconformity marks the upper contact of the BIF, which is overlain by a quartzites and shale sequence. Alternating bands of dark-coloured magnetite, grunerite and graphite and light-coloured chert, quartz and siderite comprise the iron-formation (Miyano and Beukes, 1997). The bands are laterally extensive and range from several centimetres in thickness to microscopic (Genis, 1961). The fibrous amosite asbestos is found as clearly defined lithological units (Miyano and Beukes, 1997). The amosite reefs are typically formed in several units of micro-banded magnetite-grunerite BIF (Miyano and Beukes, 1997). In most part, amosite is found in lenses of fibrous masses with their long axes lying perpendicular to the country rock (Reinecke and McClure, 1933). The quality of the amosite fibres depends on their location in the Penge/Egnep mine. Ash grey, easily separated and flexible fibres are found at the bottom levels of the mine, where the rocks are not influenced by surface waters (Reinecke and McClure, 1933). At the mine these fibres are called 'springy' fibres as they spring back to their original form after being bent (Reinecke and McClure, 1933). 'Soft white' fibres are found above the bottom level but below the ground-water level and are characterised by soft, flexible, and white fibres that do not readily revert to their original form after being bent (Reinecke and McClure, 1933). Closer to the surface, 'soft brown' fibres with the least tensile strength are found and in certain places are weathered to clayey masses (Reinecke and McClure, 1933).

The crocidolite samples were collected from the Prieska Mine in the Northern Cape where they occur as seams interbedded within BIF (Cairncross, 2004). In the Northern Cape the crocidolite fields extend > 450 km south of Prieska to the border of Botswana, where the blue fibres occur in the Asbestos Hills BIF as 1 to 50 mm cross-fibre seams (Howling, 1937; Hart, 1988). The lengths of fibres are important when considering their removal from the lungs via macrophages, the cells that

normally eliminate particles from the lungs (Strohmeier *et al.,* 2010). Fibres with lengths greater than the diameter of macrophages cannot be removed resulting in macrophage death and inflammatory cytokines release into surrounding tissues and fibrosis or asbestosis if inhaled as collagen builds up (Plumlee *et al.,* 2006). Numerous studies have indicated that fibres with lengths < 5 µm do not have any significant biological potency as they are cleared by macrophages whose sizes range between 10 to 15 µm (Ilgren, 2008). Fibres with lengths larger than 10 to 15 µm have a greater probability for persisting in the lungs for extended time periods (Ilgren, 2008). Thus, length characterisation of exposed asbestos-containing mine rock waste is important with regards to the relative health risks and effects (Strohmeier *et al.,* 2010). Crocidolite is believed to have formed from sodium-rich brines that moved through the iron formation (Genis, 1961). Unlike the host rocks, crocidolite is extremely resistant to weathering and persists at the surface (Abbot, 1983). The fibrous crocidolite asbestos deposits demonstrate significant blue colour variation (Abbot, 1983). Dark steely blue coloured crocidolite is found in the deeper mine workings of the Northern Cape, whereas lighter, lavender blue crocidolite is found in the weathered zone (Abbot, 1983). The lighter, weathered zone crocidolite contains more ferric iron and bound water and less silica than the dark fresh crocidolite (Abbot, 1983).

### 2.2.2. Polarising light microscopy (PLM)

The visible and suspected asbestos fibres extracted from their host rocks were cut with scissors and positioned on a glass slide. A small drop of eugenol (refractive oil index $n$ = 1.54) was then deposited on the fibres after, which they were covered with cover slips. The slide was scanned, and the asbestos mineral identified using its optical properties (morphology, colour, pleochroism, birefringence, extinction characteristics and sign of elongation). Coatings on the fibres sometimes obscured the optical properties of the asbestos minerals and fibres finer than the microscopes resolving power (ca. 0.3 µm) were not detectable. The colour and index of refraction of the asbestos mineral fibres may be altered or changed by acid and heat treatment.

### 2.2.3. Crushing

A simple technique of crushing, using a mortar and pestle, was used to explore whether the long, visibly elongated minerals in each of the rock samples is fibrous. Elongated minerals sometimes become matted together during crushing and form a ball and/or separate into needles or fibres; these are considered as fibrous and potentially asbestiform. Those that are easily crushed into a powder are not fibrous and therefore not asbestiform. However, cleavage fragments and asbestiform fibres may occur in association. Powdered samples were used for X-ray diffraction (XRD), X-ray fluorescence (XRF) and BET surface area analysis. A rotary splitter was used to reduce the samples, which were then powdered using a mortar and pestle.

### 2.2.4. X-ray diffraction (XRD)

The samples were analysed by X-ray diffraction (XRD) to determine the mineral phase compositions. The XRD analysis was done by using the back-loading preparation method. Diffractograms were attained by employing a Malvern Panalytical Aeris diffractometer with PIXcel detector and fixed slits with Fe filtered Co-Kα radiation. Phases were determined by means of X'Pert Highscore plus software (version 2.1. PANalytical, Malvern, UK). The Rietveld method (quantitative analysis) (Rietveld, 2014) was used to estimate the relative phase amounts (weight %). The phases were identified using X'Pert Highscore plus software. The relative phase amounts (weight %) were estimated using the Rietveld method (quantitative analysis). The relative intensities (equation 1) and *d*-spacing (equation 2) were calculated from the diffractogram data.

Relative intensity (%) = $I/I_1$ x 100 _____ Equation 1
where I is the intensity of the peak and $I_1$ is the intensity of the highest peak.

$n\lambda = 2d \sin\Theta$ _____ Equation 2 (Bragg equation)
where n = 1, λ (Co*K*α) = 1.78892 and $d = n\lambda/2*\sin(\Theta)$ (*d*-spacing value).

### 2.2.5. X-ray fluorescence (XRF)

Major and trace element concentrations of the four asbestos mineral fibre samples were determined using X-ray fluorescence (PANalytical PW2404 x-ray spectrometer) at the Earth lab, Bernard Price Building, University of the Witwatersrand, South Africa. Major elements were determined using the Norrish Fusion 1 technique (Norrish and Hutton, 1969) using in-house correction procedures outlined in Wilson (2012). Sample weight used was 0.35 gm and a flux weight of 2.5 gm. Samples were fused using Johnson Matthey Spectrolflux 105 at 1100°C and raw data corrected. Standard calibrations were made up using synthetic oxide mixtures, international standard as well as in-house controls. Calibration standards were from International Reference Materials USGS series (USA) and NIM series (South Africa). Pressed pellets were prepared for trace element analysis and the data corrected for matrix effects using Compton peak monitoring.

### 2.2.6. BET-$N_2$ specific surface area (SSA)

The specific surface area (SSA) of the asbestos rock samples was determined by the BET method (Brunauer *et al.,* 1938) using a Micromeritics TriStar 3000 V6.05 A surface area analyser with $N_2$ as absorbing gas at the School of Chemistry, University of the Witwatersrand, South Africa. A mass of ~ 0.2 g of each sample was placed in BET sample tubes and degassed for 4 hours. The samples were then loaded into the BET instrument and N2 adsorption isotherms were obtained, and the specific surface area determined.

### 2.2.7. Bio-durability tests

The ability of mineral fibres to resist chemical and/or biochemical alteration is referred to as bio-durability (Aust *et al.,* 2011; Deng *et al.,* 2012; Di Giuseppe, 2020). The bio-durability and dissolution kinetics of the asbestos rock samples was determined by dissolution batch experiments at 37°C and continuous agitation (90 rpm). Seven batch reactors were set up for each type of asbestos sample and the change in sample mass at different intervals of time was measured. The advancement of the dissolution reaction was determined at the following predetermined sampling times: 24 hours, 48 hours, 1 week, 2 weeks, 1 month, 2 months and 3 months. The batch experiments were conducted in 100 mL Erlenmeyer flasks containing water and HCl solution (50 mL) at a pH of 4

and 50 mg of sample. At each sampling time the content of the flask was vacuum filtered using 0.22 µm ϕ cellulose Merck Millipore filters (ashless grade). The mass of the solid residue was determined by measuring the weight difference of the initial NOA rock sample mass and the solid residues, after filtration and drying, known as the filter mass.

The following equation was used to calculate the dissolved mass fraction (DMF) of the chrysotile, amosite, and crocidolite:

$$\text{DMF} = 1 - \frac{Mt}{Mo} \text{ or DMF} = \frac{Mo - Mt}{Mo} \quad \text{(3)}$$

where $M_o$ is the initial mass of the solid at time = 0 and $M_t$ is the mass of the solid at time t.

The dissolution efficiency of the chrysotile, amosite and crocidolite was also calculated using the raw data of total mass loss after 720 hours. The dissolution efficiency (D%) of the asbestos rock sample in HCl-water solution was calculated according to the equation (4) (Rozalen and Huertas, 2013; Rozalen *et al.,* 2014):

$$\text{D\%} = \frac{Mi - Mt}{Mi} \; x \; 100 \quad \text{(4)}$$

where $M_i$ is the initial mass (grams), and $M_t$ is the total mass loss (g).

## 2.3. Results

### 2.3.1. Bulk macroscopic material description

The chrysotile collected from the Havelock Asbestos Mine (Bulembu) in Swaziland (Eswatini) has a homogeneously distributed fibre content within the rock (figure 2.2A). These chrysotile fibres occur in veins in the serpentinite rock deposits (figure 2.2B). The fibres within the veins display a combination of straight, curved, and contorted behaviour. A partitioning parallel to the vein walls split the cross-fibre vein and subsequently shortened the fibre length in relation to the vein width (figure 2.2D). Such partitioning affects the degree of fibre to sidewall cohesion enabling the fibres to be separated easily and dispersed from the host rock. The highly fibrous components occupy ~80

Vol% of the rock sample and are easily separable. The bundles of chrysotile fibres are pale green in colour, but separats to form a fluffy mass of white fibres (figure 2.2C).

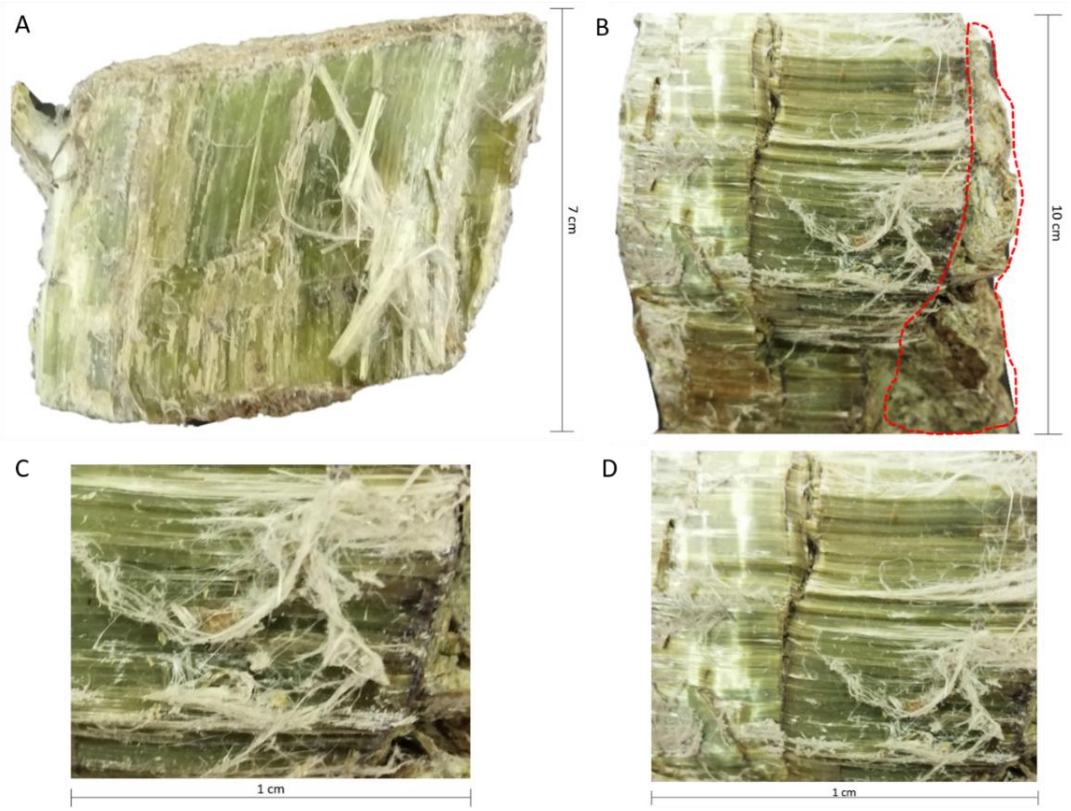


Figure 2.2: Macroscopic illustrations: (A) Chrysotile rock sample; (B) length of fibres spanning the width of the veins; (C) individual masses of matted white, silky fibres and (D) a parting at the centre of the vein width halving the length of the cross-vein fibres.

The individual fibres are extremely fine, flexible and have a curved and wavy appearance. When observed individually, the chrysotile fibres are white in colour and have a silky lustre. The crystals comprising the fibres are short (~2.5 cm) and extremely hair-like. The mineral fibres retained their fibrous form and aspect ratio upon crushing with a mortar and pestle. The fibres can be bent and twisted without breaking indicating that the chrysotile fibres have high tensile strength. Picrolite is a vein-like serpentine mineral commonly mistaken for chrysotile (Riordon, 1955).

The amosite in this sample consists of long (~20 cm), thin, straight, brown-coloured fibres that form in bundles and have a 'paintbrush-end' effect (figure 2.3A). The amosite fibres in this sample are very brittle and 'shatter' easily when brushed with the dissecting forceps. The bundle of

amosite fibres displays a slight curvature, which exists because of their long length. The surface of the amosite fibre bundle shows individual matted and splintery fibres (figure 2.3B).

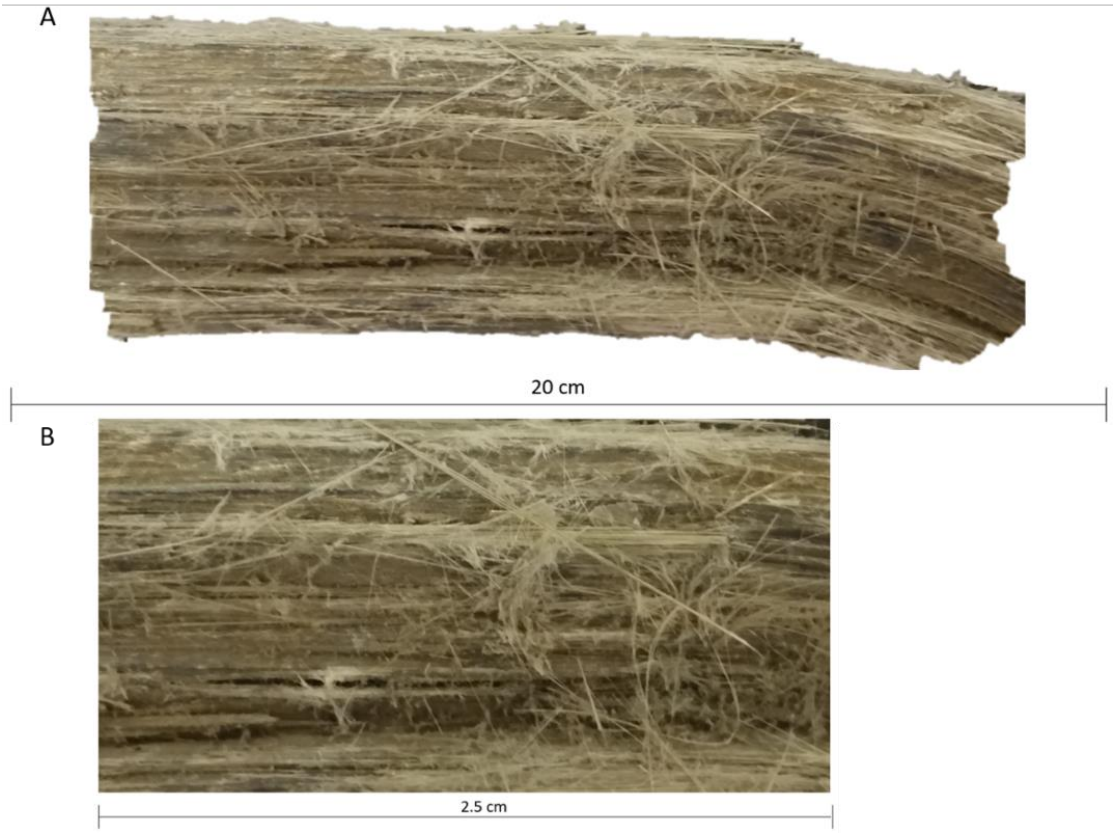


Figure 2.3: Macroscopic illustrations: (A) Amosite rock sample and (B) matted and splintery fibres

The crocidolite in this sample consists of long (~10 cm), straight, greyish to pale blue coloured fibres occurring in a bundle (figure 2.4A). The poly-filamentous bundle is macroscopically curved and contorted (figure 2.4B) indicating flexibility. The fibres are brittle and have a silky lustre. The bundle of fibres is easily parted, has a fine, longitudinal structure, and is tufted at the ends. These fibres show partial flexibility when bent.

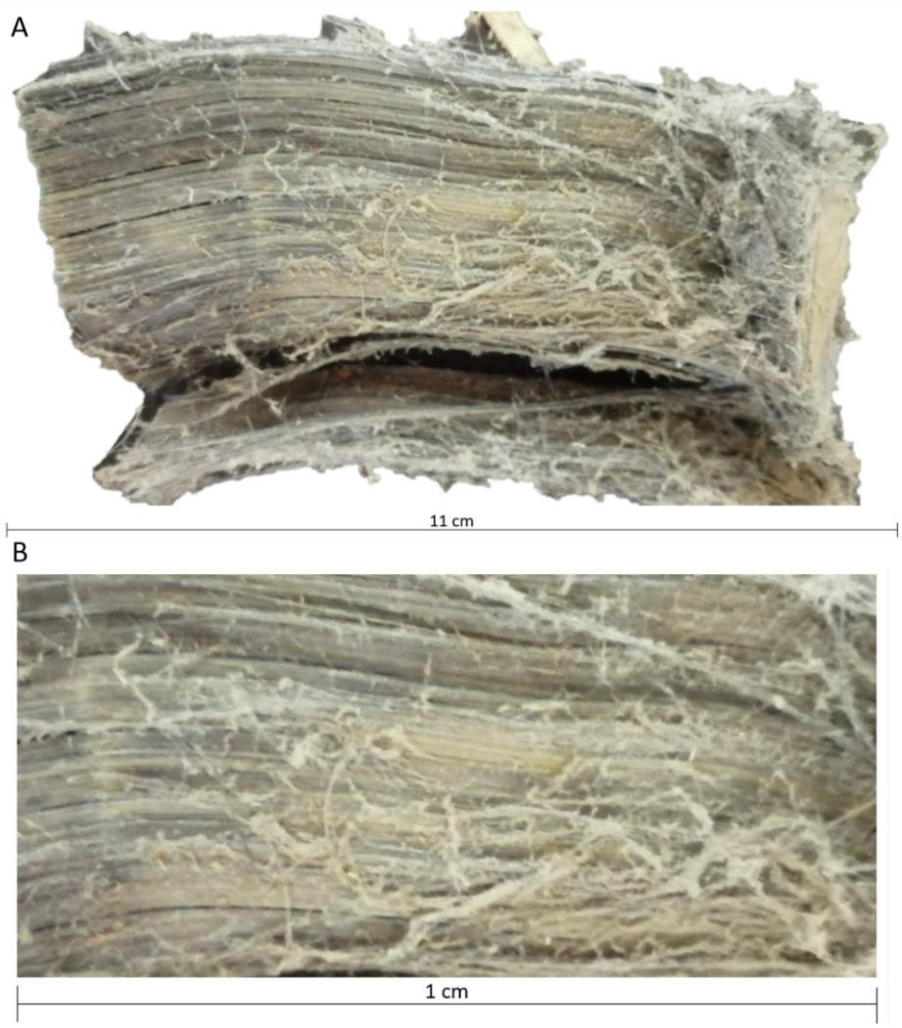


Figure 2.4: Macroscopic illustrations: (A) Crocidolite rock sample and (B) showing slight curvature of poly-filamentous bundles

The elongated shape of the minerals visibly observed in hand sample allowed direct length measurements to be taken (table 2.2).

Table 2.2: Fibre lengths for 21 counts for each mineral in hand sample

| | Chrysotile | | Amosite | | Crocidolite | |
|---|---|---|---|---|---|---|
| | | | | | | |
| Counts | Length (cm) | Width (µm) | Length (cm) | Width (µm) | Length (cm) | Width (µm) |
| 1 | 2.5 | 12.5 | 20 | 28.5 | 6 | 6.25 |
| 2 | 0.5 | 12 | 5 | 26.5 | 10 | 6.2 |
| 3 | 1.2 | 12.2 | 15 | 28 | 11 | 6.3 |
| 4 | 1.8 | 12.2 | 10 | 23.8 | 8 | 6 |
| 5 | 2.2 | 12.6 | 9 | 25.5 | 8 | 6 |
| 6 | 0.9 | 12.1 | 13 | 28 | 6 | 6 |
| 7 | 1.36 | 12.3 | 19 | 25 | 10 | 6.2 |
| 8 | 2.4 | 12.3 | 7 | 26.5 | 10 | 6.2 |
| 9 | 2.5 | 12.4 | 18 | 28 | 9 | 6.2 |
| 10 | 1.9 | 12.5 | 18 | 22.3 | 6 | 6.2 |
| 11 | 1.7 | 12 | 16 | 20.5 | 6 | 6.3 |
| 12 | 2.1 | 12.1 | 15 | 28.1 | 8 | 6 |
| 13 | 0.8 | 12.4 | 13 | 28.2 | 9 | 6.1 |
| 14 | 2 | 12.6 | 8 | 28 | 10 | 6 |
| 15 | 2 | 12.4 | 15 | 20.2 | 10 | 6.2 |
| 16 | 1.1 | 12.3 | 5 | 17 | 10 | 6.2 |
| 17 | 0.6 | 12.2 | 8 | 20 | 6 | 6.2 |
| 18 | 2.5 | 12.2 | 11 | 18.9 | 8 | 6.3 |
| 19 | 2.3 | 12.2 | 19 | 20 | 10 | 6.1 |
| 20 | 1.7 | 12.2 | 20 | 28.5 | 6 | 6.2 |
| 21 | 2 | 12.6 | 20 | 27.1 | 6 | 6.2 |
| Average | 1.72 | 12.3 | 13.52 | 24.7 | 8.24 | 6.16 |
| Minimum | 0.5 | 12 | 5 | 17 | 6 | 6 |
| Maximum | 2.5 | 12.6 | 20 | 28.57 | 11 | 6.3 |
| Variance | 0.40 | 0.30 | 25.11 | 13.87 | 3.13 | 0.01 |
| Standard dev. | 0.63 | 0.18 | 5.01 | 3.72 | 1.77 | 0.10 |

### 2.3.2. Polarising light microscopy (PLM)

The morphology of the chrysotile fibres is asbestiform containing kinks and larger bundles with splayed ends. In plane polarised light (PPL) the chrysotile fibres have low relief and show weak pleochroism with purple, light and dark brown and pale-yellow colours observed (figure 2.5). In cross-polarised light (XPL), the fibres give off pale interference colours including white, yellow, orange, red

and purple and show a parallel extinction angle (figure 2.6). The individual fibres are distinct in both PPL and XPL by various colours and birefringence. The cloudy yellow-orange character of certain bands in XPL emphasises the structure of these veins. The margins of the fibres are outlined with amorphous serpentine or material shown as irregular, slightly anisotropic, and potentially cryptocrystalline (figure 2.7 and 2.8). These margins suggest a type of colloidal replacement, where deposition of iron resulted in the cloudy nature of some of the fibre margins (Riordon, 1955).

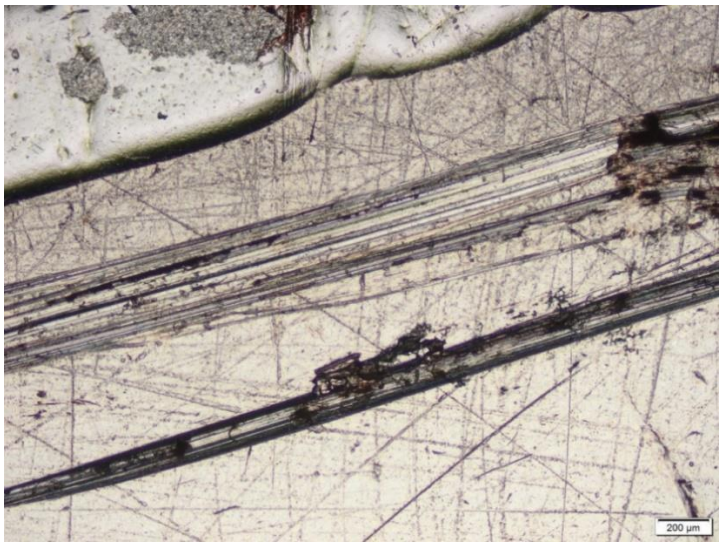


Figure 2.5: Chrysotile fibre bundle (PPL). Notice the break in the bundle in the top right.

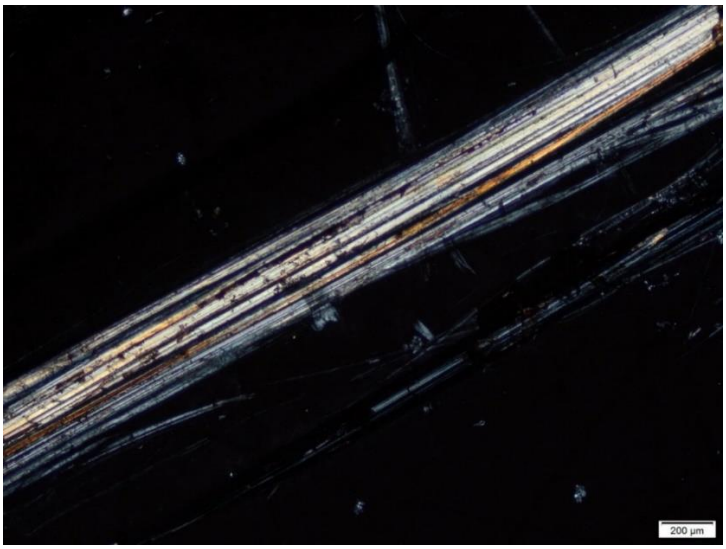


Figure 2.6: Chrysotile fibre bundle (XPL)

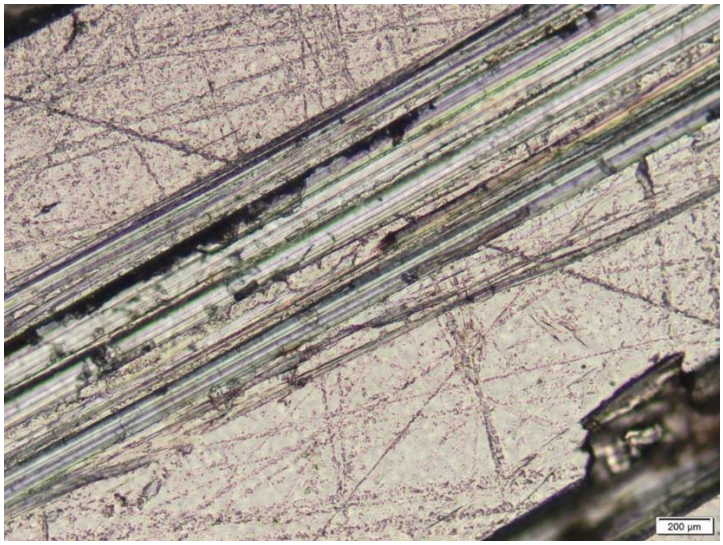


Figure 2.7: Partially altered chrysotile fibres shown by amorphous, irregular material and cloudiness (PPL).

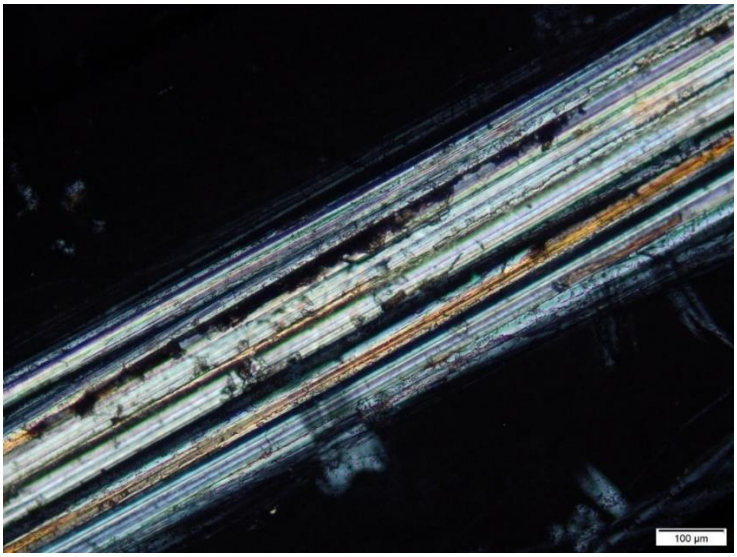


Figure 2.8: Partially altered chrysotile fibres shown by amorphous, irregular material and cloudiness (XPL).

The morphology of the amosite fibres is asbestiform with straight fibres and fibre bundles. The ends of the fibre bundles show a broom-like or splayed appearance. Under plane polarised light (PPL) the amosite has a weak to medium relief and weak to moderate pleochroism displaying brown, purple, pale green, and pale-yellow colours. In cross polarised light (XPL), pink, blue, purple, yellow, orange, and white interference colours are observed along with a parallel extinction angle. Extremely fine amosite fibres show parallel alignment and matting (figure 2.9 and 2.10). The maximum angle of pleochroism and birefringence is observed at 45° (figure 2.11 and 2.12).

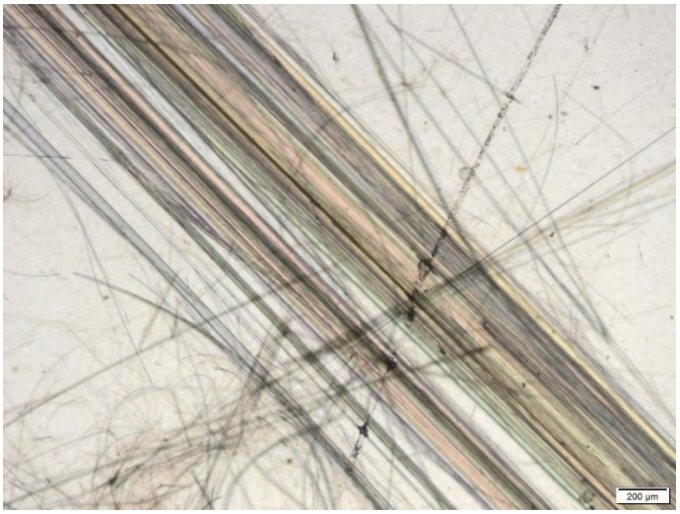


Figure 2.9: Extremely fine amosite fibres showing parallel alignment and matting (PPL).

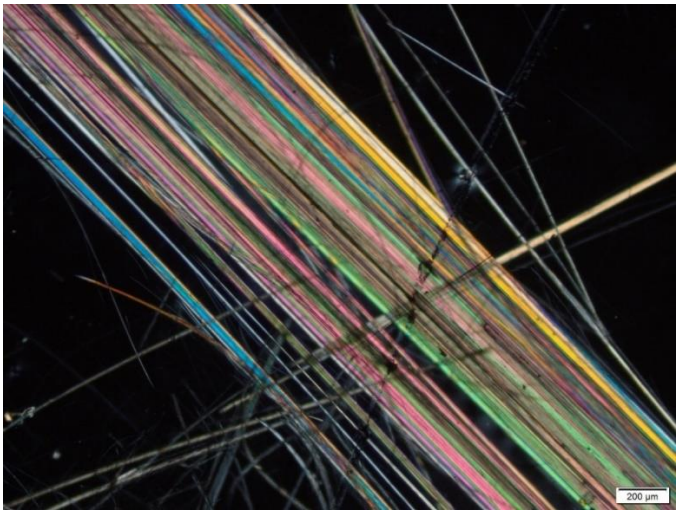


Figure 2.10: Extremely fine amosite fibres showing parallel alignment and matting (XPL).

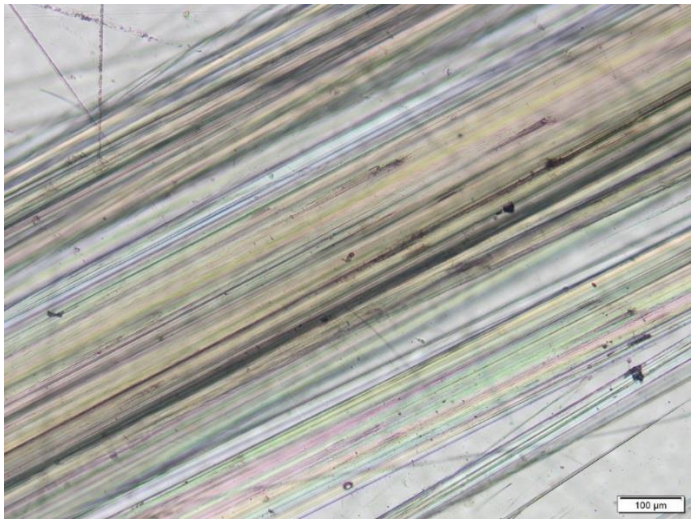


Figure 2.11: Amosite fibres at maximum angle of pleochroism showing heterogeneous colours (PPL).




Figure 2.12: Amosite fibres at maximum angle of birefringence showing heterogeneous interference colours (XPL).

The morphology of the crocidolite fibres is asbestiform with straight fibres and fibre bundles. In plane polarised light (PPL) the crocidolite fibres have moderate relief and are weakly pleochroic with blue, black, and pale-yellow colours displayed (figure 2.13). Under cross polarised light (XPL), blue and pale-yellow interference colours and a parallel extinction angle are observed (figure 2.14). The fibre bundles have clearly observed splayed ends (figure 2.15 and 2.16). Crocidolite shows the least number of interference colours amongst all four of the various asbestos mineral fibres studied.

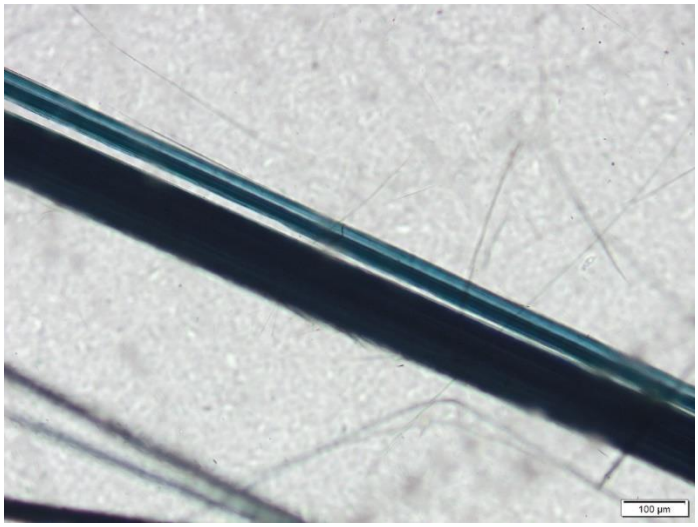


Figure 2.13: Poly-filamentous crocidolite (PPL)

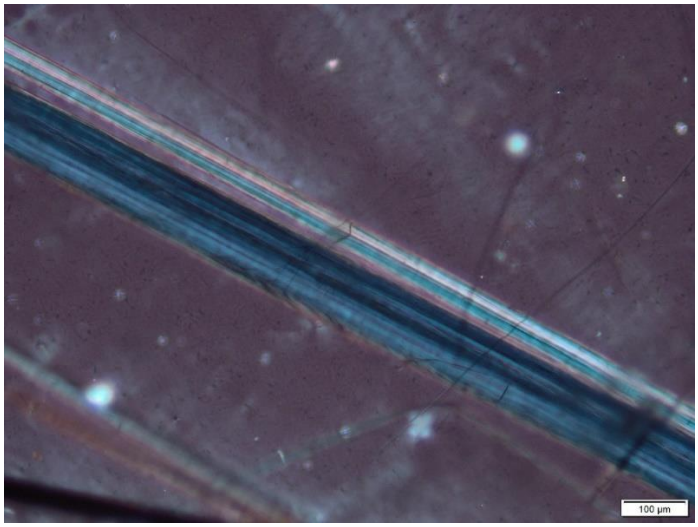


Figure 2.14: Poly-filamentous crocidolite (XPL)

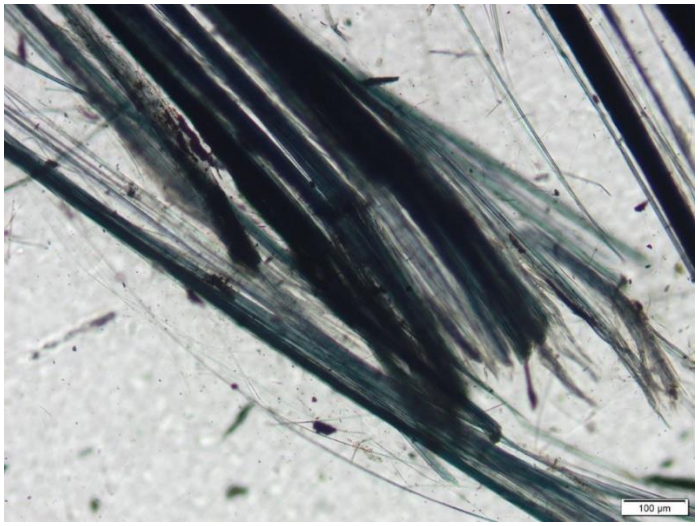


Figure 2.15: Crocidolite fibres with splayed ends (PPL)

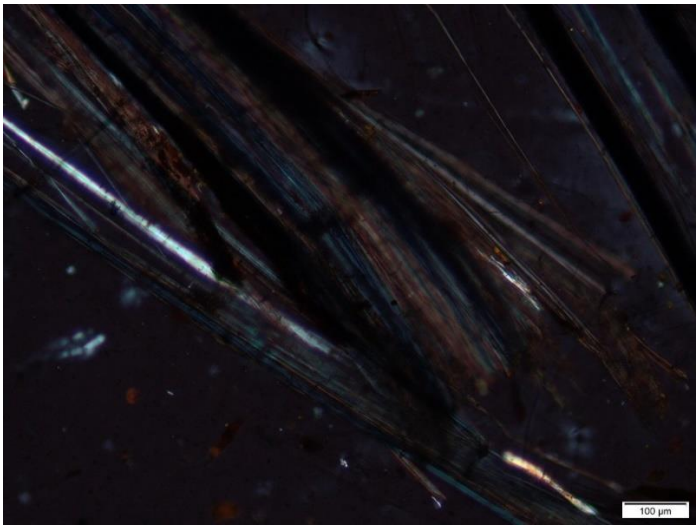


Figure 2.16: Crocidolite fibres with splayed ends (XPL)

### 2.3.3. X-ray diffraction (XRD)

Analysis by XRD allows the identification of co-occurring fine-grained minerals that are difficult to detect and distinguish in hand samples and using optical microscopy. Although the fibres were individually extracted and clearly identifiable impurities removed, some mineralogical heterogeneity is unavoidable and thus XRD was employed to determine the bulk mineralogical compositions of the asbestos samples and the recognition and identification of any impurities in each sample. The XRD ($\lambda$ (Co$K\alpha$) = 1.78892) of the samples are shown in graphs 2.1, 2.2 and 2.3 with the corresponding numerical 2$\Theta$ position and intensity data given in table 2.3.

Table 2.3: The values of 2 and intensity (I) recorded for each the peaks of each phase from the X-Ray diffraction record (λ (Co*K*α) = 1.78892)

| Peak # | Chrysotile rock sample | | Amosite rock sample | | | | | | Crocidolite rock sample | |
|---|---|---|---|---|---|---|---|---|---|---|
| | | | Amosite (grunerite) | | Quartz low | | Sepiolite | | | |
| | Intensity (counts) | Position [°2Θ] (Cobalt (Co)) | Intensity (counts) | Position [°2Θ] (Cobalt (Co)) | Intensity (counts) | Position [°2Θ] (Cobalt (Co)) | Intensity (counts) | Position [°2Θ] (Cobalt (Co)) | Intensity (counts) | Position [°2Θ] (Cobalt (Co)) |
| 1 | **15000** | 14 | 4500 | 11 | **4500** | 31 | 2000 | 4.5 | 3000 | 11.5 |
| 2 | 3000 | 22.5 | **9500** | 12 | 2200 | 59 | **3150** | 6.5 | **20000** | 12.5 |
| 3 | 6500 | 23.5 | 4000 | 30 | | | | | 1000 | 20 |
| 4 | 4000 | 26.5 | 4500 | 31.5 | | | | | 3000 | 21 |
| 5 | 8000 | 28.5 | 6100 | 33.8 | | | | | 1500 | 27 |
| 6 | 2900 | 31 | 2000 | 35 | | | | | 1800 | 28.5 |
| 7 | 2000 | 36 | 7100 | 38 | | | | | 6000 | 30.5 |
| 8 | 1200 | 39 | 5200 | 41.5 | | | | | 2500 | 32 |
| 9 | 3000 | 40 | 3100 | 45.5 | | | | | 12000 | 33.5 |
| 10 | 3100 | 42 | 4000 | 48 | | | | | 9500 | 38.5 |

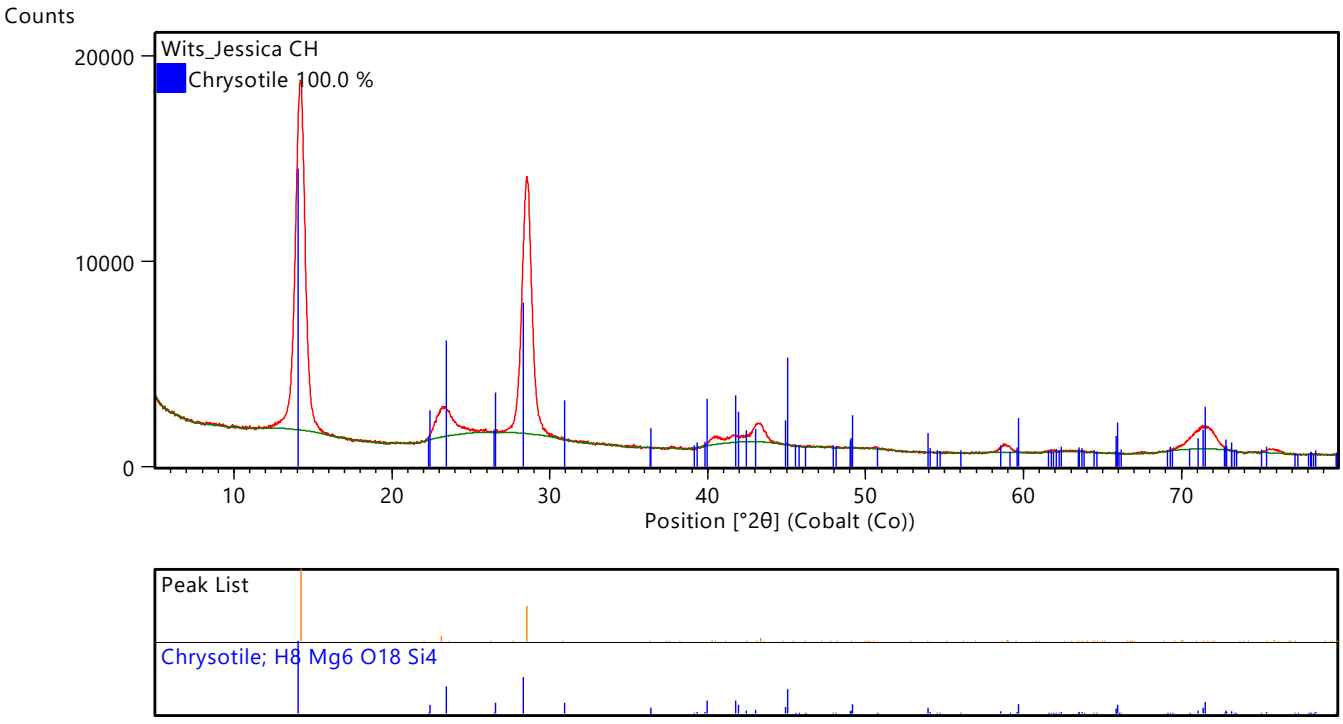


Graph 2.1: Chrysotile asbestos XRD diffractogram and Rietveld refinement phases

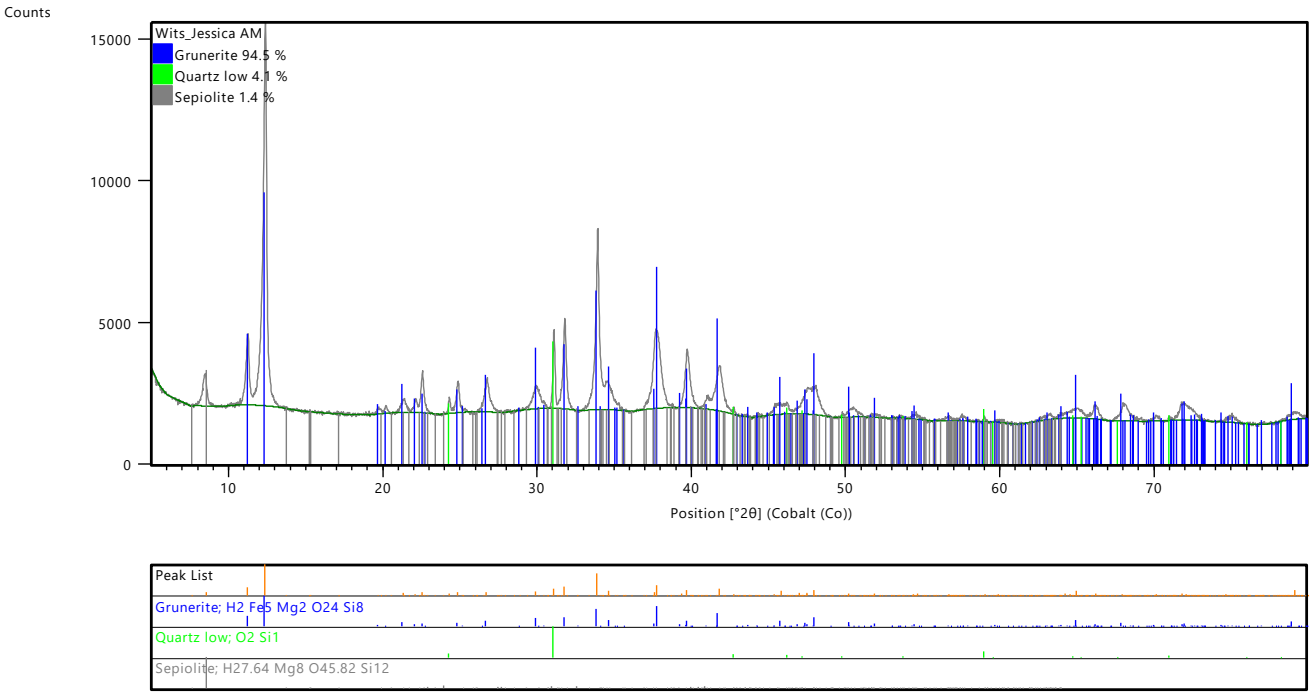


Graph 2.2: Amosite asbestos XRD diffractogram and Rietveld refinement phases

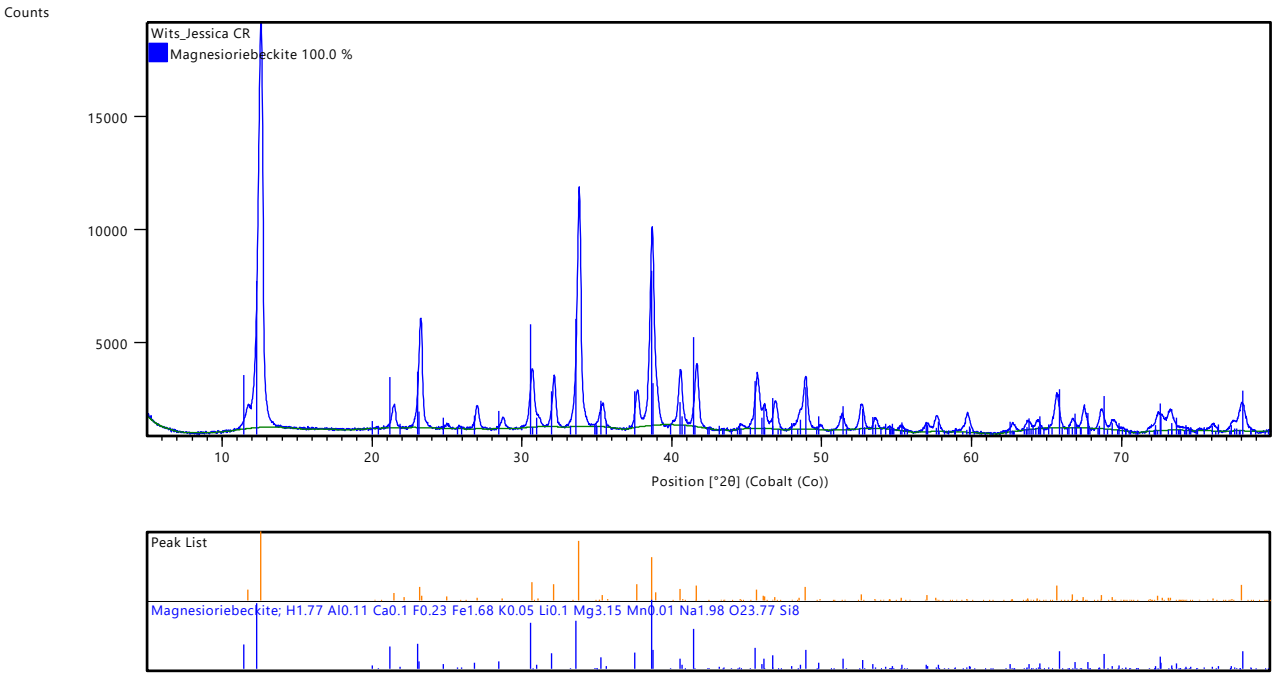


Graph 2.3: Crocidolite asbestos XRD diffractogram and Rietveld refinement phases

The relative intensity and *d*-spacing for each sample was calculated and given in table 2.4. The relative intensity and *d*-spacing calculated for the chrysotile, amosite (grunerite) and crocidolite (magnesio-riebeckite) phases (table 2.4) correspond to those of the known principle lattice spacings for each of the asbestiform minerals (Karunaratne and Fernando, 2015). The Rietveld refinement data is shown in table 2.5.

Table 2.4: Reduction of data from X-Ray Diffractogram (λ (Co*K*α) = 1.78892). The value of $I/I_1$ (relative intensity %) is determined from equation 1 where $I_1$ is intensity of the highest peak of the phase and *d* (Å) is calculated from equation 2 assuming *n* = 1.

| Peak # | Chrysotile rock sample | | Amosite rock sample | | | | | | Crocidolite rock sample | |
|---|---|---|---|---|---|---|---|---|---|---|
| | | | Amosite (grunerite) | | Quartz low | | Sepiolite | | | |
| | $I/I_1$ | *d* (Å) | $I/I_1$ | *d* (Å) | $I/I_1$ | *d* (Å) | $I/I_1$ | *d* (Å) | $I/I_1$ | *d* (Å) |
| 1 | 100 | 7.34 | 47.4 | 9.3 | 100 | 3.35 | 63.5 | 22.8 | 15 | 8.9 |
| 2 | 20 | 4.6 | 100 | 8.6 | 48.9 | 1.8 | 100 | 15.3 | 100 | 8.3 |
| 3 | 43.33 | 4.4 | 42.1 | 3.5 | | | | | 5 | 5.15 |
| 4 | 26.7 | 3.9 | 47.4 | 3.3 | | | | | 15 | 5.15 |
| 5 | 53.3 | 3.6 | 64.2 | 3.1 | | | | | 7.5 | 3.8 |
| 6 | 19.3 | 3.35 | 21.1 | 2.97 | | | | | 9 | 3.6 |
| 7 | 13.3 | 2.9 | 74.7 | 2.7 | | | | | 30 | 3.4 |
| 8 | 8 | 2.7 | 54.7 | 2.5 | | | | | 12.5 | 3.25 |
| 9 | 20 | 2.6 | 32.6 | 2.3 | | | | | 60 | 3.1 |
| 10 | 20.7 | 2.5 | 42.1 | 2.2 | | | | | 47.5 | 2.7 |

Table 2.5: Abundance (%) of mineral phases detected by XRD analysis

| **Asbestos Rock Sample** | **Phases detected (% composition)** |
|---|---|
| | |
| Chrysotile | Chrysotile (100 %) |
| Amosite | Amosite (94.5 %) >> Quarts low (4.1 %) > Sepiolite (1.4 %) |
| Crocidolite | Magnesio-riebeckite (100 %) |
| % Abundance represents the modal amounts of minerals (quantitative analysis) present in asbestos rock samples | |

Chrysotile and crocidolite were shown to be the only mineral phases indicating the purity of the fibres in each sample. In contrast, the amosite sample contained two other mineral phase impurities being quartz and sepiolite.

### 2.3.4. X-ray fluorescence (XRF) major and trace elemental analysis

X-Ray fluorescence spectroscopy (XRF) was used to quantify the major and trace elements in asbestos-containing mine waste rocks. The major and trace concentrations were investigated to define the amount of harmful elements that can potentially be released into both the environment and human body. The average major and trace elemental concentrations (n = 2) of each asbestos rock waste is presented in table 2.6 and 2.7.

Table 2.6: Major element analysis (n=2)

| **Oxides (wt%)** | **Chrysotile** | **Amosite** | **Crocidolite** |
|---|---|---|---|
| | | | |
| $SiO_2$ | 42.08 | 48.93 | 51.52 |
| $Al_2O_3$ | 0.59 | 0.36 | 0.07 |
| $Fe_2O_3$ | 2.00 | 41.37 | 38.31 |
| MnO | 0.03 | 0.64 | 0.06 |
| MgO | 40.83 | 5.84 | 2.23 |
| CaO | 0.06 | 2.02 | 0.35 |
| $Na_2O$ | 0.07 | 0.00 | 6.22 |
| $K_2O$ | 0.01 | 0.24 | 0.10 |
| $TiO_2$ | 0.03 | 0.03 | 0.03 |
| $P_2O_5$ | 0.01 | 0.02 | 0.01 |
| $Cr_2O_3$ | 0.01 | 0.02 | 0.01 |
| NiO | 0.19 | 0.01 | 0.01 |
| LOI | 12.18 | 0.48 | 1.24 |
| Total | 100.08 | 99.87 | 100.15 |

Table 2.7: Trace element analysis (n=2)

| Element (ppm) | Chrysotile | Amosite | Crocidolite |
|---|---|---|---|
| | | | |
| Sc | 6.4 | 4.64 | D.L. |
| V | 16.42 | 3.51 | 3.91 |
| Cr | 83.4 | 4.61 | D.L. |
| Co | 52.55 | D.L. | D.L. |
| Ni | 1518.54 | 51.24 | 11.86 |
| Cu | 21.99 | 36.77 | 35 |
| Zn | 16.19 | 41.62 | 12.66 |
| Ga | D.l. | D.L. | 1.63 |
| Rb | D.L. | 20.77 | 1.02 |
| Sr | 0.74 | 26.63 | 0.86 |
| Y | 0.77 | 3.78 | 1.82 |
| Zr | 0.49 | 3.7 | 0.38 |
| Nb | D.L. | 0.85 | D.L. |
| Mo | D.L. | 0.62 | D.L. |
| Ba | D.L. | 28.17 | 1.69 |
| Pb | 6.62 | 5.32 | 5.06 |
| Th | D.L. | D.L. | D.L. |
| U | D.L. | D.L. | D.L. |
| D.L. – detection limit | | | |

The samples display the following distinctive major element in geochemistry: Chrysotile samples contain the most aluminium and magnesium; amosite samples display the highest concentrations of iron and calcium; and crocidolite samples contain the greatest sodium.

### 2.3.5. BET-$N_2$ specific surface area

The specific surface area (SSA), determined by $N_2$ BET procedure, of fibrous minerals is defined as the surface area per unit volume. 'Specific' or 'reactive' are two ways in which the surface area may be defined (Fischer *et al.,* 2014). Gas absorption and the Brunauer-Emmett-Teller (BET) equation is used to determine the specific surface area, whereby the total surface area is divided by

the mass of the sample (Brunauer *et al.,* 1938). The BET $N_2$ specific surface areas and associated parameters of the extracted fibres are given in table 2.8.

Table 2.8: BET surface area report

| | Rock Sample | | |
|---|---|---|---|
| | | | |
| BET Surface Area Report | Chrysotile | Amosite | Crocidolite |
| BET SSA ($m^2/g$) | 29.6746 $\pm$ 0.1572 | 10.2856 $\pm$ 0.0535 | 18.9009 $\pm$ 0.1048 |
| Slope ($g/cm^3$ STP) | 0.145628 $\pm$ 0.000768 | 0.421158 $\pm$ 0.002177 | 0.229281 $\pm$ 0.001263 |
| Y-intercept ($g/cm^3$ STP) | 0.001070 $\pm$ 0.000116 | 0.002074 $\pm$ 0.000329 | 0.001035 $\pm$ 0.000191 |
| C | 137.071472 | 204.057744 | 222.422981 |
| Qm ($cm^3/g$ STP) | 6.8167 | 2.3628 | 4.3418 |
| Correlation coefficient | 0.9998330 | 0.9998398 | 0.9998180 |
| Molecular cross-sectional area ($nm^2$) | 0.1620 | 0.1620 | 0.1620 |

### 2.3.6. Bio-durability tests

The solid asbestos residue was separated from the solution via filtration at the end of each time interval during the bio-durability test and the mass measured (table 2.9).

Table 2.9: The measured mass (mg) of the solid asbestos sample residue after each time interval during dissolution in acidic solution

| **Time (hours)** | **Chrysotile** | **Amosite** | **Crocidolite** |
|---|---|---|---|
| | | | |
| 0 | 50 | 50 | 50 |
| 24 | 25.2 | 39.1 | 37.7 |
| 48 | 24 | 38.6 | 33.6 |
| 168 | 21 | 36.3 | 32.3 |
| 334 | 18.6 | 35.5 | 31.7 |
| 720 | 16.6 | 35.4 | 31.1 |
| Total mass loss (mg) | 33.4 | 14.6 | 18.9 |

The weight loss for all three types of asbestos reached a plateau after 186 hours indicating the completion of the chemical reaction. The mass loss of the experiments for each asbestos sample was summed up and 100% solid mass loss was never achieved. The reason is not incomplete dissolution, but rather the precipitation of silica back out of the solution (Gualtieri *et al.,* 2012). The dissolved mass fraction (DMF) calculated for the asbestos samples are given in table 2.10 and graphically represented in graph 2.4.

Table 2.10: The dissolved mass fraction (DMF) calculated for the asbestos samples

| **Time (hours)** | **Chrysotile** | **Amosite** | **Crocidolite** |
|---|---|---|---|
| | | | |
| 0 | 0 | 0 | 0 |
| 24 | 0.5 | 0.22 | 0.25 |
| 48 | 0.52 | 0.23 | 0.33 |
| 168 | 0.58 | 0.27 | 0.35 |
| 334 | 0.63 | 0.29 | 0.37 |
| 720 | 0.67 | 0.292 | 0.38 |

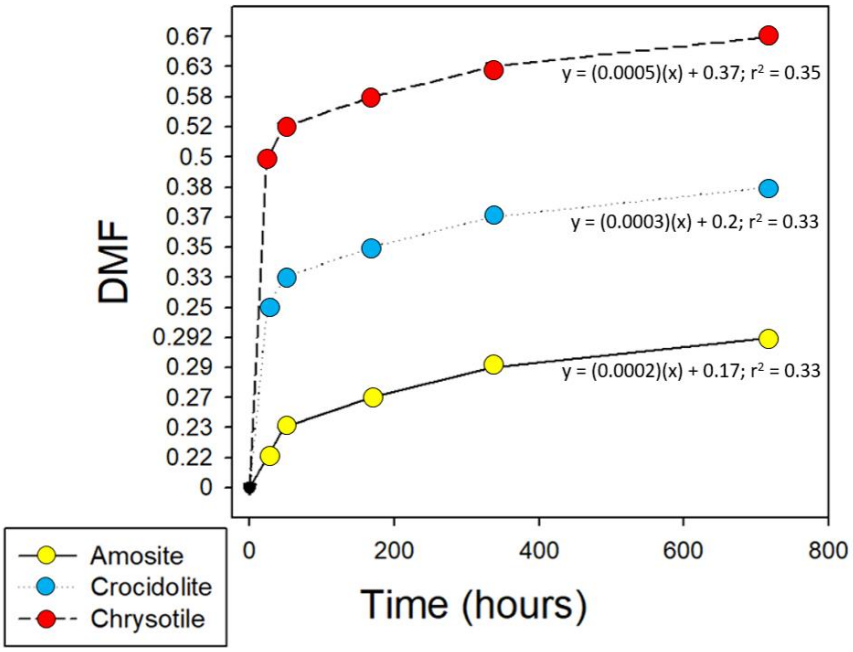


Graph 2.4: Dissolved mass fraction of the asbestos samples over time (hours)

The dissolution efficiency for chrysotile, amosite and crocidolite was calculated as 66.8 %, 29.2 % and 37.8 %, respectively.

## 2.3. Discussion

The airborne dispersion of asbestos fibres through human activities and rock weathering increases the potential for inhalation of fibres and is the basis of the risks to human health (Harper, 2008; Culley *et al.,* 2010; Bloise *et al.,* 2012; Bloise *et al.,* 2014; Punturo *et al.,* 2015). Mineralogical and geochemical characterisation of exposed asbestos-containing mine waste contributes to improved risk assessment with direct applications in predictive management. Mineral dust and fibres are heterogeneous substances with respiratory sensitising properties. The complex nature of and exposure to mineral fibres necessitates procedures that account for this complexity if the allocation and attenuation of the human health impacts is to be conducted reliably. Importantly, the selected methods are based on what is realistically practical for developing countries where funds and scientific engagement are limited.

In hand samples all three types of asbestos show asbestiform morphology, including fine thickness, parallel arrangement, separability, and flexibility. The fibres retain their aspect ratio forming numerous finer fibres during breakage caused by crushing. All samples showed moderate cohesion as fibres were released from bulk material when vigorously disturbed by hand. The three types of asbestos minerals sampled are cross-fibres in veins for chrysotile and seams for the amphiboles.

The fibre geometry (table 2.2), defined by its diameter (D) and length (L), is a key parameter in its pathogenicity, toxicity, and inflammation (Donaldson *et al.,* 2010; Gualtieri, 2018). Polarising light microscopy (PLM) is commonly used for semi-quantifying the percent of fibrous material and identifying the type of fibre (McCrone *et al.,* 1978; Middleton, 1979), but can also accurately be used to measure fibre dimensions > 1 µm in diameter (Vaughan *et al.,* 1981; Bernstein *et al.,* 2013). The dimensions provide information on the respirability and biological activity of airborne fibres (Walton, 1982). The ‘Stanton Hypothesis’ states that the optimum fibre morphology for generating intrapleural tumours is D ≤ 0.25 µm and L > 8 µm, which was derived from experimental observations succeeding fibre implantation and injection into animals (Stanton *et al.,* 1981). According to this model, ‘frustrated phagocytosis’ (Churg, 1993) results because phagocytic cells such as macrophages

are unable to eliminate 'Stanton fibres' i.e., needle-shaped particles with L > 8 µm (Stanton *et al.,* 1981).

Optical microscopy provides important knowledge on texture, mineralogy, and alteration. All samples consist of poly-filamentous fibre bundles with parallel-sided, long, thin fibres having straight extinction. Splayed ends and fibre curvature were characteristically demonstrated by the crocidolite samples. Under low magnification, amosite and crocidolite minerals do not appear compact having gaps and visible divisions between fibres, further pointing to their asbestiform nature. Unlike amosite and crocidolite, individual chrysotile fibres are not as clearly distinguishable under the polarising light microscope (PLM). Chrysotile appeared more compact however, upon closer inspection, divisions between fibres were also identified, but were less prominent than that of amosite and crocidolite. In PLM the chrysotile fibres appear to be more tightly welded together with little porosity between them.

Optically, the colours of the fibres are homogeneous or heterogeneous under PLM. Chemical heterogeneity suggested by colour variations in the fibre provides evidence of partial replacement of pre-existing fibres or generations of fibre growth. Homogenous colours were generally observed along the lengths of the amosite and crocidolite fibres (figures 2.9, 2.11, 2.13 and 2.15). Heterogeneous colours within individual fibres are only observed in chrysotile (figure 2.5 and 2.7) and implies compositional variability. This is further emphasised under cross-polarising light (figure 2.6 and 2.8). Both amphibole asbestos samples did not appear to show any modifications optically and texturally in PLM consistent with the homogeneous colouring. In comparison with the amphibole asbestos samples, the chrysotile asbestos samples exhibited a more complex microstructure matrix under PLM, in which several coexisting textures are apparent.

The asbestos-containing rock samples are natural samples collected from mines and thus the presence of mineral impurities is expected (Pollastri *et al.,* 2014; Pollastri *et al.,* 2015). Typically, natural asbestos-containing rock samples occur with other non-asbestiform morphologies and minerals (Vigliaturo *et al.,* 2018). Although these associated phases are thought to be harmless, little information on their potential toxic effects exists (Vigliaturo *et al.,* 2018). Thus, the characterisation of natural assemblages should include all phases occurring with the suspected asbestos fibres (Vigliaturo *et al.,* 2018). The results by XRD analysis allow the identification of co-occurring fine-grained minerals that are difficult to detect optically. Chrysotile (serpentine) and crocidolite (amphibole) samples are homogeneous, containing no additional mineral phases. Amosite displays

mineral phase heterogeneity and crystalline impurities of ~4.1 % quartz ($SiO_2$) and ~1.4 % sepiolite ($Mg_4Si_6O_{15}.6H_2O$). Fibrous and crystalline quartz ($SiO_2$) is known as a prolific cytotoxic particle that results in lung tumours upon inhalation (Oberdörster, 2002). The phyllosilicate mineral sepiolite ($Mg_4Si_6O_{15}.6H_2O$) belongs to the mineral group hormite and is characterised by a fibrous habit (Singer *et al.,* 1992). Given limited studies and inadequate evidence for the carcinogenic effects of sepiolite in humans, few animal studies have led the IARC to include sepiolite in the Group 3 carcinogen category (Turci *et al.,* 2017).

Based on the XRD data and published literature, there seems to be very limited research and knowledge regarding the carcinogenic and pathogenic effects of asbestos-associated mineral phases following chronic inhalation. However, asbestos-associated mineral phases should not be neglected when considering the combined factors encompassing the toxicity of asbestos-containing mine-wastes.

Of importance is the ability to quantify the amount of potentially harmful elements that can be released both into the environment and the human body. The high concentrations of Al, Mg, Mn and Fe are not unexpected as they are major rock-forming elements and are among the primary constituents in sediments and soils (Iqbal and Shah, 2014). One of the most important factors for fibre-induced patho-biological activity is the total iron content of the asbestos minerals (Gualtieri, 2018; Gualtieri *et al.,* 2019a). Siderosis is caused by the inhalation of iron-bearing compounds (Nemery, 1990). As iron acts as a catalyst for reactions involving the release of reactive oxygen species and lipid, protein, and DNA damage, it is a significant property in determining asbestos toxicity (Fubini and Mollo, 1995). Iron becomes available at the reacting surface of fibres during dissolution where, through a Haber-Weiss chain reaction sequence, it promotes hydroxyl radical formation that damages DNA (Gazzano *et al.,* 2005; 2007).

In addition to iron, other major chemical elements have been reported to participate in asbestos toxicity following inhalation (Shimizu *et al.,* 2008; Nakamura *et al.,* 2009). Silicon (Si) results in numerous pathologies such as silicosis when inhaled (Hamilton *et al.,* 2008). Asbestos minerals are silicates and therefore their silicon composition is also a factor relating to their toxicity potential. Being the 3$^{rd}$ most abundant element in the Earth's crusts, the environmental toxicology of aluminium has been revealed in recent investigations to cause numerous diseases and thus presenst a major threat to plants, animals, and humans (Barabasz *et al.,* 2002; Gupta *et al.,* 2013). The bulk chemical analysis of the chrysotile sample indicates only a slight deviation from the ideal composition

of serpentine, containing very little Fe and Al. Substitution in chrysotile may occur in both the octahedral (O) and tetrahedral (T) sheets making up this layer of silicate (Deer *et al.,* 2009). In the 1:1 T and O sheet ratio, both $Si^{4+}$ and $Mg^{2+}$ can be replaced by $Al^{3+}$, respectively, with an average $Al_2O_3$ content of <0.9 wt.% while the FeO content may be as much as 6 wt.% (Wicks and Plant, 1979). $Mg^{2+}$ in the O sheet can also be replaced by $Fe^{2+}$ and $Fe^{3+}$, while $Si^{4+}$ replacement in the T sheet is infrequent and minor. In the octahedral sheet, both $Fe^{2+}$ and $Fe^{3+}$ can replace Mg and the eventual replacement of $Si^{4+}$ by $Fe^{3+}$ may occur, although $Al^{3+}$ is preferentially hosted in this position. The presence of both $Fe^{2+}$ and $Fe^{3+}$ exclusively in 6-fold co-ordination has been suggested by Pollastri *et al.* (2015).

The different samples show considerably variable Mn concentrations with the highest amount found in the amosite. These results concur with those reported in Oberti *et al.* (2007) who explained that Mg in all the M(1), M(2), M(3) and M(4) sites of magnesium-iron-manganese-lithium amphiboles may be substituted with Mn (Bloise *et al.,* 2016). Manganese is an essential trace element for biological organisms. However, in excess, manganese poisoning ensues typically in the brain and lungs (Hudnell, 1999). Thus, managing the environmental entrance and migration of manganese is a marked health risk to humans (Aschner and Aschner, 2005).

Trace elements within mineral fibres may, in addition to the major elements, take part in the fibre toxicity (Fukuda *et al.,* 2004; Bargagli *et al.,* 2008; Wei *et al.,* 2014; Bloise *et al.,* 2016b). The presence of trace metals in fibres and their effects on the carcinogenesis of asbestos has been documented by IARC (2012). In our study the highest content of Ni, Co, Cr and V was observed in chrysotile; amosite contained the greatest concentration of Zn, Rb, Sr, Zr, Nb and Ba; and crocidolite was the only sample in which Ga was measured. Overall, the amosite rock sample contained the greatest number of detected trace elements and crocidolite had the overall lowest concentration of trace elements. Mn and trace metals such as Ni, Cr, Ni and Cu, in chrysotile almost exclusively represent isomorphous substitution of Mg (Bloise *et al.,* 2009, 2010, 2014). Unlike in antigorite and lizardite minerals, trace metal substitution in chrysotile is typically more restricted (Wicks and O'Hanley, 1988). Interestingly, although characterised by different geological conditions of formation, the detection of copper, nickel, zinc, strontium, lead, yttrium, and zirconium was shared by the three asbestos rock samples. Lead was detected in all samples and is a considerably toxic metal (Jaishankar *et al.,* 2014) serving no biological functions (Flora *et al.,* 2012). Several effects arise from the contamination of soil with lead, including the reduction of soil fertility, microbial diversity, and nutrients (Alengebawy *et al.,* 2021). Nickel was detected in all samples with chrysotile exhibiting

an exceptionally high concentration (1519 ppm). A variety of adverse human health effects such as lung fibrosis, kidney diseases, contact dermatitis, cardiovascular diseases and cancer of the respiratory tract are forms of nickel allergy that can result from contact with nickel compounds (Oller *et al.,* 1997; McGregor e*t al.,* 2000; Seilkop and Oller, 2003). Bio-available $Ni^{2+}$ toxicity at the intracellular sites was postulated by Horie *et al.* (2009). In human CD4+T lymphocytes the greatest apoptosis, DNA damage and caspase-9 positive T cells were induced by $Ni^{2+}$ at a concentration of 0.05 mM (Caicedo *et al.,* 2007).

Chromium was found in the chrysotile (83 ppm) and amosite (4.6 ppm) samples and represents a source of concern. Chromium results in the formation of hydroxyl and superoxide radicles described by the Fenton reaction (Briffa *et al.,* 2020). Fenton reactions induced by $Cr^{3+}$ damage proteins (Scharf *et al.,* 2014). The direct binding of $Cr^{3+}$ to numerous non-metallo-proteins and metallo-proteins has been shown in Cr associated with patients losing their biological functions (Gualtieri *et al.,* 2019). Chromium is also known to cause several health problems, such as vomiting, kidney failure, mouth ulcers, lung cancer, stomach cancer, indigestion and acute tubular necrosis in humans following contact (O'Flaherty, 1996; Beaumont *et al.,* 2008; Shekhawat *et al.,* 2015).
Vanadium was measured in chrysotile (16 ppm), crocidolite (3.9 ppm) and amosite (3.5 ppm) samples. Any of the three oxidation states of vanadium can produce genotoxic effects (Gualtieri *et al.,* 2019b). However, double-strand breaks are induced by $V^{4+}$ causing lesions and creating aberrations in structural chromosomes (Rodríguez-Mercado *et al.,* 2011; Gualtieri *et al.,* 2019b). Asthma, anaemia, and rhinitis can be caused by excessive amounts of vanadium in the body and even increase the possibility of lung cancer and uremia (WHO, 1990; WHO, 2001; ATSDR, 2002; Crans *et al.,* 2004). The release of vanadium from asbestos fibres into solution does not represent a concern as it is very low (Gualtieri *et al.,* 2019b).

Molybdenum was measured in amosite (0.9 ppm). Biologically, molybdenum is an essential nutrient required by humans, however, inhalation and exposure to excess levels can decrease lung functioning and cause coughing and dyspnoea (Chan *et al.,* 1998; Ott *et al.,* 2004).

The substantial presence of potentially toxic trace elements at concentrations measured in the studied chrysotile and amphibole asbestos samples may be explained, primarily, because of isomorphic substitutions in particular crystallographic positions (Bloise *et al.,* 2009; Ballirano *et al.,* 2017). The variability of potentially toxic elements amongst the studied samples, on the other hand, is best explained by the shared chemical changeability exhibited by asbestos mineral particles (Andreozzi *et al.,* 2009) and the different petrological and geochemical processes occurring during

their formation (Bloise *et al.,* 2020). High levels of heavy metals in the wastes indicate the possibility of the release into the soil, water and atmospheric environments presenting an interminable environmental hazard (Lu *et al.,* 2015).

The heavy metals hosted in fibrous minerals accumulate in the lungs via dissolution following inhalation, altering the normal human lung baseline levels of these elements (Vanoeteren *et al.,* 1986). The surface area of asbestos has been proposed to play a role in fibre toxicity (Lippmann, 1988). The surface area is a factor influencing the rate of dissolution and therefore clearance from the lungs (Fischer *et al.,* 2014; Gualtieri, 2018). Lung cancer, bronchogenic carcinoma, mesothelioma, etc. are caused when enough of these heavy metals are accumulated and the human lung tissue is damaged by metal-induced disease (Dixon *et al.,* 1970; Vanoeteren *et al.,* 1986; Nemery, 1990; Wei *et al.,* 2014; Bloise *et al.,* 2016). The threshold values in the lungs are reported in table 2.11 and indicate that the Mg, Co and Ni concentrations measured in this study significantly exceed those of the threshold lung values making its inhalation extremely dangerous with respect to its metal content. In addition, the Mn and Mg concentrations in amosite are also above those of the lung threshold.

Table 2.11: Threshold values of heavy metal in the lungs (ppm)

| **Metals (ppm)** | **Chrysotile** | **Amosite** | **Crocidolite** | **Threshold values in lungs (ppm) [1]** |
|---|---|---|---|---|
| | | | | |
| Al | 11147.8 | 6802.1 | 1322.6 | 82300 |
| Fe | 13988 | 289340 | 267940 | 56300 |
| Mn | 230 | 4987 | 465 | 950 |
| Mg | 246200 | 35220 | 13449 | 23300 |
| Cr | 83.4 | 4.61 | D.L. | 102 |
| Co | 52.55 | D.L. | D.L. | 25 |
| Ni | 1518.54 | 51.24 | 11.86 | 84 |
| Cu | 21.99 | 36.77 | 35 | 60 |
| Zn | 16.19 | 41.62 | 12.66 | 70 |
| Zr | 0.49 | 3.7 | 0.38 | 165 |
| Ba | D.L. | 28.17 | 1.69 | 425 |
| Pb | 6.62 | 5.32 | 5.06 | 14 |
| | | | | |
| [1] Vanoeteren *et al.,* 1986; Toth *et al.,* 2016 | | | | |

When the mass loss of the bio-durability experiments for each asbestos sample are summed up, 100% solid weight loss is never achieved. The reason is not incomplete dissolution but rather the precipitation of silica back out of the solution (Gualtieri *et al.,* 2012). As demonstrated by the dissolution tests, chrysotile has the lowest bio-durability and amosite the highest. Based on the close link between bio-durability and bio-persistence, it is expected that amosite fibres will have a much longer retention time following inhalation when compared to both chrysotile and amosite.

## 2.4. Implications for the environment and rehabilitation

More recently, in addition to the already stated mineralogical and geochemical properties influencing the toxicity to asbestos exposure, trace element concentrations hosted in asbestos mineral fibres and their role in fibre toxicity have come under the spotlight (Bloise *et al.,* 2020). The obvious threat of exposure to asbestos is much publicised, therefore numerous rehabilitation strategies, focused solely on mitigating the dispersion of these mineral fibres, have been considered and implemented. However, another insidious problem relevant to such mining wastes is prevalent, although understandably overshadowed by the overwhelming problem that is asbestos, but still very significant. As well as their role in determining fibre toxicity, the vast concentrations of heavy metals hosted in asbestos minerals have a profound influence on the quality of the environment. Many potentially toxic elements have been found to be hosted in all forms of asbestos minerals (Scambelluri *et al.,* 1997; Tiepolo *et al.,* 2007; Kumar and Maiti, 2015). The fundamental factor surrounding these findings is that in the natural setting, leaching, and weathering of asbestos-bearing rocks results in reduced heavy metal concentrations within the mineral particles themselves and the subsequent increase in concentrations in the surrounding soil and water ecosystems (Holmes *et al.,* 1971; Kumar and Maiti, 2015). Compared to the maximum limits imposed by environmental governments and agencies, the concentrations of heavy metals in the proximity of asbestos-bearing geological sites are typically one order of magnitude greater (Tashakor *et al.,* 2014) as documented in the serpentine-derived soils of the Gimigliano – Mount Reventino Unit (GMRU) (Punturo *et al.,* 2018). In addition to soils, the interaction of water with asbestos-bearing rocks is also characterised by exceedingly high heavy metal concentrations due to the dissolution of these minerals (Apollaro *et al.,* 2018). The sheer magnitudes of their concentrations and the fact that these toxic elements can

be mobilised and dispersed into different terrestrial environments and subsequently absorbed by humans, makes their presence in asbestos-bearing mine waste a consequential public health and environmental threat.

Substantial volumes of crushed rock-based wastes were produced during the mining of asbestos mineral resources in Southern Africa. The accumulation of these historical asbestos-mining rock wastes results in large, unmanaged mine dumps characterised by poly-mineral and rock assemblages, unstable geochemistry, poor physical structure, poor hydrological properties, and chemical conditions that are potentially toxic (Mendez and Maier, 2008; Huang *et al.,* 2012; Kumaresan *et al.,* 2017). The 'rehabilitation industry' in South Africa commonly practises vegetation establishment primarily aimed to generate surface stability and, secondary to that, to re-establish and return the site to a functional and sustainable ecosystem (Schimmer, 2017). In large, governmental and environmental agencies involved in derelict asbestos-mine land management have adopted the soil remediation approach to evaluate the rehabilitation requirements (Schimmer, 2017). Asbestos mine dumps demonstrate huge variation in physical, geochemical, and mineralogical characteristics (Northwatch *et al.,* 2008). Given the site-specific nature of mine rock wastes, a thorough investigation and characterisation is the first critical step for the formulation of a rehabilitation plan (Pentreath, 1994). Individually and interactively, the physical, mineralogical, and geochemical properties result in impediments and challenges to natural vegetation establishment during rehabilitation and thereafter sustainability. The way asbestos mine dump rehabilitation is undertaken is based on the credence that ecological restoration and remediation on all derelict and post-mining terrains can be tackled and accomplished in short deadlines. This emphasises the little to no appreciation of the influence of the geological conditions of the substrates on the community assembly and plant growth (Lamb *et al.,* 2015; Cross *et al.,* 2019). To predict the potential challenges to rehabilitation, mineralogical and geochemical characterisation of asbestos mine waste should become a standard practice.

## 2.5. Conclusion

Mineralogical and geochemical characterisations of asbestos mineral fibres left at derelict asbestos mine sites are important for two major reasons: Firstly, to identify and assess their human

health hazard and define the toxicity degree; secondly, to define the degree of potential environmental contamination in soils and (sub)surface waters in areas where these minerals occur. The results given in the study indicate that chrysotile, although being the least bio-durable, contains heavy metal concentrations that exceed those of the normal threshold concentrations in lungs beyond which functional respiratory problems start to develop. Amosite is of particular concern due to its high bio-durability and metal content above values of the safe lung threshold. These high levels of heavy metals detected in both chrysotile and amosite are potentially harmful not only to human health, but also the environment in general as they could contaminate the surrounding soil and water, which form the basis of existence for rural communities in remote locations. To conclude, the cost-effective, reliable, and easily accessible analytical methods applied here substantiate that baseline values pertinent to the geological material require revision as very little data is currently reported in literature and other official reports concerning Southern African regulations and guidelines.

## 2.6. References


Abbott, P. (1983): A review of asbestos resources. Dissertation, M. Sc. (Mineral Exploration) Degree, Rhodes University, Grahamstown, South Africa.

Alengebawy, A., Abdelkhalek, S.T., Qureshi, S.R. and Wang, M.Q. (2021): Heavy Metals and Pesticides Toxicity in Agricultural Soil and Plants: Ecological Risks and Human Health Implications. *Toxics*, **9**, 42.

Andreozzi, G.B., Ballirano, P., Gianfagna, A., Mazziotti-Tagliani, S. and Pacella, A. (2009): Structural and spectroscopic characterization of a suite of fibrous amphiboles with high environmental and health relevance from Biancavilla (Sicily, Italy). *American Mineralogist*, **94** (10), 1333–1340.

Anhaeusser, C.R. (1976): The nature of chrysotile asbestos occurrences in southern Africa: a review. *Economic Geology*, **71**, 96-116.

Apollaro, C., Fuoco, I., Vespasiano, G., De Rosa, R., Cofone, F., Miriello, D. and Bloise, A. (2018): Geochemical and mineralogical characterization of tremolite asbestos contained in the Gimigliano-Monte Reventino Unit (Calabria, south Italy). *J. Mediterr. Earth Sci.*, **10**, 5–15.

Aschner, J. L. and Aschner, M. (2005): Nutritional aspects of manganese homeostasis. *Molecular Aspect of Medicine*, **26** (4–5), 353–362.

ATSDR (Agency for Toxic substances and Disease Registry) (2002): Draft toxicological profile for several trace elements. US Dept. Health Human Services, Agency for Toxic Substances and Disease Registry, Atlanta, GA, USA.

ATSDR. Agency for toxic substances and disease registry. Toxic substances portal. Atlanta: ATSDR; 2011–2018. https://www.atsdr.cdc.gov/substances/indexAZ.asp#A .

Aust, A.E., Cook, P.M. and Dodson, R.F. (2011): Morphological and chemical mechanisms of elongated mineral particle toxicities. *Journal of Toxicology and Environmental Health, Part B*, **14**, 40–75.

Ballirano, P., Bloise, A., Gualtieri, A.F., Lezzerini, M., Pacella, A., Perchiazzi, N., Dogan, M. and Dogan, A.U. (2017): The crystal structure of mineral fibres. In: A.F. Gualtieri, Ed., Mineral fibres: Crystal chemistry, chemical physical properties, biological interaction and toxicity Vol. 18, pp. 17–64. European Mineralogical Union and the Mineralogical Society of Great Britain & Ireland, UK.

Barabasz, W., Albinska, D., Jaskowska, M. and Lipiec, J. (2002): Ecotoxicology of Aluminium. *Polish Journal of Environmental Studies*, **11** (3), 199–203.

Bargagli, E., Monaci, F., Bianchi, N., Bucci, C. and Rottoli, P. (2008): Analysis of trace elements in bronchoalveolar lavage of patients with diffuse lung diseases. *Biological Trace Element Research,* **124**, 225-235.

Beaumont, J.J., Sedman, R.M., Reynolds, S.D., Sherman, C.D., Li, L.H., Howd, R.A., Sandy, M.S., Zeise, L. and Alexeeff, G.V. (2008): Cancer mortality in a Chinese population exposed to hexavalent chromium in drinking water. *Epidemiology*, **19**, 12- 23.

Bernstein, D., Dunnigan, J., Hesterberg, T., Brown, R., Velasco, J.A.L., Barrera, R., Hoskins, J. and Gibbs, A. (2013): Health risk of chrysotile revisited. *Crit. Rev. Toxicol*., **43** (2), 154–183.

Bernstein, D.M., Dunnigan, J., Hesterberg, T., Brown, R., Velasco, J.A.L., Berrera, R., Hoskins, J. and Gibbs, A. (2013): Response to Murray M. Finkelstein, letter to editor re Bernstein et al: Health risk of chrysotile revisited. *Crit. Rev. Toxicol*., **43** (2), 154–183.

Bloise, A., Barrese, E. and Apollaro, C. (2009): Hydrothermal alteration of Ti-doped forsterite to chrysotile and characterization of the resulting chrysotile fibres. *Neues Jahrbuch für Mineralogie Abhandlungen*, **185**, 297-304.

Bloise, A., Belluso, E., Barrese, E., Miriello, D. and Apollaro, C. (2009): Synthesis of Fe-doped chrysotile and characterization of the resulting chrysotile fibres. *Crystal Research and Technology*, **44**, 590-596.

Bloise, A., Belluso, E., Fornero, E., Rinaudo, C., Barrese, E. and Capella, S. (2010): Influence of synthesis conditions on growth of Ni-doped chrysotile. *Microporous and Mesoporous Materials,* **132**, 239-245.

Bloise, A., Belluso, E., Critelli, T., Catalano, M., Apollaro, C., Miriello, D. and Barrese, E. (2012): Amphibole asbestos and other fibrous minerals in the meta-basalt of the Gimigliano-Mount Reventino unit (Calabria, South-Italy). *Rendiconti della Società Geologica Italiana*, **21**, 847-848.

Bloise, A., Critelli, T., Catalano, M., Apollaro, C., Miriello, D., Croce, A., Barrese, E., Liberi, F., Piluso, E., Rinaudo, C. and Belluso, E. (2014): Asbestos and other fibrous minerals contained in the serpentinites of the Gimigliano-Mount Reventino Unit (Calabria, S-Italy). *Environmental Earth Sciences,* **71**, 3773-3786.

Bloise, A., Barca, D., Gualtieri, A.F., Pollastri, S. and Belluso, E. (2016): Trace elements in hazardous mineral fibres. *Environmental Pollution*, **216**, 314-323.

Bloise, A., Punturo, R., Catalano, M., Miriello, D. and Cirrincione, R. (2016): Naturally occurring asbestos (NOA) in rock and soil and relation with human activities: the monitoring example of selected sites in Calabria (southern Italy). *Italian Journal of Geosciences*, **135**, 268-279.

Bloise, A., Ricchiuti, C., Punturo, R. and Pereira, D. (2020): Potentially toxic elements (PTEs) associated with asbestos chrysotile, tremolite and actinolite in the Calabria region (Italy). *Chemical Geology*, **558**, 119896.

Briffa, J., Sinagra, E. and Blundell, R. (2020): Heavy metal pollution in the environment and their toxicological effects on humans. *Heliyon*, **6** (e04691), 1–26.

Brunauer, S., Emmett, P.H. and Teller, E. (1938): Adsorption of gases in multimolecular layers. *Journal of the American Chemical Society,* **60**, 309-319.

Caicedo, M., Jacobs, J.J., Reddy, A. and Hallab, N.J. (2007): Analysis of metal ion-induced DNA damage, apoptosis, and necrosis in human (Jurkat) T-cells demonstrates Ni2+ and V3+ are more toxic than other metals: Al3+, Be2+, Co2+, Cr3+, Cu2+, Fe3+, Mo5+, Nb5+, Zr2+. *Journal of Biomedical Materials Research Part A,* **84** (4), 905–913.

Cairncross, B. (2004): Field Guide to Rocks and Minerals of Southern Africa. Struik Nature, Cape Town, South Africa.

Chan, P.C., Herbert, R.A., Roycroft, J.H., Haseman, J.K., Grumbein, S.L., Miller, R.A. and Chouf, B.J. (1998): Lung Tumour Induction by Inhalation Exposure to Molybdenum Trioxide in Rats and Mice. *Toxicological Sciences*, **45**, 58–65.

Churg, A. (1993): Asbestos lung burden and disease patterns in man. In: Guthrie, G.D. and Mossman, B.T. (Eds), Health Effects of Mineral Dust. Review in Mineralogy and Geochemistry, 28, Mineralogical Society of America, Chantilly, Virginia, USA, pp. 409–426.

Cornelissen, H., Watson, I., Adam, E. and Malefetse, T. (2019): Challenges and strategies of abandoned mine rehabilitation in South Africa: The case of asbestos mine rehabilitation. Journal of *Geochemical Exploration*, **205**, 106354.

Culley, M.R., Zorland, J. and Freire, K. (2010): Community responses to naturally occurring asbestos: implications for public health practice. *Health education research*, **25**, 877-891.

Crans, D.C., Smee, J.J., Gaidamauskas, E. and Yang, L. (2004): The chemistry and biochemistry of vanadium and the biological activities exerted by vanadium compounds. *Chemical Reviews*, **104**, 849-902.

Cross, A.T., Stevens, J.C., Sadler, R., Moreira-Grez, B., Ivanov, D., Zhong, H., Dixon, K.W. and Lambers, H. (2019): Compromised root development constrains the establishment potential of native plants in unamended alkaline post-mining substrates. *Plant Soil*. https://doi.org/10.1007/s11104-018-3876-2.

Deer, W.A., Howie, R.A. and Zussman, J. (2009): Rock Forming Minerals. 3B. Layered Silicates Excluding Micas and Clay Minerals, second ed. The Geological Society, London.

Deng, Z.J., Liang, M.L., Tóth, I., Monteiro, M.J. and Michin, R.F. (2012): Molecular interaction of poly (acrylic acid) gold nanoparticles with human fibrinogen. *ACS Nano*, **6**, 8962–8969.

Di Giuseppe, D. (2020): Characterization of Fibrous Mordenite: A First Step for the Evaluation of Its Potential Toxicity. *Crystals*, **10** (769), 1–15.

Dixon, J.R., Lowe, D.B., Richards, D.E., Cralley, L.J. and Stokinger, H.E. (1970): The role of trace metals in chemical carcinogenesis: asbestos cancers. *Cancer Research,* **30**, 1068–1074.

Donaldson, K., Murphy, F.A., Duffin, R. and Poland, C.A. (2010): Asbestos, carbon nanotubes and the pleural mesothelium: a review of the hypothesis regarding the role of long fibre retention in the parietal pleura, inflammation, and mesothelioma. *Fibre Tox*., **7**, 5.

Dreyer, C.J.B. and Söhnge, A.P.G. (1992): The Crocidolite and Amosite Deposits of the Republic of South Africa and Bophuthatswana. Pretoria: Geological Survey of South Africa, Handbook, 12, 126 pp.

Fischer, C., Kurganskaya, I., Schäfer, T. and Lüttge, A. (2014): Variability of crystal surface reactivity: what do we know? *Applications in Geochemistry,* **43**, 132–157.

Flora, S.J.S., Mittal, M. and Mehta, A. (2008): Heavy metal induced oxidative stress & its possible reversal by chelation therapy. *Indian Journal of Medical Research*, **128**, 501–523.

Fubini, B. and Mollo, L. (1995): Role of iron in the reactivity of mineral fibres. *Toxicology Letters,* **82/83**, 951-960.

Fukuda, H., Ebara, M., Yamada, H., Arimoto, M., Okabe, S., Obu, M., Yoshikawa, M., Sugiura, N. and Saisho, H. (2004): Trace elements and cancer. *Japan Medical Association Journal*, **47**, 391-395.

Gazzano, E., Foresti, E., Lesci, I.G., Tomatis, M., Riganti, C., Fubini, B., Roveri, N. and Ghigo, D. (2005): Different cellular responses evoked by natural and stoichiometric synthetic chrysotile asbestos. *Toxicology and Applied Pharmocology*, **206**, 356–364.

Gazzano, E., Turci, F., Foresti, E., Putzu, M.G., Aldieri, E., Silvagno, F., Lesci, I.G., Tomatis, M., Riganti, C., Romano, C., Fubini, B., Roveri, N. and Ghigo, D. (2007): Iron loaded synthetic chrysotile: a new model solid for studying the role of iron in asbestos toxicity. *Chemical Research in Toxicology*, **20**, 380–387.

Genis, J.H. (1961): The genesis of the blue amphibole asbestos of the Union of South Africa. PhD thesis, University of Cape Town.

Gualtieri, A.F., Viani, A., Sgarbi, G. and Lusvardi, G. (2012): *In vitro* bio-durability of the product of thermal transformation of cement–asbestos. *Journal of Hazardous Materials*, **205–206**, 63–71.

Gualtieri, A.F., Pollastri, S., Gandolfi, N.B. and Gualtieri, M.L. (2018): *In vitro* acellular dissolution of mineral fibres: A comparative study. *Science Reports*, **8**, 7071.

Gualtieri, A.F. (2018): Towards a quantitative model to predict the toxicity/pathogenicity potential of mineral fibres. *Toxicology and Applied Pharmacology*, **361**, 89–98.

Gualtieri, A.F., Andreozzi, G.B., Tomatis, M. and Turci, F. (2019): Iron from a geochemical viewpoint. Understanding toxicity/pathogenicity mechanisms in iron-bearing minerals with a special attention to mineral fibres. *Free Radical Biology and Medicine*, **133**, 21–37.

Gualtieri, A.F., Lusvardi, G., Zoboli, A., Di Giuseppe, D. and Gualtieri, M.L. (2019): Bio-durability and release of metals during the dissolution of chrysotile, crocidolite and fibrous erionite. *Environmental Research*, **171**, 550–557.

Gupta N, Gaurav SS, Kumar A. (2013). Molecular Basis of Aluminium Toxicity in Plants: A Review. *American Journal of Plant Sciences,* **4**, 21–37.

Hamilton Jr., R.F., Thakur, S.A. and Holian, A. (2008): Silica binding and toxicity in alveolar macrophages. *Free Radical Biology and Medicine*, **44** (7), 1246–1258.

Harper, M. (2008): 10th Anniversary critical review: Naturally occurring asbestos. *Journal of Environmental Monitoring*, **10**, 1394-1408.

Harris, L.V. and Kahwa, I.A. (2003): Asbestos: old foe in 21st century developing countries. *Science of the Total Environment*, **307**, 1–9.

Hart, H.P. (1988): Asbestos in South Africa. *Journal – South African Institute of Mining and Metallurgy*, **88** (6), 185-198.

Huang, L., Baumgartl, T. and Mulligan, D. (2012): Is rhizosphere remediation sufficient for sustainable revegetation of mine tailings. *Annuals Botany*, 223–238.

Higueras, P., Oyarzun, R., Iraizoz, J.M., Lorenzo, S., Esbrí, J.M. and Martínez-Coronado, A. (2012): Low-cost geochemical surveys for environmental studies in developing countries: Testing a field portable XRF instrument under quasi-realistic conditions. *Journal of Geochemical Exploration*, **113**, 3 – 12.

Hodgson, A.A. (1977): Nature and paragenesis of asbestos minerals. *Philosophical Transactions Royal Society of London A,* **286**, 611–624.

Holmes, A., Morgan, A. and Sandalls, F.J. (1971): Determination of iron, chromium, cobalt, nickel, and scandium in asbestos by neutron activation analysis. *Am. Ind. Hyg. Assoc. J*., **32** (5), 281–286.

Howlling, G.E. (1937): Asbestos. London: Imperial Institute. Pp. 88.

Hudnell, H. K. (1999): Effects from environmental Mn exposures: A review of the evidence from non-occupational exposure studies. *Neurotoxicology*, **20** (2–3), 379–398.

Hunter, D.R., and Jones, D.H. (1969): Geological Map Series (1:25,000). Sheet 2, Piggs Peak: Swaziland Geol. Survey.

IARC, (2012): A Review of Human Carcinogens. Part C: Arsenic, Metals, Fibres, and Dusts. International Agency for Research on Cancer, Lyon, France.

Ilgren, E.B. (2008): The fibre length of Coalinga chrysotile: Enhanced clearance due to its short nature in aqueous solution with a brief critique on 'Short Fibre Toxicity'. *Indoor and Built Environment*, **17**, 5–26.

Iqbal, J. and Shah, M.H. (2014): Occurrence, risk assessment, and source apportionment of heavy metals in surface sediments from Kanpur Lake, Pakistan. *Journal of Analytical Science and Technology*, **5**, 28–32.

Jaishankar, M., Tseten, T., Anbalagan, N., Mathew, B.B. and Beeregowda, K.N. (2014): Toxicity, mechanism, and health effects of some heavy metals. *Interdisciplinary Toxicology*, **7** (2), 60–72.

Karunaratne, P.C.T. and Fernando, G.W.A.R. (2015): Characterisation and radiation impact of corrugated asbestos roofing sheets in Sri Lanka. *Journal of Geological Society of Sri Lanka*, **17**, 31-40.

Kumar, A. and Maiti, S.K. (2015): Assessment of potentially toxic heavy metal contamination in agricultural fields, sediment, and water from an abandoned chromite-asbestos mine waste of Roro hill, Chaibasa, India. *Environ. Earth Sci*., **74** (3), 2617–2633.

Kumaresan, D., Cross, A.T., Moreira-Grez, B., Kariman, K., Nevill, P., Stevens, J., Allcock, R.J.N., O'Donnell, A.G., Dixon, K.W. and Whiteley, A.S. (2017): Microbial functional capacity is preserved within engineered soil formulations used in mine site restoration. *Scientific reports*, **7** (564).

Lamb, D., Erskine, P.D. and Fletcher, A. (2015): Widening gap between expectations and practice in Australian mine site rehabilitation. *Ecological Management and Restoration*, **16**, 186–195.

Lippmann, M. (1988): Asbestos Exposure Indices. *Environmental Research*, **48** (1), 86 – 106.

Lu, S., Wang, Y., Teng, Y. and Yu, X. (2015): Heavy metal pollution and ecological risk assessment of the paddy soils near a zinc-lead mining area in Hunan. *Environ Monit Assess*, **187**, 627.

Mathew, B.B., Tiwari, A. and Jatawa, S.K. (2011): Free radicals and antioxidants: A review. *Journal of Pharmacy Research,* **4** (12), 4340–4343.

McCrone, W., McCrone, L. and Delly, J. (1978): Polarized light microscopy. Ann Arbor, MI: Ann Arbor Science Publishers, Inc.

McGregor, D.B., Baan, R.A., Partensky, C., Rice, J.M. and Wilbourn, J.D. (2000): Evaluation of the carcinogenic risks to humans associated with surgical implants and other foreign bodies – a report of an IARC Monographs Programme Meeting. *European Journal of Cancer*, **36**, 307-313.

Mendez, M.O. and Maier, R.M. (2008): Phytoremediation of mine tailings in temperate and arid environments. *Reviews in Environmental Science and Biotechnology,* **7** (1), 47-59.

Middleton, A.P. (1979): The identification of asbestos in solid materials. In: Michaels L, Chissick SS, eds. Asbestos: properties applications and hazards. Chichester, UK: John Wiley and Sons, Inc.

Miyano, T. and Beukes, N.J. (1997): Mineralogy and Petrology of the Contact Metamorphosed Amphibole Asbestos-bearing Penge Iron Formation, Eastern Transvaal, South Africa. *Journal of Petrology*, **38** (5), 651–676.

Mossman, B.T., Lippmann, M., Hesterberg, T.W., Kelsey, K.T., Barchowsky, A. and Bonner, J.C. (2011): Pulmonary endpoints (lung carcinomas and asbestosis) following inhalation exposure to asbestos. *Journal of Toxicology and Environmental Health*, **14**, 76-121.

Nakamura, E., Makishima, A., Hagino, K. and Okabe, K. (2009): Accumulation of radium in ferruginous protein bodies formed in lung tissue: association of resulting radiation hotspots with malignant mesothelioma and other malignancies. *Proceedings of the Japan Academy Series B Physical and Biological Sciences*, **85**, 229–239.

Ndlovu, N., teWater Naude, J. and Murray, J. (2013): Compensation for environmental asbestos-related diseases in South Africa: a neglected issue. *Global Health Action*, **6** (19410), 82–88.

Nemery, B. (1990): Metal toxicity and the respiratory tract. *Eur. Respir. Journal,* **3**, 202–219.

Norrish, K. and Hutton, J.T. (1969): An accurate X-ray spectrographic method for the analysis of geologic samples. *Geochemica et Cosmochimica Acta*, 33, 431-454.

Northwatch, Mining Watch Canada and Associates. 2008. The Boreal Below: Mining Issues and Activities in Canada's Boreal Forest. Pp. 205.

Oberdörster, G. (2002): Toxicokinetics and effects of fibrous and nonfibrous particles. *Inhalation Toxicology*, **14**, 29–56.

Oberti, R., Hawthorne, F.C., Cannillo, E. and Camara, F. (2007): Long range order in amphiboles. In: Hawthorne, F.C., Oberti, R., Della Ventura, G., Mottana, A. (Eds.), Amphiboles: Crystal Chemistry, Occurrence, and Health Issues. Mineralogical Society of America, Chantilly, VA, USA, 125-172.

O'Flaherty E.J. (1996): A physiologically-based model of chromium kinetics in the rat. *Toxicology and Applied Pharmacology*, **138**, 54-64.

Oller, A.R., Costa, M. and Oberdörster, G. (1997): Carcinogenicity assessment of selected nickel compounds. *Toxicology and Applied Pharmacology*, **143**, 152-166.

Ott, H.C., Prior, C., Herold, M., Riha, M., Laufer, G. and Ott, G. (2004): Respiratory symptoms and bronchoalveolar lavage abnormalities in molybdenum exposed workers. *Wien. Klin. Wochenschr.*, **116**, 25-30.

Pentreath, R.J. (1994): The Discharge of Waters from Active and Abandoned Mines. In: Mining and its Environmental Impact. Edited By: R.E. Hester and R.M. Harrison. Royal Society of Chemistry (Great Britain), p. 121-131.

Plumlee, G.S., Morman, S.A. and Ziegler, T.L. (2006): The toxicological geochemistry of earth minerals: An overview of processes and the interdisciplinary methods used to understand them. *Reviews in Mineralogy and Geochemistry*, **64**, 5–57.

Pollastri, S., Gualtieri, A.F., Gualtieri, M.L., Hanuskova, M., Cavallo, A. and Gaudino, G. (2014): The zeta potential of mineral fibres. *Journal of Hazardous Materials*, **276**, 469-479.

Pollastri, S., D'Acapito, F., Trapananti, A., Colantoni, I., Andreozzi, G.B. and Gualtieri, A.F. (2015): The chemical environment of iron in mineral fibres. A combined X-ray absorption and Mossbauer spectroscopic study. *Journal of Hazardous Materials*, **298**, 282-293.

Pugnaloni, A., Giantomassi, F., Lucarini, G., Capella, S., Bloise, A., Di Primio, R. and Belluso E. (2013): Cytotoxicity induced by exposure to natural and synthetic tremolite asbestos: An *in vitro* pilot study. *Acta Histochemica*, **115**, 100-112.

Punturo, R., Bloise, A., Critelli, T., Catalano, M., Fazio, E. and Apollaro, C. (2015): Environmental implications related to natural asbestos occurrences in the ophiolites of the Gimigliano-Mount Reventino Unit (Calabria, Southern Italy). *International Journal of Environmental Research*, **9**, 405-418.

Punturo, R., Ricchiuti, C., Mengel, K., Apollaro, C., De Rosa, R. and Bloise, A. (2018): Serpentinite-derived soils in southern Italy: potential for hazardous exposure. *J. Mediterr. Earth Sci.*, **10**, 51–61.

Reinecke, L. and McClure, L. (1933): Variations in the quality of amosite asbestos at Penge, Transvaal. *Transactions of the geological society of South Africa*, **36** (1), 29 – 39.

Rietveld, H.M. (2014): The Rietveld method. *Physica Scripta*, **89** (098002), 1 – 6.

Riordon, P.H. (1955): The genesis of asbestos in ultrabasic rocks. *Economic Geology*, **50**, 67-81.

Rodríguez-Mercado, J.J., Mateos-Nava, R.A. and Altamirano-Lozano, M.A. (2011): DNA damage induction in human cells exposed to vanadium oxides *in vitro*. *Toxicology in Vitro*, **25**, 1996–2002.

Rozalen, M. and Huertas, F.J. (2013): Comparative effect of chrysotile leaching in nitric, sulfuric, and oxalic acid at room temperature. *Chemical Geology,* **352**, 134–142.

Rozalen, M., Ramos, M.E., Gervilla, F., Kerestedjian, T., Fiore, S. and Huertas, F.J. (2014): Dissolution study of tremolite and anthophyllite: pH effect on the reaction kinetics. *Applied Geochemistry*, **49**, 46–56.

Scambelluri, M., Piccardo, G.B., Philippot, P., Robbiano, A. and Negretti, L. (1997): High salinity fluid inclusions formed from recycled seawater in deeply subducted alpine serpentinite. *Earth Planet. Sci. Lett.,* **148**, 485–499.

Scharf, B., Clement, C.C., Zolla, V., Perino, G., Yan, B., Elci, G., Purdue, E., Goldring, S., Macaluso, F., Cobelli, N., Vachet, R.W. and Santambrogio, L. (2014): Molecular analysis of chromium and cobalt-related toxicity. *Science Reports*, **4**, 5729.

Schimmer, C. (2017): Synergistic use of soil microbes and plants to facilitate rehabilitation on gold tailings materials. Dissertation (MSc) School for Geo- and Spatial Sciences, North-West University, Potchefstroom.

Seilkop, S.K. and Oller, A.R. (2003): Respiratory cancer risks associated with low-level nickel exposure: an integrated assessment based on animal, epidemiological, and mechanistic data. *Regulatory Toxicology and Pharmacology*, **37**, 173-190.

Shekhawat, K., Chatterjee, S. and Joshi, B. (2015): Chromium Toxicity and its Health Hazards. *International Journal of Advanced Research*, **3**, 167-172.

Shimizu, Y., Dobashi, K., Kusakbe, T., Nagamine, T., Oikawa, M., Satoh, T., Haga, J., Ishii, Y., Ohkubo, T., Kamiya, T., Arakawa, K., Sano, T., Tanaka, S., Shimizu, K., Matsuzaki, S., Utsugi, M. and Mori, M. (2008): In-air micro-particle induced X-ray emission analysis of asbestos and metals in lung tissue. *International Journal of Immunopathology and Pharmacology*, **21**, 567–576.

Singer, A., Kirsten, W.F.A. and Buhmann, C. (1992): Occurance of sepiolite in the northern Transvaal, South Africa. *South African Journal of Geology,* **95** (5/6), 165–170.

Stanton, M.F., Layard, M., Tegeris, A., Miller, E., May, M., Morgan, E. and Smith, A. (1981): Relation of particle dimension to carcinogenicity in amphibole asbestoses and other fibrous minerals. *J. Natl. Cancer Inst.,* **67**, 965–975.

Strohmeier, B.R., Huntington, J.C., Bunker, K.L., Sanchez, M.S., Allison, K. and Lee, R.J. (2010): What is asbestos and why is it important? Challenges of defining and characterizing asbestos. *International Geology Review*, **52** (7–8), 801–872

Tashakor, M., Yaacob, W.Z.W., Mohamad, H. and Ghani, A.A. (2014): Geochemical characteristics of serpentinite soils from Malaysia. *Malays. J. Soil Sci.,* **18**, 35–49.

Tiepolo, M., Oberti, R., Zanetti, A., Vannucci, R. and Foley, S.F. (2007): Trace-element partitioning between amphibole and silicate melt. In: Hawthorne, F.C., Oberti, R., Della Ventura, G., Mottana, A. (Eds.), Amphiboles: Crystal Chemistry, Occurrence, and Health Issues. Mineralogical Society of America, Chantilly, pp. 417–452.

Toth, G., Hermann, T., Da Silva, M.R. and Montanarella, L. (2016): Heavy metals in agricultural soils of the European Union with implications for food safety. *Environ. Int.*, **88**, 299–309.

Turci, T., Tomatis, M. and Pacella, A. (2017): Surface and bulk properties of mineral fibres relevant to toxicity. *European Mineralogical Union Notes in Mineralogy,* **18**, 171–214.

Van Biljon, (1964): The chrysotile deposits of the eastern Transvaal and Swaziland, in Haughton, S. H., ed., The geology of some ore deposits in southern Africa: Johannesburg. Geological Society of South Africa, p. 625-669.

Vanoeteren, C., Cornelis, R. and Verbeeck, P. (1986): Evaluation of trace elements in human lung tissue III. Correspondence analysis. *Science of the Total Environment*, **54**, 237–245.

Vaughan, N.P, Rooker, S.J. and LeGuen, J.M. (1981): *In situ* identification of asbestos fibres collected on membrane filters for counting. *Ann. Occup. Hyg.,* **24**, 281-290.

Vigliaturo, R., Ventura, G.D., Choi, J.K., Marengo, A., Lucci, F., O'Shea, M.J., Pérez-Rodríguez, I. and Gieré, R. (2018): Mineralogical Characterization and Dissolution Experiments in Gamble's Solution of Tremolitic Amphibole from Passo di Caldenno (Sondrio, Italy). *Minerals*, **8** (557), 1–24.

Viljoen, R.P. and Viljoen, M. J. (1969): The geology and geochemistry of the layered ultramafic bodies of the Kaapmuiden area, Barberton Mountain Land. *Geological Society of South Africa Special Publication*, **1**, 661-688.

Wadhwa, N., Mathew, B.B., Jatawa, S. and Tiwari, A. (2012): Lipid peroxidation: mechanism, models, and significance. *International Journal of Current Science,* **3**, 29–38.

Walton, W.H. (1982): The nature, hazards, and assessment of occupational exposure to airborne asbestos dust: a review. *Ann. Occup. Hyg.*, **25**, 117–247.

Wei, B., Yang, L., Zhu, O., Yu, J. and Jia, X. (2014): Multivariate analysis of trace elements distribution in hair of pleural plaques patients and health group in a rural area from China. *Hair Therapy and Transplantation Journals,* **4**, 2167-3118.

WHO (1990): Environmental health criteria 81: Vanadium. 1-35. Geneva.

WHO (2001): Vanadium Pentoxide and other Inorganic Vanadium Compounds. Concise International Chemical Assessment Document: 29. Geneva.

Wicks, F.J. and O'Hanley, D.S. (1988): Serpentine minerals; structures and petrology. *Reviews in Mineralogy and Geochemistry*, **19**, 91–167.

Wicks, F.J. and Plant, A.G. (1979): Electron-Microprobe and X-Ray-Microbeam studies of serpentine textures. *Canadian Mineralogist*, **17**, 785–830.

Williams, C., Dell, L., Adams, R., Rose, T. and Van Orden, D.R. (2013): State-of-the-science assessment of non-asbestos amphibole exposure: Is there a cancer risk? *Environmental Geochemistry and Health*, **35**, 357–377.

Wilson, A.H. (2012): A chill sequence to the Bushveld Complex: Insight into the first stage of emplacement and implications for the parental magmas. *Journal of Petrology*, **53**, 1123–1168.

# Chapter 3 – Using kinetics models to study mechanisms of asbestos dissolution for inferences on chemical stability in the natural environment

Abstract

The chemical stability of asbestos fibres is a major factor characterising potential health effects and environmental persistence. The kinetics mechanisms of asbestos dissolution in batch experiments are largely based on the increase of elemental concentrations in solution. However, the chemical and mineralogical complexity of these silicates suggests this method may be unsuitable for assessing the non-constant reactivity of heterogeneous (non-isotropic) natured solids. Therefore, the aim of this study is to measure, describe and convert the increase in dissolved solid mass and investigate the dissolution kinetics and mechanisms of various asbestos rock samples according to the shrinking core and solid-state kinetic models using model-fitting methods. The chemical stability (i.e., resistance to dissolution) and dissolution reactions of chrysotile-, amosite-, crocidolite- and anthophyllite-containing mine wastes were evaluated in batch experiments with acidic (pH 4) solutions at 37°C and constant shaking using isothermal analytical approaches. The isothermal curves indicate that the order of bio-durability is chrysotile < crocidolite < amosite < anthophyllite. Chrysotile, crocidolite and anthophyllite were fitted to third order reaction models and followed at least one of the shrinking core models tested. In contrast, amosite exhibits a first order reaction and could not be fitted to any of the shrinking core models. Fitting the experimental data to a non-linear expression allows the total dissolution time of 205, 3774, 908 and 2123 days to be calculated for chrysotile, amosite, crocidolite and anthophyllite, respectively. Dissolution kinetics and mechanisms influence the potential toxicity of various fibrous minerals, and is thus an important parameter for risk assessment evaluations and its persistence in the environment.

## 3.1. Introduction

Mineral fibres, commercially termed asbestos, are widespread on the Earth (Belluso *et al.,* 2017). Asbestos is a group 1 carcinogenic mineral associated with lung and gastrointestinal cancer and asbestosis (Bernstein *et al*., 2005; Plumlee *et al.,* 2006; Gunter *et al*., 2007). Natural deposits hosting asbestos fibres, referred to as naturally occurring asbestos, are of great concern as they

represent potential environmental exposure sources of respirable mineral dust (Harper, 2008; Lucci *et al*., 2018).

Dissolution mechanisms provide insight into how a particular fibre may interact with its environment (McDonald and McDonald, 1997; Muhle and Bellmann, 1997; Guthrie, 1997) and ultimately moderate the persistence of asbestos (Oze and Solt, 2010). In the context of weathering, the dissolution of silicates is regularly classified as either congruent or incongruent (Crundwell, 2014). When there are no new phases formed during dissolution, the process is classified as congruent dissolution (Crundwell, 2014). When dissolution results in the formation of new phases, the processes are classified as incongruent dissolution (Crundwell, 2014). Additionally, the formation of an alteration layer or partially leached zone is implied by incongruent dissolution (Crundwell, 2014). The diffusion of ions through an alteration layer as a control of the rate of dissolution is a proposal made in one of the earliest models for silicate dissolution (Crundwell, 2014). The observation of alteration layers with a thickness of several Angstroms was observed on the surface by by XPS (Tsomaia *et al.,* 2003, Brantley, 2008) and presumably provides evidence in support of parabolic kinetics. However, this diffusional view is no longer predominant and there is a 'two-fold' evidence against the diffusional view: (1) The orders of reactions observed are one-half and diffusional processes are strictly first order and (ii) at longer reaction times the dissolution often becomes congruent, especially under conditions that are far from equilibrium (Crundwell, 2014). However, even if the dissolution rate is not controlled by the diffusion through the alteration layer, the surface, particularly at low pH ranges, shows the presence of layers (Crundwell, 2014). Either the re-precipitation of material post dissolution or the eventual formation of consistently thick layers due to preferential leaching at steady state may result in alteration layers such as these (Brantley, 2004).

The rate at which silicate minerals decompose via dissolution depends on both the physical and chemical properties of the fibres as different types of asbestos fibres follow different reaction kinetics (Bernstein et al., 2005). For instance, in acidic or alkaline solutions, the dissolution of silicates results in either (i) the silicate structure being completely broken down, (ii) the structure being partially broken down. The latter occurs most often, as the dissolution of the cations leaves behind a siliceous residue or (iii) no dissolution occurs (Terry, 1983a, b). Heterogeneous solid-liquid and solid-state reactions can be represented as (Levenspiel, 1972):

*aA(acid + fluid) + bB(Solid) -> products* (equation 3.1)

The rate of solid-liquid reactions is typically controlled by one of the following: (i) diffusion across a film layer, (ii) chemical reaction at the unreacted particles' core surface and (iii) diffusion through a product layer (Levenspiel 1999; Ashraf *et al*., 2005).

The kinetics of asbestos dissolution was studied by thermo-gravimetric analysis under isothermal conditions using both solid-liquid kinetic models and solid-state kinetic models. As dissolution of asbestos particles in acidic solutions is accompanied by a decrease in solid mass, measurements of weight loss are a useful parameter for tracking the dissolution kinetics. In the present study, relative kinetic parameters and overall dissolution reactions were determined using solid mass loss over time. Unlike solution kinetics, concentration measurements have little significance in solid-state kinetics models as the solid sample is not homogeneous. The heterogeneous (non-isotropic) nature of the solid means that its reactivity is not constant throughout and, therefore, the reactivity is not reflected by concentration. Thermogravimetric analysis (TGA) measures the change in solid mass as a function of time and/or temperature. The characteristics of the TGA curve relate to the nature of the solid sample under investigation (Ozawa, 2000; Sun *et al.*, 2008; Kierzkowska *et al.*, 2013; Fedunik-Hofman *et al.,* 2019). The mass loss curve is then converted into a dimensionless curve "α", from which kinetic information may be derived. The nature by which these processes proceed (slow vs. fast, non-linear vs. linear) is expressed by the modification of the conversion (α) as a function of time and/or temperature (Fedunik-Hofman *et al*., 2019). Different expressions of α (i.e., standard conversion and ash-free conversion) may be used depending on the process and characteristics of the solid material under study (Fedunik- Hofman *et al.,* 2019). As the reaction proceeds, the value of α changes as a function of time. When graphically displayed, curves with characteristic shapes are obtained (Vyazovkin and Wight, 1997). Solid-state and solid-liquid kinetic models are used to recognise and relate these shapes to various associated mechanisms (Khawam and Flanagan, 2006).

Solid-liquid reactions are investigated in a similar manner to homogeneous reactions in which the product concentration or solid phase weight change is measured as a proxy of the progress of the reaction (Grenman *et al*., 2011). During the dissolution of solids, the heterogeneous solid-liquid reaction models, which are most used, are shown in figure 3.1 (Safari *et al*., 2009).

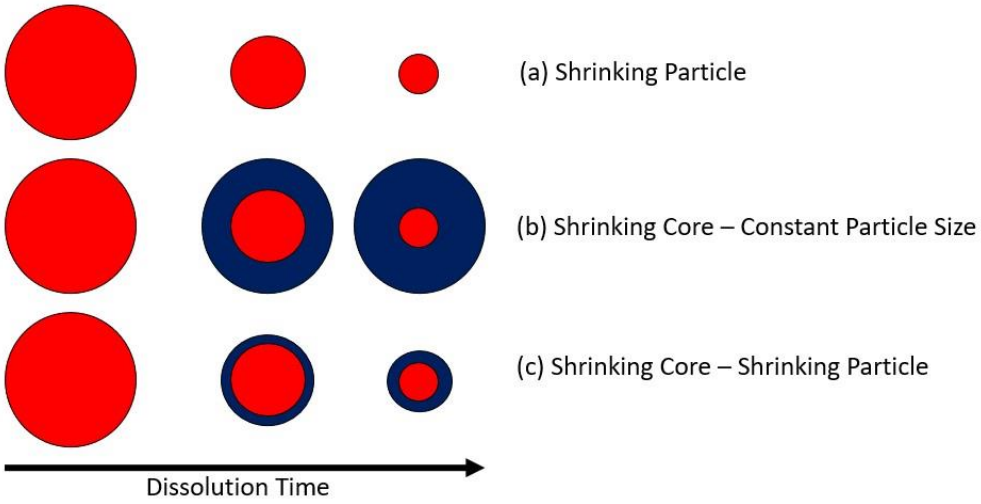


Figure 3.1.: Dissolution models of solid particles (modified from Safari *et al.,* 2009)

Model (a) describes the shrinking of a sphere over time without the surface being covered by any layer. Model (b) illustrates the shrinking of a spherical particle core over time along with an increase in the covering of the core's surface with a solid layer causing the size of the solid particle (core plus solid layer) to remain constant. Model (c) shows the progressive shrinking of the core over time together with a constant thickness of the solid layer. Solid-state kinetics is based primarily on measuring the variations in the mass of the solid sample studied to derive the conversion values of α. Solid-state reactions are described by various models (Khawam and Flanagan, 2006). All these models require conversion (α) as an input to describe the change in mass of a solid before and after the reaction (Bashir *et al.,* 2018). In most studies the proportion of the reacting mineral is used as the key quantitative variable for interpreting dissolution data (Prosser, 1996). TGA records the mass of a solid reactant mixture as it undergoes conversion to products through chemical dissolution reactions. The aim of the study was to model asbestos dissolution behaviour based on isothermal thermogravimetric (TGA) experiments to gain information about the overall reaction mechanism and determine kinetic parameters.

## 3.2. Materials and methods

### 3.2.1. Asbestos samples

Four different naturally occurring asbestos (NOA) rock samples were investigated in this study,

namely: (i) Chrysotile from Havelock Mine, Swaziland; (ii) amosite from Penge, Lydenberg District (now officially known as Mashishing in the Ehlanzeni District since June 2006), South Africa; (iii) crocidolite from Prieska Division, Northern Cape, South Africa and (iv) anthophyllite from Guelb Moghrein Mine, Akjoujt, Mauritania. All samples consist of both the host rock and the asbestos mineral fibres. The chrysotile, amosite, crocidolite and anthophyllite were separated as fibrous bundles from their host rocks. The fibres were crushed into a homogeneous powder using a sterile rotary disk mill (Dickie and Stockler, TS-250 mill) to ensure the material was representative of the bulk mineral. The powdered samples were submitted to X-ray diffraction (XRD), X-ray fluorescence (XRF) and BET surface area analysis and then used in the isothermal dissolution experiments.

### 3.2.2. Isothermal dissolution experiments

The dissolution mechanisms and kinetics of the NOA rock samples were determined by dissolution batch experiments at 37°C during continuous agitation (150 rpm). Seven batch reactors were set up for each type of NOA rock sample and the degree of dissolution was determined by measuring the change of the sample mass at different intervals of time. The advancement of the dissolution reaction was determined at the end of the following times intervals: 24 hours, 48 hours, 1 week, 2 weeks, 1 month, 2 months and 3 months. The pH of the solutions was also monitored during the experiments. The batch experiments were conducted in 100 mL Erlenmeyer flasks containing 50 mL HCl solution and 0.05 grams of sample. At each sampling time the content of the flask was vacuum filtered using 0.22 µm ϕ cellulose Merck Millipore filters (ashless grade). Knowing the filter weight, the weight of the solid residue was determined by measuring the weight difference between the initial NOA rock sample weight and one of the solid residues, after filtration and drying.

### 3.2.3. Heterogeneous solid-liquid kinetics models

Different models may be used to represent the mechanisms of mineral dissolution. In non-catalytic solid-liquid environments, the shrinking core model is one main model used to evaluate the kinetics of dissolution processes (Gharabaghi *et al.*, 2009). The dissolution of asbestos in acidic solutions results in the selective leaching of cations and this is accompanied by a reduction in the mass of the solid. The shrinking core model (Levenspiel, 1962) was used to describe the solid-liquid

dissolution kinetics. A standard conversion, αSC, is required for these models and can be calculated using (Ahn and Choi, 2017; Um, 2017):

$\alpha_{SC} = \frac{mo-mt}{mo}$ (Standard conversion, SC) (equation 3.2)

where m0 is the initial sample weight and mt is the sample weight at time t.

Mechanisms and their equations are presented in table 3.1, where αSC is the dissolved mass fraction, k is the reaction rate constant and t is the reaction time (Levenspiel, 1972; Ghassa *et al.*, 2017).

Table 3.1: Shrinking Core Models

| Equation number: | Model: | Mechanism: |
|---|---|---|
| | | |
| Equation 3.3 | $1 – (1 – \alpha)^{2/3} = kt$ | Liquid film diffusion (mixed chemical reaction control and diffusion control) |
| Equation 3.4 | $1 – (1 – \alpha)^{1/3} = kt$ | Chemical reaction control |
| Equation 3.5 | $1 – 3(1 – \alpha)^{2/3} + 2(1 – \alpha) = kt$ | Diffusion of hydrogen ions through a solid layer around the unreacted core |
| Equation 3.6 | $\frac{1}{3}\ln(1-\alpha) + ((1 - \alpha)^{-1/3} – 1) = kt$ | Interfacial transfer and diffusion through the product layer |

3.2.4. Solid-state kinetics models

Thermal analytical methods were used to study the solid-state kinetics of the isothermal dissolution of asbestos in acidic solutions. The weight loss data is converted to a normalised form known as the ash free conversion factor (α) (Johnson and Fegley, 2000; 2003). The conversion fraction (α) is a measure of the progress of the reaction as a function of time and ranges between 0 and 1 (Gualtieri *et al.,* 2012). The ash free conversion fraction (α) for isothermal thermogravimetric analysis, at any given time, can be expressed as (Yao *et al.,* 2008; Yang *et al.,* 2016):

$\alpha_{AF} = \frac{mo-mt}{mo-mf}$ (Ash free conversion, AF) (equation 3.7)

where m0 is the initial sample weight, mt is the sample weight at time t, and mf is the final sample weight.

Unlike rate laws for homogeneous kinetic reactions, differential and integral kinetic equations are used to express solid-state reaction rates (Ghaffari *et al.,* 2012). The dissolution reaction of asbestos in acidic solutions using solid-state kinetics is expressed by the following:

$\frac{d\alpha}{dt} = k(t) * f(\alpha)$ _____ (equation 3.8)

$g(\alpha) = kt$ _____ (equation 3.9)

Where t is the time, k(t) is the temperature-dependent rate constant, f(α) is the differential reaction model and g(α) is the integral reaction model. The integral reaction models are given in table 3.2.

Table 3.2: Solid-State rate expressions for different reaction models

| Number | Notation | Integral Equation<br>g(α) = kt | Type |
|---|---|---|---|
| Reaction order models | | | |
| 1 | F0/R1 | α = kt | Zero order |
| 2 | F1 | -ln (1 – α) = kt | First order |
| 3 | F2 | $[(1-\alpha)^{-1} - 1] = kt$ | Second order |
| 4 | F3 | $0.5[(1-\alpha)^{-2} - 1] = kt$ | Third order |
| Geometrical contraction models | | | |
| 5 | R2 | $[1-(1-\alpha)^{1/2}] = kt$ | Contracting area |
| 6 | R3 | $[1-(1-\alpha)^{1/3}] = kt$ | Contracting volume – chemical reaction control |
| Diffusion models | | | |
| 7 | D1 | $\alpha^2 = kt$ | 1-D Diffusion |
| 8 | D2 | $(1-\alpha)\ln(1-\alpha) + \alpha = kt$ | 2-D Diffusion |
| 9 | D3 | $[1-(1-\alpha)^{1/3}]^2 = kt$ | 3-D Diffusion-Jander |
| 10 | D4 | $1 - (2\alpha/3) - (1-\alpha)^{2/3} = kt$ | Ginstling-Brounshtein |

The regression correlation coefficients (R2) were calculated for each equation and checked graphically. Calculating the correlation coefficient, $r^2$, of the curves allows the determination of the model to best reproduce the data i.e., when the correlation coefficient is closest to 1 or -1 (Ciftci *et al.*, 2021). The apparent rate constants were determined from the slope of the calculated linear regression lines. The ability of numerous models to give excellent fits to the data obtained in the dissolution experiments is a result of the limited range ($0 \leq \alpha \geq 1$) covered by α as well as appearing in functions that further flatten the value range (i.e. ln(1 – α), (1 – α)1/2, (1 – α)1/3, (1 – α)2/3) (Lidell, 2005). The master plot method was used to confirm the most probable model as it is less influenced by experimental conditions and thus more accurate (Criado *et al*., 1989; Jin *et al*., 2009). The master plot curve is obtained by plotting the conversion fraction (α) against z(α), calculated for a selected pair of rate functions according to (Criado, 1978):

$z(\alpha) = f(\alpha) \times g(\alpha)$ _____ (equation 3.10)

The mechanism best fitting the experimental results is the most probable. The corresponding integral and differential forms of the model equations used in the master plots are given in table 3.3.

Table 3.3: Integral and Differential Forms of Model Equations used in Master Plots

| Model | Integral form $g(\alpha) = kt$ | Differential form $f(\alpha) = \frac{1}{k} * \frac{da}{dt}$ |
|---|---|---|
| | | |
| First order F1 | $-\ln(1 - \alpha)$ | $(1 - \alpha)$ |
| Second order F2 | $(1 - \alpha)^{-1} - 1$ | $(1 - \alpha)^2$ |
| Third order F3 | $0.5[(1 - \alpha)^{-2} - 1]$ | $(1 - \alpha)^3$ |

As the integral reaction model [g(α)] equations used to determine the rate constants are designed for α values ranging between 0 and 1, as a function of time t, extending to infinity, they cannot be used to calculate the total time of dissolution (Gualtieri *et al.*, 2012). To fit the data to an expression incorporating finite time, non-linear empirical equations are required. It was found that, in accordance with Gualtieri *et al.* (2012), the experimental data was best reproduced using:

$y = y_0 + A * \ln(x - x_0)$ _____ (equation 3.11)

This equation allowed the parameters y0, A and x0 to be determined. To calculate the total dissolution time, the value of y in equation 10 was set equal to 1 and the determined values were inputted into the equation:

$$t = \frac{\exp[1-\frac{y0}{A}]}{x0} \quad \text{(equation 3.12)}$$

3.2.5. Statistical analysis

Statistical analysis of the datasets was conducted using Microsoft Office Excel 2016. Linear regressions were used to fit experimental data to kinetic models and determine the reaction kinetics. Non-linear regression and solver in Excel were used to fit non-linear expressions to experimental data.

## 3.3. Results

3.3.1. Bulk geochemistry of asbestos samples

Dissolution reaction rates of silicate minerals in acidic solutions may be affected by several factors, such as the mineralogical and chemical composition, the specific surface area, the solid/liquid ratio and the granulometric distribution (Economou *et al*., 2002; Sevim *et al.*, 2003; Sengul *et al*., 2006). It is thus important to analyse these components unique to each mineral used during comparative dissolution studies. The results of the X-ray diffraction (XRD) are given in table 3.4, and the major and trace element results from X-ray fluorescence (XRF) are given in tables 3.5 and 3.6, respectively. The N2 BET specific surface area of chrysotile, amosite, crocidolite and anthophyllite were 29.7, 10.3, 19.9 and 3.5, respectively.

Table 3.4: XRD analysis showing percentage of mineral phases in asbestos-bearing rock samples (n = 2)

| Asbestos sample | Phases detected (% composition) |
|---|---|
| | |
| Chrysotile | Chrysotile (100 %) |
| Amosite | Amosite (94.5 %) >> Quarts low (4.1 %) > Sepiolite (1.4 %) |
| Crocidolite | Magnesio-riebeckite (100 %) |
| Anthophyllite asbestos | Siderite (65.7 %) > Anthophyllite-Gedrite (25.9 %) > Talc (8.3 %) |
| *% Composition represents the modal amounts of minerals (quantitative analysis) present in asbestos rock samples* | |

Table 3.5: XRF analysis of major elements (n = 2)

| Oxides (wt %) | Chrysotile | Amosite | Crocidolite | Anthophyllite |
|---|---|---|---|---|
| | | | | |
| $SiO_3$ | 42.08 | 48.93 | 51.52 | 19.71 |
| $Al_2O_3$ | 0.59 | 0.36 | 0.07 | 0.08 |
| $Fe_2O_3$ | 2.00 | 41.37 | 38.31 | 34.13 |
| MnO | 0.03 | 0.64 | 0.06 | 1.43 |
| MgO | 40.83 | 5.84 | 2.23 | 17.70 |
| CaO | 0.06 | 2.02 | 0.35 | 0.88 |
| $Na_2O$ | 0.07 | 0.00 | 6.22 | 0.00 |
| $K_2O$ | 0.01 | 0.24 | 0.10 | 0.02 |
| TiO2 | 0.03 | 0.03 | 0.03 | 0.01 |
| P2O5 | 0.01 | 0.02 | 0.01 | 0.12 |
| Cr2O3 | 0.01 | 0.02 | 0.01 | 0.00 |
| NiO | 0.19 | 0.01 | 0.01 | 0.01 |
| LOI | 12.18 | 0.46 | 1.24 | 22.02 |
| Total | 100.08 | 99.87 | 100.15 | 96.09 |

Table 3.6: XRF trace element concentrations (n = 2)

| Element (ppm) | Chrysotile | Amosite | Crocidolite | Anthophyllite |
|---|---|---|---|---|
| | | | | |
| Sc | 6.4 | 4.64 | D.L. | 100.99 |
| V | 16.42 | 3.51 | 3.91 | D.L. |
| Cr | 83.4 | 4.61 | D.L. | D.L. |
| Co | 52.55 | D.L. | D.L. | D.L. |
| Ni | 1518.54 | 51.24 | 11.86 | 43.87 |
| Cu | 21.99 | 36.77 | 35 | 7419.45 |
| Zn | 16.19 | 41.62 | 12.66 | 1.3 |
| Ga | D.L. | D.L. | 1.63 | D.L. |
| Rb | D.L. | 20.77 | 1.02 | 0.65 |
| Sr | 0.74 | 26.63 | 0.86 | 1.5 |
| Y | 0.77 | 3.78 | 1.82 | 7.01 |
| Zr | 0.49 | 3.7 | 0.38 | 0.06 |
| Nb | D.L. | 0.85 | D.L. | 0.72 |
| Mo | D.L. | 0.62 | D.L. | 1.53 |
| Ba | D.L. | 28.17 | 1.69 | D.L. |
| Pb | 6.52 | 5.32 | 5.06 | 8.42 |
| Th | D.L. | D.L. | D.L. | D.L. |
| U | D.L. | D.L. | D.L. | D.L. |
| D.L. – detection limit | | | | |

### 3.3.2. Mass loss and pH measurements

At the end of each time interval during the course of the dissolution experiments the pH of the solution was measured, and the solid asbestos was separated from the solution via filtration. Both weight loss and pH values are given in table 3.7 and 3.8, respectively.

Table 3.7: The weight of the solid residue measured at each time interval (n = 2)

| Time (hours) | Chrysotile | Amosite | Crocidolite | Anthophyllite |
|---|---|---|---|---|
| | | | | |
| 0 | 0.05 | 0.05 | 0.05 | 0.05 |
| 24 | 0.0252 | 0.0391 | 0.0377 | 0.0456 |
| 48 | 0.024 | 0.0386 | 0.0336 | 0.0451 |
| 168 | 0.021 | 0.0363 | 0.0323 | 0.0445 |
| 334 | 0.0186 | 0.0355 | 0.0317 | 0.0443 |
| 720 | 0.0166 | 0.0354 | 0.0311 | 0.0437 |
| Total mass loss | 0.0334 | 0.0146 | 0.0189 | 0.0063 |

Table 3.8: The pH of the solution measured at each time interval (n = 2)

| Time (hours) | Chrysotile | Amosite | Crocidolite | Anthophyllite |
|---|---|---|---|---|
| | | | | |
| 0 | 4.0 | 4.0 | 4.0 | 4.0 |
| 24 | 6.76 | 3.87 | 3.89 | 3.89 |
| 48 | 6.58 | 3.61 | 3.72 | 3.62 |
| 168 | 6.42 | 3.54 | 3.47 | 3.56 |
| 334 | 6.11 | 4.38 | 4.49 | 4.82 |
| 720 | 6.24 | 4.86 | 4.58 | 4.97 |

Values reach a plateau after 186 hours for all four asbestos minerals indicating the completion of the chemical reaction. The pH variations over time for each asbestos sample is displayed in figure 3.2.

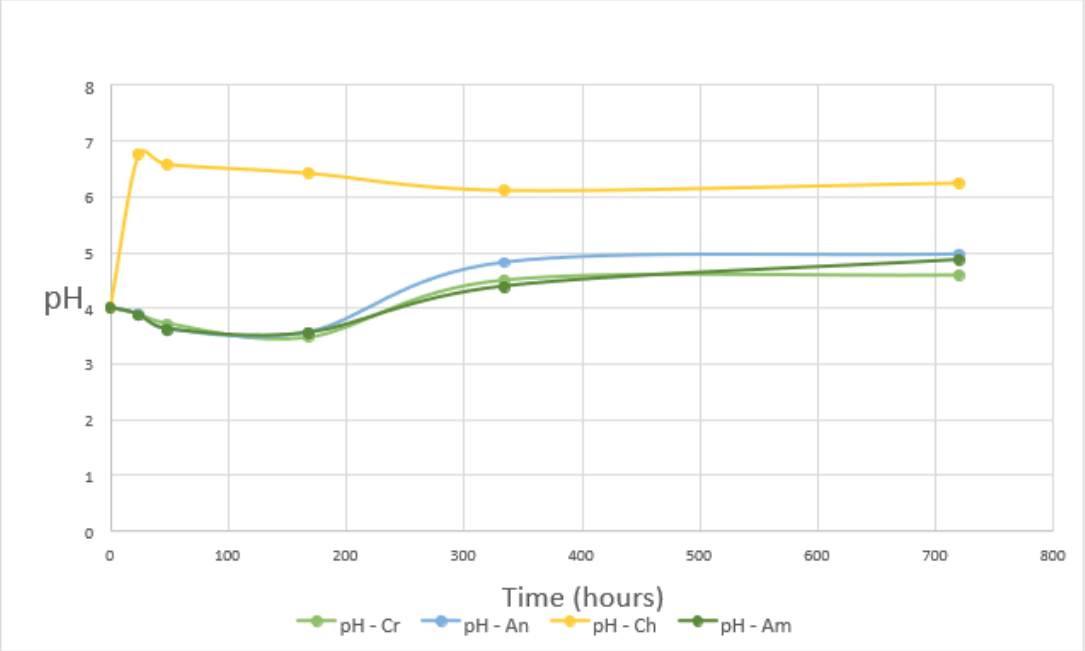


Figure 3.2: pH of the acidic solution versus time during the dissolution of asbestos particles

3.3.3. Solid-liquid kinetics

Two distinct stages occurred during the dissolution reactions as evident in figure 3.3, namely:– an initial fast stage (0 and 48 hours) and the second, slower stage (48 – 720 hours).

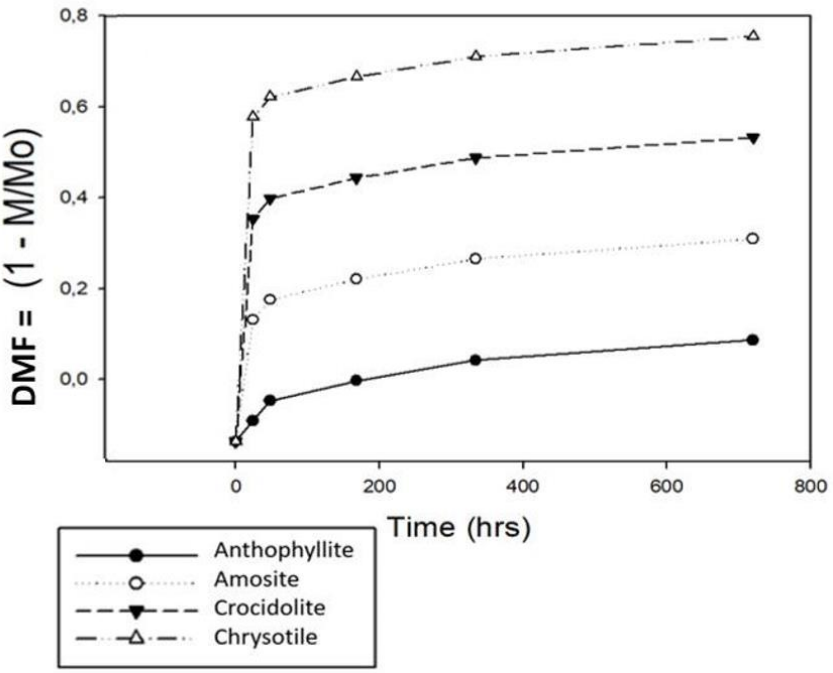


Figure 3.3: Diagram showing biphasic dissolved mass fraction, α, released from chrysotile, amosite, crocidolite and anthophyllite rocks in acidic solution consisting of an initial rapid stage followed by a slower later phase, when plotted vs t.

Therefore, the shrinking core models were examined for each stage (table 3.1). The shrinking core model was applied to the entire dissolution reaction (table 3.9 and figure 3.4).

Table 3.9: The apparent rate constants and correlation coefficients for kinetics models during the entire dissolution process.

| | Chrysotile | | Amosite | | Crocidolite | | Anthophyllite | |
|---|---|---|---|---|---|---|---|---|
| | | | | | | | | |
| Model # | *k* ($hr^{-1}$) | $r^2$ | *k* ($hr^{-1}$) | $r^2$ | *k* ($hr^{-1}$) | $r^2$ | *k* ($hr^{-1}$) | $r^2$ |
| 1 | $2 \times 10^{-4}$ | 0.86 | $7 \times 10^{-5}$ | 0.66 | $9.9 \times 10^{-5}$ | 0.51 | $3.3 \times 10^{-5}$ | 0.84 |
| 2 | $1.4 \times 10^{-4}$ | 0.91 | $4 \times 10^{-5}$ | 0.81 | $5.8 \times 10^{-5}$ | 0.54 | $1.7 \times 10^{-5}$ | 0.87 |
| 3 | $2 \times 10^{-5}$ | - | $3.3 \times 10^{-5}$ | 0.63 | $3.7 \times 10^{-5}$ | 0.58 | $3.8 \times 10^{-6}$ | 0.90 |
| 4 | $6.82 \times 10^{-5}$ | 0.94 | $4.69 \times 10^{-6}$ | 0.68 | $9.14 \times 10^{-6}$ | 0.59 | $6.95 \times 10^{-7}$ | 0.89 |
| | | | | | | | | |
| *$r^2$: 0.9 – 1.0 very highly correlated; 0.7 – 0.9 highly correlated; 0.5 – 0.7 moderately correlated; 0.3 – 0.5 low; < 0.3 no correlation* | | | | | | | | |

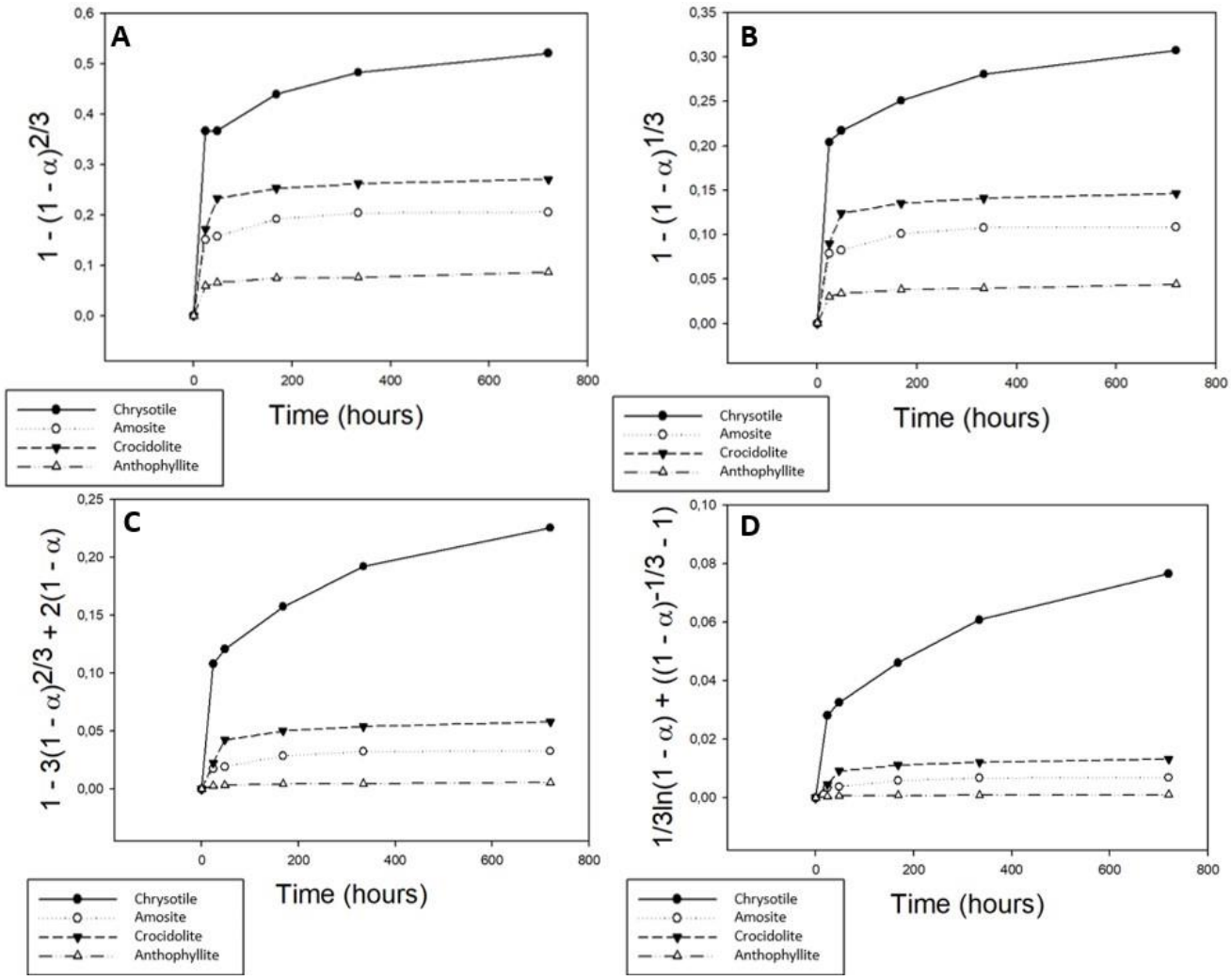


Figure 3.4: Experimental data fitted to shrinking core models for the entire dissolution reaction (0 to 720 hours). Y-axis represents the left-hand side of the shrinking core equations. The suitability of the models was evaluated using the correlation coefficient $r^2$.

The fast stage of the dissolution reaction (table 3.10 and figure 3.5), and the slow stage of the dissolution reaction (table 3.11 and figure 3.6) for each asbestos sample.

Table 3.10: Apparent rate constants and correlation coefficients for kinetics models during the fast reaction stage

| | Chrysotile | | Amosite | | Crocidolite | | Anthophyllite | |
|---|---|---|---|---|---|---|---|---|
| | | | | | | | | |
| Model # | *k* ($hr^{-1}$) | $r^2$ | *k* ($hr^{-1}$) | $r^2$ | *k* ($hr^{-1}$) | $r^2$ | *k* ($hr^{-1}$) | $r^2$ |
| 1 | $8 \times 10^{-3}$ | 0.75 | $3 \times 10^{-3}$ | 0.78 | $5 \times 10^{-3}$ | 0.93 | $1 \times 10^{-3}$ | 0.82 |
| 2 | $5 \times 10^{-3}$ | 0.79 | $2 \times 10^{-3}$ | 0.79 | $3 \times 10^{-3}$ | 0.94 | $7 \times 10^{-4}$ | 0.83 |
| 3 | $3 \times 10^{-3}$ | 0.83 | $4 \times 10^{-4}$ | 0.82 | $9 \times 10^{-4}$ | 1.00 | $7 \times 10^{-5}$ | 0.89 |
| 4 | $7 \times 10^{-4}$ | 0.85 | $8 \times 10^{-5}$ | 0.82 | $2 \times 10^{-4}$ | 1.00 | $1 \times 10^{-5}$ | 0.89 |
| *$r^2$: 0.9 – 1.0 very highly correlated; 0.7 – 0.9 highly correlated; 0.5 – 0.7 moderately correlated; 0.3 – 0.5 low; < 0.3 no correlation* | | | | | | | | |

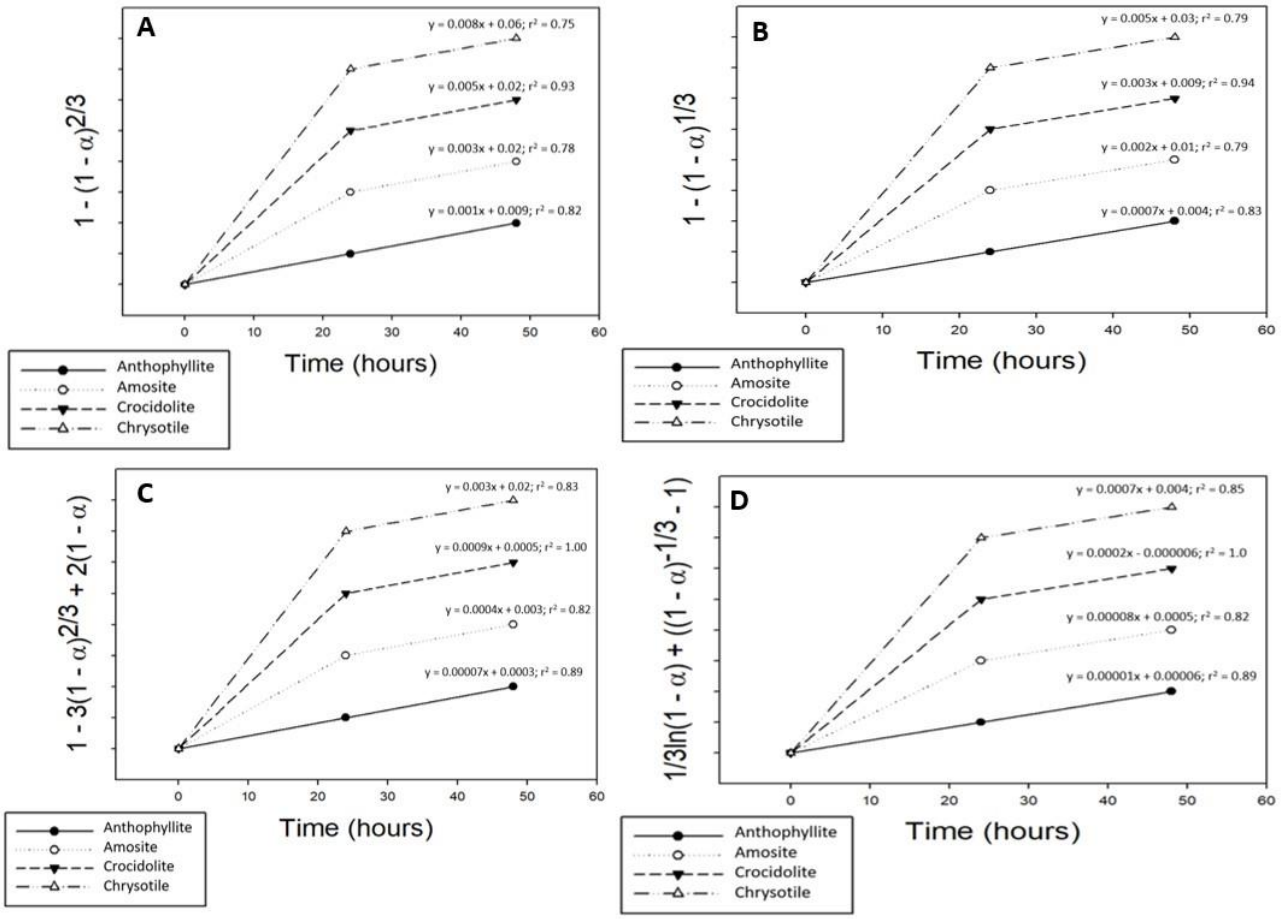


Figure 3.5: Experimental data fitted to shrinking core models for the first 48 hours (fast stage). The Y-axis represents the left-hand side of the shrinking core equations. The suitability of the models was evaluated using the correlation coefficient $r^2$.

Table 3.11: The apparent rate constants and correlation coefficients for kinetics models during the slow reaction stage.

| | Chrysotile | | Amosite | | Crocidolite | | Anthophyllite | |
|---|---|---|---|---|---|---|---|---|
| | | | | | | | | |
| Model # | *k* ($hr^{-1}$) | $r^2$ | *k* ($hr^{-1}$) | $r^2$ | *k* ($hr^{-1}$) | $r^2$ | *k* ($hr^{-1}$) | $r^2$ |
| 1 | $2 \times 10^{-4}$ | 0.83 | $6 \times 10^{-5}$ | 0.59 | $5 \times 10^{-5}$ | 0.80 | $3 \times 10^{-5}$ | 0.91 |
| 2 | $1 \times 10^{-4}$ | 0.90 | $3 \times 10^{-5}$ | 0.58 | $3 \times 10^{-5}$ | 0.81 | $1 \times 10^{-5}$ | 0.92 |
| 3 | $1 \times 10^{-4}$ | 0.91 | $2 \times 10^{-5}$ | 0.60 | $2 \times 10^{-5}$ | 0.83 | $3 \times 10^{-6}$ | 0.94 |
| 4 | $6 \times 10^{-5}$ | 0.94 | $4 \times 10^{-6}$ | 0.61 | $5 \times 10^{-6}$ | 0.83 | $6 \times 10^{-7}$ | 0.95 |
| *$r^2$: 0.9 – 1.0 very highly correlated; 0.7 – 0.9 highly correlated; 0.5 – 0.7 moderately correlated; 0.3 – 0.5 low; < 0.3 no correlation* | | | | | | | | |

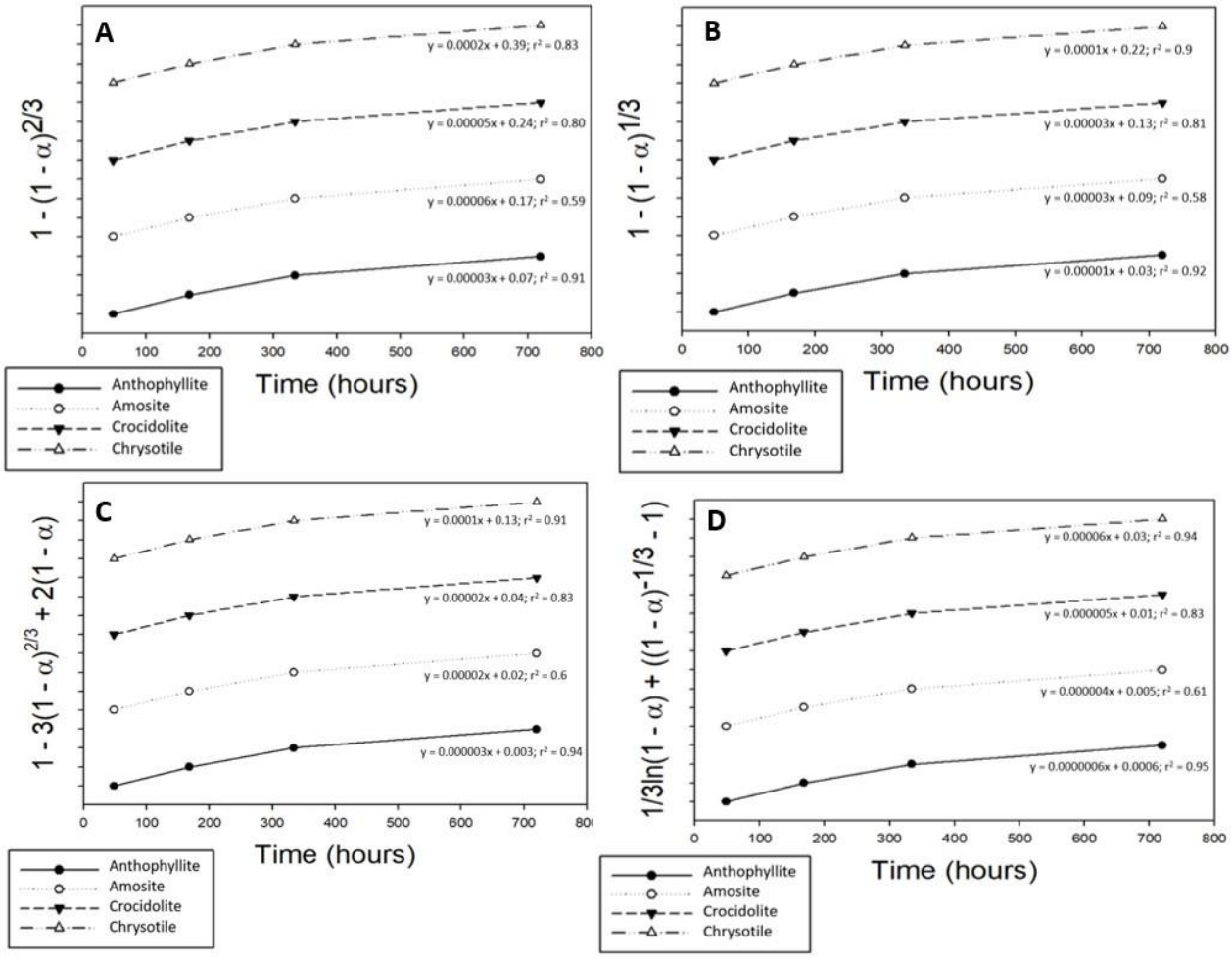


Figure 3.6: Experimental data fitted to shrinking core models for 48 – 720 hours (slow stage). The Y-axis represents the left-hand side of the shrinking core equations. The suitability of the models was evaluated using the correlation coefficient $r^2$.

Applying the shrinking core models to a time-to-given-fraction method, the rate-controlling mechanism of each state may be determined.

3.3.4. Solid-state kinetics

The rate parameter and correlation coefficients of the experimental data fitted to the various solid-state models are given in table 3.12.

Table 3.12: The overall dissolution reaction and relative kinetic parameters of each asbestos-bearing sample and their selected solid-state reaction models.

| Model | Sample | Slope | Intercept | $R^2$ |
|---|---|---|---|---|
| Reaction order models | | | | |
| $\alpha = kt$ | Chrysotile | $7.9 \times 10^{-4}$ | 0.55 | 0.35 |
| | Amosite | $7.94 \times 10^{-4}$ | 0.57 | 0.33 |
| | Crocidolite | $7.96 \times 10^{-4}$ | 0.57 | 0.33 |
| | Anthophyllite | $8 \times 10^{-4}$ | 0.54 | 0.37 |
| $-\ln(1 - \alpha) = kt$ | Chrysotile | $6.5 \times 10^{-3}$ | 0.79 | 0.77 |
| | Amosite | **$1.32 \times 10^{-2}$** | 0.61 | 0.95 |
| | Crocidolite | $8.76 \times 10^{-3}$ | 0.85 | 0.79 |
| | Anthophyllite | $5.41 \times 10^{-3}$ | 0.80 | 0.67 |
| $(1 - \alpha)^{-1} = kt$ | Chrysotile | **$4.3 \times 10^{-2}$** | 1.81 | 0.97 |
| | Amosite | 0.42 | -13.64 | 0.85 |
| | Crocidolite | **$8.94 \times 10^{-2}$** | 1.47 | 0.99 |
| | Anthophyllite | **$2.6 \times 10^{-2}$** | 2.44 | 0.92 |
| $0.5[(1 - \alpha)^{-2} - 1] = kt$ | Chrysotile | **0.4** | -9.08 | 0.91 |
| | Amosite | 30.51 | -1340.91 | 0.79 |
| | Crocidolite | **1.57** | -38.84 | 0.94 |
| | Anthophyllite | **0.16** | 1.25 | 1.00 |
| Geometrical contraction models | | | | |
| $[1 - (1 - \alpha)^{1/2}] = kt$ | Chrysotile | $3.94 \times 10^{-4}$ | 0.78 | 0.35 |
| | Amosite | $3.97 \times 10^{-4}$ | 0.79 | 0.33 |

| | | | | |
|---|---|---|---|---|
| | Crocidolite | $3.98 \times 10^{-4}$ | 0.78 | 0.33 |
| | Anthophyllite | $4 \times 10^{-4}$ | 0.77 | 0.37 |
| $[1 - (1 - \alpha)^{1/3}] = kt$ | Chrysotile | $2.63 \times 10^{-4}$ | 0.85 | 0.35 |
| | Amosite | $2.65 \times 10^{-4}$ | 0.86 | 0.33 |
| | Crocidolite | $2.65 \times 10^{-4}$ | 0.86 | 0.33 |
| | Anthophyllite | $2.67 \times 10^{-4}$ | 0.85 | 0.37 |
| Diffusion models | | | | |
| $\alpha^2 = kt$ | Chrysotile | $9.6 \times 10^{-4}$ | 0.43 | 0.56 |
| | Amosite | $9.69 \times 10^{-4}$ | 0.46 | 0.5 |
| | Crocidolite | $9.58 \times 10^{-4}$ | 0.46 | 0.47 |
| | Anthophyllite | $9.68 \times 10^{-4}$ | 0.40 | 0.59 |
| $(1 - \alpha)\ln(1 - \alpha) + \alpha = kt$ | Chrysotile | $1.77 \times 10^{-3}$ | 0.24 | 0.72 |
| | Amosite | $2.4 \times 10^{-3}$ | 0.24 | 0.82 |
| | Crocidolite | $2.1 \times 10^{-3}$ | 0.26 | 0.69 |
| | Anthophyllite | $1.58 \times 10^{-3}$ | 0.23 | 0.67 |
| $[1 - (1 - \alpha)^{1/3}]^2 = kt$ | Chrysotile | $4.57 \times 10^{-4}$ | 0.74 | 0.39 |
| | Amosite | $4.6 \times 10^{-4}$ | 0.75 | 0.37 |
| | Crocidolite | $4.6 \times 10^{-4}$ | 0.75 | 0.36 |
| | Anthophyllite | $4.63 \times 10^{-4}$ | 0.73 | 0.41 |
| $1 - (2\alpha/3) - (1 - \alpha)^{2/3} = kt$ | Chrysotile | $-3.2 \times 10^{-4}$ | 0.52 | 0.56 |
| | Amosite | $-3.2 \times 10^{-4}$ | 0.51 | 0.5 |
| | Crocidolite | $-3.2 \times 10^{-4}$ | 0.51 | 0.47 |
| | Anthophyllite | $-3.2 \times 10^{-4}$ | 0.53 | 0.59 |

The models showing the best fit to the experimental data are graphed in figure 3.7. Two models, namely F2 and F3, each show strong correlations to the experimental data for chrysotile, crocidolite and anthophyllite. Master plots were compiled to determine the best model.

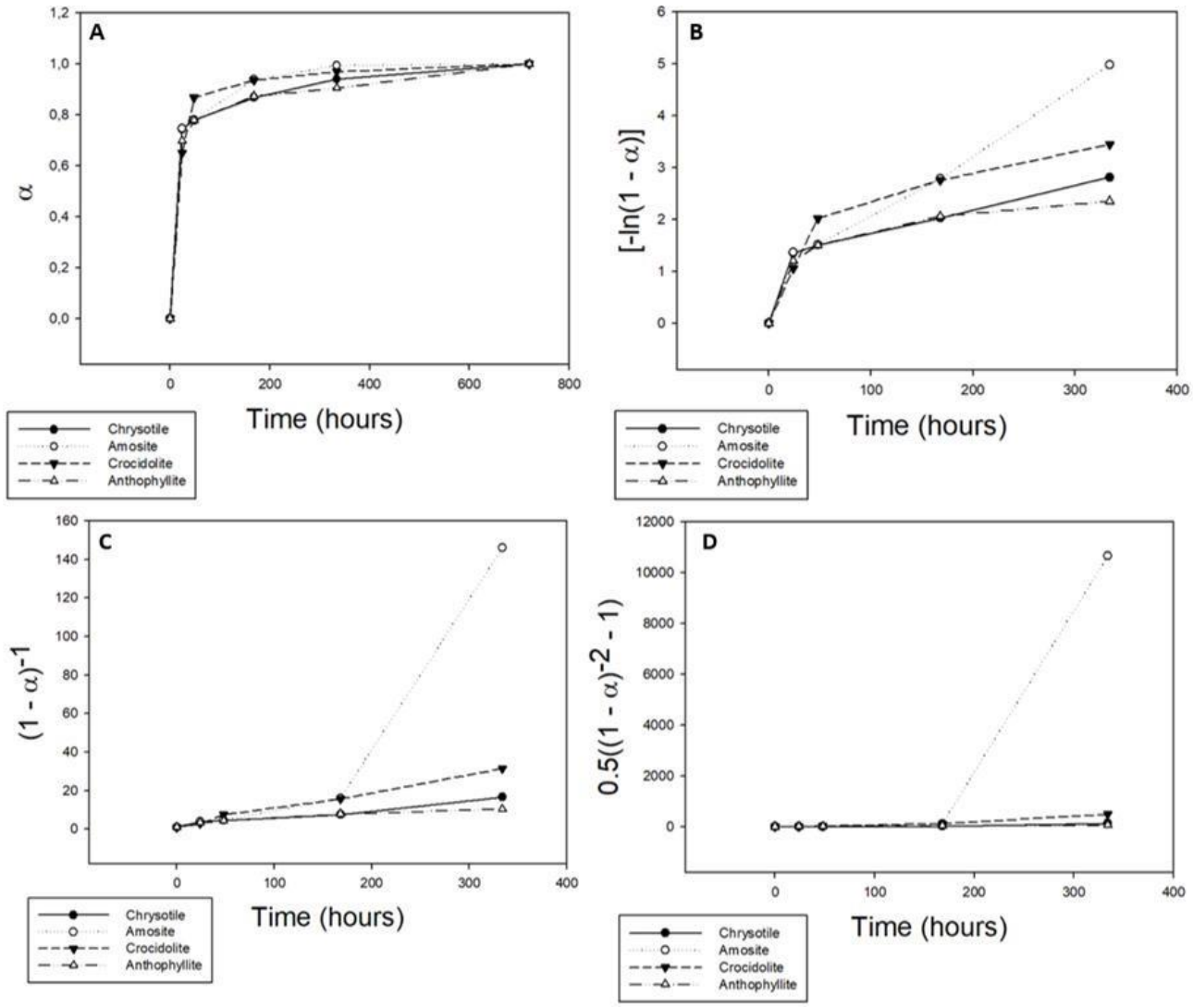


Figure 3.7: Experimental data fitted to solid-state kinetics models

The correlation coefficients of the master plots are given in table 3.13.

Table 3.13: Statistical regression and correlation values of master plots

| | $z(\alpha) = g[(1 - \alpha)^{-1} - 1] * f[(1 - \alpha)^2]$ | $z(\alpha) = g[0.5((1 - \alpha)^{-2} - 1)) * f[(1 - \alpha)^3]$ |
|---|---|---|
| | | |
| Chrysotile | $y = -9.17x10^{-3}x - 0.01$; $r^2 = 0.025$; $p > 0.05$ | $y = 0.07x + 0.02$; $\mathbf{r^2 = 0.31}$; $p > 0.05$ |
| Crocidolite | $y = -5.34x10^{-3}x - 0.02$; $r^2 = 0.004$; $p > 0.05$ | $y = 0.03x + 0.03$; $\mathbf{r^2 = 0.04}$; $p > 0.05$ |
| Anthophyllite | $y = -9x10^{-3}x - 0.01$; $r^2 = 0.02$; $p > 0.05$ | $y = 0.08x + 0.02$; $\mathbf{r^2 = 0.34}$; $p > 0.05$ |

## 3.4. Discussion

Health and environmental impact studies of naturally occurring asbestos fibres and airborne particles must take into consideration the chemical stability of asbestos and the kinetics of dissolution to clearly delineate the models and mechanisms of actions in biological systems and the environment. Research on asbestos dissolution reactions and kinetic analysis is predominantly based on measuring released elemental concentrations in solution (Hume and Rimstidt, 1992; Oze and Salt, 2010; Rozalen *et al.*, 2013; Gualtieri *et al.,* 2019; Walter *et al.*, 2019; Pacella *et al.,* 2021). Serpentine and amphibole asbestos are mineralogically complex, comprising a group of chemical-crystal systems (Lange, 1974). This complexity means that reactions occur in various steps and the dissolution mechanisms are susceptible to variations. Using single element concentrations released into solution to model dissolution reactions and kinetics may be a suitable approach for dissolution studies involving a single mineral phase. However, it may not be accurately indicative of the complete reaction kinetics in chemically complex and/or polyphasic systems. Thus, reaction models quantitatively describing the relationship between the extent and rate of solid sample conversion are adapted as mathematical translations of overall reaction progression. Reaction models are used to determine the mechanisms controlling dissolution reactions and to determine the kinetic equation that best fits the reaction isotherms (Wahab *et al.,* 2019).

### 3.4.1. Mass loss and pH

When the weight loss of the experiments for each asbestos mineral are summed up, 100% solid weight loss is never achieved. The reason is not incomplete dissolution but rather the precipitation of silica back out of the solution (Gualtieri *et al*., 2012). In both the chrysotile and amphibole asbestos minerals, magnesium is an important part, however, the difference between the two asbestos groups comes in the form of the location of the magnesium in the crystal structure (Bernstein *et al.,* 2005). Chrysotile (33% magnesium) contains the magnesium molecule on the outside of the curled structure, whereas the magnesium molecules are contained inside the crystal structure of the amphiboles (6 – 25% magnesium)

(Bernstein *et al.,* 2005). This location variation is significant for determining the solubility variations between the two groups of asbestos minerals as magnesium is soluble in the presence of fluids and is easily leached from the mineral (Bernstein *et al.,* 2005). As magnesium is present at the outer surface of chrysotile, it is readily removed from the crystal structure (Bernstein *et al.,* 2005). In contrast, the magnesium found within the amphiboles is locked within the inner I-beam type structure of the mineral (Bernstein *et al.,* 2005). This I-beam structure consists of corner linked $(SiO_4)_4$ tetrahedra bonded together in a double tetrahedral chain that sandwiches a $Ca_2Mg_5$ layer (Bernstein *et al.,* 2005). This appears to be connected to the very different solubilities of asbestos fibres exposed to acidic solutions: Being very high for chrysotile asbestos and significantly lower for the amphibole asbestos fibres (van Oss *et al.,* 1999; Taunton *et al.,* 2010). As crocidolite is more insoluble than chrysotile (Fubini and Otero Arean, 1999), acid treatment alters chrysotile more easily than crocidolite, thus deeper modifications are expected to be induced by the bacteria on chrysotile fibres (Lund and Aust, 1990; Daghino *et al.,* 2005; Daghino *et al.,* 2006). The appreciably greater solubility of chrysotile, compared to the amphibole asbestos mineral fibres, makes it less persistent (Rowlands *et al.,* 1992; Albin *et al.,* 1994; Bernstein *et al.,* 2005).

Data for the variation in the solution pH as a function of reaction time for each of the four experiments is shown in figure 3.2. The solution pH behaviour of chrysotile and amphibole asbestos sample differ greatly. In the system containing chrysotile the pH increased dramatically within the first 24 hrs after, which it essentially stabilised. In contrast, the pH measured in all three of the amphibole-containing systems gradually decreased until 168 hrs after which a rapid increase was observed. The pH value reached a final limiting value of 6.11, 4.38. 4.49 and 4.82 for chrysotile, amosite, crocidolite and anthophyllite, respectively, for all four systems at 334 hrs. The pH variations indicate that changes in the ionic concentrations of the solutions accompanied the dissolution of each of the asbestos particles (figure 3.2). The final limiting values of both pH and weight loss are reached at ~334 hrs in all four experiments. This correlation is not unexpected as the reactions controlling dissolution and pH data would be approximately equal. The behaviour of the pH data i.e., increases and decreases, is a result of the alkalinity and acidity characteristics of ionic species released into and precipitated from the solutions as a function of mineral composition. Furthermore, the

value of the final limiting pH value in each of the experiments depends on the concentrations and acidity and/or alkalinity of the released ions (Ma *et al.,* 2017).

### 3.4.2. Conversion curves and dissolution mechanisms

The conversion curves derived from the isothermal dissolution experiments at 37°C and 150 rpm show that the reactions follow a decelerating model (figures 3.3) as the reaction rate decreases with conversion. In this study the conversion refers to mass loss during dissolution because of the rock sample containing elements being released into solution. The decelerating conversion curves are used to determine the nature of the dissolution reaction (Vyazovkin *et al*., 2011). The rate of the dissolution reaction, under isothermal conditions, is only influenced by f(α) [k(T) = constant] (Dawar and Anthonysamy, 2017). Thus, isothermal experiments can delineate details of the decelerating dissolution reaction (Dawar and Anthonysamy, 2017). In an experiment performed by Turci *et al.,* 2007 chrysotile asbestos was exposed to acidic chemical weathering. Their results showed that incongruent leaching of the brucite layer, in which magnesium is substituted by iron, was promoted and the surface reactivity subsequently reduced (Turci *et al.,* 2007). In acidic solutions, amphibole asbestos fibres are less susceptible to chemical modifications as they are more stable than serpentine asbestos (Virta, 2002). Being closest to the fibre surface, as reflected in the chrysotile minerals chemical characteristics, the magnesium hydroxide portion of each layer has a poor resistance to acid compared to the amphibole asbestos substances (Bernstein *et al.,* 2008). The greater resistance of the amphibole asbestos minerals to acids derives from the fact that the hydroxides are masked within the outside silicate oxygen layers (Bernstein *et al.,* 2008). The kinetic curves indicate whether mass via ions is continuously mobilised from the asbestos minerals over the entire incubation duration. Different phases can additionally be highlighted from the curves as they show the rate of release. Variations in the rate of mass release over the incubation period are used to infer the degree of ion accessibility to the acid. An initial fast release followed by a latter slow release suggests that a fraction of the mass is more accessible and/or soluble to the acidic solution compared to the rest of the geochemical framework comprising the mineral.

### 3.4.3. Solid-liquid dissolution mechanisms

The selection of a model equation that fits the rate data is critical for developing a mechanism for the solid-liquid dissolution reaction (Prosser, 1996). There are numerous potential rate-determining steps during the reaction of silicates and acid solutions to be considered (Ross, 1967). To propose a mechanism for asbestos dissolution in acidic solutions, various forms of the shrinking core models were employed to investigate the degree of the linearisation of dissolution curves. The mechanisms controlling the dissolution behaviour of the different asbestos rock samples were investigated by dividing the dissolution reaction of each rock sample into two stages, namely a fast initial stage (0 to 48 hours) and a slow later stage (48 to 720 hours). The relationship between $1 – (1 – \alpha)2/3$ (liquid film diffusion), $1 – (1–\alpha)1/3$ (chemical reaction model), $1 – 3(1 – \alpha)2/3 + 2(1 – \alpha)$ (solid product diffusion model), $1/3 \ln(1 – \alpha) + ((1 - \alpha)^{-1/3} – 1)$ (interfacial transfer and diffusion) and experimental data against time were plotted for each time (figure 3.4, 3.5 and 3.6). Using the best fitting shrinking core models (i.e., highest regression coefficient) the rate-controlling mechanism for chrysotile was chemical surface reaction and the mechanism controlling both crocidolite and anthophyllite was interfacial transfer and diffusion through a product layer. The rate-controlling step is the slowest step in the reaction (Levenspiel, 1972). As chrysotile is controlled by a chemical surface reaction, the chemical reaction at the margin phase is significantly slower than diffusion across the margin phase (Koleini *et al.*, 2010). Conversely, if the rate of reagent diffusion across the boundary phase is far lower than of the chemical reaction at the margin phase, diffusion is the rate-determining step as exhibited during the dissolution of anthophyllite and crocidolite samples (Koleini *et al*., 2010). These controlling mechanisms are illustrated schematically in figure 3.8, where the standard SCM assumes that each solid particle of initially unreacted material is a sphere and the reaction begins at the surface of the particle and progresses inwards (Levenspiel, 1972; Roman *et al*., 1974; Crundwell, 1995).

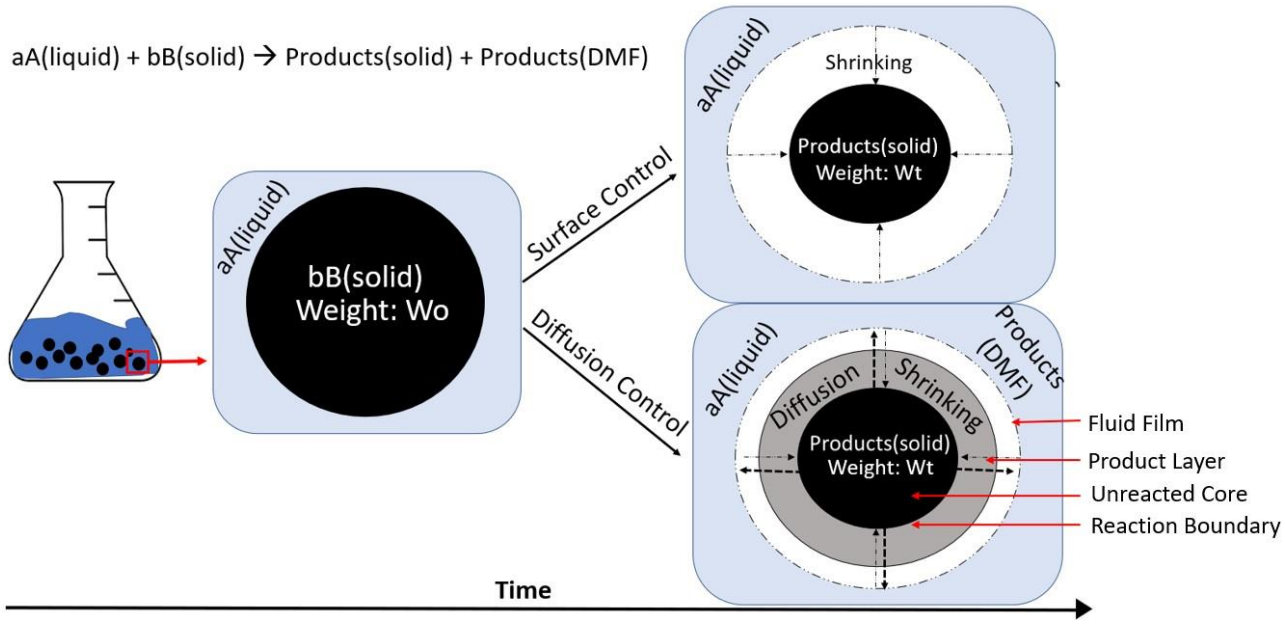


Figure 3.8: Schematic diagram showing surface chemical and diffusion control reactions of shrinking core model (SCM).

This inward progression results in the shrinking of the unreacted solids core and the subsequent formation of a permeable, inert, and solid product layer (Braun *et al*., 1974; Crundwell, 1995). In accordance with the correlation coefficient ($r2 \geq 9.0$), amosite could not be fitted to any of the shrinking core models and therefore no reaction mechanism could be determined.

### 3.4.4. Solid-state dissolution mechanisms

The experimental data was fitted to the solid-state kinetics models and the values are reported in table 14. Amosite dissolution data provides the best fit to the first-order model ($-\ln(1-\alpha) = kt$ (F1)) and chrysotile, crocidolite and anthophyllite to both second and third-order models. To determine the better model fitted to chrysotile, crocidolite and anthophyllite a master plot ($z(\alpha) = g[0.5((1-\alpha)-2-1)) * f[(1-\alpha)3]$) was created (table 3.13) showing that the third-order model best fits the experimental data for dissolution of chrysotile, crocidolite and anthophyllite. Apart from amosite, the best fit of chrysotile, crocidolite and anthophyllite also agrees with findings by Gualtieri *et al.,* 2012. First, second and third order-based solid-state reaction models follow the typical models demonstrated for solution reactions (figure 3.7; Ma *et al*., 2014). The reaction rate, in order-based models (F0 – F3), is proportional to the

conversion degree, α, raised to a power, representing the reaction order. Fitting of amosite dissolution to the first order model suggests that the rate of solid mass dissolution, $da/dt$, is directly proportional to the mass of the particles undergoing reaction (Dash *et al*., 2010; Gouda *et al*., 2017). The lack of results pertinent to amosite dissolution using shrinking core models may be explained by these solid-state model results. Specifically, the shrinking core model cannot be applied to particles exhibiting first-order kinetics (Meulenkamp, 1998; Schmidt and Vogelsberger, 2006; Ho *et al*., 2010; Liu and Hurt, 2010; Liu *et al*., 2010; Utembe *et al*., 2015). The best fitting to and application of these models to the experimental data is surprising considering that they were developed for more conventional reaction conditions where mass transfer problems are not generally considered. Regardless, these models appear valid in agreement with Ma *et al*. (2014).

The total dissolution times of the four asbestos rock samples were determined by fitting the experimental data to the non-linear expression (table 3.14).

Table 3.14: Total dissolution rates calculated for the four samples using a non-linear expression.

| **Sample** | **Estimated dissolution time (days)** |
|---|---|
| | |
| Chrysotile | 205.7 |
| Amosite | 3774.7 |
| Crocidolite | 908.8 |
| Anthophyllite | 2123.7 |

According to Gualtieri *et al.* (2018) the dissolution times of chrysotile and amphibole asbestos fibres range between 94 and 177 days and 49 to 247 years, respectively. The chrysotile sample studied here was shown by XRD analysis to be pure and gave a greater total dissolution time when compared to IUCC chrysotile (96 days); Balangero chrysotile (124 days); Valmalenco chrysotile (177 days); chrysotile (180 days) (Guldberg *et al.,* 1998); chrysotile (1 day) (Oze and Salt, 2010); chrysotile cement (KRY.AS sample 2 and 3) (20 days) (Gualtieri *et al.,* 2012) and the range given by Gualtieri *et al.* (2018) as stated above. However, this was less than the total dissolution times reported for chrysotile NIST (298 days); chrysotile cement

(KRY.AS sample 1) (253 days) (Gualtieri *et al*., 2012) and chrysotile (270 days) (Hume and Rimstidt, 1992). The studied amosite sample (3775 days) had a dissolution time less than the IUCC amosite standard (27010 days) and greater than that of the amosite (2500 days) (Guldberg *et al.,* 1998). In comparison with the total time for IUCC crocidolite standard dissolution (24090 days) and the crocidolite (5000 days) (Guldberg *et al.,* 1998), the total time determined in this study was significantly lower (909 days). Unlike chrysotile, the behaviour of amosite, and crocidolite, anthophyllite asbestos remains poorly understood. The total dissolution time measured for anthophyllite in this study is significantly lower when compared to the IUCC anthophyllite standard (83950 days) (Gualtieri *et al*., 2018). The variations in calculated total dissolution times observed for different types of asbestos minerals reported in different studies in not surprising and best explained by differences in experimental setups, including solution pH and extent of agitation, as well as mineralogical and geochemical differences among samples and the calculations of the kinetics. The apparent discrepancy between bio-durability data and the total dissolution times can be remedied by considering specific surface areas. To facilitate direct comparisons between samples, surface area must be considered (Brantley, 2003; Wu *et al*., 2007; Oze and Solt, 2010).

## 3.5. Conclusion

Isothermal mineral dissolution reactions under acidic conditions involve a change in mass. Therefore thermogravimetry (TGA) and model-fitting methods are appropriate for evaluating chemical stability, dissolution mechanisms and kinetics of complex and heterogeneous asbestos minerals. The challenges when using such methods to study asbestos dissolution relates to natural temperatures as experiments require long reaction times. The dissolution behaviour of four studied asbestos rock samples is distinct, probably reflecting variations of chemical and physical characteristics and the nature of the particle assemblages (Truesdale, 2007). Dissolution kinetics mechanisms of chrysotile, amosite, crocidolite and anthophyllite in hydrochloric solution were compared. Solid weight loss was never achieved during the reaction and both the pH values and dissolved mass fraction for all four asbestos minerals plateaued after 186 hours indicative of completion of the dissolution reactions. The

chemical stability of the four asbestos minerals studied were determined as follows: chrysotile < crocidolite < amosite < anthophyllite. This sequence confirms that chrysotile is less stable than the amphibole asbestos varieties. A first order model was fitted to amosite dissolution, whereas the third order reaction model was found more appropriate for chrysotile, crocidolite and anthophyllite. These dissolution experiments provide fundamental knowledge on determining the durability and persistence of asbestos particles in both the natural environment and the lungs.

## 3.6. References

Ahn, H. and Choi, S. (2017): A comparison of the shrinking core model and the grain model for the iron ore pellet indurator simulation. *Computers and Chemical Engineering*, **97**, 13–26.

Aierken, D., Okazaki, Y., Chew, S.H., Sakai, A., Wang, Y., Nagai, H., Misawa, N., Kohyama, N. and Toyokuni, S. (2014): Rat model demonstrates a high risk of tremolite but a low risk of anthophyllite for mesothelial carcinogenesis. *Nagoya J. Med. Sci.,* **76**, 149–160.

Ashraf, M., Zafar, Z.I. and Ansari, T.M. (2005): Selective leaching kinetics and upgrading of low-grade calcareous phosphate rock in succinic acid. *Hydrometallurgy*, **80**, 286–292.

Aust, A.E., Cook, P.M. and Dodson, R.F. (2011): Morphological and chemical mechanisms of elongated mineral particle toxicities. *Journal of Toxicology and Environmental Health, Part B*, **14**, 40–75.

Bashir, S.T., Yang, L., Liggat, J.J. and Thomason, J.L. (2018): Kinetics of dissolution of glass fibre in hot alkaline solution. *Journal of Material Sciences*, **53**, 1710–1722.

Belluso, E., Cavallo, A. and Halterman, D. (2017): Crystal habit of mineral fibres. In:
Benidire, L., Pereira, S.I.A., Castro, P.M.L. and Boularbah, A. (2016): Assessment of plant growth promoting bacterial populations in the rhizosphere of metallophytes from the Kettara mine, Marrakech. *Environmental Science and Pollution Research*, **23**, 21751–21765.

Bernstein, D. and Pavlisko, E.N. (2017): Differential pathological response and pleural transport of mineral fibres. Chapter 12. In: Gualtieri, A.F. (Ed.), Mineral fibres: crystal chemistry, chemical-physical properties, biological interaction, and toxicity. EMU Notes in Mineralogy, 18, 417–434.

Bernstein, D. M., Rogers, R. and Smith, P. (2005): The biopersistence of Canadian chrysotile asbestos following inhalation: Final Results Through 1 Year After Cessation of Exposure. *Inhalation Toxicology*, **17** (1), 1-14.

Bernstein, D., Castranova, V., Donaldson, K., Fubini, B., Hadley, J., Hesterberg, T., Kane, A., Lai, D., McConnell, E.E., Muhle, H., Oberdorster, G., Olin, S. and Warheit, D.B. (2005): Testing of fibrous particles: short-term assays and strategies: report of an ILSI Risk Science Institute Working Group. *Inhalation Toxicology*, **17**, 497-537.

Bernstein, D., Dunnigan, J., Hesterberg, T., Brown, R., Velasco, J.A.L., Barrera, R., Hoskins, J. and Gibbs, A. (2013): Health risk of chrysotile revisited. *Crit. Rev. Toxicol*., **43** (2), 154–183.

Bernstein, D.M., Donaldson, K., Decker, U., Gaering, S., Kunzendorf, P., Chevalier, J. and Holm, S.E. (2008): A biopersistence study following exposure to chrysotile asbestos alone or in combination with fine particles. *Inhal. Toxicol*., **20**, 1009–1028.

Bernstein, D.M., Dunnigan, J., Hesterberg, T., Brown, R., Velasco, J.A.L., Berrera, R., Hoskins, J. and Gibbs, A. (2013): Response to Murray M. Finkelstein, letter to editor re Bernstein et al: Health risk of chrysotile revisited. *Critical Reviews in Toxicology*, **43** (2), 154–183.

Bernstein, D.M., Dunnigan, J., Hesterberg, T., Brown, R., Velasco, J.A.L., Berrera, R.,
Berry, G. and Gibbs, G.W. (2008): Mesothelioma and asbestos. *Regul. Toxicol. Pharmacol*., **52**, S223–S231.

Brantley S. L. (2003): Reaction kinetics of primary rock-forming minerals under ambient conditions. In Treatise on Geochemistry, Surface and Ground Water, Weathering, and Soils (ed. J. I. Drever, vol. 5.). Elsevier Pergamon, pp. 73–119.

Braun, R.L., Lewis, A.E. and Wadsworth, M.E. (1974): In-place leaching of primary sulphide ores: laboratory leaching data and kinetics model. *Metallurgical Transactions*, **5** (8), 1717–1726.

Busenberg, E. and Clemency, C. V. (1976): The dissolution kinetics of feldspars at 25 °C and 1 atm C02 partial pressure. *Geochimica et Cosmochimica Acta*, **40,** 41-49.

Carbone, M., Baris, Y.I., Bertino, P., Brass, B., Comertpay, S., Dogand, A.U., Gaudino, G., Jube, S., Kanodia, S., Partridge, C.R., Pass, H.I., Rivera, Z., Steele, I., Tuncer, M., Way, S., Yang, H. and Miller, A. (2011): Erionite exposure in North Dakota and Turkish villages with mesothelioma. *Proc Natl Acad Sci USA*, **108** (33), 13618–13623.

Çiftçi, H., Arslan, B., Bilen, A., Arsoy, Z. and Ersoy, B. (2021): Optimization of leaching conditions for extraction of magnesium from a chromite beneficiation plant tailing predominantly containing lizardite. *Bulletin of the Mineral Research and Exploration*, **164**, 251-259.

Criado, J.M. (1978): Kinetic analysis of DTG data from master curves. *Thermochimica Acta*, **24**, 186-189.

Criado, J.M., Málek, J. and Ortega, A. (1989): Applicability of the master plots in kinetic analysis of non-isothermal data. *Thermochimica Acta*, **147,** 377-385.

Crundwell, F.K. (1995): Progress in the mathematical modelling of leaching reactors. *Hydrometallurgy*, **39**, 321-335.

Crundwell, F.K. (2014): The mechanism of dissolution of minerals in acidic and alkaline solutions: Part II Application of a new theory to silicates, aluminosilicates, and quartz. *Hydrometallurgy*, **149**, 265–275.

Daghino, S. (2005): Asbestos hazard in Western Alps: the use of soil fungi in bioremediation of asbestos fibres dispersed in the environment; a chemical-molecular integrated analysis. PhD thesis, University of Torino (Italy) and University "J. Fourier" of Grenoble (France).

Daghino, S., Martino, E., Fenoglio, I., Tomatis, M., Perotto, S. and Fubini, B. (2005): Inorganic Materials and Living Organisms: Surface Modifications and Fungal Responses to Various Asbestos Forms. *Chemistry: A European Journal*, **11**, 5611 – 5618.

Daghino, S., Murat, C., Sizzano, E., Girlanda, M. and Perotto, S. (2012): Fungal Diversity Is Not Determined by Mineral and Chemical Differences in Serpentine Substrates. *PLoS ONE*, **7** (9), e44233. doi:10.1371/journal.pone.0044233.

Daghino, S., Turci, F., Tomatis, M., Favier, A., Perotto, S., Douki, T. and Fubini, B. (2006): Soil fungi reduce the iron content and the DNA damaging effects of asbestos fibers. *Environmental Science and Technology*, **40**, 5793–5798.

Daghino, S., Turci, F., Tomatis, M., Girlanda, M., Fubini, B., and Perotto, S. (2009): Weathering of chrysotile asbestos by the serpentine rock-inhabiting fungus *verticillium leptobactrum*. *FEMS Microbiol. Ecol*., **69**, 132–141.

Dash, S., Murthy, P.N., Nath, L. and Chowdhury, P. (2010): Kinetic modeling on drug release from controlled drug delivery systems. *Acta Poloniae Pharmaceutica*, **67**, 217-223.

Dawar, R. and Anthonysamy, S. (2017): Kinetics of formation of lanthanum tellurate. *J Journal of Thermal Analysis and Calorimetry*, **129**, 1823–1829.

Deng, Z.J., Liang, M.L., Tóth, I., Monteiro, M.J. and Michin, R.F. (2012): Molecular interaction of poly (acrylic acid) gold nanoparticles with human fibrinogen. *ACS Nano*, **6**, 8962–8969.
Donaldson, K., Murphy, F.A., Duffin, R. and Poland, C.A. (2010): Asbestos, carbon nanotubes and the pleural mesothelium: a review of the hypothesis regarding the role of long fibre retention in the parietal pleura, inflammation, and mesothelioma. *Fibre Tox*., **7**, 5.

Donaldson, K., Poland, C.A., Murphy, F.A., MacFarlane, M., Chernova, T. and Schinwald, A. (2013): Pulmonary toxicity of carbon nanotubes and asbestos—similarities and differences. *Adv. Drug Deliv. Rev*., **65**, 2078–2086.

Duling, M.G., Stefaniak, A.B., Lawrence, R.B., Chipera, S.K. and Virji, M.A. (2012): Release of beryllium from mineral ores in artificial lung and skin surface fluids. *Environ Geochem Health*, **34**, 313–322.

Economou, E.D., Vaimakis, T.C. and Papmichael, E.M. (2002): The kinetics of dissolution of the carbonate minerals phosphate ore using dilute acetic acid solutions, the case of pH-range from 3.96 to 6.40. *Journal of Colloid Interface Science*, **245** (1), 133–41.

Fedunik-Hofman, L., Bayon, A. and Donne, S.W. (2019): Kinetics of Solid-Gas Reactions and Their Application to Carbonate Looping Systems. *Energies*, **12**, 2981.

Fubini, B. and Otero-Arèan, C. (1999): Chemical aspects of the toxicity of inhaled mineral dusts. *Chemical Society Reviews,* **28**, 373-381.

Gafney, S. H., Grespin, M., Garnick, L., Drechsel, D.A., Hazan, R., Paustenbach, D.J. and Simmons, B.D. (2017): Anthophyllite asbestos: state of the science review. *J. App. Toxicol.*, **37**, 38–49.

Gharabaghi, M., Noaparast, M. and Irannajad, M. (2009): Selective leaching kinetics of lowgrade calcareous phosphate ore in acetic acid. *Hydrometallurgy*, **95**, (3), 341–345.

Ghassa, S., Noaparast, M., Shafaei, S.Z., Abdollahi, H., Gharabaghi, M. and Borumand, Z. (2017): A study on the zinc sulphide dissolution kinetics with biological and chemical ferric reagents. *Hydrometallurgy*, **171**, 362–373.

Ghaffari, M., Ehsani, M., Khonakdar, H.A., Assche, G.V. and Terryn, H. (2012): The kinetic analysis of isothermal curing reaction of an epoxy resin-glass flake nanocomposite. *Thermochimica Acta*, **549**, 81–86.

Gouda, R., Baishya, H. and Qing, Z. (2017): Application of Mathematical Models in Drug Release Kinetics of Carbidopa and Levodopa ER Tablets. *Journal of Develop Drugs*, **6** (2), 171.

Grenman, H., Salmi, T. and Murzin, D.Y. (2011): Solid-liquid reaction kinetics – experimental aspects and model development. *Reviews in Chemical Engineering*, **27**, 53–77.

Giuseppe, D.D. (2020): Characterization of Fibrous Mordenite: A First Step for the Evaluation of Its Potential Toxicity. *Crystals*, **10** (769), 1 – 15. doi:10.3390/cryst10090769.

Guthrie, G.D. (1997): Mineral Properties and their Contributions to Toxicity. *Environmental Health Perspectives*, **105** (5), 1003 – 1011.

Grenman, H., Salmi, T. and Murzin, D.Y. (2011): Solid-liquid reaction kinetics - experimental aspects and model development. *Rev Chem Eng*, **27**, 53–77.

Gualtieri, A.F. (2017): Introduction. In A.F. Gualtieri, Ed., Mineral fibres: Crystal chemistry, chemical physical properties, biological interaction, and toxicity. Vol. 18, pp. 1–15. European Mineralogical Union and the Mineralogical Society of Great Britain & Ireland, UK.

Gualtieri, A.F. (2018): Towards a quantitative model to predict the toxicity/pathogenicity potential of mineral fibres. *Toxicology and Applied Pharmocology*, **361**, 89–98.

Gualtieri, A.F., Andreozzi, G.B., Tomatis, M. and Turci, F. (2019): Iron from a geochemical viewpoint. Understanding toxicity/pathogenicity mechanisms in iron-bearing minerals with a special attention to mineral fibres. *Free Radical Biology and Medicine*, **133**, 21–37.

Gualtieri, A.F., Lusvardi, G., Zoboli, A., Di Giuseppe, D. and Gualtieri, M.L. (2019): Bio-durability and release of metals during the dissolution of chrysotile, crocidolite and fibrous erionite. *Environmental Research*, **171**, 550–557.

Gualtieri, A.F., Mossman, B.T. and Roggli, V.L. (2017): Towards a general model to predict the toxicity and pathogenicity of mineral fibres. In: Gualtieri, A.F. (Ed.), Mineral Fibres: Crystal Chemistry, Chemical-physical Properties, Biological Interaction and Toxicity.
European Mineralogical Union, London, pp. 17–64.

Gualtieri, A.F., Pollastri, S., Gandolfi, N.B. and Gualtieri, M.L. (2018): In vitro acellular dissolution of mineral fibres: A comparative study. *Science Reports*, **8**, 7071.

Gualtieri, A.F., Viani, A., Sgarbi, G. and Lusvardi, G. (2012): In vitro bio-durability of the product of thermal transformation of cement–asbestos. *Journal of Hazardous Materials*, **205–206**, 63–71.

Guldberg, M., Christensen, V.R., Perander, M., Zoitos, B., Koenig, A.R. and Sebastian, K. (1998): Measurement of in vitro fibre dissolution rate at acidic ph. *Annual Occupational Hygiene*, **42**, 233–243.

Gunter, M.E., Belluso, E. and Mottana, A. (2007): Classification of the amphiboles. In F.C. Hawthorne, R. Oberti, G.D. Ventura, and A. Mottana, Eds., Amphiboles: Crystal Chemistry, Occurrence, and Health Issues, 67, p. 453–516. Reviews in Mineralogy and Geochemistry, Mineralogical Society of America, Chantilly, Virginia.

Harper, M. (2008): 10$^{th}$ Anniversary critical review: Naturally occurring asbestos. *Journal of Environmental Monitoring*, **10**, 1394-1408.

Ho, C.M., Yau, S.K.W., Lok, C.N., So, M.H. and Che, C.M. (2010): Oxidative dissolution of silver nanoparticles by biologically relevant oxidants: a kinetic and mechanistic study. *Chemistry - an Asian Journal*, **5**, 285–293.

Ho, C.P., Hseu, Z.Y., Chen, N.C. and Tsai, C.C. (2013): Evaluating heavy metal concentration of plants on a serpentine site for phytoremediation applications. *Environ Earth Sci*, **70**, 191–199.

Holdren, G. R., Jr. and Berner, R. A. (1979): Mechanism of feldspar weathering — Experimental studies. *Geochimica et Cosmochimica Acta*, **43**, 1161-1171.

Holdren, Jr., G.R. and Adams, J.E. (1982): Parabolic dissolution kinetics of silicate minerals: An artifact of nonequilibrium precipitation processes? *Geology*, **10**, 186 – 190.

Huang, W. H. and Kiang, W. C. (1972): Laboratory dissolution of plagioclase feldspars in water and organic acids at room temperature. *American Mineralogist*, **57**, 1849-1859.

Hume, A. and Rimstidt, J.D. (1992): The bio-durability of chrysotile asbestos. *American Mineralogy,* **77**, 1125–1128.

Jin, D., Yu, X., Yue, L. and Wang, L. (2009): Decomposition kinetics study of AlOOHcoated calcium carbonate*. Materials Chemistry and Physics*, **115** (1), 418–422.

Johnson, N.M. and Fegley Jr., B. (2000): Water on Venus: new insights from tremolite decomposition. *Icarus* ,**146**, 301–306.

Johnson, N.M. and Fegley Jr., B. (2003): Longevity of fluorine-bearing tremolite on Venus. *Icarus*, **165**, 340–348.

Khawam, A. and Flanagan, D. (2006): Solid-state kinetic models: basics and mathematical fundamentals. *Journal of Physical Chemistry B*, **110** (35), 17315–17328.

Kierzkowska, A.M., Pacciani, R. and Müller, C.R. (2013): CaO-based CO2 sorbents: From fundamentals to the development of new, highly effective materials. *ChemSusChem*, **6**, 1130–1148.

Koleini, S.M.J., Jafarian, M., Abdollahy, M. and Aghazadeh, V. (2010): Galvanic leaching of chalcopyrite in atmospheric pressure and sulphate media: Kinetic and surface studies. *Industrial and Engineering Chemistry Research*, **49** (13), 5997–6002.

Lange, A.M. (1974): Approaches and Constraints to Identification and Quantitation of Asbestos Fibres. *Environmental Health Perspectives*, **9**, 133-136.

Levenspiel, O. (1972): Chemical Reaction Engineering, second ed. Wiley, New York.

Levenspiel, O. (1999): Chemical Reaction Engineering. John Wiley & Sons.

Li, Z., Xie, Z., Deng, J., He, D., Zhao, H. and Liang, H. (2021): Leaching Kinetics of Rare Earth Elements in Phosphoric Acid from Phosphate Rock. *Metals*, **11**, 239.

Lundborg, M., Johard, U., Johansson, A., Eklund, A., Falk, R., Kreyling, W. and Camner, P. (1995): Phagolysosomal morphology and dissolution of cobalt oxide particles by human and rabbit alveolar macrophages. *Exp. Lung Res*., **21**, 51–66.

Liddell, K.C. (2005): Shrinking core models in hydrometallurgy: what students are not being told about the pseudo-steady approximation. *Hydrometallurgy*, **79**, 62–68.

Liu, B., van Gerwen, M., Bonassi, S. and Taioli, E. (2017): Epidemiology of Environmental Exposure and Malignant Mesothelioma. *Journal of Thoracic Oncology*, **12** (7), 1031-1045.

Liu, J. and Hurt, R.H. (2010): Ion release kinetics and particle persistence in aqueous nano silver colloids. *Environmental Science Technology*, **44**, 2169–2175.

Liu, J., Sonshine, D.A., Shervani, S. and Hurt, R.H. (2010): Controlled release of biologically active silver from nano silver surfaces. *ACS Nano*., **4**, 6903–6913.

Liu, J., Tian, S.P., Li, B.Q. and Qin, G.Z. (2009): Enhancing viability of two biocontrol yeasts in liquid formulation by applying sugar protectant combined with antioxidant. *Biological Control,* **54**, 817–824.

Lucci, F., Della Ventura, G., Conte, A., Nazzari, M. and Scarlato, P. (2018): Naturally occurring asbestos (NOA) in granitoid rocks, a case study from Sardinia (Italy). *Minerals*, **8**, 442.

Lucci, F., Ventura, G.D., Conte, A., Nazzari, M. and Scarlato, P. (2018): Naturally Occurring Asbestos (NOA) in Granitoid Rocks, A Case Study from Sardinia (Italy). *Minerals*, **8** (442), 1 - 23.

Lund, L.G. and Aust, A.E. (1990): Iron mobilisation from asbestos by chelators and ascorbic acid. *Archives, Biochemistry, Biophysics*, **278**, 60– 64.

Ma, L., Brow, R.K. and Schlesinger, M.E. (2017): Dissolution behaviour of Na2O–FeO– Fe2O3–P2O5 glasses. *Journal of Non-Crystalline Solids*, **463**, 90–101.

Ma, X. H., Yuan, W.B., Bell, S.E.J. and James, S.L., (2014): Better understanding of mechanochemical reactions: Raman monitoring reveals surprisingly simple 'pseudo-fluid' model for a ball milling reaction. *Chemical Communications*, **50** (13), 1585-1587.

McDonald, A., McDonald, J. and Pooley, F. (1982): Mineral fibre content of lung in mesothelial tumours in North America. *Ann Occup Hyg*, **26**, 417–422.

McDonald, J. and McDonald, A. (1997): Chrysotile, tremolite and carcinogenicity. *Annuals of Occupational Hygiene*, **41**, 699–705.

Meulenkamp, E.A. (1998): Size dependence of the dissolution of ZnO nanoparticles. *Journal of Physical Chemistry B*., **102**, 7764–7769.

Muhle, H. and Bellmann, B. (1997): Significance of the bio-durability of man-made vitreous fibres to risk assessment. *Environmental Health Perspectives*, **105**, 1045.

McClellan, R.O. and Hesterberg, T.W. (1994): Role of biopersistence in the pathogenicity of man-made fibres and methods for evaluating bio-persistence: a summary of two round-table discussions. *Environ Health Perspect*, **102** (Suppl 5), 277-283.

Moss, O. R. and Kanapilly, G.M. (1980): Dissolution of inhaled aerosols. In K. Willeke (Ed.), Generation of aerosols and facilities for exposure experiments (pp. 105–124). Ann Arbor: Ann Arbor Science Publishers Inc.

Mulak, W., Miazga, B. and Szymczycha, A. (2005): Kinetics of nickel leaching from spent catalyst in sulphuric acid solution. *Int. J. Miner. Process*., **77**, 231–235.

Oberdörster, G., Maynard, A., Donaldson, K., Castranova, V., Fitzpatrick, J., Ausman, K., Carter, J., Karn, B., Kreyling, W., Lai, D., Olin, S., Monteiro-Riviere, N., Warheit, D. and Yang, H. (2005): Principles for characterizing the potential human health effects from exposure to nanomaterials: elements of a screening strategy. *Particle and Fibre Toxicology*, **2**, 8.

Ozawa, T. (2000): Thermal analysis - review and prospect. *Thermochimica Acta*, **335**, 35-42.

Oze, C. and Solt, K.L. (2010): Bio-durability of chrysotile and tremolite asbestos in simulated lung and gastric fluids. *American Mineralogist*, **95**, 825–831.

Paces, T. (1973): Steady-state kinetics and equilibrium between groundwater and granitic rock. *Geochimica et Cosmochimica Acta*, **37**, 2641-2663.

Paces, T. (1978): Reversible control of aqueous aluminum and silica during the irreversible evolution of natural waters. *Geochimica et Cosmochimica Acta*, **42**, 1487-1493.

Pecina, T., Franco, T., Castillo, P. and Orrantia, E. (2007): Leaching of zinc concentrate in H2SO4 solutions containing H2O2 and complexing agents. *Miner. Eng*., **21**, (1), 23–30.

Pacella, A., Ballirano, P., Fantauzzi, M., Rossi, A., Nardi, E., Capitani, G., Arrizza, L. and Montereali, M.R. (2021): Surface and bulk modifications of amphibole asbestos in mimicked gamble's solution at acidic PH. *Scientific Reports*, **11**, 14249.

Plumlee, G.S. (1999): The Environmental geology of mineral deposits. In Plumlee, G.S. and Logsdon, M.J. (eds.) The Environmental Geochemistry of Mineral Deposits: Processes, Techniques and Health Issues. *Reviews in Economic Geology*, **6A**, 71-116.

Plumlee, G.S., Morman, S.A. and Ziegler, T.L. (2006) The toxicological geochemistry of earth minerals: An overview of processes and the interdisciplinary methods used to understand

them. In N. Sahai and M.A.A. Schoonen, Eds., Medical Mineralogy and Geochemistry, 64, p. 5–57. Reviews in Mineralogy and Geochemistry, Mineralogical Society of America, Chantilly, Virginia.

Plumlee, G.S., Morman, S.A. and Ziegler, T.L. (2006): The toxicological geochemistry of earth minerals: An overview of processes and the interdisciplinary methods used to understand them. *Reviews in Mineralogy and Geochemistry*, **64**, 5–57.

Prosser, A.L. (1996): Review of uncertainty in the collection and interpretation of leaching data. *Hydrometallurgy*, **41**, 119- 153.

Roman, R.J., Benner, B.R. and Becker, G.W. (1974): Diffusion model for heap leaching and its application to scale-up. *Transactions of the Society of Mining Engineers, AIME*, **256** (3), 247–252.

Ross, G.J. (1967): Kinetics of acid dissolution of an orthochlorite mineral. *Canadian Journal of Chemistry,* **45**, 3031.

Rozalen, M. and Huertas, F.J. (2013): Comparative effect of chrysotile leaching in nitric, sulfuric, and oxalic acid at room temperature. *Chemical Geology,* **352**, 134 – 142.

Rozalen, M., Ramos, M.E., Gervilla, F., Kerestedjian, T., Fiore, S. and Huertas, F.J. (2014): Dissolution study of tremolite and anthophyllite: pH effect on the reaction kinetics. *Applied Geochemistry*, **49**, 46 – 56.

Rozalen, M., Ramos, M.E., Huertas, J., Fiore, S. and Gervilla, F. (2013): Dissolution kinetics and bio-durability of tremolite particles in mimicked lung fluids: Effect of citrate and oxalate. *Journal of Asian Earth Sciences*, **77**, 318–326.

Schmidt, J. and Vogelsberger, W. (2006): Dissolution kinetics of titanium dioxide nanoparticles: the observation of an unusual kinetic size effect. *Journal of Physical Chemistry B.*, **110**, 3955–3963.

Sengul, H., Ozer, A.K. and Gulaboglu, M.S. (2006): Benefication of Mardin Mazidagi (Turkey) calcareous phosphate rock using dilute acetic acid solutions. *International Journal of Mineral Processes*, **30**, 113–25.

Sevim, F., Sarac, H. and Yartasi, A. (2003): Dissolution kinetics of phosphate ore in H2SO4 solutions. *Industrial and Engineering Chemistry Research*, **42**, 2052–2057.

Stanton, M.F., Layard, M., Tegeris, A., Miller, E., May, M., Morgan, E. and Smith, A. (1981): Relation of particle dimension to carcinogenicity in amphibole asbestoses and other fibrous minerals. *J. Natl. Cancer Inst*., **67**, 965–975.

Sun, P., Grace, J.R., Lim, C.J. and Anthony, E.J. (2008): Determination of intrinsic rate constants of the CaO-CO2 reaction. *Chemical Engineering Sciences*, **63**, 47–56.

Taunton, A.E., Druschel, G.K., Gunter, M.E. and Wood, S.A. (2010): Geochemistry in the lung: reaction-path modelling and experimental examinations of rock-forming minerals under physiologic conditions. *American Mineralogy*, **95** (11–12), 1624 - 1635.

Terry, B. (1983a): The acid decomposition of silicate minerals Part II. Hydrometallurgical applications. *Hydrometallurgy*, **10**, 151–171.

Terry, B. (1983b): Specific chemical rate constants for the acid dissolution of oxides and silicates. *Hydrometallurgy*, **11**, 315–344.

Truesdale, V.W. (2007): Batch Dissolution Kinetics: The Shrinking Sphere Model with Salts and Its Potential Application to Biogenic Silica. *Aquatic Geochem*, **13**, 267–287.

Turci, F., Favero-Longo, S. E., Tomatis, M., Martra, G., Castelli, D., Piervittori, R. and Fubini, B. (2007): A biomimetic approach to the chemical inactivation of chrysotile fibres by lichen metabolites. *Chemistry*, **13**, 4081–4093.

Turci, F., Tomatis, M., Lesci, I.G., Roveri, N. and Fubini, B. (2011): The iron-related molecular toxicity mechanism of synthetic asbestos nano fibres: a model study for high-aspect-ratio nanoparticles. *Chemistry - A European Journal*, **17**, 350–358.

Turci, F., Tomatis, M., Mantegna, S., Cravotto, G. and Fubini, B. (2007): The combination of oxalic acid with power ultrasound fully degrades chrysotile asbestos fibres. *Journal of Environmental Monitoring*, **9**, 1064–6.

Turci, T., Tomatis, M. and Pacella, A. (2017): Surface and bulk properties of mineral fibres relevant to toxicity. *European Mineralogical Union Notes in Mineralogy,* **18**, 171 – 214.

Um, N. (2017): Hydrometallurgical Recovery Process of Rare Earth Elements from Waste: Main Application of Acid Leaching with Devised τ-T Diagram, in: J.E.A. Orjuela (Ed.), Rare Earth Element, IntechOpen, pp. 41–60.

Utembe, W., Potgieter, K., Stefaniak, A.B. and Gulumian, M. (2015): Dissolution and bio-durability: Important parameters needed for risk assessment of nanomaterials. *Particle and Fibre Toxicology*, **12**, 11.

van Oss, C.J., Naim, J.O., Costanzo, P.M. Jr., Giese, R.F., Wu, W. and Sorling, A.F. (1999): Impact of different asbestos species and other mineral particles on pulmonary pathogenesis. *Clays and Clay Minerals*, **47**, 697–707.

Virta, R.L. (2002): **Asbestos: Geology, Mineralogy, Mining and Uses.** Reston, VA: US Geological Survey.

Vyazovkin, S. and Wight, C.A. (1997): Kinetics in solids. *Annual Reviews in Physical Chemistry*, **48**, 125–149.

Vyazovkin, S., Burnham, A.K., Criado, J.M., Maqueda, L.A.P., Popescu, C. and Sbirrazzuoli, N. (2011): ICTAC Kinetics Committee recommendations for performing kinetic computations on thermal analysis data. *Thermochim Acta*, **520**, 1–19.

Wahab, S.A., Rezik, A., Abdelaal, H., Khoziem, A., Khalid, E. and Abdellah, W. (2019): Kinetics of uranium carbonate leaching process from carbonaceous shale, southwestern Sinai, Egypt. *Euro-Mediterranean Journal for Environmental Integration*, **4**, 19.

Walton, W.H. (1982): The nature, hazards, and assessment of occupational exposure to airborne asbestos dust: a review. *Ann Occup Hyg*, **25**, 117–247.

Weisener, C.G., Smart, R.St.C. and Gerson, A.R. (2004): A comparison of the kinetics and mechanism of acid leaching of sphalerite containing low and high concentrations of iron. *Int. J. Miner. Process*., **74**, 239–249.

Wollast, R. (1967): Kinetics of the alteration of K-feldspar in buffered solutions at low temperature. *Geochimica et Cosmochimica Acta*, **31**, 635-648.

Wu, C.H., Wood, T.K., Mulchandani, A. and Chen, W. (2006): Engineering plant–microbe symbiosis for rhizoremediation of heavy metals. *Appl. Environ. Microbiol*, **72**, 1129–1134.

Wu, L., Jacobson, A.D., Chen, H.C. and Hausner, M. (2007): Characterization of elemental release during microbe–basalt interactions at T = 28°C. *Geochimica et Cosmochimica Acta*, **71**, 2224–2239.

Wu, S., Liu, Y., Southam, G., Robertson, L., Chiu, T.H., Cross, A.T., Dixon, K.W., Stevens, J.C., Zhong, H., Chan, T-S., Lu, Y-J. and Huang, L. (2019): Geochemical and mineralogical constraints in iron ore tailings limit soil formation for direct phytostabilization. *Science of the Total Environment*, **651**, 192–202.

Yang, S., Du, W., Shi, P., Shangguan, J., Liu, S., Zhou, C., Chen, P., Zhang, Q. and Fan, H. (2016): Mechanistic and Kinetic Analysis of Na2SO4-Modified Laterite Decomposition by Thermogravimetry Coupled with Mass Spectrometry. *PLoS ONE*, **11** (6), e0157369.

Yao, F., Wu, Q., Lei, Y., Guo, W. and Xu, Y. (2008): Thermal decomposition kinetics of natural fibres: Activation energy with dynamic thermogravimetric analysis. *Polymer Degradation and Stability*, **93**, 90 – 98.

# Chapter 4 - Preliminary characterisation of the mineralogical and microbiological constraints of banded-iron formation hosted asbestos mine dumps as substrates for the long-term revegetation and phyto-stabilisation by native plant species

Abstract

The aim of the study is to obtain information of the preliminary status of the mineralogical and microbiological conditions of derelict banded iron formation-hosted asbestos mine rock wastes in South Africa and use these baseline data sets to evaluate the appropriateness of the current rehabilitation methods. We demonstrate, using cost-effective and easily accessible analytical methods as required in capital-restricted developing countries, that current asbestos mine dump rehabilitation methods are unsuitable and non-progressive. The results of this preliminary study show that the natural habitat of the native plant species used to revegetate banded-iron formation hosted asbestos mine dumps is acidic, biologically active, highly weathered ancient soils, and hence their establishment and growth on the alkaline, biologically inert, un-weathered, poly-mineral, heterogeneous rock wastes and post-mining asbestos landforms is incipiently compromised and, in all probability, impermanent. These conditions of the substrate after rehabilitation pose a major constraint to the long-term, sustainable ecological restoration on postmining landforms of derelict asbestos mine sites. Therefore, the regulatory aims and objectives outlined by the Department of Minerals and Resources (DMR) are violated and lives are endangered. The lack of baseline data sets, literature, and research regarding the suitability of these sites, in terms of substrates for native plant revegetation, questions the benevolence of taxpayer-capitalised, governmentally managed rehabilitation practices in South Africa.

## 4.1. Introduction

Although asbestos mining has been banned for many years and its exploitation is no longer profitable, the decommissioned reserves and rock-wastes around discontinued mines present a long-standing threat and repeatedly generates environmental impairment. Derelict

asbestos mines and their associated wastes pose numerous health and environmental risks and are required by legislation to be rehabilitated. The 'rehabilitation industry' in South Africa commonly practises vegetation establishment primarily aimed to generate surface stability and secondarily to re-establish and return the site to a functional and sustainable ecosystem. The rehabilitation strategies implemented to address asbestos-related environmental pollution in South Africa have proven, in large, ineffective, and unsustainable in the long term. Improved, sustainable and long-term solutions are thus required to mitigate the risk of chronic exposure and eliminate or detoxify the deadly contaminant from or in the environment. A key challenge in asbestos mine rehabilitation is successfully establishing self-sustaining plant cover on the mine dumps, tailings, and the surrounding disturbed areas. The poor and sparse vegetation establishment, development and cover are observable outcomes characterising the rehabilitated asbestos mine dumps in South Africa (Mendez and Maier, 2008a, b; Matsabatsa, 2009; Liebenberg-Weyers, 2010; Sheoran *et al.*, 2013; Schimmer, 2017).

The soil remediation approach adopted for DAML rehabilitation at present involves methods that focus on ameliorating the chemical impediments of the soluble phase without considering the waste rock itself as a perpetual source of unfavourable and plant-restricting factors. The inability of this conventional rehabilitation approach to overcome the mineralogical and geochemical barriers in mine dumps makes it unsuitable for long-term, self-sustaining rehabilitation and restoration aspirations. The asbestos mine dumps and tailings must be reconceptualised as artificially constructed parent materials of geological emergence for the subsequent formation of soil (Li and Huang, 2015). In this study it is argued that to achieve successful rehabilitation, management, and monitoring of abandoned asbestos mine sites, the inclusion of mineralogical and microbiological characterisation of rock-wastes and predictions on their long-term behaviour and stability is imperative.

Mineralogical and microbiological characterisation of asbestos mine waste rocks and mine dumps are important to directing rehabilitation interventions (Higueras *et al.,* 2012). To establish an acceptable environment for sufficient plant cover, these parameters must be meticulously examined (Plumlee, 1999; Tordoff *et al.,* 2000). However, the costs involved in these assessments are a major issue for developing countries (Higueras *et al.,* 2012). The aim of this paper is to use cost effective mineralogical and microbiological methods to demonstrate the paramount insight provided to and the importance of incorporating

geological- and microbiological-based baseline data sets to derelict asbestos mine site rehabilitation programmes. This chapter highlights the necessity of mineralogical and microbiological data in the context of asbestos mine reclamation by emphasising its benefits and indicating its possibility in fund-limited, developing countries by using relevant scientific methods that are also cost-effective, relatively rapid, and easily accessible.

## 4.2. Materials and methods

### 4.2.1. Sample location and collection

Two different BIF-hosted asbestos rock samples were investigated in this study (table 4.1), namely: (i) Amosite from Penge, Lydenberg District, South Africa (figure 4.1) and (ii) crocidolite from Prieska Division, Northern Cape, South Africa (figure 4.2).

Table 4.1: Location co-ordinates and description of sampling locations

| | BIF hosted amosite mine rock waste | BIF hosted crocidolite mine rock waste |
|---|---|---|
| | | |
| Sampling location | Penge, Sekhukhune District, Limpopo, South Africa | Prieska Division, Northern Cape, South Africa |
| Location coordinates | 24°25’07’’S 30°20’14’’E | 28°19’01’’S 23°06’05’’E |
| Climate | Sub-tropical | Semi-arid |
| Biome | Savanna | Savanna |
| Occurrence | Cross-fibre seams in banded ironstones | Cross-fibre seams in banded ironstones |
| Number of samples | 2 | 2 |

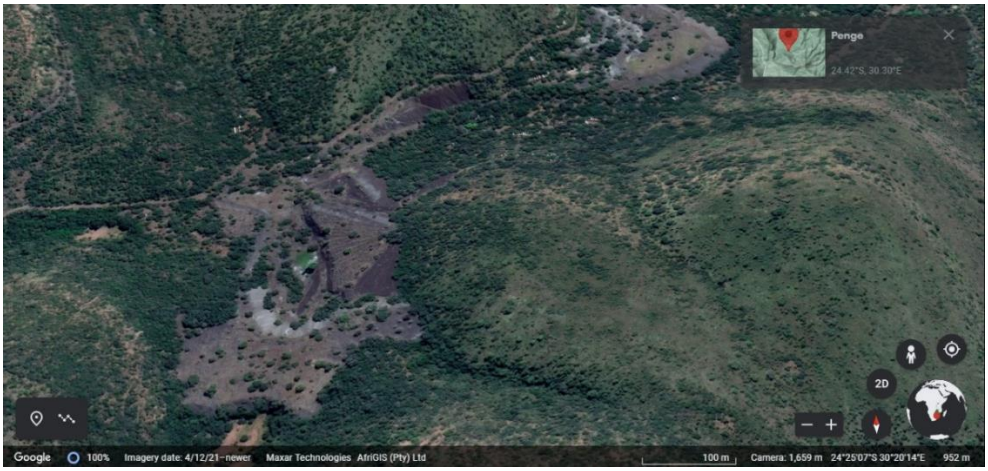


Figure 4.1: Google Earth image showing derelict amosite mine, Penge, Limpopo.




Figure 4.2: Google Earth image showing derelict crocidolite mine, Postmasburg, Northern Cape. Notice the blue colour of the crocidolite.

These mineral deposit sites were characterised in terms of their important geological characteristics (table 4.2).

Table 4.2: Description of the banded-iron formation-hosted amosite and crocidolite asbestos deposits in South Africa

| **Mineral deposits** | **Banded-iron formation – hosted amosite asbestos deposits** | **Banded-iron formation – hosted crocidolite asbestos deposits** |
|---|---|---|
| | | |
| **Host rocks** | Precambrian metamorphosed sedimentary banded iron formations | Precambrian metamorphosed sedimentary banded iron formations |
| **Ore** | Amosite (iron-magnesium silicate) | Crocidolite (complex sodium iron silicate) |
| **Nature of ore** | Seams of cross-fibre veins interbedded within alternating iron-rich and chert bands [1] | Seams of cross-fibre veins interbedded within alternating iron-rich and chert bands [1] |
| **Gangue mineralogy** | Quartz<br>Oxide facies: magnetite and hematite<br>Carbonate facies: calcite, siderite, dolomite<br>Sulphide facies: pyrite<br>Silicate facies: minnesotaite, stilpnomelane | Quartz<br>Oxide facies: magnetite and hematite<br>Carbonate facies: calcite, siderite, dolomite<br>Sulphide facies: pyrite<br>Silicate facies: stilpnomelane |
| **Secondary mineralogy** | Iron oxide minerals to iron hydroxide minerals<br>Iron silicate minerals to clay and iron hydroxide minerals | Iron oxide minerals to iron hydroxide minerals<br>Iron silicate minerals to clay and iron hydroxide minerals |
| **Deposit trace element geochemistry** | Apart from iron and silica, low abundances of other elements. | Apart from iron and silica, low abundances of other elements. |
| | | |
| Refs: [1] Hart, 1998 | | |

Bulk samples of banded iron formation-hosted amosite and crocidolite mine waste rocks were collected from mine dumps in Limpopo and the Northern Cape, respectively. A stainless-steel scoop was used to collect rock samples exposed at the surface of the mine dumps. The exposed asbestos-bearing rocks were not covered by soil and/or vegetation.

### 4.2.2. Mineralogical characterisation and paste pH-conductivity 1:10 (w/w)

The mineralogical characterisation was done using hand sample identification and referring to the XRD analysis in chapter 2. The pH-conductivity was determined using a paste of 1:10 (w/w). In 20 mL disposable tubes, 1 gram of each waste rock sample was added to 10 mL of de-ionised waster to make a 1:10 solution. The solutions were then agitated for 30 minutes on a reciprocating shaker and then left to stand. The pH and EC meters were calibrated using 4, 7 and 10 pH buffer solutions and temperature, respectively. The pH and EC were measured after 2 hours following agitation and paste pH-conductivity measurements were done in triplicate for each rock waste sample. The samples' immediate alkalinity or

acidity was determined using the paste pH-conductivity method and thus reflects the current geochemical conditions of the asbestos mine rock waste.

4.2.3. Analysis of asbestos mine waste microbial community by culture-dependent method

Rock samples were crushed into a homogeneous powder using a sterile disk mill and the powdered sample form was used in the microbiological and molecular analyses. The powdered samples do not allow for differentiation between surface and interior parts. Bacteria and fungi were isolated from the naturally occurring asbestos rock samples by a modified 'soil dilution plate' technique. All contamination-sensitive procedures were performed inside a laminar flow hood and sterile techniques were used throughout the process. For the isolation of culturable bacteria and fungi, 1 gram of powdered rock samples was taken and suspended in a test tube containing 9 mL of sterile saline solution (0.9 % w/v NaCl). The rock samples were vortexed for 10 minutes to extract lithic micro-organisms from the rock. For serial dilutions 1 mL of the suspended rock samples was added to 9 mL of sterile saline solution (0.9 % w/v NaCl) to make 1 in 10 dilution ($10^{-1}$), then 1 mL of this dilution was added to 9 mL sterile saline solution (0.9 % w/v NaCl) to make 1 in 100 dilution ($10^{-2}$). This procedure was repeated once more to reach a final $10^{-3}$ dilution. For the isolation of lithic bacteria and fungi, LB and nutrient agar, and potato dextrose and Sabauraud dextrose agar were used respectively (figure 4.3).

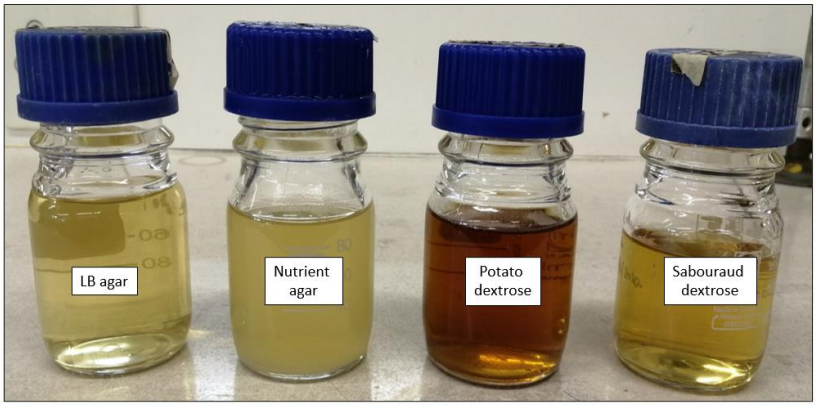


Figure 4.3: Bacterial and fungal media used for culture-dependent microbial analysis

The LB agar was prepared by mixing 5 g tryptone, 2.5 g yeast extract, 5 g sodium chloride and 7.5 g agar in distilled water to make up a 500 ml LB (agar) medium, which was then autoclaved at 121°C for 15 minutes. Nutrient agar was made from 5 g peptone, 1.5 g yeast extract, 1.5 g beef extract, 5 g sodium chloride, 15 g agar and 1 L distilled water. The LB and nutrient agar medium were allowed to cool before being poured into petri dishes (~20 ml) and left to set. The potato dextrose agar was prepared by mixing 2 g potato infusion, 10 g dextrose and 7.5 g agar to distilled water to make up a 500 ml potato dextrose (agar) medium. Sabouraund dextrose was made from 40 g dextrose (glucose), 10 g mycological peptone, 15 g agar and 1 L distilled water. Each of the media was autoclaved (20 mins at 120 °C) and allowed to cool before being poured into petri dishes. Triplicate samples of 100 µl of each dilution were spread onto agar plates for microbial counts. The plates were incubated at 37°C for bacteria and 25°C for fungi until colonies appeared. The appearance of colonies for bacterial cultures is expected within 1 to 3 days, whereas fungal cultures may be incubated for up to 10 days. Plates were monitored after 24 h and then daily for bacterial cultures, and fungal counts were monitored every 48 hours following the appearance of colonies.

### 4.2.4. Analysis of asbestos mine waste microbial community by culture-independent method

To encourage microbial growth for genomic DNA extraction, 1 gram of powdered asbestos rock waste was added into 10 mL of sterile Luria-Bartani (LB) broth in a 20 ml glass test tube. This was performed in triplicate for each sample. Additionally, microbial enrichment was also done for the non-powdered material (i.e., mineral fibres) (figure 4.4).

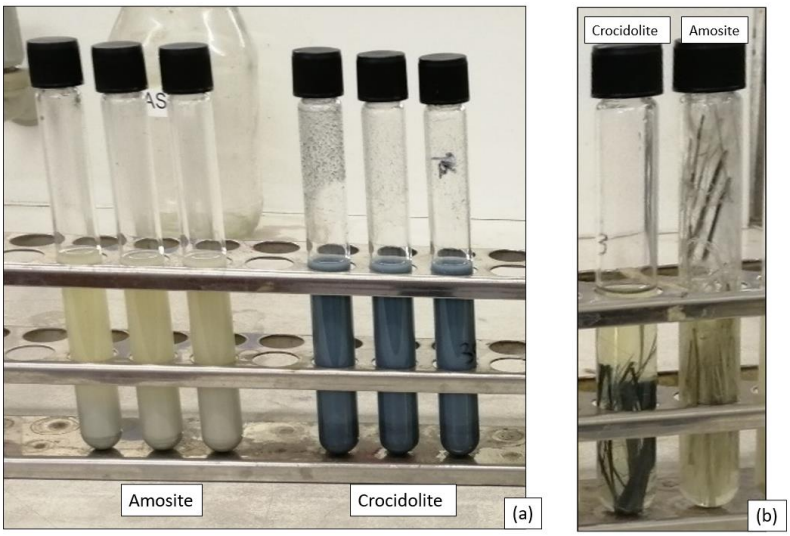


Figure 4.4: Microbial enumeration in LB broth for (a) powdered asbestos rock material and (b) asbestos mineral fibres

Each suspension was vortexed for 10 seconds and incubated at 37°C in a shaking incubator (100 rpm) for 24 hours. 1.5 ml of each culture was transferred to sterile Eppendorf tubes and subsequently centrifuged at 10 000 rpm for 5 minutes. The supernatants were discarded, and cells were resuspended in 650 µl of TE buffer (Tris/Acetic acid/EDTA). Total DNA was extracted from each microbial suspension using the ZR Soil Microbe DNA Kit Miniprep™ (Zymo Research, Irvine, CA, USA) (ZR kit) (figure 4.5).




Figure 4.5: ZR Soil Microbe DNA Kit Miniprep™ (Zymo Research, Irvine, CA, USA) (ZR kit)

This method is based on direct cell lysis and subsequent recovery and purification of nucleic acids. Approximately 250 mg of each type of asbestos fibre was weighed out and added to their individual ZR BashingBead™ Lyses tube. The DNA extraction was performed according to the manufacturer's instructions. Extractions were carried out in triplicate on all samples. The DNA concentration (ng/ml) was assessed by a Qubit 2.0 Fluorometer (figure 4.6). The Qubit® assay uses an ultrasensitive fluorescent nucleic acid stain to quantify double-stranded DNA (Invitrogen, 2010).

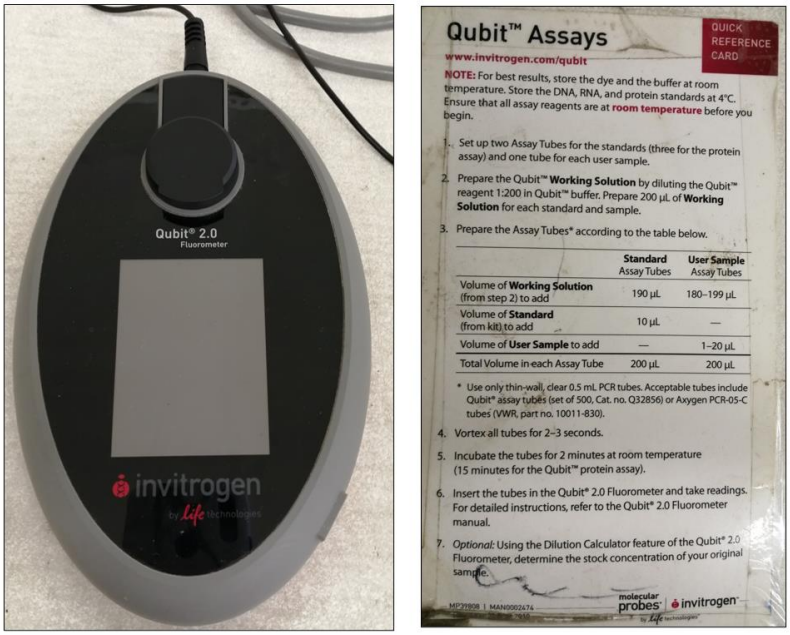


Figure 4.6: Qubit 2.0 Fluorometer

All the samples, regardless of their DNA concentration, were then subjected to Polymerase Chain Reaction (PCR) analysis. Polymerase chain reaction (PRC) is defined by Atawodi *et al. (*2010) as the '*in vitro* enzymatic amplification of specific DNA sequences (in pure form or complex mixtures) using two oligonucleotide primers that hybridise to opposite strands and flank the region of interest in the target DNA'. Amplification was performed by polymerase chain reaction (PCR) using the following primers: Universal bacterial 16S rRNA primers 8F (5'-AGAGTTTGATCCTGGCTCAG-3') and 1492R (5'-GGTTACCTTGTTACGACTT-3'); yeast primers NL1 (5`-GCATATCAATAAGCGGAGGAAAAG-3`) and NL4 (5`-GGTCCGTGTTTCAAGACGG-3`) and the fungi primers ITS1F (5'-CTTGGTCATTTAGAGGAAGTAA-3') and ITS4 (5'-TCCTCCGCTTATTGATATGC-3'). 36 amplification reactions (12 using the

bacterial primers, 12 using the yeast primers and 12 using the fungi primers) were each carried out in 25 µl volumes containing of 12.5 µl Fermentas Master Mix; 6.5 µl nuclease-free water; 2.5 µl reverse primer; 2.5 µl forward primer and 1µl DNA. The segments of DNA were amplified via the PCR in the laboratory apparatus known as a thermal cycler (figure 4.7).




Figure 4.7: Thermal cycler apparatus used for PCR analysis

The tubes containing the reaction mixtures were placed into the thermal block and the thermal cycler (2720 thermal cycler, Applied Biosystems) was programmed with the following five steps: (1) Initial denaturation at 95°C for 5 minutes; (2) followed by 35 cycles of denaturation (94°C for 30 seconds), (3) annealing (52°C for 30 seconds) and (4) elongation (72°C for 2 minutes) and (5) a final elongation step at 72°C for 5 minutes.

The method of agarose gel electrophoresis separates DNA products based on charge and size (Garibyan and Avashia, 2013). A 1.3% (*w/v*) agarose gel was made by adding 0.65 grams of agarose powder in 50 ml of 1 x Tris-acetate-ethylenediaminetetraacetate (TAE; pH 8) buffer solution. To dissolve the agarose powder, the mixture was heated in a microwave oven until it bubbled, after which it was removed and examined for suspended solids. If solid particles of agarose powder were still observed, the mixture was once again placed into the microwave oven and heated until it boiled. This was repeated until no solid particles of agarose powder remained. The solution was then left at room temperature to cool down.

After cooling, 10 µl of ethidium bromide (EtBr; 1 µl/ml) was added to the liquid gel solution. The solution was then poured into a gel casting tray, which acts as a mould and a comb (i.e., well-forming template) placed across the end of the casting tray. The liquid gel solution was then left to solidify. Following solidification, combs were removed, and the gel was placed into a horizontal gel electrophoresis tank submerged in a 1 x TAE buffer (40 mM Tris, 20 mM acetic acid and 100 mM EDTA pH 8.0) (figure 4.8).

The DNA samples were prepared by thoroughly mixing 5 µl of 6 x Fermentas DNA loading dye with 10 µl of genomic DNA/PRC product on a piece of parafilm and subsequently loaded into the previously formed wells in the solidified agarose gel. A GeneRuler DNA Ladder was also loaded into a well at the edge of the gel. This simultaneously run standardised molecular marker or GeneRuler DNA Ladder is a predetermined set of DNA products that helps determine the size of the product. The electrophoresis apparatus was connected to 100 V of direct current (DC) and the current was applied for 50 minutes.

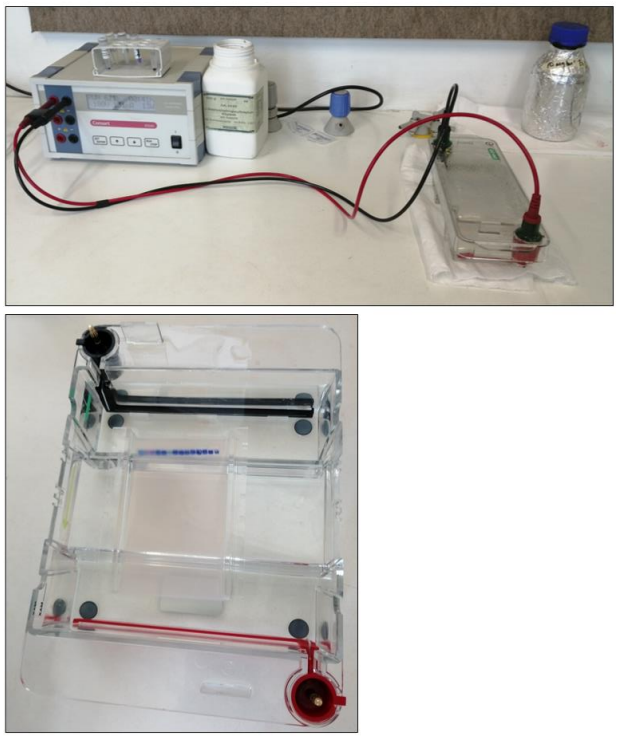

Figure 4.8: Horizontal gel electrophoresis tank

The gels were then placed into a ChemiDoc so that they could be visualised and photographed (figure 4.9).

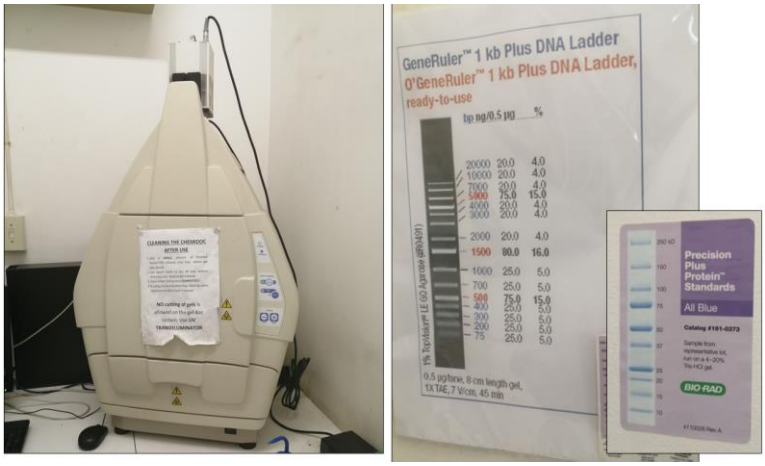


Figure 4.9: Bio-Rad ChemiDoc machine for gel visualisation of DNA

## 4.3. Results

### 4.3.1. Mineralogy, pH and EC

Predictable and important controls are exerted on the signatures of the natural environment by these geological characteristics (Plumlee, 1999). Thus, for effective mine-environment mitigation, prediction, and rehabilitation activities to be developed, a thorough comprehension of mineral deposit environmental geology is required. The mine waste was alkaline and the mineralogy is predominantly iron oxides, quartz, silicates, and carbonates (table 4.3).

Table 4.3: Mineralogical characterisation of asbestos mine waste rock samples

| **Asbestos mine waste** | **Mineral analysis of whole rock waste in hand sample** | **XRD analysis of mineral impurities in fibres extracted from host rock** |
|---|---|---|
| | | |
| Amosite waste rock | Magnetite<br>Hematite<br>Chert (quartz)<br>Carbonate<br>Amosite | Amosite (94.5 %)<br>Quartz low (4.1 %)<br>Sepiolite (1.4 %) |
| Crocidolite waste rock | Magnetite<br>Hematite<br>Chert (quartz) | Magnesio-riebeckite (100 %) |

| | | |
|---|---|---|
| | Carbonate<br>Crocidolite | |
| | | |
| | Amosite rock | Crocidolite rock |
| pH | 9.04 | 9.3 |
| EC (mS/m) | 25.4 | 27.6 |

4.3.2. Culture-dependent methods

The asbestos rock waste samples were screened for bacterial and fungal isolates residing on and within their structure by isolating and plating them on LB agar, nutrient agar, potato dextrose agar and Sabauraud dextrose media. After the appropriate incubation period for each, no growth was observed on the agar plates either bacteria or fungi. Given the dilutions used the results obtained from the plates are given as $< 1 \times 10^4$ CFU/g.

4.3.3. Culture-independent methods

DNA concentration quantification is given in table 4.4. Gel electrophoresis was unsuccessful as extremely blurry banding was visualised and further troubleshooting was ineffective at rectifying these results.

Table 4.4: DNA quantification

| Sample | Number | DNA concentration (ng/ml/DNA) |
|---|---|---|
| | | |
| Am | 1A | 4.12 |
| Am | 1B | 4.94 |
| Am | 1B | 8.79 |
| Cr | 2A | 10.4 |
| Cr | 2B | 9.01 |
| Cr | 2C | --- |

4.4. Discussion

The once prosperous industry of asbestos mining in South Africa has left a legacy of derelict mine sites and mountains of mine rock waste and tailings. In addition, the permanent closure of these mines had subsequent consequences to environmental, health and social and economic aspects as unemployment, asbestos-related diseases and environmental contamination persist (Allen *et al.,* 2018). The rehabilitation of derelict asbestos mine sites, dumps and tailings involved numerous deliberations, such as revegetation issues, health-related risks to asbestos exposure during the process and the high costs of prioritisation, implementation, and monitoring. Understanding the geological deposit and waste material geochemistry allows the formulation of a predictive strategy in which the future geochemical toxicity and ecological and human health risks, if released from their host rocks, may be predicted.

The rehabilitation and ecological restoration of alkaline, amosite and crocidolite mineral mine dumps and tailings represent a significantly large and complex challenge in South Africa. The abandoned asbestos mines and their associated waste rocks, tailings and dumps are host, in addition to asbestos mineral fibres, of a large variety of associated mineral assemblages. The mineralogical and geochemical characteristics of abandoned mine rock wastes are a significant factor for determining the acid-generating or neutralising potential of mine sites (Zhao *et al.,* 2007). Waste rock containing carbonate minerals (e.g., calcite, dolomite etc.), silicate minerals (e.g., chlorite, micas, and amphiboles) and Al and Fe (oxy)hydroxides may undergo acid-consuming reactions (Blowes *et al.,* 2003). Protons are consumed during the dissolution of these minerals and alkalinity is introduced (Amos *et al.,* 2015). In addition to introducing alkalinity by consuming protons, solutes such as Ca, Al, Mn, Mg and Fe are introduced into the leachate at considerably high levels (Plante *et al.,* 2011; Vriens *et al.,* 2019). Sulphide and iron-bearing minerals, susceptible to weathering, generate acid mine drainage (AMD) when exposed to water and oxygen results (Canovas *et al.,* 2007; Zhao *et al.,* 2007). Seepage of this acid water from waste rock dumps and tailings has detrimental effects on soils and water (Dinelli *et al.,* 2008). More so, the formation and drainage of low pH AMD intensifies the solubility of PHEs and mobilises metals, such as Zn, Mo, Al, Fe, Cu, Se and Cd into surrounding soil, surface water and groundwater (Bell and Bullock, 1996; Naicker *et al.,* 2003; Tutu *et al.,* 2008). Natural asbestos deposits are typically associated with elevated concentrations of heavy metals (Hossner and Hons, 1992). The exposed and unmanaged mining wastes generated from asbestos mining operations serve as

a continuous source of potentially hazardous elements (PHEs) (Ogola, 2010). The geochemical and mineralogical characteristics of asbestos-containing waste rock sites allow inferences of the geochemical processes that may occur, and therefore predictions on the subsequent risks to the environment and surrounding inhabitants (Vriens *et al.,* 2020).

Current asbestos mine site rehabilitation methods are conducted emphasising geotechnical and soil remediation solutions with little to no consideration on whether the mine dumps have the capacity for rehabilitation and ecological restoration, despite the return of a self-sustainable, functional environment being outlined as a regulatory requirement in the objectives. Scientific studies form the foundation for solving complex environmental issues, and thus without such studies the very standing of the methods, implementation, management, and monitoring of current asbestos mine reclamation strategies is questionable (Van Druten and Bekker, 2017). Thus, a critical restriction to successfully developing and executing asbestos mine rehabilitation is the disconnect between the scientific community and both industry and governmental sectors. This lack of co-operation indicates that asbestos mine land rehabilitation is constrained by lack of transparency and assurance issues as information sharing is yet to be established. The massive expenses involved in rehabilitation alone is another significant issue in South Africa, as in many developing countries. Furthermore, costs depend upon the rehabilitation goals and criteria and inadequate knowledge of abandoned asbestos mine sites results in poor cost estimation and therefore wastage of finances (Mhlongo and Amponsah-Dacosta, 2016). Suffice to say, to avoid squandering any funding provided, effective engagement between scientists, communities and officials is essential to implementing site management and risk mitigation strategies (Cornelissen *et al.,* 2019).

The mineralogy of the parent geology and the weathering processes in large determine soil micronutrients and their bioavailability to plants (Voss, 1998). Rehabilitating these artificial, alkaline, and un-weathered rock substrates is conducted by blending the waste with topsoil to create a ‘novel substrate’, where revegetation and ecological restoration can be achieved (Kumaresan *et al.,* 2017). The paste pH-conductivity method was done to determine the immediate pH and electrical conductivity (EC) of the asbestos rock wastes during the initial stages of interaction between water and the mine rock waste (Gomez-Arias *et al.,* 2021).

The rock wastes generated from the various asbestos mine operations were collected and assessed for microbial activity using culture-dependent (isolation) and culture-independent (molecular) methods. Apart from being indicators of ecological function and health, the microbial communities hosted by the asbestos mine rock wastes are practitioners of below-ground metabolic retrieval essential for successive above-ground rehabilitation (Harris, 2009). Although in recent years the link between below-ground and above-ground communities has been acknowledged, the mechanistic way microbial communities promote restoration of post-mining landscapes is still not understood (Bardgett and van der Putten, 2014; Kumaresan *et al.,* 2017).

The growth of the isolated bacteria and fungi was tested on bacterial and fungal agar media without the addition of any other nutrients or asbestos fibres. Banding, although unclear, was shown on the gel, which verifies that fungal DNA was in fact present and directly extracted from the asbestos rock samples. No growth was observed on either type of agar media following the incubation period. This test shows that these indigenous asbestos micro-organisms are not able to grow on either of the agar media alone. It is likely that the microbial taxa growing on the various asbestos mineral fibres in nature are mostly taxa adapted to metabolise the metals provided by the asbestos. The asbestos mineral fibres may contain non-cultivable taxa or taxa with specific nutritional requirements that were not provided during the isolation protocol used in this research (Lecomte *et al.,* 2011). It was estimated by Kirk *et al. (*2004) that the growth of only ~1 % of the soil microbial taxa from environmental samples are allowed by standard microbiological techniques. An additional reason for lack of growth, but presence of a DNA signature is that the source culture is dead.

The inability to culture microbes from the asbestos mine rock wastes and the insignificant values of DNA extracted indicate that these substrates are biologically inert. Microbial deficiencies in most rehabilitation programmes contribute to the factors resisting vegetation establishment and growth suggesting that the mine dumps are sterile, and therefore act as a negligible source of biological input into the augmented topsoil. The specific geochemical characteristics of asbestos rock wastes and the corresponding low microbial biomass make the extraction of DNA from these materials technically demanding (Barton *et al.,* 2006; Genderjahn *et al.,* 2021). Commercially sold environmental DNA extraction protocols, such as those used with the ZR Soil Microbe DNA Kit Miniprep™ (Zymo Research,

Irvine, CA, USA) (ZR kit), result in the extraction of DNA from a mixture of dead, dormant and living cells of micro-organisms (Alawi *et al.,* 2014).

The lack of investigations to characterise the mineralogical and microbial properties of asbestos mine wastes and acknowledgment of their subsequent incompatible nature for the growth and survival of the native vegetation cover (which ought to be common knowledge), which has been adapted to the surrounding but extremely different soil environment, may be interpreted in two ways. The first is that the vastly different growing conditions were not known, and thus assumed to be similar and therefore appropriate for the native vegetation. The second is that the geochemical and mineralogical conditions were known to be unsuitable for the native plants, a fundamental piece of information conveniently not stated in any of the literature regarding this topic, yet it was decided that simple agricultural techniques would provide sufficient support for growth. The lack of incorporation of this detail raises questions as to the willingness to change, modify or even accept that the currently employed methods for ensuring public safety are riddled with faults.

Asbestos mine dump rehabilitation methods require that mine dumps be revegetated using natural and indigenous plant species to restore and preserve the original biodiversity. However, the edaphic conditions of the un-weathered, biologically inert mine dumps, primarily controlled by the mineralogy, geochemical and microbiological characteristics of the waste rocks (Jamieson, 2011), are contrastingly different to the surrounding, ancient, highly weathered, biologically active, acidic natural soil substrates that host the indigenous plant species' biodiversity (figure 4.10) (Cross *et al.,* 2021). These conditions are therefore unsuitable for the long-term survival and flourishment of local plants (Cross *et al.,* 2021).

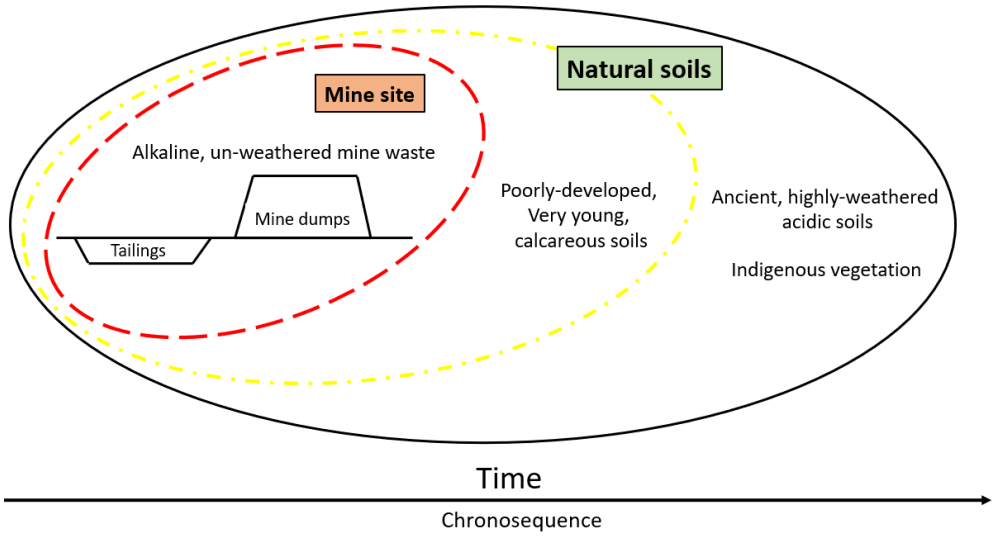


Figure 4.10: Edaphic conditions characterising DAMLs and the surrounding environments.

Rehabilitation strategies using native plant species that are genetically and phenotypically adapted to the geochemical conditions of the ancient, microbially active, heavily weathered soils of the geological region to revegetate mine dumps of contrasting conditions is hopeful at best. It is a glaring factor that compromises the entire rehabilitation programme and the entire ecological restoration efforts (Cross *et al.,* 2018). Typical native plant species used on such sites include short bushveld (*Combretum* species), trees (*Acacia* species*)* and shrubs (*Grewia* species) (Liebenberg-Weyers, 2010).

## 4.5. Conclusion

Derelict asbestos mine dumps lack macro and micronutrients, are devoid of the characteristics comprising true soil, possess extremely alkaline pH and low to no microbial abundance and diversity. To conclude, there is a perspicuous demand for significant research into the mineralogical, geochemical, and microbiological characteristics of asbestos mine dumps and how these substrates are perceived by the plants used to revegetate and phyto-stabilise the site. Specifically, consideration and knowledge are required of how factors controlling the rock wastes' substrate, such as pH, geochemistry, nutrient restrictions, physical and hydrological conditions, and native microbial alterations, influence the plant physiology in terms of development and growth.

## 4.6. References


Alawi, M., Schneider, B. and Kallmeyer, J. (2014): A procedure for separate recovery of extra- and intracellular DNA from a single marine sediment sample. *J. Microbiol. Methods*, **104**, 36–42.

Allen, L.P., Baez, J., Stern, M.E.C., Takahashi, K. and George, F. (2018): Trends and the Economic Effect of Asbestos Bans and Decline in Asbestos Consumption and Production Worldwide. *International Journal of Environmental Research and Public Health*, **15** (3), 531.

Bardgett, R. D. and van der Putten, W. H. (2014): Belowground biodiversity and ecosystem functioning. *Nature*, **515**, 505–511.

Barton, H.A., Taylor, N., Lubbers, B. and Pemberton, A. (2006): DNA extraction from low-biomass carbonate rock: An improved method with reduced contamination and the low-biomass contaminant database. *J. Microbiol. Methods*, **66**, 21–31.

Bell, F.G. and Bullock, S.E.T. (1996): The problem of acid mine drainage, with illustrative case history. *Environmental Engineering Geoscience*, **2**, 369-392.

Blowes, D.W., Ptacek, C.J., Jambor, J.L. and Weisener, C.G. (2003): The geochemistry of acid mine drainage. *Environ. Geochem*., **9**, 149–204.

Canovas, C.R., Olias, M., Nieto, J.M., Sarmiento, A.M. and Ceron, J.C. (2007): Hydrogeochemical characteristics of the Tinto and Odiel Rivers (SW Spain). Factors controlling metal contents. *Science Total Environment*, **373**, 363–382.

Cornelissen, H. (2017): The Development of a Qualitative Ranking Tool for the Preliminary Selection of Abandoned Asbestos Mine Sites for Rehabilitation. Proceedings of the 3rd World Congress on New Technologies (NewTech'17) Rome, Italy. Paper No. ICEPR 145.

Cornelissen, H., Watson, I., Adam, E. and Malefetse, T. (2019): Challenges and strategies of abandoned mine rehabilitation in South Africa: The case of asbestos mine rehabilitation. *Journal of Geochemical Exploration*, **205**, 106354.

Cross, A.T. and Lambers, H. (2017): Young calcareous soil chrono sequences as a model for ecological restoration on alkaline mine tailings. *Science of the Total Environment*, **607–608**, 168–175.

Cross, A.T., Stevens, J.C., Sadler, R., Moreira-Grez, B., Ivanov, D., Zhong, H., Dixon, K.W. and Lambers, H. (2019): Compromised root development constrains the establishment potential of native plants in unamended alkaline post-mining substrates. *Plant Soil*. https://doi.org/10.1007/s11104-018-3876-2

Cross, A.T., Young, R., Nevill, P., McDonald, T., Prach, K., Aronson, J., Wardell-Johnson, G. and Dixon, K.W. (2018): Appropriate aspirations for effective post-mining restoration and rehabilitation: a response to Kaźmierczak et al. *Environ. Earth Sciences,* **77**, 256.

Dinelli, E., Lucchhini, F., Fabbri, M. and Cortecci, G. (2001): Metal distribution and environmental problems related to sulphide oxidation in the Libiola copper mine area (Ligurian Apennines, (Italy). *Journal of Geochemical Exploration*, **74**, 141–152.

Garibyan, L. and Avashia, N. (2013): Research Techniques Made Simple: Polymerase Chain Reaction (PCR). *Journal of Investigative Dermatology*, **133** (3), e6.

Genderjahn, S., Lewin, S., Horn, F., Schleicher, A.M., Mangelsdorf, K. and Wagner, D. (2021): Living Lithic and Sublithic Bacterial Communities in Namibian Drylands. *Microorganisms*, **9**, 235.

Gomez-Arias, A., Yesares, L., Caraballo, M.A., Maleke, M., Vermeulen, D., Nieto, J.M., van Heerden, E. and Castillo, J. (2021): Environmental and geochemical characterization of alkaline mine wastes from Phalaborwa (Palabora) Complex, South Africa. *Journal of Geochemical Exploration*, **224,** 106757.

Harris, J. (2009): Soil microbial communities and restoration ecology: facilitators or followers? *Science*, **325**, 573–574.

Higueras, P., Oyarzun, R., Iraizoz, J.M., Lorenzo, S., Esbrí, J.M. and Martínez-Coronado, A. (2012): Low-cost geochemical surveys for environmental studies in developing countries: Testing a field portable XRF instrument under quasi-realistic conditions. *Journal of Geochemical Exploration*, **113**, 3 – 12.

Hossner, L.R and Hons, F.M. (1992): Reclamation of mine tailings. *Advances in soil sciences*, **17**, 311-350.

Jamieson, H.E. (2011): Geochemistry and mineralogy of solid mine waste: essential knowledge for predicting environmental impact. *Elements*, **7**, 381–386.

Kirk, J.L., Beaudette, L.A., Hart, M., Moutoglis, P., Klironomos, J.N., Lee, H. and Trevors, J.T. (2004): Methods of studying soil microbial diversity. *Journal of Microbiology Methods*, **58**, 169–188.

Kumaresan, D., Cross, A.T., Moreira-Grez, B., Kariman, K., Nevill, P., Stevens, J., Allcock, R.J.N., O'Donnell, A.G., Dixon, K.W. and Whiteley, A.S. (2017): Microbial functional capacity is preserved within engineered soil formulations used in mine site restoration. *Scientific reports*, **7** (564).

Lecomte, J., St-Arnaud, M. and Hijri, M. (2011): Isolation and identification of soil bacteria growing at the expense of arbuscular mycorrhizal fungi. *FEMS Microbiology Letters*, **317**, 43 – 51.

Li, X. and Huang, L. (2015): Toward a new paradigm for tailings phyto-stabilization—nature of the substrates, amendment options, and anthropogenic pedogenesis. *Critical Reviews in Environmental Science and Technology*, **45**, 813–839.

Liebenberg-Weyers, D. (2010): A multidisciplinary approach for the assessment of rehabilitation at asbestos mines in South Africa. MSc dissertation, Northwest University, Potchefstroom.

Matsabatsa, G.M. (2009): Post-closure environmental impacts of asbestos mining in Penge, Limpopo Province, South Africa. MSc dissertation, University of the Witwatersrand, Johannesburg.

Mendez, M.O. and Maier, R.M. (2008a): Phytoremediation of mine tailings in temperate and arid environments. *Reviews in Environmental Science and Biotechnology,* **7** (1), 47-59.

Mendez, M.O. and Maier, R.M. (2008b): Phyto-stabilization of mine tailings in arid and semiarid environments- an emerging remediation technology. *Environmental Health Perspectives*, **116** (3), 278-283.

Mhlongo, S.E. and Amponsah-Dacosta, F. (2016): A review of problems and solutions of abandoned mines in South Africa. International Journal of Mining. *Reclamation and Environment*, **30** (4), 279–294.

Naicker, K., Cukrowska, E. and McCarthy, T.S. (2003): Acid mine drainage arising from gold mining activity in Johannesburg, South Africa, and environs. *Environmental Pollution*, **122**, 29–40.

Ogola, J.S. (2010): Dispersion of Heavy Metals and their potential impacts on the Environment: A case study of Gold Tailings Dam in Giyani Belt, Limpopo Province, South Africa. University of Venda, Thohoyandou.

Plante, B., Benzaazoua, M. and Bussière, B. (2011): Predicting Geochemical Behaviour of Waste Rock with Low Acid Generating Potential Using Laboratory Kinetic Tests. *Mine Water Environ.*, **30**, 2–21.

Plumlee, G.S. (1999): The environmental geology of mineral deposits. In: Plumlee, G.S. and Logsdon, M.J. (eds.) The Environmental Geochemistry of Mineral Deposits: Processes, Techniques and Health Issues. *Reviews in Economic Geology*, **6A**, 71-116.

Plumlee, G.S., Morman, S.A. and Ziegler, T.L. (2006) The toxicological geochemistry of earth minerals: An overview of processes and the interdisciplinary methods used to understand them. In: N. Sahai and M.A.A. Schoonen, Eds., Medical Mineralogy and Geochemistry, 64, p. 5–57. Reviews in Mineralogy and Geochemistry, Mineralogical Society of America, Chantilly, Virginia.

Plumlee, G.S., Morman, S.A. and Ziegler, T.L. (2006): The toxicological geochemistry of earth minerals: An overview of processes and the interdisciplinary methods used to understand them. *Reviews in Mineralogy and Geochemistry*, **64**, 5–57.

Schimmer, C. (2017): Synergistic use of soil microbes and plants to facilitate rehabilitation on gold tailings materials. Dissertation (MSc) School for Geo- and Spatial Sciences, Northwest University, Potchefstroom.

Sheoran, V., Sheoran, A.S. and Poonia, P. (2013): Phytostabilization of metalliferous mine waste. *Journal of Industrial Pollution Control*, **29** (2).

Tutu, H., McCarthy, T.S. and Cukrowska, E. (2008): The chemical characteristics of acid mine drainage with particular reference to sources, distribution and remediation: The Witwatersrand Basin, South Africa, as a case study. *Application Geochem*, **23**, 3666–3684.

Van Druten, E. and Bekker, M. C. (2017): Towards an inclusive model to address unsuccessful mine closures in South Africa. *Journal of the Southern African Institute of Mining and Metallurgy*, **117** (5), 485–490.

Voss, R. (1998): Micronutrients. Department of Agronomy Iowa State University Ames, IA 50011.

Vriens, B., Plante, B., Seigneur, N. and Jamieson, H. (2020): Mine Waste Rock: Insights for Sustainable Hydrogeochemical Management. *Minerals*, **10** (728).

Zhao, F., Cong, Z., Sun, H. and Ren, D. (2007): The geochemistry of rare earth elements (REE) in acid mine drainage from the Sitai coal mine, Shanxi Province, North China. *International Journal of Coal Geology*, **70**, 184–192.

# Chapter 5 - Rhizosphere competence and abiotic stress tolerance of commercially-sold *Pseudomonas fluorescens* biofertilizers: Implications for its bioremediation potential

Abstract

Microbial remediation research has become front and centre gaining momentum for numerous environmental biotechnological applications. Agronomical bioproducts have been widely used for many years and their availability, low costs and safety make them potentially suitable for alternative biotechnological applications, specifically environmental remediation. In this study, the commercially available biofertilizer, *Pseudomonas fluorescens* (Rizofos), was examined for its rhizosphere competence, abiotic stress tolerance and heavy metal tolerance using relatively rapid and economically feasible, standard culture-based laboratory methods to determine their potential use in the field of bioremediation. This plant growth promoting-bacteria biofertilizer shows phase variation, metabolic versatility, and mobility, all of which are necessary for rhizosphere fitness and colonisation. In addition, both exceptional abiotic stress tolerance (pH, NaCl and temperature) and heavy metal (HM) tolerance was exhibited by this biofertilizer. To conclude, this study demonstrates that the prospect of using already available, well-studied, safe, and environmentally friendly agronomic bioproducts as alternative biotechnologies, including bioremediation is realistic, offering a more rapid solution to environmental problems extending beyond identifying, testing and formulating new liquid bio-inoculants specifically for contaminated soils.

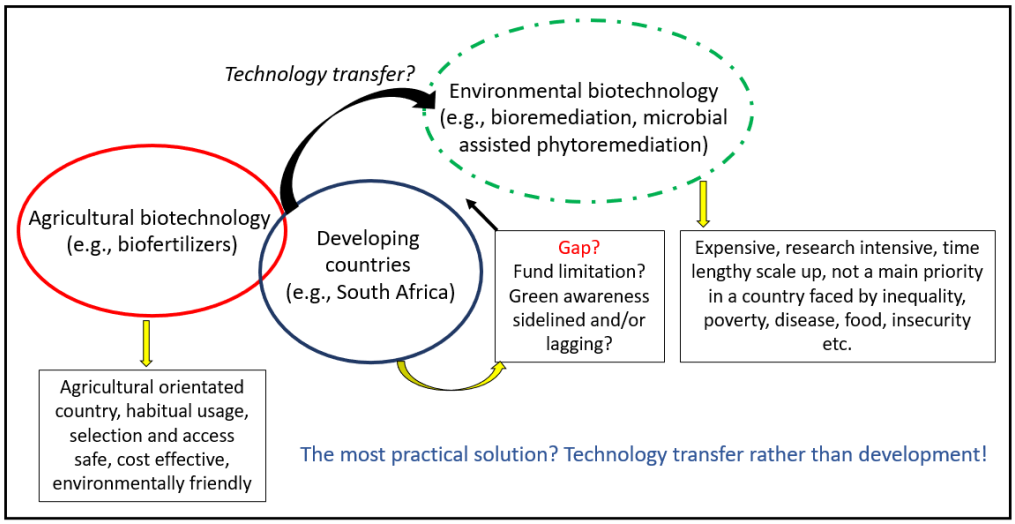


Figure 5.1: Practical science for allowing environmental sustainability progress under the biotechnology development limitations of developing countries

The scarcity and slow development of environmental biotechnology in developing countries, such as South Africa, can be explained in length by a myriad of nation-specific factors, and therefore the study acknowledges such limitations regarding national environmental biotechnological capabilities and presents a practical solution using effective methods to explore the potential for agricultural technology transfer.

## 5.1. Introduction

The use of biofertilizers for sustainable agriculture represents one of the most advanced biotechnological tools in modern times. Across the world, at an annual increase of ~10 %, there is an expanding market for microbial inoculants (Berg, 2009). When compared to chemical pesticides and fertilisers, microbial inoculants offer several advantages: They are safer with more targeted activity and reduced environmental damage. They are also effective in smaller quantities with the ability to multiply, and have decomposition procedures that are quicker (Berg, 2009).

The legacy of environmental pollution has followed in the wake of worldwide industrialisation and extensive agricultural and anthropogenic practices (Shinwari *et al.,* 2015). Toxic compounds, metals and effluents have heavily contaminated soils, water and air leaving an environment that is unsuitable for sustaining life. Conventional methods for the

remediation of contaminated soils and mine sites are high energy consuming, costly and in largely unsustainable (Jeyasingh and Philip, 2005). In this regard, microbial-based technologies, known as bioremediation, to remediate or assist remediation practices, have gained considerable attention over the last few decades due to their superior performance, low cost, and environmentally friendly nature (Iqbal and Edyvean, 2004; Wu *et al.*, 2006). Bioremediation is defined as the implementation of biological systems, almost universally micro-organisms, to clean up or restore contaminated sites (Bains, 1993).

The *Pseudomonas* genus is one of the best-studied and most important bacterial taxa in soil (Raaijmakers *et al.,* 2002). The reasons for this are that the *Pseudomonas* species is isolated easily from the natural environment, effortless to cultivate and easy to manipulate genetically (Whipps, 2001; Raaijmakers *et al.,* 2002). The members of the genus can colonise a wide range of niches as they demonstrate wide metabolic diversity (Palleroni and Cornelis, 2008). Other important characteristics of the genus *Pseudomonas* include rapid growth, production of metabolites (siderophores and growth promoters) and their ability to adapt to environmental stress and compete with other micro-organisms (Goldberg, 2000; Kraemer, 2004; Hider and Kong*,* 2010; Cornelis, 2010; David *et al.,* 2018). These features combine to make this microbial inoculant a strongly desired agent in applications, such as bioremediation and biocontrol (Kloepper *et al.,* 2004; Weller, 2007). *Pseudomonas fluorescens* is one species of this diverse group of bacteria that is particularly well-known for its role in biocontrol, biodegradation, and bioremediation (Roca and Olsson, 2001; Palleroni, 2010).

The environmental-biotechnological applicability of certain microbial species is generally performed by isolating soil microbes from the contaminated site and testing whether they possess the capacity to accomplish the desired function. This technique is, however, limited by being site-specific and if the microbe presents as being applicable for bioremediation, further time, money and workforce are required for developing the bacteria into a formulated inoculant that is safe for both the environment and human handling. This process is in all regard paradigmatic in the developing world, where environmental conciseness and funds are not as broadly or extensively prioritised. Considering this, the use of commercially available, safe, and relatively cheap Plant Growth Promoting Bacteria (PGPB) biofertilizers exhibiting multiple plant beneficial properties, abiotic stress and metal tolerance is an encouraging, environmentally friendly and cost competitive soil bioremediating tool. The prospect of using commercially available biofertilizers for bioremediation technology and

establishing whether the administration of Plant Growth Promoting Rhizobacteria (PGPR) biofertilizers, largely used to improve agricultural yields, for solving environmental problems, is a concept that has largely been overlooked (figure 5.2).

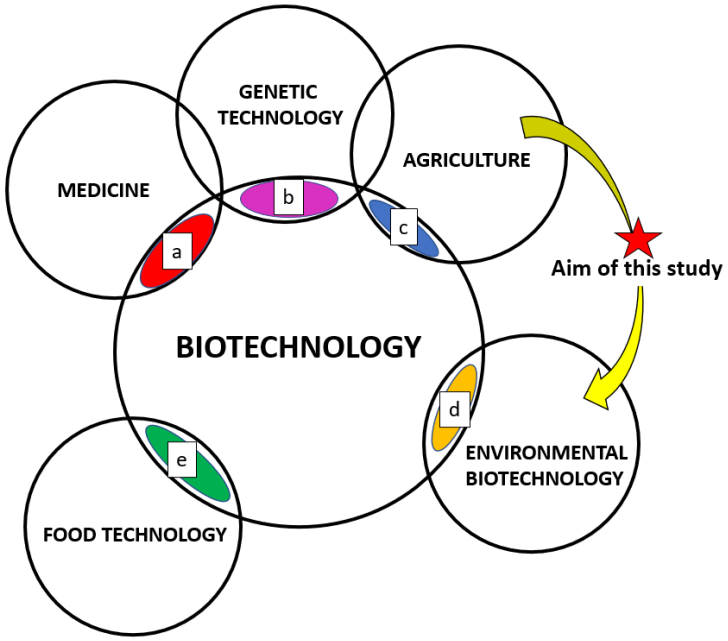


Figure 5.2: Applications of biotechnology and alternative applications of agricultural biotechnology in environmental biotechnology. (a) Antibiotic production; (b) genetic engineering for human application; (c) genetic engineering for plant and animal applications; (d) decontamination, biomonitoring, biosensors, and pollution prevention and (e) fermentation products (adapted from Gavrilescu, 2010).

*Pseudomonas fluorescens*-containing biofertilizers produced specifically for their phosphate solubilising properties are a commercially available agricultural biotechnology (Goddard *et al.,* 2001). Compared to fungi, the faster growth rate and ease for manipulation of bacteria make them convenient to culture. Thus, they may serve potentially as more suitable effectors for the bioremediation of soil. Being commercially available and widely used, its performance for scale-up and field employment has already been confirmed and is a significant factor to why the commission of bio-inoculants developed for biotechnological employment are commonly short-lived (Goddard *et al.,* 2001). Numerous in-depth studies have exposed the bioremediation potentials of *Pseudomonas fluorescens* (Rainey, 1999; Juhasz and Naidu, 2000; Barathi and Vasudevan, 2001; Janek *et al*., 2010), and therefore this

species was selected for this research. Thus, the microbial biofertilizer was investigated for its potential to be used beyond its current agricultural purpose in the realm of bioremediation and bio-augmentation-assisted rehabilitation of soils.

The aim of this study was to use a culture-based strategy to examine colony morphology expressions, abiotic stress tolerance and heavy metal tolerance of *Pseudomonas fluorescens*. PGPR *Pseudomonas fluorescens* was cultured on a variety of variable culture media and colony growth times and the observed phenotypic expressions (colony morphology, alterations in colony traits, growth rate, fluorescent pigments, and colouration) were examined and compared. Abiotic stress and heavy metal tolerance was also studied using standard culturing techniques and determined by adjusting the individual environmental parameters for each and inspecting the effects on growth. Identifying the impacts of some variables on the microbiological effects and phenotypic expressions of *Pseudomonas fluorescens* provides inferences on their potential environmental adaptability, virulence and resistance following introduction into the soil environment (Sousa *et al.,* 2013). As this microbe is already used in agriculture for its plant growth-promoting abilities, these properties were not studied, as the goal of this study was to determine if the use of this agricultural bioproduct in environmental biotechnological applications is a feasible recourse, mainly relying on its ability to survive, replicate, tolerate and perform the desired biotechnological appointment.

## 5.2. Materials and Methods

### 5.2.1. Micro-organism, maintenance, and storage

The bacterial strain of *Pseudomonas fluorescens* used in this study was donated as a commercially-sold inoculant labelled Rizofos Maize from Microbial Biological Fertilizers International (MBFi), Delmas, South Africa. Rizofos Maize is a liquid inoculant containing the phosphorus solubilizing bacteria *(Pseudomonas fluorescens)* (1 x $10^9$ cfu/mL in a sterile liquid broth culture). This strain is, however, also capable of producing siderophores under iron-limited conditions, a trait desired for this experiment. This biofertilizer is a special liquid formulation that contains not only the desired micro-organism and their nutrients, but also

special cell protectants or substances that encourage longer shelf life and tolerance to stressful condition. The *Pseudomonas fluorescens* was maintained at 4 °C on nutrient agar (Merck, Darmstadt, Germany) plates. For long time storage, stock cultures were made from liquid cultures (1200 µl culture, 300 µl 80% glycerol) and frozen at -20 °C.

Several growth-based assays were used to phenotypically characterise the *Pseudomonas fluorescens* biofertilizer. These assays are important to increase understanding of the ecology of this significant rhizosphere-related micro-organism, with major implications for its application as a bio-inoculant in environmental restoration and remediation biotechnologies.

### 5.2.2. Media composition and preparation of experimental plates

*Pseudomonas fluorescens* was cultured in four different media: Pseudomonas agar, Kings B agar, LB agar and nutrient agar to investigate the effects of the composition of different media and growth time on (i) morphological features (i.e., colony growth, colour, and edge), (ii) rate of bacterial growth and (iii) physiological features (i.e., colour changes and fluorescence). To assess the impact of solid media composition on colony morphology, growth and fluorescence, *Pseudomonas fluorescens* was streaked on different solid media (table 5.1).

Table 5.1: Media used and their composition

| **Media** | **Composition** |
|---|---|
| | |
| Pseudomonas agar | Tryptone (10 g/l)<br>Gelatin peptone (16 g/l)<br>Potassium sulphate (10 g/l)<br>Magnesium chloride (anhydrous) (1.4 g/l)<br>Agar (11 g/l) |
| Kings B agar | Peptone (20 g/l)<br>Dipotassium hydrogen phosphate (1.5 g/l)<br>Magnesium sulphate heptahydrate (3 g/l)<br>Glycerol (10 ml/l)<br>Agar (15 g/l) |
| LB agar | Sodium chloride (10 g/l)<br>Tryptone (10 g/l)<br>Yeast extract (5 g/l)<br>Agar (15 g/l) |
| Nutrient agar | Beef extract (10 g/l)<br>Peptone (10 g/l)<br>Sodium chloride (5 g/l)<br>Agar (15 g/l) |

The media were prepared, autoclaved at 121 °C for 20 minutes, allowed to cool and poured into Petri dishes under sterile conditions in triplicate. As the amount of solid medium in the Petri plates has been observed to impact colony morphogenesis (Sousa *et al.,* 2013), the height of the solid media in each plate was standardised to 0.5 cm thick or ~15 mL of medium per 9 cm diameter plates with an area of 7226.4 $mm^2$.

### 5.2.3. Detection of motility

Motility can be divided into (i) swimming and (ii) swarming forms (Robertson *et al.,* 2013). A positive result for swimming motility is shown by a ring of colony expansion after 24 to 48 hours of growth. Swarming motility is observed if the edge of isolated colonies demonstrates irregular extensions and/or projections after 24 to 48 hours of growth. Colony morphogenesis and motility were monitored visually over the incubation period.

### 5.2.4. Detection of fluorescence

After 24, 48 and 72 hours of incubation the plates were examined for fluorescence under an ultraviolet light at 360 nm.

### 5.2.5. pH tolerance tests

To study the effect of temperature on growth of *P. fluorescens*, a loopful of 24-hour old culture growth in nutrient broth was streaked onto nutrient agar plates with different pH values (4, 5, 6, 7, 8, 9 and 10). The final pH of the medium was adjusted using 1 mol/L HCl or 1 mol/L NaOH. The plates were incubated at 25 °C for 48 hours and visually inspected for the absence or presence of growth, which were then documented as intolerant (I) and tolerant (T), respectively.

### 5.2.6. Temperature tolerance tests

To study the effect of temperature on growth of *P. fluorescens*, a loopful of 24-hour old culture growth in nutrient broth was streaked onto nutrient agar plates and incubated at different temperatures of 5, 10, 15, 20, 25, 30, 35 and 40 °C for 48–96 hours (Bruno *et al.,* 2020). The plates were visually inspected for the absence or presence of growth which were then documented as intolerant (I) and tolerant (T), respectively.

### 5.2.7. Salinity tolerance tests

To study the effect of temperature on growth of *P. fluorescens*, a loopful of 24-hour old culture growth in nutrient broth was streaked onto nutrient agar plates amended with different concentrations of NaCl (0.1, 1, 2, 3, 4, 5, 6 and 7%). The plates were incubated at 25°C for 48 hours and visually inspected for the absence or presence of growth, which were then documented as intolerant (I) and tolerant (T), respectively.

### 5.2.8. Heavy metal (HM) tolerance

The heavy metals used in the tolerance tests were iron, manganese, cobalt, zinc, copper, lead and chromium from $FeSO_4.6H_2O$, $MnSO_4.4H_2O$, $CoCl_2.6H_2O$, $ZnCl_2$, $CuO_4S.5H_2O$,

$Pb(NO_3)_2$ and $CrO_3$, respectively. A 1 mol/L stock solution for each metal salt was made from which the appropriate volumes were taken to get the desired concentration of heavy metals in each of the 25 mL agar plates using $C_1V_1 = C_2V_2$ (table 5.2).

Table 5.2: Heavy metal concentrations and volumes added to agar plates

| | Iron | Manganese | Cobalt | Zinc | Copper | Lead | Chromium |
|---|---|---|---|---|---|---|---|
| Concentration | | | | | | | |
| ppm | µM | | | | | | |
| 10 | 38.46 | 66.22 | 42.03 | 73.37 | 40.05 | 30.193 | 100 |
| 50 | 192.3 | 331.1 | 210.15 | 366.84 | 200.25 | 150.97 | 500 |
| 100 | 384.6 | 662.2 | 420.3 | 733.7 | 400.5 | 301.93 | 1000 |
| 200 | 769.2 | 1324.5 | 840.6 | 1467.4 | 801 | 603.9 | 2000 |
| 300 | 1153.8 | 1986.7 | 1261 | 2201 | 1201.5 | 903.8 | 3000 |
| | | | | | | | |
| ppm | Volume (mL) to add to agar ($(C_1)(V_1) = (C_2)(V_2)$) | | | | | | |
| 10 | 0.01 | 0.02 | 0.01 | 0.02 | 0.01 | 0.008 | 0.025 |
| 50 | 0.05 | 0.08 | 0.05 | 0.09 | 0.05 | 0.04 | 0.125 |
| 100 | 0.09 | 0.2 | 0.1 | 0.2 | 0.1 | 0.08 | 0.25 |
| 200 | 0.2 | 0.3 | 0.2 | 0.4 | 0.2 | 0.15 | 0.5 |
| 300 | 0.3 | 0.5 | 0.3 | 0.55 | 0.3 | 0.22 | 0.75 |

The heavy metal (HM) tolerance of the PGPR *Pseudomonas fluorescens* was tested using the agar dilution method (Lee *et al.,* 2009). The *Pseudomonas fluorescens* was grown in a nutrient broth for 24 hours and then, using an inoculating loop, streaked onto nutrient agar plates amended individually with increasing concentrations (10, 50, 100, 200 and 300 ppm) of different heavy metals. Unamended nutrient agar plates were used as controls to examine tolerance. The plates were incubated at 25°C for 48 hours and visually inspected for the absence or presence of growth which were then documented as intolerant (I) and tolerant (T), respectively.

## 5.3. Results

### 5.3.1. Effect of medium composition on colony morphology, colour, and growth

The PGPR *P. fluorescens* was plated onto different agar media to assess the effect of nutritional composition on colony morphology and biomass production. The time-lapse images of the plates at 24, 48 and 72 hours are given for each medium in figures 5.3 - 5.6.

Colony growth and expansion of the *Pseudomonas fluorescens* strain over the course of 72 hours showed variations in rate and extent amongst the four media types. Colony growth, degree of expansion and rate of expansion was greatest on the Kings B agar medium and slowest on the Nutrient agar medium.

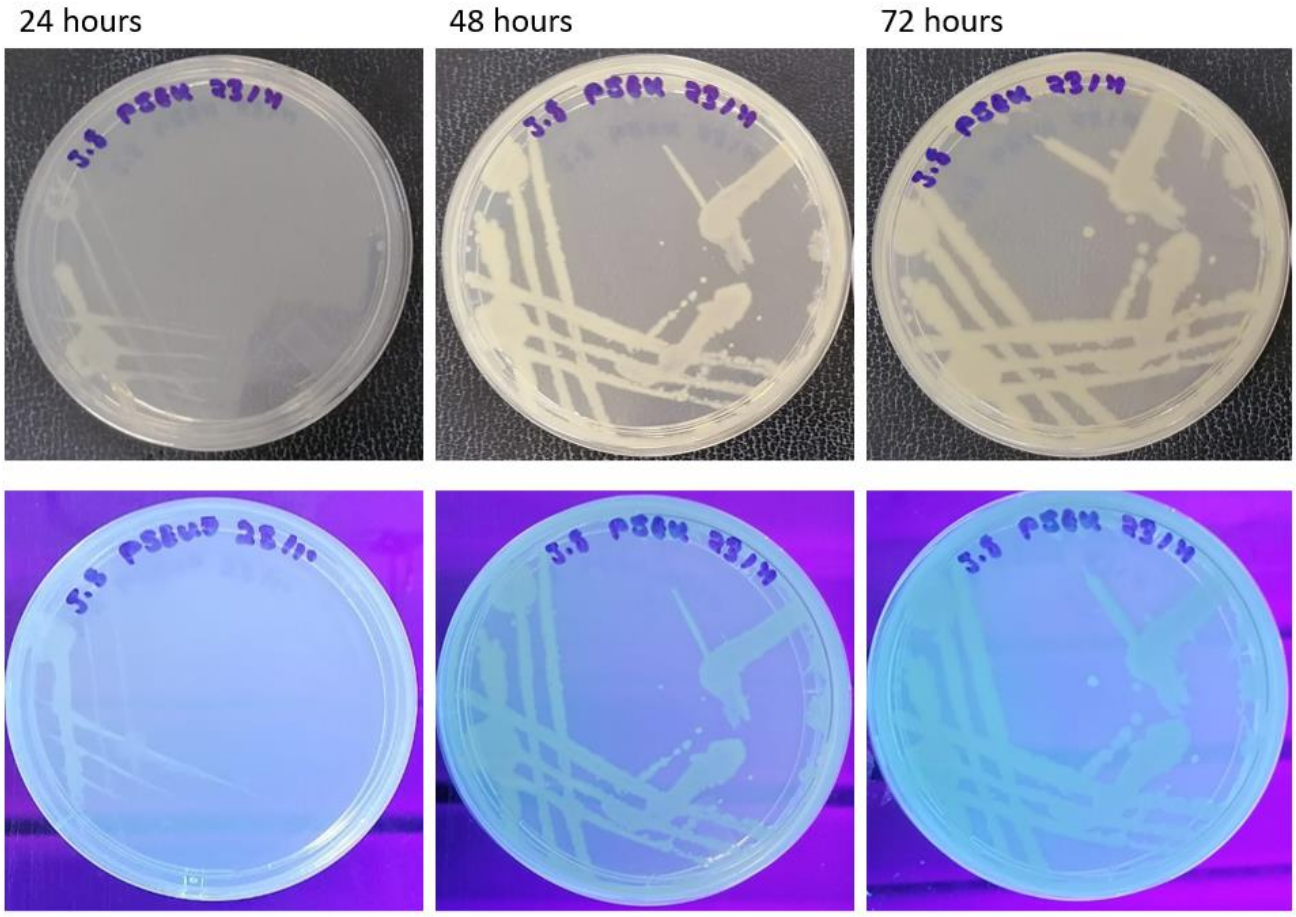


Figure 5.3: The (a) morphology and (b) *fluorescens* of PGPR *Pseudomonas fluorescens* of Pseudomonas agar over 3 days of incubation

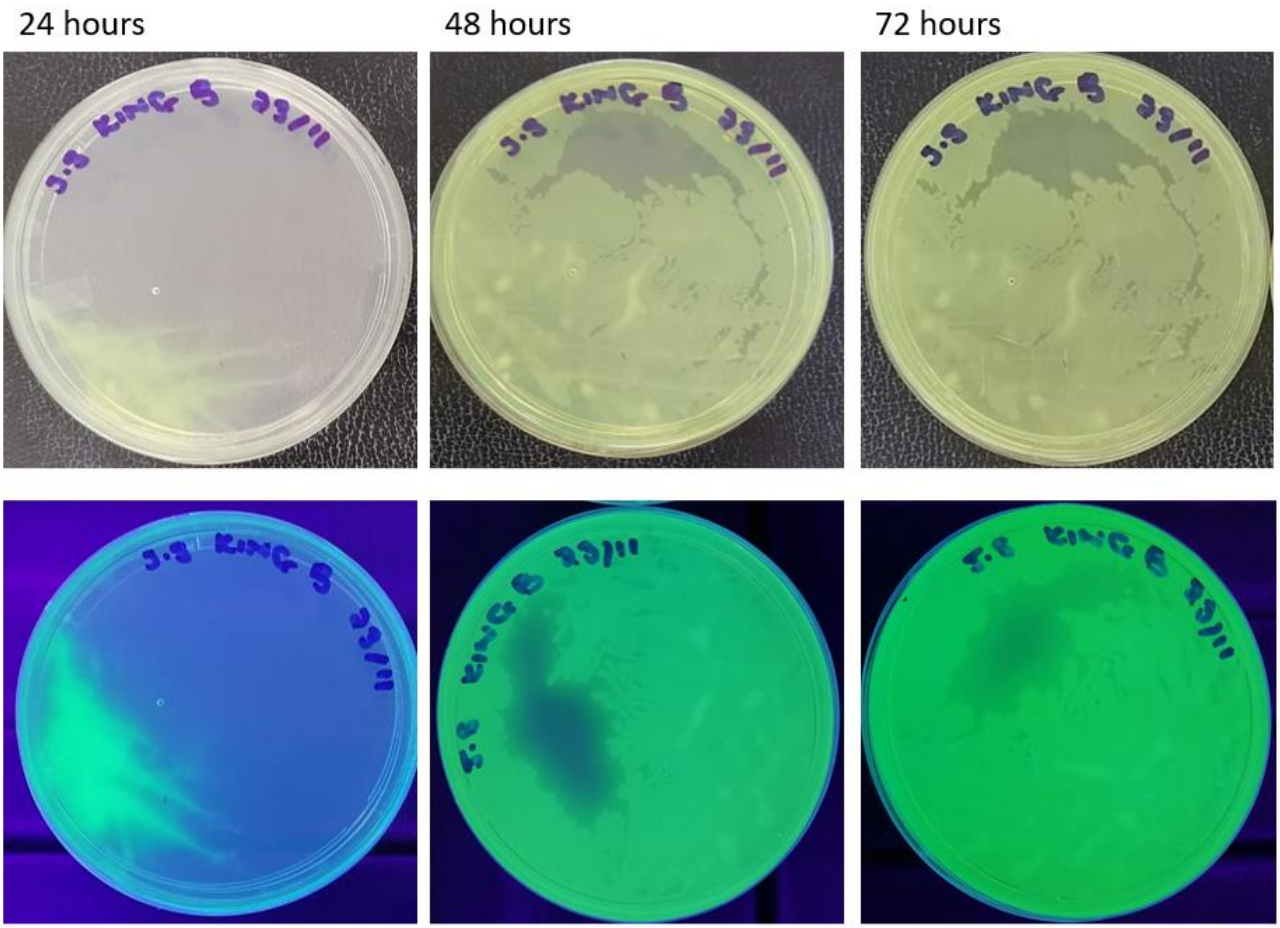


Figure 5.4: The (a) morphology and (b) fluorescence of PGPR *Pseudomonas fluorescens* on Kings B agar over 3 days of incubation

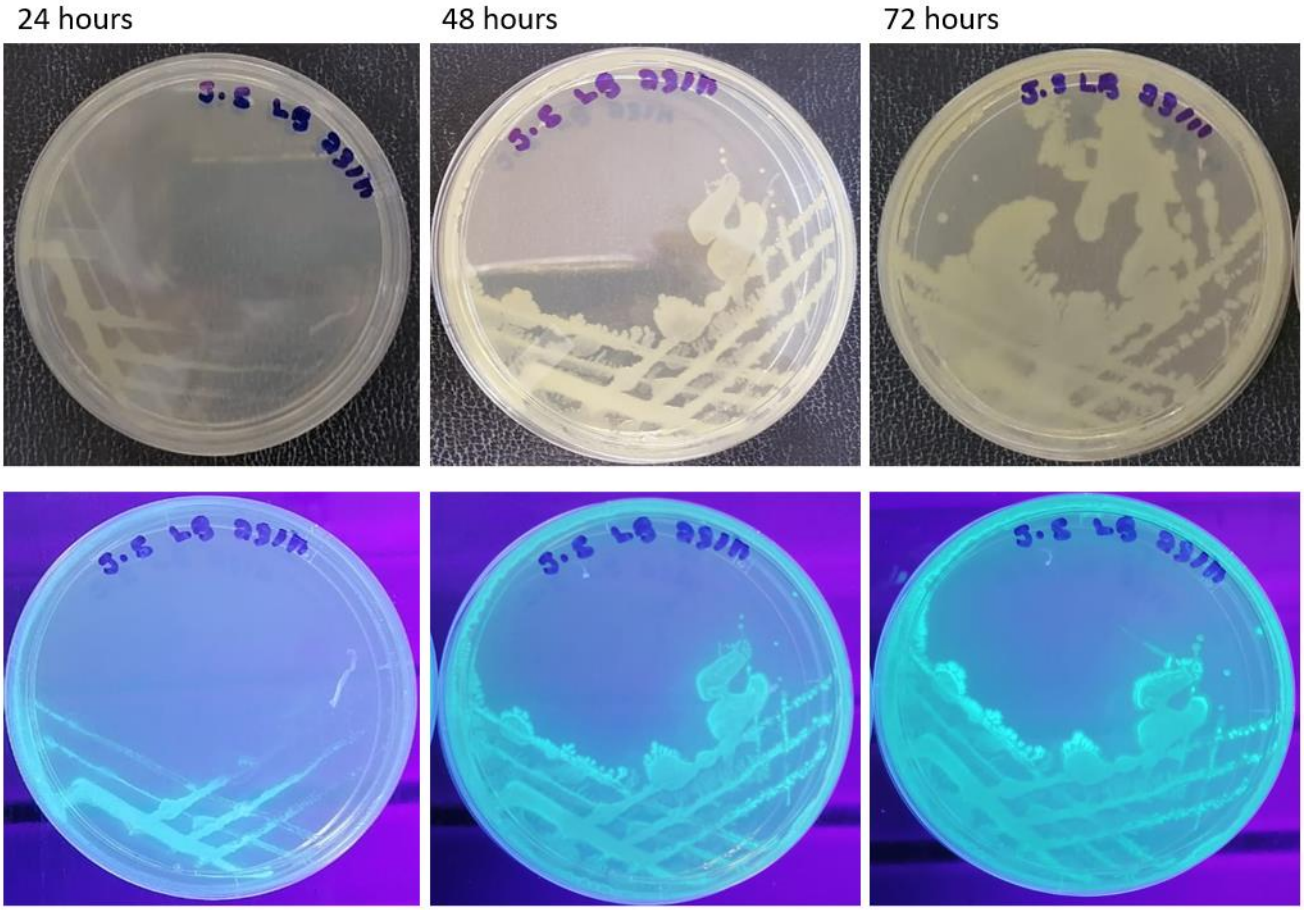


Figure 5.5: The (a) morphology and (b) fluorescence of PGPR *Pseudomonas fluorescens* on LB agar over 3 days of incubation

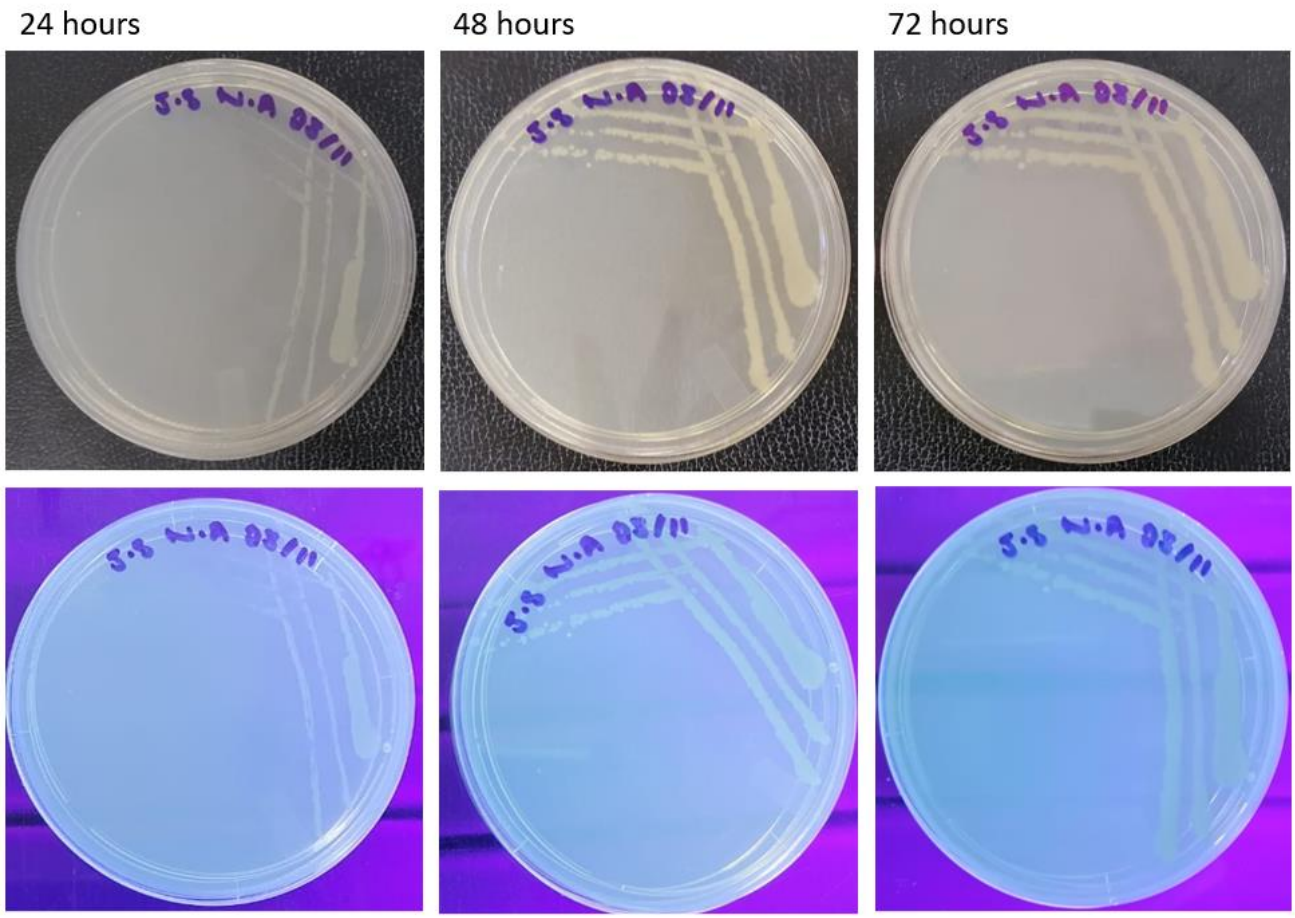


Figure 5.6: The (a) morphology and (b) fluorescence of PGPR *Pseudomonas fluorescens* on Nutrient agar over 3 days of incubation. Colony growth and expansion increased gradually and steadily over the 72-hour incubation period.

Motility was not observed on the Nutrient agar medium. Swimming motility was observed on the Pseudomonas agar medium. The Kings B agar medium was dominated by swarming motility growth. The LB agar medium showed both swimming and swarming motility and growth behaviours. Unlike the thick irregular tendrils observed on the Kings B agar, those on the LB agar plates were longer and slenderer. Colony growth and expansion on the Pseudomonas agar medium showed three stages beginning with an initial slow stage (24 hrs), followed by a fast stage (48 hrs) and lastly a slow stage (72 hrs) (figure 5.3). The colony spread observed on this medium was swimming dependent with colony growth and expansion occurring as distinct, expanding rings. Colony growth and expansion on the Kings B agar plates showed an initial slow stage up until ~ 24 hours of incubation after which rapid growth and expansion occurred to nearly cover the plate (figure 5.4). Colony growth and expansion on the LB agar increased gradually and steadily over the 72-hour incubation period

(figure 5.5). However, compared to that observed on the Nutrient agar, the growth and expansion rate was faster. Several irregular swarming extensions appeared at different sites on the swimming colony boarders at 48 hours resulting in further expansion from the primary streak culture across the plate. Colony growth and expansion on the Nutrient agar medium increased gradually and steadily over the 72-hour incubation period (figure 5.6). The growth observed on the Nutrient agar medium appears to be non-motile, which also explains the lack of colony expansion across the agar surface.

The results indicate that all the media used were suitable for the growth of *Pseudomonas fluorescens.* However, the type and composition of the solid media used noticeably influence the colony morphogenesis of *P. fluorescens* as exhibited by distinct colony morphologies and growth patterns according to the culture media used (table 5.3).

Table 5.3: Effect of media composition on colony morphology and growth

| **Colony morphology** | **Culture medium** | | | |
|---|---|---|---|---|
| | | | | |
| | *Pseudomonas agar* | *Kings B agar* | *LB agar* | *Nutrient agar* |
| | | | | |
| **Growth** | Medium to fast growth | Fast growth | Fast growth | Medium growth |
| | | | | |
| **Form** | Small, irregular colonies | Irregular, rhizoid, spreading, swarming colonies | Medium to large irregular, rhizoid colony shape, spreading or swarming colonies | Small, irregular and round colonies |
| | | | | |
| **Margin** | Entire margin | Entire margin | Entire margin | Entire margin |
| | | | | |
| **Surface** | Dull, smooth surface | Mucoid to glistening surface | Dull, smooth surface | Sull, smooth surface |
| | | | | |
| **Elevation** | Slightly raised, convex | Slightly raised, convex | Slightly raised, convex | Slightly raised, convex |
| | | | | |
| **Opacity** | Translucent | Translucent | Translucent | Translucent |
| | | | | |
| **Colour** | Cream to dull yellow | Bright yellow to green | Cream to yellow | Cream to dull yellow |
| | | | | |
| **Mobility** | Positive | Positive | Positive | Negative |

The motility, auto-aggregation, colour, and pigment production were features that were visually verified to be the most strikingly affected (table 5.4).

Table 5.4: Effect of media composition on pigmentation and fluorescence

| **Media** | **Pigmentation** | **Diffusible pigment** | **Fluorescens** |
|---|---|---|---|
| | | | |
| Pseudomonas agar | + | - | ++ |
| Kings B agar | +++ | +++ | +++ |
| LB agar | ++ | ++ | +++ |
| Nutrient agar | + | - | + |
| | | | |
| +++ high/bright pigmentation/diffusible pigment/fluorescence<br>++ medium pigmentation/diffusible pigment/fluorescence<br>+ low/dull pigmentation/diffusible pigment/fluorescence<br>- no pigmentation/diffusible pigment/fluorescence | | | |

The results indicate that the PGPR *P. fluorescens* is a fast growing, nutritionally versatile, pigment-producing, fluorescing bio-inoculant that exhibits phase variation, all of which strengthen its ability to survive, colonise and proliferate in the soil environment following introduction.

### 5.3.2. Abiotic stress tolerance and growth

The pH, temperature and salinity tolerance and growth limitations of the PGPR *P. fluorescens* are given in table 5.5.

Table 5.5: Abiotic stress tolerance and growth results of PGPR *P. fluorescens*

| **pH tolerance** | | | | | | | |
|---|---|---|---|---|---|---|---|
| 4 | 5 | 6 | 7 | 8 | 9 | 10 | |
| - | + | + (OG) | + | + | - | - | |
| I | T | T | T | T | I | I | |
| **Temperature tolerance (°C)** | | | | | | | |
| 5 | 10 | 15 | 20 | 25 | 30 | 35 | 40 |
| + | + | + | + | + (OG) | + | + | - |
| T | T | T | T | T | T | T | I |
| **Salinity tolerance (%)** | | | | | | | |
| 0.1 | 1 | 2 | 3 | 4 | 5 | 6 | 7 |
| + (OG) | + | + | + | + | - | - | - |
| T | T | T | T | T | I | I | I |
| | | | | | | | |
| + Growth, - no growth<br>T tolerant, I intolerant<br>OG optimal growth | | | | | | | |

Growth was observed for a pH ranging between 5 (acidic) and 8 (alkaline), which indicates that it is not bound to a specific pH region and thus should not be sensitive to pH fluctuations above or below neutral (pH 7), which are common in soil remediation methods. Extreme pH values of acidity and alkalinity would, however, impede the survival of this bio-inoculant, regardless of liming and/or addition of alkaline amendments typically used during the rehabilitation of pH extreme sites. This biofertilizer exhibits temperature tolerance between 5 and 35 $\pm$ 2 °C, which is sufficient for soil environments. Salinity tolerance was restricted to 4 % NaCl, which allows the use of this biofertilizer for all but sodic soils. As sodic soils are not typically associated with metal sites or metalliferous mining areas, this result only provides information for the few cases where the PGPR *P. fluorescens* should not be considered as a biological inoculant.

### 5.3.3. Heavy metal (HM) tolerance

The HM tolerance and growth limitations of the PGPR *P. fluorescens* are given in table 5.6.

Table 5.6: Heavy metal (HM) tolerance results of PGPR *P. fluorescens*

| Heavy metals | Concentrations (ppm or μg/ml) | | | | | % |
|---|---|---|---|---|---|---|
| | 10 | 50 | 100 | 200 | 300 | (R) |
| Iron | T | T | T | T | T | 100 |
| Manganese | T | T | T | T | T | 100 |
| Cobalt | T | T | T | T | T | 100 |
| Zinc | T | T | T | T | T | 100 |
| Copper | T | T | T | T | T | 100 |
| Lead | T | T | T | T | T | 100 |
| Chromium | T | T | T | I | I | 60 |
| | | | | | | |
| T – tolerable<br>I – intolerable<br>R - resistance | | | | | | |

The microbial inoculant demonstrated 100 % tolerance to all concentrations for all the HM tested except chromium, with concentrations > 200 ppm inhibiting growth. This finding once again allows for identifying contaminated soils and/or mine sites where the use of PGPR *P. fluorescens* would be suitable. As different soils and mine lands possess unique geochemical properties and heavy metal associations, understanding of HM and the degree of their concentration effects will allow the determination of the usefulness of a particular microbial agent as the appropriate inoculants.

## 5.4. Discussion

For decades the introduction of desired bacteria and fungi into the soil has occurred for agricultural purposes (Van Veen *et al.,* 1997). These inoculations have been done to stimulate plant growth, supply nutrients, improve the structure of soil and control plant pathogen activity (Wilson and Lindow, 1993). In more recent years, there have been other objectives for the introduction of microbial organisms into the soil (Van Veen *et al.,* 1997). These include the bioaccumulation of inorganic compounds, microbial leaching (Van Veen *et al.,* 1997) and the bioremediation of pollutants in the soil (Middeldorp *et al.,* 1990). Many inoculations of micro-organisms into the soil have successfully fulfilled their purpose, however, many failures have also been reported (van Elsas and Heijnen, 1990; Akkermans, 1994). Such failures raise concern about the degree to which these microbial releases have sufficient practical potential

in soil remediation objectives (Van Veen *et al.,* 1997). Following the introduction into the soil, a pivotal factor for failure is the rapid decline in the size of the active cell population below levels required for the objective to be achieved, rendering them ineffective to their purpose (Van Veen *et al.,* 1997).

The application requires that certain ecological conditions be present allowing an effective level of introduced micro-organisms (Van Veen *et al.,* 1997). The survival of introduced micro-organisms is largely determined by abiotic soil factors, such as temperature, pH, substrate availability, moisture content and texture. Thus, a critical assessment of these factors is required before each introduction (Gray, 1975). The physiological and genetic constitution of the inoculant determines its response to the prevailing conditions of the soil (Gray, 1975). Therefore, the ability of the introduced micro-organisms to deal with the effects of the various soil factors differs in accordance with the inoculant's ability to cope with fluctuation and adverse conditions (Gray, 1975).

Insight into micro-organisms displaying multifaceted beneficial traits, such as plant growth promotion, rhizosphere competence, abiotic stress tolerance and/or heavy metal stress tolerance is of great importance in the realm of environmental biotechnology. Such micro-organisms present novel agents in regulated and legally obligated ecological restoration efforts. The prospect of identifying and making use of already available and commercially sold bioproducts for environmental applications other than in agriculture is significant, especially in developing countries where research and funds restrict remediation practices. To the best knowledge, this study is the first of its kind with regards to exploring the bioremediation potential of agronomic products sold in South Africa.

Phenotypic or phase variation is an important characteristic demonstrated in rhizosphere competent bacteria as it allows the achievement of population diversification within a species crucial in niche adaptation and enhanced bacterial fitness when subjected to certain unfavourable conditions (van den Broek *et al.,* 2005). Colony morphotyping has been shown to be a definitive technique for assessing phenotypic variation, which is an important measure of colonisation, survival, and adaptive competence in the soil system (Sousa *et al.,* 2013). The colony morphology method was applied in this study as a means of rapidly predicting the competence of a selected strain and therefore its enduring performance following introduction into the field.

During colonisation of the different media, *Pseudomonas fluorescens* underwent phenotypic variation, which resulted in the emergence of colonies having different morphologies. The appearance of colony morphology variation of the *Pseudomonas fluorescens* on and between each of the different media, representing structured environments, demonstrates the capability for both stress tolerance and niche specialisation. Additionally, the diffuse morphology observed for some colonies indicates that motility on the agar substrates may have occurred. This is not an unusual observation as *Pseudomonas fluorescens* possesses flagella required for swarming and swimming (Harshey, 1994). Mobility has several advantages related to rhizosphere competence as it allows the microbe to colonise a greater area of the rhizosphere and populating potentially less microbially dense parts under competitive stress (Sanchez-Contreras *et al.,* 2002). Colony colour and pigmentation variation was also observed for *Pseudomonas fluorescens* on the different agar substrates. Under UV light the *Pseudomonas fluorescens* demonstrated a blue pigmentation and fluorescence on the *Pseudomonas* agar, LB and nutrient agar and a vibrant green on Kings B. Pigmentation and fluorescence appears to be linked to the nutritional composition of the growth media. Pigment production is an important parameter as it is correlated to stress tolerance and survival under different environmental conditions (Ahmad *et al.,* 2016).

Environmental stress is a major challenge for the sustainability of rehabilitation and therefore ecosystem recovery of mine sites, soils, and rock wastes (Goswami and Deka*,* 2020; Khan *et al.,* 2020). For a microbial inoculant to be considered effective in stress environments it is necessary that they display the ability to survive in adverse conditions. The results of this study suggest that the commercially available PGPR *P. fluorescens* demonstrates such a capacity for survival and persistence in unfavourable abiotic environments, further supporting its suitability in applications of bioremediation.

The global repositioning to a greener economy and the subsequent biotechnological potentials of heavy metal tolerant microbes and their cellular products provided major momentum into their research. In general, micro-organisms have many beneficial applications in the environment and are largely used for agricultural purposes, such as promoting crop yields and/or increasing soil fertility (Nazli *et al.,* 2020). However, biotechnological processes in large require that for microbial species to play a significant role, especially in matters regarding environmental and ecosystem recovery and/or heath, they

need to demonstrate heavy metal tolerance (Nazli *et al.,* 2020). This study shows that PGPR *Pseudomonas fluorescens* is 100 % tolerant to all heavy metals tested except for chromium, although the extent of growth was affected by increasing heavy metal concentrations for all metals tested, implying increased sensitivity to higher metal concentrations. Apart from chromium, the heavy metal tolerance of the PGPR *Pseudomonas fluorescens* strain indicates that they could survive and have bioremediation potential for HM-polluted environments. Tolerance to heavy metals by certain PGPR micro-organisms indicates their suitability as bio-inoculants to be applied to contaminated environments in terms of their probable survival. Based on the demonstrated heavy metal tolerance, PGPR *Pseudomonas fluorescens* strain should be further investigated for the possibility of being used for soil bioremediation purposes in heavy metal contaminated soils.

## 5.5. Conclusion

The success of using microbial agents as bio-inoculants for soil bioremediation technologies will depend on our ability to manage the rhizosphere to enhance survival and competitiveness of these beneficial micro-organisms. The use of commercially available PGPR *P. fluorescens* as a bio-inoculant for the bio-augmentation and bioremediation of contaminated soils relies on its ability to survive, replicate, and perform the desired biotechnological appointment. Rhizosphere competence, abiotic stress and heavy metal tolerance to certain common environmental parameters associated with mine lands and/or contaminated soils enables the survivability of the microbial inoculant to be gauged. This study shows that common, widely applied, and available agronomic biofertilizers, *P. fluorescens* exhibits an exceptional capacity to withstand hostile environmental conditions which, in addition to its numerous plant growth promoting traits, makes it a desirable micro-organism for use in environmental biotechnologies applied to ecosystem restoration.

## 5.6. References

Ahmad, S., Lee, S.Y., Kong, H.G., Jo, E.J., Choi, H.K., Khan, R. and Lee, S.W. (2016): Genetic Determinants for Pyomelanin Production and Its Protective Effect against Oxidative Stress in *Ralstonia solanacearum. PLOS ONE*, **11**, e0160845.

Bains, W. (1993): Biotechnology from A-Z. 1st edition. Oxford University Press, Oxford.

Berg, G. (2009): Plant-microbe interactions promoting plant growth and health: perspectives for controlled use of microorganisms in agriculture. *Applied Microbiology and Biotechnology*, **84**, 11-18.

Bruno, L.B., Karthik, C., Ma, Y., Kadirvelu, K., Freitas, H. and Rajkumar, M. (2020): Amelioration of chromium and heat stresses in Sorghum bicolor by Cr6+ reducing-thermotolerant plant growth promoting bacteria. *Chemosphere*, **244**, 125521.

Cornelis, P. (2010): Iron uptake and metabolism in pseudomonads. *Appl. Microbiol. Biotechnol*., **86**, 1637–1645.

David, B.V., Chandrasehar, G. and Selvam, P.N. (2018): Chapter 10-Pseudomonas fluorescens: A plant-growth-promoting rhizobacterium (PGPR) with potential role in biocontrol of pests of crops. In Crop Improvement through Microbial Biotechnology; Prasad, R., Gill, S.S., Tuteja, N., Eds.; Elsevier: Amsterdam, The Netherlands, pp. 221–243. ISBN 978-0-444-63987-5.

Gavrilescu, M. (2010): Environmental Biotechnology: Achievements, Opportunities and Challenges. Dynamic Biochemistry, Process Biotechnology and Molecular Biology 4 (1): 1-36. Goddard VJ, Bailey MJ, Darrah P, Lilley AK, Thompson IP (2001). Monitoring temporal and spatial variation in rhizosphere bacterial population diversity: A community approach for the improved selection of rhizosphere competent bacteria. *Plant and Soil*, **232**, 181–193.

Goldberg, J.B. (2000): Pseudomonas: Global bacteria. *Trends Microbiol*., **8**, 55–57.

Goswami, M. and Deka, S. (2020): Plant growth-promoting rhizobacteria—Alleviators of abiotic stresses in soil: A review. *Pedosphere*, **30**, 40–61.

Harshey, R.M. (1994): Bees aren't the only ones: swarming in gram-negative bacteria. *Molecular Microbiology*, **13**, 389-394.

Hider, R.C. and Kong, X. (2010): Chemistry and biology of siderophores. *Nat. Prod. Rep*., **27**, 637–657.

Iqbal, M. and Edyvean, R.G.J. (2004): Biosorption of lead, copper and zinc on loofa sponge immobilized biomass of *Phanerochaete chrysosporium*. *Mineral Engineering*, **17**, 217-223.

Jeyasingh, J. and Philip, L. (2005): Bioremediation of chromium contaminated soil: optimization of operating parameters under laboratory conditions. *Journal of Hazardous Materials*, **118**, 113–120.

Khan, N., Ali, S., Tariq, H., Latif, S., Yasmin, H., Mehmood, A. and Shahid, M.A. (2020): Water conservation and plant survival strategies of rhizobacteria under drought stress. *Agronomy*, **10** (1683).

Kloepper, J., Ryu, C. and Zhang, S. (2004): Induced systemic resistance and promotion of plant growth by *Bacillus* spp. *Phytopathology*, **94**, 1259-66.

Kraemer, S.M. (2004): Iron oxide dissolution and solubility in the presence of siderophores. *Aquat. Sci*., **66**, 3–18.

Nazli, F., Mustafa, A., Ahmad, M., Hussain, A., Jamil, M., Wang, X., Shakeel, Q., Imtiaz, M. and Esawi, M.A.E. (2020): A Review on Practical Application and Potentials of Phytohormone-Producing Plant Growth-Promoting Rhizobacteria for Inducing Heavy Metal Tolerance in Crops. *Sustainability*, **12** (9056).

Palleroni, N.J. and Cornelis, P. (2008): The road to the taxonomy of Pseudomonas. *Pseudomonas: Genomics and Molecular Biology,* Caister Academic Press, U.K., pp.1-18.

Palleroni, N.J. (2010): Pseudomonas. *Topley and Wilson's Microbiology and Microbial Infections,* John Wiley & Sons, Ltd.

Raaijmakers, J.M., Vlami, M. and de Souza, J.T. (2002): Antibiotic production by bacterial biocontrol agents. *Antonie Van Leeuwenhoek International Journal of General and Molecular Microbiology*, **81** (1-4), 537-547.

Roca, C. and Olsson, L. (2001): Dynamic responses of Pseudomonas fluorescens DF57 to nitrogen or carbon source addition. *Journal of Biotechnology*, **86** (1), 39-50.

Sánchez-Contreras, M., Martın, M., Villacieros, M., O'Gara, F., Bonilla, I. and Rivilla, R. (2002): Phenotypic Selection and Phase Variation Occur during Alfalfa Root Colonization by *Pseudomonas fluorescens* F113. *Journal of Bacteriology*, **184** (6), 1587 – 1596.

Shinwari, K.I., Shah, A., Afridi, M.I., Zeeshan, M., Hussain, H., Hussain, J., Ahmad, O. and Jamil, M. (2015): Application of Plant Growth Promoting Rhizobacteria in Bioremediation of Heavy Metal Polluted Soil. *Asian journal of multidisciplinary studies*, **3** (4), 179 – 185.

Sousa, A.M., Machado, I., Nicolau, A. and Pereira, M.O. (2013): Improvements on colony morphology identification towards bacterial profiling. *Journal of Microbiological Methods*, **95**, 327–335.

van den Broek, D., Bloemberg, G.V. and Lugtenberg, B. (2005): The role of phenotypic variation in rhizosphere *Pseudomonas* bacteria. *Environmental Microbiology*, **7** (11), 1686–1697.

Weller, D. (2007): *Pseudomonas* biocontrol agents of soil-borne pathogens: looking back over 30 Years. *Phytopathology*, **97** (250).

Whipps, J.M. (2001): Microbial Interactions and Biocontrol in the Rhizosphere. *Journal of Experimental Botany*, **52**, 487 – 511.

Wu, C.H., Wood, T.K., Mulchandani, A. and Chen, W. (2006): Engineering plant–microbe symbiosis for rhizoremediation of heavy metals. *Appl. Environ. Microbiol*., **72**, 1129–1134.

# Chapter 6 - Crocidolite and amosite asbestos occurrences and mineralisation in the Precambrian Banded Iron Formations of South Africa: Implications for iron and manganese ore mining and significance for field identification and *in situ* hazard evaluation

Abstract

The literature on asbestos minerals fibres and their subsequent health and environmental hazard is currently extensive and of much interest. However, research and literature regarding natural occurrences of two of the most carcinogenic asbestos varieties, crocidolite and amosite, are minimal, specifically in the non-commercial perspective. The study presents a collection of photographic records outlining the variability of macroscopic morphologies, host rock lithologies, structural characters, alteration and cohesion states of crocidolite and amosite asbestos-containing rock specimens. In this study, various structural features in the rock specimens are used to assign and constrain time of formation and mechanisms of deformation to amphibole-asbestos mineralisation so as to better understand the geological conditions and structural aspects controlling their occurrence. This is done within context of a predictive approach during iron and manganese ore mining. The various structures observed in the representative samples indicate that numerous mechanisms of formation and deformation potentially occurred during different periods of time within the geological history of the Lower Griqualand Stage of the Transvaal Supergroup.

## 6.1. Introduction

The term asbestos, habitually and in accordance with South African legislation, applies specifically to a group of six naturally occurring fibrous silicate minerals known commonly as tremolite, actinolite, crocidolite, amosite, anthophyllite and chrysotile (Hodgson, 1977; Williams *et al.,* 2013; Gualtieri, 2021). This definition of the term asbestos is, for most practical purposes, adequate. However, currently this definition connects various regulatory and scientific disciplines causing ongoing and unresolved controversial debate on a more comprehensive and exclusive definition of the term (Gualtieri, 2017). On that note, the

definition of asbestos has, over the years, customarily been applied and defined in no less than four disparate ways, subject to the specified situations, including commercial, regulatory, mineralogical, and geological and analytical asbestos definitions (Glenn *et al.,* 2008).

Extensive research aimed at identifying and defining the hazardous morphological parameters of these six commercially mined and regulated asbestos fibre mineral types has been done over the last few decades and is well detailed. However, these hazard and risk assessments are based on and designed for occupational asbestos exposures (Petriglieri *et al.,* 2021).

Naturally occurring asbestos (NOA) defines fibrous minerals that are natural components of soils and rocks (Harper, 2008; Baumann *et al.,* 2015). In the natural environment asbestos occurrences are common (Case *et al.,* 2011). These NOA sites present an asbestos hazard whenever airborne fibres, both fibrillar bundles and individual fibrils, are produced because of disturbance processes (Vignaroli *et al.,* 2014). The low density and small size of asbestos fibres easily facilitates their airborne transport and dispersion into surrounding environmental ecosystems (Petriglieri *et al.,* 2021). Fibre dispersion is naturally constituted by weathering, erosion, and wind mobilisation (Petriglieri *et al.,* 2021). The asbestos hazard posed by airborne fibres is twofold, affecting both the abiotic and biotic environment. Areas with soil and sediment containing NOA are potential exposure sources for nearby populations and disturbances, such as human activities and erosion, increase this risk as fibres become airborne and disperse (Carbone *et al.,* 2011; Baumann *et al.,* 2013). Weathering of naturally occurring asbestos (NOA) is a major health and environmental concern as the environmental dispersion of hazardous trace elements is mainly caused by weathering processes (Buccianti *et al.,* 2009; Guagliardi *et al.,* 2013a; Guagliardi *et al.,* 2013b, Guagliardi *et al.,* 2016a; Guagliardi *et al.,* 2016b; Perri *et al.*, 2015; Perri *et al.*, 2016; Apollaro *et al.,* 2018). Potential environmental exposure to respirable mineral dust from NOA is of great concern.

Unlike asbestos fibres emitted from occupational exposure sources, those occurring in their natural environment have compositions that are heterogeneous with mixtures of fibre morphologies, intermediate shapes, and many mineral phases (Petriglieri *et al.,* 2021). The natural environmental contexts of NOA have massive intrinsic diversity and are considered as unconfined sites. This complexity is not accounted for in the risk evaluation, based on

their hazardous morphological parameters, outlined in the guidelines compiled for occupational exposure to commercial asbestos fibres.

In this study, numerous South African crocidolite and amosite rock samples were evaluated with the aim of (i) connecting the expected occurrence of hazardous fibrous minerals to geo-diversities and recurrent lithotypes to predict and prevent accidental disturbance to asbestos-bearing geo-sites and (ii) understanding and identifying the complex nature and wide spectrum of colours, morphologies, natural shapes and alteration modes exhibited by asbestos rocks in the natural setting.

## 6.2. The geographical and geological context of amphibole asbestos-hosting BIF in South Africa

The amphibole asbestos deposits of South Africa are found in the banded iron formation of the Neoarchaean-Palaeoproterozoic Transvaal Supergroup (Eriksson *et al.,* 2006). Two structural basins of the Transvaal Supergroup are preserved in South Africa, namely (1) the Transvaal Basin (Northwest, Limpopo, Mpumalanga and Gauteng provinces) and (2) the Griqualand West Basin (Northern Cape and Northwest provinces) (figure 6.1) (Eriksson *et al.,* 2006).

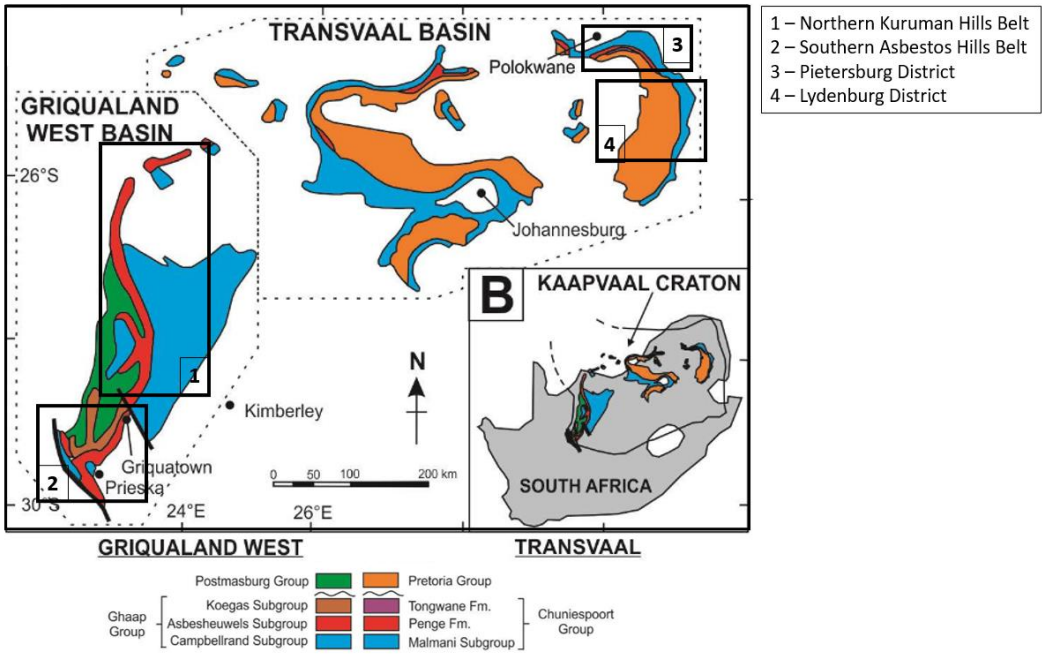


Figure 6.1: The two structural basins of the Transvaal Supergroup: Griqualand West Basin and the Transvaal Basin (adapted from Warke, 2016 ).

The rocks of the Transvaal Supergroup are exposed on a wide arc spanning from the Orange River in the Northern Cape province some 1000 km to Botswana and then east and south into the Limpopo province (du Toit, 1952). The crocidolite and amosite asbestos minerals found in these strata have notable differences with respect to their origin (Cilliers and Genis, 1964). The Asbestos Hills in the Northern Cape province host crocidolite deposits only and seem to be reliant on changes in the host rock structure occurring at the convergences of cross-folding and consecutive folding (Hodgson, 1977). Cross fibre veins of crocidolite asbestos form seams between 0.5 to 100 mm thick provided that the correct chemical composition and dynamic forces were imposed in the correct locations (Hodgson, 1977).

The amosite asbestos fields in the eastern Limpopo (Transvaal) are characterised by the sample depositional history as those of the crocidolite fields in the Northern Cape Province, however, that is where the comparison between the two ends (Hodgson, 1977). The generally thicker and more numerous amosite fibre seams are ash grey in colour and their host rocks are dense and dark grey (Hodgson, 1977).

## 6.3. Methodology

Three methods of the investigation were employed: (1) thorough review of the literature, (2) sampling, photographic documentation and visual characterisation, including a alteration, relevant to field identification in all aspects and sectors affected by NOA and (3) field tests to determine the presence of carbonate and to distinguish whether the minerals are fibrous or pseudo-fibrous. Additionally, rock specimens with features important to current debates on certain topics will be elucidated on.

### 6.3.1. Samples

In this study, 18 naturally occurring asbestos-bearing rock samples were collected and studied, of which 15 were crocidolite and 3 were amosite. The samples were collected from numerous locations scattered across three South African provinces. To provide an overview and connect lithologies and general characteristics, the samples where characterised based on their regional occurrence and discussed using an 'area-type' approach. This approach provides more useful criteria in the mining context that occupy large areas of land as well as remote communities scattered across more 'rural' provinces, where population density is low and distributed over great lateral expanse. Four 'type-areas' were chosen, although part of the same geological units of the Transvaal Supergroup demonstrate geological characteristics that distinguish each. These 'type-areas' include the: (1) Northern Kuruman Hills Asbestos Belt; (2) Southern Asbestos Hills Asbestos Belt; (3) Pietersburg Asbestos Belt and (4) Lydenburg Asbestos Belt. The Northern Kuruman Hills Asbestos Belt and Southern Asbestos Hills Asbestos Belt occur in the Griqualand West Basin (Northern Cape and Northwest provinces) of the Transvaal Supergroup, and the Pietersburg Asbestos Belt and Lydenburg Asbestos Belt occur in the Limpopo Province portion of the Transvaal Basin (Northwest, Limpopo, Mpumalanga, and Gauteng provinces) of the Transvaal Supergroup. The 'type-area' and associated sample numbers, sizes, fibre-lengths, and magnetic properties of the asbestos-bearing rock specimens are summarised in table 6.1.

Table 6.1: General parameters of the naturally occurring asbestos-bearing rock specimens studied including 'type-area', sample number, sizes, fibre-lengths, and magnetic properties.

| **Sample #** | **Size (cm)** | **Fibre length (cm)** | **(1) Associated magnetite and (2) host rock magnetism? (yes/no)** | **Magnetic strength** |
|---|---|---|---|---|
| | | | | |
| **Northern Kuruman Hills Asbestos Belt (figure 1)** | | | | |
| | | | | |
| 1 | 4 (L); 2.5 (W); 5.5 (H) | 3.9 | (1) Yes<br>(2) Yes | Strongly magnetic |
| 2 | 2.3 (L); 2 (W); 1.9 (H) | 1.5 | (1) Yes<br>(2) Yes | Strongly magnetic |
| 3 | 5.5 (L); 5.2 (W); 4.4 (H) | Three seams: 1.8; 0.1; 0.3 | (1) Yes<br>(2) Yes | Moderately magnetic |
| 4 | 6.5 (L); 2.5 (W); 3.5 (H) | 1.7 | (1) Yes<br>(2) Yes | Strongly magnetic |
| 5 | 10 (L); 9 (W); 5.5 (H) | Top seam: 1; middle seam: 2; bottom seam: 0.5 | (1) Yes<br>(2) Yes | Moderately magnetic |
| | | | | |
| **Southern Asbestos Hills Asbestos Belt (figure 1)** | | | | |
| | | | | |
| 6 | 11.5 (L); 6.5 (W); 2.1 (H) | 0.2 – 0.9 | (1) Yes<br>(2) Yes | Moderately magnetic |
| 7 | 7 (L); 3 (W); 3.5 (H) | 2.5 | (1) Yes<br>(2) Yes | Weakly magnetic |
| 8 | 6.5 (L); 3 (W); 4 (H) | 7 | (1) Yes<br>(2) Yes | Moderately magnetic |
| 9 | 15.5 (L); 4 (W); 8.5 (H) | 3.3 | (1) Yes<br>(2) Yes | Strongly magnetic |
| 10 | 10.5 (L); 4 (W); 2 (H) | 6 | (1) Yes<br>(2) Yes | Moderately magnetic |
| 11 | 6.5 (L); 4.5 (W); 3.8 (H) | 3.2 | (1) Yes<br>(2) Yes | Strongly magnetic |
| 12 | 8 (L); 6 (W); 5 (H) | 1.8 | (1) Yes<br>(2) Yes | Strongly magnetic |
| 13 | 13.5 (L); 7.5 (W); 3.5 (H) | 2 | (1) Yes<br>(2) Yes | Weakly magnetic |
| 14 | 9 (L); 7.5 (W); 4.5 (H) | 4 | (1) Yes<br>(2) Yes | Moderately magnetic |

| | | | | |
|---|---|---|---|---|
| | | | | |
| **Pietersburg Asbestos Belt (figure 1)** | | | | |
| | | | | |
| 15 | 13.5 (L); 9.5 (W); 5 (H) | 3 – 4.5 | (1) Unknown - can't be determined in hand sample<br>(2) Yes | Moderately magnetic |
| | | | | |
| **Lydenburg Asbestos Belt (figure 1)** | | | | |
| | | | | |
| 16 | 14.5 (L); 7 (W); 5.5 (H) | 2 | (1) No<br>(2) No | Non-magnetic |
| 17 | 15 (L); 6 (W); 8.5 (H) | 1.5 – 4.5 | (1) No<br>(2) No | Non-magnetic |
| 18 | 12.5 (L); 5.5 (W); 6.5 (H) | 4.5 | (1) No<br>(2) No | Non-magnetic |

The rock specimens were thoroughly examined in detail regarding their host-rock lithologies, seam morphologies, structures associated with mineralisation, structures associated with deformation, secondary mineralisation, degree of weathering and alteration status. Photographic were taken to illustrate and classify amphibole asbestos mineralisation in banded iron formations to provide a geological, field-based record of the geo-diversities and heterogeneities expressed by naturally occurring amphibole asbestos rocks.

### 6.3.2. Determination of carbonate presence

A weak solution of hydrochloric acid (10 %) was used to determine whether carbonate minerals were present in the host rock lithologies of each of the samples. A drop of the HCL solution was placed on the rock specimen and the determination of carbonates was done by observing whether fizzing occurs, indicating that carbon dioxide gas bubbles are released.

### 6.3.3. Distinguishing fibrous and pseudo-fibrous minerals

The material appearing fibrous in each sample was identified and a small amount removed from the rock specimen and crushed using a mortar and pestle along with alcohol. The crushed material was observed with a hand lens to distinguish whether it formed (i) a powder or (ii) separable fibres or needles or (iii) matted together to form a ball. If the sample was crushed to a powder, it is classified as not fibrous, however, if a matted ball or separable fibres resulted following crushing the material is considered fibrous and potentially asbestiform.

## 6.4. Results

Amphibole asbestos occurring in the natural environment is characterised by various lithologies, colours, lengths, complex structural features relating to both mineralisation and deformation, intermixed fibre morphologies and mineral phases, heterogeneous composition and appearance as related to degree of alteration. The sample description, lithology and carbonates, deformation character and morphological and structural features are summarised in table 6.2.

Table 6.2: Summary of the sample description, lithology and carbonates, deformation character and morphological and structural features

| **Sample #** | **General description** | **Host rock lithology** | **Carbonates?** | **Morphological and structural features, deformation character (brittle vs. ductile)** |
|---|---|---|---|---|
| | | | | |
| 1 | Oxidised composite seam | Banded ironstone | Yes | Planar upper surface, corrugated and irregular lower bounding surface, bifurcation of magnetite laminae, fibre cones, ridge-like structures formed by wavy magnetite laminae, cone-in-cone structures, disseminated magnetite crystals dispersed along cross-fibre length |
| 2 | Oxidised simple seam | Banded ironstone | No | Planar upper and lower bounding surface; kinked cross-fibre band |
| 3 | Three separate simple seams, discoloured | 'Sandy' jasper | No | Three simple seams of varying fibre length; planar upper surface for all three and irregular lower surface for all due to marginal magnetite disruptions and wavy behaviour; inclined fibres in largest most upper seam |

| | | | | |
|---|---|---|---|---|
| 4 | Discoloured composite seam | Banded chert | No | Irregular bounding surfaces; internal magnetite screens; infilled planes of fracture cutting irregularly across lower portion of seam; randomly distributed spherulite riebeckite occurrence associated with planes of fracture in lower portion of seam |
| 5 | Discoloured, oxidised, silicified composite seam | Jasper | No | Locally and restricted warped bedding planes; cones; cone-in-cones; ridge-like protrusions; mixed fibre orientations; central magnetite partings; marginal magnetite disruptions and magnetite laminae oscillating between upper and lower bounding surfaces in a sinusoidal manner |
| 6 | Brown band of acicular amphibole arranged in cross-fibre manner, simple seam | Jasper | No | Planar upper and lower bounding surfaces; narrowing and widening seam behaviour; bend to curved cross-fibres |
| 7 | Composite seam | Massive riebeckite (both blue bands and orange bands). Orange massive riebeckite result from large amount of dispersed magnetite | No | Rapid variation in cross-fibre length; pinch and swell structures; cusp and lobe interface buckling; highly irregular, lenses of cross-fibres |
| 8 | Brown acicular cross-fibre amphibole simple seam | Banded quartz, carbonate and stilpnomelane | Yes | Wavy seam bounding surfaces; curved cross-fibre orientation; cones structures; large magnetite crystals disseminated through cross-fibres and at bounding surfaces |
| 9 | Silicified composite seam | Banded jasper and ironstone | No | Planar boundings surface; cone-in-cone structures; internal magnetite partings; marginal disruption of magnetite; bifurcation of magnetite laminae; ridge-like protrusions due to irregular behaviour of magnetite screens across cross-fibres |
| 10 | Silicified simple seam (Hawks-eye) | Ferruginous black shale | No | Planer bounding surfaces; mixed fibre orientation |
| 11 | Silicified simple seam (Hawks-eye and Tigers-eye mixture) | Mudstone | No | Planer bounding surfaces; mixed fibre orientation |

| | | | | |
|---|---|---|---|---|
| 12 | Silicified simple seam (Hawks-eye) | Banded jasper and ironstone | No | Marginal fibrous quartz; upper planar and lower irregular structures; disrupted magnetite screen; cone-in-cone structures; plastic turbulence structures on cone margins; minute fractures; slip fibres; bedding parallel fibrous quartz veins; mixed fibre orientation |
| 13 | Silicified composite seam (Tigers-eye) | Banded mudstone and ironstone | No | Cone structures; marginal ridge-like protrusions; central discontinuities in seam; marginal disruptions of magnetite |
| 14 | Silicified simple seam (Tigers-eye) | Banded mudstone and ironstone | No | Planar bounding surfaces; mixed fibre orientations |
| 15 | Folded simple seam | Banded ironstone | No | Inclined fibres; folded host rock |
| 16 | Simple amosite seam | Shaley type banded ironstone | Yes (weak – siderite?) | Wavy bounding surfaces; fibre cones |
| 17 | Composite amosite seam | Shaley type banded ironstone | Yes (weak – siderite?) | Internal continuous and discontinuous dark non-magnetitic black laminae (dark lines); planes of fracture; curved and inclined fibre orientations; jagged and uneven upper bounding surface; unequal fibre length across cross-fibre seam; fibres truncating bedding planes |
| 18 | Simple amosite seam | Shaley type banded ironstone | Yes (weak – siderite?) | Uneven and wavy bounding surfaces; cone structures (waste cones); dark lines and associated ridge-like protrusions; disorientated grunerite crystals and rosettes dispersed through the cross-fibres |

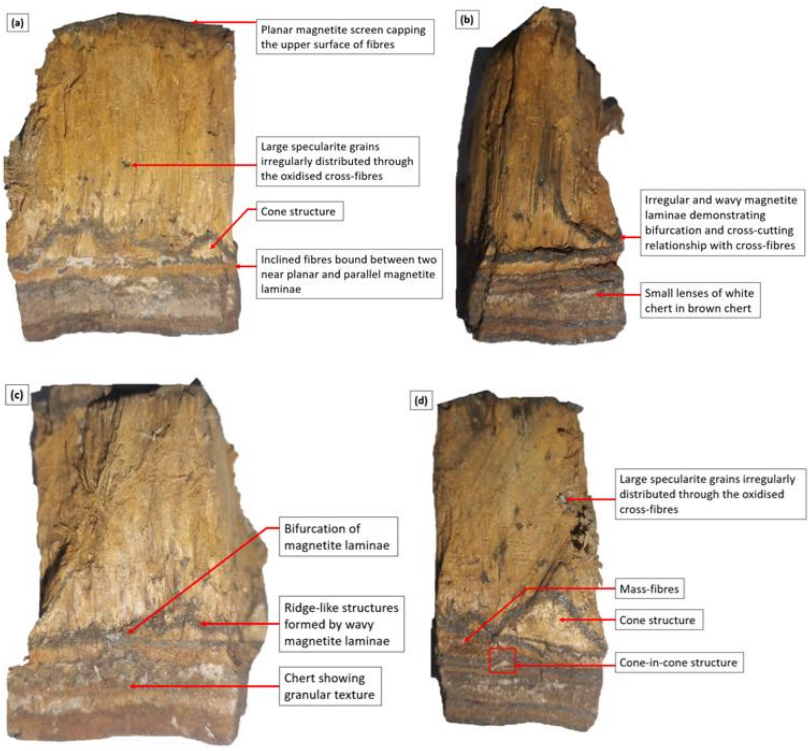


Figure 6.2: (sample 1) Composite seam of oxidised crocidolite (griqualandite) displaying 'corrugated' or cone structures and bifurcation of thin magnetite seams.

The banded ironstone host rock in sample 1 is only observed underlying the cross-fibre and is well-bedded, demonstrating conspicuous banding composed of fine to moderate laminations. The alternating ferruginous and siliceous layers are distinctly distinguished in hand sample. The fibres are bound by magnetite screens on both the upper and lower surfaces. The magnetite bands have a black colour and are generally thinner than those representing the siliceous layers. In addition, the magnetite layers show a general uniformity with respect to the thickness of the various individual layers. The chert layers are, in large, thicker than those of magnetite and have a general patchiness with respect to their colour both within and between individual bands. Brown, yellow, and whitish colours are all observed, and the individual chert laminae vary substantially in thickness. In hand sample, the thickest chert laminae are observed to have a lenticular texture in places, while lenses or elongated bodies of whitish and/or lighter coloured chert occur within the brown chert layers giving it a speckled appearance. This rock sample also contains a considerable amount of magnetite crystals (~ 0.5 – 1 mm) dispersed throughout the upper and lower portions of the cross-fibre material (figure 6.3a). The cross-fibres are approximately 3.9 cm in length, and

although a distinct fibrous structure can be recognised, they are characterised by an ochreous, orange-brown colour (figure 6.3b, c). This highly oxidised fibrous material is soft and easily powdered when rubbed between the fingers.

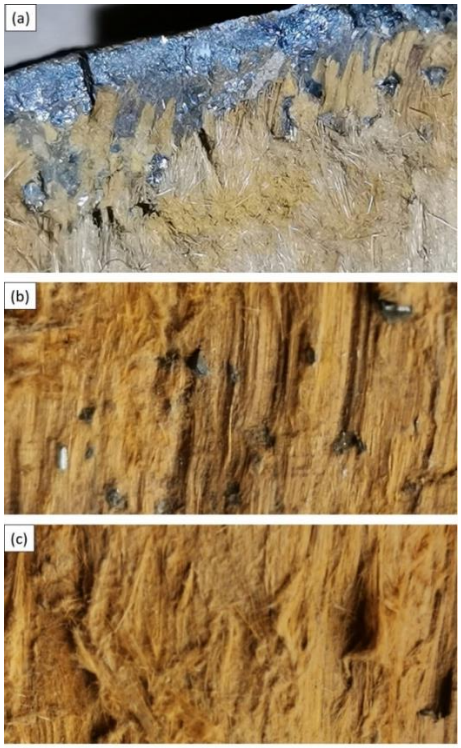


Figure 6.3: (sample 1) Oxidised crocidolite fibres (a) disseminated magnetite crystals in the upper portion of the fibre seam derived from the upper magnetite screen; (b) fragments of the magnetite layers scattered throughout the fibres derived from the magnetite bands overlying and underlying the cross-fibre and (c) texture and colour of the soft, ochreous, matted fibrous griqualandite material that resulted from the oxidation of crocidolite.

This sample represents a composite seam as it contains several, thin magnetite partings roughly parallel to both bounding surfaces and persist across the seam. The seam is distinctly asymmetrical due to the nature of the outer bounding surfaces. A planar and irregular magnetite screen forms the upper and lower bounding surface, respectively. In hand sample, distinct and small-scale variations in the lengths of the fibres are identified and reflected on only the lower seam surface by cone-like and corrugated structures. A smaller, thinner fibre seam below the thick composite seam is identified in the hand sample. This seam has relatively thick, distinct planar to sub-planar magnetite contacts on both surfaces. The fibres in this narrow seam have an inclined orientation and mostly retain a uniform thickness.

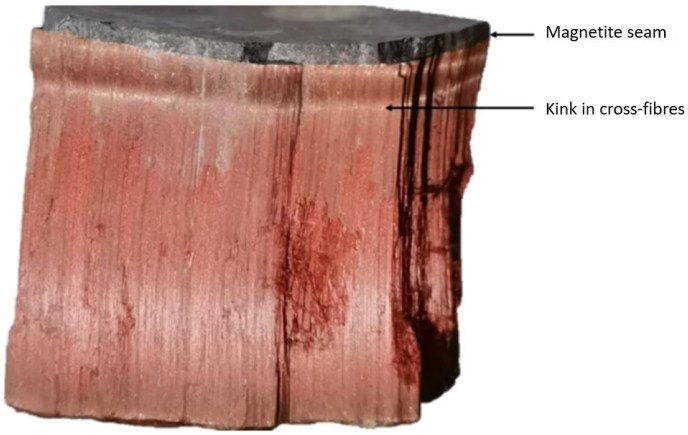


Figure 6.4: (sample 2) Oxidised, simple crocidolite cross-fibre seam showing magnetite seam at the upper bounding surface (scale ~ 1cm x 1 cm)

Sample 2 is composed of crocidolite cross-fibres and a 2 mm-thick black magnetite seam. A single, pronounced kink is observed in the upper portion of the seam nearest to the magnetite seam. The pronounced red colour of the fibres observed in this sample indicates oxidation, resulting in the soft red fibrous material. Although the fibrous structure is clearly preserved in this sample the material readily powders when touched.




Figure 6.5: (sample 3) Three silvery crocidolite seams within a ‘sandy’ jasper host rock.

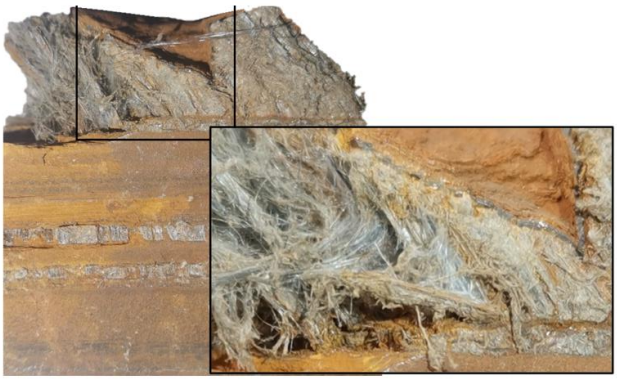

Figure 6.6: (sample 3) Irregular upper bounding surface of thickest seam due to local warping of bedding.

Sample 3 resembles a soft, porous, light brown to leached brown shale or mudstone and represents a 'sandy' jasper. Alternating beds of yellowy-brown chert and reddish-brown thickly banded jasper with thin, dark grey magnetite layers comprise the host rock. The magnetic properties of this sample are a result of both the thin magnetite bands and fibre-associated magnetite screens. Unlike the magnetite layers within the host rock, the magnetite crystals making up the screens are larger in size and less well linearly and cohesively arranged in the layers. The fine, sandy texture and porous nature of the rock suggests that possible leaching may have removed some material.

The thickest fibre seam in the sample contains inclined fibres and the two thinner seams are perpendicular to the bedding. All three seams are associated with magnetite screens. The crocidolite fibres in the three seams observed in the sample are distinctly silvery-greyish blue in colour and those in the thickest upper seam exhibit a soft and fluffy nature with fibres being easily detached from bundles upon disturbance. The two thinner lower seams display distinct lateral variations in cross-fibre length and in certain areas complete disruptions in the seam resembling pinch-and-swell and boudinage structures.

When the sample is observed from the side, a thin, warped, and contorted bed covering the inclined fibres at the top of the sample is identified in the otherwise unfolded banded specimen (figure 6.6). The single 'tiny fold' in the upper bedding plane protrudes into the crocidolite fibres and is characterised by a steeply angled axial plane. The pale, greyish to silvery blue colour of the fibres in this samples indicates that this sample has experienced incipient alteration resulting in discolouration. Accompanying the change in colour is

noticeable loss of fibre stringiness, with the fibres being fleecier and finer and having an overall woolly appearance.



Figure 6.7: (sample 4) Composite crocidolite seam in banded chert.

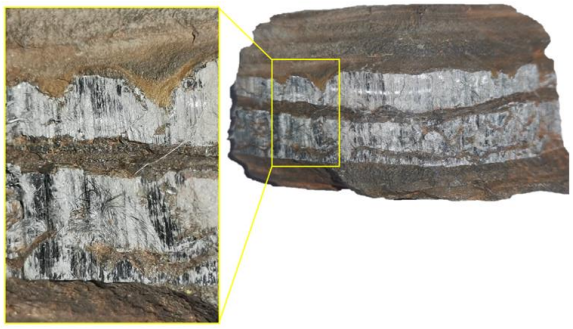

Figure 6.8: (sample 4) Composite seam of cross-fibre crocidolite having a wavy central magnetite parting and interface buckling at the upper bounding surface.



Figure 6.9: (sample 4) Composite cross-fibre seam that exhibits small-scale variation in fibre lengths. The seam in the upper portion of the image has irregular and wavy bounding surfaces resulting in length variations in cross-fibres. The seam in the lower portion of the image shows wavelike patterns of the fibres due to irregular wave-like magnetite partings resulting in variations in fibre length.

Thick, poorly-bedded grey to black banded chert that are in large devoid of ferruginous layers. Equi-granular, magnetite grains are dispersed through the microcrystalline quartz matrix in certain places of the sample. In this specimen, these areas containing exposed magnetite grains in the sample are observed as a reddish-brown coating and represent alteration of magnetite to goethite and/or hematite. In other instances, the surface of the chert layers observed in the rock sample appears to be minutely pitted and resembles fine-to-medium-grained quartzite. This is attributed to the complete removal of magnetite grains from the chert matrix through weathering. The finely spotted surfaces in other chert layers indicate the presence of the iron-oxides within the microcrystalline quartz matric. Thin, conspicuous, and persistent magnetite bands are observed to be restricted to between and within the cross-fibre seams. The composite seam is formed by a relatively thick, wavy central parting of magnetite and the host rock of the upper bounding surface displays cusp and lobate folds giving the seam an irregular upper bounding surface (figure 6.8). Fractures infilled with magnetite are numerous in the lower portion of the composite seam and appear to be associated with riebeckite spherulites (figures 6.9 and 6.10).

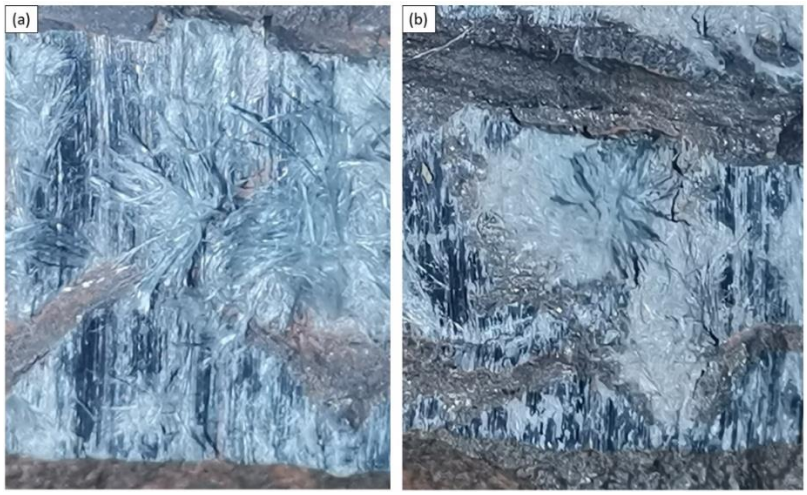


Figure 6.10: (sample 4) Spherulites of fibrous riebeckite associated with irregular magnetite layers disrupting crocidolite cross-fibres.

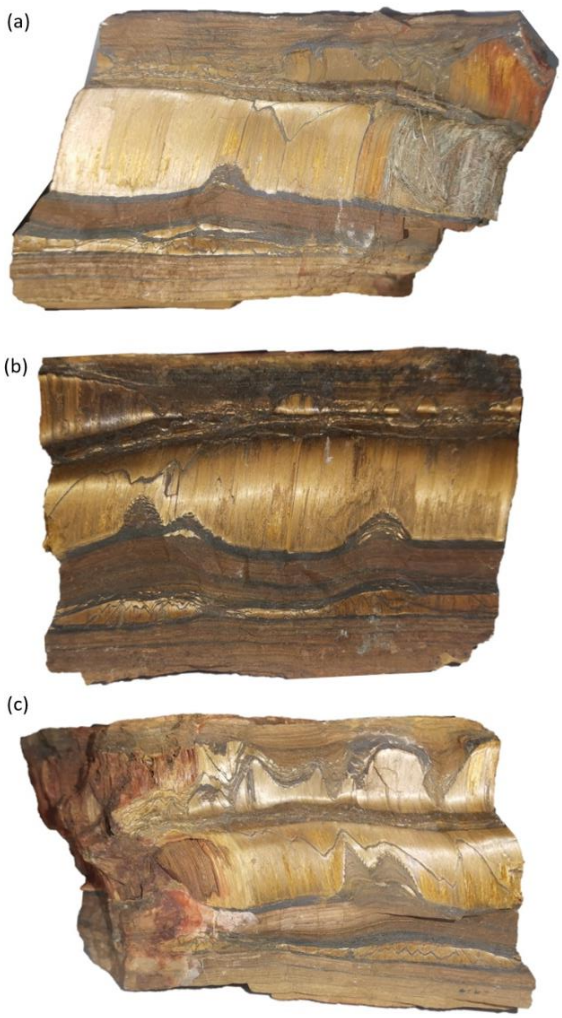


Figure 6.11: (sample 5) Discoloured, oxidised and silicified composite seam in thinly banded shaly material and brown jasper. Side views are shown in (a) and (c) and the back view in (b).

Thinly bedded, soft, very fine-grained, yellowish brown shaley/argillaceous layers and finely, well-bedded brown chert or jasper bands make up the host rock. The bedding of the host rock shows very restricted, small-scale warping in specific localities within a largely un-disturbed bedding plane sequence. The degree of weathering and alteration varies in different parts of this specimen showing blue to grey discoloured fibres, red and orange oxidised fibres and golden silicified fibres.

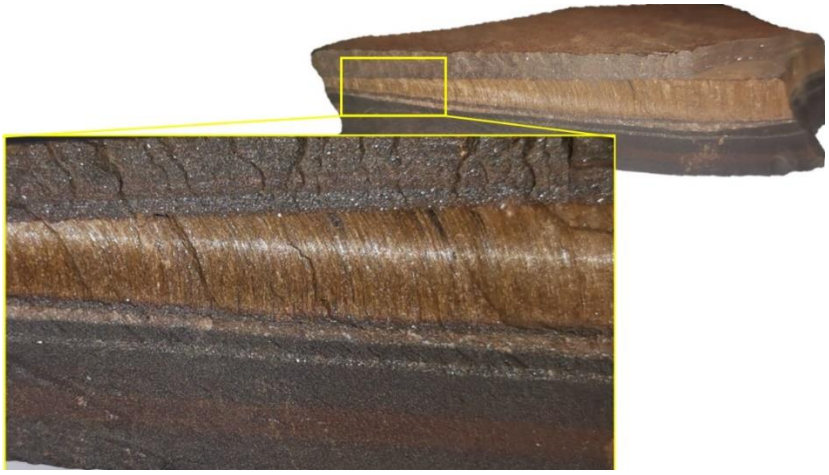

Figure 6.12: (sample 6) Brown acicular amphibole cross-fibre seam with planar bounding surfaces.

The sample is divided into three portions consisting of different mineralogy. The upper portion (i.e., rock above the fibre seam) is magnetic and composed of finely laminated, extremely thin, alternating silvery and brown layers with perfect slaty cleavage giving the rock a massive appearance. The portion below the fibre seam is composed of black and red jaspers with poor and uneven bedding planes having conchoidal fractures. The complete lack of interbedded bands of magnetite in this lower rock portion means that it is devoid of magnetic properties. The fibres are composed of brown amphibole cross-fibres and show a narrowing of the seam along the bedding planes.

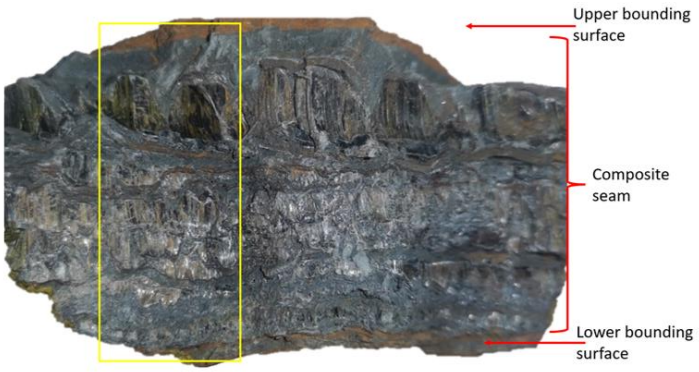


Figure 6.13: (sample 7) Composite seam composed of cross-fibre crocidolite in lenses of mass fibre riebeckite.



Figure 6.14: (sample 7) Blue coloured riebeckite rich bands composed of complex, interwoven, dis-orientated acicular crystals.

This rock specimen shows a composite asbestos seam composed of irregular-sized and -distributed cross-fibre crocidolite and hard, blue, massive riebeckite. The blue coloured bands are rich in riebeckite and crocidolite and contain very little magnetite. The top portion of the rock sample is composed of a layer of greenish-grey cross-fibre asbestos known as Prieskaite. Riebeckite layers in the banded ironstones are composed of randomly orientated and intimately interlocked riebeckite needles (figure 6.14). These cross-fibre lenses are various shapes and sizes with little lateral continuity (figure 6.15).



Figure 6.15: (sample 7) Section through the seam to show the variation in the small fibre seams due to irregular pinch and swell behaviour of bounding surfaces.

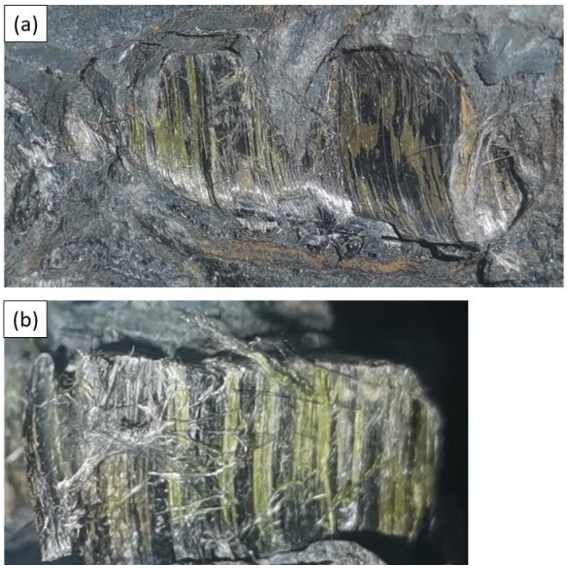


Figure 6.16: (sample 7) Showing (a) pinch-and-swell structures and (b) green and black cross-fibres characterising the sample.

The sample shown in figure 6.16 is described by Cilliers (1961) as Prieskaite. These layers of greenish-grey cross-fibre asbestos have a significantly lower ferric iron content than crocidolite, however, the morphology indicates their potential toxicity. To the best of knowledge such mineral fibres have not been reported in terms of hazardous fibrous minerals and present an interesting subject for future research.

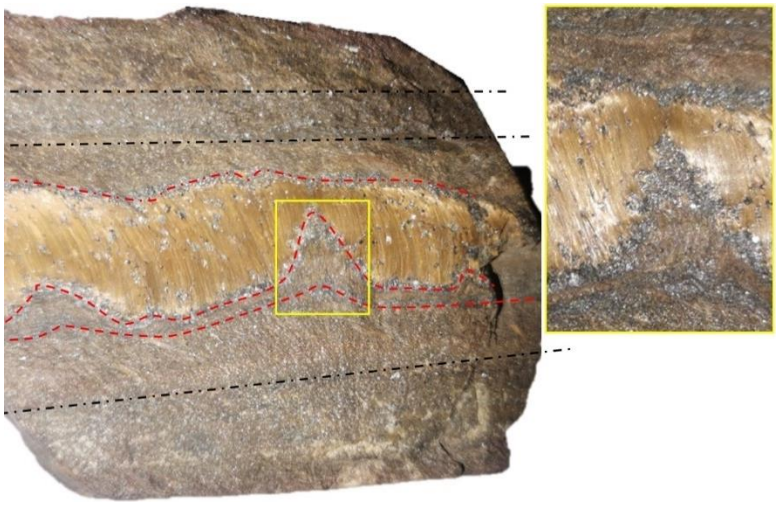

Figure 6.17: (sample 8) Carbonate-rich rock containing cross-fibre brown acicular amphibole with large magnetite dispersed through the fibres and concentrated at the bounding surfaces.

The sample is composed of darker brown, iron-rich layers composed of alternating quartz and carbonate layers, and lighter brown iron poor layers composed of mainly quartz and carbonate with abundant needles and sprays of brown stilpnomelane crystals. The boundaries between the bands are wavy and they have uneven thickness throughout the sample. The cross-fibre seam is composed of compact acicular amphibole and the lower bounding surface contains cone structures.

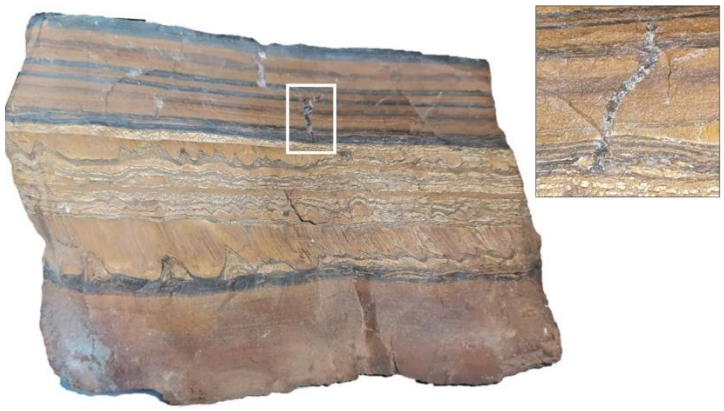

Figure 6.18: (sample 9) Silicified crocidolite seam in banded jasper and ironstone showing a complex composite structure.

Thick unevenly-bedded bands of light to dark brown jasper contain an abundance of black magnetite bands. The jasper bands have been silicified and thus the rock is hard and resistant to weathering. The sample contains quartz-filled, fissure-like vertical cracks cross cutting the bedding, which is a feature that always coincides with silicified hard jasper (Schoeman, 1929). A composite seam of silicified crocidolite containing numerous thin and persistent partings is observed within the host rock. These partings have resulted in the average fibre length in the seam bearing no relation to the total width of the seam from one bounding surface to the other. The complex nature of this crocidolite seam potentially indicates that the commencement of fibre growth, simultaneously or elsewhere, at the base, middle or top of a seam and the overall irregular crystallisation of crocidolite over disrupted intervals results in this composite structure (figure 6.19). Marginal cone-in-cone structures of fibre layers between nested conical magnetite structures are show in figure 6.20.

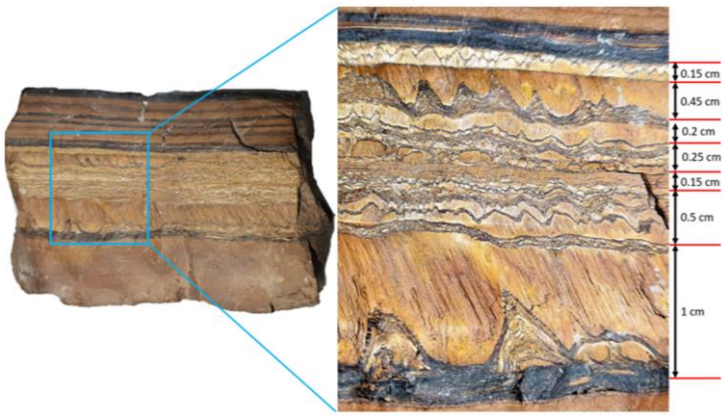


Figure 6.19: (sample 9) Wavelike patterns and the small-scale variation of fibre lengths. The wavy seams that occur above and below one another have similar profiles and formed during fibre growth.

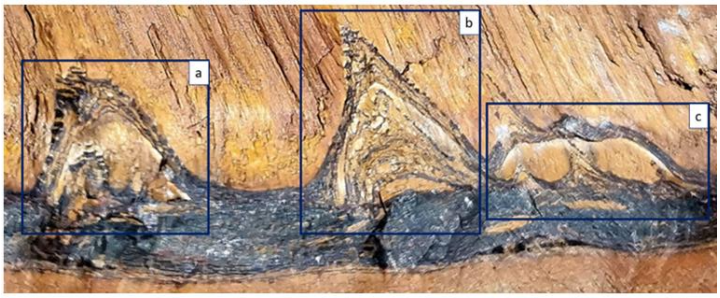


Figure 6.20: (sample 9) Shows three different cone-in-cone structures lying next to one another along the same plane (a) (0.8 cm L x 0.7 cm H); (b) (0.8 cm L x 1 cm H); (c) (0.9 cm L x 0.4 cm H) (L = length; H = height). Cone in the seam that contains several subsidiary cone-shaped layers of magnetite resulting in cone-in-cone structures.

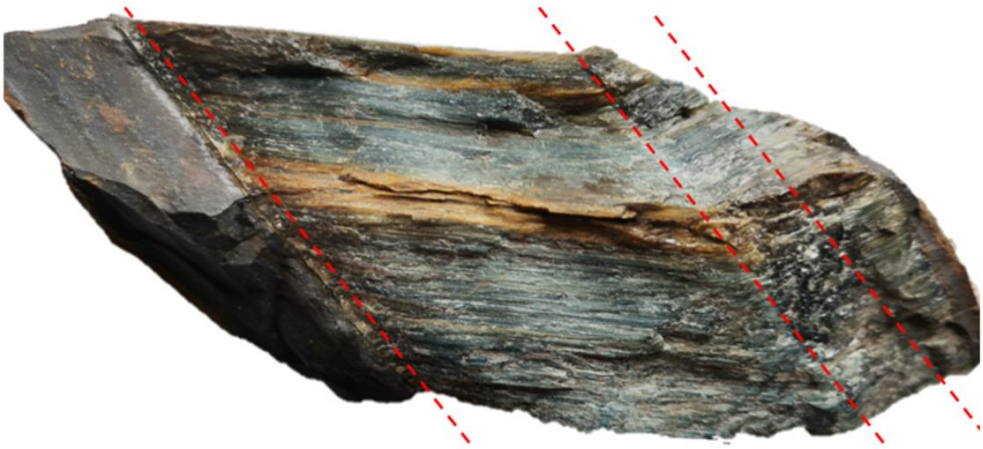

Figure 6.21: (sample 10) Silicified mixed Hawks-eye and Tigers-eye simple seam showing many kink bands across length of seam.



Figure 6.22: (sample 10) Compact, columnar quartz material comprising the bedding-parallel cross-fibre seam.

The host rock is composed of a ferruginous black shale that is oxidised on the top of the exposed surface to a yellow-brown colour. The ferruginous black shale contains small grains of visibly reflective minerals. The fibres are silicified 'Hawks eye' and represent a simple seam bounded by magnetite on only one enclosing surface. Three distinct kinks delineating a change in fibre orientation are observed in the cross-fibre structure indicating that the seam is a mixed fibre orientation seam. The textures of the columnar quartz comprising this seam are showing in figure 6.22.

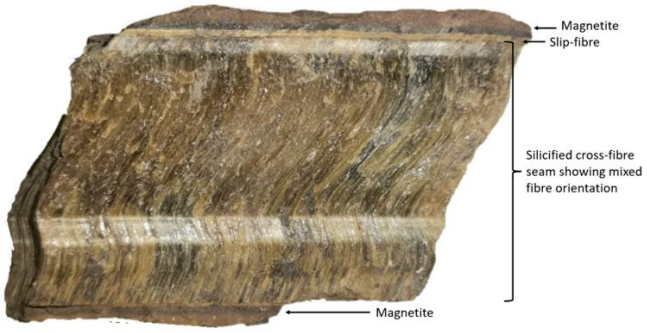


Figure 6.23: (sample 11) Silicified simple cross-fibre seam

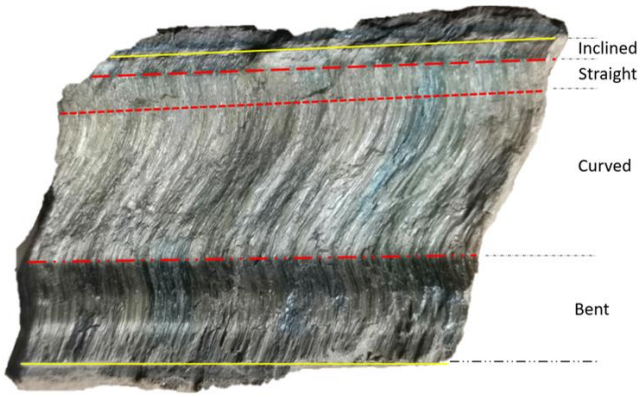


Figure 6.24: (sample 11) Various orientations assumed by fibres across the width of seam

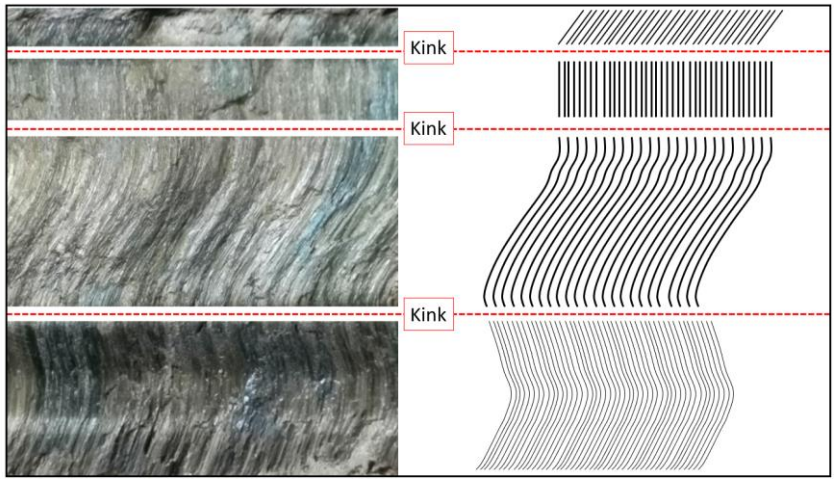


Figure 6.25: (sample 11) Mixed fibre orientations exhibited across the length of the seam.

Brown, thinly bedded, fine-grained mudstone showing a moderate degree of weathering and sub-conchoidal fracturing. The brown colour of the mudstone is likely a result of iron oxidation. On the flat surface, minute and visibly reflective mineral grains are observed within the mudstone layer. The platy, rusty appearance of the mudstone bedding is likely due

to biotite being a dominant mineral in this sample. The thinly bedded mudstone layers alternate with thin, black magnetite layers, which give the sample its strong magnetic properties. The magnetite bands are horizontally bedded with a constant and uniform thickness. The cross-fibres observed in this sample are bound by magnetite layers at both the upper and lower surfaces and are an example of Hawks-eye. The fibres display mixed orientation having several kinks throughout the width of the seam (figures 6.24 and 6.25). This sample is classified as a simple seam and does not contain any subordinate magnetite partings within the fibre seam.



Figure 6.26: (sample 12) Silicified Hawks-eye seam showing a cone-in-cone structure at the lower margins, marginal 'fibrous' quartz at the lower seam margin and deformation structures.

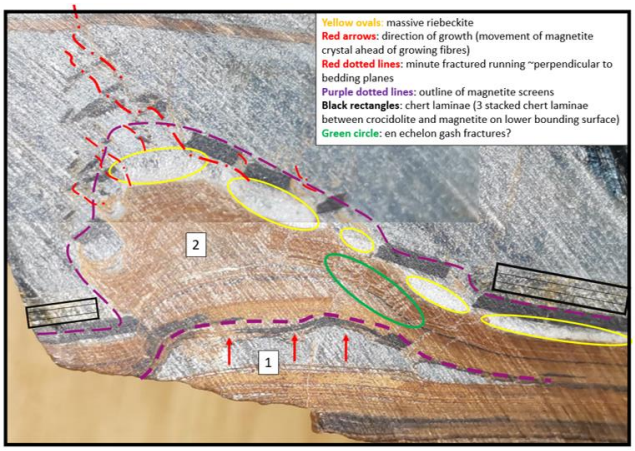


Figure 6.27: (sample 12) Shows the different structural features associated with the cone-in-cone structure.

The dashed purple lines outline two magnetite laminae below? the two separate cone structures. The lower dashed purple line shows the discontinuous magnetic screen following the upper surface of the cone-shaped cross-fibre crocidolite seam indicating that unequal growth of the fibres resulted in their movement and shape. The ruptured magnetite is separated by orange-brown chert. The upper dashed purple line shows warped, curved and disrupted segments and or remenants of what was a previously connected and continuous magnetite band situated between the crocidolite seam and lower contant chert wall rock. The pinch-and-swell and subsequent conical character of the chert laminae observed in the figure indicate some type of pressure phenomenon resulting in the upward transfer of wall material in isolated areas along the lower seam contact. Minute fractures trend more or less perpendicular to the bedding planes crest of the cone shown by the red dashed lines and represent small-scale faulting, which typically accompanies folding of rock laminae (figure 6.27). The magnetite laminae display drag structures on either sides of these fractures, which can be visibly observed in the top left portion of figure (6.27). The above features provide evidence for small scale folding after consolodation of the rock. Formation of the fibres resulted in the observed conical proturbance of the enclosing rock into the crocidolite seam. Massive reibeckite pods (infered, in hand sample and shown in the yellow ovals) are composed of randomly orientated, slender riebeckite needles that are intricately interlocking aggregates giving a mesh appearance. These reibeckite pods occur between the cone and the fragmented piece of the magnetite bands following the curvature of the outer cone surface.

The specimen examined in this study is a Hawks-eye sample from Griqualand West, obtained from the collection belonging to Oliver Barker, Banzi Geotechnics cc, Johannesburg. This sample is silicified and is composed of alternating bands of jasper and magnetite that are evenly and thinly bedded. To the best knowledge, this rock specimen is the first of its kind in that it illustrates the preservation of a cone-in-cone structure in Hawks-eye, which has implications for the development of Hawks-eye/Tigers-eye. The main seam is an example of the simplest crocidolite band representation being a parallel-sided planar seam concordant with the banding of the bedding planes of the enclosing ironstone. The width of the ‘main seam’ is abruptly constricted by a conical marginal protrusion, from the lower bounding surface, into the crocidolite. This conical protrusion appears only on the one side of the seam

(i.e., lower surface) and is therefore classified as a 'single cone' (Trendall and Blockley, 1970). The cone-in-cone structure protruding into the main seam from the lower bounding surface is characterised by ruptured and spatially complex magnetite structures and fragments preserved within the blue, silicified cross-fibrous quartz seam. The cone-in-cone structure appears to have occurred by dilation growth, resulting in the distortion/disruption of the rock during or before compaction/lithification and not due to any tectonic origin as the rock specimen shows little to no other signs of rock deformation and the cone-in-cone structure is restricted in both vertical and lateral extent (within a stratigraphic interval of 3.5 cm). The turbulence structures defining the margin of the cone clearly indicate that the crocidolite seam-and-ironstone experienced plastic deformation as these structures clearly occurred under plastic conditions. Moreso, unlike the magnetite laminae associated with the cone-in-cone structure, the micro-banding of the chert layers with plastic deformation appear to have, in large, retained their continuity across the cone.

The cone structure shown in figure 6.27 results from the conical protuberance of the lower portion of the enclosing rock into the cross-fibre crocidolite seam. The lower cone structure (1) is an isolated feature composed entirely of cross-fibre crocidolite and the upper cone structure (2) is composed of alternating layers of chert protruding into a separated conformable cross-fibre crocidolite seam. The two cones pointed out in the specimen have characteristic features indicating that their formation resulted from two different processes. Distinctly elongated microcrystalline crystals ~1 mm in length, forming three separate bands parallel to the bedding, are located in the black rectangles. These three laminae of microcrystaline quarts are found between the cross-fibre crocidolite and the magnetite screen of the lower bounding surface. The laminae are more or less the same thinckness containing similar length, elongated quartz crystals that are arranged parallel to one another and perpendicular to the bedding planes of the rock. The three laminae of quartz lie directly adjacent to one another between the crocidolite and magnetite, and can be distinguished by distinct kinks and slightly different colours and orientations. The bottom chert lamina, lying directly above the magnetite lamina, has a slightly darker yellow colour and the top chert lamina, directly below the crocidolite, has the lightest yellow colour. Each of these individual quartz laminae consists of coarse, elongated quartz crystals arranged parallel to one another and perpendicular to the bedding plane. The contact with the crocidolite and that between each of the marginal fibrous quartz laminae are in large sharp and smooth. The direction of

crocidolite fibres at the junction between the two minerals, i.e., the fibrous quartz and crocidolite, is inclined to the banding. There is no relationship between the thickness of the marginal fibrous quartz and the cross-fibre crocidolite seam (Trendall and Blockley, 1970). These marginal fibrous quartz veins have a distinctive 'zebra' colouring pattern, in which elongated yellow quartz crystals alternate with thinner blue elongated quartz crystals. In certain confined portions of the rock specimen, the blue colour in these bedding parallel fibrous quartz veins becomes dominant and indicates an increased inclusion of riebeckite minerals (Trendall and Blockley, 1970). Fibrous quartz forms thin bedding-parallel veins that are clearly observed in hand-sample throughout this rock specimen. The principle component of these coarse, parallel crystals forming veins is yellow to clear fibrous quartz crystals, elongated perpendicular to the bedding planes, which appear blue in certain areas due to scattered patches of fibrous riebeckite occurrences in small portions (Trendall and Blockley, 1970). Figure 6.28 shows bedding-parallel quartz veins and associated structures.

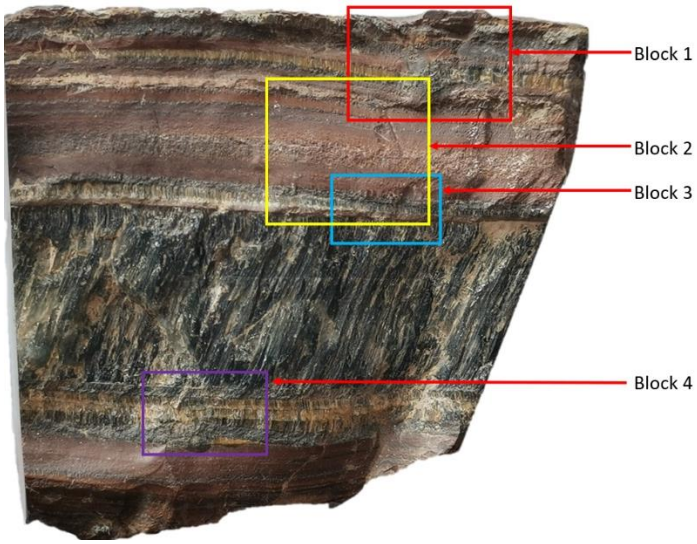


Figure 6.28: (sample 12) Back view showing various structures that are described in the images corresponding to the blocks.

Slip-fibre riebeckite is observed in thin, concordant fibrous bands (1 mm). The fibres' orientation at a high angle to the bedding planes are observed in this rock specimen and show associations with magnetite layers marginal to chert. Additionally, the slip-fibre riebeckite bands appear to be related to magnetite and chert bands exhibiting slight bending or fracture (figure 6.29).




Figure 6.29: (sample 12) Complex dislocation structures between magnetite and bedding parallel fibrous quartz veins. Greyish blue slip fibre riebeckite at upper left part of the image.




Figure 6.30: (sample 12) Thin bedding-parallel quartz veins lying above the seam between chert and magnetite laminae.




Figure 6.31: (sample 12) Gradation of colour across the direction of the fibrous quartz vein from yellow to blue indicating an increased infilling of fibrous riebeckite material within the bedding-parallel fibrous quartz veins.

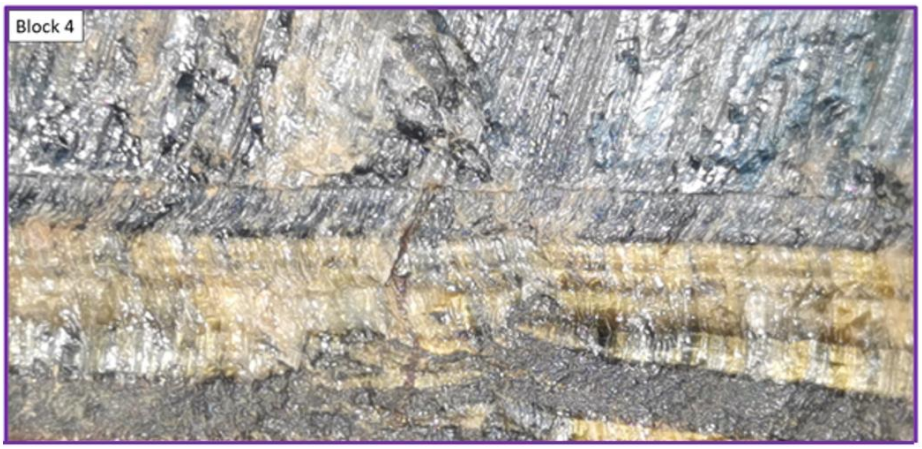


Figure 6.32: (sample 12) Dislocation structures formed between magnetite layers and marginal fibrous quartz.

Numerous bedding parallel 'fibrous' quartz veins are observed in this specimen having different associations with the seam and host rock (figures 6.30, 6.31, 6.32 and 6.33).

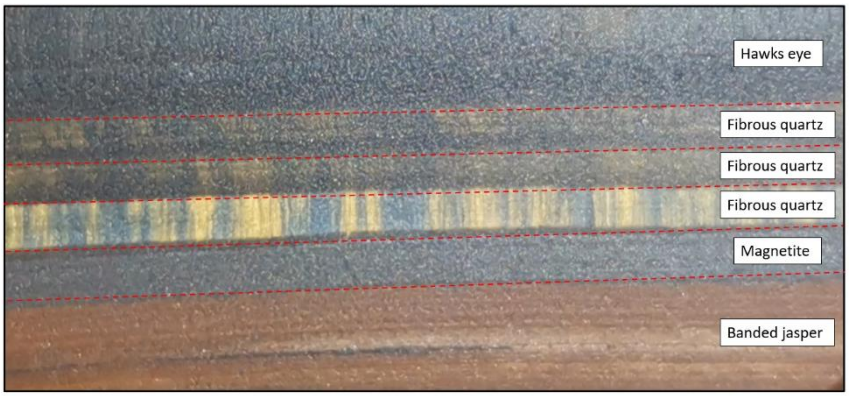


Figure 6.33: (sample 12) Close-up image of the planar features observed in this specimen

Complex dislocation structures formed between the marginal fibrous quartz bands and the adjacent magnetite layers are shown in figures 6.29 and 6.32. These dislocation structures are like those observed at the margins of conical protuberances in crocidolite, in which the fibre direction shows sharp curvatures (Trendall and Blockley, 1970). Unlike those found in crocidolite, kink bands, internal discontinuities and magnetite screens having elaborate shapes are never found in fibrous quartz laminae (Trendall and Blockley, 1970).




Figure 6.34: (sample 13) The images above show the (a) side view (1); (b) side view (2) and (c) front view of a Tigers-eye rock specimen.

This sample is an example of Tigers-eye and is hosted in a very fine-grained mudstone with intercalated magnetite laminae. The sample has planar upper and lower bounding surfaces and a medial planar and persistent discontinuity that clearly separates the width of the seam into an upper and low portion. This sample is completely atypical with respect to most Tigers-eye specimens in that it contains an abundance of cone and cone-in-cone structures composed of a variety of minerals, including host rock, Tigers-eye, interlocking coarse quartz and magnetite laminae. The unusual microstructures observed in this Tigers-eye sample have major implications for the origin and mechanisms of formation (figures 6.35, 6.36 and 6.37).



Figure 6.35: (sample 13) Cone microstructures observed on the upper bounding surface and protruding from persistent central partings dividing the seam into two portions. Notice the magnetite screens making up the marginal bounding surface and the central discontinuity across the seam.

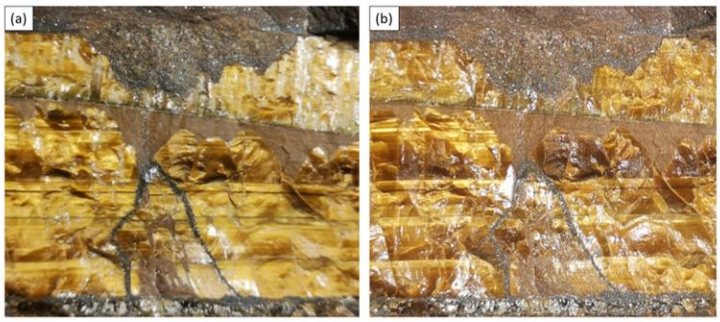


Figure 6.36: (sample 13) Same cone structure photographed using different light sources to highlight the various components of this peculiar structure.



Figure 6.37: (sample 13) Highly unusual cone structure formed by large, coarse, multi-coloured, and interlocking quartz crystals. The cone shape is outlined by dark-grey magnetite laminae of varying thickness.



Figure 6.38: (sample 14) Silicified crocidolite cross-fibre seam showing mixed fibre orientations.

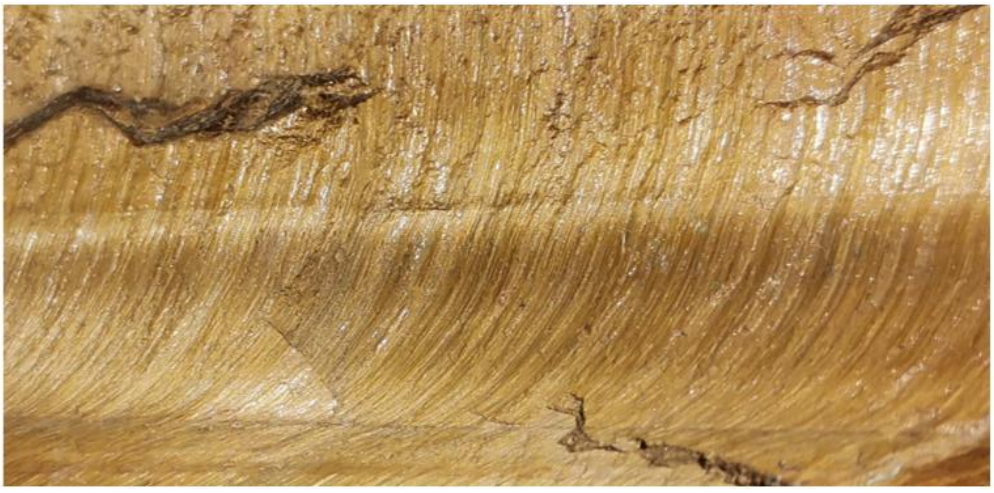

Figure 6.39: (sample 14) Silicified, mixed fibres orientation and extremely compact cross-fibres.

Sample 14 represents a silicified, simple cross-fibre seam having planar bounding surfaces hosted in a very finely laminated, poorly bedded banded magnetite and japer layers. The surface of brown jasper bands of the host rock shows sub-conchoidal to conchoidal fracture surfaces. The mixed orientation ‘fibre’ striations spanning the width of the seam demonstrates a shining, golden brown to yellow colour. No discernible upper or lower magnetite screen can be identified upon visual examination. No conclusive information on the origin can be obtained without further analysis s plane polarising light microscopy, XRF and XRD etc. The cross-fibre striations in this rock specimen represent the original crocidolite

fibres pre-silicification (figure 6.39). The fibres in this sample are compact and cannot be discerned into individual fibre units, therefore not presenting any hazard to both human health and the environment.



Figure 6.40: (sample 15) Crocidolite from Malips Drift area of Pietersburg District of Limpopo

This sample comes from Malips Drift, Pietersburg District. Intense overfolding of the rocks occurred in the Malips Drift area resulting in highly deformed strata and numerous small-scale isoclinal overfolds (Genis, 1961). The numerous examples of asbestos seams demonstrating slip, bent and steeply inclined fibres indicate that the large extend of folding in this area occurred post-fibre formation (Genis, 1961). In addition, fibres that have been cross-cut by large magnetite porphyroblasts and partial recrystallisation to needle-like riebeckite indicate that substantial recrystallisation also occurred (Genis, 1961). The partial alignment of minerals observed in the barren strata further denote the recrystallisation event due to directed pressure (Genis, 1961).

The host rock is a moderately magnetic, finely-bedded, poorly-banded, dark- coloured banded iron formation rock. The surface is characterised by a brown to maroon iron oxide coating. The rock has been folded. The crocidolite fibres are loosely compact on the surface of the sample becoming progressively compact below the surface. They exhibit a grey-blue colour with surface exposed fibres losing their blue colour and becoming greyer. The fibres have a length of 3 to 4.5 cm. The host rock is comprised of a siliceous type of ironstone of

broad, irregular, white chert bands that are separated by paper thin, poorly defined, massive-looking, black, magnetite-bearing bands, which impart a weak to moderate magnetic property. The exposed bedding plane surfaces are characterised by a patchy brown to maroon coloured iron-oxide coating resulting from weathering. The bedding in the Malips Drift area has been substantially folded and the bulk of the fibres constituting this area are inclined or obliquely-orientated fibres (Dreyer, 1974). The fibres are generally orientated parallel to the axial planes in the hinges of the folds (figure 6.41a and b). There is a slight tendency for a splaying of the fibres on the limbs. Pear to lenticular shaped bodies of crocidolite fibre bundles are shown in figure 6.41b.

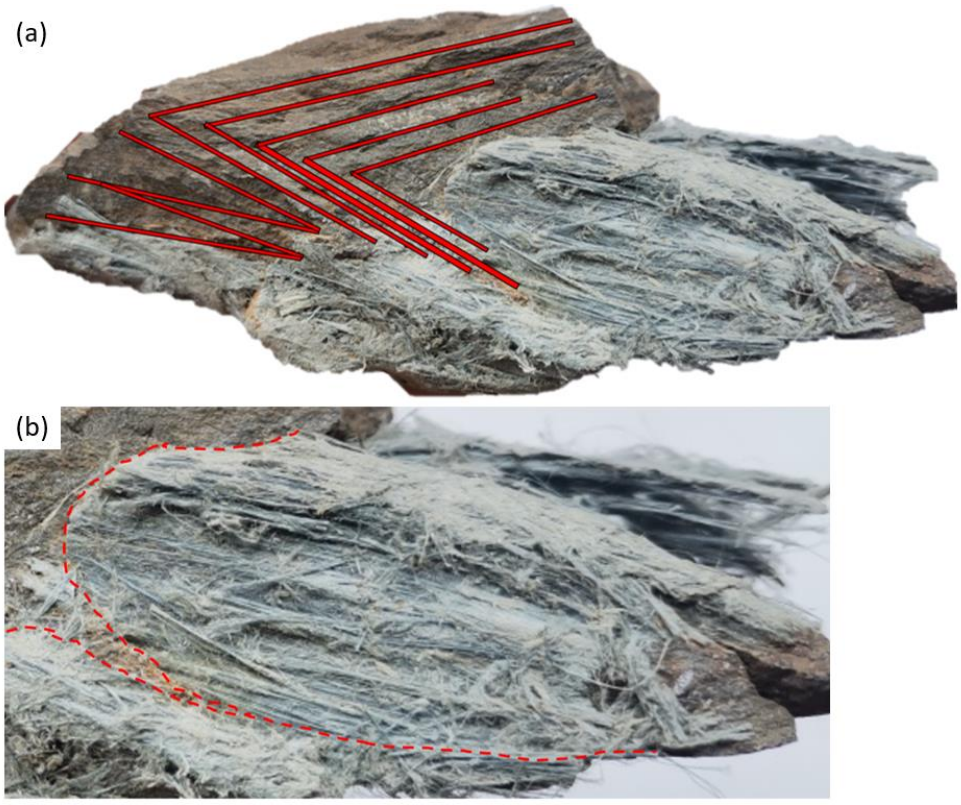


Figure 6.41: (sample 15) Single folded crocidolite cross-fibre seam.

The sample shows that the crocidolite fibres near the fold-hinges are orientated parallel to the axial plane of the folds and those that are along the inner limbs of the folds splay outwards slightly. Examination of this sample leaves indicates that folding occurred after the growth of fibres without any relationship between both. The crocidolite fibre seams follow the folds . This sample represents folds that have been sharply compressed as the seam has been contorted and the associated fibres transitioned to slip-fibres as they became

inclined to the bedding planes. The seam shows various degrees of discolouration and cohesion (figures 6.42 and 6.43). These fibres can readily be detached when touched or disturbed, indefinitely disintegrating into threads of unlimited fineness.

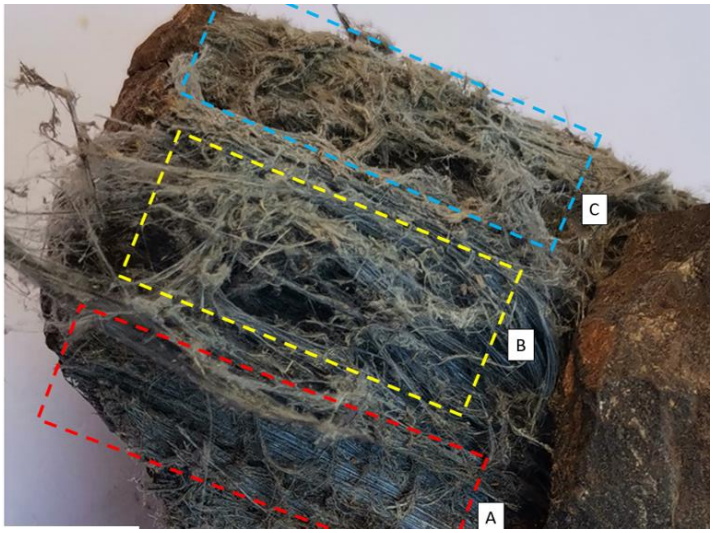


Figure 6.42: (sample 15) Different stages of weathering and subsequent effects on cohesion of fibres within a single sample: (A) The fibrous mass presents a deep blue, compact, smooth, silky-lustrous surface, parallel-oriented fibres, fibre bundles; (B) Lavender blue, non-lustrous, fluffy, moderately compact fibre bundles and, (C) grey, ashy, dull, fluffy, loose, poorly compact fibrous mass rather than bundles of parallel fibres.




Figure 6.43: (sample 15) Close-up view showing different stages of alteration reflected in fibre colour, ‘wooliness’ and cohesion.



Figure 6.44: (Sample 16) Amosite asbestos cross-fibre seam in host rock containing grunerite needles giving the rock a speckled or ‘sugary’ appearance.



Figure 6.45: (Sample 16) The walls of the cross-fibre bands are irregular and wavy with the upper bounding surface being the more pronounced of the two.



Figure 6.46: (Sample 16) Cusp and lobe upper bounding surface and approximately planar lower bounding surface with cone structure filled with fibres. Notice the loose, long, and relatively hard amosite fibres on the surface of the seam.

Medium to coarsely banded assemblage of dark graphitic and lighter chert and the presence of fine rosettes and needles of amphibole give the speckled appearance to the host

rock. The seam bounding surfaces are largely irregular, however, this is distinctly marked in the upper surfaces of the seam (figure 6.45). Two fibre cone structures are shown on the lower bounding surface. The loss of fibre bundle cohesion on the exposed surface of the seam is shown in figure 6.45, where the fibres can be separated easily. The cone structures observed in the specimen are composed of the amosite fibres (figure 6.46).



Figure 6.47: (sample 17) Amosite rock sample (side view 1)



Figure 6.48: (sample 17) Amosite rock sample (side view 2)

The host rock is a light brown to cream coloured, soft, friable, and finely-laminated shale containing darker brown mass-fibre bands and scattered needles of amphibole minerals giving the rock an overall speckled appearance. The amphibole minerals giving the speckled

appearance to the host rock occur as both fine rosettes and needles. The upper surface of the seam shows a jagged and uneven boundary (figure 6.49). Additionally, the amosite seam appears to cut across the bedding of the upper surface (figure 6.50).



Figure 6.49: (Sample 17) Jagged and uneven upper bounding surface formed due to the unequal growth of fibres.



Figure 6.50: (Sample 17) Jagged and uneven upper bounding surface formed due to the unequal growth of fibres and the cross-cutting relationship of the fibres with the bedding-planes of the host rock.



Figure 6.51: (Sample 18) Amosite asbestos rock sample; notice the wavy, uneven, and unclear bounding surfaces due to overgrowth of grunerite needles.



Figure 6.52: (Sample 18) Amosite seam having a waste cone without any amosite fibres

This rock is mainly composed of dark brown mass-fibre bands and scattered needles of amphibole minerals giving the rock an overall speckled appearance with occasional black hematite laminae. The sample contains a waste cone at the lower seam surface without fibres (figure 6.52).

The alteration status, fibrous or pseudo-fibrous classification, cohesion, releasability and potential hazard for each of the studied amphibole asbestos-bearing rock samples are given in table 6.3.

Table 6.3: Summary of alteration, fibrous or pseudo-fibrous classification, cohesion, releasability and potential hazard

| Sample # | Alteration status | Fibrous vs pseudo-fibrous? | Cohesion | Potential releasability and dispersion | Hazard? |
|---|---|---|---|---|---|
| | | | | | |
| 1 | Oxidised, non-fibrous | Powdered, pseudo-fibrous | Low | Low (pseudo-fibrous) | Low |
| 2 | Oxidised, non-fibrous | Powdered, pseudo-fibrous | Low | Low (pseudo-fibrous) | Low |
| 3 | Discoloured | Fibrous, matted fibre balls | Low | High | High |
| 4 | Discoloured | Fibrous, matted fibre balls | Moderate to low | Moderate to low | Moderate |
| 5 | Discoloured, oxidised, silicified | Mixture: Ash grey blue discoloured fibres matted into a ball (fibrous) and the red, orange, and golden fibres powdered (pseudo-fibrous) | Low | High to low | High to low |
| 6 | Oxidised or brown acicular amphibole cross fibre | Powdered, pseudo-fibrous | High | Low | Low |
| 7 | Discoloured | Separate fibres, fibrous | High to moderate | Moderate | Moderate |
| 8 | Oxidised or brown acicular amphibole cross fibre | Both needles, fibrous and powdered, pseudo-fibrous | High | Low | Low |
| 9 | Silicified | Powdered, pseudo-fibrous | High | Low | Low |
| 10 | Silicified | Shards (not powder and not fibres) | High | Low | Low |
| 11 | Silicified | Shards (not powder and not fibres) | High | Low | Low |
| 12 | Silicified | Shards (not powder and not fibres) | High | Low | Low |
| 13 | Silicified | Shards (not powder and not fibres) | High | Low | Low |
| 14 | Silicified | Both powdered, pseudo-fibrous and shards (not powder and not fibres) | High | Low | Low |

| | | | | | |
|---|---|---|---|---|---|
| 15 | Mix normal to discoloured fibres | Matted balls, fibrous | Low | High | Very high |
| 16 | Unaltered to slightly altered | Separate fibres, fibrous | Low | High | High |
| 17 | Unaltered to slightly altered | Separate fibres, fibrous | Low | High | High |
| 18 | Moderate to highly altered | Separate fibres, fibrous | High | Moderate to low | Moderate to low |

## 6.5. Discussion

The geological complexities at the hand-scale (mesoscale) were defined and geological-structural heterogeneities described. Implications for recognising natural amphibole asbestos geo-types are import for *in situ* identification, fibre content and quantity in rock masses.

The crocidolite fibre seams are formed in true banded ironstone-type host rocks, whereas amosite cross-fibres predominantly occur in entirely non-magnetite, soft 'amosite slates' (a term proposed by Hall, 1930), which have a soft graphitic, very fine, shaly character, unlike those hosting crocidolite, which are entirely non-magnetic. In addition to the typical banded ironstone, crocidolite cross-fibre seams, both simple and composite, are shown to be hosted in banded chert (sample 4), jasper (sample 3, 5, 6, 9, 12, 14), massive riebeckite (sample 7), ferruginous shaley (sample 10 and 13), and rocks dominated by carbonates, quartz and/or stilpnomelane (sample 8 and 11). The host rock colouring, nature and thickness of banding, and degree of weathering vary substantially both within the individual and between the different samples. Carbonate and grunerite minerals are a large constituent of the amosite hosted lithologies with grunerite needles dispersed throughout both the rock and amosite cross-fibre seams. The asbestos-bearing rock specimens show lithological heterogeneity with respect to amphibole asbestos host rocks indicating that the cross-fibre mineralisation was not primarily controlled by the rock types within BIF.

The crocidolite and amosite cross-fibre seams range in fibre lengths from < cm to several centimetres. The seams show small-scale variations in width corresponding to noticable rapid variations in fibre lengths over short distances controlled by both the nature of the bounding surfaces and the presence of internal persistent and non-persistent cross-cutting mineral screens. A variety of colours is observed and can be related to their degree of alteration.

Sample 2, 6, 8, 10, 11, 12, 14, 15, 16 and 18 show cross-fibre seams that are classified as simple seams, whereas samples 1, 3, 4, 5, 7, 9, 13 and 17 represent composite seams. Simple seams are those that have fibre bundles spanning from one bounding surface to the other without any partings or only subordinate magnetite partings between surfaces (Hanekom, 1966). Composite seams are those that contain several persistent magnetite partings roughly parallel to the bounding surfaces of the total seam (Hanekom, 1966). These magnetite partings result in an individual seam bounded between distinct bounding surfaces consisting of numerous, approximately parallel layers that each host fibre bundles of differing lengths (Hanekom, 1966). The major difference separating simple and composite seams is that the asbestos fibre length in simple seams equates to the total width of the seam, whereas there is no relation of the average asbestos fibre length in composite seams to that of the total seam width (Hanekom, 1966). The structures observed in composite seams are thought to be due to the variations in the growth of fibres or slight displacement under pressure during folding (Schoeman, 1929). Kneebend-type folds may be associated with seams of crocidolite having curls or curves at one or both bounding surfaces (Schoeman, 1929). Lines of weakness running parallel to the host rock bedding planes resulted from this bending in the fibres (Schoeman, 1929). The composite and dual structure of seams often form in folds, where these lines of weakness transition into fracture planes (Schoeman, 1929). However, the consensus is that uneven crystallisation over disrupted intervals caused the composite seam structure as the growth of the fibres commenced, simultaneously or otherwise, at the base, middle or top of the seam (Schoeman, 1929).

Sample 1 shows magnetite impurities within the cross-fibres. Magnetite is the most common impurity in the cross-fibre seams (Genis, 1961). These magnetite impurities are interpreted as being the remains of broken magnetite screens that remained within the seam during the growth of the fibres (Genis, 1961). Sample 4 shows fibrous riebeckite spherulites in contact with magnetite on the surface of the lower portion of the composite seam. The spherulites form along a geometric pattern that begins with a single nucleus and develop by a fanning mechanism or fringing dendritic growth as illustrated in figure 6.53.

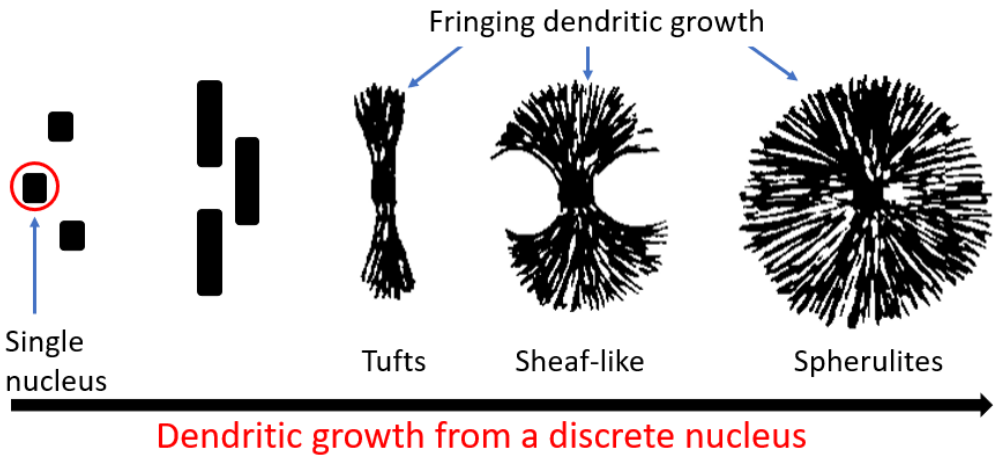


Figure 6.53: The five stages in the development of spherulite fibres (adapted from Keller, 1958 and Genis, 1961).

The spherical form, under this mechanism (figure 6.53), is progressively developed via a series of intermediate shapes (Keller, 1958). Grunerite needles are shown to be a major impurity within the amosite seam in sample 18.

In sample 12 the primary seam shows an intimate relationship with elongated, blocky quartz at its margins. Several thin (0.5 to ~2 mm), parallel-sided (or planar), bedding-parallel 'fibrous' quartz veins are observed across the sample. The three-stacked bedding parallel 'fibrous' quartz veins at the lower seam margin are approximately 3 mm thick with each being ~1 mm thick. Each of these is strictly parallel to one another, the seam and the bedding planes of the host rock. Sharp boundaries define the individual marginal quartz veins from one another and the associated upper seam and lower magnetite band. It is a common occurrence to observe perpendicular fibrous quartz along either one or both crocidolite seam margins (Trendall and Blockley, 1970). The marginal 'fibrous' quartz may either maintain its thickness or sympathetically vary with corrugations of the adjoining seam, typically magnetite, thus resembling the fibrous quartz related with small-scale folds isolated from crocidolite (Trendall and Blockley, 1970). The contact between fibrous quartz and crocidolite may be sharp and smooth or slightly ragged (Trendall and Blockley, 1970). The formation of the veins occurred via a planar control as indicated by the planar shape and matching upper and lower bounding surfaces (Kronyak *et al.,* 2019). Thin, planar, bedding-parallel 'fibrous' quartz veins are interpreted as sites of fracturing and crack-seal vein filling during numerous post amphibole asbestos seam deformational periods (Ramsay, 1980). Their location at the margin of

asbestos seams as shown in sample 12 is consistent with planes of weakness within the rocks (Ramsay, 1980). In complex dislocation structures, marginal fibrous quartz may be concerned with adjoining magnetite like those of rapid curvatures of fibre orientation and at the cone margins in crocidolite (Trendall and Blockley, 1970). However fibrous quartz margins never have magnetite screens that create the shapes like those of crocidolite, kink bands or internal discontinuities (Trendall and Blockley, 1970). The bedding parallel fibrous quartz veins in sample 12 show gradational and sectional colour dominance. In certain parts of the sample these quartz veins appear atypically blue, indicating an increase in fibrous riebeckite as infilling material (Trendall and Blockley, 1970).

Structural features related to mineralisation and deformation are fundamental for interpreting the geological history and therefore the conditions that were accompanied by amphibole asbestos formation. The geological processes responsible for hazardous amphibole asbestos mineralisation in BIF geological settings and the subsequent weathering and alteration processes are recorded in the variety and complexity of rock fabrics, structures, mineral associations, and textures observed in natural rock samples. Visual morpho-structural investigation of various seam morphologies, conical, ridge-like and cone-in-cone (CIC) structures in asbestos seams hand specimens give insight and provide various explanations to their formation, and in most instances lead to the generation of more questions than answers. Corrugated, convoluted, and conical structures are observed within the asbestos seams (samples 1, 5 and 9), probably illustrating plane intersections with certain internal planar breaks of the fibres across which they diagonally dissect in the direction of the fibres at low angles (Trendall and Blockley, 1970). Sample 1, 5, 8, 9, 13, 16 and 18 contain cone structures composed of either the fibres themselves or the enclosing rock protruding into the seam. Normal and inverted cone structures occur when the fibres in composite asbestos seams grew in opposite directions (Hanekom, 1966). Cone-structures formed during crocidolite growth from opposite bounding surface could only occur if a magnetite lamina originally separated the parent-material from which the crystallisation of crocidolite originated (Hanekom, 1966). Crystallisation of adjoining layers of parent-material commenced under pressure conditions with one of the layers developing into the mould for the adjacent layer (Hanekom, 1966). Cones that are represented by ridge-like protrusions have irregular outlines that to a certain degree mimic small-scale folding (Hanekom, 1966).

Ridge-like protrusions are commonly formed by (sub)parallel arrangement of cones (Hanekom, 1966). Waste cones are formed due to the folding of the bedding planes into the cross-fibre seams resulting in a cone-shape devoid of fibres (Dreyer, 1974). These cones formed strictly because of folding and not due to unequal fibre growth (Dreyer, 1974).

Samples 5, 9, 12, 13 show several cone-in-cone structures characterised by copious co-axial layers constructed from different materials. Cone-in-cone structures are found in numerous geological settings and rock types (Pettijohn, 1957). There is general acceptance that their formation required pressure (Fockema, 1967). Cone-in-cone structures formed by fibrous layers commonly display the following characteristics (Cobbold *et al.,* 2013): (i) Layers of fibres are situated between nesting conical surfaces that have a common axis; (ii) the fibres in these layers are orientated parallel or fairly obliquely to the axis of the conical surfaces in which they are nested; (iii) thin screens of magnetite (in crocidolite samples) and grunerite (in amosite) either line the margins or form the conical surfaces themselves; and (iv) cone and/or cone-in-cone aggregates formed by the parallel arrangement of coaxial cone nests. Samples 17 and 18 show waste cones and ribbon rock textures.

Many cone-bearing composite seams are composed of a crocidolite and a mass-fibre layer and the cones in these bands contain mass-fibre and interrelated funnel-shaped or inverted cones in the adjoining crocidolite seam (Fockema, 1967). Such cones could not have formed by growth variations of riebeckite crystals as if specific crocidolite crystals took preference during growth, then similar structures would also occur in single asbestos layers, which is never the instance (Fockema, 1967).

Cones found in the asbestos samples containing features not conforming to crystal growth can be explained by expansion of a prior compressed material into tensile stress zones or potentially even tensile spaces generated during folding (Fockema, 1967). The formation of cones under this assumption occurred during (i) an early deformation period, which resulted in tension zones; where (ii) definite spaces formed below or above competent rock layers in fold troughs and crests; (iii) plastic proto-asbestos bands above or below such spaces; (iv) originally compressed incompetent material expanded and took the form of cones and associated ridge-like structures (figure 6.55) (Fockema, 1967).

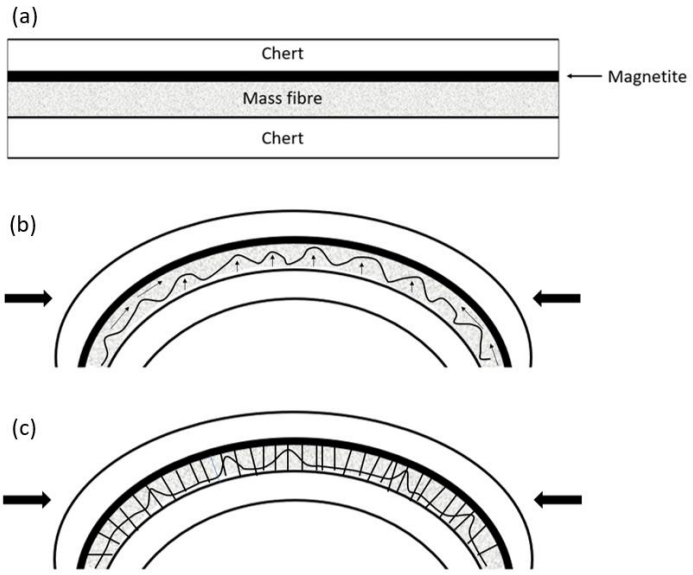


Figure 6.55: The conversion of layers of mass fibre into composite crocidolite seams with partings of magnetite. The conical structures occur in the lower portion of the seam only (adapted from Fockema, 1967).

Cones that have a perfect circular base suggest that these structures did not experience any lateral stresses during their formation (Fockema, 1967). However, long ridges and aligned cones may have also formed during rapid enlargement of proto-riebeckite (Fockema, 1967). The appearance of small fractures just before or at the same time as this enlargement probably controlled the shape of the cones (Fockema, 1967). Areas subjected to the existence of a horizontal stress field may have also resulted in the alignment of elliptical cones (Fockema, 1967). In all instances the expanding material of mass fibre was incapable of completely filling the open spaces and material from the portions adjacent to the folds moved in, resulting in the formation of a composite band containing two layers of proto-asbestos (Fockema, 1967). This explains why even outer surfaces are always found bounding cone-bearing composite bands (Fockema, 1967). This theory assumes that cone-formation ended prior to the completion of crocidolisation (Fockema, 1967).

Numerous angles between perpendicular and nearly parallel seam contacts are assumed by mutually parallel crocidolite and amosite fibres comprising cross-fibre seams (Genis, 1961). The orientation of fibres other than normal to the bounding surfaces is hypothesised to have occurred post fibre development via the application of vertical pressure

to the seam (Genis, 1961). The formation of these orientations is facilitated by the finely fibrous nature of the amphibole asbestos (Genis, 1961). Several orientations are described here namely (a) inclined fibres; (b) slip-fibres; (c) kinked fibres; (d) doubly inclined fibres; (e) bent and curved fibres; and (f) mixed fibre orientations. Sample 2 exhibits a single kink in the upper portion of the seam running parallel to the bounding surfaces. Individual fibre seams may display a sudden switch in crocidolite fibre orientation resulting in 'kinking' (Fockema, 1967). Kinked fibres are observed in numerous cases where only a portion of the seam width has inclined fibres (Genis, 1961). In such instances the fibres at one contact are perpendicular to the bounding surface while those at the other are inclined (Genis, 1961). A definite kink exists along which the orientation of the fibre change is presented in such seams and typically trends parallel to the seams bounding contacts (Genis, 1961; Cilliers, 1961). Sample 3 shows uniform low-angle inclined fibre orientation within the upper seam. Inclined fibres are those that are slanted at an angle to the contacts of the seam (Genis, 1961). Low angle, singly inclined seams develop because of being subjected to a small component of horizontal shearing stress (Genis, 1961). Samples 6 and 8 show curved fibre orientations. Cross-fibre seams often contain fibres that display a curved or bent nature formed post-fibre formation (Dreyer, 1974). Bent and curved fibres are a result of seams containing doubly-inclined fibres with no definite kink between the change in orientation of the fibres within the seam (Genis, 1961). Instead of a distinct kink, the fibres are present as being gently bent or curved (Genis, 1961). Samples 10, 11 and 14 show mixed fibre orientations across the length of the fibres. The most common form of mixed fibre orientation is presented in the seam as straight fibre orientation in the inner portion and curved and/or curled fibres at both or one of the upper and lower portions of the seam (Trendall and Blockley, 1970). Mixed fibre type of fibre inclination within a seam is unquestionably a result of post-crystallisation movement (Schoeman, 1929).

Structures and grooves occurring on the host-rock bedding planes, such as those resembling slickensides, provide evidence for large-scale motion across the bedding-planes, which make up the banded ironstones (Hanekom, 1966). Different periods of folding can be identified in folded reef strata (Genis, 1961). Evidence of folding that took place post cross-fibre seam formation is observed and appears to have been a frequent occurrence in amphibole asbestos-bearing banded iron formation (Genis, 1961). Brecciation and/or inclination of the cross-fibres in crocidolite and amosite seams are due to post-formation

folding, unlike the host strata that behaved incompetentl (Genis, 1961). Small-scale nappe structures and slip-fibre development in shear planes have been observed in specimens as the result of extreme cases of overfolding (Genis, 1961). Such examples of overfolding in crocidolite horizons are frequently found in the rocks at Klipfontein and Orange View in the Prieska, region where numerous low-angle, singly inclined seams developed because of the shearing stress (Genis, 1961). Recrystallisation in the beds of mass-fibres also emerged due to the stresses resulting in the formation of thin patches of flake-like slip-fibres across the shear planes, which slightly resemble mica flakes (Genis, 1961).

The movement of one bounding surface and not the other results in inclined fibre orientation and occurs due to parallel or low angle tension with respect to the bedding-planes (figure 6.54a) (Hanekom, 1966). Differential movement, when both bounding surfaces slide past one another, may take place during folding and/or small-scale thrust-faulting (figure 6.54b) (Hanekom, 1966). Fibre bundles in a single asbestos seam that have perpendicular orientation at one bounding surface and are inclined at the other bounding surface provide evidence of selective movement of these surfaces (Hanekom, 1966). Such observations indicate that under the control of directed pressure during the initial stages of fibre-crystallisation the maximum tension operated in a vertical orientation (Hanekom, 1966). The one bounding surface of the seam moved laterally, while the other remained fixed or moved to a smaller degree (Hanekom, 1966). Shearing of the fibre bundles within the seam resulted in their growth in the direction of maximum tension and at an angle to which movement was the greatest (figure 6.54c) (Hanekom, 1966).

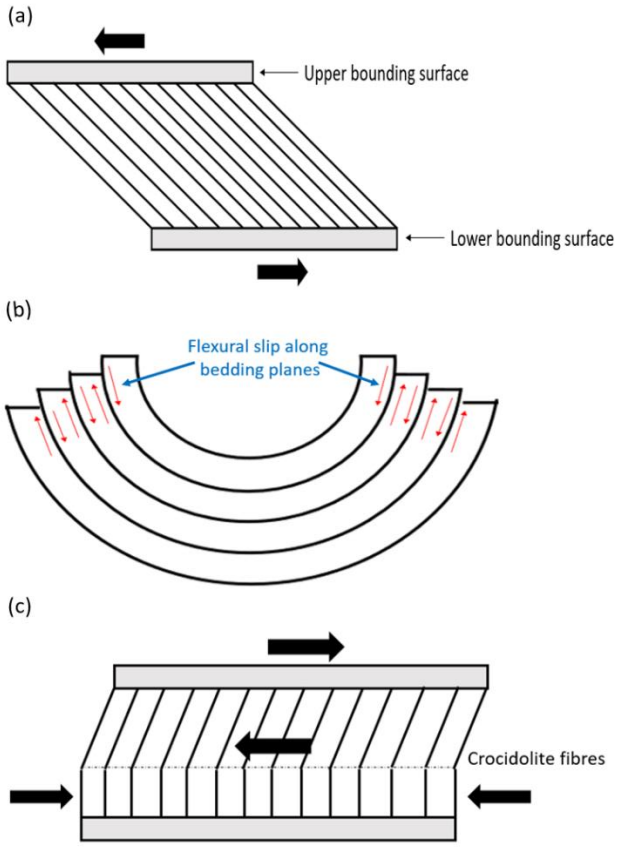


Figure 6.45: Inclined orientation of fibres owing to sliding of opposite bounding surfaces. (a) Movement along one bounding surface; (b) movement along both bounding surfaces; (c) shearing of cross-fibres in direction of greatest movement (adapted from Hanekom, 1966).

The fibre-length to seam-thickness ratio is enhanced in seams having inclinations and/or kinks in the fibres (Genis, 1961). Thus, seams having such fibre attitudes were considered when evaluating the reef values providing partial recrystallisation and hardening of the fibres had not occurred (Genis, 1961).

In sample 4 the composite seam is characterised by a planar lower bounding surface and an irregular upper bounding surface that shows cusp-and-lobate morphology typical of interface buckling. Small-scale intra-stratal folding may result due to perpendicular to oblique uneven loading, layer-parallel compression or surface irregularity amplification during deformation flow. Bending and buckling are two mechanisms by which folding may be achieved. Bending involves forces that are applied to the layers, which may or may not demonstrate contrast in competence at high angles. Competent rocks enclosed in

incompetent mediums of adequate contrast in viscosity may develop rounded folds via the active mechanism referred to as buckling. At a specific force the rapid transformation from planar to buckled (curved) results due to the development of mechanical instability. Interface buckling occurs when the planar interface between two contrasting viscosity materials is affected by buckle folding. This type of buckling generates a characteristic form of folds known as lobate folds. Lobate folds have a broad rounded shape closing in a single direction with cusps pointing towards the higher viscosity material.

Sample 7 exhibits layers displaying a continuity loss being represented by a sequence of lenticular bodies. Such features are common in amphibole cross-fibre seams and are referred to as pinch-and-swell and/or boudinage (Fockema, 1967). Pinch and swell structures are visible on both the microscopic and macroscopic scale (Fockema, 1967). Chert is the primary mineral composing these 'boudins', however any mineral mixtures typical of banded iron formations may make up these structures (Fockema, 1967). Beds displaying pinch and swell irregularities often pass into bands that have irregular 'nodular' bodies, which are observed as irregular elliptical or circular mound-like structures in plan-view (Kettenbrink, 1970). These structures were most likely the result of intra-stratal flowage of sediments that were either unconsolidated or weakly consolidated (Kettenbrink, 1970).

Sample 12 shows turbulence structures in the chert of the outer margin of the cone emplaced into the cross-fibre seam. The development of turbulence structures occurs in crocidolite seams that have undisturbed and straight fibres and planar sides (Trendall and Blockley, 1970). Any small marginal inward-projecting magnetite irregularity results in the inward crocidolite for it to have a characteristic twisted structure (Trendall and Blockley, 1970). The even fibres on both sides of the twisted crocidolite mirrors patches of flowing liquid arising from obstructions encountered by an otherwise laminar flowing fluid (Trendall and Blockley, 1970).

Sample 5 images 14, 15, 16 and 17 show cone and cone-in-cone structures that result from the emplacement of host-rock material into the seam. Minute fibre layers or lenses within these structures can be observed in hand sample and in figures 6.16, 6.17 and 6.18,, however the small size allows the inference that these structures are not controlled primarily

due to fibre growth, but are rather syn-sedimentary deformation structures. The fibre lenses within these three structures may have resulted as infilling material when small openings were created between the bedding planes of the deformed material composing the structures. The upper contact of the deformation structures shown in figures 6.16 and 6.18 appears to be somewhat sharp, whereas that in figure 6.17 is gradational. An examination of the morphology of these structures indicates that both ductile and brittle features are present. The brittle features are presented mainly in the magnetite laminae as fragmented and bead-like boudinage features on the millimetre size (Toro and Pratt, 2015). The ruptured and brittle features of the magnetite bands are observed at the front or margins of the folded structures. Plastic and brittle deformation features found in co-existence indicates a complex reaction of differing rheological characterised semi-cohesive sediments exposed to external stresses (El Taki and Pratt, 2012; Toro and Pratt, 2015).

## 6.6. Geological factors potentially responsible for BIF-hosted asbestos mineralisation

The variety and abundance of naturally occurring asbestos and other fibrous minerals across South Africa in both geographical extent and geological diversity raises great concern over potential environmental asbestos exposure to the public. The fact that all three principle types of asbestos are found in South Africa and their diversity and extent makes South Africa unique compared to the rest of the world. In this study, numerous naturally occurring BIF-hosted amphibole asbestos were presented and examined to better understand the correspondence between asbestos mineralisation and fabric of the host rocks. Mitigating asbestos hazards requires that its occurrence may be predicted before activities such as mining disrupt the geological site (Vignaroli *et al.,* 2011).

A systematic description and classification of crocidolite and amosite seams within their host rocks was done to better understand the geological conditions related to their natural mode of occurrence. The morphology, internal structure and orientation of crocidolite and amosite seams preserve information on the asbestos seam-forming mechanisms, diagenesis, rock deformation and palaeostress (Meng *et al.,* 2017). The meso-structural (hand sample scale) investigation reveals that numerous mechanisms may be responsible for conformable

cross-fibre asbestos seam formation, allowing to infer their relative position during the geological history of the Lower Griquatown Stage.

The geological setting and the subsequent rock-associated history of BIF-hosted amphibole asbestos mineralisation in the Transvaal Supergroup can be divided, briefly, into five sections (table 6.4): (1) Deposition of the Lower Griquatown Stage; (2) penecontemporaneous deformation; (3) pre-Matsap folding; (4) deposition of the Gamagara and Matsap Formations in the Griqualand Basin and corresponding Loskop and Waterberg Systems in the Transvaal Basin, respectively; and (5) post-Matsap folding (Cilliers and Genis, 1964).

Table 6.4: Geological history, meso-structural analysis of different crocidolite and amosite seams, primary and secondary structural elements, and potential mechanisms of formation

| **Geological history** | **Major geological processes** | **Seam characterisation** | **Seam formation mechanisms** | **Structures associated with seam formation and deformation** | **Stress regime** | **Characteristic samples** |
|---|---|---|---|---|---|---|
| | | | | | | |
| Deposition of Lower Griquatown Stage | Deposition, burial, and diagenesis | Simple? Composite? Both? | Force of fibre crystallisation (dilation growth mechanisms)? | | Plastic/ductile | |
| | | | | | | |
| Synsedimentary-penecontemporaneous deformation | Deposition, burial, and diagenesis | Simple? Composite? Both? | Force of fibre crystallisation (dilation growth mechanisms)? | Bedding plane restricted: Slump structures, instrastratal folding | | Sample 5, 17 (Sample 8 and 16?) |
| Increase overpressure | | | | | | |
| Latest stages of burial history – basin is extensional stress | Burial = greater depths = High fluid pressure under low differential stress = initiation of extensional fractures | Pre-tectonic (pre-folding, seams (extensional) – regional extensional or tensional stress fracture event | Hydro fracture - extensional seams | Planar, simple seams | Extension – dilatant fracture propagates though brittle rock | Sample 2, 3, 6, 9, 10, 11, 14 Sample 13? |
| | | | | | | |

| | | | | | | |
|---|---|---|---|---|---|---|
| Initial manifestations of compressional stress regime – onset of pre-Matsap deformation | Onset of tectonic switch from extensional to compressional stress regimes | Layer-parallel shortening – structures formed due to incompetent and competent strata contrasts | | Cuspate-lobate, boudinage and pinch-and-swell structures | Mixed brittle-ductile (competent and incompetent bedding behaviour) | Sample 4 (Sample 7?) |
| | | | | | | |
| Pre-Matsap deformation | 1st period of folding – gentle | Post-tectonic seams (compressional) | | Folded seams | Brittle | Sample 15? |
| | | | | | | |
| Deposition of Gamagara and Matsap Formations | | Post-tectonic seams (compressional) | | | Brittle | |
| | | | | | | |
| Post-Matsap deformation | 2nd period of folding – intense | Post-tectonic seams (compressional)? | | Folded seams? | Brittle | Sample 15? |

The morphological analysis of the characteristics of the different seams and their structural features allows for the construction of the relative geological and structural paragenesis important for understanding the geological and structural conditions controlling the formation and occurrence of crocidolite and amosite cross-fibre mineralisation, regardless of their past economic importance.

The deposition of the BIF of the Lower Griquatown Stage took place between 2.2 to 2.5 Ga and the origin of asbestos mineralisation is thought to have occurred during succeeding diagenesis at low pressures and low-grade metamorphism during the extensional stress regime of the basin (Dreyer, 1982; Abbott, 1983; Dreyer and Sohnge, 1992; Gibbons, 2000). The samples studied here support this theory, however, also provide evidence pointing to a much earlier asbestos seam development period and a later asbestos seam development period. What follows provides a discussion on this.

The lower portion of the Banded Ironstone Zone, throughout the Northern Cape, is exceptionally contorted and wrinkled, even in locations showing an absence of regional large-scale folding (Genis, 1964). The small amplitude of this penecontemporaneous folding appears to have resulted from slumping and flowage of the bedding just after deposition but prior to lithification (Genis, 1964). Syn-sedimentary or penecontemporaneous deformation occurs fundamentally at a certain stage straight after deposition of the Lower Griquatown

Stage and before notable burial and diagenesis with the rheological properties of the rocks ranging from semi-consolidated to unconsolidated (Toro and Pratt, 2015). The formation of deformation structure styles during this period can be classified as either ductile, ductile-brittle or brittle types and are a direct result of the response and susceptibility of the sediments to different stresses (El Taki and Pratt, 2012).

In sample 5 the predominance of penecontemporaneous (soft sediment) deformation structures associated with the BIF at the margins of the cross-fibre seams indicates that the sediments were semi-consolidated having a relatively high porosity. The soft-sediment deformation structures observed indicate that during authigenic fibre growth of crocidolite, semi-lithified conditions were capable of inciting penecontemporaneous deformation in the adjacent BIF. Additional evidence supporting early burial dilation growth are the cone and cone-in-cone structures and associated fractured magnetite laminae indicating unequal fibre growth and disruption along the direction of fibre growth. The high degree of microstructure preservation (cone and cone-in-cone structures) on the seam surface indicates that surface weathering was avoided potentially by a rapid deposition rate during early stages of burial. From this it is postulated that seam formation may have occurred in semi-consolidated sediments during the early burial stages via dilation growth before any significant overpressure accumulation occurred.

The accumulation of fluid overpressure above rock strength at low differential pressure during the later stages of burial resulted in hydraulic or extensional fracturing causing tension partings along the bedding planes (Van Noten *et al.,* 2011). Extensional fractures form in sediments that are more deeply buried under progressively increasing gravitational stress. Extensional veins initiated as fractures under a regionally constant stress field are characterised by planar seams having flat upper and lower contacts and no displacement along the seam walls that extend uniformly along their lengths over large areas (Van Noten *et al.,* 2011). This morphology of the seams indicates that they formed extensionally in horizontally positioned host-rock strata. The cross-fibre seams formed as crack-seal infilling in extensional veins may have curved and straight fibre orientations but are always bound by sharp contacts irrespective of fibre orientation. Samples 2, 3, 6, 9, 10, 11, 13 and 14 all show such seam morphologies indicating their formation because of crack-seal of extensional fractures during the latest stages of burial.

Sample 13 shows seam morphology that presents an enigma when considering both mechanisms and timing of formation. Sample 13 shows a composite seam that is divided into an upper and lower portion by a persistent thin, fine-grained median band approximately sub-horizontal and parallel to the bedding of the host rock. Seams displaying fibres emanating from a median band at the centre indicate that an initial hydrofracture was formed, sealed, and later expanded (Bons *et al.,* 2012). The argillaceous material comprising the median zone contains numerous scattered argillaceous cones projecting into the lower half of the seam below the median zone. The maximum lengths of the cross-fibres in the upper and lower seams are commonly constant each side of the median zone and may either be the same as or significantly different to those on the opposite side of the median band. A large cone structure composed of coarse, equant quartz grains is observed protruding from the lower seam contact into the lower portion of the composite seam and intersects the median band. The elongated crystals comprising the lower portion of the seam do not penetrate the cone but rather end at its margins.

Sample 12 shows seam-intersecting and cross-cutting relationships that are important for inferring the relative timing of cross-fibre seam formation. The banded jasper and ironstone on either side of the later, discrete cross-fibre lens is mostly horizontal unlike the displaced laminae above the cross-fibre vein, which have been displaced to their current position above their lateral correlatives (figures 6.36 and 6.37). This displacement, along with the ruptured magnetite laminae, are interpreted as being a result of vertical fibre growth with the extent of plastic deformation being confined to a restricted range of centimetres above the margin of the vein. The upper seam is interpreted as forming prior to the smaller, lens-shaped, lower seam as it shows to be cross-cut by the lower discrete seam cell. The initial seam is planar and regular indicating it formed during late burial via extensional fracturing and crack-seal. The widening of the later, small, irregular, and discrete seam below the initial regular seam resulted in the upward vertical compaction of the enclosing BIF gently folding the laminae around and ahead of the emplacement of the small seam to accommodate expansion. This finding indicates that both extensional and displacive mechanisms may be responsible for crocidolite seam formation with the latter resulting in the sporadic occurrence of smaller more irregularly distributed asbestos deposits.

Sample 4 shows the presence of a cross-fibre crocidolite seam in both the cusp and lobate folds of the upper bounding surface suggesting that the seam formed prior to the

interface buckle folds of the upper bounding surface. The extensional conformable cross-fibre seam formed prior to the formation of interface buckling, which formed later as progressive shortening caused buckling of incompetent layers. The planar lower contact and cusp-and-lobate upper contact geometry may be interpreted as a brittle-ductile transition (Kenis and Sintubin, 2007) reflecting the onset of compressional tectonic inversion (Kenis *et al.,* 2002) prior to the pre-Matsap folding period. This cuspate-lobate geometry at the interface between the cross-fibre seam and chert indicate a difference in competence between two lithological bands (Van Noten *et al.,* 2011). Based on this structural observation it may be concluded that extensional seams showing mullions (cusp-and-lobate buckling) are the initial indication of the compressional regime at the beginning of pre-Matsap contraction.

Sample 12 shows that 'fibrous' (blocky) bedding-parallel quartz veins associated with the extensional crocidolite seams formed during later fracturing events and subsequent crack-seal. This later event can clearly be justified based on the contrasting morphology and thickness of the crocidolite seams and 'fibrous' quartz veins (Zhang *et al.,* 2015). Unlike the thick cross-fibre asbestos seam these thin, bedding parallel 'fibrous' quartz veins are composed of thick elongate quartz crystals. These veins are interpreted as slip-reactivated veins that formed primarily along the contacts of the asbestos seams by bedding-parallel shearing and slippage (Rodrigues *et al.*, 2009). This event must have occurred during or after the sealing of the extensional fractures by cross-fibre asbestos during some form of slip/shear deformation, but prior to the onset of compression. Evidence supporting this is seen by the distinct band of localised change in crocidolite fibre orientation at the lower contact of the seam near the region of shearing and thus the marginal quartz vein.

The iron-formation and associated sediments related to the asbestos deposits of the Transvaal have been folded along two major axes, one trending east-west (strongest set) and the other trending north-south (weaker set) (Whittaker, 1979). A series of large dome and basin structures formed at interference points between the two sets (Abbott, 1983). The first folding event known as the pre-Matsap folding event occurred prior to the deposition of the Gamagara and Matsap Formations and is characterised by mild stratal deformation (Visser, 1944; Hanekom, 1966). During the event the state of the sediments were still highly plastic and the material within certain individual layers of the banded ironstones experienced lateral movement resulting in the flanks of these folds having thicker anticline crests and syncline troughs (Abbott, 1983). Following the deposition of Gamagara and Matsap Formations in the

Griqualand Basin (Loskop and Waterberg Systems in the Transvaal Basin) a second period of folding took place known as the post-Matsap event in which intense pressure directed from the west resulted in the rocks along the western edge of the primary depositional basins being intensely folded (Genis, 1961). The development of numerous low angle thrust faults occurred in areas, such as Postmasburg, where maximum pressure was experienced (Genis, 1961).

Sample 15 shows a single crocidolite seam that is continuous around fold hinges where the fibres are orientated at a high angle to the seam wall. This indicates that the seam was already formed when the final post-Matsap folding event took place. The study shows that amphibole asbestos seam formation has a complex geological and deformation history. In all theories regarding the mechanisms of bedding-parallel cross-fibre amosite and crocidolite mineralisation in BIF, there is one single factor universally accepted: Regardless of the chemical conditions required, bedding-parallel space is essential for the development of cross-fibre amphibole asbestos seam formation. With this said, that is where the agreement between the scientists involved in this research ends as this necessary area for fibre development can be generated in a variety of ways, some of which include: (1) Hydro-facture due to porewater pressure exceeding overburden pressure (i.e. principle stress) during horizontal compression (figure 6.56) (Heaney and Fisher, 2003; Hilgers and Urai, 2005); (2) the force of mineral crystallisation (figure 6.57) (Means and Li, 2001; Wiltschko and Morse, 2001; Hilgers and Urai, 2005); and (3) combined effective tension and hydraulic fracturing during the enhancement of porewater overpressure by seepage forces opening up bedding-parallel fractures (Cosgrove, 1995; Cobbold and Rodriguez, 2007).

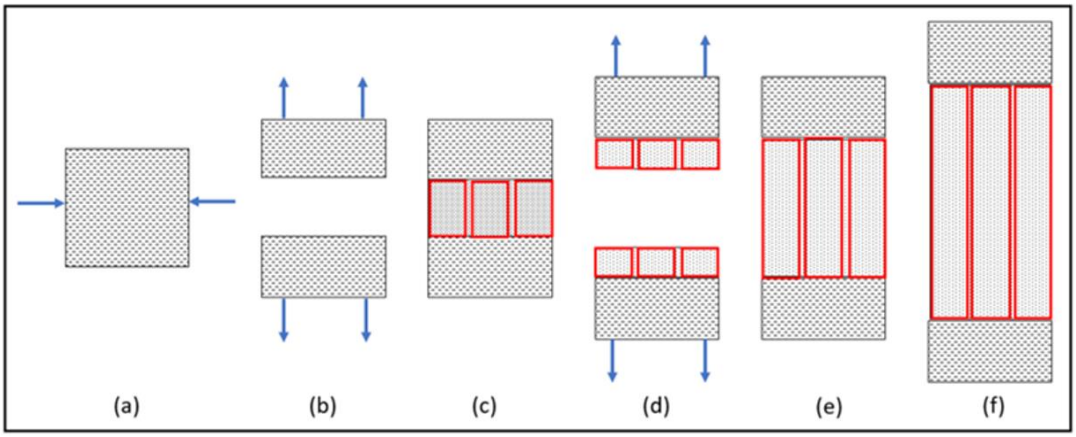

Figure 6.56: Crack-seal deformation mechanism sequence of events (a) elastic strain, (b) fracture, (c) sealing, (d) later fracture, (e) overgrowth and sealing, and (f) development of fibrous microstructure by repeated crack-seal increments (adapted from Cox and Etheridge, 1983).

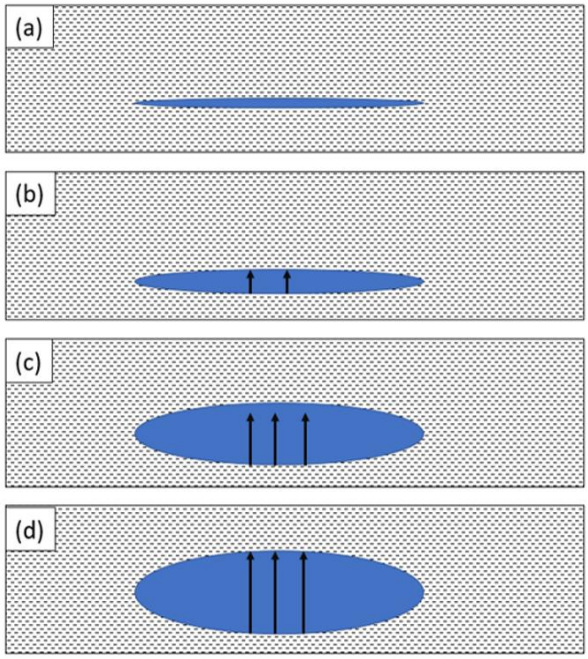


Figure 6.57: Dilation growth during the force of asbestos fibre crystallisation/growth. The amphibole asbestos cross-fibre seams are formed by dilation growth shown in (a) to (d), in which space is progressively created by the force of crocidolite/amosite fibre growth along their lengths

## 6.7. Hawks-eye (sample 12): Pseudo-morphic replacement of crocidolite by quartz or crack-seal fracture filling?

Bedding-parallel fibrous quartz veins and cone-in-cone structures composed of fibrous quartz is a topic of debate, i.e. whether this quartz is a primary mineral or the product of secondary alteration (i.e., silicification and pseudomorphic replacement) (Woodland, 1964; Heany and Fisher, 2003, 2004; Gutzmer *et al.,* 2004). The following discussion is based on the visual examination of sample 12. Small-scale mining and benefaction of the beautiful and fascinating semi-precious gemstones, Tigers-eye, and Hawks-eye, hosted in the banded iron

formation of the Asbestos Hills Subgroup, occur near the Niekerkshoop, Prieska, Hay and Griquatown areas in the Northern Cape Province (Ledwaba, 2014; Rasmeni *et al.,* 2016).

The sample has a macroscopic appearance of vivid blue 'fibrous' quartz spanning the width of the seam. Unlike most Tigers-eye and Hawks-eye rock specimens this sample shows both structural strain and post-crystallisation deformation having significant inference on the formation mechanisms. In accordance with the most recent, two opposing theories being that (1) quartz is a later pseudomorphic replacement of crocidolite and (2) quartz and crocidolite grew as crocidolite, the following hypotheses are outlined and objectively deconstructed based on this Hawks-eye rock specimen alone: **Null hypothesis -** crocidolite grew as crocidolite and was later pseudo-morphically replaced by quartz resulting in the formation of Tigers-eye and Hawks-eye. The **alternative hypothesis** - synchronous growth of crocidolite and quartz (Tigers-eye and Hawks-eye): Crocidolite grew as crocidolite and quartz grew as quartz through the processes of crack seal vein filling, therefore Tigers-eye and Hawks-eye are primary minerals formed synchronously with crocidolite during the same geological event. As no published literature regarding the structures observed in this Hawks-eye seam is available, this rock specimen will be described using the terminology associated with cross-fibre crocidolite seams.

It is important to note that the evidence put forth by the two major parties, namely Heaney and Fisher (2003) and Gutzmer *et al.* (2004), to support their theory and dismiss the contrasting theory presents issues. Heaney and Fisher (2003) argue for crack-seal based on mineralogical, textural, and crystallographic evidence, whereas Gutzmer *et al.* (2004) argue for pseudo-morphic replacement based on field relations and geological setting evidence.

The structures, morphologies, mineral associations and apparent paragenetic relationships observed in hand sample for sample 12 (figure 6.58) were used to make a general inference of the most likely structural evolution followed during the development of this rock specimen. The clear overprinting of the planar conformable cross-fibre seam by the cone-in-cone structure indicates that the simultaneous formation of the two is incompatible and that the most probable explanation involves a two-stage history. However, if all details regarding mineral paragenesis are considered, a more complex, multi-stage history can be outlined.

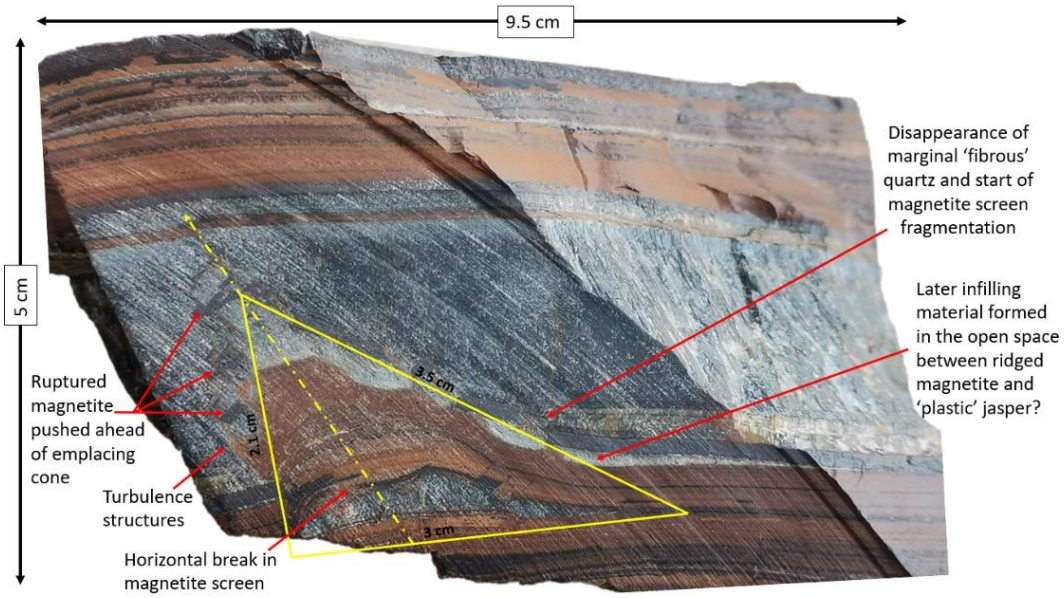


Figure 6.58: (Sample 12) Hawks-eye rock sample

The shapes of the ruptured magnetite laminae above this marginal conical structure is a common feature observed in crocidolite seam morphologies. It may indicate disruption ahead of the growing fibre direction. This also supports dilation growth in which the force of crocidolite or Hawks-eye crystallisation was the primary control for the initiation, upper and lateral spread and steady outward wedging, resulting in the discrete 'lenses' of fibre growth within the final cone-in-cone structure observed in this specimen.

The magnetite fragments associated with the emplacement of the cone-in-cone structure into the pre-existing bedding-parallel cross-fibre vein are largely isolated bodies (i.e., have not resulted in major disruptions). They are perfectly preserved and indicate their movement into their current position occurred when the material comprising the rock behaved in a somewhat pliable manner, allowing structural penetration without being deformed in a brittle manner (brecciating). The entrained magnetite fragments conform to fabric and turbulence structures defining the outer cone margin. These geometrical features indicate that during displacive or dilation growth the material into which emplacement occurred was unconsolidated allowing moulding. In this sample, the minute oblique micro-fractures radiating from the cone indicate that, although the material behaved plastically and allowed moulding, it was consolidated. However, the material being emplaced allowed for accommodation (figure 6.59). Based on this, it is reasonable to assume that very fine and

flexible cross-fibres, such as those of crocidolite, most probably existed during the formation of this dissecting, isolated and scale-restricted non-shear deformation structure.

To further support this is the apparent consumption of marginal quartz, but not Hawks-eye, which also being quartz, would then be expected. This cone-in-cone growth would presumably alter the local stress field in its immediate area, explaining the rapid disappearance of the marginal quartz and break in the lower magnetite screen of the primary seam. The numerous micro-fractures emerging and propagating from the upper parts of cone-in-cone structure reflect this confined stress state and would explain the sudden disappearance of the marginal quartz as being mechanically sensitive to this local stress field. This may account for the lost material as being redistributed in the form of fluid within, and later forming the infilling material of the minute conduit fractures.

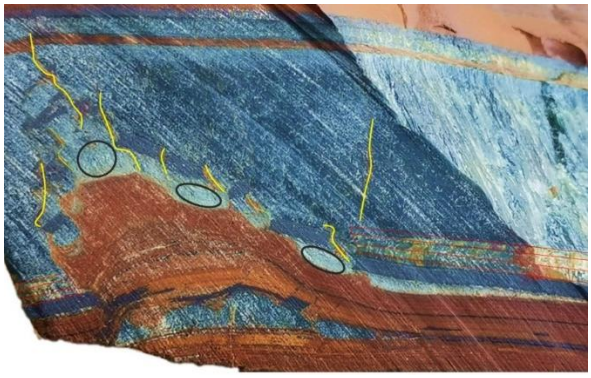

Figure 6.59: (sample 12) Small deformation structures observed in Hawks-eye rock sample.

Additionally, the position of the cone-in-cone emplacement suggests that during its formation by dilation growth the overlying material posed the least resistance compared to the underlying material. The preferential upwards displacement indicates easier material to penetrate and wedge across.

In accordance with the above, a new explanation for both crocidolite and Hawks-eye mineralisation is provided and schematically illustrated (figure 6.60 and 6.61):

(1) Hydro fracture of the host rocks during gentle E-W and/or N-S compression resulting in planar fractures parallel to the jasper bedding planes (representing regional scale shear deformation) (figure 6.60 a,b).

(2) Crack-seal vein-filling of these fractures by very fine, flexible and compliant fibrous crocidolite asbestos (figure 6.60 c).

(3) Later, minor hydrofracturing forming thinner, planer fractures parallel to the jasper bedding and at planes of weakness, such as those found between the contacts of crocidolite cross-fibres and their bounding surfaces. Subsequent crack-seal vein-filling of these with 'fibrous' quartz (i.e., elongated, block quartz crystals arranged parallel to one another and perpendicular to the bedding planes) (figure 6.60d and 6.61e).

(4) The transition from the halt in fibrous crocidolite growth followed by marginal 'fibrous' quartz is potentially associated with progressive lithification associated with an increasing depth.

(5) Non-shear deformational event resulting from the force of crystallisation during dilation growth of crocidolite (or Hawks-eye?) resulting in the cone-in-cone structure. Discrete, horizontally and vertically restricted, non-planar, sporadic body of fibre growth in the core of the cone-in-cone structure (and being the origin of the cone-in-cone structure), which overprinted the earlier formed seam (figure 6.61 f, g).

(6) Later silicification (and pseudomorphic replacement) of both crocidolite seams (earlier and later), resulting in the uniform colour and mineralogy, and the preservation of crocidolite-like structures within the 'fibrous' quartz (Hawks-eye) veins (figure 6.61 h).

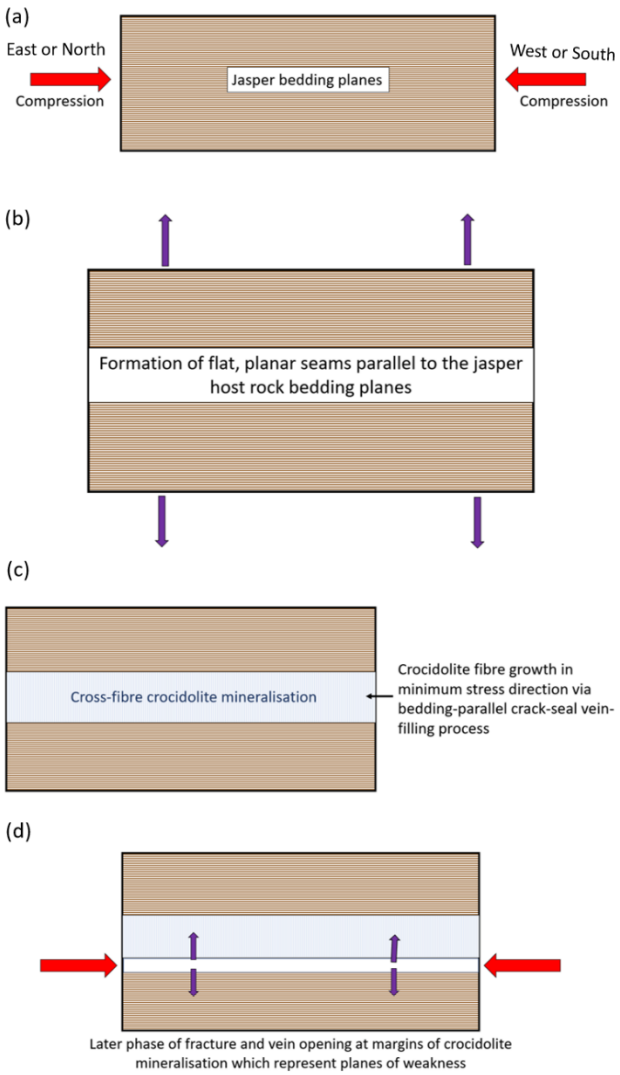


Figure 6.60: Proposed model for formation of crocidolite and Hawks-eye in sample 12.

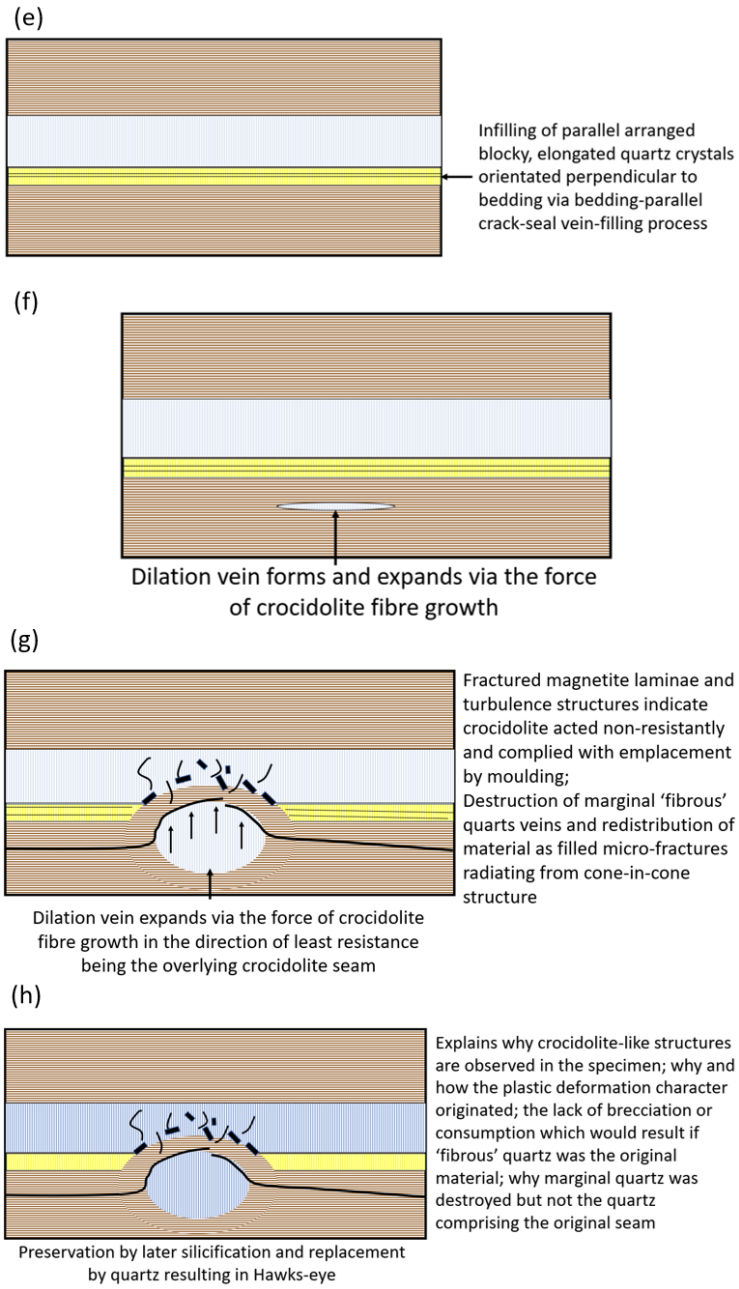


Figure 6.61: Proposed model for formation of crocidolite and Hawks-eye in sample 12.

The model presented here is in accordance with the statement by Vignaroli *et al.* (2011) that fibrous mineral mineralisation and their textures result from both regional shear deformation events and local (small-scale, confined) non-shear deformational processes. It therefore supports both a crack-seal and dilational vein origin for crocidolite formation. This paper supports crocidolite growth in dilation veins, contradicting the study by Dreyer and Sohnge (1992). Moreso, the alternative hypothesis by Heaney and Fisher (2003; 2004) is rejected based on evidence that (i) Tiger-eye and Hawks-eye form as flat, planar intergrowth

within banded iron formations and (ii) the rock is cross-cut by the boarders of Tigers-eye and Hawks-eye implying later-stage infiltration fronts. Both of which can discounted based on the visual observations of structural features in this specimen, if Hawks-eye formed as a primary mineral. Additionally, Heaney and Fisher (2003) stated that ‘’little signs of both structural strain and post-crystallisation deformation are exhibited within the ‘fibrous’ quartz of Tigers-eye and Hawks-eye’’. The observations made in the Hawks-eye sample in this study are a result of being preserved by later replacement of the original fibrous crocidolite and directly contradicts their statement.

## 6.8. Implications for *in-situ* asbestos identification and hazard assessment

The samples presented in this study all exhibited a fibrous nature in hand sample, however, the potential risks associated with these specimens could not be simply correlated with this macroscopic observation as some specimens had highly compact fibres and others disintegrated into a powder, both of which do not present a risk in regulatory terms.

These natural amphibole-asbestos rock specimen prototypes highlight that a lack of correspondence between the fibrous nature observed in hand sample and the regulated morphological parameters guiding asbestos risk assessment studies, especially those in the mining context. The complete lack of connection between the macroscopic morphology and that of microscopic character present a clear flaw in the visual, *in situ* identification and discrimination criteria used by the mining sector n distinguishing hazardous asbestos-like elongated material particles from non-hazardous mineral look-alikes. The spatial extent of amphibole asbestos bearing Precambrian BIF across South Africa means that the outcropping or anthropogenically exposed NOA occurrences experiences weathering processes controlled by differing climatic conditions (i.e., humid, arid, sub-tropical) and therefore exhibit physico-mechanical modifications (alteration statuses). Recognising, attributing, and assessing the vast assortment of morphologies and alteration degrees of potentially hazardous asbestiform and/or fibrous minerals in the context of the mining industry requires that visual data bases available for field application be compiled and made available to industry and the public. The degree of alteration and its relevance to airborne and waterborne dispersion are graphically illustrated in figure 6.62.

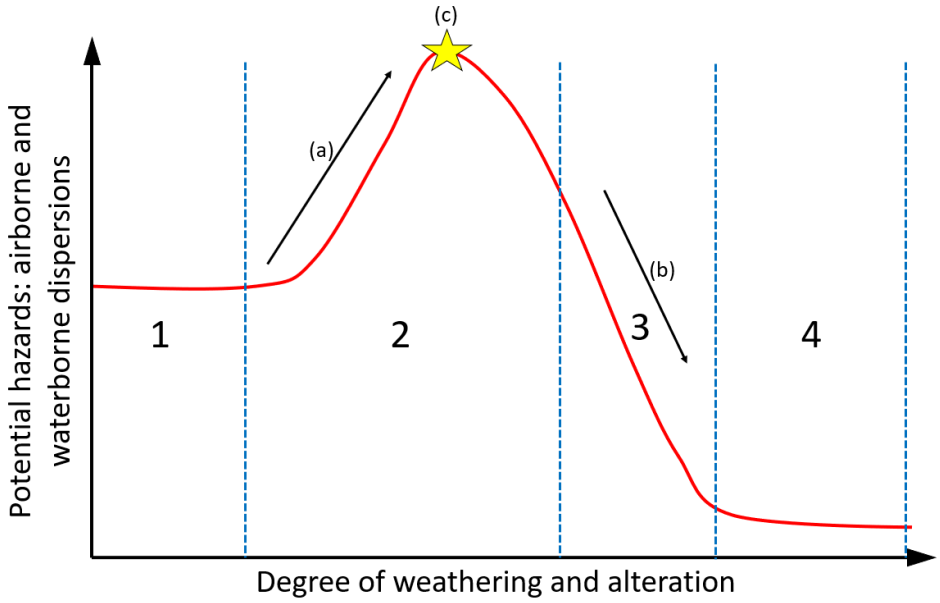


Figure 6.62: (1) Unaltered sample, cohesion is substantial, releasability is low; (2) beginning of alteration, discolouration, cohesion progressively decreases, releasability is the greatest; (3) moderate alteration, oxidation, pseudo-fibrous, loss of aerodynamic fibrous morphology, low dispersibility potential and, (4) silicification, cohesion is great, no potential of airborne and waterborne releasability and dispersion. The progressive loss of cohesion of fibres in host rock followed by release of fibre bundles and subsequent fibre release is shown by the arrow in (a), however the integrity of the fibrous structure is intact and thus the highest potential for airborne release is approached (c). Following (c) the structural integrity of the fibres breaks down and therefore the hazards of fibre dispersion decrease along (b) with loss of morphological parameters pertinent to toxicity.

The observations provided in this study are extremely significant in making inferences about the potential release of hazardous fibres from naturally occurring asbestos-bearing rocks. Furthermore, in the context of mining, understanding, and interpreting the great diversity of potentially intersected NOA minerals during geologically disruptive activities *in situ* is of great importance for mitigating the risks of asbestos exposure.

## 6.9. Conclusion

In recent years considerable progress has been made regarding asbestos in all scientific fields, covering all aspects related to the health and environmental concerns, risks and hazards surrounding all asbestos minerals and other non-asbestos fibrous minerals. In this study, BIF-hosted amphibole asbestos rock samples were examined at hand scale and characterised based on morphology, colour, cohesion, structure, deformation character and host rock lithologies. The samples are photographically documented to show the extensive variation portrayed by natural amphibole asbestos. The importance of this work is to add to the knowledge about amphibole asbestos relevant to predicting natural occurrences of asbestos. And to provide a baseline for mitigating and preventing the risk of asbestos exposure both to persons involved in geologically disturbing activities and the general population. A greater understanding of the geological setting allows for progressive asbestos management strategies to be set with the goal of saving lives.

## 6.10. References

Abbot, P. (1983): A review of asbestos resources. M.Sc. Dissertation, Rhodes University, Grahams-town, South Africa, http://vital.seals.ac.za:8080/vital/access/services/Download/vital:4910/SOURCEPDF.

Alsop, G.I., and Marco, S. (2011): Soft-sediment deformation within seismogenic slumps of the Dead Sea Basin. *Journal of Structural Geology*, **33**, 433–457, https://doi.org/10.1016/j.jsg.2011.02.003.

Apollaro, C., Fuoco, I., Vespasiano, G., De Rosa, R., Cofone, F., Miriello, D., and Bloise, A. (2018): Geochemical and mineralogical characterization of tremolite asbestos contained in the Gimigliano-Mount Reventino Unit (Calabria, south Italy). *Journal of Mediterranean Earth Sciences*, **10**, 5-15, https://doi.org/10.3304/JMES.2018.011.

Baumann, F., Ambrosi, J.P. and Carbone, M. (2013): Asbestos is not just asbestos: an unrecognised health hazard. *Lancet Oncology*, **14** (7), 576–578, https://doi.org/10.1016/S1470-2045 (13)70257-2.

Baumann, F., Buck, B.J., Metcalf, R.V., McLaurin, B.T., Merkler, D., and Carbone, M. (2015): The presence of asbestos in the natural environment is likely related to mesothelioma in young individuals and women from Southern Nevada. *Journal of Thoracic Oncology,* **10** (5), 731–737, https://www.ncbi.nlm.nih.gov/pmc/articles/PMC4406807/.

Beukes, N.J. (1973): Precambrian iron-formations of Southern Africa. *Economic geology*, **68**, 960 – 1004, https://doi.org/10.2113/gsecongeo.68.7.960.

Boggs, S. Jr. (2006): Principles of Sedimentology and Stratigraphy (4th edition). Pearson Prentice Hall, Upper Saddle River, New Jersey, USA.

Bons, P. D., Elburg, M.A., and Gomez-Rivas, E. (2012): A review of the formation of tectonic veins and their microstructures. *Journal of Structural Geology*, **43**, 33-62,

https://doi.org/10.1016/j.jsg.2012.07.005.

Buccianti, A., Apollaro, C., Bloise, A., De Rosa, R., Falcone, G., Scarciglia, F., Tallarico, A., and Vecchio, G. (2009): Natural radioactivity levels (K, Th, U and Rn) in the Cecita Lake area (Sila Massif, Calabria, Southern Italy): an attempt to discover correlations with soil features on a statistical base. *Geoderma*, **152**, 145-156, http://dx.doi.org/10.1016/j.geoderma.2009.05.027.

Button, A. (1976): Transvaal and Hamersley Basins: A review of basin development and mineral deposits. *Minerals Science and Engineering*, **8** (4), 262 – 293, https://www.wits.ac.za/media/migration/files/cs-38933-fix/migrated-pdf/pdfs-8/EGRU%20107.pdf.

Carbone, M., Baris, Y.I., Bertino, P., Brass, B., Comertpay, S., Dogand, A.U., Gaudino, G., Jube, S., Kanodia, S., Partridge, C.R., Pass, H.I., Rivera, Z., Steele, I., Tuncer, M., Way, S., Yang, H., and Miller, A. (2011): Erionite exposure in North Dakota and Turkish villages with mesothelioma. *Proc Natl Acad Sci USA*, **108** (33), 13618–13623, https://doi.org/10.1073/pnas.1105887108.

Case, B.W., Abraham, J.L., Meeker, G.P., Pooley, F.D., and Pinkerton, K.E. (2011): Applying definitions of "asbestos" to environmental and "low-dose" exposure levels and health effects, particularly malignant mesothelioma. *J. Toxicol. Environ. Heal. Part B Crit. Rev*., **14**, 3–39, https://www.ncbi.nlm.nih.gov/pmc/articles/PMC3118487/.

Cobbold, P.R., Zanella, A., Rodrigues, N., and Løseth, H. (2013): Bedding-parallel fibrous veins (beef and cone-in-cone): Worldwide occurrence and possible significance in terms of fluid overpressure, hydrocarbon generation and mineralization. *Marine and Petroleum Geology*, **43**, 1 – 20, https://doi.org/10.1016/j.marpetgeo.2013.01.010.

Cox, S.F., and Etheridge, M.A. (1983): Crack-seal fibre growth mechanisms and their significance in the development of oriented layer silicate microstructures. *Tectonophysics*, **92**, 147 – 170, https://doi.org/10.1016/0040-1951(83)90088-4.

Dreyer, C.J.B. (1974): The geology of the Bewaarkloof area, Pietersburg Asbestos Field. M. Sc. Thesis, University of the Witwatersrand, Johannesburg, South Africa, https://www.wits.ac.za/media/migration/files/cs-38933-fix/migrated-pdf/pdfs-7/EGRU%20195.pdf.

Dreyer, C.J.B. (1982): Amphibole asbestos in South Africa. Ph.D. thesis, Rand Afrikaans University, Johannesburg.

Dreyer, C.J.B., and Söhnge, A.P.G. (1992): The crocidolite and amosite deposits of the Republics of South Africa and Bophuthatswana. *Geological Survey of South Africa, Handbook* **12**,.

Du Toit, A.L. (1945): The origin of the Amphibole Asbestos deposits of South Africa. *Transactions geological Society of South Africa*, **48**, 161 – 206.

El Taki, H., and Pratt, B.R. (2012): Syndepositional tectonic activity in an epicontinental basin revealed by deformation of subaqueous carbonate laminites and evaporites: seismites in Red River strata (Upper Ordovician) of southern Saskatchewan, Canada. *Bulletin of Canadian Petroleum Geology*, **60**, 37–58, https://doi.org/10.2113/gscpgbull.60.1.37.

Eriksson, P.G., Altermann, W., and Hartzer, F.J. (2006): The Transvaal Supergroup and its precursors. In: Johnson, M.R., Anhaeusser, C.R. and Thoms, R.J., Eds., The Geology of South Africa, pp. 237-260. https://www.researchgate.net/publication/302559973_The_Transvaal_Supergroup_and_its_precursors, 2006.

Fockema, P.D. (1967): Crocidolite and associated rocks of Kuruman area in the Northern Cape. Ph.D. thesis, University of the Witwatersrand, Johannesburg, South Africa.

Genis, J.H. (1961): The genesis of the blue amphibole asbestos of the Union of South Africa. D. Sc. Thesis, University of Cape Town, Cape Town, South Africa,

https://open.uct.ac.za/bitstream/handle/11427/25590/Genis_genesis_blue_1961_1.pdf?sequence=1.

Genis, J.H. (1964): The formation of crocidolite asbestos. In: Haughton, S.H., Ed.,The geology of some ore deposits in Southern Africa. *The Geological Society of South Africa*, **2**, 571 – 578.

Gibbons, W. (2000): Amphibole asbestos in Africa and Australia: geology, health hazard and mining legacy. *Journal of the Geological Society, London*, **157**, 851–858, https://doi.org/10.1144/jgs.157.4.851.

Glenn, R.E., Lee, R.J., Jastrem, L.M., Bunker, K.L., Van Orden, D.R., and Strohmeier, B.R. (2008): Asbestos: By any other name, is it still? *Chemical Regulation Reporter*, **32** (21), 22–33.

Guagliardi, I., Buttafuoco, G., Apollaro, C., Bloise, A., De Rosa, R., and Cicchella, D. (2013a): Using gamma-ray spectrometry and geostatistics for assessing geochemical behaviour of radioactive elements in the Lese catchment (Southern Italy). *International Journal of Environmental Research*, **7**, 645-658, https://dx.doi.org/10.22059/ijer.2013.644.

Guagliardi, I., Apollaro, C., Scarciglia, F., and De Rosa, R. (2013b): Influence of particle-size on geochemical distribution of stream sediments in the Lese River catchment, Southern Italy. *Biotechnologie, Agronomie, Société et Environnement*, **17**, 43-55, https://www.researchgate.net/publication/235734347_Influence_of_particle-size_on_geochemical_distribution_of_stream_sediments_in_the_Lese_river_catchment_southern_Italy.

Guagliardi, I., Rovella, N., Apollaro, C., Bloise, A., De Rosa, R., Scarciglia, F., and Buttafuoco, G. (2016a): Effects of source rocks, soil features and climate on natural gamma radioactivity in the Crati valley (Calabria, southern Italy). *Chemosphere*, **150**, 97-108, https://doi.org/10.1016/j.chemosphere.2016.02.011.

Guagliardi, I., Rovella, N., Apollaro, C., Bloise, A., De Rosa, R., Scarciglia, F., and Buttafuoco, G. (2016b): Modelling seasonal variations of natural radioactivity in soils: A case study in southern Italy. *Journal of Earth System Science*, **125**, 1569- 1578, https://www.researchgate.net/publication/311246488_Modelling_seasonal_variations_of_natural_radioactivity_in_soils_A_case_study_in_southern_Italy.

Gualtieri, A.F. (2017): Introduction. In A.F. Gualtieri, Ed., Mineral fibres: Crystal chemistry, chemical physical properties, biological interaction, and toxicity. Vol. 18, pp. 1–15. European Mineralogical Union and the Mineralogical Society of Great Britain & Ireland, UK https://doi.org/10.1180/EMU-notes.18.

Gutzmer, J., Beukes, N.J., and Cairncross, B. (2004(: New interpretation of the origin of tiger's-eye: Comment. *Geology*, **31** (4), e44, https://doi.org/10.1130/0091-7613-32.1.e44.

Hall, A.L. (1918): Asbestos in the Union of South Africa. *Mem. Geological Survey Union of South Africa*, **12**.

Hall, A.L. (1930): Asbestos in the Union of South Africa, Second Edition. *Mem. Geological Survey Union of South Africa*, **12**.

Hanekom, H.J. (1966): The crocidolite deposits of the Northern Cape Province. D. Sc. Thesis, University of Pretoria, Pretoria, South Africa, http://hdl.handle.net/2263/29089.

Harper, M. (2008): 10th Anniversary critical review: Naturally occurring asbestos. *Journal of Environmental Monitoring*, **10**, 1394-1408, https://doi.org/10.1039/B810541N.

Heaney, P.J., and Fisher, D.M. (2003): New interpretation of the origin of tiger's-eye. *Geology*, **31** (4), 323 – 326, http://dx.doi.org/10.1130/0091-7613(2003)031%3C0323:NIOTOO%3E2.0.CO;2.

Heaney, P.J., and Fisher, D.M. (2003): New interpretation of the origin of tiger's-eye: Reply. *Geology*, **31** (4), e45, https://doi.org/10.1130/0091-7613-32.1.e44.

Hendrickx, M. (2009): Naturally occurring asbestos in eastern Australia: a review of geological occurrence, disturbance and mesothelioma risk. *Environmental Geology*, **57**, 909–926, https://link.springer.com/content/pdf/10.1007/s00254-008-1370-5.pdf.

Hodgson, A.A. (1977): Nature and paragenesis of asbestos minerals. *Philosophical Transactions in the Royal Society of London A*, **286**, 611 – 624, https://www.jstor.org/stable/74736?seq=1.

Keller, A. (1958): Morphology of crystalline polymers. Growth and perfection of crystals, ed. Doremus, Roberts and Turnbull, John Wiley, New York. Pp. 499 – 528, https://www.researchgate.net/publication/230286151_The_morphology_of_crystalline_polymers.

Kenis, I., Sintubin, M., Muchez, Ph., and Burke, E.A.J. (2002): The 'boudinage' question in the High-Ardenne Slate Belt (Belgium): a combined structural and fluid-inclusion approach. *Tectonophysics*, **348**, 93–110, https://doi.org/10.1016/S0040-1951(01)00251-7.

Kenis, I., and Sintubin, M. (2007): About boudins and mullions in the Ardenne–Eifel area (Belgium, Germany). *Geologica Belgica*, **10**, 79–91, https://www.researchgate.net/publication/286545817_About_boudins_and_mullions_in_the_Ardenne-Eifel_area_Belgium_Germany.

Kettenbrink Jr., E.C. (1970): Petrology and diagenesis of the cyclic Maquoketa Formation (Upper Ordovician) Pike County, Missouri. Masters Thesis, Missouri University of Science and Technology, 5514, https://scholarsmine.mst.edu/masters_theses/5514.

Kronyak, R.E., Kah, L.C., Edgett, K.S., Van Bommel, S.J., Thompson, L.M., Wiens, R.C., Sun, V.Z., and Nachon, M. (2019): Mineral-filled fractures as indicators of multigenerational fluid flow

in the Pahrump Hills member of the Murray formation, Gale crater, Mars. *Earth and Space Science*, **6**, 238–265, https://doi.org/10.1029/2018EA000482.

Lugli, S., Reimold, W.U., and Koeberl, C. (2005): Silicified Cone-in-Cone Structures from Erfoud (Morocco): A Comparison with Impact-Generated Shatter Cones. In Koeberl, C. and Henkel, H., Eds. (2005) Impact Tectonics. *Impact Studies* (vol. **6**), Springer, Heidelberg, https://www.researchgate.net/publication/226367958.

Meng, Q., Hooker, J., and Cartwright, J. (2017): Early over-pressuring in organic-rich shales during burial: evidence from fibrous calcite veins in the lower Jurassic shales-with-beef member in the Wessex Basin, UK. *Journal of the Geological Society*, **174** (5), 869–882, https://www.researchgate.net/publication/316205963.

Meng, Q., Hooker, J.N., and Cartwright, J. (2018): Displacive Widening of Calcite Veins in Shale: Insights Into the Force of Crystallization. *Journal of Sedimentary Research*, **88** (3), 327-343, https://www.researchgate.net/publication/323888670.

Miles, K.R. (1942): The blue asbestos bearing banded iron formations of the Hamersley Ranges, Western-Australia. *West. Austr. Geol. Surv. Bull*., **100**, part 1.

Peacock, M.A. (1928(: The nature and origin of Amphibole Asbestos of South Africa. *American mineralogist*, **13**, 241 – 284, https://watermark.silverchair.com/am-1928 241.pdf.

Perri, F., Scarciglia, F., Apollaro, C., and Marini, L. (2015): Characterization of granitoid profiles in the Sila Massif (Calabria, southern Italy) and reconstruction of weathering processes by mineralogy, chemistry, and reaction path modeling. *Journal of Soils and Sediments*, **15**, 1351-1372, https://link.springer.com/article/10.1007/s11368-014-0856-x.

Perri, F., Letto, F., Le Pera, E., and Apollaro, C. (2016): Weathering processes affecting granitoid profiles of Capo Vaticano (Calabria, southern Italy) based on petrographic, mineralogic and reaction path modeling approaches. *Geological Journal*, **51**, 368-386, https://doi.org/10.1002/gj.2635.

Pettijohn, F.J. (1957): Sedimentary rocks. Harper and Row, 2nd ed., New York, USA.

Petriglieri, J.R., Laporte-Magoni, C., Salvioli-Mariani, E., Ferrando, S., Tomatis, M., Fubini, B., and Turci, F. (2021a): Morphological and chemical properties of fibrous antigorite from lateritic deposit of New Caledonia in view of hazard assessment. *Science of the Total Environment*, **777**, 146185, https://doi.org/10.1016/j.scitotenv.2021.146185.

Petriglieri, J.R., Bersani, D., Laporte-Magoni, C., Tribaudino, M., Cavallo, A., Salvioli-Mariani, E., and Turci, F. (2021b): Portable Raman Spectrometer for *In Situ* Analysis of Asbestos and Fibrous Minerals. *Appl. Sci*., **11**, 287, https://doi.org/10.3390/app11010287.

Ramsay, J.G. (1980): The crack-seal mechanism of rock deformation. *Nature*, **284**, 135-139 https://www.nature.com/articles/284135a0.

Rodrigues, N., Cobbold, P.R., Løseth, H., and Ruffet, G. (2009): Widespread bedding-parallel veins of fibrous calcite ("beef") in a mature source rock (Vaca Muerta Fm, Neuquén Basin, Argentina): Evidence for overpressure and horizontal compression. *J. Geol. Soc*., **166**, 695–709,
https://www.researchgate.net/publication/230743872.

Schoeman, H.E. (1929): Crocidolite in the districts of Prieska and Hay. Thesis. Rhodes University College, Grahamstown, South Africa.
http://vital.seals.ac.za:8080/vital/access/services/Download/vital:21133/SOURCE1.

Toro, B., and Pratt, B.R. (2015): Eocene paleoseismic record of the Green River Formation, Fossil Basin, Wyoming, USA: implications of synsedimentary deformation structures in lacustrine carbonate mudstones. *Journal of Sedimentary Research*, **85**, 855–884,
https://www.researchgate.net/publication/280851513.

Trendall, A.F., and Blockley, J.G. (1970): The iron formations of the Precambrian Hamersley Group, Western Australia. *Australian Institute of Mineralogy and Metallurgy Proclamations*, **206**.

Van Noten, K., Muchez, P., and Sintubin, M. (2011): Stress-state evolution of the brittle upper crust during compressional tectonic inversion as defined by successive quartz vein types (High-Ardenne slate belt, Germany). *Journal of the Geological Society of London*, **168**, 407–422, https://www.researchgate.net/publication/228117252.

Vignaroli, G., Rossetti, F., Belardi, G., and Billi, A. (2011): Linking rock fabric to fibrous mineralisation: a basic tool for the asbestos hazard. *Nat. Hazards Earth Syst. Sci*., **11**, 1267–1280, https://www.researchgate.net/publication/230736253.

Vignaroli, G., Ballirano, P., Belardi, G., and Rossetti, F. (2014): Asbestos fibre identification vs. evaluation of asbestos hazard in ophiolitic rock melanges, a case study from the Ligurian Alps (Italy). *Environ. Earth Sci*., **72**, 3679–3698, https://www.researchgate.net/publication/268518110.

Warke, M.R. (2016): Stratigraphic and geochemical framework of the Paleoproterozoic rise in atmospheric oxygen: Transvaal Supergroup (South Africa. Thesis for PhD in Engineering and Science, University of Manchester, Manchester, England. https://pure.manchester.ac.uk/ws/portalfiles/portal/60830743/FULL_TEXT.PDF

Williams, C., Dell, L., Adams, R., Rose, T., and Van Orden, D.R. (2013): State-of-the-science assessment of non-asbestos amphibole exposure: Is there a cancer risk? *Environmental Geochemistry and Health***, 35**, 357–377, https://doi.org/10.1007/s10653-012-9500-0.

Zhang, B., Yin, C.Y., Gu, Z.D., Zhang, J.J., Yan, S.Y., and Wang, Y. (2015): New indicators from bedding-parallel beef veins for the fault valve mechanism. *Science China Earth Sciences*, **58**, 1320–1336, https://www.researchgate.net/publication/277690712.

# Chapter 7 - Fibrous minerals and Naturally Occurring Asbestos (NOA) in the metacarbonate hosted Fe oxide-Cu-Au-Co mineralized rocks from the Guelb Moghrein Mine, Akjoujt, Mauritania: Implications for *in situ* hazard assessment and mitigation protocols

Abstract

The awareness of the potential risks associated with the environmental exposition of asbestos is on the rise and has facilitated new interest in *in situ* identification and assessment of hazards of fibrous minerals. The mineralised metacarbonate rocks of Guelb Moghrein deposit have not been studied regarding the identification and characterisation of fibrous minerals occurrences. Thus, the aim of this study is to collect samples from different lithotypes with visually identifiable fibrous minerals and examine the geological-structural features pertaining to their mode of occurrence and formation. The mineral fibre components of the rock samples demonstrate that fibrous and asbestiform mineralisation occurred via several modes, including fracture fill, slip-fibre recrystallisation and replacement. The geological diversity of fibrous amphibole mineralisation points to the chemistry of the rocks in this area as well as open space being the major factors controlling the presence of NOA in this deposit. The variability of NOA due to different fibrous mineral intergrowths is investigated in this work by determining the bulk mineralogical and geochemical properties of the fibrous mineral content of each sample. The identification of the asbestiform features exhibited by siderite, anthophyllite and talc in the mineralised metacarbonate of the Guelb Moghrein deposit underlines the necessity for further mineralogical research to enhance our understanding of fibrous minerals and how we assess their potential hazards to health.

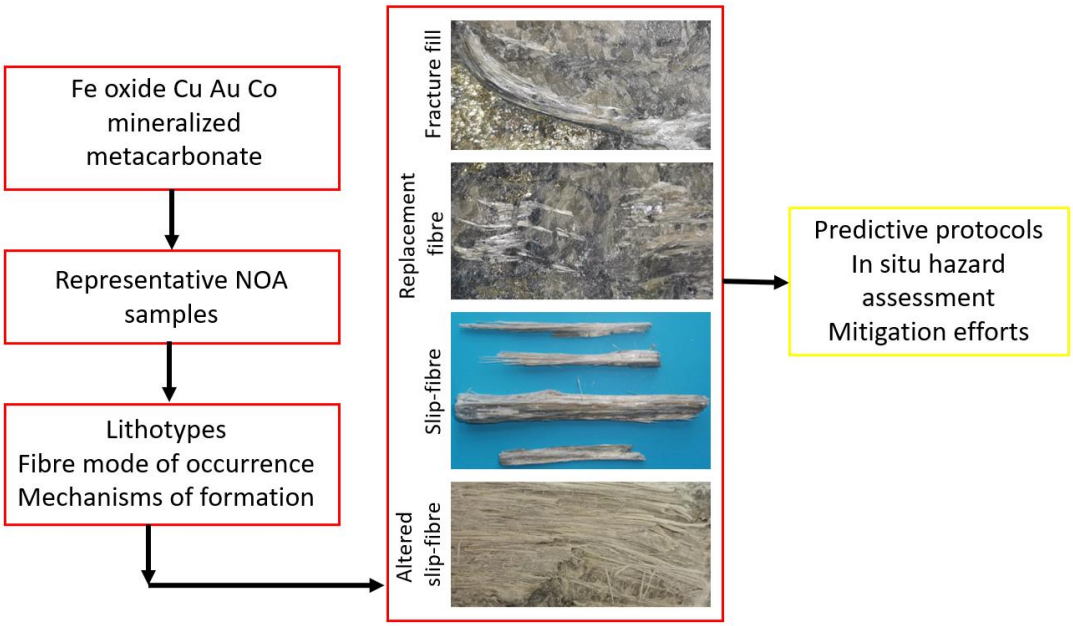


Figure 7.1: Graphical abstract of work investigated in the study

## 7.1. Introduction

The commercially applied term asbestos encompasses a group of six naturally occurring fibrous silicates used in numerous past industrial and commercial applications for their unique and desirable characteristics (Lahondère *et al.,* 2019). However, unlike commercially used UICC asbestos, naturally occurring asbestos (NOA) samples are characterised by different fibre morphologies, intermixed mineral phases and heterogeneous chemical compositions (Wagner, 2015). Thus, conventional geological, health-based or legal definitions for the term asbestos cannot be easily used when studying NOA fibres (Meeker *et al.,* 2003; Wagner, 2015).

Growing concerns of the potential health effects from disturbed NOA have also facilitated investigations worldwide. Increasing attention to mineral fibre and NOA occurrences in their natural geological settings have ensued over recent years in view of environmental hazard assessment (Lucci *et al.,* 2018). Naturally occurring asbestos (NOA) is a term used to define fibrous minerals that are natural components of soils and rocks (Harper, 2008; Metcalf and Buck, 2015). Natural and anthropogenic disturbances to the NOA-hosted geological material represents a major source of asbestos dispersion and subsequent exposure presenting an aggressive environmental hazard (Vignaroli *et al.,* 2014).

Anticipating and/or predicting natural occurrences of asbestos in their geological environment offers a fundamental strategy for mitigating the hazards of asbestos exposure and dispersion (Vignaroli *et al.,* 2011). However, to administer such progressive and prognostic hazard identification and mitigation, guidelines for reducing the risks of environmental exposure to asbestos and increased understanding of the relationship between asbestos mineralisation and the geological conditions are required (Giacomini *et al.,* 2010; Vignaroli *et al.,* 2011; Lescano *et al.,* 2013; Lucci *et al.,* 2018). Fibrous minerals, including asbestos are found in a broad spectrum of geological settings (Vignaroli *et al.,* 2011). Predicting and quantifying the asbestos hazard and associated risks in the natural environment requires knowledge on the geological setting and conditions relevant for NOA environments. Thus, if saving lives is to be accomplished in such heterogeneous and unconfined (exposed to the atmosphere) settings it is imperative that greater attention be devoted to applying geological-structural based research for discerning the correspondence between potential asbestos occurrences, geo-and-lithological diversities, and any other impacting geological factors, such as deformation (Vignaroli *et al.,* 2020).

In this work, an example of an NOA occurrence in mineralised metacarbonate rocks from the Guelb Moghrein Mine, Akjoujt, Inchiri Region, Mauritania, is investigated. The geological conditions directly control the formation of the asbestiform or fibrous crystal habit of minerals during crystallisation (Van Orden *et al.,* 2008). This site-specific geological-structural investigation identifies the presence of NOA and provides insight into non-asbestos fibrous mineral associated with asbestos has not yet documented.

## 7.2. Geological background and mineralisation

The Guelb Moghrein Mine is located close to a town known as Akjoujt, ~260 km northeast of Nouakchott (capital city) in the Inchiri Province of Mauritania (Gray *et al.,* 2016). The Guelb Moghrein Fe oxide-Cu-Au deposit is situated within the Mauritanide fold-and-thrust belt that accreted during the Variscan orogeny along the western edge of the West African craton (Lecorche *et al.,* 1989; Martyn and Strickland, 2004) (figure 7.2).

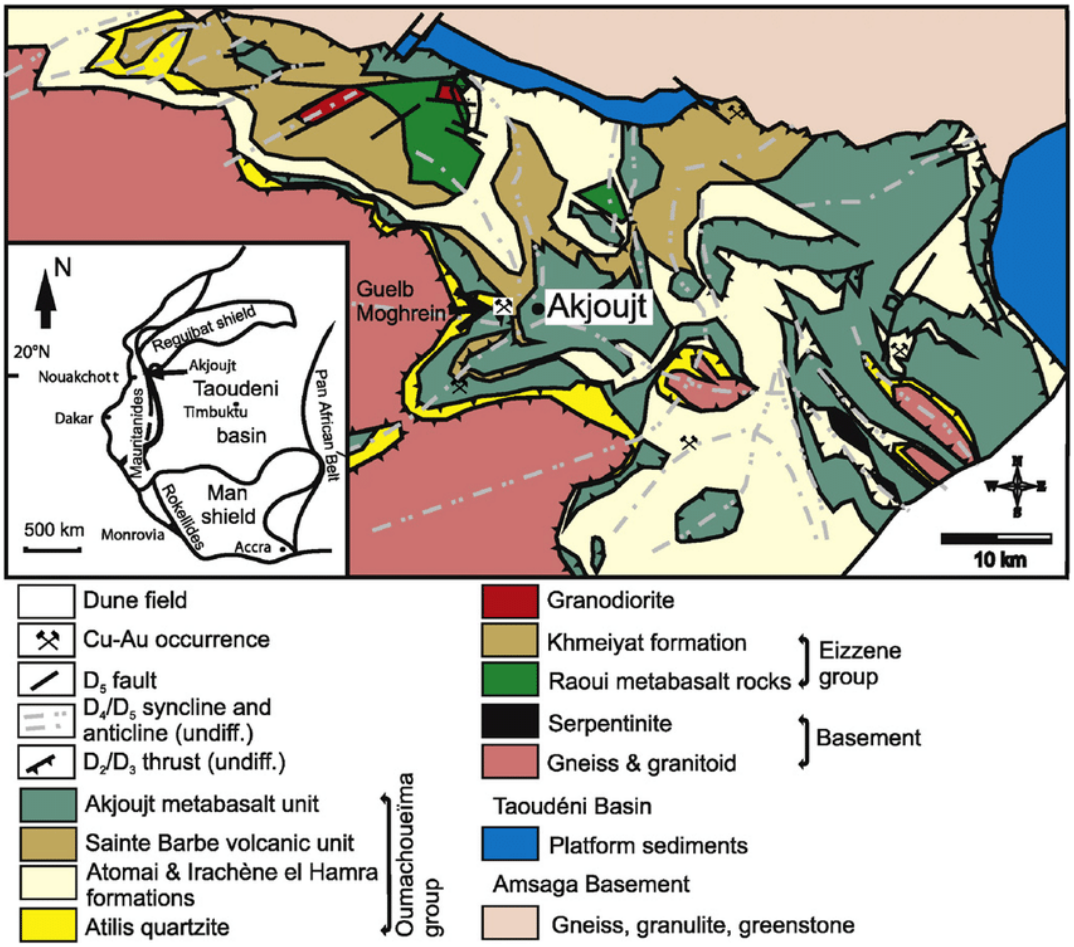


Figure 7.2: Regional geological setting of the Guelb Moghrein Fe oxide Cu-Au deposit (taken from Kolb and Petrov, 2016)

Bound by thrust-faults, a Ferro-Magnesian Carbonate unit (FMC) hosts the two outcropping and lensoid Oriental and Occidental deposits of the Guelb Moghrein (Kirschbaum and Hitzman, 2016). The FMC is situated between meta-basalt and mafic schists along its contacts (Gray *et al.,* 2016). The coarse-grained, massive metacarbonate Oriental and Occidental bodies are host to the iron oxide-copper-gold mineralisation (Kirschbaum and Hitzman, 2016). These metacarbonate bodies primarily consist of siderite with accompanying ore and alteration minerals of chalcopyrite, pyrrhotite, pentlandite, gold, graphite magnetite and Fe-Mg clinoamphibole (Strickland and Martyn, 2002). Surrounding the mineralised metacarbonate bodies is an extensive zone of oxidation that formed during weathering and is characterised by hematite, goethite, and siderite with minor graphite and anthophyllite (Sakellaris, 2007). The epigenetic Fe oxide-Cu-Au mineralisation is controlled by a range of shear and fault zones (Kolb *et al.,* 2006). The metacarbonate is truncated by discrete $D_2$ shear

zones characterising brittle deformation along which the Fe oxide-Cu-Au-Co mineralisation is concentrated (Kolb *et al.,* 2006). The stage of mineralisation is regarded as coeval with $D_2$ shearing as the resulting breccia developed in the metacarbonate are always host to some Fe oxide-Cu-Au-Co mineralisation (Sakellaris, 2007). Multiple, merging breccia zones up to 30 cm in width and consisting of siderite, magnetite, Fe-Mg clinoamphibole, graphite and sulphide assemblages constitute the $D_2$ shear zones in the mineralised metacarbonate (figure 7.3) (Sakellaris, 2007).

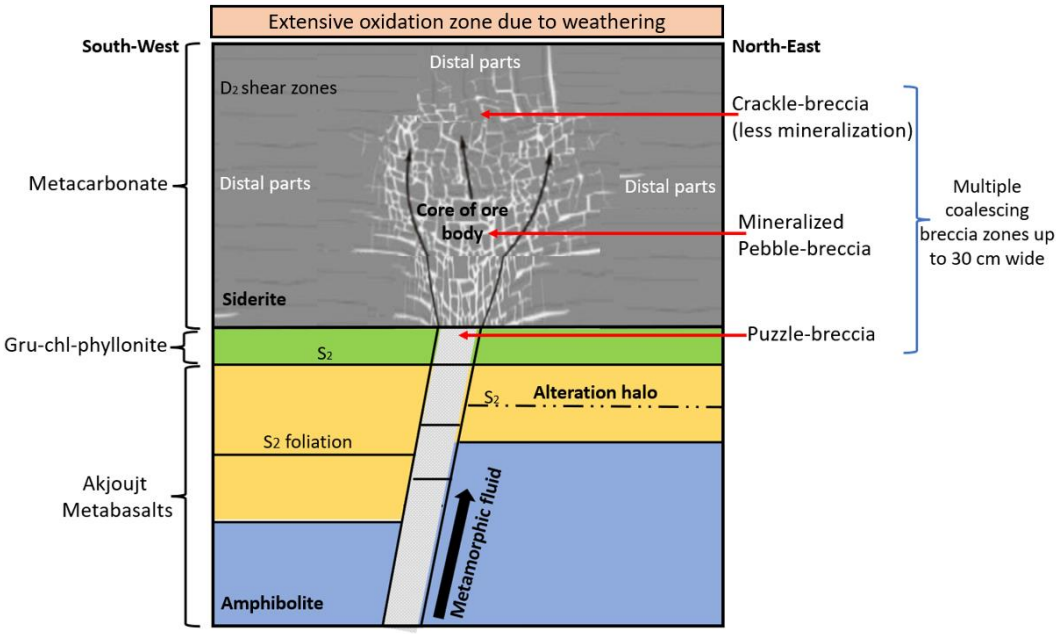


Figure 7.3: Schematic illustration of the Fe oxide-Cu-Au-Co mineralised metacarbonate deposit of the Guelb Moghrein (adapted from Sakellaris, 2007)

The lithology and associated textures are characterised by their horizontal location transversing along the distal least altered and mineralised wall rocks through to the zones of alteration and eventually the massive ore zones at the core of the mineralised metacarbonate body (figure 7.3). Progressing with horizontal distance towards the central ore zones is a systematic increase in brecciation (fragment size and clast-matrix ratio: Sakellaris, 2007).

## 7.3. Materials and methods

### 7.3.1. Sample location and collection

Fibrous mineral-containing rock fragments representing different lithotypes, textures and modes of NOA occurrence and mineralisation were collected from the Guelb Moghrein Mine (19°44’45’’ latitude and 14°25’40’’ longitude) (figure 7.4).



Figure 7.4.: Photographs of different parts of the Guelb Moghrein mine

The Guelb Moghrein mine comprises a single open pit, 141 m above sea level, from which the ore body is removed and stockpiled (Gray *et al.,* 2016). The ore mined from the pit

can be classified as structurally-modified iron oxide-copper-gold (IOCG) mineralisation and it is hosted in a unit of coarse-grained ferro-magnesian carbonate. The deposit is marked by a siliceous gossan that outcrops as two hills (Bargmann and Dominy, 2008). The samples were collected from the open mine pit based on their visually apparent fibrous mineral content and varying lithotypes. The rock fragment lithologies are easily assigned because in-pit geology exposures allow for a greater understanding of close space grade and geological continuity (Gray *et al.,* 2016).

### 7.3.2. Sample characterisation

The samples were examined using a geological-structural approach to characterise the rock fabric and structural heterogeneities related to fibrous mineral occurrence and formation (figure 7.5).

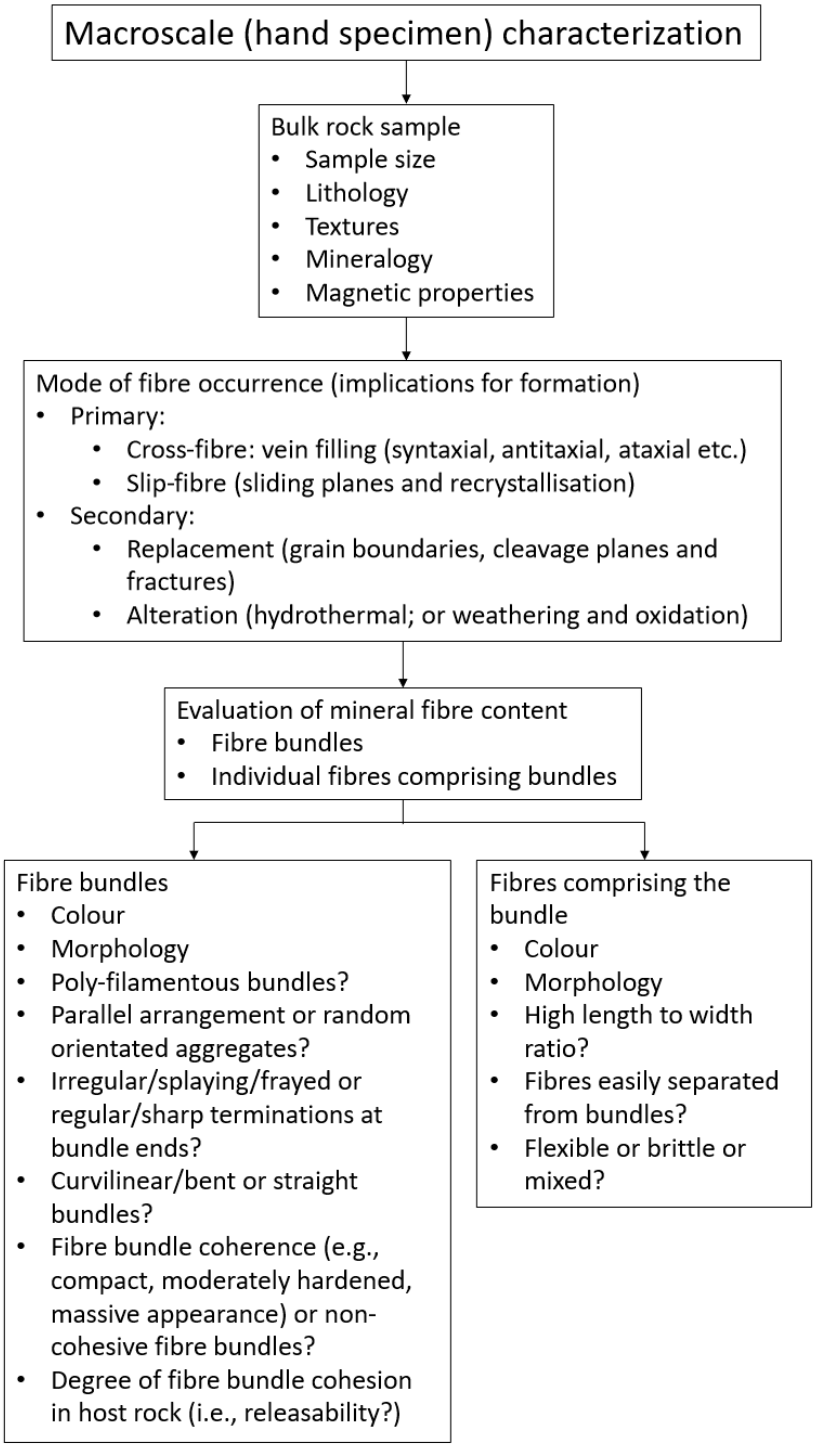


Figure 7.5: Flowchart for macroscale characterisation of the metacarbonate rocks

A geological-mineralogical description of the samples was done, and they were assigned to their respective lithological and corresponding structural classes. A total of 11 hand sample specimens were collected. The fibrous minerals identified in the rock samples

were classified based on colour, morphology, habit, and properties (figure 7.5). Additionally, each sample was documented photographically.

### 7.3.3. Fibre subsample extraction; distinguishing fibrous and pseudo-fibrous minerals, and acid test on fibres (determination of carbonate presence)

Fibres in each sample were identified and a small amount removed from the rock specimen using sterile stainless-steel forceps. The removed fibrous material was placed in a mortar and pestle and crushed to determine whether it was genuinely fibrous or pseudo-fibrous. This was accomplished by observing whether the crushed material formed (i) separable fibres or needles, (ii) matted together to form a ball, (iii) cleavage fragments or (iv) a powder, under a binocular microscope. Carbonate impurities or fibrous minerals were determined by exposing the extracted fibres to a weak solution of hydrochloric acid (10 %).

### 7.3.4. Mineralogical and geochemical investigation

From the entire suite of studied samples, sample 1 was selected for mineralogical and geochemical analysis based on the peculiar characteristics of its fibrous mineral content. The mixed fibrous morphological types identified in sample 1 include (i) flexible to ridged fibrous crystals (asbestiform), (ii) brittle acicular crystals and (iii) coarsely acicular crystals with a more massive appearance. All occur within a large poly-filamentous bundle of parallel-arranged crystals within the metacarbonate host rock surface surrounding a siderite matrix. The long crystal lengths (up to 10 cm) and their restriction to the surface plane surrounding the pebble-like siderite matrix implies that the fibres are slip-fibre type that formed by recrystallisation in highly sheared zones (Abbott, 1983). However, unlike those of the same lithology and slip-fibre origin demonstrated in samples 2 to 6, the fibrous bundles in sample 1 exhibited a strong reaction to the acid test and produced many morphological-type by-products (i.e., fibres, cleavage fragments and powder) following mechanical abrasion via crushing.

### 7.3.5. Polarised light microscopy (PLM)

The intact subsampled fibres from sample 1 were placed on a slide, covered and examined by Polarising Light Microscopy. The thin sections were made parallel to the c-axis of the fibres to determine the textural and composition relationships within and between individual fibres comprising parallel-arranged fibre bundles. The optical properties under plane polarising light (PPL) and cross-polarising light (XPL) were determined.

### 7.3.6. X-Ray Diffraction (XRD)

The fibrous subsamples from sample 1 were disaggregated and crushed in a mortar and pestle and submitted for XRD analysis to assess the bulk mineralogical composition. Diffractograms were obtained using a Malvern Panalytical Aeris diffractometer with PIXcel detector and fixed slits with Fe filtered Co-Kα radiation. The phases were identified using X'Pert Highscore plus software. The relative phase amounts (weight %) were estimated using the Rietveld method (quantitative analysis). The relative intensities (equation 1) and *d*-spacing (equation 2) were calculated from the diffractogram data.

Relative intensity (%) = $I/I_1$ x 100 _____ Equation 1

where I is the intensity of the peak and $I_1$ is the intensity of the highest peak.

$n\lambda = 2d \sin\Theta$ _____ Equation 2 (Bragg equation)

where n = 1, λ (Co*K*α) = 1.78892 and $d = n\lambda/2*\sin(\Theta)$ (*d*-spacing value).

### 7.3.7. X-Ray Fluorescence (XRF)

Major and trace element concentrations of the four asbestos mineral fibre samples were determined using X-ray fluorescence (PANalytical Axios Max and Panalytical Philips PW2404 X-ray spectrometer) at the Earth lab, Bernard Price Building, University of the Witwatersrand, South Africa. Major elements were determined using the Norrish Fusion 1 technique using in-house correction procedures. Calibration standards were from International Reference Materials USGS series (USA) and NIM series (South Africa). Precision

is taken as 1 % for elements in abundance greater than 5% by weight, and 5% for elements in abundance less than 5%. Pressed pellets were prepared for trace element analysis.

### 7.3.8. BET-$N_2$ Specific surface area

The specific surface area of the asbestos rock samples was determined by the BET method using a Micromeritics TriStar 3000 V6.05 and a surface area analyser with $N_2$ as absorbing gas at the School of Chemistry, University of the Witwatersrand, South Africa. A mass of ~ 0.2 g of each sample was placed in BET sample tubes and degassed for 4 hours. The samples were then loaded into the BET instrument and $N_2$ absorption isotherms were obtained, and the specific surface area determined.

## 7.4. Results

### 7.4.1. Sample characterisation

Sizes, lithological and textural assignment, mineralogy, and magnetic properties for all samples as identified macroscopically, are given in table 7.1.

Table 7.1: General macroscopic description and lithotype category of the different fibrous mineral-containing rock fragments

| Sample # | Sample size (cm) | Lithologies | Texture | Mineralogy | Magnetic properties? |
|---|---|---|---|---|---|
| 1 | Length 12.5<br>Width 6.5 | Least altered zone | | Siderite<br>Fibrous minerals (siderite, anthophyllite-gedrite, talc)<br>Magnetite | Yes – weakly magnetic |
| 2 | Length 11<br>Width 3.8 | Inner alteration zone | Pebble-like breccia | Siderite<br>Fibrous minerals<br>Magnetite | Yes – moderately magnetic |
| 3 | Length 11<br>Width 1.3 | Inner alteration zone | Pebble-like breccia? | Siderite<br>Fibrous minerals<br>Magnetite | Yes – moderately magnetic |

| | | | | | |
|---|---|---|---|---|---|
| 4 | Length 8.5<br>Width 0.5 | Inner alteration zone | Pebble-like breccia? | Siderite<br>Fibrous minerals<br>Magnetite | Yes – moderately magnetic |
| 5 | Length 8<br>Width 0.8 | Inner alteration zone | Pebble-like breccia? | Siderite<br>Fibrous minerals<br>Magnetite | Yes – moderately magnetic |
| 6 | Length 6<br>Width 0.7 | Inner alteration zone | Pebble-like breccia? | Siderite<br>Fibrous minerals<br>Magnetite | Yes – moderately magnetic |
| 7 | Length 5.3<br>Width 2.7 | Outer alteration zone | Crackle breccia | Siderite<br>Magnetite<br>Chalcopyrite<br>Fibrous minerals<br>Pyrrhotite | Yes – strongly magnetic |
| 8 | Length 4<br>Width 3.2 | Outer alteration zone | Crackle breccia | Siderite<br>Magnetite<br>Chalcopyrite<br>Fibrous minerals<br>Pyrrhotite | Yes – strongly magnetic |
| 9 | Length 2.8<br>Width 2 | Outer alteration zone | Crackle breccia | Siderite<br>Magnetite<br>Chalcopyrite<br>Fibrous minerals<br>Pyrrhotite | Yes – strongly magnetic |
| 10 | Length 3.5<br>Width 2.5 | Outer alteration zone | Crackle breccia | Siderite<br>Magnetite<br>Chalcopyrite<br>Fibrous minerals<br>Pyrrhotite | Yes – strongly magnetic |
| 11 | Length 4.2<br>Width 2.8 | Outer alteration zone | Crackle breccia | Siderite<br>Magnetite<br>Fibrous minerals | Yes – strongly magnetic |

Rock sample 1 (figure 7.6) is composed of coarse-grained (~2 cm), light and dark coloured, compact siderite crystals that exhibit perfect cleavage. Small magnetite crystals are disseminated throughout the siderite crystal mass imparting weak magnetism to the sample.

The fibrous material is restricted to the surface of the carbonate rock and has a white to clove brown colour. The fibres occur in parallel fibre bundles showing a preferred orientation with the longest fibre length being 10 cm and having a high aspect ratio. The poly-filamentous fibre bundles show curvature and have splayed and/or irregular ends. The fibres constituting the parallel fibrous aggregates and show mixed morphologies: from fine, flexible asbestiform habits with individual fibres being readily separated from bundles to coarser, more brittle acicular and lamellar habits that are less easily resolved into individual fibrils and more tightly welded together. The mixed and heterogeneous morphology, habit, and tensile strength across parts of this sample suggest some alteration. Crushing of the fibrous material subsamples resulted in a combination of fibres, cleavage fragments and powder material.

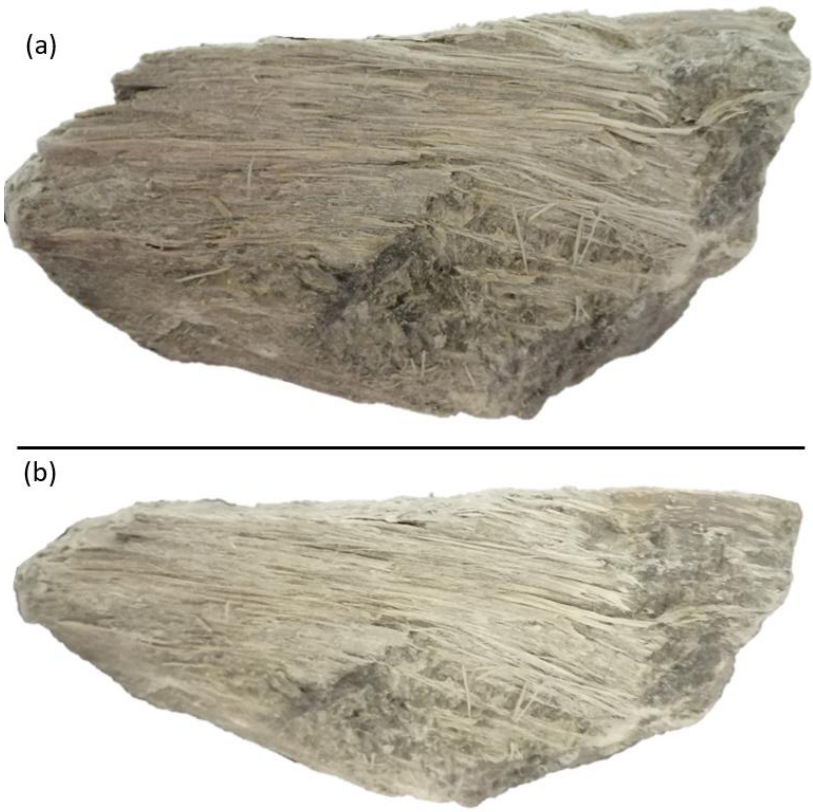


Figure 7.6: Rock sample 1 showing least-altered siderite with white to clove brown-coloured, ‘slip-fibre’ type poly-filamentous, parallel-arranged fibre bundles on the surfaces. Curvature of fibres and bundles and splayed and/or frayed fibre bundle ends are observed.

In sample 2 (figure 7.7), the extremely long, fine, white to clove and dark brown fibrous amphibole surround a matrix of pebble-like siderite breccia. The length of these fibres

and the slip-fibre occurrence indicates that their formation is a result of recrystallization along shear planes. The subsampled fibrous material is clearly asbestiform being flexible and retaining its original aspect ratio and forming matted fibrous balls when crushed. Additionally, these fibres did not react to exposure to acid indicating that they are not fibrous siderite or other carbonate minerals.

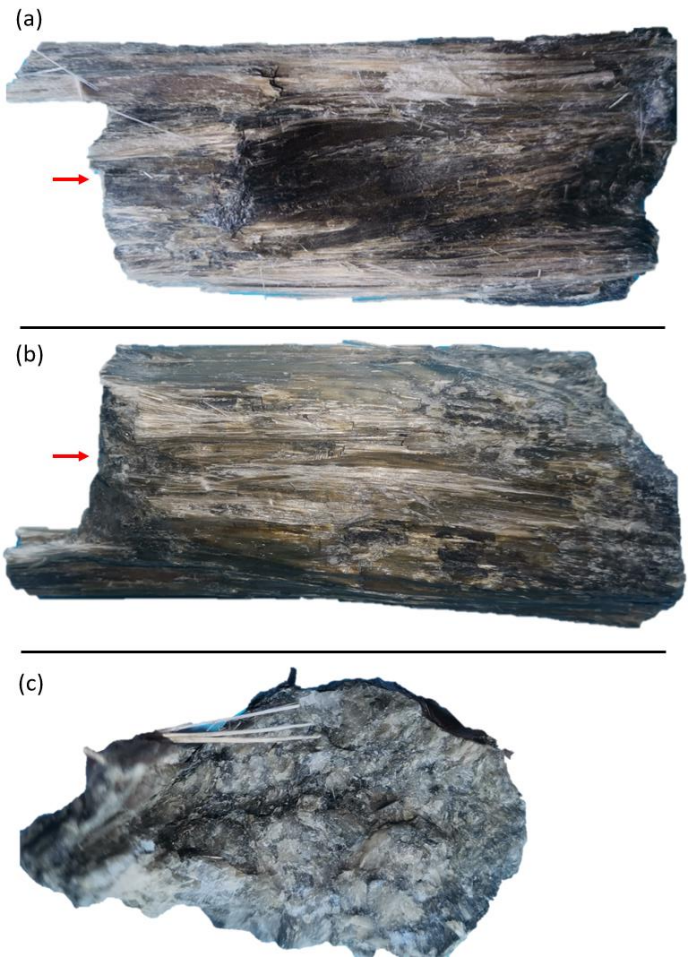


Figure 7.7: Rock sample 2 showing long pebble-like, low clast/matrix ratio siderite breccia surrounded by very long, fine fibrous amphibole.

The four fibre bundles represented by samples 3 – 6 (figure 7.8) show both fibrous and acicular morphology having mixed flexible and brittle fibrous portions. The fibres are white to clove brown in colour and are arranged in parallel bundles. Sample 4 has splayed fibre bundle terminations and sample 5 shows matted fibre on the surface indicating that, although the fibres in these four bundles appear quite straight and ridged, they do possess a degree of flexibility.

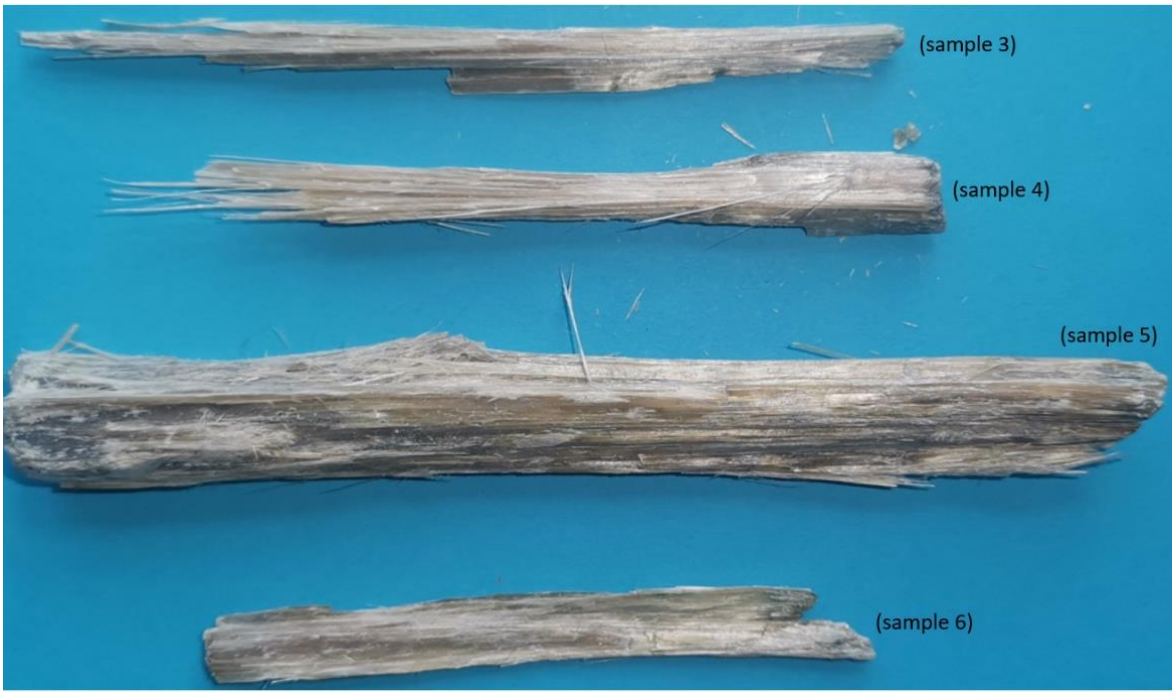


Figure 7.8: Samples 3 to 6 showing discrete, white to clove brown parallel-arranged fibre bundles ranging in length from 11 to 6 cm. The bundles of fibres demonstrate quite rigid acicular habit. The bundle ends in sample 4 are splayed and have longitudinal splitting in flexible fibres. Matted fibre masses are observed on the surface of sample 5.

The rock samples 7 to 11 are dark grey in colour and composed mainly of siderite and magnetite with white, fibrous amphiboles and sulphide intergrowths, which appear to have a replacement paragenetic association of siderite. The texture in these samples is a crackle breccia where incipient brecciation of the siderite is identified by less-mineralisation and weakly fractured appearance. These samples show structures that include variably orientated and healed microfractures filled with both sulphides and fibrous amphiboles. These veins resulted during *in situ* fragmentation of the primary siderite and subsequent syntaxial vein filling (Sakellaris, 2007). The very weak response of the fibrous material in these samples (besides sample 10 and 12) to acid implies that their bulk composition is most likely that of typical of silicates. Additionally, the mechanical crushing test resulted in the formation of numerous individual finer fibres that have retained their original aspect ratio in fibre bundles and can therefore be interpreted as asbestiform particles. Sample 7 (figure 7.9 and 7.10) shows the textures and rock fabrics associated with the growth and occurrence of fibrous amphiboles. Sample 8 (figure 7.11 and 7.12), sample 9 (figure 7.13), sample 10 (figure 7.14)

and sample 11 (figure 7.15) show fibrous amphibole occurrences because of vein filling and replacement growth.

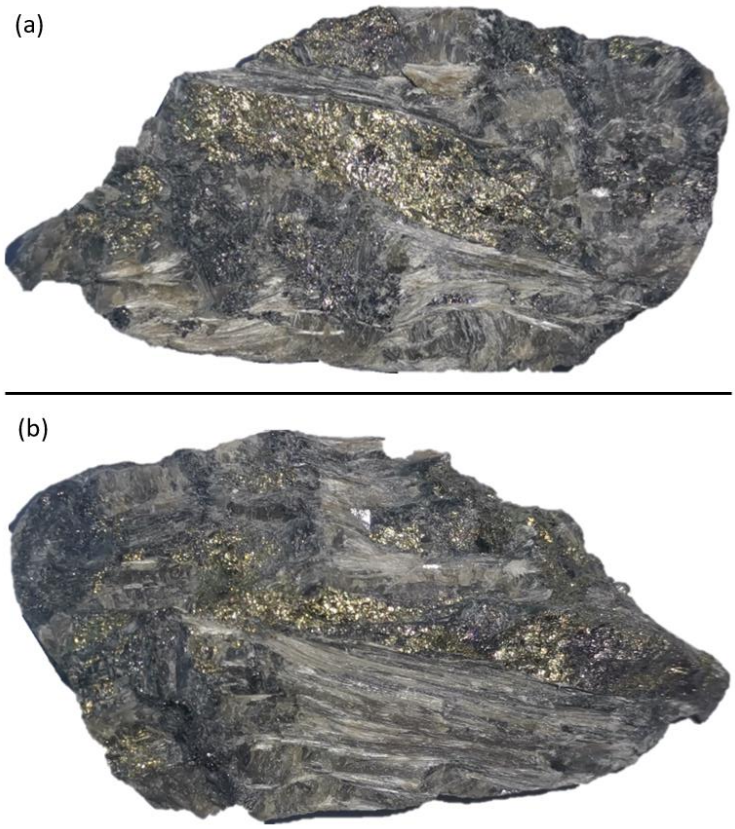


Figure 7.9: Sample 7 showing (a) white fibres occurring as mats encompassing and surrounding different minerals. The flexible white fibrous bundles formed around mineral grain boundaries; within cleavage planes and fractures they directly replace siderite, and (b) fibre bundles as fracture filling in siderite crystals. The fibrous amphibole grew as fracture filling material in siderite microfractures and shows clear crystallographic preferred orientation with respect to the fracture.

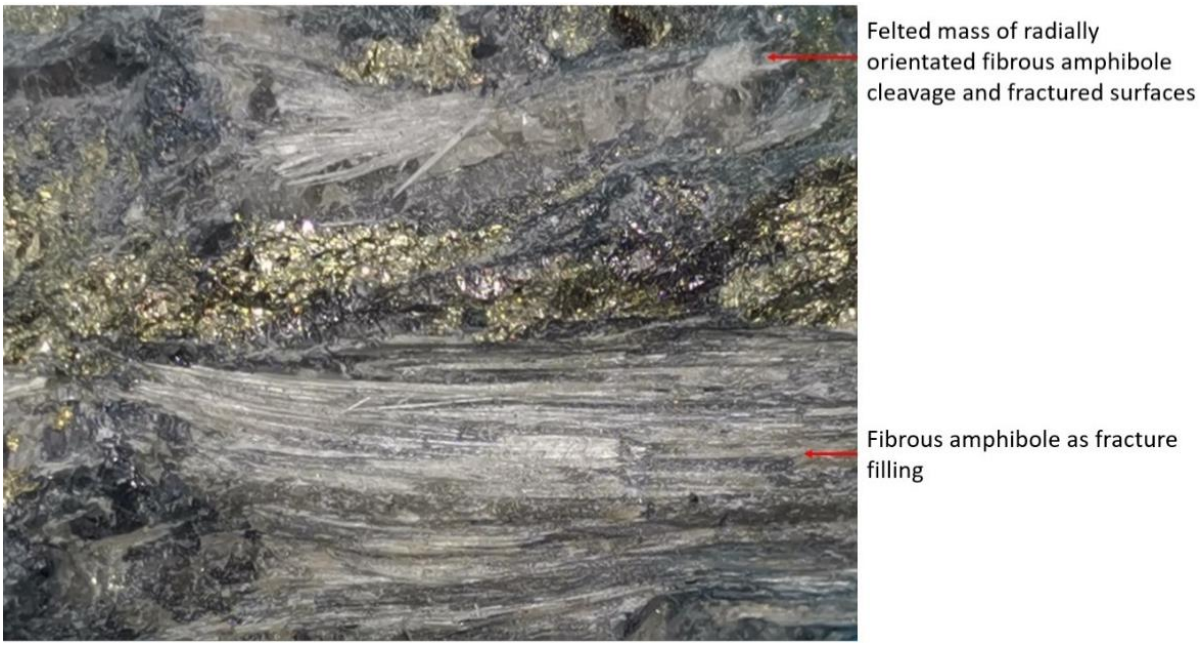


Figure 7.10: Textures observed in fibrous amphiboles, sulphides, and magnetite within the siderite host rock.

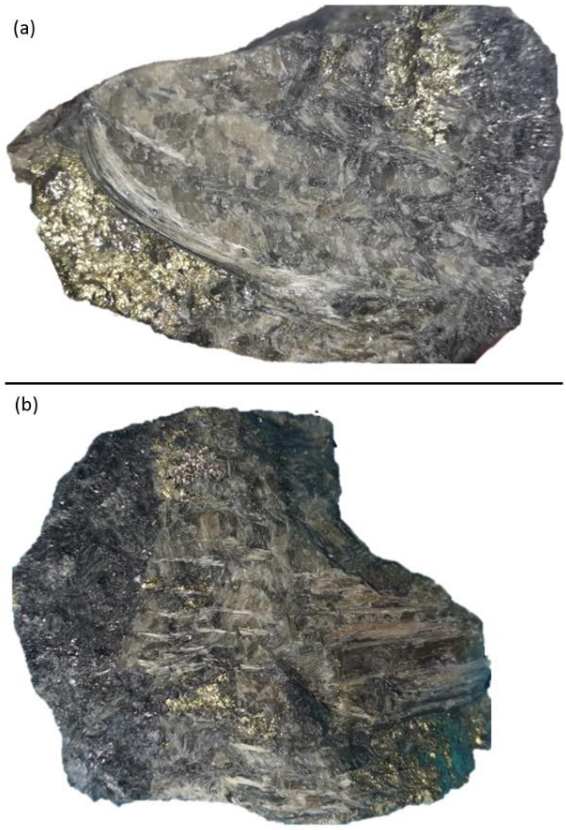


Figure 7.11: Sample 8 showing (a) white to tan coloured vein filling asbestos in siderite organised in bundles; bundles have a curvilinear trend orientated parallel to vein wall. Fibre bundle ends show individual fibrils disseminated/splaying into the siderite matrix and the

boundary between the vein and the host rock is sharp and (b) showing replacement of siderite along cleavage cracks by fibrous amphiboles.

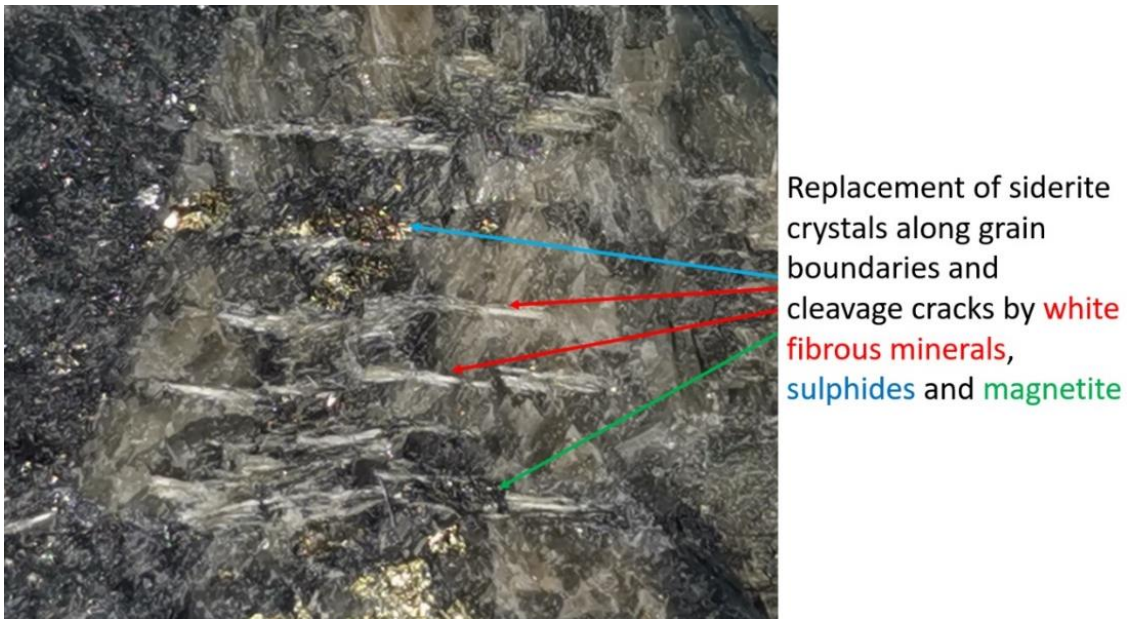


Figure 7.12: Fibrous amphibole mesh textures observed in sample 8 replacing siderite along cleavage cracks and grain boundaries forming thin sub-parallel bands.

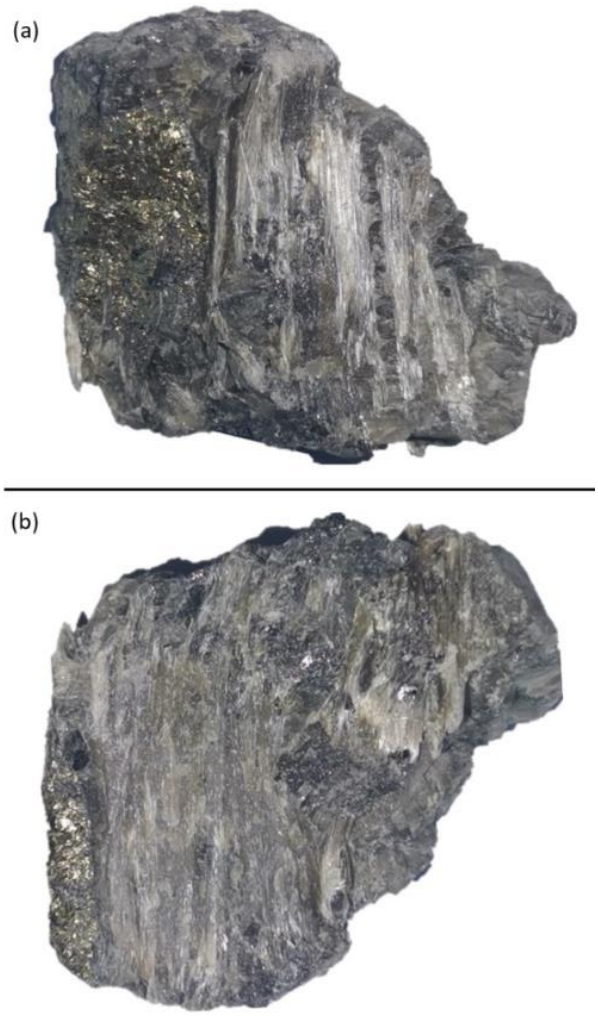


Figure 7.13: Sample 9 showing large mats of fibrous mineral replacement of siderite overprinting original rock mineralogy and texture in both (a) and (b).

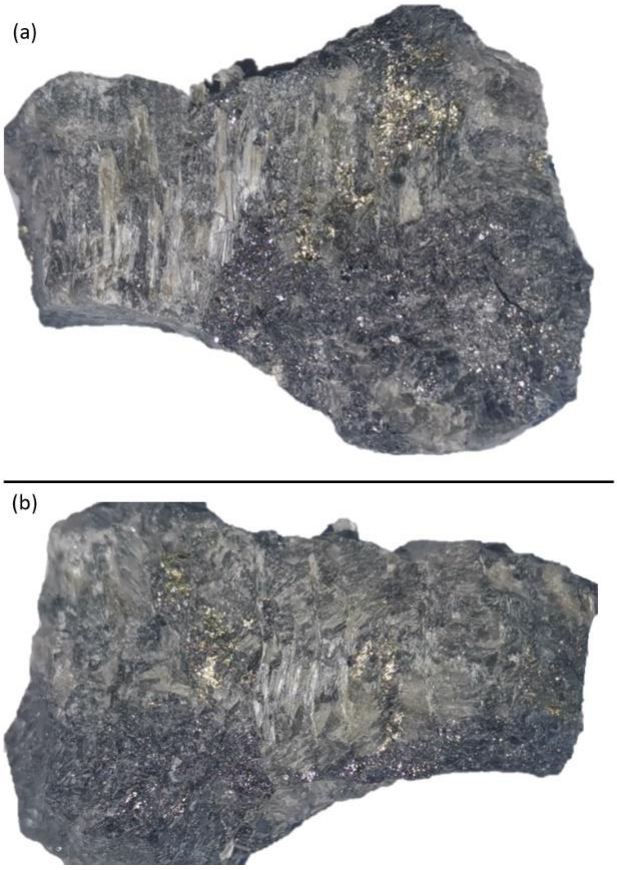


Figure 7.14: Sample 10 (a and b) shows replacement of siderite by fibrous amphiboles along grain boundaries and cleavage cracks. The orientation of fibre growth conforms to that of the cleavage microcracks and boundaries of the siderite grains.



Figure 7.15: Sample 11 showing large mats of replacement material having an elongated crystal habit covering original mineralogy and rock textures.

### 7.4.2. Polarised light microscopy (PLM)

The photomicrographs of sample 1 are given in figure 7.16 and 7.17, showing a range of pleochroic and birefringence colours within and between fibres along the c-axis indicating compositional heterogeneity. The PLM images show straight fibres forming parallel- arranged bundles. The fibres show both asbestiform (figure 7.16) and acicular habits (figure 7.17). The colours observed in PPL include a mixture of pale-yellow-and-green, blue and light and dark shades of brown. Vibrant pink, blue, yellow, orange, green and white birefringent colours are observed under XPL and the sample has a parallel extinction angle.

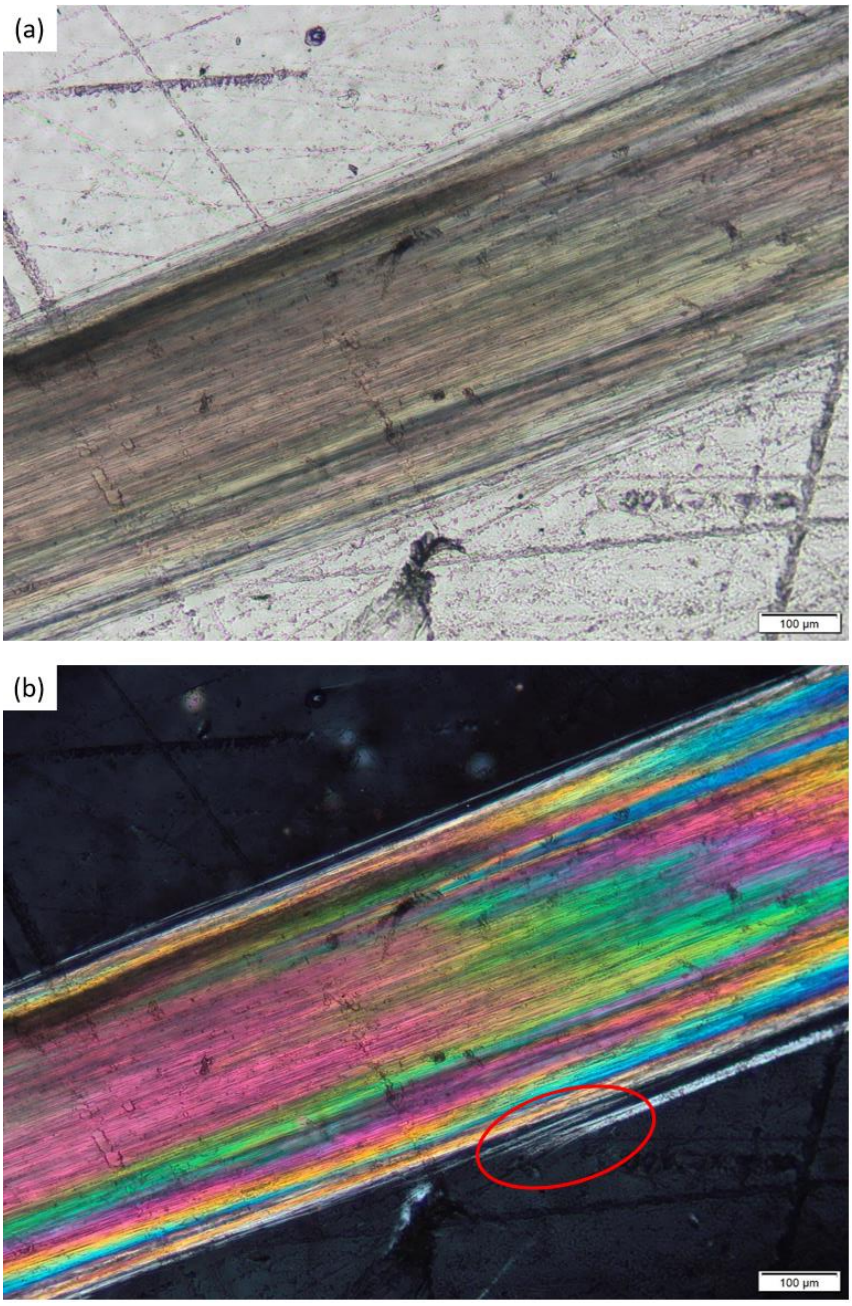


Figure 7.16: Sample 1: Photomicrographs of fibrous-acicular bundles in (a) plane polarising light and (b) cross-polarising light. The fibre bundles show heterogeneous birefringence colours and the red oval highlights splayed ends of the asbestiform component.

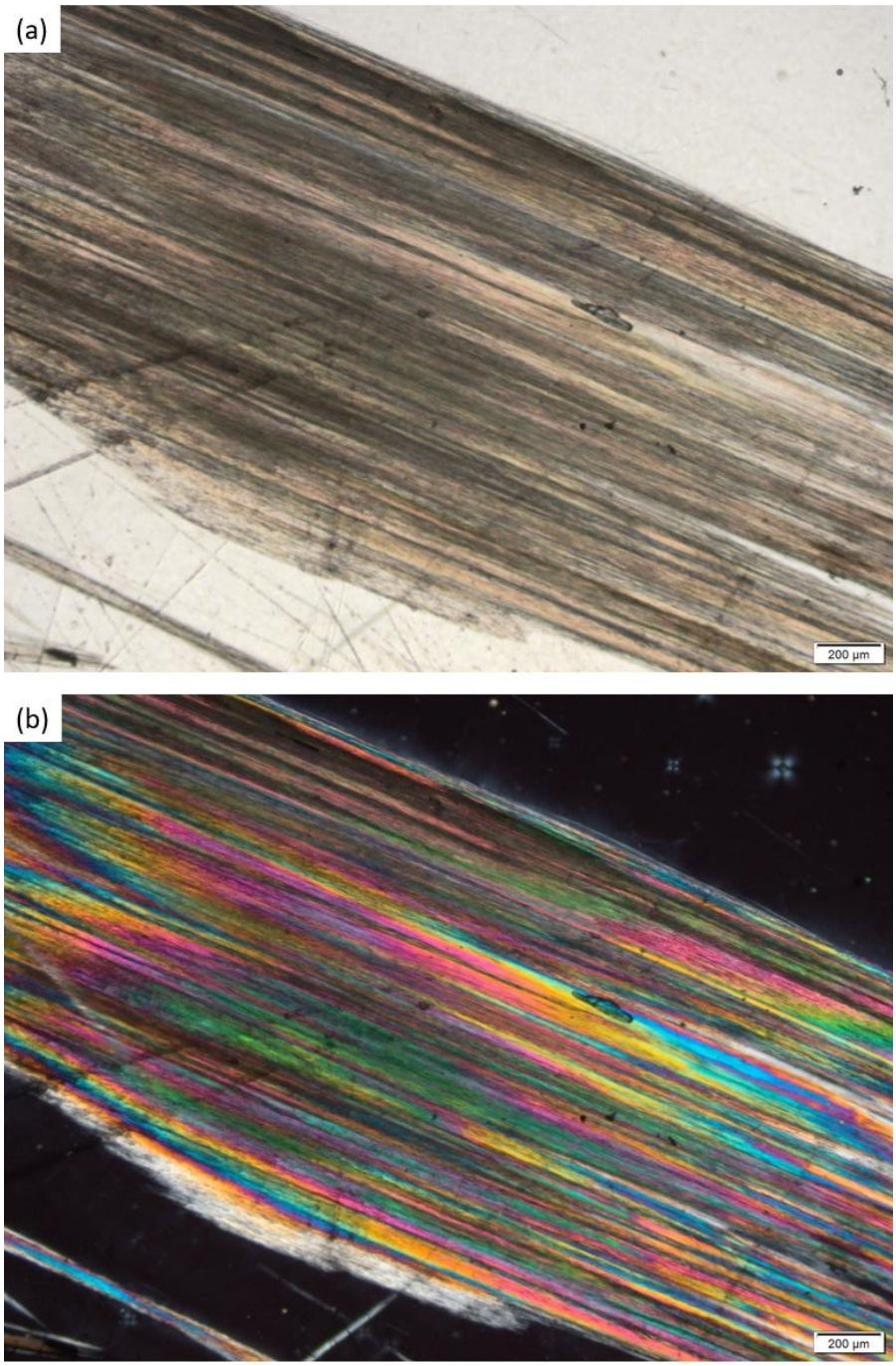


Figure 7.17: Sample 1: Photomicrographs of fibrous-acicular bundles in (a) plane polarising light and (b) cross-polarising light. Heterogeneous pleochroic and birefringence colours are observed along the length of the crystals. Notice the lenticular inclusion within the fibre bundle.

### 7.4.3. X-Ray Diffraction (XRD), X-Ray Fluorescence (XRF) and BET-$N_2$-pecific surface area

The XRD (λ (Co*K*α) = 1.78892) and Rietveld refinement data of the minerals detected in the fibrous material of sample 1 are shown in figure 7.18, and the corresponding numerical position and intensity data given in table 7.2.

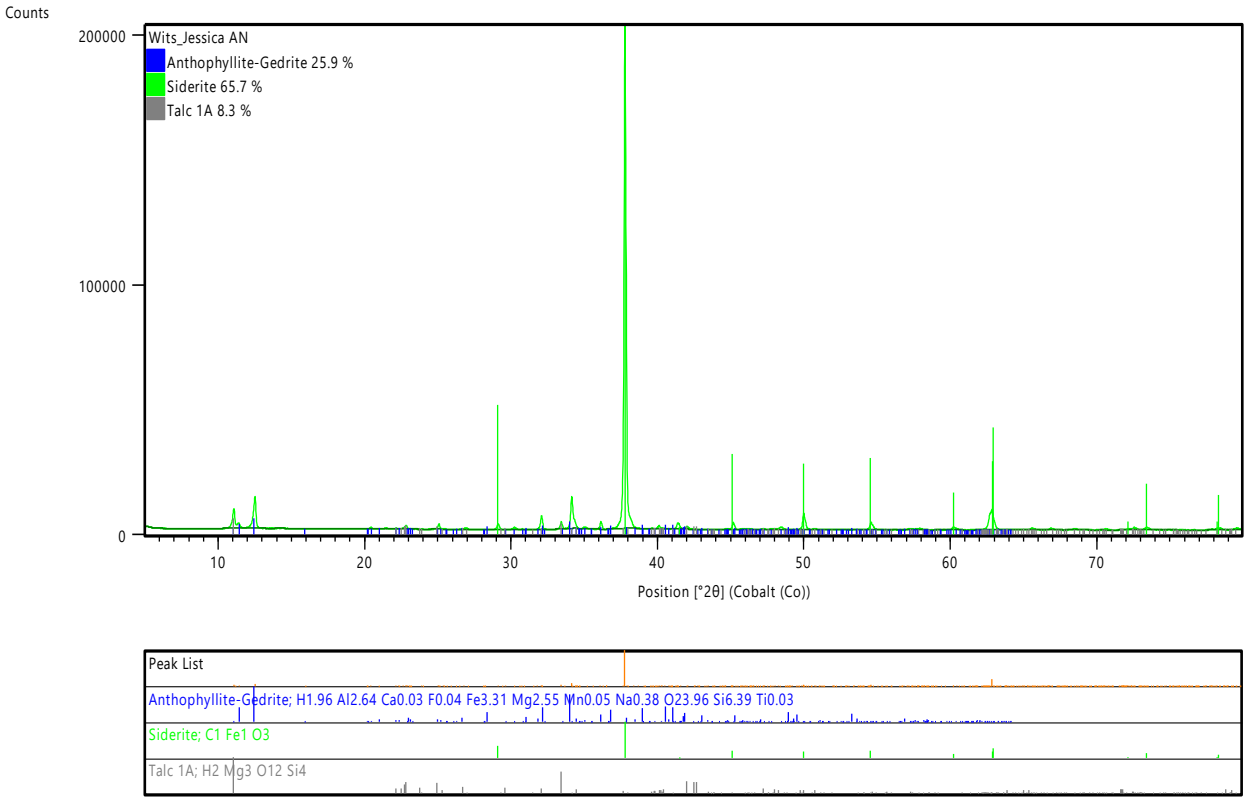


Figure 7.18: X-Ray Diffraction and Rietveld refinement diffractogram of the fibrous material subsampled from sample 1.

Table 7.2: Values of °2Θ and intensity (I) recorded for each the peaks of each phase from the X-Ray Diffraction record (λ (Co*K*α) = 1.78892)

| Peak # | Anthophyllite-Gedrite | | Siderite | | Talc | |
|---|---|---|---|---|---|---|
| | Intensity (counts) | Position [°2Θ] (Cobalt (Co)) | Intensity (counts) | Position [°2Θ] (Cobalt (Co)) | Intensity (counts) | Position [°2Θ] (Cobalt (Co)) |
| 1 | 500 | 11.5 | 5500 | 29 | **750** | 11 |
| 2 | **750** | 12.5 | **200000** | 37.6 | 250 | 22.5 |
| 3 | 250 | 15.8 | 3250 | 45 | 250 | 25 |
| 4 | 250 | 20.2 | 2750 | 50 | 500 | 33.5 |
| 5 | 250 | 20.5 | 2700 | 54.5 | 250 | 42 |
| 6 | 250 | 21 | 1750 | 60 | 250 | 42.5 |
| 7 | 300 | 28 | 3750 | 63 | | |
| 8 | 750 | 34 | 1550 | 73.5 | | |
| 9 | | | 1000 | 78 | | |

The relative intensity and *d*-spacing determined for the anthophyllite-gedrite phase (Table 7.3) is consistent with that of the known principle lattice spacings of anthophyllite (Karunaratne and Fernando, 2015).

Table 7.3: Reduction of data from X-Ray Diffractogram (λ (Co*K*α) = 1.78892). The value of $I/I_1$ (relative intensity %) is determined from equation 1, where $I_1$ is intensity of the highest peak of the phase and *d* (Å) is calculated from equation 2 assuming *n* = 1.

| Peak # | Anthophyllite-Gedrite | | Siderite | | Talc | |
|---|---|---|---|---|---|---|
| | $I/I_1$ | *d* (Å) | $I/I_1$ | *d* (Å) | $I/I_1$ | *d* (Å) |
| 1 | 66.66 | 8.9 | 2.75 | 3.6 | 100 | 9.3 |
| 2 | 100 | 8.2 | 100 | 2.8 | 33.33 | 4.6 |
| 3 | 33.33 | 6.5 | 1.63 | 2.3 | 33.33 | 4.1 |
| 4 | 33.33 | 5.1 | 1.38 | 2.1 | 66.66 | 3.1 |
| 5 | 33.33 | 5.0 | 1.35 | 1.95 | 33.33 | 2.5 |
| 6 | 33.33 | 4.9 | 0.88 | 1.8 | 33.33 | 2.5 |
| 7 | 40 | 3.7 | 1.88 | 1.7 | | |
| 8 | 100 | 3.0 | 0.78 | 1.5 | | |
| 9 | | | 0.5 | 1.4 | | |

X-ray fluorescence (XRF) was used to obtain the bulk geochemical major and trace elements of the fibrous material extracted from sample 1 (table 7.4). The BET-$N_2$-specific surface area of the fibrous material subsampled from sample 1 is 3.26 $m^2/g$.

Table 7.4: Major (oxide wt%) and trace element (ppm) concentrations of fibrous material subsamples extracted from sample 1, values of elements in the human lungs (ppm) (Vanoeteren *et al.,* 1986) and the threshold values (ppm) of metals in soils (Toth *et al.,* 2016)

| Oxides (wt%) | | Trace elements (ppm) | | Elements in human lungs (ppm) (Vanoeteren *et al.,* 1986) | Threshold values (ppm) (Toth *et al.,* 2016) |
|---|---|---|---|---|---|
| $SiO_2$ | 19.73 | Sc | 100.99 | ND | NA |
| $Al_2O_3$ | 0.08 | V | DL | 0.50 | 100 |
| $Fe_2O_3$ | 34.13 | Cr | DL | 0.50 | 100 |
| MnO | 1.43 | Co | DL | 0.10 | 20 |
| MgO | 17.70 | Ni | 43.87 | 1.00 | 50 |
| CaO | 0.88 | Cu | 7419.45 | 5.00 | NA |
| $Na_2O$ | 0.00 | Zn | 1.3 | 30 | 200 |
| $K_2O$ | 0.02 | Ga | DL | NA | NA |
| $TiO_2$ | 0.01 | Rb | 0.65 | 10 | NA |
| $P_2O_5$ | 0.12 | Sr | 1.5 | 1 | NA |
| $Cr_2O_3$ | 0.00 | Y | 7.01 | ND | NA |
| NiO | 0.01 | Zr | 0.06 | NA | NA |
| LOI | 22.02 | Nb | 0.72 | NA | NA |
| | | Mo | 1.53 | NA | NA |
| | | Ba | DL | >1.10 | NA |
| | | Pb | 8.42 | 0,50 | 60 |
| | | Th | DL | ND | NA |
| | | U | DL | 0.005 | NA |
| | | | | | |
| Total | 96.09 | | 7585.5 | | |
| | | | | | |
| DL: detection limit; NA: not available; ND: not detected | | | | | |

## 7.5. Discussion

Fibrous amphiboles, including anthophyllite, actinolite and tremolite constitute 2 % of the Guelb Moghrein deposit, where they commonly occur attached to the carbonate minerals, along fractures or as discrete fibrous aggregates (Strickland and Martyn, 2002). Samples 1 to 6 represent slip-fibres that form in localised planes of shearing resulting is the siderite being recrystallised to amphibole fibre that is orientated in the direction of shear. Slip-fibre inference is based on the long-lengths of the fibres, observed in samples 1 to 6, as well as their occurrence as slip-fibre coatings on the surfaces of metacarbonate host rocks. The nature of fibres observed in samples 2 to 6 is unlike that in sample 1, which appears to have been altered by weathering processes to some degree. Fracture-filling hydrothermal fibrous and replacement-type fibrous mineral occurrences, as shown in samples 7 to 11, represent an early hydrothermal event and late replacement stages, respectively. The fibrous mineral content of samples 7 to 11 are smaller and more irregularly distributed than that of samples 1 to 6. Additionally, much longer fibre lengths are observed in samples 1 to 6 (>6 cm), whereas those in samples 7 to 11 do not exceed ~2 cm. Asbestiform habit was established for the fibrous minerals in all 11 samples, however, unlike samples 2 to 11, sample 1 showed mixed and interlocking elongated crystal habits within its fibrous mineral content, with asbestiform being subordinate relative to acicular. The asbestiform habit of the minute fibres in samples 7 to 11 are easily identified using a hand lens; they project from the fibrous bundle or aggregate mass. The macroscale habit of fibrous minerals is often not corresponding to that observed at the microscale, aiding in the difficulty of distinguishing asbestos and non-asbestiform mineral fibres under regulatory and scientific guidelines (Punturo *et al.,* 2018; Militello *et al.,* 2019). However, simple crushing tests allow fibrous material from non-or pseudo-fibrous material to be distinguished based on flexibility and aspect ratio retention of the crushed material using a binocular microscope. The development of secondary textures of fibrous amphiboles is observed in samples 7 to 11, where the fibres appear to have originated at the siderite crystal boundaries, cleavage planes and fracture. Those formed by siderite replacement along cleavage planes are generally no longer than 4 mm in length; their preferred direction of growth is related to the nature of the siderite surface. When fibre development due to siderite replacement is advanced, mats of both parallel and/or random

amphibole fibres are found surrounding and covering the rock mineral substrate. The parallel mineral fibres displayed in samples 9 and 11 appear to produce a foliation covering the original rock minerals. Replacement during late-stage, distal hydrothermal alteration has produced mesh textures in samples 8 and 10, where tiny fibrous minerals of interpenetrating and orientated bundles are arranged along the siderite cleavage cracks. The samples studied here illustrate that within a single deposit type several modes of fibrous mineral occurrences, textures, and mineral assemblages can occur.

The fibrous Fe-Mg clino-amphibole (i.e., cummingtonite, grunerite, tremolite and actinolite) minerals formed during equilibrium reactions, and directly replace siderite (Sakellaris, 2007). Hydrothermal metamorphism caused the siderite of the metacarbonate to metamorphically react with silica-bearing hydrothermal fluids leading to the paragenetic association of quartz-free magnetite and fibrous amphibole minerals (Ellis and Hiroy, 1997).

The unusual, intermixed fibre morphologies and compositions identified during crushing and acid tests of sample 1 were confirmed by bulk mineralogical and geochemical analysis. The fibrous mineral content of sample 1 is unique in that it embodies all the attributes of asbestos occurrences in complex mineralogical environments showing a wide range of morphologies and intergrown mineral varieties. Bulk mineralogical and geochemical analysis was performed only on sample 1 as its fibrous phases appear unlike those observed in samples 2 to 11. Research pertaining to unusual but potentially harmful fibrous minerals not using the established parameters for defining asbestos in the regulatory sense, are greatly lacking due to challenges involved in identifying and characterising non-conventional fibrous minerals in the natural environment. Optically, fibre colours observed in sample 1 are heterogeneous on the micrometre scale exhibiting colour banding within and between individual fibres (figure 7.16 and 7.17). This variation in colour suggests that the fibres are chemically heterogeneous providing evidence to either multiple generations of mineral fibre growth or partial replacement of original fibres (Dutrow and Henry, 2016). The variety of pleochroic colours observed under PPL (figure 7.16a and 7.17a) suggests that transition elements are incorporated within the mineral fibre structure (Dutrow and Henry, 2016). The irregular colour zoning forms distinct colour patches along the c axis (figure 7.16b and 7.17b) are compatible with formation during dissolution and reprecipitation (Dutrow and Henry, 2016). Despite their minute size, the fibres show complex and strong colour zoning in PLM,

representing compositional heterogeneity most likely reflecting features typical of complex mineral fibre dissolution and reprecipitation reactions (Dutrow and Henry, 2000).

This compositional heterogeneity observed in PLM is confirmed in XRD, XRF and BET specific surface area measurements that are unlike those of UICC anthophyllite asbestos. The quantitative phase analysis of XRD data, using the Rietveld method, shows that fibrous material of sample 1 is composed of three intergrown mineral phases being siderite (65.7 %), anthophyllite-gedrite (25.9 %) and talc (8.3 %). This mineral and therefore chemical heterogeneity accounts for the anomalous and heterogeneous pleochroic and birefringent colours observed within and between the crystals under PLM. Although talc (8.3 %), as observed in sample 1, is known to occur as in intergrowth within anthophyllite at the submicrometric scale (Bloise *et al.,* 2016), to the best of knowledge, this is the first documented case of fibrous anthophyllite coexisting with fibrous siderite. Talc, whether in the fibrous or non-fibrous form, has been shown to result in the induction of lung tumours in rats following chronic particle inhalation (Oberdörster, 2002). There is no research and knowledge on the carcinogenic and pathogenic effects of asbestos-associated fibrous siderite mineral phases. Although these associated phases are thought to be harmless, little information on their potential toxic effects is known (Vigliaturo *et al.,* 2018), although asbestos-associated mineral phases should not be neglected when considering the combined factors encompassing the toxicity of NOA. Thus, the characterisation of natural assemblages should include all phases occurring with asbestos fibres (Vigliaturo *et al.,* 2018).

Bulk rock geochemistry of the fibrous material subsampled from sample 1 shows that $Fe_2O_3$ (34.1 wt%), $SiO_2$ (19.7 wt%) and MgO (17.7 wt%) are the main components of the fibrous content. The iron, magnesium, calcium, and manganese values are consistent with those of the siderite previously reported for this deposit by Sakellaris (2007). The significantly higher $SiO_2$ content measured here is a result of the anthophyllite-gedrite and talc mineral phases as identified by XRD. The elevated Ni and Cu values are also consistent with those given by Sakellaris (2007), however, the Sr concentration is significantly greater and may also be attributed to the additional mineral phase. Sakellaris (2007) interpreted Cu values > 1500 ppm to the occurrence of local sulphide (chalcopyrite) mineralisation in the siderite rock, however, the lack of sulphide mineral phase detection by XRD indicates that the 7420 ppm Cu measured by XRF must be incorporated within the structure of one or more of the three

mineral phases reported by XRD in this study. This is an interesting finding and should be considered for further examination.

The metal concentrations measured in the bulk, mixed mineral phase fibrous material of sample 1 are above the threshold values (ppm) in soil (Toth *et al.,* 2016) and human lungs (Vanoeteren *et al.,* 1986) (table 7.4) are copper (7491.45 ppm), nickel (43.87 ppm), lead (8.42 ppm) and strontium (1.5 ppm) and are to be considered an ecological and human health risk. The fibrous minerals isolated in sample 1 are composed of an intergrowth of three mineral phases namely siderite, anthophyllite-gedrite and talc, and therefore it is important to regard their contribution to the bulk major and trace elemental composition determined by XRF or XRD analysis. The trace element concentrations are highly variable compared to UICC standards due to the different mineral phase intergrowths and the independent geochemical mechanisms influencing their genesis (Bloise *et al.,* 2017; Bloise *et al.,* 2020). Apoptosis and cellular damage are caused by exposure of cells to Ni ions and the subsequent induction of tumours (Lee *et al.,* 2016). Lead is highly toxic and has extensively contaminated the environment and led to numerous health issues in numerous parts of the globe (Jaishankar *et al.,* 2014). Brain damage, mental retardation, kidney damage and birth defects are some of the effects caused by chronic exposure to lead (Martin and Griswold, 2009). The specific surface area of UICC anthophyllite asbestos is 4.4 $m^2/g$ (Gualtieri *et al.,* 2018), which is greater than measured here (3.26 $m^2/g$). The heterogeneous and mixed mineral phase nature of NOA in natural environmental settings is excellently depicted in sample 1.

## 7.6. Implications for *in-situ* identification and health risk assessment

The samples and their fibrous mineral content represent different lithotypes within the deposit, and their various textural associations are attributed to distinct geological processes. This study highlights that the nucleation and growth of fibrous amphiboles occurs in numerous environments via different mechanisms within a single type of deposit. The length of fibre growth also appears to be dependent upon the location or occurrence. Replacement at siderite cleavage planes and grain boundaries having short fibre lengths (maximum of 4 mm) and recrystallisation at shear planes or slip-fibre type resulted in the longest lengths (11 cm shown in sample 2 and 3). Fibres formed as a product of fracture filling show intermediate

lengths between replacement and recrystallisation mechanisms of formation. The study identifies that fibrous amphibole and/or fibrous mineral formation requires open space (i.e., cleavage cracks, fractures and/or shear planes). Mitigating the potential risks of NOA exposure from mining activities requires an extensive understanding of the geological setting and associated conditions favouring asbestos mineralisation. Knowledge pertaining to NOA geological environments allows predictive asbestos management tools to be developed that are critical for protecting public health.

## 7.7. Conclusion

In this study, metacarbonate rocks with visible fibrous minerals were collected from Guelb Moghrein mining site. The fibrous minerals correspond to fracture fill, slip-fibre, and replacement fibre modes. The asbestiform nature of the fibrous material content was easily discernible in hand sample or under hand lens. The variable compositions obtained for the fibrous mineral content of sample 1 is due to the mixed fibre content and mineral phases. NOA occurrences are highly dependent upon the geological conditions, and understanding these in a various settings may allow the development of predictive strategies necessary for *in situ* identification and hazard assessment required for health risk mitigation in the context of mining and other geologically disruptive activities.

## 7.8. References

Bargmann, C. J. and Dominy, S. C. (2008): Technical Report on the Mauritania Copper Mines: Guelb Moghrein resource estimation Project No. L00131. NI 43-101 Technical Report for Mauritania Copper Mines by Snowden Mining Industry Consultants Limited.

Bloise, A., Barca, D., Gualtieri, A.F., Pollastri, S. and Belluso, E. (2016a): Trace elements in hazardous mineral fibres. *Environmental Pollution*, **216**, 314-323.

Bloise, A., Catalano, M., Barrese, E., Gualtieri, A.F., Gandolfi, N.B., Capella, S. and Belluso, E. (2016b): TG/DSC study of the thermal behaviour of hazardous mineral fibres. *Journal of Thermal Analysis and Calorimetry*, **123**, 2225 - 2239.

Bloise, A., Punturo, R., Catalano, M., Miriello, D. and Cirrincione, R. (2016c): Naturally occurring asbestos (NOA) in rock and soil and relation with human activities: the monitoring example of selected sites in Calabria (southern Italy). *Italian Journal of Geosciences*, **135**, 268-279.

Bloise, A., Catalano, M., Critelli, T., Apollaro, C. and Miriello, D. (2017): Naturally occurring asbestos: Potential for human exposure, San Severino Lucano (Basilicata, southern Italy). *Environ. Earth Sci.*, **76** (19), 648.

Bloise, A., Ricchiuti, C., Punturo, R. and Pereira, D. (2020): Potentially toxic elements (PTEs) associated with asbestos chrysotile, tremolite and actinolite in the Calabria region (Italy). *Chem. Geol.*, **558**, 119896.

Dutrow, B.L. and Henry, D.J. (2000): Complexly zoned fibrous tourmaline, Cruzeiro mine, Minas Gerais, Brazil: A record of evolving magmatic and hydrothermal fluids. *Canadian Mineralogist*, **38**, 131–143.

Dutrow, B.L. and Henry, D.J. (2016): Fibrous tourmaline: a sensitive probe of fluid compositions and petrologic environments. *The Canadian Mineralogist*, **54**, 311-335.

Ellis, D.J. and Hiroi, Y. (1997): Secondary siderite–oxide–sulphide and carbonate–andalusite assemblages in cordierite granulites from Sri Lanka: post-granulite facies fluid evolution during uplift. *Contributions to Mineralogy and Petrology*, **127**, 315-335.

Giacomini, F., Boerio, V., Polattini, S., Tiepolo, M., Tribuzio, R. and Zanetti, A. (2010): Evaluating asbestos fibre concentration in meta-ophiolites: A case study from the Voltri Massif and Sestri–Voltaggio Zone (Liguria; NW Italy). *Environ. Earth Sci.*, **61**, 1621–1639.

Gualtieri, A.F., Pollastri, S., Gandolfi, N.B. and Gualtier, M.L. (2018): *In vitro* acellular dissolution of mineral fibres: A comparative study. *Scientific Reports,* **8** (7071), 1–12.

Gray, D., Cameron, T. and Briggs, A. (2016): Guelb Moghrein Copper Gold Mine, Inchiri, Mauritania. Guelb Moghrein Copper Gold Mine Technical Report NI 43-101, pp. 109. https://www.miningdataonline.com/reports/GuelbMoghrein_Technical_032016.pdf .

Harper, M. (2008): 10th Anniversary critical review: Naturally occurring asbestos. *Journal of Environmental Monitoring*, **10**, 1394–1408.

Jaishankar, M., Tseten, T., Anbalagan, N., Mathew, B.B. and Beeregowda, K.N. (2014): Toxicity, mechanism, and health effects of some heavy metals. *Interdiscip. Toxicol.,* **7** (2), 60–72.

Karunaratne, P.C.T. and Fernando, G.W.A.R. (2015): Characterisation and radiation impact of corrugated asbestos roofing sheets in Sri Lanka. *Journal of Geological Society of Sri Lanka*, **17**, 31-40.

Kirschbaum, M.J. and Hitzman, M.W. (2016): Guelb Moghrein: An unusual carbonate-hosted iron oxide copper-gold deposit in Mauritania, Northwest Africa. *Economic Geology,* **111**, 763–770.

Kolb, J., Sakellaris, G.A. and Meyer, F.M. (2006): Controls on hydrothermal Fe oxide–Cu–Au–Co mineralization at the Guelb Moghrein deposit, Akjoujt area, Mauritania. *Mineral. Deposita*, **41**, 68–81.

Kolb, J. and Petrov, N. (2016): The Guelb Moghrein Cu–Au deposit: Neoarchaean hydrothermal sulfide mineralization in carbonate-facies iron formation. *Ore Geology Reviews*, **78**, 573–577.

Lahondère, D., Cagnard, F., Wille, G. and Duron, J. (2019): Naturally occurring asbestos in an alpine ophiolitic complex (northern Corsica, France). *Environmental Earth Sciences*, **78** (540), 1 – 23.

Lécorché, J.P., Dallmeyer, R.D. and Villeneuve, M. (1989): Definition of tectonostratigraphic terranes in the Mauritanide, Bassaride, and Rokelide orogens, West Africa, *in* Dallmeyer, R.D. ed., Terranes in the circum-Atlantic Paleozoic orogens: Geological Society of America Special Paper, 131–144.

Lee, Y.J., Lim, S.S., Baek, B.J., An, J.M., Nam, H.S., Woo, K.M., Cho, M.K., Kim, S.H. and Lee, S.H. (2016): Nickel (II)-induced nasal epithelial toxicity and oxidative mitochondrial damage. *Environ. Toxicol. Pharmacol*., **42**, 76–84.

Lescano, L., Marfil, S., Maiza, P., Sfragulla, J. and Bonalumi, A. (2013): Amphibole in vermiculite mined in Argentina: Morphology; quantitative and chemical studies on the different phases of production and their environmental impact. *Environ. Earth. Sci.*, **70**, 1809–1821.

Lucci, F., Della Ventura, G., Conte, A., Nazzari, M. and Scarlato, P. (2018): Naturally Occurring Asbestos (NOA) in Granitoid Rocks, A Case Study from Sardinia (Italy). *Minerals,* **8** (442), 1 – 23.

Martin, S. and Griswold, W. (2009): Human health effects of heavy metals. *Environmental Science and Technology Briefs for Citizens*, **15**, 1–6.

Martyn, J.E. and Strickland, C.D. (2004): Stratigraphy, structure, and mineralization of the Akjoujt area, Mauritania. *Journal of African Earth Sciences*, **38**, 489–503.

Meeker, G., Bern, A., Brownfield, I., Lower, H., Sutley, S., Hoefen, T. and Vance, J. (2003): The Composition and Morphology of Amphiboles from the Rainy Creek Complex, Near Libby, Montana. *Am. Mineral*., **88**, 1955–1969.

Metcalf, R.V. and Buck, B.J. (2015): Genesis and health risk implication of an unusual occurrence of $NaFe_3^+$ amphibole. *Geology*, **43**, 63-66.

Militello, G.M., Bloise, A., Gaggero, L., Lanzafame, G. and Punturo, R. (2019): Multi-Analytical Approach for Asbestos Minerals and Their Non-Asbestiform Analogues: Inferences from Host Rock Textural Constraints. *Fibers*, **7** (42), 1 – 16.

Oberdörster, G. (2002): Toxicokinetics and effects of fibrous and nonfibrous particles. *Inhalation Toxicology*, **14**, 29 – 56.

Punturo, R., Cirrincione, R., Pappalardo, G., Mineo, S., Fazio, E. and Bloise, A. (2018): Preliminary laboratory characterization of serpentinite rocks from Calabria (southern Italy) employed as stone material. *J. Mediterr. Earth Sci*., **10**.

Sakellaris, G.A. (2007): Petrology, Geochemistry, Stable and Radiogenic Isotopy of the Guelb Moghrein Iron oxide-Copper-Gold-Cobalt Deposit, Mauritania (Ph.D. Thesis), RWTH Aachen University, Aachen, 444 p.

Strickland, C.D. and Martyn, J.E. (2002): The Guelb Moghrein Fe-oxide copper–gold–cobalt deposit and associated mineral occurrences, Mauritania: A geological introduction. In: Porter, T.M. (Ed.), Hydrothermal Iron Oxide Copper–Gold & Related Deposits: A Global Perspective. PGC Publishing, Adelaide, pp. 275–291.

Toth, G., Hermann, T., Da Silva, M.R. and Montanarella, L. (2016): Heavy metals in agricultural soils of the European Union with implications for food safety. *Environ. Int.*, **88**, 299–309.

Vanoeteren, C., Cornelis, R. and Verbeeck, P. (1986): Evaluation of trace elements in human lung tissue III. Correspondence analysis. *Sci. Total Environ*., **54**, 237–245.

Van Orden, D., Allison, K. and Lee, R. (2008): Differentiating amphibole asbestos from non-asbestos in a complex mineral environment. *Indoor Built Environ*., **17**, 58–68.

Vignaroli, G., Rossetti, F., Belardi, G. and Billi, A. (2011): Linking rock fabric to fibrous mineralisation: A basic tool for the asbestos hazard. *Nat. Hazards Earth Syst. Sci.*, **11**, 1267–1280.

Vignaroli, G., Ballirano, P., Belardi, G. and Rossetti, F. (2014): Asbestos fibre identification vs. evaluation of asbestos hazard in ophiolitic rock mélanges, a case study from the Ligurian Alps (Italy). *Environ. Earth Sci.*, **72**, 3679–3698.

Vigliaturo, R., Ventura, G.D., Choi, J.K., Marengo, A., Lucci, F., O'Shea, M.J., Pérez-Rodríguez, I. and Gieré, R. (2018): Mineralogical Characterization and Dissolution Experiments in Gamble's Solution of Tremolitic Amphibole from Passo di Caldenno (Sondrio, Italy). *Minerals*, **8** (557), 1–24.

Vignaroli, G., Rossetti, F., Billi, A., Theye, T. and Belardi, G. (2020): Structurally controlled growth of fibrous amphibole in tectonised metagabbro: constraints on asbestos concentration in non-serpentinised rocks. *Journal of the Geological Society*, **177** (1), 103–119.

Wagner, J. (2015): Analysis of serpentine polymorphs in investigations of natural occurrences of asbestos. *Environ. Sci.: Processes Impacts*, **17**, 985–996.

# Chapter 8 – Toxic element enrichment and potential ecological risks from asbestos-bearing mine wastes


## Abstract

Historical asbestos mining operations have left a legacy of widespread environmental contamination globally. However, in comparison to North America and Europe, the number of modern environmental asbestos exposure sources in rural provinces of South Africa is considerable. In developing countries, such as those in Africa, the existence of empirical data characterising the chemical composition and ecological and health risks of solid mine wastes, such as asbestos, is extremely limited. The geological properties and carcinogenic risks of asbestos fibres are long known and well researched. However, the potential ecological impacts of exposed asbestos mine wastes and asbestos-bearing geological deposits have largely been ignored. This chapter provides a preliminary assessment of extent of heavy metal pollution hosted in asbestos-mine wastes using different pollution indices in exposed geological mining materials in the context of source contamination. The quantitative contamination indices (enrichment factor, geo-accumulation index ($I_{geo}$), contamination factor ($C_f$), degree of contamination ($C_{degree}$) and pollution load index (PLI)), ecological risks and hazard quotient (HQ) where determined for chrysotile, amosite, crocidolite and anthophyllite mine wastes examined previously in chapter 2 and 7. The results indicate that the asbestos mine wastes contain high heavy metal concentrations, greater than their respective background levels, with significant implications for ecological and human health risks.


## 8.1. Introduction

One of the greatest life-threatening concerns for the mining milieu is that of mine dumps, wastes, and tailings, as they remain a persistent environmental issue causing catastrophic ecosystem pollution (Agboola *et al.,* 2020). The soil, air, aquatic and biotic environments, and human health are severely affected by the end-results of mine wastes, which in turn affects the economy (Agboola, 2019). Heavy metal pollution of air, water and soil is currently one of the most challenging environmental concerns that has gained

exponential interest (Babula *et al.,* 2008). This is attributed to the increasing toxicity of the environment and negative impacts on ecosystems and human health (Chaturvedi *et al.,* 2018; Chen *et al.,* 2018). Exposure of humans to heavy metals occurs through the inhalation of heavy metal-enriched airborne particles or via the consumption of contaminated food or water (Yi *et al.,* 2017).

The growing public concern regarding the impact of heavy metals on human health and the environment has led to increasing research involving the assessment of heavy metals contamination and health risks in soils (Rao *et al.,* 2010; Ali *et al.,* 2013; Bansah and Addo, 2016; Ibrahim, 2016; Akoto and Anning, 2021). These studies quantify heavy metal concentrations in the certain environment (typically soil and water), use pollution indices to determine the extent of heavy metal pollution in soils and estimate both the ecological and human health risks. Although such studies show that there is pollution of the investigated environment, they do not consider the source as the primary concern and how to prevent further contamination because of release from the source, which in most cases are the solid geological materials. To emphasise this, typically, heavy metals contamination studies focus on anthropogenic input sources, such as sewage sludges, fertilizers, atmospheric deposition from industrial sites, etc. However, contamination via the release of the geological parent materials can pollute soils with concentrations that are 10 – 1000 greater (He *et al.,* 2005a, He *et al.,* 2005b).

The rationale behind this research idea follows previou pioneering studies (Bloise *et al.,* 2016; Gualtieria *et al.,* 2019 and Bloise *et al.,* 2020), which demonstrate the severe degree of heavy metals concentrations in asbestos minerals and their significance with respect to the environment. The objective of the present study is to determine the metal enrichment and potential ecological and human health risks of the heavy metal contents in four different asbestos mine wastes already examined in chapter 2 and 7 to propose probable detrimental environmental outcomes arising from neglected and improperly handled solid mine wastes.

## 8.2. Methodology

### 8.2.1. Chemical analysis of asbestos

The chemical analysis obtained for chrysotile, crocidolite, amosite (chapter 2) and anthophyllite (chapter 8) is used for determining quantitative contamination indices of these solid mine wastes.

### 8.2.2. Pollution Indices for assessing metal contamination in asbestos rock samples

The degree of contamination may be comprehensively evaluated with the use of pollution indices (Gong *et al.,* 2008; Mazurek *et al.,* 2017). Due to the comprehensive nature of pollution indices, both the degree of degradation and the environmental risks may be estimated (Adamu and Nganje, 2010). There are two groups of indices, namely: Individual and complex (Kowalska *et al.,* 2018). A geochemical background (GB) is required for pollution indices calculations from which abnormal and/or enriched heavy metal concentrations may be distinguished (Reimann and Garret, 2005; Kowalska *et al.,* 2018). The background levels chosen for this study were crustal abundances, WHO permissible limits in soils and UICC asbestos standards (compositions).

*Enrichment factor (EF)*

The enrichment factor was used to assess the degree of heavy metal pollutant enrichment. Using iron as a reference element (Taylor and McLennon, 1995) the enrichment factor was calculated by equation 1 (Salomons and Forstner, 1984):

$$EF = \frac{Mx * FeB}{Mb * Fex} \quad \text{(1)},$$

where Mx is the concentration of the heavy metal (ppm), FeB is the average continental crust abundance of iron (ppm), Mb is the average continental crust abundance of the heavy metal (ppm) and Fex is the concentration of iron in the sample (ppm). Using the approach (Sutherland, 2000), the enrichment factors could be evaluated (table 8.1).

Table 8.1: Classification of degree of enrichment based on the enrichment factor values

| Factor | Degree of enrichment |
|---|---|
| | |

| | |
|---|---|
| < 2 | Minimal enrichment |
| 2 – 5 | Moderate enrichment |
| 5 - 20 | Significant enrichment |
| 20 - 40 | Very high enrichment |
| > 40 | Extremely high enrichment |
| | |
| Sutherland (2000) | |

*Geo-accumulation Index ($I_{geo}$)*

The $I_{geo}$ allows the assessment of heavy metal contamination in soils and minerals by referencing the measured concentrations to a specified geochemical background (Muller, 1969). The Muller's expression was used to determine the geo-accumulation index values:

Geo-accumulation Index = $\log_2(\frac{Cn}{1.5\ x\ GB})$ _____ (2),

where Cn is the concentration of the individual heavy metal, GB is the geochemical background value and 1.5 is a constant that allows the variability of heavy metals due to natural processes to be analysed by providing a lithogenic correction (Iwegbue *et al.,* 2018). The values of $I_{geo}$ for the asbestos minerals allow the different minerals to be divided into classes based on quality (Muller 1969; Ji *et al.,* 2008; Nowrouzi and Pourhabbaz 2014).

Table 8.2: Division of $I_{geo}$ values into quality classes

| Value | Interpretation |
|---|---|
| | |
| $I_{geo} \leq 0$ | Uncontaminated |
| $0 < I_{geo} < 1$ | Uncontaminated to moderately contaminated |
| $1 < I_{geo} < 2$ | Moderately contaminated |
| $2 < I_{geo} < 3$ | Moderately to heavily contaminated |
| $3 < I_{geo} < 4$ | Heavily contaminated |
| $4 < I_{geo} < 5$ | Heavily to extremely contaminated |
| $5 < I_{geo}$ | Extremely contaminated |

*Contamination factor ($C_f$)*

Contamination factors are used to assess the degree of heavy metal contamination in the hosting rocks (i.e. the asbestos rock samples). The contamination factors were calculated using the equation given by Forstner and Wittmann (1983):

$C_f = C_s/C_b$ _____ (3),

where $C_s$ is the concentration of the toxic metal in the asbestos and $C_b$ is the concentration of toxic metal in the background sample (Iwegbue *et al.,* 2018).

Environmental geochemical studies are significantly influenced by the chosen background values (Islam *et al.,* 2015). The average crustal abundance values are primarily chosen as reference baselines in contamination studies (Singh *et al.,* 2005; Sekabira *et al.,* 2010; Kowalska *et al.,* 2018). The crustal abundance, WHO permissible limits and UICC asbestos standards, were all chosen to evaluate the degree of heavy metal contamination in the four samples (table 8.3).

Table 8.3: Crustal abundance, WHO permissible limits and UICC asbestos standards

| Metal | Crustal abundance (ppm) [a] | Permissible limits in soils (ppm) (WHO) [b] | UICC standard asbestos samples (ppm) [c] | | | |
|---|---|---|---|---|---|---|
| | | | Chrysotile | Amosite | Crocidolite | Anthophyllite |
| | | | | | | |
| Al | 82300 | - | 15682 | 0 | 0 | 26074 |
| Fe | 56300 | 50000 | 35870 | 476065 | 512564 | 68595 |
| Mn | 950 | 2000 | 903 | 23242 | 1549 | 1936 |
| Mg | 23300 | - | 663310 | 112099 | 45105 | 479739 |
| Cr | 102 | 100 | 2600 | < 15 | < 15 | 1330 |
| Co | 25 | 50 | 103 | 25 | 20 | 70 |
| Ni | 84 | 50 | 1850 | 33 | 18 | 1125 |
| Cu | 60 | 100 | 7 | 16 | 8 | 30 |
| Zn | 70 | 300 | < 3 | 16 | 14 | 234 |
| Zr | 165 | - | 15 | 20 | 10 | 15 |
| Ba | 425 | 9 | < 20 | < 20 | < 20 | < 20 |
| Pb | 14 | 100 | 38 | 11 | 6 | < 5 |
| | | | | | | |
| [a] David R. Lide, ed., 'Atomic Masses and Abundances', 2005; [b] WHO, 1996; [c] Bowes and Farrow, 1997 | | | | | | |

To evaluate whether the three background values chosen are not unreasonably different, analysis of variance (ANOVA) was performed to determine if they are statistically significant. The ANOVA results indicate that the mean values of all the background values are statistically equal with $Pr(F_{stat} < F_{critical} \mid H_o) = \alpha$ ($\alpha = 0.05$). The contamination factor can be classified based on the level of contamination given in table 8.4 (Kusin *et al.,* 2018).

Table 8.4: Classification of contamination factor into degree of contamination

| Range of contamination factor (CF) | Risk level of contamination factor |
|---|---|
| | |
| CF < 1 | Low degree |
| 1 ≤ CF < 3 | Moderate degree |
| 3 ≤ CF < 6 | Considerable degree |
| CF > 6 | Very high degree |
| | |
| Pandey *et al. (*2019) | |

*Degree of contamination ($C_{degree}$)*

The degree of contamination is the sum of the contamination factors and is calculated according to equation:

$C_{degree} = \sum C_f = \sum C_s/C_b$ _____ (4)

Table 8.5: Classification of degrees of contamination based on $C_d$ values

| Factor | Interpretation |
|---|---|
| | |
| $C_d < 8$ | Low degree of contamination |
| $8 \leq C_d \leq 16$ | Moderate degree of contamination |
| $16 \leq C_d \leq 32$ | Considerable degree of contamination |
| $32 \leq C_d$ | Very high degree of contamination |

*Modified degree of contamination ($mC_d$)*

The modified degree of contamination is the sum of the contamination factors divided by the number of heavy metals measured. The modified degree of contamination is given according to equation:

$mC_d = \frac{\sum Cf}{n}$ _____ (5)

Table 8.6: Interpretation of contamination using modified degree of contamination values

| Factor | Interpretation |
|---|---|

| | |
|---|---|
| $mC_d \leq 1.5$ | Very low contamination |
| $1.5 \leq mC_d \leq 2$ | Low contamination |
| $2 \leq mC_d \leq 4$ | Moderate contamination |
| $4 \leq mC_d \leq 8$ | High contamination |
| $8 \leq mC_d \leq 16$ | Very high contamination |
| $16 \leq mC_d \leq 32$ | Extremely high contamination |
| $32 \leq mC_d$ | Ultra high contamination |

*Pollution load index (PLI)*

The pollution load index was calculated using the equation (Tomllinson *et al.,* 1980; Angulo, 1996):

$PLI = (CF1 \times CF2 \times CF3 \ldots CFn)^{1/n}$ _____ (6),

with CF being the contamination factor of each metal in the asbestos fibres and n the number of toxic metals assessed.

Table 8.7: Interpretation of pollution load index based on PLI values

| Factor | Interpretation |
|---|---|
| | |
| PLI ≥ 1 | Indicates the existence of pollution (undesirable condition) |
| PLI = 1 | Indicates existence of pollution by at the background level, a more detailed study is required |
| PLI < 1 | Indicates that immediate mitigation measures may not be necessary |

### 8.2.3. Ecological risk assessment

To evaluate the likelihood of events of any unfavourable ecological effects through subjection to one or many of the heavy metal contaminants contained in the asbestos samples, the Potential Ecological Risk Index (PERI) was employed (Hakanson, 1980). The linkage of toxicity level, heavy metal concentration and ecological sensitivity of heavy metals are comprehensively considered in this method (Singh *et al*., 2010; Douay *et al*., 2013). Contamination degree, toxic-response factor and potential ecological risk factor are the three basic modules make up the Potential Ecological Risk Index (Hakanson, 1980).

*Individual potential ecological risk factor*

The potential risk index for individual heavy metal contaminants can be calculated using equation 7 (Guo *et al.,* 2010):

$E_r^i = T_r^i \times C_f^j$ _____ (7),

where $T_r^i$ is the toxic response factor for the individual heavy metal pollutants and $C_f^j$ is the contamination factor for the given heavy metal.

Table 8.8: Classification of ecological risk level using potential ecological risk index ($E_r^i$) values

| Scope of potential ecological risk index ($E_r^i$) | Ecological risk level of single factor pollution |
|---|---|
| | |
| $E_r^i < 40$ | Low |
| $40 \leq E_r^i < 80$ | Moderate |
| $80 \leq E_r^i < 160$ | High |
| $160 \leq E_r^i < 320$ | Higher |
| $320 \leq E_r^i$ | Serious |
| | |
| Guo *et al. (*2010) | |

*Ecological risk index*

The total risk index of potential ecological risks was calculated using equation 8 (Guo *et al.,* 2010):

$RI = \sum_{i=1}^{n} E^i_r$ _____ (8),

where RI is the sum of all the potential risk factors for all the heavy metals measured in each of the samples.

Table 8.9: Ecological risk level interpretation of risk index (RI) values

| Scope of potential toxicity index (RI) | Ecological risk level |
|---|---|
| | |
| RI < 150 | Low-grade |

| | |
|---|---|
| 150 ≤ RI < 300 | Moderate |
| 300 ≤ RI < 600 | Severe |
| 600 > RI | Serious |
| | |
| Guo *et al. (*2010) | |

### 8.2.4. Health risk assessment

As the source rock was studied here a full human health risk assessment could not be done as in dust, water, and soil samples. However, the human risk associated with the heavy metals could be assessed using the hazard quotient (HQ) (Kim *et al*., 1998; Nishida *et al*., 1982). The HQ was calculated as the ratio of the element's concentration ($C_c$) and the threshold values in the lungs ($C_p$) (Vanoeteren *et al.,* 1986; Toth *et al.,* 2016).

$$HQ = \frac{Cc}{Cp} \quad \text{(9)}$$

Table 8.10: Threshold values for heavy metal (ppm) in the lungs

| Metal | Threshold values in lungs (ppm) [a] |
|---|---|
| | |
| Al | 82300 |
| Fe | 56300 |
| Mn | 950 |
| Mg | 23300 |
| Cr | 102 |
| Co | 25 |
| Ni | 84 |
| Cu | 60 |
| Zn | 70 |
| Zr | 165 |
| Ba | 425 |
| Pb | 14 |
| | |
| [a] Vanoeteren *et al. (*1986); Toth *et al. (*2016) | |
| | |
| HQ < 1 | No adverse effect on human health is expected due to the exposure to elemental concentrations in the asbestos. |
| HQ > 1 | This indicates that adverse human health effects from the contamination exposure are possible. The estimation of individual elements using the HQ could potentially underestimate the level of hazards in an area, relative to synergistic and simultaneous exposures to different elements. |

### 8.2.5. Statistical analysis

Statistical analysis of the datasets was conducted using Microsoft Office Excel 2016. The concentrations of heavy metals, their enrichment factors, geo-accumulation indices, contamination factors and toxic responses determined for each sample was compared using Pearson's correlation matrix analysis. The pollution load index, contamination degree and potential ecological risk index values for were compared among the four different asbestos analysis of variance (ANOVA), followed by theTurkey (HSD) test where significant differences existed.

## 8.3. Results

### 8.3.1. Heavy metal concentrations

The concentrations (ppm) of 12 elements (Al, Fe, Mn, Mg, Cr, Co, Ni, Cu, Zn, Zr, Ba and Pb) in chrysotile, amosite, crocidolite and anthophyllite mine waste are listed in table 8.11.

Table 8.11: The chemical composition of major heavy metals (ppm) of concern in the asbestos mine wastes studied.

| Metal (ppm) | Chrysotile* | Amosite* | Crocidolite* | Anthophyllite* |
|---|---|---|---|---|
| | | | | |
| Al | 11147 | 6802 | 1322 | 1511.57 |
| Fe | 13988 | 289340 | 267940 | 238705 |
| Mn | 230 | 4987 | 465 | 11075 |
| Mg | 246200 | 35220 | 13449 | 106748 |
| Cr | 83 | 4 | D.L. | D.L. |
| Co | 52 | D.L. | D.L. | D.L. |
| Ni | 1518 | 51 | 11 | 43 |
| Cu | 21 | 36 | 35 | 7419 |
| Zn | 16 | 41 | 12 | 1 |
| Zr | 0.5 | 3 | 0.4 | 0.06 |
| Ba | D.L. | 28 | 1 | D.L. |
| Pb | 6.6 | 5 | 5 | 8 |
| | | | | |
| * Average value (n = 2) | | | | |

The means of three background values selected (crustal abundances, WHO permissible limits in soils and UICC asbestos standards) were shown to be statistically significant at the 0.05 level, the three sets of values were averaged to make direct

comparisons between the mean (n = 2) concentrations measured. The mean concentrations of Mg and Ni (chrysotile), Fe (amosite and crocidolite) and Fe, Mn, and Cu (anthophyllite) in the asbestos mine wastes were significantly higher ($p < 0.05$) than their respective background values.

The results show that the average concentrations of heavy metals in each asbestos sample vary significantly and decrease in the order of: Chrysotile: Mg > Fe > Al > Ni > Mn > Cr > Co > Cu > Zn > Pb > Zr; amosite: Fe > Mg > Al > Mn > Ni > Zn > Cu > Ba > Pb > Cr, crocidolite: Fe > Mg > Al > Mn > Cu > Zn > Ni > Pb > Ba > Zr and anthophyllite: Fe > Mg > Mn > Cu >Al > Ni > Pb > Zn > Zr.

A general comparison between concentrations of metals in the asbestos mine waste show that certain heavy metals in each sample are significantly higher than their respective background levels. The concentrations of Mg, Co and Ni are similar to crustal abundances; Al, Mg, Co, Ni and Zr are similar to permissible limits in soils, and Cu and Zn are similar to IUCC asbestos samples in chrysotile are greater than those background levels. The concentrations of Fe, Mn and Mg are similar to crustal abundances; Al, Fe, Mn, Mg, Ni and Zr are similar to permissible limits in soils, and Al, Mn, Mg, Ni, Cu, Zn and Ba are similar to IUCC asbestos samples in amosite and are greater than background levels. The concentrations of Fe are similar to crustal abundances; Al, Fe and Mg are similar to permissible limits in soils, and Al, Fe, Mg and Cu are similar to IUCC asbestos samples in crocidolite and greater than background levels. The concentrations of Fe, Mn, Mg and Cu are similar to crustal abundances; Al, Fe, Mn, Mg and Cu are similar to permissible limits in soils and Fe, Mn, Cu and Pb are simiar to IUCC asbestos samples in anthophyllite and greater than background levels.

### 8.3.2. Contamination level of heavy metals in different asbestos mine wastes

Pollution indices were used to make geochemical assessments on the degree of heavy metal enrichment in each of the samples. The enrichment factor values of heavy metals in the four asbestos samples are given in table 8.12.

Table 8.12: Enrichment factor values of the studied asbestos mine wastes

| Metal | Chrysotile | Amosite | Crocidolite | Anthophyllite |
|---|---|---|---|---|
| | | | | |
| Al | 0.55 | 0.02 | 0.0034 | 0.004 |
| Fe | 1 | 1 | 1 | 1 |
| Mn | 0.97 | 1.02 | 0.103 | 2.75 |
| Mg | 42.53 | 0.29 | 0.12 | 1.08 |
| Cr | 3.29 | 0.009 | - | - |
| Co | 8.46 | - | - | - |
| Ni | 72.76 | 0.2 | 0.03 | 0.12 |
| Cu | 1.48 | 0.12 | 0.12 | 29.17 |
| Zn | 0.93 | 0.12 | 0.04 | 0.004 |
| Zr | 0.012 | 0.004 | 0.0005 | 0.00009 |
| Ba | - | 0.01 | 0.0008 | - |
| Pb | 1.9 | 0.07 | 0.08 | 0.14 |
| | | | | |
| Total | 133.9 | 2.86 | 1.5 | 34.27 |

Chrysotile recorded extreme magnesium (42.53) and nickel (72.76) enrichment, significantly high cobalt (8.46) enrichment and moderate chromium (3.29) enrichment. All the heavy metals studied in both amosite and crocidolite showed minimal enrichment factors. Copper (29.17) was extremely enriched in anthophyllite accompanied by moderate manganese (2.75) enrichment. The elevated enrichment factors for the four asbestos samples indicate that these mine wastes, under the appropriate conditions, are capable of appreciably enhancing the surrounding environmental compartments with many pollutants.

The geo-accumulation indices of the metals in the samples are given in table 8.13.

Table 8.13: Geo-accumulation indices of the metals in the studied asbestos mine wastes

| Metal | Chrysotile | Amosite | Crocidolite | Anthophyllite |
|---|---|---|---|---|
| | | | | |
| Al | -3.47 | -4.18 | -6.54 | 6.35 |
| Fe | -2.59 | 1.78 | 1.67 | 1.5 |
| Mn | -2.63 | 1.81 | -1.62 | 2.96 |
| Mg | 2.816 | 0.011 | -1.38 | 1.61 |
| Cr | -0.88 | -5.05 | - | - |
| Co | 0.49 | - | - | - |
| Ni | 3.59 | -1.298 | -3.41 | -1.52 |
| Cu | -2.03 | -1.29 | -1.36 | 6.37 |
| Zn | -2.7 | -1.34 | -3.05 | -6.34 |
| Zr | -8.98 | -6.06 | -9.35 | -12.01 |
| Ba | - | -4.5 | -8.56 | - |
| Pb | -1.67 | -1.98 | -2.05 | -1.32 |

The geo-accumulation index of magnesium (2.82) and nickel (3.59) in chrysotile indicate that these metals are heavily accumulated. Amosite shows moderate accumulation of iron (1.78) and manganese (1.81), and crocidolite moderate accumulation of iron (1.67). Extremely heavy accumulation of aluminium (6.35) and copper (6.37), and moderate to heavy accumulation of iron (1.5), magnesium (1.61) and manganese (2.96) are shown in anthophyllite.

Table 8.14: Contamination factors of the studied asbestos mine wastes

| Metal | Contamination factors (CF) | | | |
|---|---|---|---|---|
| | Chrysotile | Amosite | Crocidolite | Anthophyllite |
| | | | | |
| | Crustal abundance | | | |
| | | | | |
| Al | 0.14 | 0.083 | 0.017 | 0.018 |
| Fe | 0.25 | 5.14 | 4.76 | 4.24 |
| Mn | 0.24 | 5.25 | 0.49 | 11.66 |
| Mg | 10.57 | 1.512 | 0.58 | 4.58 |
| Cr | 0.82 | 0.05 | - | - |
| Co | 2.102 | - | - | - |
| Ni | 18.08 | 0.61 | 0.14 | 0.52 |
| Cu | 0.37 | 0.613 | 0.58 | 123.66 |
| Zn | 0.23 | 0.59 | 0.18 | 0.019 |
| Zr | 0.003 | 0.02 | 0.002 | 0.0004 |
| Ba | - | 0.07 | 0.004 | - |
| Pb | 0.47 | 0.38 | 0.36 | 0.6 |
| | | | | |
| | Permissible limits | | | |
| | | | | |
| Al | - | - | - | - |
| Fe | 0.28 | 5.79 | 5.36 | 4.77 |
| Mn | 0.115 | 2.49 | 0.23 | 5.538 |
| Mg | - | - | - | - |
| Cr | 0.834 | 0.05 | - | - |
| Co | 1.05 | - | - | - |
| Ni | 30.37 | 1.025 | 0.24 | 0.88 |
| Cu | 0.22 | 0.368 | 0.35 | 74.19 |
| Zn | 0.05 | 0.139 | 0.04 | 0.004 |
| Zr | - | - | - | - |
| Ba | - | 3.13 | 0.19 | - |
| Pb | 0.07 | 0.05 | 0.05 | 0.084 |
| | | | | |
| | IUCC asbestos standards | | | |
| | | | | |
| Al | 0.711 | 6802.1 | 1322.6 | 0.058 |
| Fe | 0.39 | 0.608 | 0.523 | 3.48 |
| Mn | 0.25 | 0.215 | 0.3 | 5.718 |
| Mg | 0.37 | 0.314 | 0.298 | 0.223 |
| Cr | 0.03 | 0.307 | - | - |
| Co | 0.51 | - | - | - |

| | | | | |
|---|---|---|---|---|
| Ni | 0.821 | 1.55 | 0.66 | 0.039 |
| Cu | 3.14 | 2.298 | 4.375 | 247.315 |
| Zn | 5.397 | 2.6 | 0.9 | 0.0056 |
| Zr | 0.03 | 0.185 | 0.038 | 0.004 |
| Ba | - | 1.4085 | 0.085 | - |
| Pb | 0.17 | 0.48 | 0.84 | 1.68 |

Chrysotile shows a very high degree of Ni (30.37) and Mg (10.57) contamination; a considerable degree of Zn (5.397) and Cu (3.14) contamination, and a low degree of Co (2.102) contamination. Amosite shows a very high degree of Al (6802) contamination; considerable degree of Fe (5.79), Mn (5.25) and Ba (3.13) contamination, and a low degree of Zn (2.6), Ni (1.55), Mg (1.51) and Cu (2.29) contamination. Crocidolite showed a very high degree of Al (1322) contamination and a considerable degree of Fe (5.36) and Cu (4.38) contamination. Anthophyllite demonstrated a very high degree of Cu (247.3) and Mn (11.66) contamination; a considerable degree of Fe (4.77) contamination and a low degree of Pb (1.68) contamination.

Table 8.15: Values for degree of contamination in samples using respective background values.

Table 8.15: Degree of contamination values of the studied asbestos mine wastes

| Background value used in contamination factor | Contamination degree ($C_{degree}$) | | | |
|---|---|---|---|---|
| | Chrysotile | Amosite | Crocidolite | Anthophyllite |
| | | | | |
| CF – C.A. | 33.28 | 14.32 | 7.11 | 145.3 |
| CF – P.L | 32.99 | 13.04 | 6.46 | 85.47 |
| CF – IUCC | 11.82 | 6812.07 | 1330.62 | 258.52 |
| | | | | |
| CF – C.A.: Contamination factor using crustal abundance as background value<br>CF – P.L: Contamination factor using permissible limits in soil as background value<br>CF – IUCC: Contamination factor using IUCC standard reference asbestos samples as background value | | | | |

Chrysotile shows a very high degree of contamination when both crustal abundance and WHO permissible limits are used as geochemical background values and a moderate degree of contamination when referenced against the IUCC chrysotile standard. Conversely, amosite shows a moderate degree of contamination using crustal abundance and WHO permissible limits as reference values, and very high degree of contamination when IUCC amosite standards are set as geochemical backgrounds. Crocidolite exhibits a low degree of

contamination using crustal abundance and WHO permissible limits, and very high degree of contamination using UICC crocidolite standard. A very high degree of contamination was reported for all three geochemical backgrounds in the anthophyllite sample.

Table 8.16: Modified degree of contamination values of the studied asbestos mine wastes for each background value

| | Chrysotile | Amosite | Crocidolite | Anthophyllite |
|---|---|---|---|---|
| Crustal abundances | | | | |
| $mC_d$ | 3.025 | 1.3 | 0.7 | 16.14 |
| | | | | |
| Permissible limits | | | | |
| $mC_d$ | 4.12 | 1.63 | 0.92 | 14.24 |
| | | | | |
| IUCC asbestos standards | | | | |
| $mC_d$ | 1.07 | 619.28 | 133.06 | 28.7 |

The modified degree of contamination for chrysotile shows moderate, high and very low contamination for crustal abundance, permissible limits in soil and IUCC asbestos standard background levels, respectively. The modified degree of contamination for amosite and crocidolite shows very low, low and ultra-high contamination for crustal abundance, permissible limits in soil and IUCC asbestos standard background levels, respectively. The modified degree of contamination for anthophyllite shows extremely high, very high and extremely high contamination for crustal abundance, permissible limits in soil and IUCC asbestos standard background levels, respectively.

Table 8.17: Pollution load index values of the studied asbestos mine wastes

| Reference values used | Chrysotile | Amosite | Crocidolite | Anthophyllite |
|---|---|---|---|---|
| | | | | |
| Crustal abundances | 0.48 | 0.37 | 0.13 | 0.47 |
| Permissible limits in soil | 0.4 | 0.53 | 0.24 | 0.91 |
| UICC standards for asbestos | 0.39 | 1.52 | 0.92 | 0.36 |

The pollution load index values of all four asbestos samples using crustal abundance and WHO permissible limits as backgrounds all report as low, indicating immediate mitigation measures are not a necessity. Chrysotile, crocidolite and anthophyllite all report the same as above using UICC standards as reference values. However, amosite is categorised for the existence of pollution.

### 8.3.3. Ecological risk assessment

The individual potential ecological risk coefficients ($E_r$) and comprehensive potential ecological risk index (RI) values were calculated according to Hakanson (1980) to evaluate the potential ecological risk index of heavy metals in each type of asbestos waste.

Table 8.18: Individual potential ecological risk factors of the studied asbestos mine wastes

| Metal | Toxic response factor | CF – C.A | CF - PL | CF – IUCC |
|---|---|---|---|---|
| | Chrysotile | | | |
| Mn | 1 | 0.2 | 0.1 | 0.3 |
| Cr | 2 | 1.6 | 1.7 | 0.06 |
| Co | 5 | 10.5 | 5.3 | 2.6 |
| Ni | 5 | 90.4 | 151.8 | 4.1 |
| Cu | 5 | 1.9 | 1.1 | 15.7 |
| Zn | 1 | 0.2 | 0.05 | 5.4 |
| Pb | 5 | 2.4 | 0.4 | 0.9 |
| | | | | |
| | Amosite | | | |
| Mn | 1 | 5.3 | 5.8 | 0.2 |
| Cr | 2 | 0.1 | 0.1 | 0.6 |
| Co | 5 | - | - | - |
| Ni | 5 | 3.05 | 5.1 | 7.8 |
| Cu | 5 | 3.07 | 1.8 | 11.5 |
| Zn | 1 | 0.6 | 0.1 | 2.6 |
| Pb | 5 | 1.9 | 0.3 | 2.4 |
| | | | | |
| | Crocidolite | | | |
| Mn | 1 | 0.5 | 5.4 | 0.3 |
| Cr | 2 | - | - | - |
| Co | 5 | - | - | - |
| Ni | 5 | 0.7 | 1.2 | 3.3 |
| Cu | 5 | 2.9 | 1.8 | 21.9 |
| Zn | 1 | 0.2 | 0.04 | 0.9 |
| Pb | 5 | 1.8 | 0.3 | 4.2 |
| | | | | |
| | Anthophyllite | | | |
| Mn | 1 | 11.7 | 4.8 | 5.7 |
| Cr | 2 | - | - | - |
| Co | 5 | - | - | - |
| Ni | 5 | 2.6 | 4.4 | 0.2 |
| Cu | 5 | 618.3 | 370.9 | 1236.6 |
| Zn | 1 | 0.02 | 0.004 | 0.006 |
| Pb | 5 | 3 | 0.4 | 8.4 |
| | | | | |
| CF – C.A.: Contamination factor using crustal abundance as background value<br>CF – P.L: Contamination factor using permissible limits in soil as background value<br>CF – IUCC: Contamination factor using IUCC standard reference asbestos samples as background value | | | | |

Ecological risk level of nickel (152) in chrysotile is shown to be high and that of copper (1237) in anthophyllite serious when referenced to crustal abundances. In addition, both amosite and crocidolite indicate a low ecological risk level. The ecological risk levels of the four asbestos samples using WHO permissible limits are classified as identical to those of the crustal background abundances. The ecological risk level calculated for the samples with IUCC asbestos standards backgrounds designated chrysotile, amosite and crocidolite as low risk. However, the copper level in anthophyllite is again shown as a serious ecological health risk.

Table 8.19: Ecological risk index values of the studied asbestos mine wastes

| Background value used in contamination factor | Potential ecological risk index (RI) | | | |
|---|---|---|---|---|
| | Chrysotile | Amosite | Crocidolite | Anthophyllite |
| | | | | |
| CF – C.A. | 107.24 | 13.96 | 6.07 | 635.58 |
| CF – P.L | 160.38 | 13.24 | 8.6 | 380.5 |
| CF - IUCC | 28.9 | 25.07 | 30.6 | 1250.9 |
| | | | | |
| CF – C.A.: Contamination factor using crustal abundance as background value<br>CF – P.L: Contamination factor using permissible limits in soil as background value<br>CF – IUCC: Contamination factor using IUCC standard reference asbestos samples as background value | | | | |

The results of the ecological risk index (RI) are very similar to those give above in the individual potential ecological risk factor. Using crustal abundance and IUCC asbestos standards as background values chrysotile, amosite and crocidolite can be defined as low risk, whereas anthophyllite indicates a serious ecological risk. Chrysotile can be characterised as a moderate ecological risk using permissible limit backgrounds, and amosite, crocidolite and anthophyllite are the same as the previous background values.

### 8.3.4. Health risk assessment

The health risks of the heavy metals contained in the asbestos mine wastes can be evaluated from their calculated hazard quotient (HQ) values given in table 8.20.

Table 8.20: HQ values of the studied asbestos mine wastes

| Metal | Chrysotile | Amosite | Crocidolite | Anthophyllite |
|---|---|---|---|---|
| | | | | |

| | | | | |
|---|---|---|---|---|
| Al | 0.14 | 0.08 | 0.02 | 0.02 |
| Fe | 0.25 | **5.13** | **4.76** | **4.24** |
| Mn | 0.24 | **5.25** | 0.49 | **11.66** |
| Mg | **10.6** | **1.5** | 0.58 | **4.58** |
| Cr | 0.8 | 0.05 | - | - |
| Co | **2.1** | - | - | - |
| Ni | **18.08** | 0.61 | 0.14 | 0.52 |
| Cu | 0.37 | 0.61 | 0.58 | **123.66** |
| Zn | 0.23 | 0.59 | 0.18 | 0.02 |
| Zr | 0.003 | 0.02 | 0.002 | 0.0004 |
| Ba | - | 0.07 | 0.004 | - |
| Pb | 0.47 | 0.38 | 0.36 | 0.6 |

Mg, Co and Ni in chrysotile, Fe, Mn and Mg in amosite, Fe in crocidolite and Fe, Mn, Mg and Cu in anthophyllite are shown to have HQ values greater than 1, and therefore are considered to have adverse human health effects.

### 8.3.5. Statistical analysis

The inter-element associations between heavy metals in each rock sample is examined using a correlation matrix. Heavy metals that show high correlation coefficients may indicate similar origins and low correlation coefficients may reflect variable sources closely related with weathering processes (Ma *et al.,* 2016). Tables 8.21, 8.22, 8.23 and 8.24 summarise the Pearson's correlation between metals within each sample at both $p < 0.05$ and $p < 0.01$ statistical significance. The correlation coefficient can be separated into four correlation classes: Low $r \leq 0.1$; medium $0.1 \leq r \leq 0.3$; high $0.3 \leq r \leq 0.5$ and very high $r \geq 0.5$ (Weissmannová *et al.,* 2019).

Table 8.21: Pearson's Rank correlation matrix for chrysotile (n = 66)

| | *Al* | *Fe* | *Mn* | *Mg* | *Cr* | *Co* | *Ni* | *Cu* | *Zn* | *Zr* | *Pb* |
|---|---|---|---|---|---|---|---|---|---|---|---|
| Al | 1.00** | | | | | | | | | | |
| Fe | 1.00** | 1.00** | | | | | | | | | |
| Mn | 1.00** | 1.00** | 1.00** | | | | | | | | |
| Mg | 1.00** | 1.00** | 1.00** | 1.00** | | | | | | | |
| Cr | 1.00** | 1.00** | 1.00** | 1.00** | 1.00** | | | | | | |
| Co | 0.99** | 0.99** | 0.98** | 0.99** | 0.98** | 1.00** | | | | | |
| Ni | 1.00** | 1.00** | 1.00** | 1.00** | 1.00** | 0.99** | 1.00** | | | | |
| Cu | 0.98** | 0.98** | 0.79** | 0.98** | 0.78** | 0.76** | 0.76** | 1.00** | | | |
| Zn | 0.92** | 0.92** | 0.89** | 0.92** | 0.88** | 0.85** | 0.87** | 0.92** | 1.00** | | |
| Zr | **0.25*** | **0.25*** | **0.26*** | **0.25*** | **0.27*** | **0.30*** | **0.27*** | 0.39** | 0.48** | 1.00** | |
| Pb | 0.92** | 0.92** | 0.87** | 0.92** | 0.89** | 0.94** | 0.89** | 0.77** | 0.84** | 0.54** | 1.00** |

*Pearson's correlation significant at 0.05 level (the bold font)

**Pearson's correlation significant at 0.01 level

Table 8.22: Pearson's Rank correlation matrix for amosite (n = 66)

| | *Al* | *Fe* | *Mn* | *Mg* | *Cr* | *Ni* | *Cu* | *Zn* | *Zr* | *Ba* | *Pb* |
|---|---|---|---|---|---|---|---|---|---|---|---|
| Al | 1.00** | | | | | | | | | | |
| Fe | 0.63** | 1.00** | | | | | | | | | |
| Mn | 0.63** | 1.00** | 1.00** | | | | | | | | |
| Mg | 0.63** | 1.00** | 1.00** | 1.00** | | | | | | | |
| Cr | 0.62** | 0.74** | 0.70** | 0.74** | 1.00** | | | | | | |
| Ni | 0.65** | 1.00** | 0.99** | 1.00** | 0.75** | 1.00** | | | | | |
| Cu | 0.68** | 1.00** | 0.95** | 1.00** | 0.77** | 0.98** | 1.00** | | | | |
| Zn | 0.68** | 1.00** | 1.00** | 1.00** | 0.74** | 0.99** | 0.97** | 1.00** | | | |
| Zr | 0.57** | 0.63** | 0.53** | 0.63** | 0.95** | 0.61** | 0.68** | 0.59** | 1.00** | | |
| Ba | 0.66** | 0.98** | 0.98** | 0.98** | 0.85** | 0.98** | 0.99** | 0.98** | 0.77** | 1.00** | |
| Pb | 0.70** | 0.93** | 0.80** | 0.93** | 0.90** | 0.86** | 0.91** | 0.83** | 0.88** | 0.97** | 1.00** |

*Pearson's correlation significant at 0.05 level (the bold font)

**Pearson's correlation significant at 0.01 level

Table 8.23: Pearson's Rank correlation matrix for crocidolite (n = 55)

| | *Al* | *Fe* | *Mn* | *Mg* | *Ni* | *Cu* | *Zn* | *Zr* | *Ba* | *Pb* |
|---|---|---|---|---|---|---|---|---|---|---|
| Al | 1.00** | | | | | | | | | |
| Fe | 0.63** | 1.00** | | | | | | | | |
| Mn | 0.63** | 1.00** | 1.00** | | | | | | | |
| Mg | 0.63** | 1.00** | 1.00** | 1.00** | | | | | | |
| Ni | 0.69** | 0.96** | 0.91** | 0.96** | 1.00** | | | | | |
| Cu | 0.72** | 0.99** | 0.83** | 0.99** | 0.93** | 1.00** | | | | |
| Zn | 0.70** | 0.97** | 0.97** | 0.97** | 0.98** | 0.87** | 1.00** | | | |
| Zr | 0.34** | 0.24 | 0.24 | 0.24 | 0.50** | **0.31*** | 0.47** | 1.00** | | |
| Ba | 0.42** | 0.37** | 0.37** | 0.37** | 0.61** | 0.44** | 0.58** | 0.99** | 1.00** | |
| Pb | 0.74** | 0.91** | 0.66** | 0.91** | 0.88** | 0.92** | 0.79** | 0.61** | 0.71** | 1.00** |

*Pearson's correlation significant at 0.05 level (the bold font)

**Pearson's correlation significant at 0.01 level

Table 8.24: Pearson's Rank correlation matrix for anthophyllite (n = 45)

| | *Al* | *Fe* | *Mn* | *Mg* | *Ni* | *Cu* | *Zn* | *Zr* | *Pb* |
|---|---|---|---|---|---|---|---|---|---|
| Al | 1.00** | | | | | | | | |
| Fe | 1.00** | 1.00** | | | | | | | |
| Mn | 1.00** | 1.00** | 1.00** | | | | | | |
| Mg | 1.00** | 1.00** | 1.00** | 1.00** | | | | | |
| Ni | 1.00** | 1.00** | 0.99** | 1.00** | 1.00** | | | | |
| Cu | 1.00** | 1.00** | 0.99** | 1.00** | 0.98** | 1.00** | | | |
| Zn | **0.38*** | 0.38** | **0.31*** | 0.38** | **0.37*** | **0.36*** | 1.00** | | |
| Zr | 0.20 | 0.20 | 0.20 | 0.20 | 0.25 | 0.22 | 0.98** | 1.00** | |
| Pb | 0.96** | 0.96** | 0.63** | 0.96** | 0.63** | 0.74** | 0.49** | 0.42** | 1.00** |

*Pearson's correlation significant at 0.05 level (the bold font)
**Pearson's correlation significant at 0.01 level

## 8.4. Discussion

Mining has emerged as a major cause of the enhanced loading of metals to soil, water and atmospheric systems worldwide. Contributing to this problem is the inadequate and/or neglected management of exposed mine wastes. Increased weathering and metal leaching from these exposed metalliferous mine rocks, tailings and dumps are additional factors magnifying the heavy metal problem (Malmström *et al.,* 2008; Thorslund *et al.,* 2012; Chalov *et al.,* 2017). The present study focusses on the geo-toxicity of asbestos-bearing materials in the surface environment as hosts to enormous reserves of potentially toxic elements. Explanation of the heavy metal content of each asbestos mine waste is fundamental for determining the potential impact on public health and surrounding ecosystems. As the South African metal polluted lands (MPLs) values come from geochemical research and characterisation of soil types South Africa, these values should only be considered as general estimates for the assessment of contamination (Chonokhuu *et al.,* 2019). A more accurate approach is to distinguishing contamination levels in the four asbestos rocks using pollution indices.

Significant quantities of potential toxic elements are hosted in solid mine wastes that, under conducive conditions, may be released into the surrounding environments contaminating and altering their geochemical characteristics (Cobbina *et al.,* 2013; Wang *et al.,* 2017; Aznar-Sánchez *et al.,* 2018). In the present study high concentrations of Fe, Mn, Mg,

Al, Cu, Zn and Pb are observed in the asbestos mine wastes relative to the background levels. Furthermore, higher contamination factors and geo-accumulation indices are recorded in the four asbestos mine wastes compared to background levels. The higher enrichment factors, contamination factors and geo-accumulation indices demonstrated for various heavy metals in the four asbestos mine wastes provide evidence supporting the hypothesis that they are heavy metal sources and indicating their potential to cause adverse effects on surrounding environments (Swartjes *et al.,* 2012; Alfaro *et al.,* 2015; Bello *et al.,* 2016).

In environmental media the extent of heavy metal enrichment is commonly determined by the enrichment factor (EF) (Nowrouzi and Pourkhabbaz, 2015). The asbestos mine wastes in the present study have EF values of Mg, Cr, Co, Ni, Cu and Pb greater than 1.5, indicating concentrations above background values (Zhang and Liu, 2002) and suggesting high enrichment of these metals. It is evident that the degree of metal enrichment varies among the types of asbestos mine wastes, which is likely a result of the different processes accounting for their formation. The elevated EF values for the four asbestos mine wastes indicate, in general, that each of these solid wastes are, under the appropriate circumstances, able to notably enrich the encompassing environmental media (Liakopoulos *et al.,* 2010).

Above certain concentrations heavy metals have known significant effects on plants, animals and humans (Singh *et al.,* 2011; Mishra *et al.,* 2017), such as DNA damage, cytoplasmic enzyme inhibition and carcinogenic effects in animals and plants (Ali *et al.,* 2013). The high HQ values above 1 documented in this study for the four asbestos mine wastes indicate that metal enrichment associated with their related locations is sufficient to induce significant human health effects. The asbestos mine waste type determines the health risks associated with the heavy metal contaminant enrichment.

The contamination and risk characterisation of the toxic elements measured in the four types of asbestos samples are summarised in the correlation matrixes. These matrixes are essentially the toxicity array identifying each of the measured heavy metals in terms of their concentrations, enrichment factors, geo-accumulation indices, contamination factors and toxic responses. The four-toxicity matrix are used as an initial approximation to classify the geo-toxicity of heavy metals in surface-exposed asbestos rocks and waste as a means of

guiding future efforts. Calculation of indices characterized by various features aids in establishing the suitable theoretical basis for appropriate interpretation of future soil conditions. Elements with high correlation values indicate that they may share a common source (Wang *et al.,* 2014). In soil, high correlations between elements indicate their alignment with their parent source (Diami *et al.,* 2016). In addition to sharing a common source (Diami *et al.,* 2016), high correlation values between elements may exhibit analogous behaviours during transformation and migration processes (Wang *et al.,* 2014). Accordingly, the resources and their trajectories may be derived for inter-elemental relationships between different metals (Oliva and Espinosa, 2007).

## 8.5. Conclusion

The environmental threats posed by asbestos mine wastes via heavy metal contamination into the surrounding environment is demonstrated in this study. The four studied asbestos mine wastes show that they host heavy metals in high amounts, which can be leached out into and enriching surrounding environmental media. Site specific environmental management decisions are required as the type of asbestos mine waste determines the extent of heavy metal enrichment and subsequently the potential ecological risk.

## 8.6. References


Adamu, C. L. and Nganje, T. N. (2010): Heavy metal contamination of surface soil in relationship to land use patterns: A case study of Benue State. Nigeria. *Materials Sciences and Applications*, **1**, 127–134.

Agboola, O (2019): The role of membrane technology in acid mine water treatment: a review. *Kor. J. Chem. Eng*, **36** (9), 1389–1400.

Agboola, O., Babatunde, D.E., Fayomi, O.S.I., Sadiku, E.R., Popoola, P., Moropeng, L., Yahaya, A. and Mamudu, O.A. (2020): A review on the impact of mining operation: Monitoring, assessment and management. *Results in Engineering*, **8**, 100181

Akoto, R. and Anning, A.K. (2021): Heavy metal enrichment and potential ecological risks from different solid mine wastes at a mine site in Ghana. *Environmental Advances*, **3**, 100028

Alfaro, M.R., Montero, A., Ugarte, O.M., Nascimento, Do, A., C.W., De Aguiar Accioly, A.M., Biondi, C.M. and Da Silva, Y.J.A.B. (2015): Background concentrations and reference values for heavy metals in soils of Cuba. *Environ. Monit. Assess*., **187** (4198), 1–10. doi:10.1007/s10661-014-4198-3

Ali, H., Khan, E. and Sajad, A.M. (2013): Phytoremediation of heavy metals – concepts and applications. *Chemosphere*, **91**, 869–881

Apollaro, C., Fuoco, I., Vespasiano, G., De Rosa, R., Cofone, F., Miriello, D. and Bloise, A. (2018): Geochemical and mineralogical characterization of tremolite asbestos contained in the Gimigliano-Monte Reventino Unit (Calabria, south Italy). *J. Mediterr. Earth Sci*, **10**, 5–15.

Angulo, E. (1996): The Tomlinson pollution load index applied to heavy metals “mussel–watch” data: a useful index to assess coastal pollution. *Sci Total Environ*, **187**, 19–56.

Aznar-Sánchez, J.A., García-Gómez, J.J., Velasco-Muñoz, J.F. and Carretero-Gómez, A. (2018): Mining waste and its sustainable management: advances in worldwide research. *Minerals*, **8**, 1–27.

Babula, P., Adam, V., Opatrilova, R., Zehnalek, J., Havel, L. and Kizek, R. (2008): Uncommon heavy metals, metalloids and their plant toxicity: A review. *Environ. Chem. Lett*., **6**, 189–213

Ballirano, P., Bloise, A., Gualtieri, A.F., Lezzerini, M., Pacella, A., Perchiazzi, N., Dogan, M. and Dogan, A.U. (2017): The crystal structure of mineral fibres. In: Gualtieri, A.F. (Ed.), Mineral Fibres: Crystal Chemistry, Chemical-Physical Properties, Biological Interaction and Toxicity. European Mineralogical Union, London, pp. 17–53.

Bansah, K.J. and Addo, W.K. (2016): Phytoremediation potential of plants grown on reclaimed spoil lands. *Ghana Min. J*., **16** (1), 68–75.

Baumann, F., Buck, B.J., Metcalf, R.V., McLaurin, B.T., Merkler, D.J. and Carbone, M. (2015): The presence of asbestos in the natural environment is likely related to mesothelioma in young individuals and women from Southern Nevada. *J. Thorac. Oncol*., **10**, 731–737

Bello, S., Zakari, Y.I., Ibeanu, I.G.E. and Muhammad, B.G. (2016): Characterization and assessment of heavy metal pollution levels in soils of Dana steel limited dumpsite, Katsina state, Nigeria using geo-accumulation, ecological risk and hazard indices. *Am. J. Eng. Res*., **5** (1), 49–61.

Berry, G. and Gibbs, G.W. (2008): Mesothelioma and asbestos. *Regul. Toxicol. Pharmacol*., **52**, S223–S231.

Bloise, A., Belluso, E., Barrese, E., Miriello, D. and Apollaro, C. (2009): Synthesis of Fedoped chrysotile and characterization of the resulting chrysotile fibers. Cryst. Res. Technol., 44 (6), 590–596.

Bloise, A., Barca, D., Gualtieri, A.F., Pollastri, S. and Belluso, E. (2016): Trace elements in hazardous mineral fibres. *Environmental Pollution*, **216**, 314e323

Bloise, A., Ricchiuti, C., Punturo, R. and Pereira, D. (2020): Potentially toxic elements (PTEs) associated with asbestos chrysotile, tremolite and actinolite in the Calabria region (Italy). *Chemical geology*, **558**, 119896

Bowes, D.R. and Farrow, C.M. (1997): Major and Trace Element Compositions of the UICC Standard Asbestos Samples. *American Journal of Industrial Medicine*, **32**, 592–594

Briffa, J., Sinagra, E. and Blundell, R. (2020): Heavy metal pollution in the environment and their toxicological effects on humans. *Heliyon*, **6**, e04691

Caeiro, S., Costa, M.H., Ramos, T.B., Fernandes, F., Silveira, N., Coimbra, A., Medeiros, G. and Painho, M. (2005): Assessing heavy metal contamination in Sado Estuary sediment: an index analysis approach. *Ecol. Indic*., **5**, 151–169.

Chalov, S.R., Thorslund, J., Kasimov, N., Aybullatov, D., Ilyicheva, E., Karthe, D., Kositsky, A., Lychagin, M., Nittrouer, J., Pavlov, M., Pietroń, J., Shinkareva, G., Tarasov, M., Garmaev, E., Akhtman, Y. and Jarsjö, J. (2017): The Selenga River delta—a geochemical barrier protecting Lake Baikal waters. *Reg Environ Change*, **17**, 2039–2053

Chaturvedi, A., Bhattacharjee, S., Singh, A. K. and Kumar, V. A. (2018): A new approach for indexing groundwater heavy metal pollution. *Ecological Indicators*, **87**, 323–331.

Chen, Q., Pan, X.-D., Huang, B.-F. and Han, J.-L. (2018): Distribution of metals and metalloids in dried seaweeds and health risk to population in southeastern China. *Scientifc Reports*, **8**, 3578.

Chonokhuu, S., Batbold, C., Chuluunpurev, B., Battsengel, E., Dorjsuren, B. and Byambaa, B. (2019): Contamination and Health Risk Assessment of Heavy Metals in the Soil of Major Cities in Mongolia. *Int. J. Environ. Res. Public Health*, **16**, 2552

Cobbina, S.J., Myilla, M. and Michael, K. (2013): Small scale gold mining and heavy metal pollution: assessment of drinking water sources in datuku in the Talensi-Nabdam district. *Int. J. Sci. Technol. Res*., **2** (1), 96–100.

David R. Lide, ed., ''Atomic Masses and Abundances'', in *CRC Handbook of Chemistry and Physics, Internet Version 2005,* David R. Lide, ed., http://www.hbcpnetbase.com, CRC Press, Boca Raton, FL, 2005, p. 15-18.

Diami, S.M., Kusin, F.M. and Madzin, Z. (2016): Potential ecological and human health risk of heavy metals in surface soils associated with iron ore mining in Pahang, Malaysia. *Environ. Sci. Pollut. Res*., **23** (20), 21086–21097.

Douay, F., Pelfrêne, A., Planque, J., Fourrier, H., Richard, A., Roussel, H. and Girondelot, B. (2013): Assessment of potential health risk for inhabitants living near a former lead smelter, Part 1: metal concentrations in soils, agricultural crops, and homegrown vegetables. *Environ. Monit. Assess*., **185**, 3665–3680.

Forstner, U. and Wittmann, G.T.W. (1983): Metal pollution in aquatic environment. Springer, New York

Gamble, J.F. and Gibbs, G.W. (2008): An evaluation of the risks of lung cancer and mesothelioma from exposure to amphibole cleavage fragment. *Regul. Toxicol. Pharmacol*., **52**, 154–186.

Gong, Q., Deng, J., Xiang, Y., Wang, Q. and Yang, L. (2008): Calculating pollution indices by heavy metals in ecological geochemistry assessment and a case study in parks of Beijing. *Journal of China University of Geosciences*, **19**, 230–241.

Gualtieria, A.F., Lusvardia, G., Zobolia, A., Di Giuseppea, D. and Gualtieri, M.L. (2019): Biodurability and release of metals during the dissolution of chrysotile, crocidolite and fibrous erionite. *Environmental Research*, **171**, 550–557

Guo, W., Liu, X., Liu, Z. and Li, G. (2010): Pollution and potential ecological risk evaluation of heavy metals in the sediments around Dongjiang Harbor, Tianjin. *Procedia Environ. Sci*., **2**, 729–736.

Grant, A. and Middleton, R. (1990): An assessment of metal contamination of sediments in the humber estuary. *U.K. Estuar. Coast. Shelf Sci*., **31**, 71–85.

Hakanson, L. (1980): An Ecological Risk Index for Aquatic Pollution Control: A Sedimentological Approach. *Water Res*., **14**, 975–1001.

Harris, L.V. and Kahwa, I.A. (2003): Asbestos: old foe in 21st century developing countries. *Sci Total Environ*, **307**, 1–9

He, Z. L., Xu, H. P., Zhu, Y.M., Yang, X.E. and Chen, G.C. (2005a): Adsorption-desorption characteristics of cadmiumin variable charge soils. *Journal of Environmental Science and Health*, Part A, **40** (4), 805–822.

He, Z.L., Yang, X.E. and Stoffella, P.J. (2005b): Trace elements in agroecosystems and impacts on the environment. *Journal of Trace Elements in Medicine and Biology*, **19** (2–3), 125–140.

Hillerdal, G. (1999): Mesothelioma: Cases associated with non-occupational and low dose exposures. *Int. J. Occup. Environ. Med*., **56**, 505–513.

Holmes, A., Morgan, A. and Sandalls, F.J. (1971): Determination of iron, chromium, cobalt, nickel, and scandium in asbestos by neutron activation analysis. *Am. Ind. Hyg. Assoc. J*., **32** (5), 281–286.

IARC: International Agency for Research on Cancer. Agents Classifed by the IARC Monographs. 2020. Available online: https://monographs.iarc.fr/list-of-classifications

Ibrahim, I.M.N. (2016): The relations between concentration of Iron and the pH of ground water (Case Study Zulfi Ground Water). *Int. J. Environ. Monit. Anal*., **4** (6), 140.

Islam, M.S., Ahmed, M.K., Raknuzzaman, M., Habibullah-Al-Mamun, M. and Islam, M.K. (2015): Heavy metal pollution in surface water and sediment: A preliminary assessment of an urban river in a developing country. *Ecol. Indic*., **48**, 282–291.

Iwegbue, C.M.A., Obi, G., Emoyan, O.O., Odali, E.W., Egobueze, F.E., Tesi, G.O., Nwajei, G.E. and Martincigh, B.S. (2018): Characterization of metals in indoor dusts from electronic workshops, cybercafés and offices in southern Nigeria: implications for onsite human exposure. *Ecotoxicol Environ Saf*, **159**, 342–353.

Ji, Y., Feng, Y., Wu, J., Zhu, T., Bai, Z. and Duan, C. (2008): Using geo-accumulation index to study source profiles of soil dust in China. *J. Environ. Sci*., **20**, 571–578.

Kim, K.W., Lee, H.K. and Yoo, B.C. (1998): The environmental impact of gold mines in the Yugu-Kwangcheon Au-Ag metallogenic province, Republic of Korea. *Environ. Technology*, **19**, 291–298.

Kowalska, J.B., Mazurek, R., Gasiorek, M. and Zaleski, T. (2018): Pollution indices as useful tools for the comprehensive evaluation of the degree of soil contamination–A review. *Environ Geochem Health*, **40**, 2395–2420

Kumar, A. and Maiti, S.K. (2015): Assessment of potentially toxic heavy metal contamination in agricultural fields, sediment, and water from an abandoned chromite-asbestos mine waste of Roro hill, Chaibasa, India. *Environ. Earth Sci*., **74** (3), 2617–2633.

Kusin, F.M., Azani, N.N.M., Hasan, S.N.M.S. and Sulong, N.A. (2018): Distribution of heavy metals and metalloid in surface sediments of heavily mined area for bauxite ore in Pengerang, Malaysia and associated risk assessment. *Catena*, **165**, 454–464

Li, Y., Zhang, Z., Zhou, H., Fan, Z., Wu, D. and Xia, B. (2016): Characteristics, sources and health risk assessment of toxic heavy metals in PM2.5 at a megacity of southwest China. *Environ. Geochem. Health*, **38**, 353–362.

Liakopoulos, A., Lemiere, B., Michael, K., Crouzet, C., Laperche, V., Romaidis, I., Drougas, I. and Lassin, A. (2010): Environmental impacts of unmanaged solid waste at a former base metal mining and ore processing site (Kirki, Greece). *Waste Manag. Res*., **28**, (11), 996–1009.

Ma, Y., Egodawatta, P., McGree, J., Liu, A. and Goonetilleke, A. (2016): Human health risk assessment of heavy metals in urban stormwater. *Sci. Total Environ*., **557**, 764–772.

Malmström, M.E., Berglund, S. and Jarsjö, J. (2008): Combined effects of spatially variable flow and mineralogy on the attenuation of acid mine drainage in groundwater. *Appl Geochem*, **23**, 1419–1436.

Mazurek, R., Kowalska, J., Gasiorek, M., Zadrozny, P., Jozefowska, A. and Zaleski, T. (2017): Assessment of heavy metals contamination in surface layers of Roztocze National Park forest soils (SE Poland) by indices of pollution. *Chemosphere*, **168**, 839–850.

Mishra, J., Singh, R. and Arora, N.K. (2017): Alleviation of heavy metal stress in plants and remediation of soil by rhizosphere microorganisms. *Front. Microbiol*., **8**, 1–7. doi:10.3389/fmicb.2017.01706, (1706).

Muller, G. (1969): Index of geo-accumulation in sediments of the Rhine River. *GeoJournal*, **2**, 108–118.

Ndlovu, N., Naude, J.T. and Murray, J. (2013): Compensation for environmental asbestos-related diseases in South Africa: a neglected issue. *Global Health Action,* **6**, 19410.

Nishida, H., Miyai, M., Tada, F. and Suzuki, S. (1982): Computation of the index of pollution caused by heavy metals in river sediment. *Environ. Pollut*., **B4**, 241–248.

Nowrouzi, M. and Pourkhabbaz, A. (2014): Application of geoaccumulation index and enrichment factor for assessing metal contamination in the sediments of Hara Biosphere Reserve, Iran. *Chemical Speciation & Bioavailability*, **26**, 99.

Nowrouzi, M. and Pourkhabbaz, A. (2015): Application of geoaccumulation index and enrichment factor for assessing metal contamination in the sediments of Hara Biosphere Reserve, Iran. *Chem. Speciat. Bioavail.*, **26** (2), 99–105. doi:10.3184/095422914X13951584546986

Olawoyin, R., Schweitzer, L., Zhang, K., Okareh, O. and Slates, K. (2018): Index analysis and human health risk model application for evaluating ambient air-heavy metal contamination in Chemical Valley Sarnia. *Ecotoxicology and Environmental Safety*, **148**, 72 – 81.

Oliva, S.R. and Espinosa, A.F. (2007): Monitoring of heavy metals in topsoils, atmospheric particles and plant leaves to identify possible contamination sources. *Microchem. J.*, **86**, 131–139

Pandey, L.K., Park, J., Son, D.H., Kim, W., Islam, M.S., Choi, S., Lee, H. and Han, T. (2019): Assessment of metal contamination in water and sediments from major rivers in South Korea from 2008 to 2015. *Sci. Total Environ.*, **651**, 323–333.

Punturo, R., Ricchiuti, C., Mengel, K., Apollaro, C., De Rosa, R. and Bloise, A. (2018): Serpentinite-derived soils in southern Italy: potential for hazardous exposure. *J. Mediterr. Earth Sci*, **10**, 51–61.

Rachwał, M., Wawer, M., Jabłonska, M., Rogula-Kozłowska, W. and Rogula-Kopiec, P. (2020): Geochemical and Mineralogical Characteristics of Airborne Particulate Matter in Relation to Human Health Risk. *Minerals*, **10** (866). doi:10.3390/min10100866

Rao, K., Mohapatra, M., Anand, S. and Venkateswarlu, P. (2010): Review on cadmium removal from aqueous solutions. *Int. J. Eng. Sci. Technol.*, **2** (7), 81–103.

Reimann, C. and Garret, R. G. (2005): Geochemical background: Concept and reality. *Science of the Total Environment*, **350**, 12–27.

Salomons, W. and Forstner, U. (1984): Metals in the Hydrocycle. Berlin-Heidelberg: Springer.

Sekabira, K., Oryem Origa, H., Basamba, T.A., Mutumba, G. and Kakudidi, E. (2010): Assessment of heavy metal pollution in the urban stream sediments and its tributaries. *Int. J. Environ. Sci. Technol*., **7**, 435–446.

Scambelluri, M., Piccardo, G.B., Philippot, P., Robbiano, A. and Negretti, L. (1997): High salinity fluid inclusions formed from recycled seawater in deeply subducted alpine serpentinite. *Earth Planet. Sci. Lett.,* **148**, 485–499.

Singh, K.P., Malik, A., Sinha, S., Singh, V.K. and Murthy, R.C. (2005): Estimation of source of heavy metal contamination in sediments of Gomti River (India) using principal component analysis. *Water Air Soil Pollut*., **166**, 321–341.

Singh, A., Sharma, R. K., Agrawal, M. and Marshall, F. M. (2010): Health risk assessment of heavy metals via dietary intake of foodstuffs from the wastewater irrigated site of a dry tropical area of India. *Food Chem. Toxicol*., **48**, 611–619.

Singh, R., Gautam, N., Mishra, A. and Gupta, R. (2011): Heavy metals and living systems: an overview. *Indian J. Pharmacol*., 5–8. doi:10.4103/0253-7613.81505.

Sutherland, R. A. (2000): Bed sediment-associated trace metals in an urban stream, Oahu, Hawaii. *Environmental Geology*, **39**, 611–627

Swartjes, F.A., Rutgers, M., Lijzen, J.P.A., Janssen, P.J.C.M., Otte, P.F., Wintersen, A., Brand, E. and Posthuma, L. (2012): State of the art of contaminated site management in The Netherlands: policy framework and risk assessment tools. *Sci. Total Environ*., **427** (428), 1–10.

Tashakor, M., Yaacob, W.Z.W., Mohamad, H. and Ghani, A.A. (2014): Geochemical characteristics of serpentinite soils from Malaysia. *Malays. J. Soil Sci.,* **18**, 35–49.

Taylor, S.R. and McLennon, S.M. (1995): The geochemical evolution of the continental crust. *Reviews Geophysics*, **33**, 241 – 265.

Thorslund, J., Jarsjö, J., Chalov, S.R. and Belozerova, E.V. (2012): Gold mining impact on riverine heavy metal transport in a sparsely monitored region: the upper Lake Baikal Basin case. *J Environ Monitor*, **14**, 2780–2792

Tiepolo, M., Oberti, R., Zanetti, A., Vannucci, R. and Foley, S.F. (2007): Trace-element partitioning between amphibole and silicate melt. In: Hawthorne, F.C., Oberti, R., Della Ventura, G., Mottana, A. (Eds.), Amphiboles: Crystal Chemistry, Occurrence, and Health Issues. Mineralogical Society of America, Chantilly, pp. 417–452.

Tomllinson, D.C., Wilson, J.G., Harris, C.R. and Jefery, D.W. (1980): Problems in the Assessment of Heavy metals levels in Estuaries and the formation of pollution index. *Helgolander Wissenschaftliche Meeresunters Uchunge*, **33**, 566–569.

U.S. Environmental Protection Agency. Toxics Release Inventory: Public Data Release Report. 2001. Available online: www.epa.gov/tri/tridata/tri01.

USEPA: US Environmental Protection Agency (2009): Part F, Supplemental guidance for inhalation risk assessment. In Risk Assessment Guidance for Superfund Volume I: Human Health Evaluation Manual; Office of Superfund Remediation and Technology Innovation: Potomac Yards, VA, USA, p. 68.

Wang, Y., Yang, L., Kong, L., Liu, E., Wang, L. and Zhu, J. (2014): Spatial distribution, ecological risk assessment and source identification for heavy metals in surface sediments from Dongping Lake, Shandong, East China. *Catena*, **125**, 200–205.

Wang, L., Ji, B., Hu, Y., Liu, R. and Sun, W. (2017): A review on in situ phytoremediation of mine tailings. *Chemosphere*, **184**, 594–600.

Weissmannová, H.D., Mihocová, S., Chovanec, P. and Pavlovský, J. (2019): Potential Ecological Risk and Human Health Risk Assessment of Heavy Metal Pollution in Industrial Affected Soils by Coal Mining and Metallurgy in Ostrava, Czech Republic. *Int. J. Environ. Res. Public Health*, **16**, 4495

WHO (1996): Permissible limits of heavy metals in soil and plants (Geneva: World Health Organization), Switzerland.

Yi, Y., Tang, C., Yi, T., Yang, Z. and Zhang, S. (2017): Health risk assessment of heavy metals in fish and accumulation patterns in food web in the upper Yangtze River, China. *Ecotoxicology and Environmental Safety*, **145**, 295–302.

Zhang, J. and Liu, C.L. (2002): Riverine composition and estuarine geochemistry of particulate metals in China-weathering features, anthropogenic impact and chemical fluxes. Estuar. Coast. *Shelf Sci*., **54**, 1051–1070

Zheng, J., Zhan, C., Yao, R., Zhang, J., Liu, H., Liu, T. and Cao, J. (2017): Levels, sources, markers and health risks of heavy metals in PM2.5 over a typical mining and metallurgical city of Central China. *Aerosol Sci. Eng*., **2**, 1–10.

# Chapter 9 - The Importance of Functional Integration of Independent Studies to the Environmental Management of Asbestos-polluted Mine Land

## 9.1. Introduction

A multi-perspective analysis is performed in this thesis to approach the complex dimensions impacting the management of environmental asbestos. Bioremediation, the purposeful use of micro-organisms to degrade or remove toxic compounds from the environment, is the method proposed for the management of environmental asbestos. It can be implemented with a remarkable range of treatment approaches to enhance the efficacy of removing toxic compounds, such as asbestos. The process is adaptable and is more effective in the long-term than present methods. Additionally, bioremediation technology reduces the cost of a remediation project. In recent years, bioremediation has gained significant attention due to its eco-friendly and economical nature. The treatment of toxic contaminants/minerals by specific micro-organisms has become one of the most promising technologies for the remediation of contaminated sites, such as abandoned asbestos mines. However, bioremediation of these toxic materials in natural settings is a complicated process due to the heterogeneous nature and interactions occurring in these natural environments. Therefore the successful application of *in situ* bioremediation is dependent upon a comprehensive understanding of the properties, interactions, and effects of the environment in question, hence the need for a multi-perspective analysis . Targeting? inorganic or organic material/chemical and the microbial strains selected (i.e., selected bio-remediator), as well as knowledge of its biodegrading abilities and activities, in both controlled and indigenous environments, are required in the bioremediation process.

## 9.2. A Multi-faceted Approach to Remediation

At the Earth's surface, an unconsolidated, naturally occurring mineral and organic material horizon known as 'soil' provides an environment to an extreme diversity of living organisms (Voroney, 2007). As this horizon is in contact with the atmosphere it is susceptible to contamination. Human activities, such as mining and industrialisation, disrupt, expose, and

mobilise, into the air, asbestos fibres from the host rocks (Daghino *et al.,* 2005). The mobilised fibres may be deposited in large areas of soil resulting in its contamination with bio-persistent asbestos minerals (Daghino *et al.,* 2005). In the soil environment, asbestos contamination can occur either in the form of bulk material or as scattered fibres and/or fragments (Nelson *et al.,* 2011). Bulk material contaminants occur in primary sites, such as waste dumps, whereas fragmentary material is involved in secondary contamination and more widely distributed (Nelson *et al.,* 2011). The notion that asbestos fibres contained in soils are immobile is a long-standing paradigm that may be challenged based on new findings. Asbestos fibre remobilisation into the environment and toxicity alterations may occur when physical and chemical changes affect asbestos in soils (Willenbring *et al.,* 2016). The potential for inhalation is increased by a decrease in the length of the fibres (Willenbring *et al.,* 2016). The first-order control on asbestos toxicity is exerted by the iron content of the fibres as it results in reactive oxygen species production following inhalation (Willenbring *et al.,* 2016). Fungi, bacteria, and plant exudate such as organic acids. Siderophore compounds, and dissolved organic matter are often contained in natural soil environments and geo-engineered soil caps. They alter the surface charge and chemistry of the asbestos fibres (Willenbring *et al.,* 2016). Iron removal from both the structure and surface of chrysotile asbestos fibres can increase significantly when exposed to siderophore exudates (Willenbring *et al.,* 2016). Dissolved organic carbon, pH and ionic strength are other soil conditions, varying from soil to soil, that potentially allow asbestos fibres to move through the soil (Willenbring *et al.,* 2016). In the presence of dissolved organic matter (DOM), Willenbring *et al.* (2016) documented that fluvic acid (DOM) affects asbestos fibre mobility through the soil. The organic matter was reported to transform the fibres by reversing the charges of the asbestos from positive to negative, thereby reducing its ability for attachment to the individual soil grains (Willenbring *et al.,* 2016). From such results, the long-term effectiveness of current asbestos-contaminated soil remediation strategies appears to require re- valuation as possible exposure and alteration of asbestos fibres contained in soils are not adequately considered (Willenbring *et al.,* 2016).

The technology needed for the remediation of such sites is currently unavailable as asbestos is neither removable nor degradable under all conventional remediation protocols (Daghino *et al.,* 2005). Furthermore, asbestos-contaminated soils cover wide areas and disruptions could lead to even higher dispersion of fibres, representing problems with current

remediation strategies (Daghino *et al.,* 2005). The soil constitutes one of the major terrestrial habitats for micro-organisms (Ellis, 2004) with one gram containing up to $10^6$ microbial cells (Bundt *et al.,* 2001). The total number of living organisms inhabiting the soil and their abiotic surroundings define the biologically-rich region known as the soil habitat (Voroney, 2007). Many natural soil environments show microhabitats, where both fungi and bacteria reside and co-operate (Johansson *et al*., 2004). Microbial communities residing within the soil are among the most diverse and abundant on Earth (Bardgett and van der Putten, 2014). The recovery of soil from chemical contamination is primarily dependent on the presence of a microbial community with the ability to remove it (Bardgett and van der Putten, 2014). This forms the basis of a bioremediation prospective.

The micro-organisms, physicochemical conditions and their environment are all factors governing how the balance between metal immobilisation and mobilisation varies (Gadd, 2004). The removal of metal contaminants from solid matrices, in the context of bioremediation, is achieved through solubilisation (Gadd, 2004). Mobilisation or immobilisation processes mediated by micro-organisms occur when microbes are able to influence the balance between insoluble and soluble phases (Gadd, 2004). Chelation is one way of metal mobilisation (Gadd, 2004). For the natural environment, the research and application of mineral-microbe interactions, especially the action of bacteria and fungi to remove or detoxify xenobiotic compounds, is known as bioremediation. This remediation option, which relies upon the enzymatic activities of microbes to transform or degrade contaminants in the environment, offers a green technology solution to the global problem of environmental pollution.

When human beings are exposed to these toxic fibres, predominantly through inhalation, the development of various fatal diseases may result, such as lung mesothelioma (cancer), peritoneal mesothelioma, pleural plaques, bronchogenic carcinoma and asbestosis (Fubini *et al.,* 1990). Removal of the iron from asbestos structure would largely permit its detoxification (Moldoveanu *et al.*, 2009).

Despite being highly resistant to weathering, asbestos minerals have been documented to be biodegraded by certain fungal species (Daghino *et al.,* 2008). Although the

morphological and chemical modifications of asbestos induced by fungi are widely suggested as being instrumental for reducing the asbestos-related environmental hazard (Fubini, 1997), this thesis documents that bacteria could also play an important role in asbestos bioremediation. Asbestos weathering and/or detoxification proceeds either via the siderophore-mediated extraction of iron or by the disruption of the magnesium-silicate framework (Daghino *et al.,* 2008).

A) Siderophore-mediated iron removal

Bioremediation in natural ecosystems relies strongly on the availability of micronutrients, including iron. The chemical status and solubility of metals in the environment may be modified by the activities of numerous micro-organisms residing in the soil environment (Daghino *et al.,* 2005). Bioremediation employs such micro-organisms to polluted sites to improve the quality of the environment through the degradation of the pollutants by the metabolic activities of the microbes (Daghino *et al.,* 2005). Asbestos itself cannot biodegrade (Milne *et al.,* 2013), however, the elemental composition contributing to its toxicity may be biologically altered to reduce its toxicity. As iron is both a surface and structural component of most asbestos minerals and is a key contributor to the asbestos toxicity, bioremediation strategies may be a possibility (Martino *et al.,* 2003). In water, the recalcitrant asbestos fibres are very poorly soluble (Lund and Aust, 1990), however, iron may be extracted from the fibres and taken into solution when exposed to potent chelators, such as siderophores produced and excreted by a variety of soil micro-organisms under iron-limiting conditions (Werner *et al.,* 1995; Martino *et al.,* 2003). Additionally, iron-specific chelators or siderophores may modify the surface properties of asbestos and promote the eventual disruption of several subsurface layers (Prandi *et al.,* 2002). When extraction of iron proceeds through several layers below the surface of the fibres, the mineral lattice may be destabilised (Daghino *et al.,* 2005). Thus, as the pathogenicity of asbestos fibres involves both the chemical reactivity and the fibrous habit, the removal of iron is a possible strategy for the inactivation of the fibres and subsequent reduction of asbestos-associated toxicity (Daghino *et al.,* 2005).

The study of iron-containing fibres confirms the toxic effect as iron is continuously undergoing redox cycling along with surface iron activation – reactivation promoting the formation and release of toxic free radicles (Fubini *et al.*, 1995).

Results obtained by Gonneau *et al.* (2016) highlight the importance of the characteristics of the pollutants, but also all soil-limiting parameters, when considering the feasibility of bioremediation of asbestos-contaminated soils. Their research proposes a novel approach to the remediation of asbestos-polluted soil. The Fertility Capability Classification, pertinent to soil properties and toxicity using an ecotoxicological test, were determined at three locations with different asbestiform minerals (Gonneau *et al.,* 2016) to evaluate the feasibility of phytoremediaton of asbestos contaminated soils. The percentage of inhibition of seed germination and root growth was determined on three species (one *Poaceae*, two *Brassicaceae*) (Gonneau *et al.,* 2016). In the various soil parameters, all locations tested differed significantly (Gonneau *et al.,* 2016). The percentage of gravel, pH, P, K, total concentrations of Ni and Cr were, among 23 soils parameters and 12 modifiers, the factors determined as limiting the fertility (Gonneau *et al.,* 2016). Seed germination in all three asbestiform sites had, as shown in the ecotoxicological test, been reduced by 5-30 % of the control (Gonneau *et al.,* 2016). A 2-50 % reduction of control was observed in the root growth with Poaceae demonstrating the greatest reduction (Gonneau *et al.,* 2016). Alongside a pH decrease and soil fertility increase, the utilisation of compost was also noted to cause an increase in the bioavailability of trace elements (Ni or Cr) (Gonneau *et al.,* 2016). Their study concluded that serpentinophytes provide a possible method for the phytoremediation on asbestiform contaminated sites.

Following such research, bioremediation is now being thought of as an innovative approach towards the biotransformation of asbestos to a less toxic or nontoxic entity. The probability of several more microbial species in both bacterial and fungal classifications as having the potential for asbestos bioremediation cannot be ruled out, simply due to the plethora of microbial diversity in nature.

B) Disruption of the magnesium-silicate framework

When combined with aluminium, iron, calcium and oxides of magnesium, silicon dioxide forms the silicate minerals in soil and rocks (Bergna, 1994). Making up 90 % of the crust and comprising 30 % of all minerals, silicates form the largest class of minerals on Earth (Ehrlich, 1998; Ehrlich and Newman, 2009). Physical, chemical, and biological processes all weather silicates, silica, and aluminosilicates in rocks (Brehm *et al*., 2005). In nature, an important factor in the operating biogeochemical cycles is the biological weathering of silicate minerals.

Minerals are typically defined, in geochemical terms, as inorganic compounds that are of a described structure and chemical composition (Ehrlich, 1981). All classes of minerals are, to different degrees, vulnerable to natural weathering processes, which includes mechanical, chemical, and biological weathering (Ehrlich, 1996; Ehrlich, 2001). The composition, chemical structure, and stability of the minerals in the environment are all factors controlling depends (Ehrlich, 1998).

Weathering of minerals by biological processes involves a combination of diverse and complex interactions between the micro-organism and the mineral (Mapelli *et al.,* 2012). The mineralogy, textural and crystallo-chemical properties of the mineral impose both kinetic and thermodynamic constraints, which are, however, likely to be overcome by these abiotic and biotic interactions, resulting in the mobilisation and release of structural iron, which becomes biologically available for the microbial uptake and use (Mapelli *et al.,* 2012).

The physiological activities and structure of microbial communities associated with soil are affected by the soil's mineral composition (Boyd *et al*., 2007; Carson *et al*., 2007; Carson *et al*., 2009). Through bio-weathering processes, micro-organisms have a profound effect on extracting the nutritional elements from minerals into the soil environment (Certini *et al*., 2004). One major mechanism, termed acidification, is involved in mineral weathering (Uroz *et al.,* 2009), whereby minerals are susceptible to numerous biotic by-products formed during the metabolic activities of bacteria (Welch and Ullman, 1993). These by-products include organic acids, complex molecules and protons (Welch and Ullman, 1993). Chelating molecules, such as siderophores, have a triple action on mineral weathering: (i) They extract nutrients from the minerals by a transfer of electrons following their adherence to the surface of the mineral; (ii) they break the oxygen links in the mineral structure and (iii) they create an

imbalance between the concentrations of anions and cations in the solution, indirectly causing the rate of mineral dissolution to accelerate as their hydroxyl and carboxyl groups chelate ions in solution (Welch *et al.,* 2002). The simultaneous use of the two processes, acidolysis and complexolysis by bacteria, are well known for their ability to have an impact on the stability of minerals (Leyval and Berthelin, 1989).

In soils, the mineral surface-colonising microbial communities are different to those inhabiting the soil surroundings (Certini *et al*., 2004). A micro-environment is formed when microbes attach to the surfaces of minerals and protect them against environmental stresses (Liermann *et al*., 2000; Ojeda *et al*., 2006). Mineral nutrients in micro-environments can either be shared amongst surrounding micro-organisms or directly chelated from the soil (Roberts Rogers and Bennett, 2004). The mineral weathering of insoluble phases can be promoted by siderophores produced by the micro-organisms in the soil (Certini *et al*., 2004). Even those silicates characterised by chemical and physical resistance can be attacked by microbial activities (Brehm *et al*., 2005). In conjunction with biomechanical effects, microbial action is largely indirect through the production of either chelates, other metabolites or organic or mineral acids (Cromack *et al*., 1979; De La Torre *et al*., 1992; Mandal *et al*., 2002). The silicate lattice structure may collapse during bio-weathering of rock aluminosilicates and silicates through either cation removal from the crystal lattice of the silicate or cleavage of Mg-O, Al-O or Si-O-Si (siloxane) bonds (Mandal *et al*., 2002).

In earlier reports (e.g., Paris *et al.,* 1994; Daghino *et al.,* 2009,) bacteria have been documented to weather phyllosilicates, such as clays and micas. Essential element extraction from minerals forms the core of microbe-mineral interactions.

## 9.3. Conclusion

For more than ninety years, South Africa extensively mined asbestos minerals (Petja *et al.,* 2007). Numerous countries implemented a ban on the use of asbestos because of the associated health problems. However, following decades of intensive asbestos mining, vast tracts of asbestos-contaminated soils, dumps and tailings still confront communities in past mining regions globally and, particularly, in South Africa (Braun and Kisting, 2006).

Compared to Europe or North America, the aggregate of contemporary sources of environmental asbestos exposure sources in the Northern Cape, Mpumalanga and Limpopo provinces of South Africa is considerable, and so is the number of people who still suffer and die from asbestos-related diseases (ARDs) (Braun and Kisting, 2006). The realisation of the health issues and environmental impacts created by asbestos mining lead to the closure of the mines and the commissioning of rehabilitation processes (Petja *et al.,* 2007). However, following decades of asbestos mining and industrialisation, large tracts of soil polluted with exposed harmful fibrous asbestos minerals persist and pose a monumental contemporary health and environmental hazard (Petja *et al.,* 2007). Since establishment of mine rehabilitation processes, rehabilitation by capping and vegetating asbestos-contaminated soils has been largely ineffective (Petja *et al.,* 2007), and therefore a more multi-perspective approach should prove to have better results.

## 9.4. References


Baath, E. (1989): Effects of Heavy Metals in Soil on Microbial Processes and Populations: A Review. *J. of Water, Air & Soil Pollution*, **47**, 335-379.

Bardgett, R.D. and van der Putten, W.H. (2014): Belowground biodiversity and ecosystem functioning. *Nature*, **515**, 505–511.

Barra Caracciolo, A., Bottoni, P. and Grenni, P. (2010): Fluorescence *in situ* Hybridization in soil and water ecosystems: a useful method for studying the effect of xenobiotics on bacterial community structure. *Toxicological and Environmental Chemistry*, *92*, 567-579

Bazylinski, D. A. and Schubbe, S. (2007)**:** Controlled biomineralization by and applications of magnetotactic bacteria. *Advanced Applied Microbiology,* **62**, 21-62.

Bergna, H.E. (1994): Colloid chemistry of silica – an overview. *Colloid Chem Silica*, **234**, 1-47.

Bhattacharya, K., Dopp, E., Kakkar, P., Jaffery, F.N., Schiffmann, D., Jaurand, M.C., Rahman, I. and Rahman Q. (2005): Biomarkers in risk assessment of asbestos exposure. *Mutation Research,* **579**, 6-21.

Blagodatskaya, E. and Kuzyakov, Y. (2008): Mechanisms of real and apparent priming effects and their dependence on soil microbial biomass and community structure: critical review. *Biology and Fertility of Soils*, **45**, 115–131.

Bogan, B.W. and Sullivan, W.R. (2003): Physio-Chemical Soil Parameters Affecting Sequestration and Mycobacterial Biodegradation of Polycyclic Aromatic Hydrocarbons (PAHs) in Soil. *Journal of the Chemosphere*, **52**, 1717- 1726.

Boyd, P.W., Jickells, T., Law, C.S., Blain, E.A., Buesseler, K.O., Coale, K.H., Cullen, J.J., de Baar, H.J.W., Follows, M., Harvey, M., Lancelot, C., Levasseur, M., Owens, N.P.J., Pollard, R., Rivkin,

R.B., Sarmiento, J., Schoemann, V., Smetacek, V., Takeda, S., Tsuda, A., Turner, S. and Watson, A.J. (2007): Mesoscale iron enrichment experiments 1993-2005: Synthesis and future directions. *Science*, **315**, 612-617.

Brehm, U., Gorbushina, A. and Mottershead, D. (2005): The role of microorganisms and biofilms in the breakdown and dissolution of quartz and glass. *Palaeogeography, Palaeoclimatology, Palaeoecology*, **219**, 117–129.

Brown, G.M., Bonnesen, P.V., Moyer, B.A., Gu, B., Alexandratos, S.D. and Patel, V. (1999): Design of selective resins for the removal of pertechnetate and perchlorate from groundwater. Abstracts of Papers American Chemical Society, 218th National Meeting of the American Chemical Society, Part 1 & 2. New Orleans, Louisiana.

Bundt, M., Widmer, F., Pesaro, M., Zeyer, J. and Blaser, P. (2001): Preferential flow paths: biological 'hot spots' in soil. *Soil Biology and Biochemistry*, **33**, 729–738.

Campbell, W.J. and co-workers (1977): Selected Silicate Minerals and Their Asbestiform **Varieties**. IC 8751, U.S. Bureau of Mines, Washington, D.C., p. 5 - 33.

Carson, J.K., Rooney, D., Gleeson, D.B. and Clipson, N. (2007): Altering the mineral, composition of soil causes a shift in microbial community structure. *FEMS Microbiology Ecology*, **61**, 414–423.

Carson J.K., Campbell L., Rooney D., Clipson N. and Gleeson D.B. (2009): Minerals in soil select distinct bacterial communities in their microhabitats. *FEMS Microbiology Ecology*, **67**, 381-388.

Certini, G., Campbell, C.D. and Edwards, A.C. (2004): Rock fragments in soil support a different microbial community from the fine earth. *Soil Biology and Biochemistry,* **36**, 1119-1128.

Chiapello, M., Daghino, S., Martino, E. and Perotto, S. (2010): Cellular response of *Fusarium oxysporium* to crocidolite asbestos as revealed by a combined proteomic approach. *Journal of Proteome Resources,* **9** (8), 3923- 3931.

Cromack, K., Jr, Solkins, P., Grausten, W.C., Speidel, K., Todd, A.W., Spycher, G., Li, C.Y. and Todd, R.L. (1979): Calcium oxalate accumulation and soil weathering in mats of the hypogeous fungus *Hysterangium crassum*. *Soil Biology and Biochemistry*, **11**, 463–468.

Daghino, S., Martino, E., Fenoglio, I., Tomatis, M., Perotto, S. and Fubini, B. (2005): Inorganic Materials and Living Organisms: Surface Modifications and Fungal Responses to Various Asbestos Forms. *Chemistry: A European Journal*, **11**, 5611 – 5618

Daghino, S. (2005): Asbestos hazard in Western Alps: the use of soil fungi in bioremediation of asbestos fibres dispersed in the environment; a chemical molecular integrated analysis. Other. Università degli studi di Torino; Université Joseph-Fourier - Grenoble I.

Daghino, S., Turci, F., Tomatis, M., Favier, A., Perotto, S., Douki, T. and Fubini, B. (2006): Soil fungi reduce the iron content and the DNA damaging effects of asbestos fibers. *Environmental Science and Technology*, **40**, 5793-5798.

Daghino, S., Martino, E., Vurro, E., Tomatis, M., Girlanda, M., Fubini, B. and Perotto, S. (2008): Bioweathering of chrysotile by fungi isolated in ophiolitic sites. *FEMS Microbiology Letters*, **285**, 242-249.

Daghino, S., Turci, F., Tomatis, M., Girlanda, M., Fubini, B. and Perotto, S. (2009): Weathering of chrysotile asbestos by the serpentine rock inhabiting fungus *Verticillium leptobactrum. FEMS Microbiology Ecology*, **69**, 132-141.

Daghino, S., Martino, E. and Perotto, S. (2010): Fungal weathering and implications in the solubilization of metals from soil and from asbestos fibres. *Current research, technologies and education topics in Applied Microbiology and Microbial Biotechnology,* **1**, 329-338.

Donmez, H., Ozkul, Y. and Ucak, R. (1996): Sister chromatid exchange frequency in inhabitants exposed to asbestos in Turkey. *Mutation Research*, **361**, 129-132.

Ehrlich, H.L. (1981): **Geomicrobiology**. Marcel Dekker Inc., New York, USA.

Ehrlich, H.L. (1996): How microbes influence mineral growth and dissolution. *Chemical Geology*, **132**, 5-9.

Ehrlich, H. L. (1998): Geomicrobiology: its significance for geology. *Earth Sci Rev*, **45**, 45–60.

Ehrlich, H.L. (2001): Past, present and future of biohydrometallurgy. *Hydrometallurgy*, **59**, 127-134.

Ehrlich, H. L. and Newman, D. K. (2009): **Geomicrobiology** (5th edition). CRC Press/Taylor & Francis, Boca Raton, FL.

Ellis, R.J. (2004): Artificial soil microcosms: a tool for studying microbial autecology under controlled conditions. *Journal of Microbiological Methods*, **56**, 287– 290.

Faver-Longo, S.E., Siniscalco, C. and Piervittori, R. (2006): Plant and lichen colonization in an asbestos mine; Spontaneous bioattenuation limits air dispersion of fibres. *Plant Biosystems*, **140** (2), 190- 205.

Favero-Longo, S.E., Girlanda, M., Honegger, R., Fubini, B. and Piervittori, R. (2007): Interactions of sterile-cultured lichen-forming ascomycetes with asbestos fibres. *Mycological Research*, **111**, 473-481.

Fenoglio, I., Prandi, L., Tomatis, M. and Fubini, B. (2001): Free radical generation in the toxicity of inhaled mineral particles: the role of iron speciation at the surface of asbestos and silica. *Redox Report,* **6**, 235-241.

Fubini, B., Gianello, E., Volante, M. and Bolis, V. (1990): Chemical functionalities at the silica surface determining its reactivity when inhaled: formation and reactivity of surface radicals. *Toxicology and Industrial Health,* **6**, 571-94.

Fubini, B. (1997): Surface reactivity in the pathogenic response to particulates. *Environmental Health Perspectives,* **105** (5), 1013-1020.

Gadd, G.M. (2004): Microbial influence on metal mobility and application for bioremediation. *Geoderma*, **122**, 109 – 119. doi: 10.1016/j.geoderma.2004.01.002

Gadd, G.M. (2008): Bacterial and fungal geomicrobiology: a problem with communities? *Geobiology*, **6**, 278–284.

Gadd, G.M. (2010): Metals, minerals and microbes: geomicrobiology and bioremediation. *Microbiology*, **156** (3), 609 - 43.

Gadd, G.M. (2017): Geomicrobiology of the built environment. *Nature Microbiology,* **2**, 1 – 9. [16275]. https://doi.org/10.1038/nmicrobiol.2016.275

Gazzano, E., Foresti, E., Lesci, I.G., Tomatis, M., Riganti, C., Fubini, B., Roveri, N. and Ghigo, D. (2005): Different cellular responses evoked by natural and stoichiometric synthetic chrysotile asbestos. *Toxicology and Applied Pharmacology*, **206**, 356–364.

Girma, G. (2015): Microbial Bioremediation of Some Heavy Metals in Soils: An Updated Review. *Indian Journal of Science Research,* **6** (1), 147 – 161.

Glazer, A.N. and Nikaido, H. (1995): **Microbial biotechnology: fundamentals of applied microbiology**. Freeman, New York.

Grenni, P., Gibello, A., Barra Caracciolo, A., Fajardo, C., Nande, M., Vargas, R., Saccà, M.L., MartinezIñigo, M.J., Ciccoli, R. and Martín, M. (2009): A new fluorescent oligonucleotide

probe for *in situ* detection of s-triazine-degrading *Rhodococcus wratislaviensis* in contaminated groundwater and soil samples. *Water Research*, **43**, 2999-3008.

Guenet, B., Leloup, J., Hartmann, C., Barot, S. and Abbadie, L. (2011): A new protocol for an artificial soil to analyse soil microbiological processes. *Applied Soil Ecology*, **48**, 243–246. doi: 10.1016/j.apsoil.2011.04.002

Guthrie, G.D. (1997): Mineral properties and their contributions to particle toxicity. *Environmental Health Perspectives*, **105**, 1003.

Hart, H.P. (1988): Asbestos in South Africa. *Journal of the Southern African Institute of Mining and Metallurgy,* **88** (6), 185 – 198.

Hinsinger, P., Bengough, A.G., Vetterlein, D. and Young, I.M. (2009): Rhizosphere: biophysics, biogeochemistry and ecological relevance. *Plant Soil*, **321**, 117–152.

Hodgson, A.A. (1986): **Scientific Advances in Asbestos, 1967 to 1985**. Anjalena Publication, Crowthorne, UK, p. 10 -117.

Johansson, J.F., Paul, L.R. and Finlay, R.D. (2004): Microbial interactions in the mycorrhizosphere and their significance for sustainable agriculture. *FEMS Microbiology Ecology,* **48**, 1-13.

Kilburn, K.H. (2000): Indoor air effects after building renovation and in manufactured homes. *American Journal of the Medical Sciences*, **320** (4), 249 - 254.

Konhauser, K.O. (2007): **Introduction to Geomicrobiology**. Blackwell, Oxford, United Kingdom.

Konhauser, K.O., Kappler, A. and Roden, E.E. (2011): Iron in Microbial Metabolisms. *Elements*, **7**, 89 – 93. DOI: 10.2113/gselements.7.2.89

Laossi, K.L., Noguera, D.C., Bartolomé-Lasa, A., Mathieu, J., Blouin, M. and Barot, S. (2009): Effects of endogeic and anecic earthworms on the competition between four annual plants and their relative reproduction potential. *Soil Biology and Biochemistry*, **41**, 1668–1773.

Lewis, R. (2003): Bioremediation. In R. Robinson (Ed.), *Genetics*. New York: Macmillian Reference USA.

Leyval, C. and Berthelin, J. (1989): Interactions between *Laccaria laccata, Agrobacterium radiobacter* and beech roots: influence on P, K, Mg and Fe mobilization from minerals and plant growth. *Plant Soil*, **117**, 103–110

Liermann, L.J., Kalinowski, B.E., Brantley, S.L. and Ferry, J.G. (2000): Role of bacterial siderophores in dissolution of hornblende. *Geochimica et Cosmochimica Acta*, **64**, 587-602.

Liermann, L.J., Barnes, A. S., Kalinowski, B. E., Zhou, X. and Brantley, S. L. (2000): Microenvironments of pH in biofilms grown on dissolving silicate surfaces. *Chemical Geology,* **171**, 1 - 16.

Lin, F.C. and Clemency, C.V. (1981): The dissolution kinetics of brucite, antigorite, talc, and phlogopite at room-temperature and pressure. *American Mineralogist*, **66**, 801–806.

Lujan, A.M., Gomez, P. and Buckling, A. (2015): Siderophore cooperation of the bacterium *Pseudomonas fluorescens* in soil. *Biology Letters,* **11** (20140934), 1–4. http://dx.doi.org/10.1098/rsbl.2014.0934

Lund, L.G. and Aust, A.E. (1990): Iron mobilisation from asbestos by chelators and ascorbic acid. *Archives, Biochemistry, Biophysics*, **278**, 60– 64.

Manning, C.B., Vallyathan, V. and Mossman, B.T. (2002): Diseases caused by asbestos: Mechanisms of injury and disease development. *International Immunopharmacology,* **2**, 191-200.

Mapelli, F., Marasco, R., Balloi, A., Rolli, E., Cappitelli, F., Daffonchio, D. and Borin, S. (2012): Mineral–microbe interactions: Biotechnological potential of bioweathering. *Journal of Biotechnology*, **157** (4), 473–481

Martino, E., Prandi, L., Fenoglio, I., Bonfante, P., Perotto, S. and Fubini, B. (2003): Soil Fungal Hyphae Bind and Attack Asbestos Fibers. *Angewandte Chemie International Edition,* **42** (2), 219 – 222. DOI:10.1002/anie.200390083

Martino, E., Cerminara, S., Prandi, L., Fubini, B. and Perotto, S. (2004): Physical and biochemical interactions of soil fungi with asbestos fibers. *Environmental Toxicology and Chemistry*, **23**, 938 – 944.

McCulloch, J. (2003): Asbestos mining In Southern Africa, 1893-2002. *International Journal of Occupational and Environmental Health*, **9**, 230-235.

Meeks, M.E. (1982): Pathogenesis of asbestos-associated diseases. *The New England Journal of Medicine*, **307**, 1526 - 1527.

Milne, S.J., Garton, E., Nelson, G., Murray, J., Davies, J.C.A. and Phillips, J.I. (2013): A South African database of samples analysed for the presence of asbestos. *Occupational Health Southern Africa*, **19** (6), 14 – 21.

Morgan, P. and Watkinson, R.J. (1989): Hydrocarbons Degradation in Soils and Methods for Soil Biotreatment. *CRC Critical Reviews in Biotechnology*, **8**, 305-333.

Mossman, B.T. and Gee, J.B.L. (1989): Asbestos-related diseases. *The New England Journal of Medicine,* **320**, 1724 -1730.

Mossman, B.T., Bignon, J. and Corn, M. (1990): Asbestos: scientific developments and implications for public policy. *Science,* **247**, 294-301.

Nagai, H., Ishihara, T., Lee, W.H., Ohara, H., Okazaki, Y., Okawa, K. and Toyokuni, S. (2011): Asbestos surface provides a niche for oxidative modification. *Cancer Science*, **102** (12), 2118-25.

Ojeda, L., Keller, G., Mühlenhoff, U., Rutherford, J.C., Lill, R. and Winge, D.R. (2006): Role of glutaredoxin-3 and glutaredoxin-4 in the iron regulation of the Aft1 transcriptional activator in *Saccharomyces cerevisiae*. *Journal of Biological Chemistry*. **281**, 17661–17669.

Okayasu, R., Takahashi, S., Yamada, S., Hei, T.K. and Ullrich, R.L. (1999): Asbestos and DNA double strand breaks. *Cancer Research,* **59**, 298-300.

Paris, F., Bonnaud, P., Ranger, J. and Lapeyrie, F. (1994): Phyllosilicate alteration by ectomycorrhizal fungi *in-vitro*. *Acta Bot Gallica*, **141**, 529–532

Pascolo, L., Gianoncelli, A., Schneider, G., Salome, M., Schneider, M., Calligaro, C., Kiskinova, M., Melato, M. and Rizzardi, C. (2013): The interaction of asbestos and iron in lung tissue revealed by synchrotron-based scanning X-ray microscopy. *Scientific Reports*, **3**, 1123.

Pollastri, S., D'Acapito, F., Trapananti, A., Colantoni, I., Andreozzi, G.B. and Gualtieri, A.F. (2015): The chemical environment of iron in mineral fibres. A combined X-ray absorption and Mössbauer spectroscopic study. *Journal of Hazardous Materials*, **298**, 282–293.

Pumpel, T. and Paknikar, K.M. (2001)**:** Bioremediation technologies for metal-containing wastewaters using metabolically active microorganisms. *Advanced Applied Microbiology,* **48**, 135-169.

Ramsey, M.J., Moore, D.H., Briner, J.F., Lee, D.A., Olsen, L., Senft, J.R. and Tucker, J.D. (1995): The effects of age and lifestyle factors on the accumulation of cytogenetic damage as measured by chromosome painting. *Mutation Research*, **338**, 95-106.

Roberts Rogers, J. and Bennett, P.C. (2004): Mineral stimulation of subsurface microorganisms: release of limiting nutrients from silicates. *Chemical Geology*, **203**, 91-108.

Shukla, A., Gulumian, M., Hei, T.K., Kamp, D., Rahman, Q. and Mossman, B.T. (2003): Multiple roles of oxidants in the pathogenesis of asbestos induced diseases. *Free Radical Biology and Medicine*, **34**, 1117-1129.

Skinner, H.C.W., Ross, M. and Frondel, C. (1988): **Asbestos and other fibrous materials – mineralogy, crystal chemistry, and health effects**. Oxford University Press, New York (NY).

Srivastava, J., Naraian, R., Kalra, S.J.S. and Chandra, H. (2014): Advances in microbial bioremediation and the factors influencing the process. *International Journal of Environmental Sciences and Technology*, **11**, 1787–1800. DOI 10.1007/s13762-013-0412-z

Thassitou, P.K. and Arvanitoyannis, I.S. (2001): Bioremediation: a novel approach to food waste management. *Trends in Food Science and Technology*, **12,** 185-196.

Tomatis, M., Turci, F., Ceschino, R., Riganti, C., Gazzano, E., Martra, G., Ghigo, D. and Fubini, B. (2010): High aspect ratio materials: role of surface chemistry vs. length in the historical long and short amosite asbestos fibers. *Inhalation Toxicology*, **22**, 984–998.

Toyokuni, S. (2009): Mechanisms of asbestos-induced carcinogenesis. *Nagoya Journal of Medical Science*, **71**, 1 - 10.

Unfried, K., Schurkes, C. and Abe, J., (2002): Distinct spectrum of mutations induced by crocidolite asbestos: clue for 8-hydroxydeoxyguanosine dependent mutagenesis *in vivo*. *Cancer Research*, **62**, 99-104.

Uroz, S., Calvaruso, C., Turpault, M.P. and Frey-Klett, P. (2009): Mineral weathering by bacteria: ecology, actors and mechanisms. *Trends in Microbiology*, **17**, 378–387.

US Geological Survey, (2001): Some Facts about Asbestos (USGS Fact Sheet FS-012-01).

Voroney, R.P. (2007): The Soil Habitat. In: *Soil Microbiology, Ecology, and Biochemistry*. Academic Press, Oxford, United Kingdom, 25 – 49.

Welch, S.A. and Ullman, W.J. (1993): The effect of organic acids on plagioclase dissolution rates and stoichiometry. *Geochimica Cosmochimica Acta*, **57**, 2725–2736

Welch, S.A., Taunton, A.E. and Banfield, J.F. (2002): Effect of microorganisms and microbial metabolites on apatite dissolution. *Geomicrobiology Journal*, **19**, 343–367.

Whatteau, F. and Berthelin, J. (1994): Microbial dissolution of iron and aluminium from soil minerals; efficiency and specificity of hydroxamate siderophores compared to aliphatic acids. *European Journal of Soil Biology*, **30**, 1-9.

Whittaker, E.J.W. (1979): **Short Course in Mineralogical Techniques of Asbestos Determination** (Volume 4). Mineralogical Association of Canada, Quebec, Canada, p. 16 - 30.

Willenbring, J.K., Mohanty, S.K., Salamatipour, A., Gonneau, C., Jerolmack, D. and Casper, B. (2016): The Fate of Asbestos in Soil: Remediation Prospects and Paradigms. 252nd American Chemical Society National Meeting, Philadelphia, August 21 - 2

# Chapter 10 – Conclusion

Chrysotile, crocidolite, and amosite compose the three principle types of asbestos (Hart, 1988). South Africa contains all three varieties making it unique (Hart, 1988). In South Africa, which was the third largest producer of asbestos, the mining of this industrial mineral occurred from the late 1800s to 2002, and was used for a wide variety of industrial applications (Nelson *et al.,* 2011). The long history of mining and manufacturing has made asbestos a priority contaminant concern in South Africa with a large number of potentially contaminated sites (Nelson *et al.,* 2011).

Rich deposits of asbestos and decades of mining in South Africa have left a prominent and persistent legacy of asbestos-contaminated soils, mines, dumps, and tailings throughout several rural parts of provinces that represent a significant and fatal health risk to local communities. Repeated experimentations have proven the association between asbestos exposure and carcinoma (Okayasu *et al*., 1999; Kilburn, 2000; Unfried *et al*., 2002). The toxicity and carcinogenic effects of asbestos-mineral fibres are related to the physical and chemical properties, including durability and/or bio-persistence, high aspect-ratio and chemical composition of these fibrous minerals (Mossman *et al.,* 2011; Pugnaloni *et al.,* 2013; Bloise *et al.,* 2016). There are numerous types of asbestos-related diseases, including both diseases of the pleura and of the lung parenchyma (Ndlovu *et al.,* 2013). Malignant mesothelioma, thickening and pleural plaques comprises the pleura diseases category, and asbestosis and lung cancer comprise the lung parenchyma diseases category (Rees *et al.,* 1999; Ndlovu *et al.,* 2013). The current consensus, based on scientific evidence, is that there is no safe level or threshold of asbestos fibre exposure below which the risk of mesothelioma is negligible (Ramazzini, 2011; Gualtieri *et al.,* 2012). Different fibrous minerals have been extensively demonstrated to have different toxicities due to their different physical and chemical properties (Fubini and Otero Arean, 1999; Fubini and Fenoglio, 2007).

Derelict asbestos mines are distributed throughout the rural landscapes of Southern Africa. These massive pollution sources directly influence the environment serving as perennial sources of metal contamination disrupting abiotic and biotic operational ecosystem balance, thereby challenging productivity and sustainability. Additionally, exposed asbestos-containing geological material, such as that characterising DAMLs, may release fibres that

become airborne representing a direct pathway for their incorporation into the human body via inhalation. The rehabilitation of derelict asbestos mine sites, dumps and tailings involves numerous deliberations, such as revegetation issues, health-related risks to asbestos exposure during the process and the high costs of prioritisation, implementation, and monitoring. The conventional encapsulation method for derelict asbestos mine wastes focuses on soil remediation and has proven to be slow, expensive, self-restricted and not site-feasible with regards to long-term and effective ecological restoration. Soil remediation methods focus on ameliorating the chemical impediments of the soluble phase at present without considering the waste rock itself as a perpetual source of unfavourable and plant growth restricting factors. The inability of this conventional rehabilitation to overcome the mineralogical and geochemical barriers in mine dumps makes it unsuitable for long-term, self-sustaining rehabilitation and restoration aspirations.

The health risks, environmental impacts and rehabilitation challenges associated with derelict asbestos mine waste in Southern Africa were evaluated in this study. Geochemical and mineralogical investigations of asbestos-containing rock wastes in abandoned mine environments should be performed as a prerequisite for both human and environmental health risk assessments. Chapter 2 provides the first comprehensive geochemical and mineralogical investigation of the actual, exposed asbestos mine waste from derelict asbestos mine sites in Southern Africa. Here, the importance of characterizing the geochemical and mineralogical components of the asbestos-bearing rock waste for both human and environmental risk assessments and rehabilitation design is highlighted. The actual asbestos waste at these sites has been overlooked by most studies concerned with secondary asbestos occurrences, such as asbestos dusts and asbestos in soils. The argument presented is that to make realistic assessments, the focus of such studies should commence at the source of the asbestos pollution, being the asbestos mine wastes themselves, as it provides the framework and explanations for all other consequent asbestos occurrences. This perspective allows for predictive geological modeling and relative human and environmental risk estimations, both of which, as it is argued, are more valuable than the insight gained from secondary asbestos pollution sources.

The potential environmental and human hazards associated with the geological material comprising the mine wastes generated during mining was investigated. The

petrological, morphological, and chemical data provide valuable information on the potential toxicity of the certain asbestos minerals to surrounding communities and environments. This data provides a baseline from which communities and industries in proximity to these environmental exposure sources can assess the risks, and subsequently act on or implement the appropriate safety measures.

The chemical stability of chrysotile, amosite, crocidolite and anthophyllite asbestos was investigated in chapter 3. The mechanisms and kinetics of the four asbestos rock samples were distinct, indicating variations of chemical and physical characteristics and the nature of the particle assemblages. The batch isothermal dissolution experiments in acidic solutions showed that the chemical stability between the types were as follows: Chrysotile < crocidolite < amosite < anthophyllite. Dissolution mechanisms and kinetics models of asbestos are important for estimating the residence time in the soil. This study is important as it allows inferences of the chemical stability and therefore persistence of certain fibre types in the natural environment intended for rehabilitation.

Mineralogical, physicochemical, and microbiological baseline data provide insight into site-specific ecosystem risks posed by asbestos sites to restoration sustainability. In chapter 4, methods practical to developing countries for predictive planning were outlined. Current asbestos management strategies employ a universal approach for all asbestos sites, precluding site-unique factors challenging environmental restoration. This approach, as a novel idea, allows the biotically adverse geological conditions to be predetermined and initial remedies employed. The geological and mineralogical conditions characterising un-weathered alkaline amosite and crocidolite asbestos mine rock wastes, mine dumps and tailings, are not conducive to the development and long-term establishment of local, native, indigenous vegetation adapted to the ancient, highly weathered acidic soil conditions characterising the region. Recent studies of plant-growth on alkaline mine wastes attribute this post rehabilitation plant growth failure primarily to N deficiency and high pH (Cross *et al.,* 2019; 2020; Cross and Lambers, 2021). Also, the soil microbial abundance and diversity of mine waste substrates appear to be one of the most important traits influencing the long-term success of rehabilitation strategies in terms of vegetation establishment and cover. The present study indicates that asbestos mine rock wastes are, in large, biologically inert substrates, and therefore act as a negligible source of microbiological input into the augmented overlying soil.

Bio-augmentation-assisted asbestos mine dump rehabilitation was considered in chapter 5 in terms of biotechnology available in context of developing countries, such as South Africa. The suitability of using the commercially available PGPR *Pseudomonas fluorescens* bio-fortifier as a bio-inoculant for asbestos mine lands was tested using growth-assay based microbiological methods. These tests demonstrate that *P. fluorescens* has an exceptional capacity to withstand hostile environmental conditions, which, with its numerous plant growth promoting traits, makes it a promising contemporary solution for improving asbestos rehabilitation success.

The increased awareness of the risks posed by the environmental exposition of asbestos from NOA geological units has led to novel interest in the *in-situ* identification and characterisation of regulated asbestiform and non-regulated fibrous minerals. The ability to recognise the numerous forms presented by asbestos in their natural setting and discerning NOA geological environments is crucial in mitigating the risks of environmental exposure. Predictive and informed understanding of geological units potentially hosting asbestos mineralisation allows for managing and mitigation strategies to be put in place prior to land-disturbing activities, thereby securing public health. This geological approach allows for a greater understanding of asbestos geology and the recognition of geological environments that are likely to bear asbestos mineralisation. Such a strategy aids in the identification of asbestos-bearing regions and spares the costs and efforts of monitoring and regulating asbestos in locations where it is not necessary.

Asbestos mineralisation occurs in specific and anticipatable geological settings, and thus understanding and applying principles of asbestos geology allows asbestos-dust exposures to be managed, thereby assisting industries and agencies involved in natural deposit disturbances. Chapters 6 and 7 provide geological knowledge of asbestos-mineralisation used for site development design and exposure safety protocols required by mining industries. The geological approach in this study provides guidelines, which mining sectors may use to predict and therefore appropriately manage risk mitigating procedures upon encountering asbestos.